# Geochemistry and Geochronology of Palaeoproterozoic Fe-rich Tholeiites and Metasediments from the Georgetown Inlier, North Queensland: their Petrogenesis, Metamorphic History, Tectonic Setting, and Implications for Relationship with the Broken Hill and Mt Isa Sequences.

by

Michael J Baker, B.Sc. (Hons.)

Submitted in fulfilment of the
Requirements for the Degree of

Doctor of Philosophy


University of Tasmania, September, 2007

## Declaration

This thesis contains no material that has been accepted for the award of a degree or diploma at any other institution. To the best of the author's knowledge, this thesis contains no material previously written or published by another person, except where due reference is given in the text. All referenced material is listed in the back of the thesis.

## Authority of Access

This thesis may be made available for limited loan or photocopying in accordance with the *Copyright Act 1968.*

# Geochemistry and geochronology of Palaeoproterozoic Fe-rich tholeiites and metasediments from the Georgetown Inlier, North Queensland: their petrogenesis, metamorphic history, tectonic setting, and implications for relationship with the Broken Hill and Mt Isa sequences.

## Abstract

Fe-rich tholeiites intruded the lower Etheridge Group of the Georgetown Inlier of north Queensland during the late-Palaeoproterozoic (ca. 1680-1640 Ma), during a prolonged period of rift-related sedimentation associated with extension in the Georgetown basin. The tholeiites comprise two lithologically distinct units: the extrusive Dead Horse Metabasalt (DHM), a conformable 1000m-thick series of fine- to coarse-grained basalts and pillow lavas; and the intrusive Cobbold Metadolerite (CMD), a multitude of sills and lesser dykes that range from a few metres to over 500 m in thickness. U-Pb LA-ICPMS dating of igneous zircons indicate the tholeiites were intruded in at least two pulses. The first coincided with the extrusion of the DHM and associated CMD sills at ca. 1670 Ma, while a younger pulse occurred during the deposition of the overlying Lane Creek Formation at ca. 1640 Ma.

The DHM and CMD are co-magmatic, and have compositions typical of relatively evolved, low-K, Fe-rich continental tholeiites and tholeiites generated in plume-triggered volcanic passive margins leading up to continental breakup. Immobile major and trace element patterns suggest that the tholeiites were derived from partial melting of the convecting depleted upper mantle depleted mantle melt, and melts evolved along a trend of increasing Fe-enrichment to strongly Fe-enriched (21.11 wt% total Fe as $Fe_2O_3$) ferro-tholeiites. Initial $\varepsilon_{Nd}$ values range between +2.6 and +5.3 (average +4.0), confirming a depleted mantle source for the tholeiites. $T_{DM}$ ages range between 1.85 Ga and 3.39 Ga (average 2.5 Ga). Several samples show slight LILE- and LREE-enrichment and have low initial $\varepsilon_{Nd}$ values (+2.6-2.9) consistent with limited crustal contamination involving local host sedimentary rocks of the lower Etheridge Group.

Between ca. 1600 and 1500 Ma, the lower Etheridge Group was deformed and metamorphosed by at least two regionally significant orogenic events. The first event ($D_1$) was the most intense, producing a pervasive foliation and metamorphism ($M_1$) that varied in intensity from upper amphibolite facies in the east, through to lower greenschist facies in the south-west. Metasediments in the south of the inlier record *P-T* conditions of up to 650°C and 7.5 kbar for $M_1$. $D_1$ was followed by a period of retrogressive metamorphism that lasted until ca. 1550 Ma, when voluminous granitoids of the Forsayth Batholith were intruded into the lower Etheridge Group. High-temperature, low-pressure metamorphism ($M_2$) was associated with this event. Initial *P-T* conditions for $M_2$ are inferred from a retrogressive mineral assemblage that returned conditions of 550°C and 3 kbar. EMPA monazite dating returned a possible ca. 1585 Ma age for $M_1$ and a ca. 1550-1530 Ma age for $M_2$. A younger monazite population (ca. 1500

Ma) suggests either $M_2$ continued for a further 30-50 million years, or an additional weak thermal event affected the Etheridge Group at this time.

The DHM and CMD are broadly correlated temporally and geochemically to basic gneisses of the Broken Hill Group in the Willyama Inlier, and amphibolites of the Soldiers Cap Group in the Mt Isa Eastern Succession. In particular, immobile trace element ratios and REE patterns between these tholeiitic suites are virtually indistinguishable. The crystallisation ages of the DHM and CMD, as determined by U-Pb LA-ICPMS zircon dating also closely resembles established ages for the Broken Hill (ca. 1685 Ma) and Mt Isa Eastern Succession (ca. 1670 Ma) tholeiitic rocks. This relationship is of regional significance, as it suggests the terranes were spatially associated during the Palaeoproterozoic, and places the Georgetown Inlier within the Proterozoic framework of northern Australia, and likely a part of the North Australian Craton in the Palaeoproterozoic.

# Geochemistry and geochronology of Palaeoproterozoic Fe-rich tholeiites and metasediments from the Georgetown Inlier, North Queensland: their petrogenesis, metamorphic history, tectonic setting, and implications for relationship with the Broken Hill and Mt Isa sequences.

## Contents

## List of Figures

## List of Tables

# Acknowledgements

There are a number of people who I wish to acknowledge for their help and support over the course of this project, for without their assistance completing this thesis would have been next to impossible. First and foremost, my sincere thanks must go to my supervisor Tony Crawford for providing the topic, logistical and financial support in the field and for his careful editorial work and guidance throughout. For work in the field and additional editing and guidance with mineral chemistry and the analysis of monazites, I also give sincere thanks to my associate supervisor Ron Berry.

A number of people in north Queensland require thanks for their assistance in enabling me to complete the fieldwork component of this project. Significantly, the hospitality and generosity of Eddie, Adelia, and Shannon Hoolihan at Ortona Station is greatly appreciated. In particular, the Eddie's knowledge of the location of the best outcrops saved a lot of time and effort! Thanks also to Ian Withnall of the Queensland Geological Survey for his assistance with organising contacts in north Queensland, for his suggestions on where to go, and for providing maps of the field area. Thanks to Kevin for his assistance in the field, particularly with carrying a backpack full of basalt samples without complaint, and for the field surgery he successfully performed on my sledgehammer, giving it an extra two weeks of life. Mick is also thanked for his cooking at Ortona, and for the colourful stories which dragged on long into the night. In addition, Barry Hughes, Major Elgey, Kevin Hoolihan, Alan Zabel, and the owners of Robinhood Station are thanked for granting access to their respective properties. Terrasearch Pty. Ltd. in Townsville is also thanked for the use of one of their 4WD vehicles.

My analytical work at the University of Tasmania was made possible with the assistance of several people; most notably Sebastian Meffre whose considerable help with preparing zircon separates, using the LA-ICPMS, and reducing the resultant complex datasets is greatly appreciated. Thanks also to Phil Robinson, Katie McGoldrick, and Sarah Gilbert for the preparation and analysis of all the geochemistry samples, and for lending me their keys on countless occasions! David Steele and Karsten Gömann are thanked for their assistance with the use of both the EMP and SEM at the Central Science Laboratory. Simon Stephens and his assistants are thanked for the preparation of the 300+ thin sections for this project. Roland Maas at the University of Melbourne is also thanked for the preparation and analysis of the Nd-isotope samples used in the geochemistry section of this thesis.

Finally, thank-you to my all my family, in particular to Dad, Mum and Renée, for their continued interest in my progress and their encouragement despite the distance between us. Last but certainly not least, a huge thank-you to my partner Ashleigh. Her patience, love, and support have been a source of tremendous encouragement to me, and have made these last few years the most fulfilling of my life.

# Chapter 1.

# Introduction

## 1.1 Outline of the Study

Proterozoic basement complexes in eastern Australia include the Willyama Inlier of western NSW and eastern SA, the Mt Isa – Macarthur Basin Inliers of western Queensland and the Northern Territory, the Georgetown Inlier of north Queensland, and several smaller inlier (Coen, Yambo and Dargalong) north of the Georgetown Inlier. Two of these, the Mt Isa and Willyama Inliers, contain immense base-metal ore deposits. A growing body of evidence is showing strong similarities between these crustal blocks in terms of the nature and timing of Palaeoproterozoic magmatism and subsequent metamorphism. This has led to a number of tectonic models suggesting that these diverse crustal blocks all derive from fragmentation of a Palaeoproterozoic continental block (Giles *et al.*, 2002).

This study focuses on the geological development and magmatic, metamorphic and tectonic evolution of Proterozoic rocks in the central part of the Georgetown Inlier, the largest area of exposed Precambrian rocks in northeastern Queensland, Australia (Fig. 1.1). A major emphasis is on the timing of magmatic and metamorphic events in the western Georgetown Inlier, as this information is critical to a detailed evaluation of tectonic models claiming that the Georgetown, Mt Isa and Willyama Inliers were once contiguous as part of a Palaeozoic continental block. The geochemistry of extensive mafic igneous rocks in the central Georgetown Inlier are of particular interest to my study, and their characteristics are compared with essentially contemporaneous metabasic igneous rocks in the Broken Hill region of the Willyama Inlier (New South Wales) and in the Mt Isa Inlier of far western Queensland.

## 1.2 Previous Work - a Brief Review

The main features of the Georgetown Inlier were first outlined by reconnaissance mapping in the late 1950s by the Bureau of Mineral Resources (BMR) and the Geological Survey of Queensland (GSQ) (White, 1965). From 1972, BMR and GSQ began more detailed studies of the inlier that included geological mapping at

1:100,000 scale as well as geochronological, geochemical and geophysical studies (Withnall *et al.*, 1988a). Subsequent mapping of the area has been reported by Bain *et al.* (1985), Withnall (1985), and further 1:100,000 scale mapping was released in 2003 by the Queensland Department of Natural Resources and Mines (Withnall & Blight, 2003; Withnall *et al.*, 2003a; Withnall *et al.*, 2003b). Petrological studies focussing on the oldest rocks in the Georgetown Inlier have been carried out at numerous locations within central and western parts of the Inlier. Dating of various igneous and metamorphic rocks of the inlier was completed by Black *et al.* (1979), Black & McCulloch (1984, 1990), Black & Withnall (1993), Black *et al.* (1998, 2005) and Hoskin & Black (2000). Studies involving petrology, structural analysis, geochronology and geochemistry for the purpose of developing a model for the regional tectonic evolution of the Inlier include the work of Withnall (1985; 1996), Withnall *et al.* (1988a), Black *et al.* (1998, 2005), Boger & Hansen (2004), and Cihan & Parsons (2005).

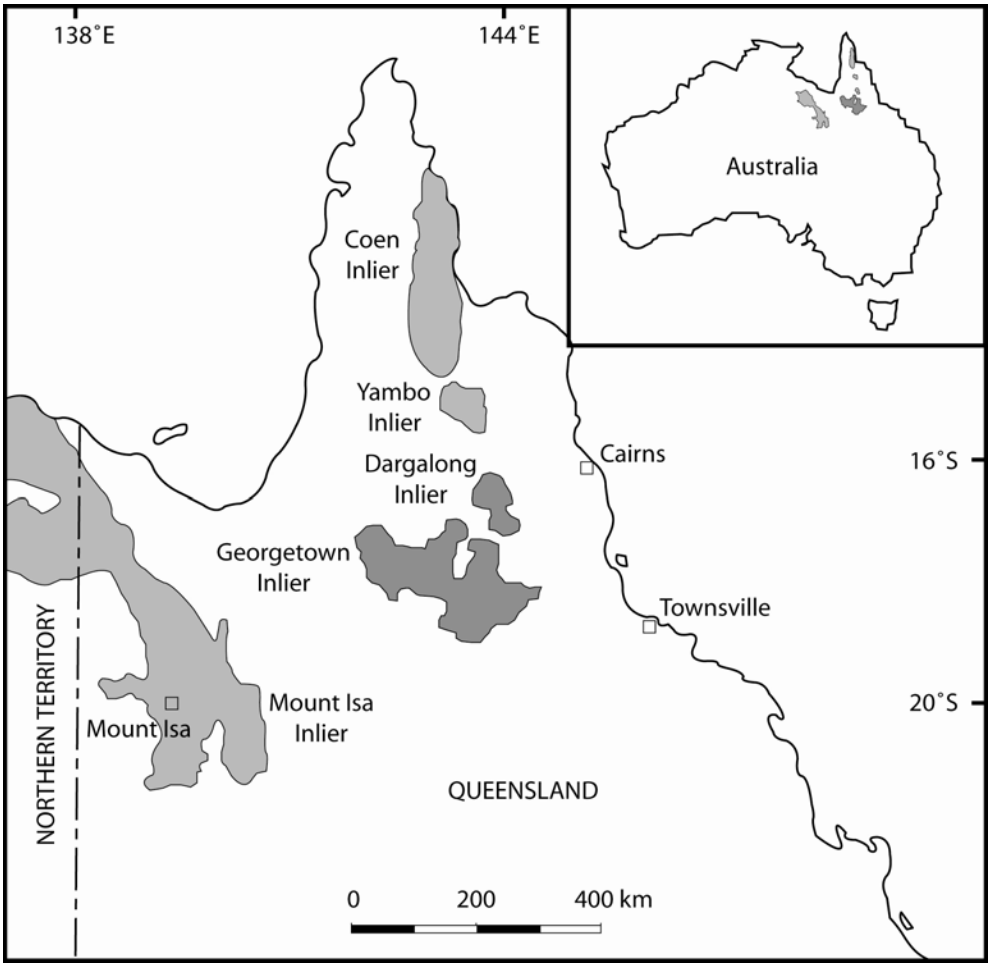


**Figure 1.1: Location map of the Georgetown Inlier. Georgetown and Dargalong Inliers are highlighted in darker grey.**

## 1.3 Background – Extensive Proterozoic and Phanerozoic Mafic Magmatism

Earth history is punctuated by numerous episodes in which rapid pulses of mafic magmatism formed extensive provinces of flood basalts, on either continental crust or oceanic crust, known as Large Igneous Provinces or LIP (Coffin & Eldholm, 1994). Well studied Phanerozoic examples include the Karoo, Parana-Entendeka, Deccan, Siberian and Emeishan flood basalts, but Proterozoic examples are also known (eg. Coppermine Range – Cape Smith Fold Belt, Canada; Griselin *et al.*, 1997). All contain vast amounts of igneous material (often in excess of $10^5$ $km^3$), and almost always consist of an extrusive component accompanied by an often voluminous suite of doleritic and gabbroic feeder sills and dykes in the underlying country rocks. The extensional environments in which flood basalt provinces occur vary from intracontinental settings in which rifting does not progress to generation of oceanic crust (eg. Siberian Traps), to regions of successful continental fragmentation and the generation of new ocean basins (eg. Parana - Entendeka, leading to opening of the South Atlantic). Consequently, the geochemistry (including isotopic characteristics) of flood basalts varies significantly. This, in turn, assists in the determination of mantle-source components and the types of contamination the magmas may have encountered through their evolution. LIP are generally interpreted to be the prime manifestation of the arrival at the Earth's surface of the head of a mantle plume (White & McKenzie, 1995; Coffin & Eldholm, 1994). Starting mantle plume heads ascend from deep in the mantle, and eventually impinge on the base of the lithosphere. The hot plume material spreads laterally, ponding beneath the lithosphere and leading to epeirogenic uplift (Nyblade & Sleep, 2003). Adiabatic decompression melting within the flattened starting-heads of upwelling mantle plumes is widely believed to be responsible for the genesis of the enormous volumes of magma forming LIP, which may form lava piles several kilometers thick (Self *et al.*, 1997). Eventually the plume material transfers its excess heat to the overlying lithosphere, thinning the lithosphere, and in some instances, leading to creation of an ocean basin.

A second form of LIP occurs on volcanic passive continental margins, and forms at the time of final breakup of continental crust and initiation of steady state ocean crust accretion. Consequent upon final rupture of the continental crust and lithospheric mantle, massive volumes of basalt are erupted in a short time interval (up to 10 m/1000 yr; Larsen & Jakobsdóttir, 1988), leading to the formation of seaward-dipping

reflector packages (SDRS). SDRS comprise lava flows that dip towards the centre of zones of rifting, probably largely due to post-depositional subsidence (e.g. SDRS of east Greenland; Larsen & Jakobsdóttir, 1988). Their occurrence is believed to result from the breakup and spreading of thinned continental basement adjacent to thick, pre-breakup, sediment-filled basins, with the thickest parts of the newly formed mafic crust associated with seaward-dipping reflectors (Mutter & Zehnder, 1988). Flood basalt provinces were originally considered to be characterised by the eruption of chemically homogeneous, relatively Fe-rich tholeiitic basalts (Kuno, 1969). Since the advent of more detailed geochemical analysis, studies have revealed significant compositional diversity both within and between individual provinces. In a general sense, most continental flood basalts (CFB) have the geochemical characteristics of enriched mid-oceanic ridge tholeiitic basalts, and isotopic compositions vary from MORB to oceanic-island basalt (OIB) affinities (Mahoney, 1987). However, SDRS basalts are generally MORB-like, as are some basalts in oceanic LIP such as the Ontong Java Plateau (Neal *et al.*, 1997).

The presence of abundant mafic rocks, including dykes, sills and lavas, all of similar geochemical affinities (Withnall, 1985) interbedded with and intruding sedimentary rocks in the Georgetown Inlier, suggests that similar processes that produced CFB provinces described above may have also have been involved in the development of the Georgetown Inlier mafic rocks. The tectonic setting for the deposition of the major rock package hosting the mafic volcanics in the Georgetown Inlier, the Etheridge Group, is the focus of current debate. It has been linked with the formation of the North Australian Craton (Myers *et al.*, 1996) during the Palaeoproterozoic and Mesoproterozoic, and in recent years a number of models have been put forward to describe this relationship (Etheridge *et al.*, 1987; Withnall *et al.*, 1988; Black *et al.*, 1998; Giles *et al.*, 2002; Boger & Hansen, 2004). The key features of each of these models are described in the following chapter, following a summary of the Proterozoic basement blocks of northeastern Australia, and leading into an outline of the geological evolution of the Georgetown Inlier.

## 1.4 Aims

This project is primarily aimed at providing a detailed understanding of the petrology, geochemistry, geochronology and tectonic significance of the mafic-igneous rocks

and enclosing sedimentary rock packages that comprise the western, low metamorphic grade part of the Palaeoproterozoic Georgetown Inlier. Such detailed information is critical for a more rigorous comparison of the Georgetown Inlier with other Proterozoic crustal blocks in northern Australia to test whether or not they were once contiguous parts of the same continental block. In particular, the formation and emplacement of the mafic rocks in the Georgetown Inlier and the 'adjacent' Mt Isa Inlier have important implications for the development of continental crust, its rifting and dispersal in forming the North Australian Craton during the Palaeoproterozoic. Other key questions that will be addressed in this project include:

1. Do the mafic rocks in the Georgetown Inlier show temporal and spatial variations in composition?
2. Are the intrusive dolerites and extrusive basalts geochemically related, as suggested by Withnall (1985) on the basis of reconnaissance data?
3. What are the magmatic affinities of the mafic rocks in the Georgetown Inlier, and how do they compare with Phanerozoic and other Proterozoic continental flood basalts?
4. How does the mafic magmatism in the Georgetown Inlier compare or contrast with Palaeoproterozoic mafic magmatism in the Broken Hill region in western New South Wales, and the Mt Isa Inlier in western Queensland? In particular, do the high-Fe mafic rocks that characterise the near-ore settings in the Broken Hill region and Mt Isa Inlier occur also in the Georgetown Inlier?
5. How similar are detrital zircon populations from the sedimentary packages above and below the major basaltic sequences in the Georgetown Inlier to those from the Mt Isa Inlier and Broken Hill region?
6. What do the structure and metamorphism tell us about the post-depositional tectonic evolution of the Etheridge Group? In particular, do the observed structural fabrics correspond to particular monazite age populations or other features of geological significance.

# Chapter 2.

# Overview of the Regional Geological Setting and Lithologies of the Georgetown Inlier and Etheridge Group, Northeast Queensland

## 2.1 Regional geology overview

### 2.1.1 Proterozoic Crustal Blocks of Northern Australia

The North Australian Craton contains several Proterozoic blocks that are inferred to have formed through the accretion of older crustal fragments, along with younger Proterozoic orogenic belts and sedimentary basins. Blocks that accumulated as sedimentary basins of Proterozoic age include those in McArthur and Mt Isa Inliers, Georgetown Inlier, and Victoria River basin (Fig. 2.1; Etheridge *et al*., 1987; Myers *et al*., 1996; Scott *et al*., 2000). Between the older cratonic blocks the structure of the Precambrian basement has mostly been interpreted from combined aeromagnetic and gravity data due to varying amounts of Phanerozoic cover (Myers *et al*., 1996). Geophysical and isotopic evidence suggests that Archaean and Proterozoic basement rocks were amalgamated to form the North Australian Craton by 1800 Ma (Myers *et al*., 1996; Tyler *et al*., 1998; Scott *et al*., 2000).

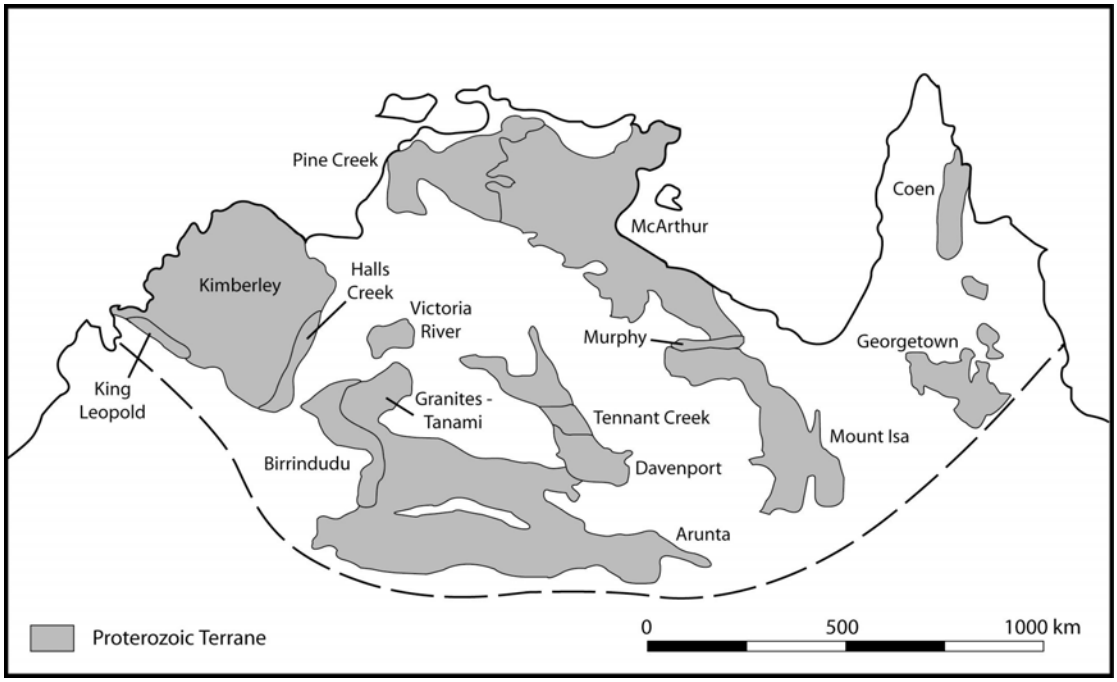


**Figure 2.1: Cartoon depicting early- to mid-Proterozoic terranes of the North Australian Craton, after Etheridge *et al.* (1987) and Myers *et al.* (1996).**

Proterozoic basement complexes in northern Australia show evidence for two main periods of deposition and orogeny (Page, 1988; Etheridge *et al*., 1987). The first depositional cycle is best represented in the Halls Creek and Pine Creek domains of western and central Australia (Etheridge *et al*., 1987). It was characterised by shallow-marine clastic sedimentary sequences containing predominately mafic volcanic rocks, overlain by dominantly carbonaceous and turbiditic sedimentary rocks. Limited study of the first cycle mafic volcanic rocks suggested they have 'both MORB and continental affinities' (Etheridge *et al*., 1987), with some examples showing geochemical similarities to tholeiitic flood basalts of the Karoo province of southern Africa (O'Dea *et al*., 1997; Giles *et al*., 2002). The first cycle of basin formation ended with the onset of a period of inter-cratonic orogeny between 1900-1870 Ma (O'Dea *et al*., 1997) that affected most of the northern Australian Proterozoic terranes. This orogeny was termed the "Barramundian" by Etheridge *et al*. (1987). The second inter-cratonic cycle of sedimentation and basin formation is generally thought to have begun around ca. 1730-1670 Ma (Etheridge *et al*., 1987). Characteristics of this orogenic cycle are described in more detail below, as it directly affected the evolution of the Georgetown Inlier.

A largely convergent setting is proposed for the cratonic elements of the North Australian Craton between 1800 and 1575 Ma (Scott *et al*., 2000). Jackson *et al*. (2000) have divided the period covered by rocks of the Victoria River, Pine Creek, McArthur, Murphy and Mt. Isa regions into the Leichhardt (c. 1800-1750 Ma), the Calvert (c. 1735-1690 Ma), and the Isa (c. 1665-1575 Ma) superbasins (Fig. 2.1). Extension in the north-east of the region began with the opening of the Davenport and Mt Isa rifts between 1835-1780 Ma, and the McArthur rift between 1750-1710 Ma (Myers *et al*., 1996). Felsic intrusives are also recorded in the western part of the North Australian Craton at this time, in the Pine Creek and Tanami regions (1835-1815 Ma; Myers *et al*., 1996). The rift stages of northern basins comprise 'continental-type' basalts, and felsic volcanics and intrusives. The igneous rocks are typically overlain by, or interbedded with, diverse terrestrial, peritidal to deep marine sediments that are characterised by extensive fine-grained carbonaceous siltstones and shales (Myers *et al*., 1996; Scott *et al*., 2000).

Extension and deposition in the northern basins continued until c. 1710 Ma, with granite intrusion occurring near the Davenport rift at this time. Further extension in

the Mt Isa region between 1680-1650 Ma led to emplacement of granitic rocks, as well as renewed deposition of sedimentary rocks (Mt Isa Group rocks; Myers *et al*., 1996; Betts & Lister, 2001). In addition to felsic magmatism, at least five discrete major, mafic magmatic events at c. 1780, 1725, 1710, 1590, and 1300 Ma are recognised in the north and central Australian terranes over this period (Scott *et al*., 2000). Although the presence of bimodal magmatism is often linked to episodes of crustal extension, Scott *et al*. (2000) preferred the interpretation that this magmatism was rather a consequence of a large mantle thermal anomaly beneath the North Australian Craton.

### 2.1.2 North-eastern Queensland Proterozoic Crustal Blocks

The Georgetown Inlier, at approximately 30,000 km$^2$, is the largest of four regions of contemporaneous Precambrian rocks in north-east Queensland. The other areas are the Dargalong, Yambo, and Coen Inliers, which all lie to the north of the Georgetown Inlier (Fig. 1.1).

The Coen Inlier is comprised of a number of Proterozoic metamorphic and granitic rocks, intruded by mid-Palaeozoic granites, and overlain locally by mid- to late-Palaeozoic sedimentary rocks (Blewett *et al.*, 1992). The Proterozoic rocks are comprised of predominately mid- to upper-amphibolite facies schist, gneiss, and some quartzite. The age of deposition and Proterozoic metamorphism in the Coen Inlier is uncertain, however zircon age dating on paragneiss from the group has returned ages of between 1590-1550 Ma (Blewett *et al.*, 1997).

The Yambo Metamorphic Group is comprised of high-grade metasedimentary and meta-igneous rocks including schist, quartzite, ortho- and paragneiss, amphibolite, and mafic granulite. A major thermal event that occurred during the mid-Proterozoic is thought to be associated to metamorphism that locally reached granulite facies conditions (Blewett & Black, 1998). The age of deposition of the sedimentary protoliths to the group is believed to have commenced after about 1643 Ma (Blewett *et al.*, 1997).

The Dargalong Metamorphic Group is comprised of a variety of rock types including migmatitic gneiss, orthogneiss, and amphibolites, along with some medium- to coarse-grained schists and lesser calc-silicate gneiss (Bultitude *et al.*, 1995). During

the mid-Proterozoic the rocks of this group experienced relatively high temperatures associated with a period of regional metamorphism. The metamorphic grade associated with this event reaches upper amphibolite facies. The age of the group is uncertain, but dating of metasedimentary rocks in the adjacent Yambo Inlier indicate deposition probably occurred towards the end of the Palaeoproterozoic (Donchak & Bultitude, 1998). Withnall *et al.* (1997) included the Dargalong Metamorphic Group into the geological framework of the Georgetown Inlier.

## 2.2 Tectonostratigraphic setting and development of the Georgetown Inlier and Etheridge Group

### 2.2.1 Geological framework

The location of this study is the regionally extensive Palaeoproterozoic to late Palaeozoic Georgetown Inlier of central northern Queensland (Fig. 1.1). The region is bounded to the west by the Carpentaria Lowlands Region and to the east by the Cairns and Clarke River Regions (Fig. 2.2). The Georgetown Inlier was originally separated into three tectonic subprovinces termed the Croydon, Forsayth, and Greenvale Subprovinces (Withnall *et al.*, 1980). The subdivisions have since been incorporated into the Etheridge Province and Croydon Province of Withnall *et al.* (1997) (Fig. 2.3).

The Mesoproterozoic Croydon Province corresponds to the Croydon Subprovince of Withnall *et al.* (1980). It is comprised of the S-type Croydon Volcanic Group and associated granites of the Esmeralda Supersuite (Fig. 2.3). The age of the province has been dated to about 1550 Ma (Black & McCulloch, 1990; Black & Withnall, 1993). The rocks are disconformably overlain by the Neoproterozoic to early Palaeozoic Inorunie Group (Fig. 2.2; Mackenzie *et al.*, 1985).

The Palaeoproterozoic Etheridge Province is divided into the Forsayth and Yambo Subprovinces (Withnall *et al.*, 1997), and corresponds to the Forsayth Subprovince of Withnall *et al.* (1980). The Yambo Subprovince is represented by the Dargalong Metamorphic Group (Fig. 2.2). The Forsayth Subprovince includes the Etheridge and Langlovale Groups, McDevitt Metamorphics, and various mafic intrusive rocks and Mesoproterozoic granites of the Forest Home and Forsayth Supersuites. Rocks of the Greenvale Subprovince of Withnall *et al.* (1980) including the Halls Reward

Metamorphics are correlated with the Etheridge Group (Withnall, 1989), and have subsequently been included with it (Fig. 2.3; Withnall *et al.*, 1997).

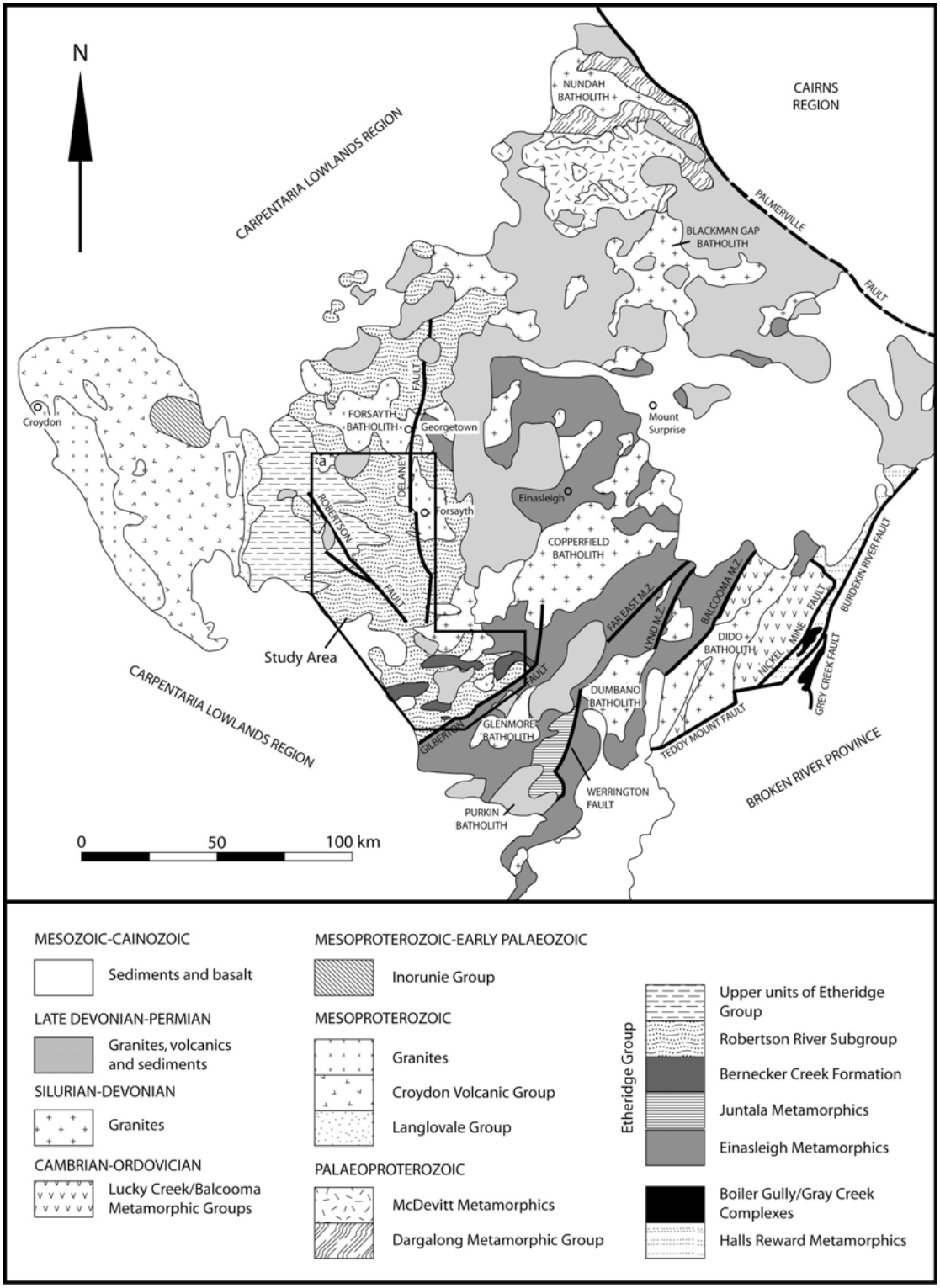


**Figure 2.2: Simplified geological map of the Georgetown Inlier (after Withnall *et al.*, 1997). (a) Area of study.**

The Etheridge Group represents the main focus of this study. It contains the majority of Palaeoproterozoic rocks in the Georgetown Inlier and crops out over approximately half of the region. The group consists predominately of shallow-marine clastic meta-sedimentary rocks, along with lesser doleritic intrusions and associated basaltic lavas. Biotite-schist, calc-silicate, and leuco-gneiss, and amphibolite occur predominately in the eastern part of the group where the metamorphic grade is higher. The Etheridge Group is thought to have been deposited between 1700-1550 Ma, based on zircon ages obtained from a number of igneous and metasedimentary rock samples within the group (Black *et al.*, 1998, 2005). The Etheridge Group is unconformably overlain to the west by the Langlovale Group and to the north by various Mesozoic and Cainozoic sediments (Fig. 2.2). The eastern and southern parts of the group are overlain by various Palaeozoic volcanics and sediments, and are bounded by the Palmerville and Burdekin River Fault systems (Fig. 2.2).

The Mesoproterozoic Langlovale Group consists of poorly sorted, feldspathic sandstone grading into massive to laminated shales, mudstones, siltstones, and sporadic sandstone beds (Withnall, 1996). The rocks are unconformably overlain by the Croydon Volcanic Group (Fig. 2.2). Due to the Langlovale Groups stratigraphic relationship with the Etheridge and Croydon Volcanic Groups, its age is constrained to about 1550 Ma (Withnall *et al.*, 1997).

The Palaeoproterozoic McDevitt Metamorphics are exposed in the northern part of the Etheridge Group alongside the Dargalong Metamorphic Group (Fig. 2.2). The rocks consist predominately of metapelites (mica schist) and subordinate micaceous meta-arenite and quartzite (Withnall *et al.*, 1997). The rocks appear to have followed a similar metamorphic history to the Etheridge Group, with grades locally reaching upper-greenschist to lower-amphibolite facies. The highest grade rocks commonly occur adjacent to contacts with the Dargalong Metamorphic Group (Withnall *et al.*, 1997). The McDevitt Metamorphics have not been directly dated, but are probably of a similar age to the Etheridge Group. The rocks are unconformably overlain by Carboniferous felsic-volcanic rocks, Mesozoic sediments, and Cainozoic basalts, and are intruded by Proterozoic mafic-igneous, and Palaeozoic granitic rocks (Fig. 2.2; Withnall *et al.*, 1997; Donchak & Bultitude, 1998).

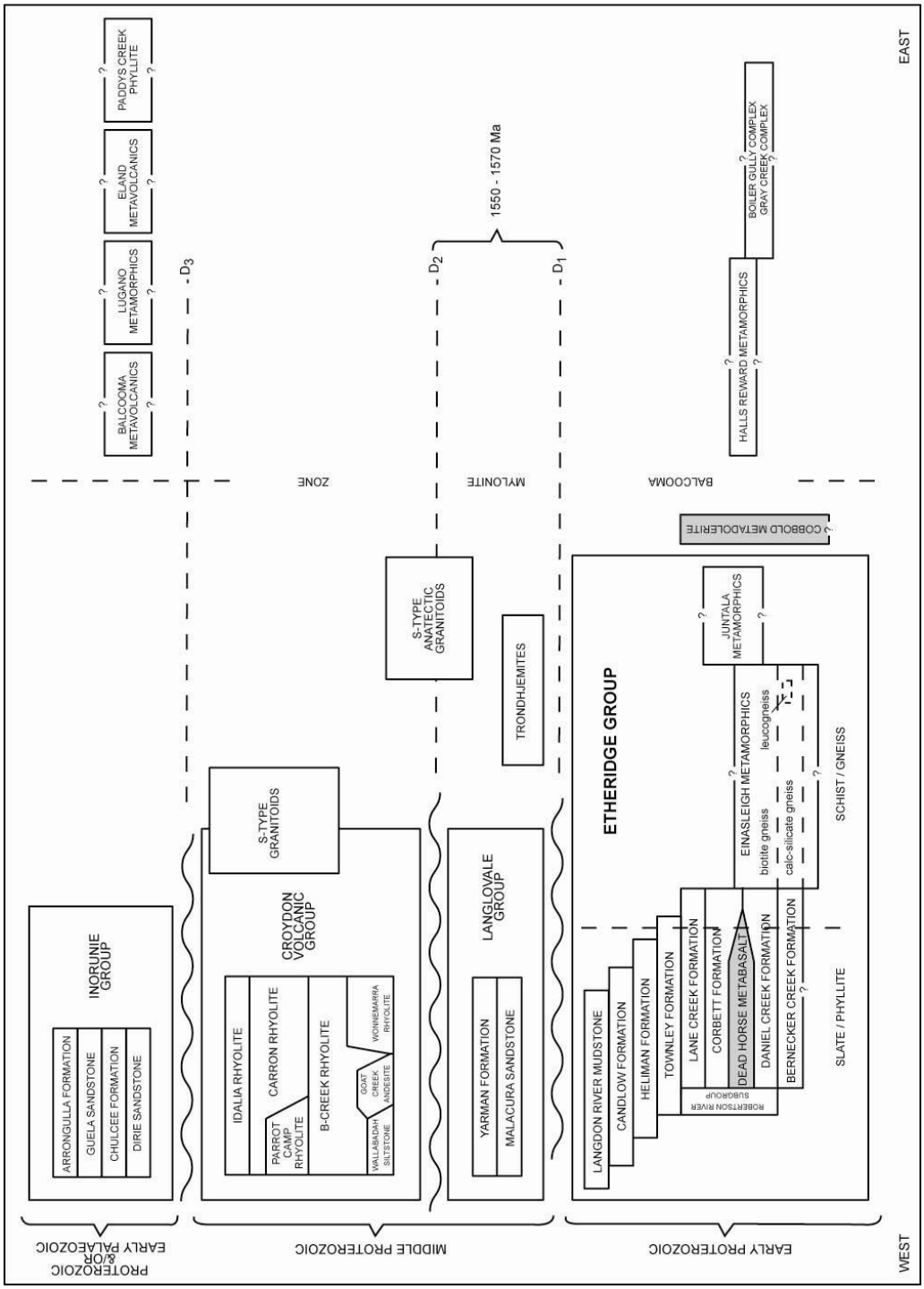


**Figure 2.3: Proterozoic stratigraphic relationships in the Georgetown Inlier (after Withnall, 1996).**

The metasedimentary rocks of the Etheridge Group are intruded by various Mesoproterozoic granites that include the Forest Home and Forsayth Supersuites. The Forsayth Supersuite is mainly S-type, but contains some I-type granites. It intrudes the Etheridge Group in a number of areas, with the main outcrop situated around Forsayth in the western half of the region (Fig. 2.2). The Forest Home Supersuite is dominantly

I-type, and is comprised of a number of small intrusive bodies found in the central part of the region. Numerous unnamed granites have also been identified throughout the higher grade areas of the Etheridge Group (Withnall *et al.*, 1997). Recent zircon age dating and structural observations indicate they may also be of Mesoproterozoic age (Black *et al.*, 1998).

### 2.2.2 Tectonic setting

The key characteristic which links all models for the formation of the Etheridge Group is that the deposition of sediments comprising the basal units of the group formed during extension of continental crust, which resulted in the formation of a shallow epi-continental or intra-continental sea. This was thought to have occurred during the second of two cycles of episodic extension, sedimentation, and magmatism (ca. 1.73-1.67 Ga; Etheridge et al., 1987) that affected several northern Australian Proterozoic terranes, including the McArthur basin, the Mt Isa Inlier, and the Georgetown Inlier (Etheridge *et al.*, 1987; Withnall 1985; Giles *et al.*, 2002).

In the Georgetown Inlier, deposition commenced with predominantly fine-grained calcareous to dolomitic sandstone, siltstone and mudstone, containing sedimentary structures indicative of a shallow-water or shoreline environment (Withnall *et al.* 1988a). Immediately following this phase of sedimentation, a phase of tholeiitic mafic magmatism occurred (ca. 1.69-1.65 Ga). This magmatic phase is also recorded within the eastern Mt Isa Inlier (Withnall 1985; Giles *et al.*, 2002). Sedimentation in the northeastern Australian basins continued until around 1.59 Ga (Page & Sun, 1998), and included rift-related sediments in the eastern Mt Isa Inlier (O'Dea *et al.*, 1997) and deep-water sediments in the Etheridge Group.

During the Mesoproterozoic a number of tectonothermal events deformed the Etheridge Group, producing definitive structural and metamorphic features. Metamorphic grade ranges from low-greenschist facies in the west and south-west through to granulite facies in the north-east, with peak metamorphic conditions probably reached in the Mesoproterozoic. Although there appears to be general consensus as to the metamorphic history of the region, conjecture still exists as to the tectonic events which led to sedimentation of the Etheridge Group: was it related to similar areas of sedimentation in northern Australia? Or did it form as a separate and

unrelated sequence, only to be amalgamated into the north Australian craton after deposition ceased?

### 2.2.3 Models for the Tectonic Evolution of the Etheridge Group

Although there appears to be consensus on the style of deposition recorded in the Georgetown Inlier, the various models (Etheridge *et al.,* 1987; Withnall *et al.,* 1988; Black *et al.,* 1998; Giles *et al.*, 2002; Boger & Hansen, 2004) differ with respect to the tectonic conditions prior to its deposition. Etheridge *et al.* (1987) proposed an ensialic model for northern Australian Proterozoic tectonics. It involved processes largely independent of plate-boundary forces, including lithospheric stretching, mantle-derived magmatism and contemporaneous underplating of the crust prior to sedimentation. The processes were all initiated by the onset of small-scale mantle convection between 2.2-2.0 Ga (Etheridge *et al*., 1987).

The second cycle, as described above, commenced with a period of crustal extension and rifting followed by post-extensional thermal subsidence with associated fine-grained clastic and carbonaceous sedimentary sequences. Felsic, dominantly A-type plutonic rocks were emplaced throughout the second cycle, such as in the Mt Isa Inlier (Etheridge *et al*., 1987; Scott *et al*., 2000), whereas mafic rocks were generally emplaced and erupted in periods of crustal extension (Etheridge *et al*., 1987; Withnall *et al*., 1988a).

The absence of felsic igneous rocks in the Etheridge Group has also been observed in other northern Australia Proterozoic terranes, such as the Pine Creek Inlier (Withnall *et al*., 1988a). The absence of coarse clastic rift-related sediments (i.e. associated with rift margin faulting) from the lowermost exposed sections of the Etheridge Group suggests that it may be related to a period of thermal subsidence during the second depositional cycle (Withnall *et al*., 1988a). The rift-related sequences, if they do exist, must occur below the Etheridge Group and have therefore not been identified. U-Pb zircon ages in more recent work (Black *et al.* 1998; Hoskin & Black 2000) confirm that ages of the oldest recognisable units of the Etheridge Group are around 1700-1650 Ma. As the mafic rocks in the Etheridge Group were emplaced close to the interpreted base of the sequence after 1700 Ma, it has been argued that they may relate to the final stages of the extensional part of the cycle (Withnall *et al*., 1988a).

The genesis of the mafic rocks in the Etheridge Group has been interpreted by Withnall (1985) and Withnall *et al.* (1988a) using a similar framework to that of Etheridge *et al.* (1987). However, in the model of Withnall *et al*. (1988a) the mafic rocks are considered to be derived directly from the convective mantle upwelling which produced crustal extension. The deposition of the Etheridge Group is interpreted to have taken place on continental crust, in either a stable shelf or epi-continental sea. As no evidence of rifting has been found in the lower parts of the sequence, the cause of the apparent rapid change from a shallow-marine to deep-marine environment that followed the eruption of mafic rocks in the formation remains unclear. Withnall (1985) suggested that the subsidence may be caused by the thinning of ductile crust rather than via rifting, as some authors have previously postulated that continental crust in the early Proterozoic may still have been hot enough to allow sub-solidus ductile flow (Wynne-Edwards 1972; Kröner 1979). Once convection and associated crustal thinning ceased, rapid subsidence would then commence. Withnall (1985) also noted that the mafic rocks show similarities to modern enriched mid-ocean ridge basalts (E-MORB), although they also share characteristics with the low-K flood basalts of Greenland and the Karoo (Cox & Hornung 1967; Clarke 1970; Brooks *et al.*, 1976). In this instance it is the extension and accelerated subsidence of the continental basement that is proposed to have led to the eruption and emplacement of the mafic rocks.

In recent times, as an increasing amount of evidence has become available suggesting that subduction operated in the Proterozoic, plate-tectonic models of the Australian Proterozoic have become more popular (Myers *et al*., 1996; Scott *et al.*, 2000; Giles *et al*., 2002). In contrast to the model of Etheridge *et al.* (1987) that involved a combination of lithospheric stretching and mantle-derived magmatism, Giles *et al.* (2002) proposed that the Georgetown Inlier represents a far-field back-arc basin formed in a period of subduction driven extension. They suggested that the northern Australian Proterozoic terranes were originally part of a contiguous crustal block, and that they show contemporaneous tectono-thermal events. The formation of a back-arc basin into which the Etheridge Group was deposited was linked to a continental scale region of intermittently extended crust, which also contained the McArthur Basin and Mt Isa Inlier. A north-dipping subduction system driving the extension is believed to have existed along the Palaeo-southern edge of the central Australian Arunta Inlier

(Zhao, 1994). It would have provided, along with hypothesized slab-rollback, the necessary slab-pull force to initiate the wide region of continental extension (Fig. 2.4).

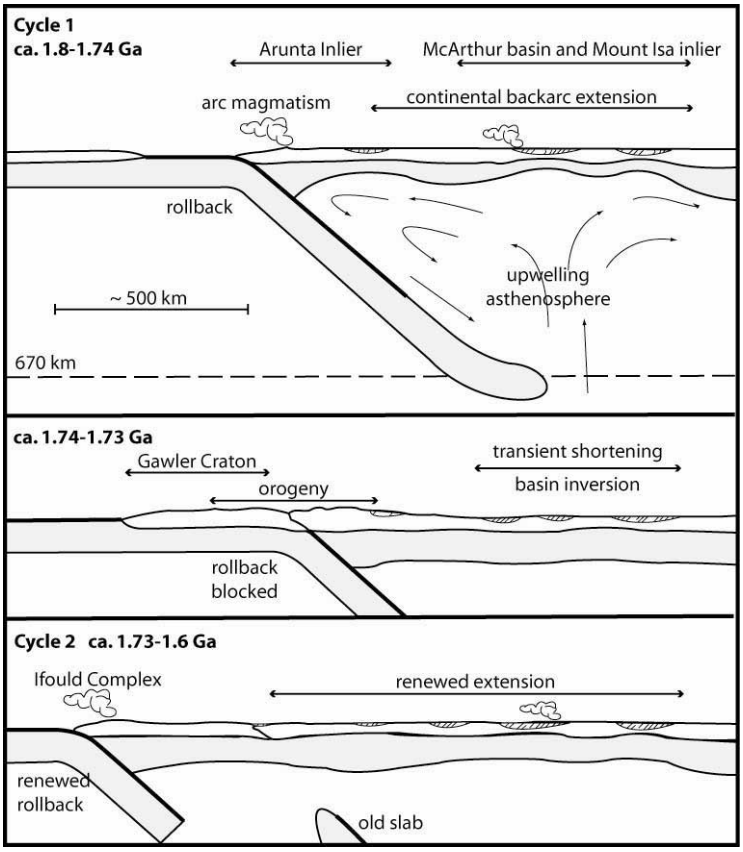


**Figure 2.4: Cartoon depicting relationship between convergent margin near Arunta Inlier and wide zone of intermittent extension (after Giles *et al.*, 2002).**

Alternatively, Boger & Hansen (2004) suggested that the Georgetown Inlier is unrelated to the other Australian Palaeoproterozoic terranes. They pointed to a number of key differences in metamorphic evolution and structural history between the Georgetown Inlier and adjacent Proterozoic inliers, including preservation of a two-stage metamorphic event in the Georgetown Inlier, the level of heat flow through both terranes, and the gross structural trend across the region. They propose that the Georgetown Inlier may have been accreted onto the margin of the North Australian Craton prior to 1550 Ma, rather than having always been part of it. This theory has significant implications, as it would imply the Palaeoproterozoic eastern margin of Australia was ocean-facing, and hence would not allow for plate-reconstructions of Rodinia that rely on the continuation of pre-1550 Ma features from Australia to Laurentia (e.g. Burrett & Berry 2000; Karlstrom *et al.* 2001). They also note that the metamorphism experienced by the Georgetown Inlier and the Eastern Fold Belt of the

Mt Isa Inlier differ in both style and intensity. They indicated that substantial low-pressure high-temperature metamorphism and anomalously high geothermal gradients (40-60 °C $km^{-1}$) are absent from the geological record of the Georgetown Inlier. On the other hand, the metamorphic evolution of the Georgetown Inlier involved burial and a 'normal' geotherm (20-30 °C $km^{-1}$) followed by localized contact metamorphism. However, it is possible that the effects of orogenesis in the Mt Isa Inlier prior to the onset of deposition in the Georgetown Inlier would have substantially affected the "local" geotherm underlying the Mt Isa Inlier. The emplacement of voluminous granites in the Mt Isa Inlier, including the Weberra and Sybella Granites (O'Dea *et al.* 1997), prior to deposition of sediments considered contemporaneous with those of the Etheridge Group, also supports the case that geothermal gradients and later styles of metamorphism may have been affected by tectonic processes prior to 1550 Ma.

Boger & Hansen (2004) also noted that the gross structural grain of the Georgetown Inlier is orthogonal to that of the Mt Isa Inlier and the Coen and Yambo Inliers to the north. Proterozoic structures in the Georgetown Inlier generally trend east-west, whereas Proterozoic structures in surrounding terranes predominantly trend north-south. Although this is partly true, Proterozoic structural fabrics orthogonal to those described above for the Georgetown Inlier also exist. Withnall (1996) noted that the main episodes of deformation that affected the Georgetown Inlier during the Proterozoic exhibited some variation in the trend of structural fabric across the terrane. He suggested this may be caused by either 'mega-folding' related to one of the later deformation events, or that the terrane may have been part of an arcuate fold belt. He also noted the orthogonal nature of fold trends between the first ($D_1$) and second ($D_2$) deformation events in the Georgetown region, and presented U-Pb zircon ages for syn-$D_2$ granites that questioned the separation of the two events (Black & McCulloch, 1990; Black & Withnall, 1993).

Despite these observations, the inferred structural disparity along with the differing styles of metamorphism between the Georgetown Inlier and other Proterozoic terranes in north-eastern Australia led Boger & Hansen (2004) to conclude that the Georgetown Inlier may have been part of a separate and unrelated lithospheric block prior to 1550 Ma. Their work has important ramifications not only for models of the

eastern Proterozoic margin of Australia, but also for Australia's place in the Proterozoic make-up of Rodinia.

The work of Black *et al.* (1998) focussed on constraining the age of deposition of the Etheridge Group. Their study showed that the lower portion of the Etheridge Group, including the mafic igneous rocks was deposited over a period of more than 40 m.y. A U-Pb zircon age of 1695.8 ± 1.5 Ma was determined for a granite that intrudes the sequence, indicating that deposition must have begun prior to 1700 Ma. They also noted that the age of deposition correlates with younger units in the Eastern Fold Belt of the Mt Isa Inlier, where dating by Page & Sun (1998) limited the deposition of the sedimentary precursor to felsic gneiss within the Soldiers Cap Group to before 1676 ± 5 Ma. O'Dea *et al.* (1997) showed that the upper units of the Eastern Fold Belt correlate in age to that of the Surprise Creek Formation in the western Mt Isa Inlier. This formation is composed of conglomerate, sandstone and thinly-bedded sandstone and siltstone and is overlain by the predominantly carbonaceous siltstones of the Mt Isa Group (1652 ± 7 Ma; Page & Sun, 1998), which hosts several world-class Pb-Zn-Ag deposits. The Mt Isa Group is thought to have been deposited in a shallow marine environment (Neudert & Russell 1981).

Subsequent work done by Black *et al*. (2005) on the age of the Etheridge Group has provided further constraints on the maximum age of deposition. They collected zircons from leucogneiss of the Einasleigh Metamorphics which returned ages in two populations of 1707 ± 8 and 1703 ± 14 Ma. Should the leucogneiss represents the altered remains of sediments derived from volcanics or epiclastic deposits, then the ages would appear to constrain the maximum age of deposition of that part of the sequence to around 1700 Ma.

The minimum ages for sedimentation noted above also match those determined for another major region of base-metal mineralisation, the Broken Hill region of the Willyama Inlier of western New South Wales. SHRIMP U-Pb zircon dating of amphibolite facies felsic metavolcanics in the Broken Hill Group by Page & Laing (1992) defined a major magmatic population at 1690 ± 5 Ma. The upper part of this group contains the Hores Gneiss, a formation containing metamorphosed tuffaceous sediments and rhyodacitic tuff that hosts the massive Pb-Zn-Ag orebodies at Broken Hill. Noting these similarities, Black *et al.* (1998) suggested that the Georgetown

region may have also provided a favourable environment for base-metal mineralisation.

The absence of exposed features that relate the Georgetown Inlier to an intra-continental rift basin raises the possibility that the terrane may in fact represent a continental margin rift setting, with no continental material existing outboard (east) of the terrane. The absence of felsic volcanics of a similar age to the Etheridge Group also suggest that the terrane was deposited in a tectonically quiet environment, possibly a passive-margin setting. Sedimentary features in the lowermost exposed members of the Etheridge Group indicate the depositional environment varied from wave-dominated shoreline to deep sub-tidal settings (Withnall, 1985). The upward fining of sediments in the sequence is also indicative of a relatively calm, uniformly subsiding shallow-water environment.

## 2.3 Review of Etheridge Group lithostratigraphy

The Etheridge Group, that contains over half of all exposed Palaeoproterozoic rocks in the Georgetown Inlier, is estimated to be between 6 and 11 km thick (Withnall, 1996), and its base is not exposed. Exposed rocks of the Etheridge Group have been subdivided into a number of lithologically distinct units (Fig. 2.2; Withnall & MacKenzie, 1980; Withnall, 1996). These include the Einasleigh Metamorphics, Juntala Metamorphics, Bernecker Creek Formation, Robertson River Subgroup, the Townley, Heliman, and Candlow Formations, and the Langdon River Mudstone. The Cobbold Metadolerite is also included with the Etheridge Group due to its relationship with members of the Robertson River Subgroup in the study area; however it is not stratigraphically considered a part of the Etheridge Group (Withnall, 1996). A detailed summary of the lithologies listed above, based primarily on the work of previous authors, is presented here, with detailed information on lithologies collected over the course of this study presented in the following chapter.

### 2.3.1 Einasleigh Metamorphics

The Einasleigh Metamorphics is exposed mostly in the south and east of the Georgetown Inlier (Fig. 2.2). It consists of biotite gneiss, calc-silicate gneiss, migmatite, and lesser leucogneiss, amphibolite, schist, and quartzite. The dominant

units are biotite and calc-silicate gneiss that generally form well-layered, laterally continuous units which appear to reflect original sedimentary layering (Fig. 2.5). Hornblende-gneiss occurs in places and is thought to be intermediate between the biotite and calc-silicate gneiss (Withnall, 1996). The calc-silicate gneiss is thought to be derived at least in part from calcareous to dolomitic psammitic rocks similar to those of the Bernecker Creek Formation (Withnall *et al*., 1988a); however it is uncertain whether all calc-silicate gneiss in the Einasleigh Metamorphics is equivalent to the Bernecker Creek Formation. Most of the larger amphibolite bodies are believed to be of intrusive origin, and are thought to be equivalent to the Cobbold Metadolerite (Withnall, 1996). The leucogneiss has no known low grade equivalent, but is thought to have been derived from sediments of igneous origin (Black *et al*., 2005).

**Figure 2.5: Einasleigh Metamorphics biotite gneiss. Grain size variation and mineralogy possibly reflect original sedimentary layering. Percy River near Percyvale.**

The regional increase in metamorphic grade eastwards in the Etheridge Group has enabled the recognition of stratigraphy traced from lower grade rocks into the higher grade and more intensely deformed Einasleigh Metamorphics. On this basis Withnall (1984, 1996) and Withnall *et al*. (1988a) suggested that the Einasleigh Metamorphics are probably equivalent to the Bernecker Creek and Daniel Creek Formations, and that parts of the Einasleigh Metamorphics may also represent units of the Etheridge Group below the basal exposed unit, the Bernecker Creek Formation. However, this correlation is less certain in the easternmost parts of the region where metamorphic grade has all but obliterated pre-metamorphic detail.

### 2.3.2 Juntala Metamorphics

The Juntala Metamorphics are located in the southern part of the Georgetown Inlier (Fig. 2.2). The unit consists predominately of mica schist that is believed to have originally formed from either mudstone or shale (Withnall, 1996). It has a gradational contact to the west and north with calc-silicate and biotite gneiss of the Einasleigh Metamorphics. To the east it is bounded by the Werrington Fault which juxtaposes the rocks against calc-silicate gneiss of the Einasleigh Metamorphics (Withnall, 1996). Withnall (1996) tentatively correlated the Juntala Metamorphics to the schist facies of the Corbett Formation.

### 2.3.3 Bernecker Creek Formation

The Bernecker Creek Formation is the lowermost exposed unit of the Etheridge Group (Fig. 2.3), cropping out mainly in the cores of regional-scale anticlines in the south-western part of the Georgetown Inlier (Fig. 2.6). However, due to the higher grade of metamorphism further east in the Etheridge Group obliterating original sedimentary features and stratigraphic relationships, Withnall (1996) has suggested that parts of the Einasleigh Metamorphics could be stratigraphically lower. The Bernecker Creek Formation consists predominantly of calcareous to dolomitic, fine-grained, subfeldspathic sandstone, siltstone, and mudstone. It is at least 2000 m thick, and its base is not exposed. Bedding in the sandstones is rarely more than a metre thick, and sedimentary layers are commonly between a few cm and a metre thick. Calc-silicate gneiss and granofels belonging to the Bernecker Creek Formation are observed further east near ‘Welfern’, and are considered equivalent to calc-silicate gneiss of the Einasleigh Metamorphics (Withnall, 1996). The formation is conformably overlain by the Daniel Creek Formation.

The lowermost section in the formation consists mainly of up to 100 m of laminated mudstone, siltstone, and minor fine-grained sandstone (Withnall & Mackenzie, 1980). Higher in the sequence, the frequency and thickness of sandstone layers increase, and they are interbedded with thin laminated siltstone and mudstone beds. In the uppermost part of the unit, carbonaceous mudstone or shale, and siltstone layers are overlain by relatively thick, fine-grained sandstone layers. In the larger sandstone

beds, sedimentary features include (but are not limited to) trough-cross-bedding (Fig. 2.7), ripple marks, and soft-sediment deformation. Observed soft-sediment deformation structures include load casts, boudinaged layers, and contorted or disturbed bedding (Fig. 2.8). The observed sedimentary features have led previous authors (Withnall & Mackenzie, 1980; Withnall *et al*., 1988a; Withnall, 1996) to suggest a wave-dominated shore-line to tidal flat as the possible environment of deposition for the formation.

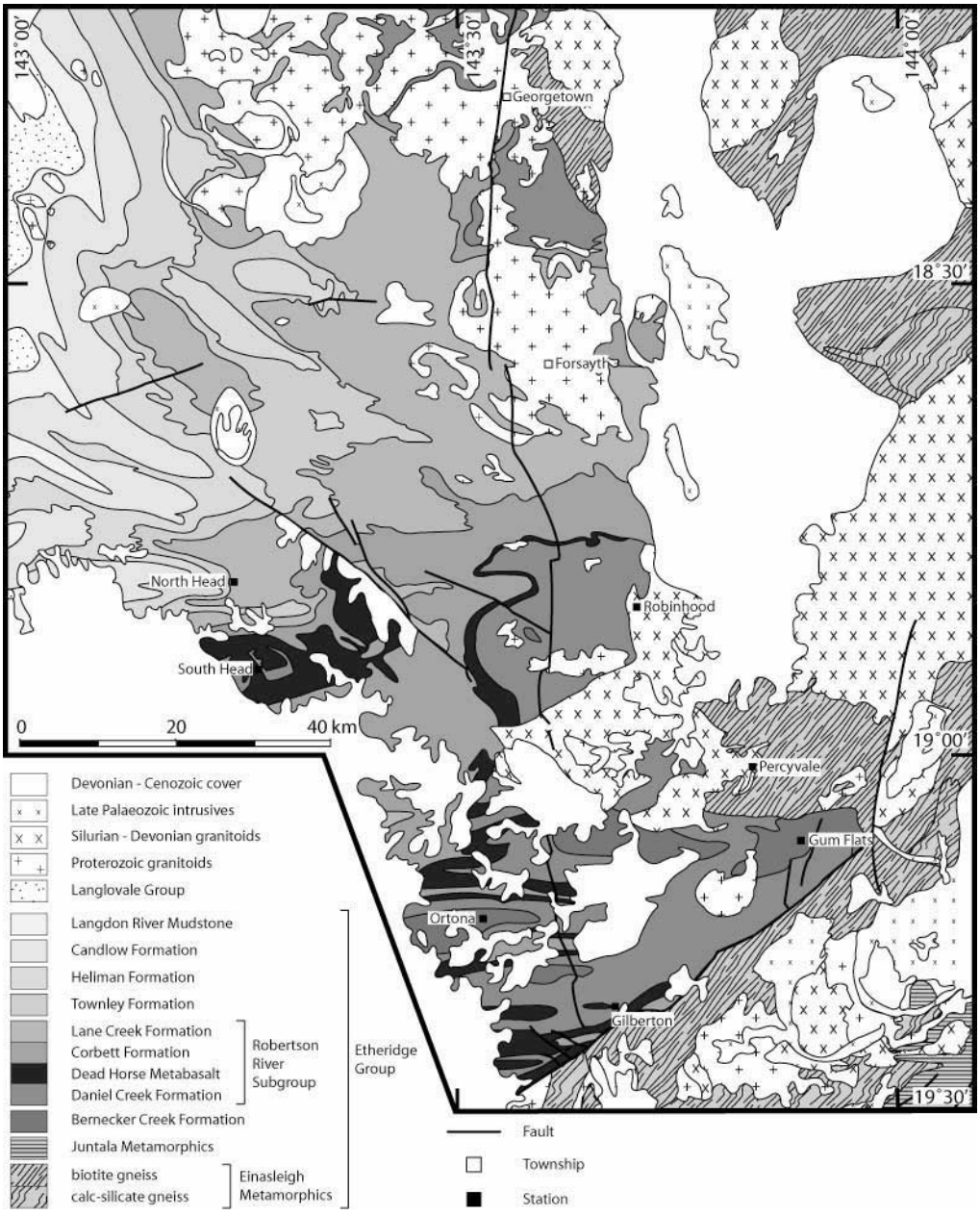


**Figure 2.6: Generalised geology of the central Georgetown Inlier (after Withnall, 1996). Outcrop too small for this scale, including individual units of the Cobbold Metadolerite, have been omitted.**

**Figure 2.7: Cross-bedding in Bernecker Creek Formation sandstone; Percy River near Ortona.**

**Figure 2.8: Soft-sediment deformation in Bernecker Creek Formation sandstone; Percy River near Ortona.**

### 2.3.4 Robertson River Subgroup

The Robertson River Subgroup is subdivided into the Daniel Creek Formation, Dead Horse Metabasalt, and the Corbett and Lane Creek Formations (Fig. 2.3; Withnall, 1983). The subgroup consists predominately of low-grade metasedimentary rocks and metabasalt in the south (Ortona area; Fig. 2.2), and higher-grade 'schist-facies' equivalent rocks and amphibolite north of the Robertson River, and to the east near

Gum Flats (Fig. 2.2; Withnall, 1996). Metamorphosed mafic rocks of the Cobbold Metadolerite are stratigraphically bounded by the metasedimentary rocks of the Robertson River Subgroup. The subgroup is conformably overlain by the Townley Formation to the north and north-west, and unconformably overlain to the south-west by Mesozoic sediments (Fig. 2.2).

#### 2.3.4.1 Daniel Creek Formation

The Daniel Creek Formation conformably overlies the Bernecker Creek Formation. It differs from the Bernecker Creek Formation in being less calcareous or dolomitic, and generally more pelitic (Fig. 2.9; Withnall *et al*., 1988a). The Daniel Creek Formation is composed of mudstone, shale or siltstone, and fine-grained sandstone, and is 1000-2000 m thick (Withnall *et al*., 1988a). The formation is suggested to have been deposited in a sandy-deltaic environment (Withnall *et al*., 1988a). A sequence of alternating quartzite and mica schist mapped as the Mount Helpman Member in the 'Robinhood' area (Withnall & Blight, 2003) is compositionally similar to the Daniel Creek Formation, and was therefore included within it; however the mica schist phase only becomes dominant in the Daniel Creek Formation proper (Withnall, 1996).

**Figure 2.9: Lensoid bedding (centre-left) and cross-bedding (centre-right) in the Daniel Creek Formation; Percy River near Ortona.**

The lower part of the formation consists of mudstone, siltstone, and lesser fine-grained sandstone. The siltstone and sandstone are commonly laminated and preserve

some sedimentary features including cross-bedding and lensoid bedding (Fig. 2.9). Further up in the formation, fine-grained sandstone including calcareous sandstone is more abundant (Withnall, 1996), and form beds up to 1 m thick. Mudstone and siltstone with lesser sandstone form the uppermost part of the formation, underlying the Dead Horse Metabasalt; however in the Gilbert River near 'Rungulla' the metabasalt overlies a sequence containing more abundant sandstone. This observation also prompted Withnall (1996) to suggest that the sedimentary facies in the Daniel Creek Formation are partly diachronous.

#### 2.3.4.2 Dead Horse Metabasalt

The Dead Horse Metabasalt lies between the Daniel Creek and Corbett Formations, and consists of several hundred metres of metamorphosed mafic pillow lava, hyaloclastic breccia and structureless, massive aphanitic flows, along with some minor interbedded mudstone and siltstone. Lower grade metabasalts are metamorphosed to lower greenschist facies, and igneous textures are generally well preserved. The main outcrop area is between 'North Head', 'Gilberton' and 'Robinhood' (Fig. 2.6; Withnall *et al*., 2003a; Withnall *et al*., 2003b). Previous studies of mafic rocks in the Etheridge Group have focussed on their classification as either doleritic or basaltic, especially where the two layers do not overlap. However, it has become apparent over the course of this study that significant variation exists within the metabasalt layers, particularly in respect to grain size and texture. Consequently, ground truthing of areas mapped via airborne surveys as metabasalt has in fact revealed numerous metadolerite layers.

In the lower grade area of the Robertson River Subgroup, the base of the mapped metabasalt units is mostly composed of massive, fine- to medium-grained structureless flows, which commonly resemble metadolerite in texture and grainsize. The rocks are green to dark-green, and consist of randomly oriented albite laths, acicular actinolite or hornblende (at higher metamorphic grades), epidote/clinozoisite, chlorite, calcite, and minor titanite and magnetite. The middle part of the formation generally consists of fine- to very fine-grained, locally aphyric basalt flows, and the upper part consists of layers of pillow lavas and hyaloclastic breccias (metabasalt clasts in siliceous matrix), with thin inter-layered, fine-grained sheet flows or sills and minor sedimentary rocks (Fig. 2.10). In many outcrops the metabasalt is weakly to

strongly foliated, which along with metamorphism has obliterated most igneous textures, and locally flattened pillowed basalts parallel to the foliation.

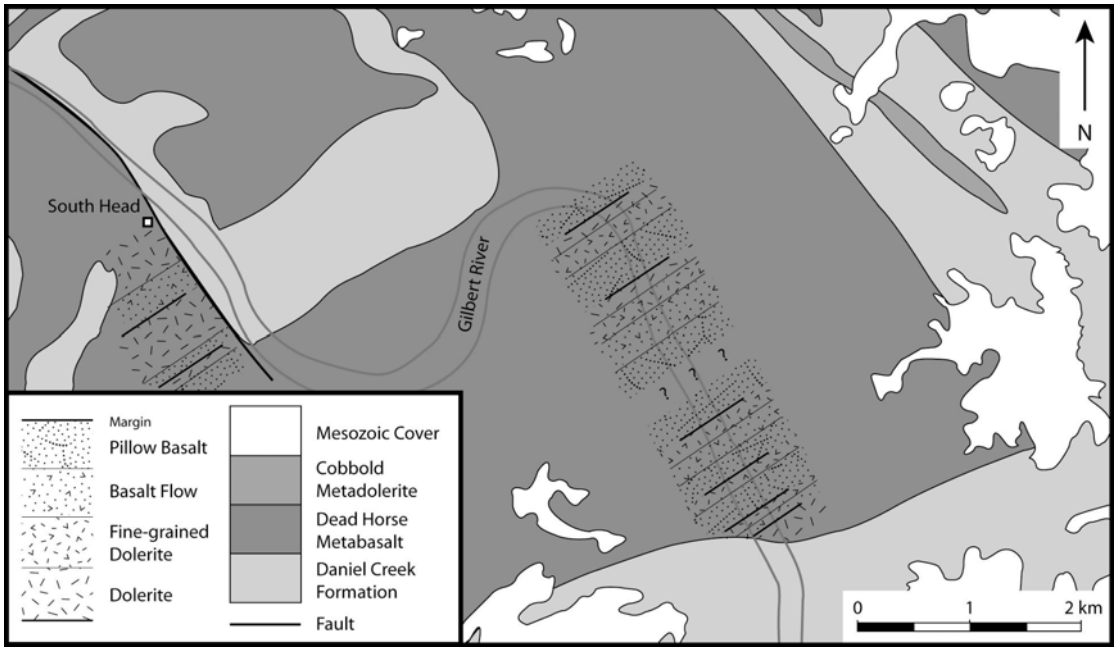


**Figure 2.10: Stratigraphic relationships of the 'South Head' area. Compositional changes within Dead Horse Metabasalt outcrop also shown.**

### 2.3.4.3 Corbett Formation

The Corbett Formation overlies the Dead Horse Metabasalt, and differs from the Daniel Creek Formation in consisting almost entirely of mudstone. The formation crops out between Gilberton in the south, and as far north as Forsayth and 'Ironhurst' (Fig. 2.6; Withnall & Blight, 2003; Withnall *et al*., 2003a; Withnall *et al*., 2003b). The formation is approximately 1000 m thick, and is suggested to have been deposited in a subtidal to deep-subtidal environment (Withnall *et al*., 1988a).

The lower part of the formation consists of grey, slightly carbonaceous laminated mudstone. The upper part consists of generally green, sparsely laminated mudstone or phyllite. A quartz-rich phyllite layer marks the top of the formation (Withnall, 1996). In higher grade areas the mudstone grades into mica schist similar to that of the Daniel Creek Formation. The mica schist of the Corbett Formation differs from that of the Daniel Creek Formation in that it is generally poorly layered and contains abundant biotite porphyroblasts (Withnall, 1996). Staurolite is locally present in the mica schist as large poikiloblasts containing small quartz grains, and breaks down to form garnet plus kyanite with increasing grade. Where the quartz-rich phyllite marker

bed is absent in the higher-grade rocks, the presence of biotite porphyroblasts distinguish the Corbett Formation from the overlying Lane Creek Formation (Withnall, 1996).

A series of outcrops containing almost exclusively thickly bedded quartzite has been mapped as the Tin Hill Quartzite Member of the Corbett Formation in the area between 'Robinhood' and the Forsayth road (Withnall & Blight, 2003). It consists of a single layer of massive quartzite 5-40 m thick, and has been traced east towards the Newcastle Range. No low grade equivalent has been recognised. Withnall (1996) suggested that the quartzite was originally a chemical sediment or chert.

#### 2.3.4.4 Lane Creek Formation

The Lane Creek Formation conformably overlies the Corbett Formation, and is the uppermost formation in the Robertson River Subgroup. It is composed of commonly carbonaceous and locally calcareous mudstone and siltstone, and lesser sandstone and limestone (Withnall *et al*., 1988a). Its main outcrop extends in a broad belt from Forsayth in the south to 'Ironhurst' in the north, where it is overlain unconformably by Palaeozoic-Cainozoic sediments (Withnall, 1996). Various smaller outcrops occur to the west and south around 'North Head' and the Robertson River, where it is overlain by the Townley Formation (Withnall & Blight, 2003; Withnall *et al*., 2003b). The formation is up to 2000 m thick, and suggests a continuation of the deep-water facies conditions that are inferred for the Corbett Formation (Withnall *et al*., 1988a). Withnall *et al*. (1988a) also noted the presence towards the top of the formation of minor mudclast-sandstone containing sedimentary features that may indicate a return to a shallow-water depositional environment.

Highly carbonaceous, laminated mudstone and siltstone is characteristic of the low grade part of the Lane Creek Formation, and distinguish it from the underlying Corbett Formation (Withnall, 1996). Minor components of the formation include fine-grained sandstone and thinly bedded limestone, which are interbedded with the more dominant lithologies. The mudstone and siltstone grade into mica schist in the central part of the region (Fig. 2.6), along with minor quartzite and calc-silicate rocks. The schists commonly contain andalusite and cordierite porphyroblasts, and at higher grades muscovite and sillimanite. Sillimanite porphyroblasts are commonly

retrogressed to sericite. In the 'Ironhurst' area migmatite has developed (Withnall, 1996).

### 2.3.5 Upper Etheridge Group lithologies

The upper units of the Etheridge Group include, in order of decreasing age: the Townley, Heliman, and Candlow Formations, and the Langdon River Mudstone (Fig. 2.3). They are made up of varying proportions of siltstone, carbonaceous mudstone, silicious siltstone, fine-grained sandstone and rare limestone. The formations have been metamorphosed from greenschist through to lower amphibolite facies (Withnall, 1996). They are unconformably overlain the Mesoproterozoic Langlovale Group to the west, and by Palaeozoic and Mesozoic felsic-volcanic and sedimentary rocks to the east and north (Fig. 2.2).

### 2.3.6 Cobbold Metadolerite

The Cobbold Metadolerite occurs as numerous largely conformable intrusions throughout the Robertson River Subgroup (Withnall & Blight, 2003; Withnall *et al*., 2003a; Withnall *et al*., 2003b). The intrusions occur mostly as sills, and are anywhere between a few metres to over 500 m in thickness. Many of the outcrops can be followed along strike for several km. Dykes are uncommon, although some examples are present around 'Ortona' (Withnall, 1981; Withnall *et al*., 2003a). The Cobbold Metadolerite is believed to have been intruded in at least two pulses (Withnall, 1985). One is believed to have coincided with the extrusion of the Dead Horse Metabasalt, with a second, younger pulse thought to have occurred immediately after the deposition of the Lane Creek Formation (Withnall, 1996). No mafic intrusive rocks of Proterozoic age occur above the Lane Creek Formation in the Etheridge Group.

## 2.4 Mesoproterozoic Granites

Mesoproterozoic granites in the central part of the Georgetown Inlier form the Forsayth Batholith. The batholith outcrops over ~700 $km^2$ and is subdivided into nine named, and several other unnamed plutons (Black & Withnall, 1993). Units relevant to this study are mentioned here; however a comprehensive list of Proterozoic granites of the Georgetown Inlier is given by Withnall *et al*. (1997).

### 2.4.1 Forsayth Granite

The Forsayth Granite's main exposure occurs just to the north of Forsayth (Fig. 2.6; Withnall & Blight, 2003). It consists of commonly foliated, grey to dark-grey, medium- to coarse-grained, strongly porphyritic biotite granite. Conventional U-Pb zircon dating has returned an age of 1550 ± 7 Ma for the Forsayth Granite (Black & McCulloch, 1990).

### 2.4.2 Digger Creek Granite

The Digger Creek Granite consists of numerous small exposures that outcrop between Forsayth and as far south as 'Percyvale' (Fig. 2.6; Withnall & Blight, 2003). The main exposures occur near 'Robinhood' station (Fig 2.6), where the granite has caused the recrystallization of 'schist-facies' rocks of the Robertson River Subgroup. The granite consists of medium- to coarse-grained muscovite leuco-granite and muscovite pegmatite. A U-Pb zircon SHRIMP ion-microprobe age of 1554 ± 10 Ma has been obtained for the Digger Creek Granite (Black & Withnall, 1993).

### 2.4.3 Ropewalk Granite

The Ropewalk Granite is also composed of numerous small exposures, the largest of which are between Forsayth and 'Robinhood' (Fig. 2.6; Withnall & Blight, 2003). The granite consists of grey to dark-grey, foliated, medium-grained muscovite-biotite and quartz granite, and commonly contains melanocratic pockets of biotite (Sample 208; Appendix 1).

### 2.4.4 Mount Hogan Granite

The Mount Hogan Granite is exposed in the south of the region near 'Mount Hogan' station (Fig. 2.6; Withnall *et al*., 2003a). The granite consists of pink to reddish-brown, medium- to coarse-grained biotite-muscovite granite. A U-Pb zircon SHRIMP ion-microprobe age of 1549 ± 25 Ma has been obtained for the Mount Hogan Granite (Black & Withnall, 1993).

## 2.5 Review of the Structural evolution of the Etheridge Group

Previous authors have identified six major deformation events that have affected the Etheridge Group ($D_1$-$D_6$; Withnall *et al.*, 1997). The first two folding events ($D_1$ & $D_2$) were inferred to have occurred close to each other at about 1550 Ma, and are both associated with metamorphism. The metamorphism ranges from lower-greenschist to upper-amphibolite and locally granulite facies, with peak metamorphic conditions reached during $D_2$ (Withnall, 1996). $D_1$ is best preserved in the western, lower grade part of the region, where later overprinting effects are at their weakest. Withnall (1996) indicated that $D_1$ appears to be of a relatively uniform intensity over the entire region. $D_1$ generally produced tight to isoclinal, upright to overturned folds, with a strong axial-plane foliation. $F_1$ wavelengths are generally of the order of 1-10 km (Withnall *et al.*, 1997).

The age of $D_1$ remains uncertain. It was directly dated by Black *et al*. (1979) using Rb-Sr whole-rock and mineral techniques to 1570 ± 20 Ma. However, the Rb-Sr whole-rock technique for dating metamorphic rocks has long been considered obsolete (Black & Withnall, 1993). Subsequent dating of post-$D_2$ granitoids (Black & McCulloch, 1990; Black & Withnall, 1993) has shown that the age of $D_1$ obtained using the Rb-Sr technique was anomalously young. Recent dating of leucogneiss from the Einasleigh Metamorphics by Black *et al*. (2005) showed that a significant metamorphic event occurred at 1562 ± 4 Ma. However, it remains unclear whether this age is representative of $D_1$, or alternatively represents the onset of the second major episode of regional deformation and metamorphism. If the latter is correct, it would indicate that $D_2$ lasted for at least 12 million years, and that $D_1$ is likely to have occurred ~20 million years earlier at ca. 1580 Ma, when peak tectonothermal events were drawing to a close in the Broken Hill Block and the Mt Isa Eastern Succession (Black *et al*., 2005). EMPA dating of monazites from amphibolite facies metasedimentary rocks of the Robertson River Subgroup by Cihan *et al*. (2006) suggest the latter is true and they give a weighted average age for the peak metamorphic conditions associated with $D_1$ of 1586 ± 6 Ma.

The effects of $D_2$ are best seen in the eastern half of the Georgetown Inlier, as both the intensity of folding and deformation increase eastwards. In westernmost outcrops of the Etheridge Group $D_2$ forms local, weak, northerly trending crenulations that lie sub-parallel to the axial planes of large open folds which deform $F_1$ folds (Withnall,

1996). In easternmost outcrops $D_2$ forms generally north trending tight to isoclinal folds with wavelengths up to 2 km, which are associated with either a strong crenulation cleavage, or schistosity (Withnall, 1996). Where this deformation is strongest, $D_2$ overprints the earlier metamorphic fabric as well as primary features including sedimentary layering.

Using Rb-Sr techniques Black *et al*. (1979) obtained an age of 1469 ± 20 Ma for $D_2$. However, subsequent dating of Proterozoic felsic granites and volcanic rocks that postdate $D_2$ using SHRIMP and conventional multi-grain zircon techniques (Black & McCulloch, 1990; Black & Withnall, 1993) has shown that this age is obsolete, and that $D_2$ is about 80 Ma older, probably occurring at around 1550 Ma (Black & Withnall, 1993). Recent dating of leucogneiss from the Einasleigh Metamorphics by Black *et al*. (2005) returned an age of 1555 ± 3 Ma, which they correlated to the peak of metamorphism associated with the $D_2$ event. Monazites analysed by Cihan *et al*. (2006) yielded a weighted average age of 1542 ± 8 Ma, which they correlate to marking the beginning of $D_2$ in the Robertson River Subgroup.

$D_3$ produced folding of varying intensity across the Georgetown Inlier. In the central part of the inlier near 'Robinhood', $D_3$ produced generally open to tight, upright to overturned folds with axial planes striking approximately south-easterly to easterly (Withnall, 1996). Further east, and to the south of the Gilberton Fault, $D_3$ produced generally weak open folds with wavelengths of less than 1 km to over 10 km (Withnall, 1996). In these areas, $D_3$ is also associated with small-scale folds, weak crenulations, and low-grade retrogressive metamorphism, although due to the weak development of $D_3$ foliations, it is difficult to distinguish these features from later events.

The age of $D_3$ was dated at 967±28 Ma using Rb-Sr techniques from samples of outcrops supposedly possessing well-developed $S_3$ schistosities (Black *et al*., 1979). Subsequent studies of the same outcrops have suggested that the foliation $S_3$ may in fact be $S_2$, and that the age obtained by Black *et al*. (1979) may represent a partially reset $D_2$ age (Withnall, 1996). Bell (pers. comm., 1984 in Withnall, 1996), on the basis of shallowly dipping axial planes in some $F_3$ folds, suggests that $D_3$ may be early Palaeozoic in age, and related to deformation in the Greenvale Subprovince of Withnall (1989). Cihan *et al*. (2006) noted a large grouping of monazite ages in their study which gave a weighted mean age of 1512 ± 5 Ma. They postulated that this age

may represent a thermal pulse or hydrothermal activity that may or may not have been associated with the later stages of $D_2$, and could therefore represent the age of $D_3$.

$D_4$ has had little effect on the western and southern parts of the Etheridge Group, and the event is best recorded in the eastern, higher-grade parts of the inlier. $F_4$ folds are rare; however, Withnall (1996) suggests open, mesoscopic $F_4$ folds are common near Einasleigh and further north. Black *et al.* (1979) suggested an age of about 400 Ma for $D_4$ based on K-Ar and Rb-Sr mica ages, but did not directly attempt to date the event. McNaughton (1980) obtained K-Ar muscovite ages of 410 ± 12 Ma and 414 ± 12 Ma from the Einasleigh Metamorphics east of the study area, which he interpreted to have crystallised syn-$D_4$. Other geochronological studies from areas surrounding the Georgetown Inlier have also returned ages around 400 Ma (e.g. Withnall *et al*., 1991) indicating that this age is of regional significance; however, it is yet to be determined conclusively that this age corresponds to $D_4$.

Later deformation events ($D_5$-$D_6$) produced open folding and weak crenulations in the Etheridge Group. $D_5$ is represented by open folds with east-striking axial planes (Withnall, 1996). Minor crenulations have also been recognised in the Robertson River area. $D_6$ is mainly represented by crenulations. The ages of D5 and D6 have not been determined, but are believed to be of late-Palaeozoic age (Withnall, 1996).

## 2.6 Faulting

Three major fault systems can be found in the central part of the Georgetown Inlier (Fig. 2.6). The Robertson, Gilberton and Delaney fault systems all or partly occur within the study area, and are described in detail below.

### 2.6.1 Robertson Fault System

The Robertson Fault System has been mapped for approximately 45 km northwest from the northern end of the Agate Creek Volcanics to 2 km south of the Gongora Granodiorite (Withnall & Blight, 2003; Withnall *et al*., 2003b). The fault system splits into two branches north of the Robertson River (Fig. 2.6; Withnall *et al*., 2003b).

The eastern branch and main stem of the Robertson Fault both show a sinistral movement of 5 km, while at least 2 km of dextral movement has occurred on the western branch (Withnall, 1996). Vertical displacement involving west-block-down

movement of up to 150 m also occurred along the western and main stems of the fault during the Pliocene (Withnall, 1996). This displacement is observable along the section of the fault which runs parallel to the Robertson River, where the Jurassic Hampstead Sandstone is now in fault-contact with metasediments of the Etheridge Group (Fig. 2.6; Withnall *et al*., 2003b).

The age of the Robertson Fault is uncertain. It is thought to be at least Pliocene in age, but could possibly be as old as late Palaeozoic, based on late Palaeozoic volcanics and intrusives lying along the south-easterly projection of the fault system (Withnall, 1996).

### 2.6.2 Gilberton Fault System

The Gilberton Fault System has been mapped for approximately 55 km northeast from its southern contact with Jurassic sediments 20 km southwest of Gilberton, to its intersection with the Ballynure Fault, east of 'Gum Flats' station (Fig. 2.6; Withnall *et al*., 2003a).

Considerable dextral movement of at least 50 km along the Gilberton Fault has been hypothesised (Withnall *et al*., 1980), as along the southern half of the fault high grade rocks of the Einasleigh Metamorphics are in contact with low grade rocks of the Robertson River Subgroup. The juxtaposition of rocks of different metamorphic grades can also be explained by vertical movement; however, the distance over which faulting is thought to have occurred makes this unlikely (Withnall *et al*., 1980).

In outcrop, the Gilberton Fault ranges from narrow zones of fault gouge (Withnall, 1996), through to zones of intense shearing and fracturing up to 100 m wide. Mylonitic leucogranite is recognised close to the southern side of the fault south of 'Gum Flats', indicating that some ductile deformation was involved during movement along parts of the fault.

The age of the Gilberton Fault is thought to be late Ordovician or early Silurian (Withnall, 1989), based on the presence of mylonite pebbles in early Silurian conglomerates in the Broken River Province to the southeast of the Georgetown Inlier (Withnall *et al*., 1988b). Mylonitisation along the Gilberton Fault is believed to have occurred at this time.

### 2.6.3 Delaney Fault System

The Delaney Fault is discontinuous, and forms a series of north-striking, narrowly offset segments that continue for at least 100 km (Fig. 2.2; Withnall, 1996). The northern limit of the fault has been mapped to 3 km south of the Yataga Granodiorite, and the southern limit is mapped to the Gilberton Fault, approximately 5 km southwest of Gilberton (Fig. 2.6; Withnall *et al*., 2003a). A number of small, mafic dykes occur along the length of the fault, and are interpreted to be Carboniferous to early Permian in age (Withnall & Blight, 2003).

In most areas, the fault has caused no observable displacement of stratigraphy. One notable exception is in the central part of the region, where the fault has displaced the contact of the Robin Hood Granodiorite by approximately 1 km (Withnall, 1996; Withnall & Blight, 2003). Small vertical displacements have otherwise been suggested to account for the lack of lateral movement (Withnall, 1996).

The age of the Delaney Fault is uncertain. Withnall (1996) suggests that it may have formed between the early Devonian and Permian, based on the displacement of the Robin Hood Granodiorite and the intrusion of mafic dykes.

# Chapter 3.

# Geology and Structure of key lithologies within the lower Etheridge Group

## 3.1 Introduction

Based on geological maps by Withnall & Blight (2003), Withnall *et al*. (2003a), and Withnall *et al*. (2003b), I spent four weeks carrying out detailed geological sampling of key units across the western Georgetown Inlier, and completed several transects aimed at elucidating the geochemical, structural and metamorphic evolution of the relatively low-grade section of the inlier. Over 300 samples were collected for this study, and a representative selection is listed in Appendix 1.

This chapter describes in detail the composition, structure and field relationships of the lower Etheridge Group lithologies which form the focus of this study, in particular the mafic igneous rocks of the Dead Horse Metabasalt and Cobbold Metadolerite. Geological relationships that clarify the timing, relative ages, and geological sequence of events for the various lithologies are also described. The result is a geological framework which allows the tectonic significance of the mafic igneous units to be confidently examined.

The location of the area of study is shown in Figure 2.2. A geological map encompassing the area of study is shown in Figure 2.6. Lithologies not shown include Palaeozoic and younger rocks, felsic pegmatites, and various small mafic igneous veins, sills and dykes belonging to the Cobbold Metadolerite and Einasleigh Metamorphics.

## 3.2 Etheridge Group

Apart from several granitoid samples of the Forsayth Batholith and Mt Hogan Granite, the remaining samples from this study were collected from lithologies belonging to the lower Etheridge Group. Sampling was concentrated on the Dead Horse Metabasalt and Cobbold Metadolerite members; however numerous samples of surrounding metasediments including the Einasleigh Metamorphics, Bernecker Creek Formation, and Robertson River Subgroup were also collected. Outcrop of

metaigneous and metasedimentary rock is generally poor across the region, with best exposures found in road cuttings and in river beds where seasonal water flow and sand abrasion have exposed fresh outcrops.

### 3.2.1 Einasleigh Metamorphics

Biotite gneiss belonging to the Einasleigh Metamorphics in the Gum Flats area (Fig. 2.6) is generally grey and consists mainly of coarse-grained biotite, quartz, andesine to albite, calcite, locally garnet, and accessory haematite (Fig. 3.1; Sample 317, Appendix 1). Thin discontinuous layers composed of aggregates of retrogressive sericite replacing sillimanite are also visible in the gneiss. With decreasing feldspar and increasing muscovite, biotite gneiss grades into mica schist. With increasing grade, the biotite gneiss grades into migmatite near 'Percyvale' (Fig. 2.6); and consist mainly of concordant leuco-granitic pods (leucosomes) and biotite-rich selvedges (melanosomes) ranging in thickness from <1 cm to up to 50 cm (Fig. 3.2).

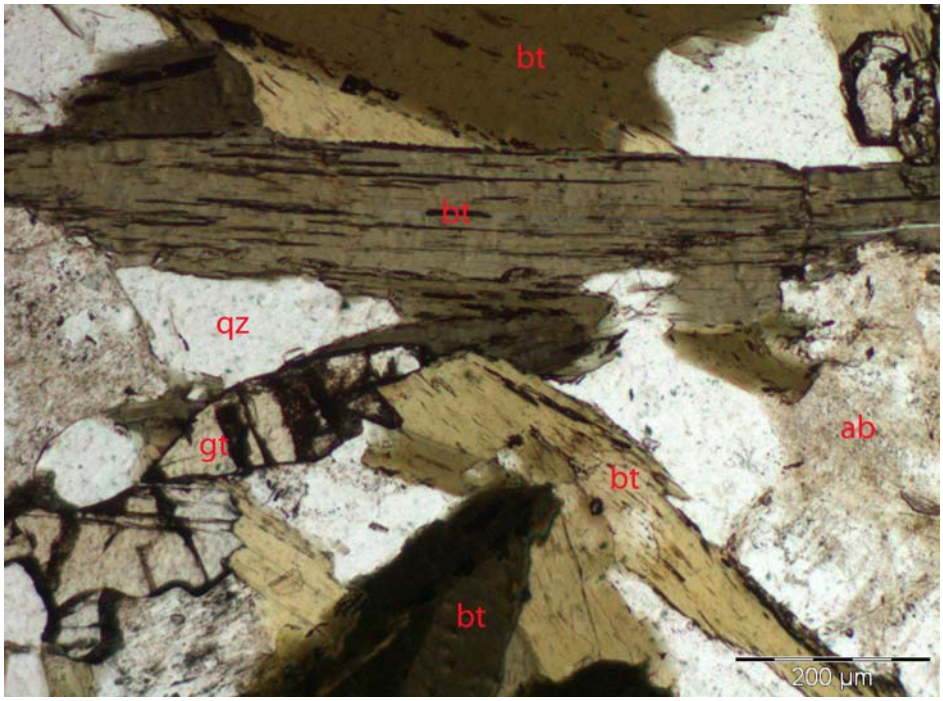


**Figure 3.1: Thin section photo of Einasleigh Metamorphics biotite gneiss. Mineral labels: bt = biotite; qz = quartz; ab = albite; gt = garnet. Sample 317, Appendix 1.**

Mafic layers up to 1 m across are found in areas of migmatisation, and are probably equivalent to amphibolites from lower grade areas. Samples of the amphibolite contain foliated, euhedral hornblende, albite, and minor quartz, clinopyroxene, and magnetite (Sample 318, Appendix 1). Samples of calc-silicate gneiss vary from pink

through to grey and green, and contain varying proportions of quartz, microcline, plagioclase, hornblende, clinopyroxene, sphene, and locally garnet, epidote/clinozoisite, and calcite. Magnetite and haematite/ilmenite are also present as accessory minerals.

**Figure 3.2: Migmatitic Einasleigh Metamorphics; Percy River near Percyvale.**

### 3.2.2 Bernecker Creek Formation

Representative samples of the Bernecker Creek Formation were collected from the Percy River north of 'Ortona' (Fig. 2.6), and are mostly fine- to very fine-grained sandstones (Appendix 1). Representative samples 7, 13 and 124 contain a high percentage of grain-supported quartz (60-70% in sample 7, 50-60% in sample 13, 50% in sample 124). Minor mineral phases include calcite (Sample 7) and epidote (Sample 13). In sample 124, calcite comprises approximately 30% of the sample, and muscovite comprises a further 5-10% (Fig. 3.3; Sample 124, Appendix 1). Accessory opaque minerals are predominately magnetite and chalcopyrite. Detrital zircon is rare, but can be found in some samples of fine-grained sandstone. Grainsize variation in sedimentary minerals, such as quartz, is minimal, indicating that sandy layers in the formation are generally well sorted and mature. However, metamorphic minerals,

such as epidote in sample 13, show greater variation in grainsize, with larger grains forming microscopic layering in the sediments (Fig. 3.4; Sample 13, Appendix 1).

The Bernecker Creek Formation grades eastwards into calcareous mica-schist and quartzite that contains calc-silicate minerals including hornblende, plagioclase, epidote, and clinopyroxene. With increasing metamorphic grade and intensity of deformation, most sedimentary features observable in the lower grade rocks are obliterated. Bedding is usually preserved, but becomes increasingly difficult to distinguish from tectonic structures.

Higher grade samples of the Bernecker Creek Formation were collected near ‘Gum Flats’ station to the east of ‘Ortona’ (Fig. 2.6). Samples from this area are mostly of mica schist, and sedimentary features are mostly obliterated by overprinting of metamorphic textures. Mineral texture varies from coarse- to fine-grained depending on the sedimentary precursor, and the dominant mineral phases include calcite, muscovite, biotite, quartz, and lesser plagioclase feldspar and scapolite (Fig. 3.5, Samples 292; Appendix 1).

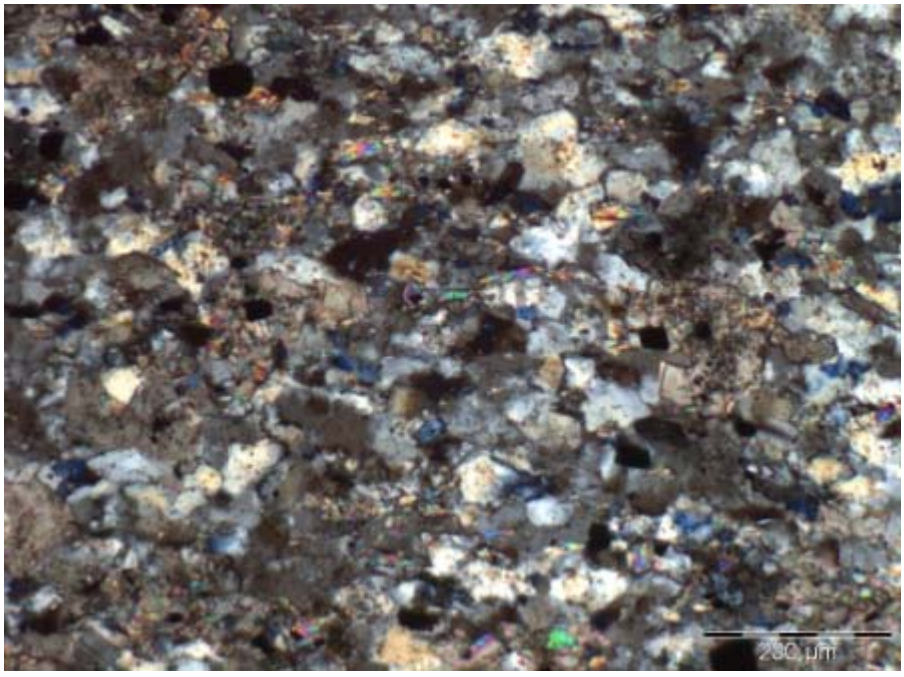


**Figure 3.3: Crossed-polarised thin section photo of Bernecker Creek Formation fine-grained sandstone; Gilbert River, Ortona. Sample 124, Appendix 1.**

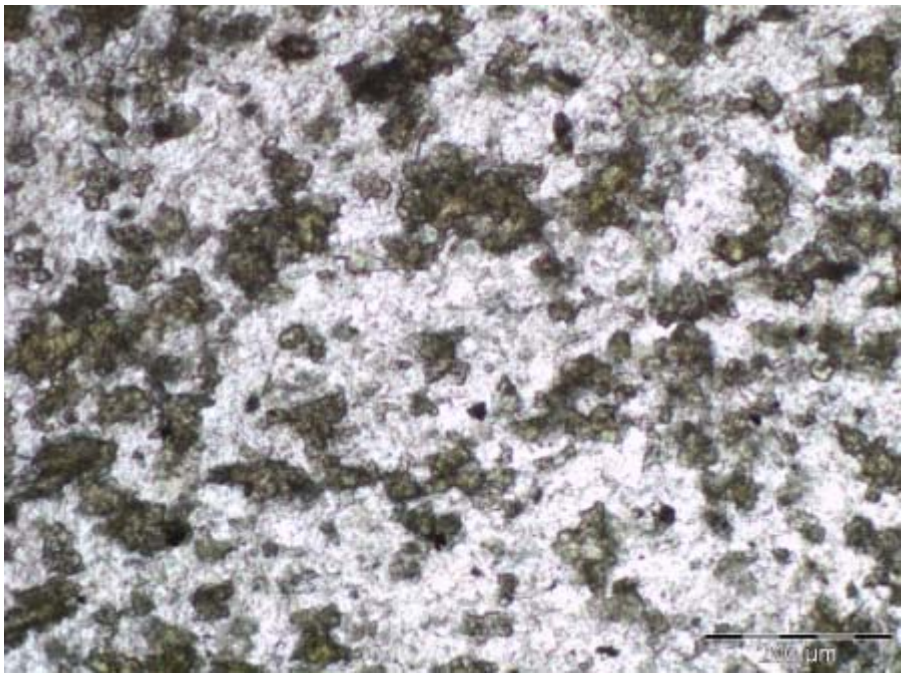

**Figure 3.4: Thin section photo of Bernecker Creek Formation sandstone containing metamorphic epidote; Percy River, Ortona. Sample 13, Appendix 1.**

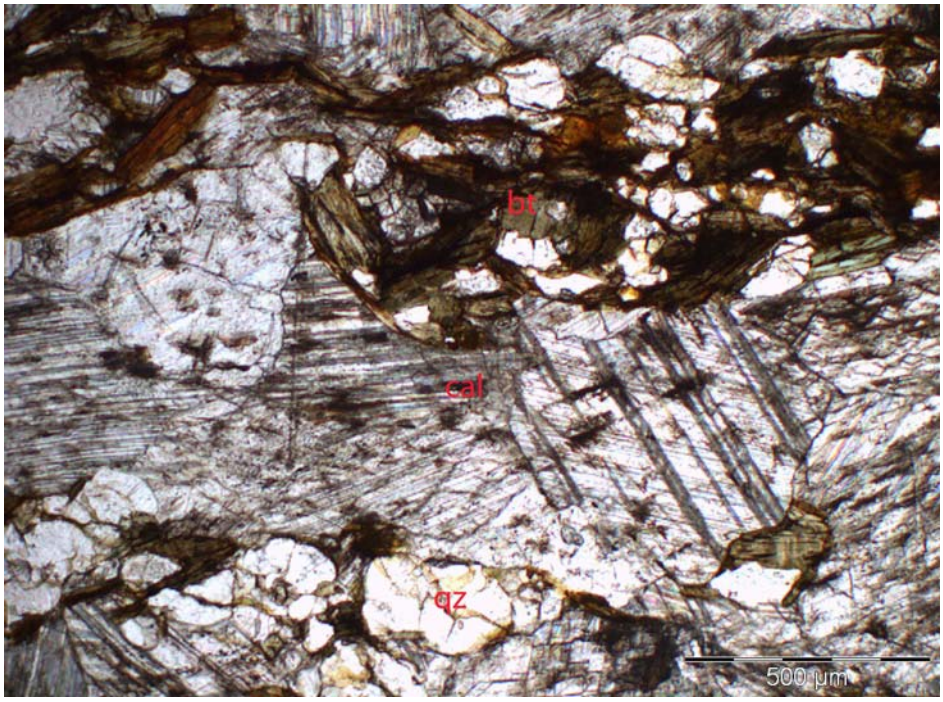


**Figure 3.5: Thin section photo of coarse-grained, calcareous Bernecker Creek Formation mica schist. Mineral labels: cal = calcite; bt = biotite; qtz = quartz. Sample 292, Appendix 1.**

### 3.2.3 Robertson River Subgroup

Numerous samples of the constituent lithologies within the Robertson River Subgroup were collected over the course of this study. Samples of the Dead Horse Metabasalt

were primarily collected for geochemical analysis, with several samples also employed for geochronological and lithological analysis. Samples of the Daniel Creek Formation, Corbett Formation, and Lane Creek Formation were also collected for lithological, structural, geochronological, and thermobarometric analysis as described in this and the following chapters.

#### 3.2.3.1 Daniel Creek Formation

Representative low-grade samples of the Daniel Creek Formation were collected from the Percy River north of 'Ortona' (Fig. 2.6), and are mostly siltstone (Appendix 1). Sample 97 from this locality contains very fine-grained, aligned quartz and muscovite, porphyroblasts of a prograde metamorphic mineral (possibly staurolite) pseudomorphed by chlorite, and biotite (Sample 97, Appendix 1). In thin section, muscovite-rich/quartz-poor and muscovite-poor/quartz-rich layering is visible, and probably indicates small-scale changes in the clastic composition of original sedimentary layers. Metamorphic biotite has grown in the matrix along with quartz.

Low-grade rocks of the Daniel Creek Formation are mainly located between Gilberton and the Agate Creek gemfields (Fig. 2.6; Withnall *et al*., 2003a), and near 'South Head' (Fig. 2.6; Withnall *et al*., 2003b). Elsewhere the low-grade rocks grade into mica schist and quartzite. As with the Bernecker Creek Formation, the higher grade of metamorphism and more intense deformation have obliterated most small-scale sedimentary structures; however bedding is generally preserved. Mica schist belonging to the Daniel Creek Formation was sampled from the 'Gum Flats' area (Fig. 2.6). Samples of the mica schist mostly contain fine-grained quartz, biotite, muscovite, lesser plagioclase, and in some samples small garnet porphyroblasts and aluminosilicate (Fig. 3.6; Sample 311, Appendix 1). Biotite is generally the dominant mica phase. Aluminosilicate in the mica-schist was probably andalusite, and where originally present, has been mostly retrogressed to sericite. The quartzite contains mostly quartz, plagioclase, and lesser white mica.

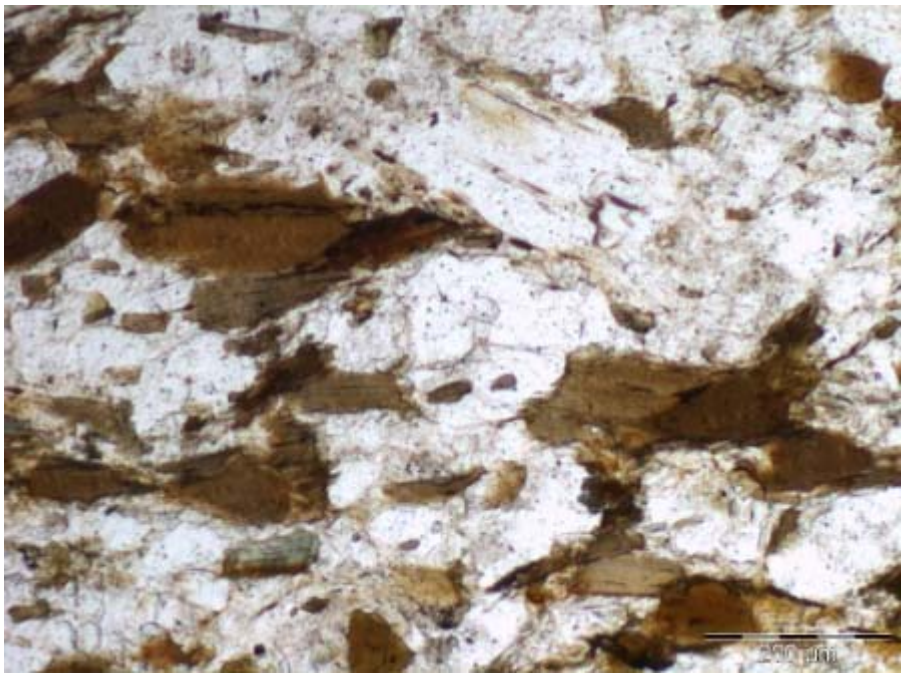

**Figure 3.6: Thin section photo of Daniel Creek Formation biotite schist containing fine-grained quartz, biotite, muscovite, and lesser plagioclase. Sample 311, Appendix 1.**

### 3.2.3.2 Dead Horse Metabasalt

Samples of the Dead Horse Metabasalt collected for this study can be split into two groups based on their sampling location. The South Head rocks were collected from the Gilbert River southeast of 'South Head' station (Fig. 2.6; Withnall *et al*., 2003b), and the Ortona rocks were sampled from the area surrounding 'Ortona' station (Fig. 2.6; Withnall *et al*., 2003a). In both localities the metamorphic grade of the rocks is predominantly greenschist facies.

The South Head rocks are best exposed to the southeast of 'South Head' station, where they occur as a discontinuous series of outcrops along the base of the Gilbert River for over 4 km (Fig. 2.10). Over the length of the section, the dominant texture of the metabasalt varies considerably, from an inferred margin of fine grained doleritic material, through coarser grained dolerite, then fine grained basalt flows, to predominantly pillowed basalt layers (Fig. 2.10). The predominantly coarse-grained dolerite layers are up to 700 m thick, and are composed of actinolite, albite, and chlorite, along with minor sericite, epidote, relic igneous plagioclase and clinopyroxene, and accessory haematite and chalcopyrite (Fig. 3.7; Sample 241, Appendix 1). They are similar in appearance and mineralogy to samples of the

Cobbold Metadolerite from ‘Ortona’ that occur stratigraphically below the Dead Horse Metabasalt, and may correlate with it.

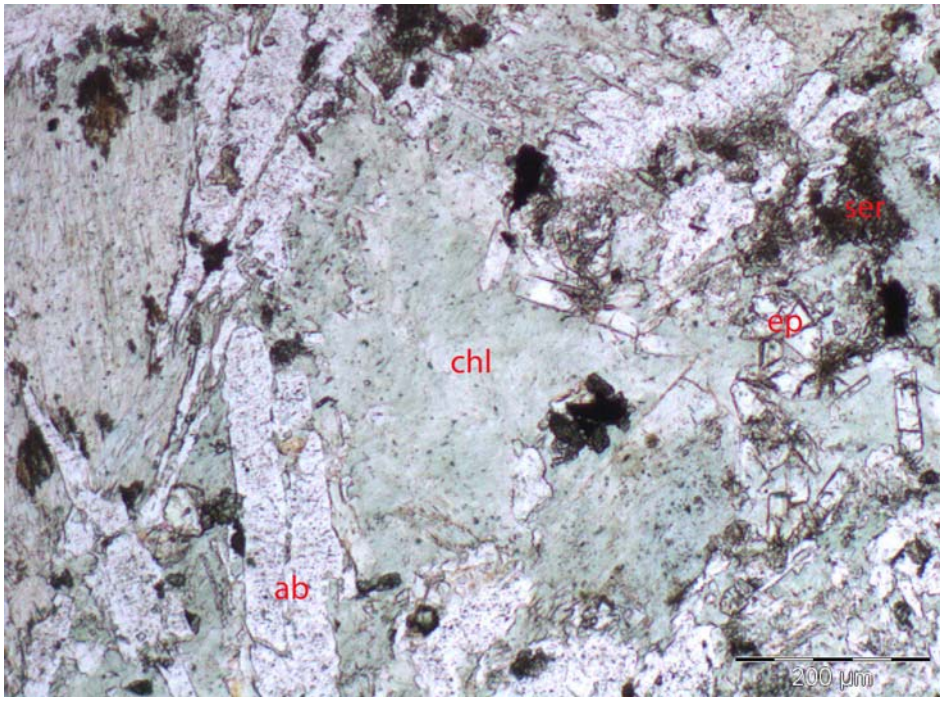


**Figure 3.7: Thin section photo of doleritic Dead Horse Metabasalt showing low-grade metamorphic assemblage. Mineral labels: chl = chlorite; ab = albite; ep = epidote; ser = sericite. Sample 241, Appendix 1.**

Stratigraphically overlying the doleritic layers are predominantly fine-grained, locally massive basalt flows up to 500 m thick. Individual basalt flows are generally no thicker than 20m, and are usually separated by thin doleritic layers and minor pillowed layers. The basalt flows are generally finer-grained, yet mineralogically similar to the doleritic layers. In both the basaltic and doleritic samples accessory haematite and chalcopyrite are metamorphic, and have grown in place with quartz. Haematite primarily occurs as concentric growth bands around chalcopyrite, and the growth bands may also include limonite (Fig. 3.8; Sample 229, Appendix 1). The growth bands may have formed by supergene alteration of the chalcopyrite grains.

The inferred top of the sequence is composed predominantly of a thick sequence of pillowed basalt layers up to 300 m thick. Individual pillows are generally no larger than 1 m in diameter, and pillowed basalt layers are generally less than 10 m thick (Fig. 3.9). Pillow cores and rims are mineralogically similar, containing very fine-grained chlorite, igneous plagioclase, and minor actinolite, epidote, haematite, and magnetite. Pillow rims generally contained a higher proportion of matrix glass,

primarily altered to chlorite (Fig. 3.10; Sample 234, Appendix 1). Spaces between pillows were most likely filled by quenched, basaltic glass that has subsequently weathered (Fig. 3.9).

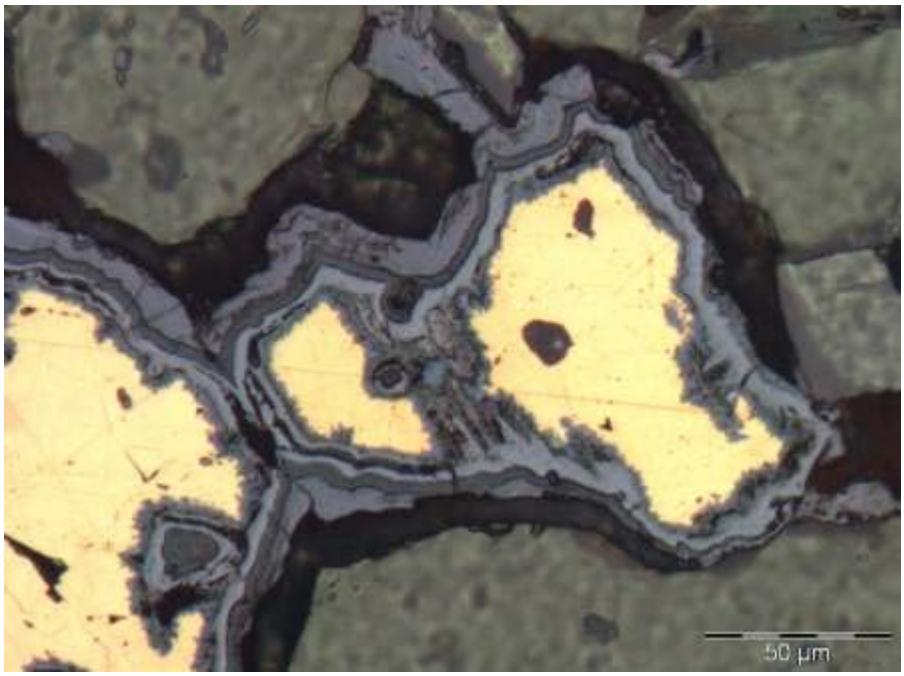


**Figure 3.8: Thin section photo of concentric haematite bands surrounding chalcopyrite grain in aphyric metabasalt; Dead Horse Metabasalt, South Head. Sample 229, Appendix 1.**

**Figure 3.9: Pillowed basalt outcrop; Gilbert River, South Head.**

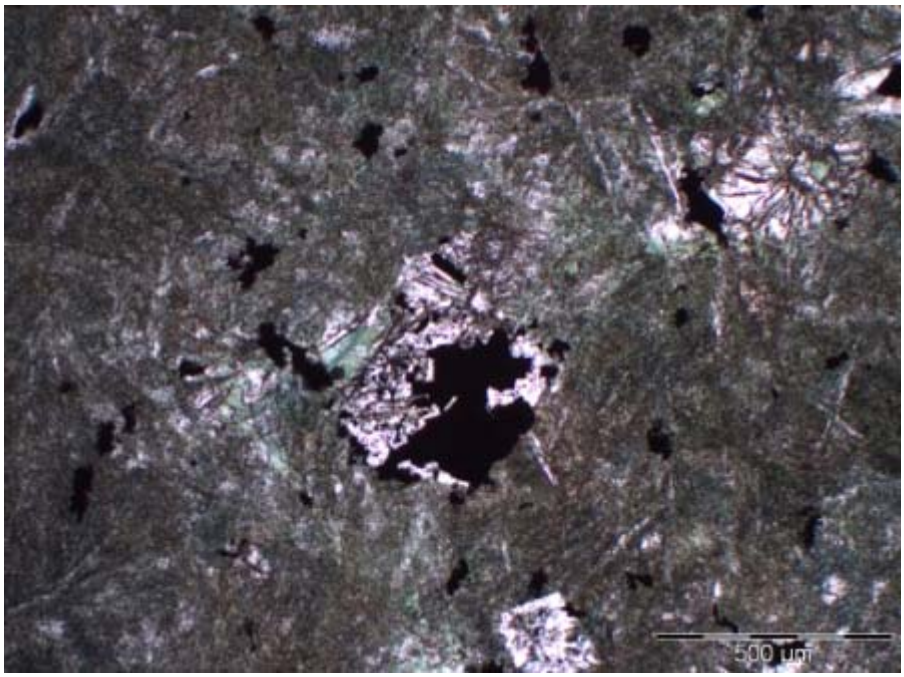


**Figure 3.10: Thin section photo of Dead Horse Metabasalt pillowed basalt rim containing fine-grained chlorite, albite, and lesser calcite; Gilbert River, South Head. Sample 234, Appendix 1.**

The Ortona rocks are best exposed to the north and south of 'Ortona' station, where they occur as numerous, laterally extensive layers up to 1 km thick (Fig. 2.6; Withnall *et al*., 2003a). Samples of the metabasalt were collected mostly from outcrops in the Percy and Gilbert River beds, with the largest sequence of outcrops occurring to the northwest of 'Ortona' in the Gilbert River. Here the metabasalt has been folded by a west-recumbent regional scale $F_1$ anticline (Fig. 2.6; Withnall, pers. comm., 2003). The Ortona metabasalts generally display the same variation in texture as the South Head samples, but on a smaller scale. Alternating layers of fine-grained metabasalt, and coarser-grained metadolerite can be found in all sections; however, pillowed basalt layers are restricted to the largest exposed sequence of outcrops in the Gilbert River. The exact sequence of layering is difficult to identify in the metabasalt due to the randomly occurring nature of outcrops; however, metadolerite sills have been mapped stratigraphically below some metabasalt layers in the region (Withnall *et al*., 2003a), and therefore may lie at the base of the sequence.

The fine-grained metabasalt and coarser-grained metadolerite layers are each less than 30 m in thickness and are mineralogically similar, containing actinolite, chlorite, albite, and minor epidote, magnetite, and relic igneous clinopyroxene and plagioclase (Fig. 3.11; Sample 111, Appendix 1). Samples of pillowed basalt from outcrops in the area are composed primarily of albite and chlorite. Accessory minerals include

actinolite, epidote, titanite, and relic igneous clinopyroxene and plagioclase grains (Fig. 3.12; Sample 80, Appendix 1).

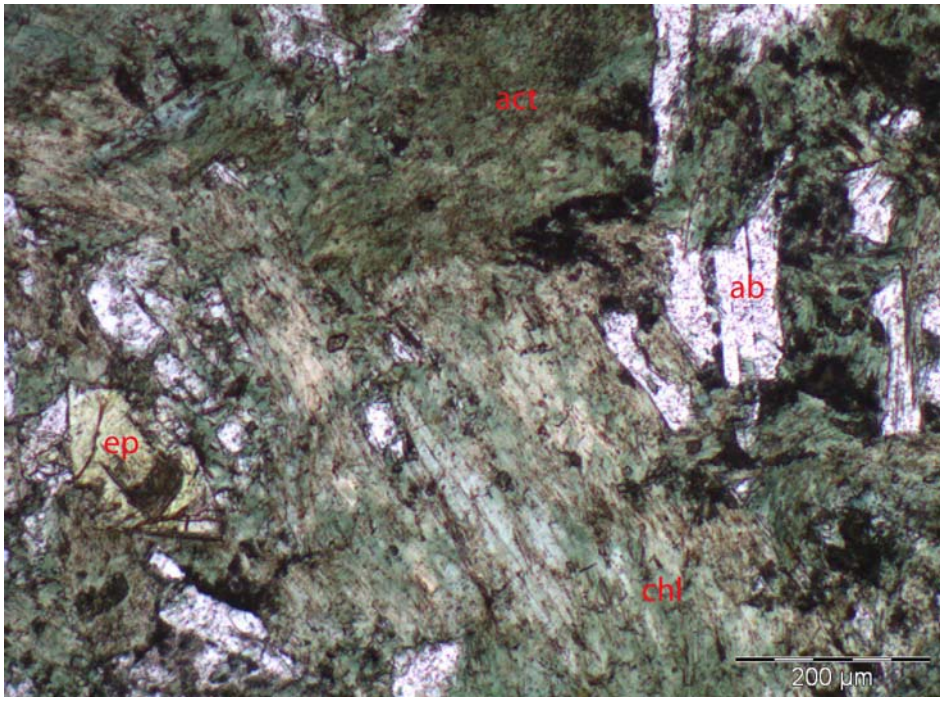


**Figure 3.11: Thin section photo of fine-grained Dead Horse Metabasalt; Percy River, Ortona. Mineral labels: act = actinolite; chl = chlorite; ab = albite; ep = epidote. Sample 111, Appendix 1.**

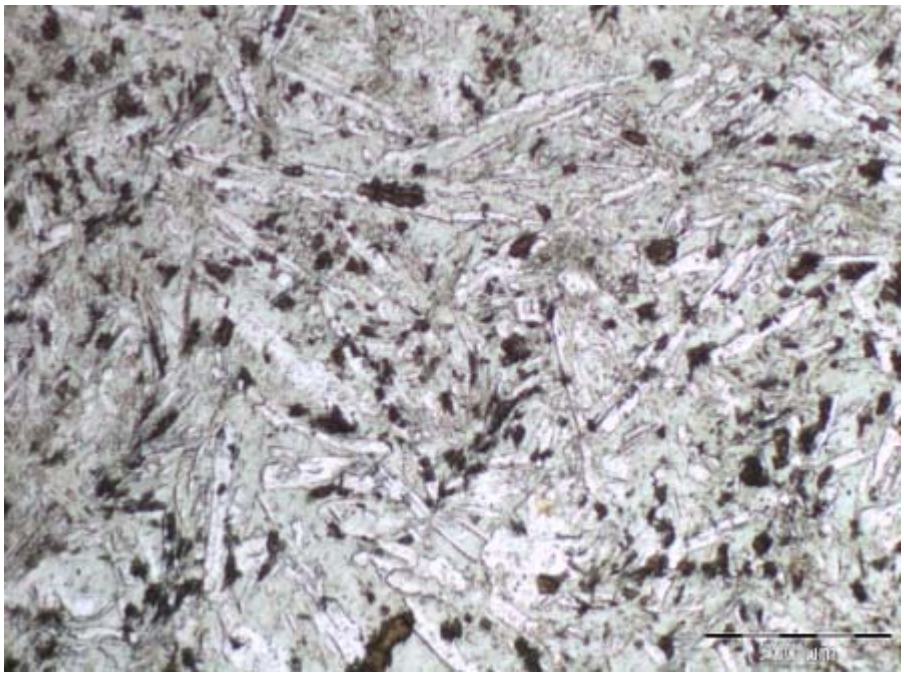

**Figure 3.12: Thin section photo of Dead Horse Metabasalt pillowed basalt containing fine-grained chlorite, albite, and accessory epidote and titanite; Gilbert River, Ortona. Sample 80, Appendix 1.**

In the higher grade area of the Robertson River Subgroup around ‘Robinhood’, the Dead Horse Metabasalt consists of fine-grained, foliated amphibolite. In samples of the higher grade rocks, the dominant amphibole is actinolite grading into hornblende, chlorite is absent, and metamorphic albite is present along with quartz and minor Ti-magnetite (Fig. 3.13; Sample 261, Appendix 1). Some outcrops of the amphibolite in the Robertson River are coarser-grained with a gneissic appearance, and have been intruded by thin dioritic veins containing a higher percentage of quartz and plagioclase, and less hornblende (Fig. 3.14).

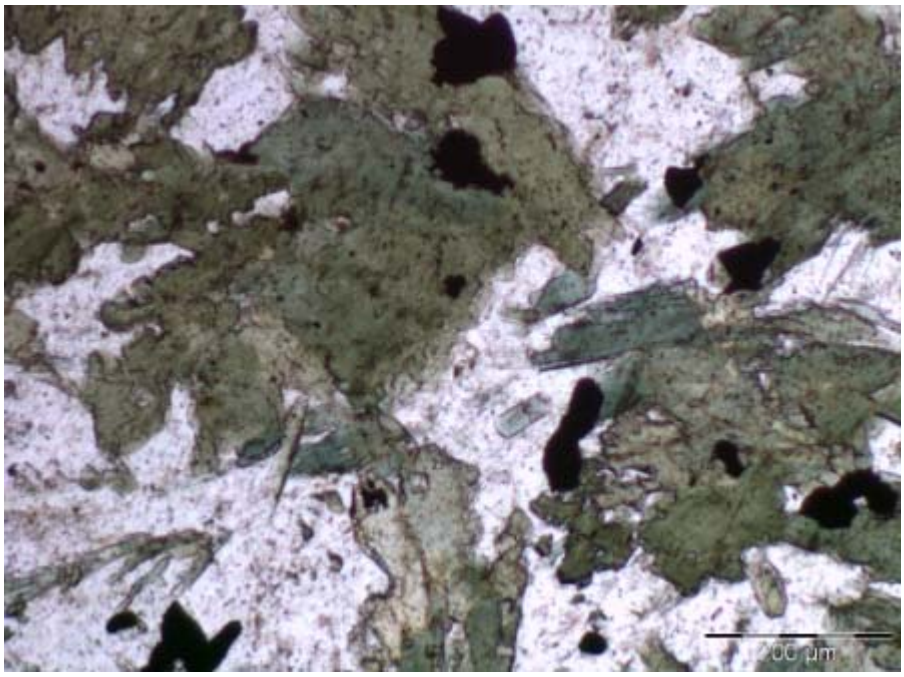

**Figure 3.13: Thin section photo of Dead Horse Metabasalt amphibolite containing fine-grained hornblende, quartz, albite, and minor Fe-Ti oxide; Robertson River, Robinhood. Sample 261, Appendix 1.**

### 3.2.3.3 Corbett Formation

Representative low-grade samples of the Corbett Formation were collected from the Percy River north of ‘Ortona’ (Fig. 2.6), and vary from siltstone to mudstone (Appendix 1). Sample 278B from Ortona contains very fine-grained, aligned quartz, muscovite, and lesser biotite (Fig. 3.15; Sample 278B, Appendix 1). Higher grade samples were collected from between Forsayth and ‘Robinhood’ (Fig. 2.6), and are predominately mica schist. Representative samples commonly contain fine-grained foliated biotite, muscovite, and blocky quartz (Fig. 3.16; Sample 306; Appendix 1). Garnet and staurolite are also identified in some samples. Garnet is commonly fine-

grained and surrounded by very fine-grained biotite. Staurolite is poikiloblastic, containing fine-grained quartz and retrogressive muscovite.

**Figure 3.14: Dead Horse Metabasalt amphibolite containing dioritic vein; Robertson River near Robinhood.**

**Figure 3.15: Thin section photo of Corbett Formation mica schist; Gum Flats. Sample 278B, Appendix 1.**

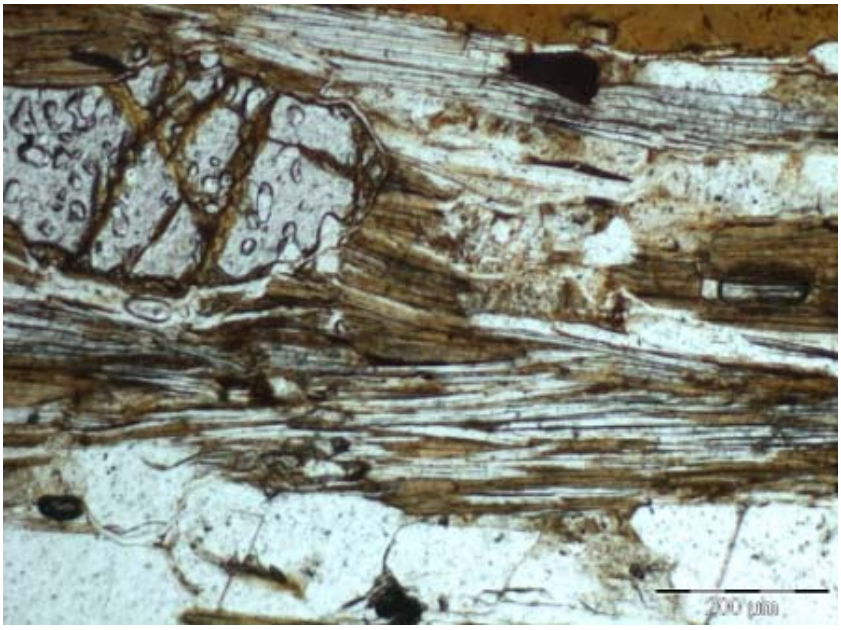

**Figure 3.16: Thin section photo of Corbett Formation mica-schist containing metamorphic garnet porphyroblasts wrapped by later biotite and muscovite. Sample 306, Appendix 1.**

### 3.2.3.4 Lane Creek Formation

Representative low-grade samples of the Lane Creek Formation were collected from west of Georgetown near Stockyard Creek and South Head (Fig. 2.6), and are predominately comprised of siltstone (Appendix 1). Samples of the siltstone from South Head contain very fine-grained, foliated, quartz and muscovite (Fig. 3.17; Sample 245, Appendix 1). Higher grade samples were collected from between Forsayth and 'Robinhood' (Fig. 2.6), and are predominately mica schist (Fig. 3.18; Sample 304, Appendix 1).

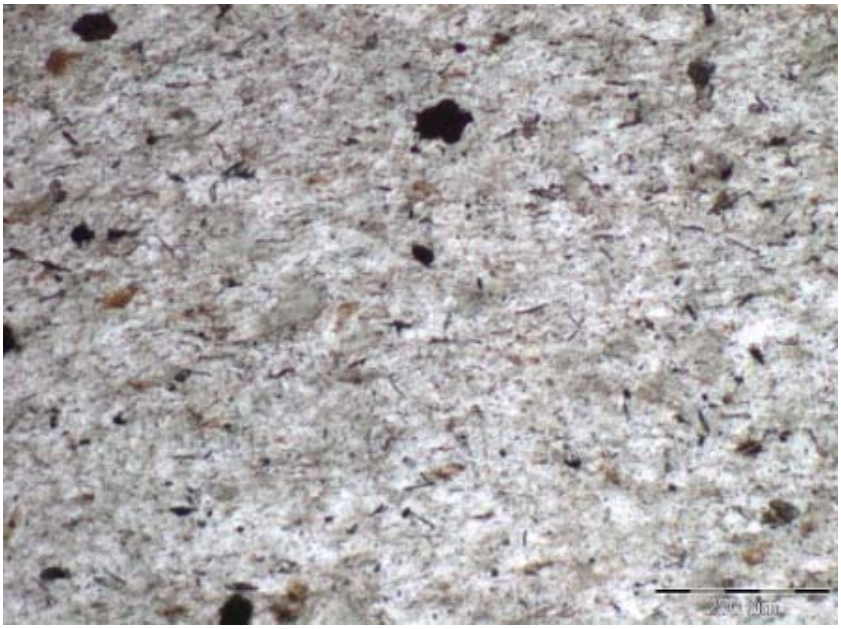

**← Figure 3.17: Thin section photo of very fine-grained Lane Creek Formation quartz-muscovite schist; South Head. Sample 245, Appendix 1.**

The higher grade mica schist commonly contains foliated, elongate muscovite that is microscopically layered between blocky quartz grains. Minor mineral phases include biotite, and locally garnet. Patches of unfoliated quartz, chlorite and muscovite occur throughout the sample, and may represent replacement of metamorphic andalusite.

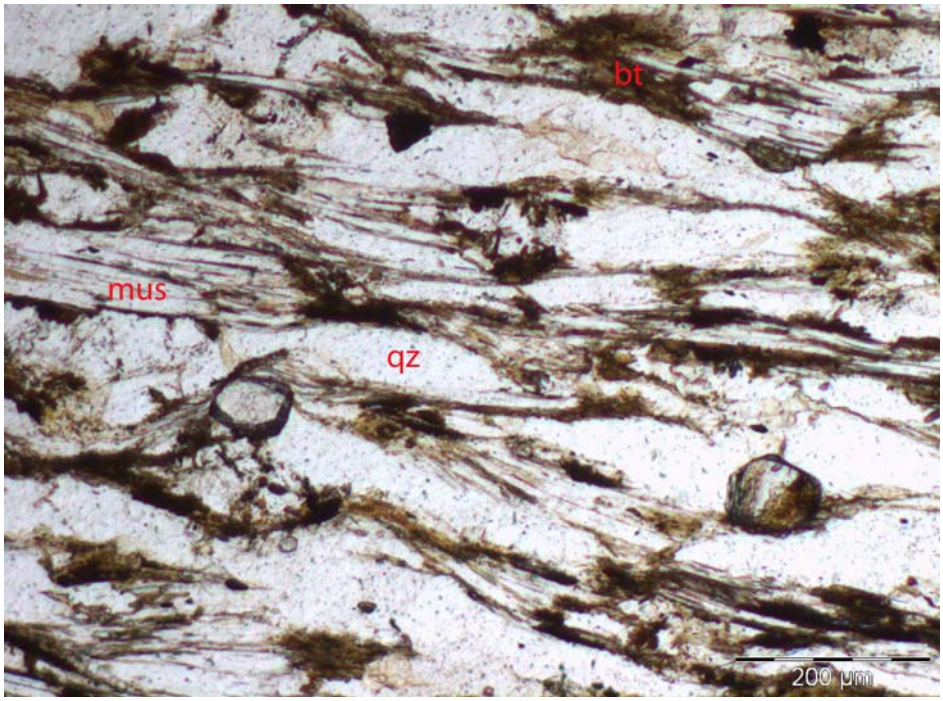


**Figure 3.18: Thin section photo of fine-grained Lane Creek Formation mica-schist; Robinhood. Sample 304, Appendix 1.**

### 3.2.4 Cobbold Metadolerite

In the low grade area of the Robertson River Subgroup, including near 'Ortona' and Stockyard Creek, the metamorphic grade of the metadolerite is lower- to mid-greenschist facies. Samples interlayered with or below the Dead Horse Metabasalt are fine- to coarse-grained, and commonly contain anhedral metamorphic actinolite, albite, chlorite, quartz, epidote, and sericite replacing igneous plagioclase feldspar (primarily labradorite), rare igneous clinopyroxene, and accessory magnetite and chalcopyrite (Fig. 3.19; Sample 121; Appendix 1).

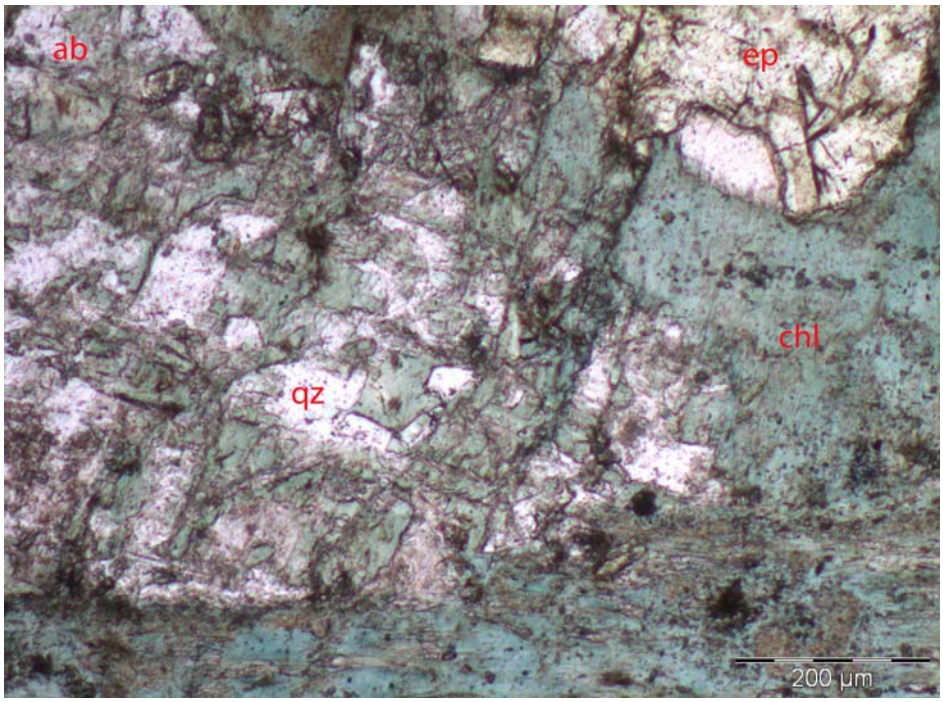


**Figure 3.19: Thin section photo of Cobbold Metadolerite from layer adjacent to Dead Horse Metabasalt; Ortona. Mineral labels: ab = albite; chl = chlorite; ep = epidote; qz = quartz. Sample 121, Appendix 1.**

Samples of the metadolerite from stratigraphically above the Dead Horse Metabasalt are petrographically similar to those that occur with the metabasalt. Variations between the two metadolerite groupings, if they exist, would be observed in the concentrations of some trace elements, and are therefore described in Chapter 6. Metadolerite outcrops from lower grade areas contain in places minor felsic segregations that have possibly formed as late-stage felsic differentiates, or as peprites along the margins of the intrusion and sediments (Fig. 3.20). Where the felsic segregations occur within the metadolerite, a decrease in the modal percentage of felsic minerals is observable around their margin (Fig. 3.21). Felsic components of the metadolerite are commonly composed of coarse-grained calcite, albite, quartz, and muscovite, and minor chlorite, sphene, magnetite, and accessory zircon.

**Figure 3.20: Peperite at contact of Bernecker Creek Formation (left) and Cobbold Metadolerite (to right of photo, not shown); Percy River, Ortona.**

One interesting section of exposed metadolerite in the Percy River near 'Ortona' is composed of spheroidal 'felsic' xenoliths surrounded by dolerite (Fig. 3.22). The section is approximately 1 m wide, and is in contact with the Bernecker Creek Formation. However, the xenoliths mineralogically different to other felsic segregations found within the metadolerite as these contain coarse-grained, anhedral clinozoisite and lesser epidote (Fig. 3.23; Sample 178, Appendix 1). The mineralogy of metadolerite surrounding the xenoliths appears equivalent to metadolerite from other locations (Fig. 3.23). The origin of the xenoliths is unclear, but they may have been locally derived from adjacent Bernecker Creek Formation calcareous quartz sandstones, and were possibly rounded by chemical reaction rather than mechanical abrasion.

**Figure 3.21: Felsic segregations in low-grade Cobbold Metadolerite; Percy River, Ortona.**

**Figure 3.22: 'Felsic' xenoliths in low-grade Cobbold Metadolerite, Percy River, Ortona. Red colouration in blebs is a weathering effect unrelated to mineralogy.**

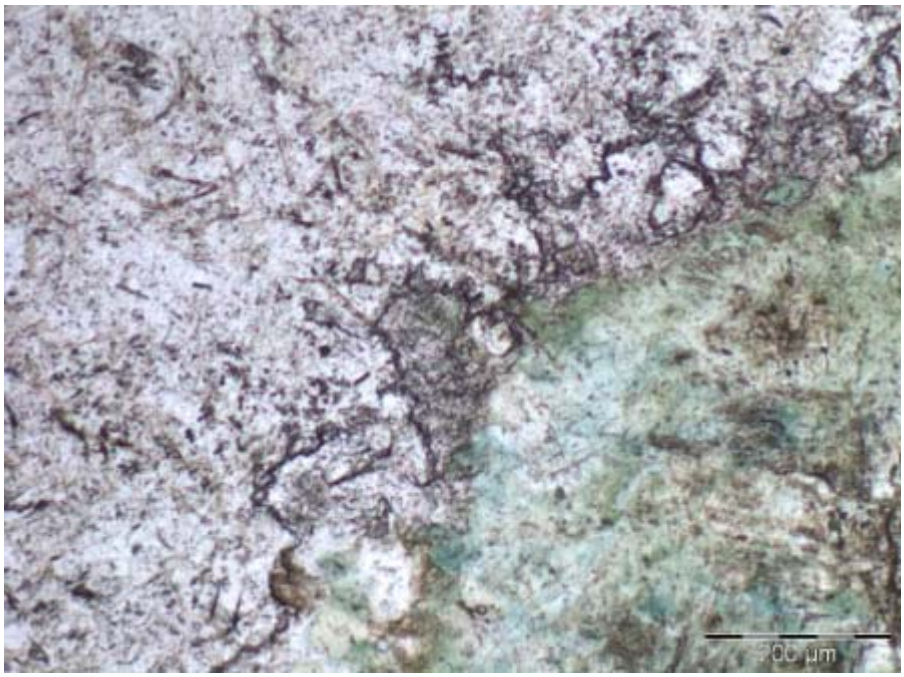

**Figure 3.23: Thin section photo of clinozoisite-epidote-rich 'felsic' xenolith (left) and low-grade Cobbold Metadolerite (lower right); Percy River, Ortona. Sample 178, Appendix 1.**

In the high grade areas of the Robertson River Subgroup, including near 'Robinhood' and 'Gum Flats', actinolite in the metadolerite is replaced by blue-green hornblende, and albite is the dominant feldspar. Epidote and chlorite become minor phases, and are absent in amphibolite facies samples. As with the surrounding metasediments and metabasalt, the metadolerite is commonly deformed, and igneous textures and minerals are rarely preserved. Samples from the 'Robinhood' area mostly reached amphibolite facies, and are generally foliated. They commonly contain euhedral hornblende, quartz, albite, minor anhedral biotite, and magnetite (Fig. 3.24; Sample 215, Appendix 1). Samples from the 'Gum Flats' area reflect a change in metamorphic grade from upper greenschist facies to amphibolite facies. Samples of the metadolerite from close to the Gilberton Fault are at greenschist facies, containing actinolite (e.g.: Sample 291; Appendix 1). Further north, hornblende replaces actinolite and albite, while quartz and magnetite are common (e.g.: Sample 300, Appendix 1). Hornblende and quartz show evidence of recrystallising igneous clinopyroxene, and sericite replacing igneous plagioclase. Higher grade metadolerite samples were collected from within areas mapped as the Einasleigh Metamorphics by Withnall *et al*. (2003a), and are described in that section.

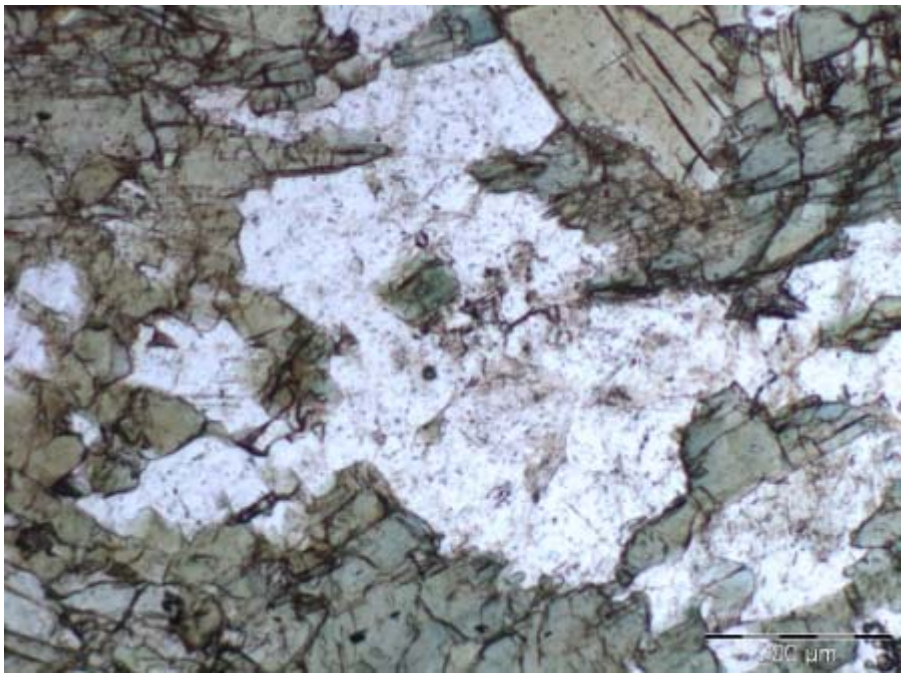

**Figure 3.24: Thin section photo of amphibolite facies Cobbold Metadolerite containing fine-grained hornblende, quartz, albite, and minor biotite; Robinhood. Sample 215, Appendix 1.**

## 3.3 Mesoproterozoic Granites

Four samples of Mesoproterozoic granite that intruded the Etheridge Group were collected during this study, including three samples of the Ropewalk Granite, and one sample of the Mount Hogan Granite. Samples of the Ropewalk Granite consist of medium- to coarse-grained biotite and lesser muscovite, along with quartz, titanite, orthoclase, and lesser plagioclase (Samples 208, 209, 210; Appendix 1). The sample of the Mount Hogan Granite consists of medium- to coarse-grained quartz, microcline, and fine-grained muscovite (Sample 135; Appendix 1).

## 3.4 Folding in the Etheridge Group

Of the six episodes of deformation recognised in the Etheridge Group, only the first four events are described in detail below. $D_5$ and $D_6$ had limited effect on the Etheridge Group and were not recognised in outcrops over the course of this study; as such they are not described here.

### 3.4.1 First Deformation Event

Rocks of the study area generally show well-developed axial planar foliations ($S_1$) that have intensely folded bedding ($S_0$), and vary from a slaty cleavage through to schistosity depending on the grade of metamorphism. In the study area $F_1$ folds are generally between 4-8 km in wavelength and isoclinal (Fig. 3.25). Near 'Ortona' the axial planes of $F_1$ folds are generally steep to vertical and trend west-southwest (Fig. 3.26a). Eastwards, in the area south of 'Gum Flats', axial planes retain their steep to sub-vertical nature but trend northeast (Fig. 3.27). North of 'Gum Flats' the steeply dipping nature of the event is maintained; however, the trend is more easterly (Fig. 3.27).

**Figure 3.25: Core of isoclinal, upright $F_1$ fold, Bernecker Creek Formation; Percy River, Ortona.**

In the north of the study area, approximately 20 km west of 'Robinhood' (Fig. 2.6), the majority of $D_1$ structures have been overprinted by the more intense $D_2$ event, hence the location and nature of $F_1$ folds in this area is uncertain. Structural data obtained from this area indicate the overprinting effects of $D_2$ (Fig. 3.28). In Figure 3.28, the general trend recognised for $S_1$ at 'Ortona' and 'Gum Flats' appears to continue, with steeply dipping west-southwesterly planes denoting $S_1$. The repetition

of stratigraphy in the area may relate to a later stage of folding, most likely $F_3$; however, the overall northward younging of the stratigraphy from 'Ortona' through to 'Robinhood' has previously led Withnall (1996) to suggest the rocks may lie on the northern limb of a major $F_1$ anticline.

### 3.4.2 Second Deformation Event

Within the study area the effects of $D_2$ are variable. Near 'Ortona' there is little or no folding associated with it; however, local, weak crenulation cleavages are attributed to $D_2$. They generally form a steeply dipping, east-northeasterly trending cleavage (Fig. 3.26b). Towards the east and north of 'Ortona' $D_2$ forms generally open folds associated with a weak crenulation cleavage. $D_2$ is more prominent in the north of the study area near 'Robinhood' and east near 'Gum Flats' and 'Percyvale'. At these localities $D_2$ has resulted in tight to isoclinal, short wavelength folding associated with a strong, differentiated cleavage or schistosity. Structural data collected from the area surrounding 'Robinhood' indicates a clustering of poles to $S_2$ in the southwest quadrant (Fig. 3.28). Withnall (1996) has attributed this effect to later folding associated with $D_3$.

$S_2$ crenulation cleavages in the area south of 'Gum Flats' strike northeast to north and are steeply to sub-vertically dipping (Fig. 3.27). North of 'Gum Flats' $S_2$ remains steeply dipping; however, the strike is generally towards the east (Fig. 3.27). Large northeast-trending folds in the area that fold both $S_0$ and $S_1$ are interpreted to be $F_2$. Poles to $S_1$ in the north of the area illustrate the northeast trending nature of these folds (Fig. 3.27). The change in the general trends of both $S_1$ and $S_2$ in the area surrounding 'Gum Flats': from northeast in the south, to east in the north, is consistent with the presence of a major, open $F_3$ fold in the area. Withnall (1996) suggested that this fold has an axial plane which passes through the middle of the area, and strikes approximately east. North of 'Gum Flats', further rotation of axial planes to $F_2$ folds towards the southeast support this argument (Fig. 3.27).

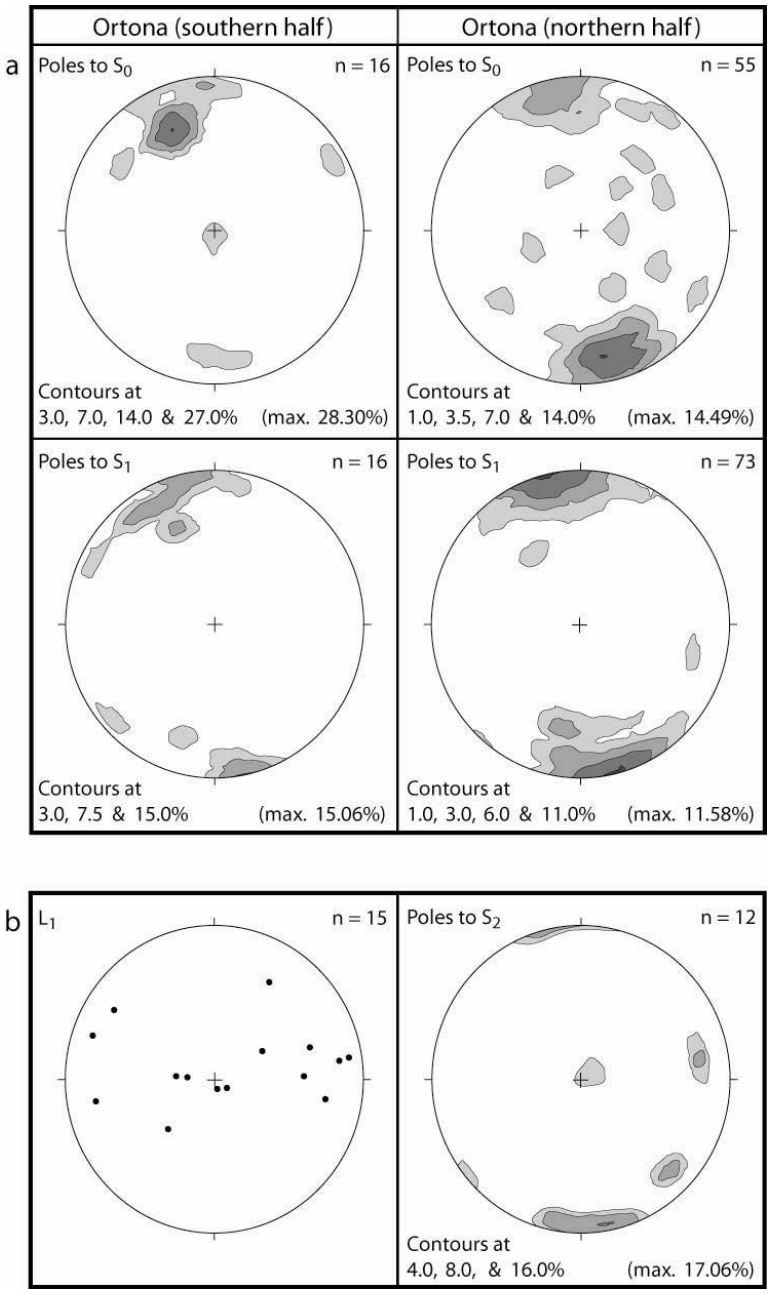


**Figure 3.26: Structural data for the area near 'Ortona' station. The area corresponds to the 'Ortona domain' of Withnall (1996). (a) $S_0$ and $S_1$ data for north and south Ortona. Boundary between areas is northing 7876000 ('Ortona' station). (b) Combined $L_1$ and $S_2$ data for 'Ortona' area. Equal area stereonet projection used.**

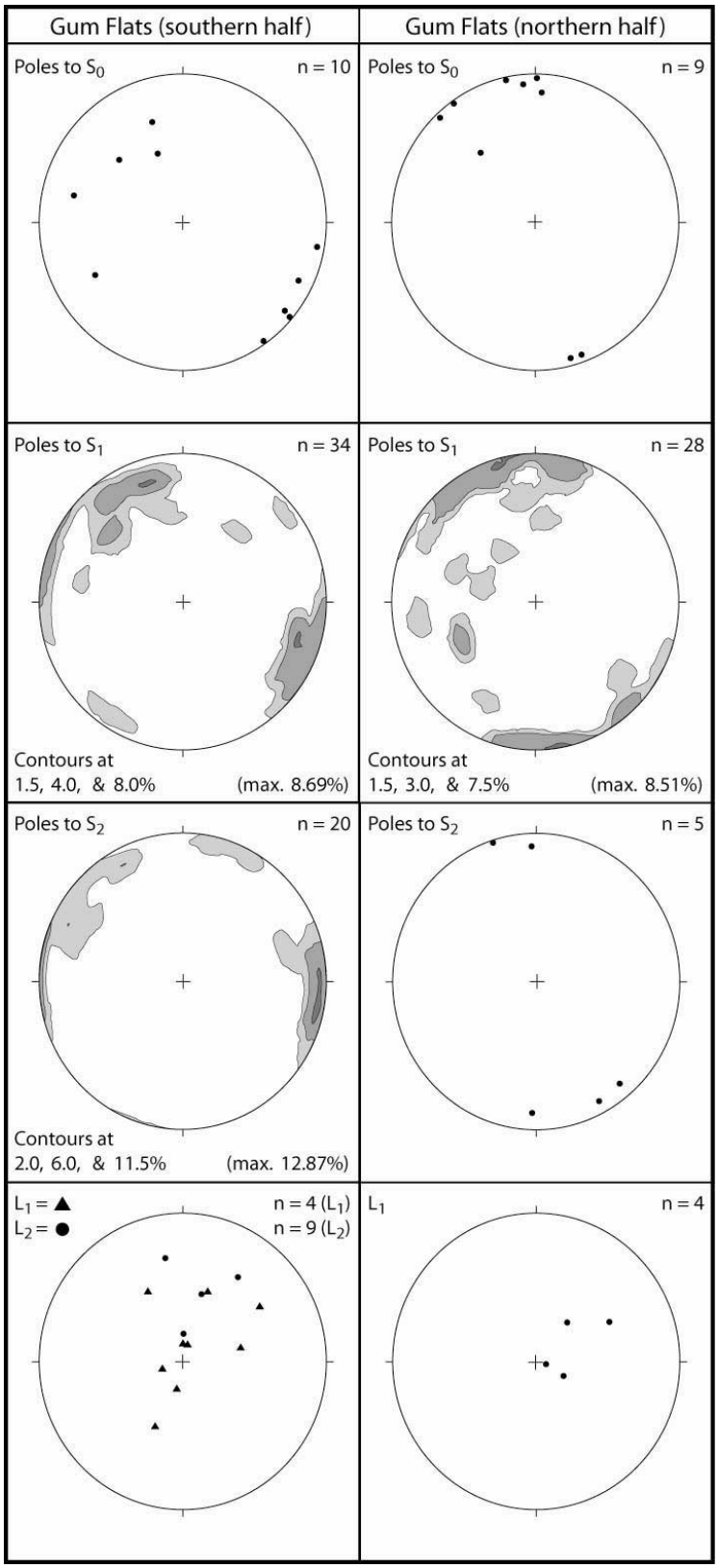


**Figure 3.27: Structural data for the area near 'Gum Flats' and 'Percyvale' stations. The area corresponds to the eastern 'Mount Hogan domain' and western 'Welfern domain' of Withnall (1996). Boundary between areas is northing 7885100 ('Gum Flats' station). Equal area stereonet projection used.**

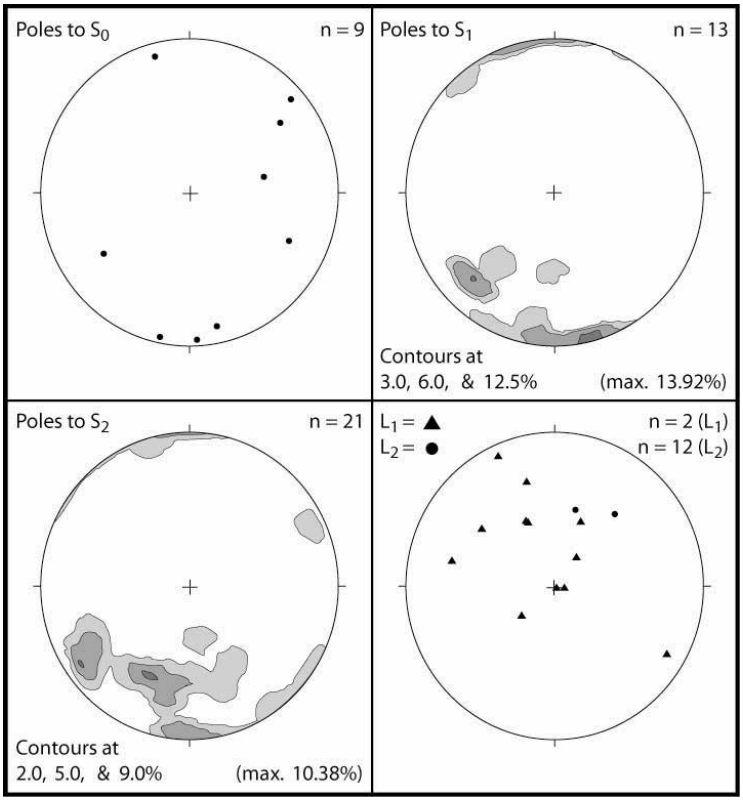


**Figure 3.28: Structural data for the area near 'Robinhood' station. The area corresponds to the 'Robinhood domain' of Withnall (1996). Equal area stereonet projection used.**

### 3.4.3 Third Deformation Event

In the study area, the effects of $D_3$ are variable. Foliation associated with $D_3$ has not been recognised in the study area except as the axial planes of crenulations of $S_2$. North-west of 'Robinhood' $D_3$ is dominant, and has produced tight overturned folds with northerly dipping axial planes and fold axes plunging towards the northwest (Withnall, 1996). As discussed above, this has effectively confined poles to $S_2$ to the southern hemisphere (Fig. 3.28). Near 'Ortona' $F_3$ folds have not been recognised. However, Withnall (1996) suggested that in this area the effect of $D_3$ may have been to further tighten $F_1$ folds, with no separate $F_3$ folds being generated.

### 3.4.4 Fourth Deformation Event

$D_4$ has had little effect on the study area, apart from possibly producing a broad warping in the trends of $F_3$ axial planes near 'Robinhood'. As such, no definitive qualitative structural data relating to this event was obtained. Elsewhere the effects of

$D_4$ are minor, including forming small kinks and crenulations in pre-existing fabrics. In the south of the study area near ‘Ortona’ and ‘Gum Flats’, no $D_4$-related structures were recognised.

# Chapter 4.

# U-Pb igneous and detrital zircon, and EMPA monazite age constraints on the deposition, igneous emplacement, and post-depositional evolution of the lower Etheridge Group

## 4.1 Introduction

A combination of conventional multigrain LA-ICPMS U-Pb zircon dating and electron microprobe U-Th-Pb analysis of monazite (EMPA) is used on a number of igneous and metasedimentary samples in order to better constrain the evolution, emplacement and depositional ages the lower Etheridge Group. Zircons were primarily sourced from samples of the Cobbold Metadolerite and Dead Horse Metabasalt exhibiting granophyric or peperitic textures and high Zr contents (Zr > 150 ppm), and were collected from a number of localities within the central Georgetown Inlier (Fig. 4.1). In addition, detrital zircons were obtained from samples of metasedimentary rocks surrounding the mafic units. Samples containing monazite were primarily sourced from metapelitic schists of the lower Etheridge Group in the areas surrounding Gum Flats and Robinhood stations (Fig. 4.1).

In this chapter, U-Pb dating of igneous zircons from the mafic rocks of the lower Etheridge Group is used to test, in conjunction with available geochemical data, whether they relate to a single magmatic event, or multiple events. It is also an aim of this study to better constrain the timing of this magmatism, as well as that of the main deformation events, in order to establish a realistic estimate for the timing of deposition and deformation of the lower Etheridge Group. The results of this study are also compared to magmatic, detrital, and metamorphic ages obtained from similarly aged terranes in eastern Australia, to investigate regional correlations between the terranes, and what implications this has for the Proterozoic history of the Georgetown Inlier.

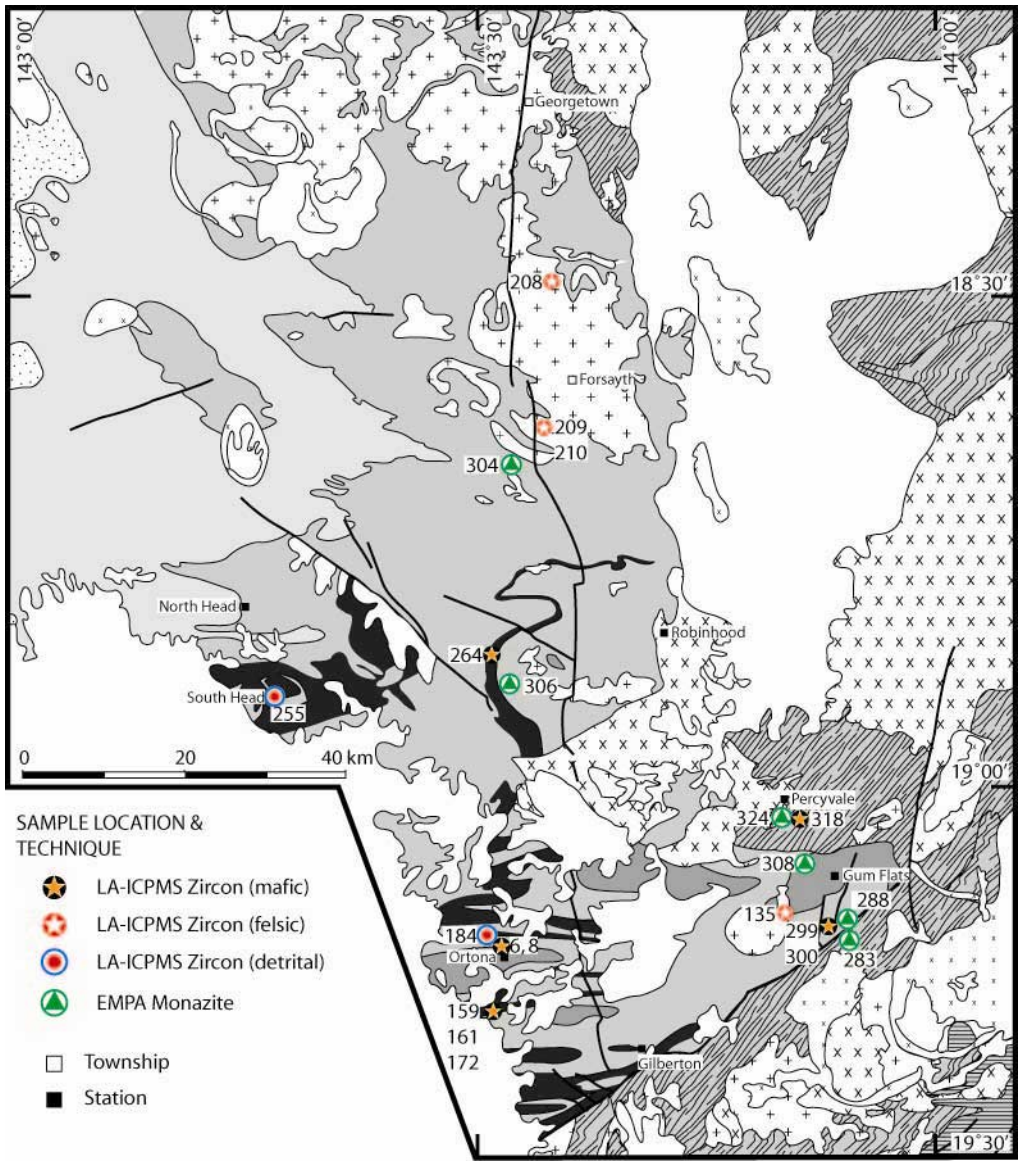


**Figure 4.1: Geological setting of the central Georgetown Inlier, with locations for analysed samples of zircon and monazite. Geological units as for Figure 2.6.**

## 4.2 Previous work

A lack of suitable rock types has hampered previous efforts to directly measure the depositional age of the lower Etheridge Group. However, these studies have proved more successful in constraining the deformation history of the Etheridge Group, and have placed a minimum age on its deposition. Deposition of the Etheridge Group was thought to have occurred prior to 1570 ± 20 Ma, based on a combination of detailed structural analysis and Rb-Sr whole-rock isochron ages, which suggested that $D_1$ and $D_2$ occurred at 1570 ± 20 Ma and 1470 ± 20 Ma, respectively (Black *et al.*, 1979). However, subsequent SHRIMP and conventional multi-grain zircon dating has shown

that at least the younger of these two estimated ages is too young (Black & McCulloch, 1990; Black & Withnall, 1993; Black *et al*., 1998, 2005).

Recent work has established a minimum age of around 1550 Ma for deposition of the Etheridge Group. Support for this age comes from a conventional multi-grain U-Pb zircon age of 1552 ± 2 Ma (Black & McCulloch, 1990) and a SHRIMP zircon age of 1548 ± 18 Ma (Black & Withnall, 1993), both obtained from the overlying Croydon Volcanic Group. Multi-grain zircon ages for both the Forsayth (1550 ± 7 Ma) and Mistletoe (1544 ± 7 Ma) Granites also support this minimum age (Black & McCulloch, 1990). Similar ages have also been obtained for the Lighthouse, Digger Creek and Mt Hogan Granites (Black & Withnall, 1993). Leucogneiss from the Einasleigh Metamorphics within the Etheridge Group has also returned an age of 1555 ± 3 Ma (Black *et al*., 2005).

Establishing a maximum age limit for the Etheridge Group has proven difficult due to the absence of exposed basement rocks. Black & McCulloch (1984), using Sm-Nd data from a diverse range of lithologies, arrived at an age of 2490 ± 70 Ma for the initial formation of the Etheridge Group. Subsequent work (Withnall *et al*., 1988; Black & Withnall, 1993) identified similar-aged zircon in some metasedimentary and igneous rocks, and has since established the ca. 2500 Ma age more likely represents the provenance rather than the age of onset of deposition for the Etheridge Group. This led Black *et al*. (1998) to suggest the 2490 ± 70 Ma age as an upper age limit for the deposition of the Etheridge Group.

EMPA monazite dating of metasedimentary samples from the Robertson River Subgroup was recently conducted by Cihan *et al*. (2006). They suggested that peak conditions for $M_1$ and $M_2$ were reached at 1586 ± 6 Ma and 1542 ± 8 Ma respectively. Based on ages obtained from the oldest monazites analysed, they also suggested that metamorphism leading into $M_1$ may have begun as early as 1655 ± 2 Ma for some sedimentary components of the lower Etheridge Group. A younger group of monazite ages yielded a weighted mean age of 1512 ± 5 Ma, which they inferred to represent a later stage of hydrothermal or thermal activity in the lower Etheridge Group.

The Etheridge Group is now thought to have been deposited prior to 1656 ± 2 Ma, based on the U-Pb zircon age obtained from a leucogabbro sill intruded into the Lane Creek Formation in the middle of the Group (Black *et al*., 1998). An age obtained

from granite gneiss intruded into the Einasleigh Metamorphics (1696 ± 2 Ma) also indicates that deposition of the older part of the Etheridge Group, below the Lane Creek Formation, took at least 40 million years (Black *et al*., 1998). The 1707 ± 8 Ma and 1703 ± 14 Ma zircon populations from leucogneiss of the Einasleigh Metamorphics may also provide constraints on the maximum depositional age for at least part of the lower Etheridge Group (Black *et al*., 2005). However, to date no definitive age exists for the onset of deposition across the entire Etheridge Group.

## 4.3 Objectives of the geochronological study

Apart from the studies of Black *et al*. (1998, 2005), little data exists relating to geochronological studies of the mafic and metasedimentary rocks from the lower Etheridge Group. The analysis of metasedimentary rocks has previously concentrated on areas that reached high grades of metamorphism; consequently, lower-grade areas are poorly constrained. Therefore, the key objectives of this geochronological study are:

- To determine the age of emplacement for the Dead Horse Metabasalt and Cobbold Metadolerite members.
- To determine if the magmatism that led to the emplacement of the Dead Horse Metabasalt and Cobbold Metadolerite was synchronous, and short-lived; or if it was related to a number of 'pulses' that were not temporally associated.
- To provide realistic estimates for the maximum and minimum ages of deposition of the lowermost units of the Etheridge Group based on magmatic and detrital zircon ages.
- To compare mafic and detrital zircon populations from the Etheridge Group to those from sections of the Mt Isa Inlier and Broken Hill Block in eastern Australia, to determine if any regional correlation exists, and to support the comparative geochemical study of Chapter 7.
- To determine the age(s) of metamorphic monazite growth, and where possible relate these to significant structural and metamorphic events in the lower Etheridge Group.

Details of the sampling and analytical techniques used and additional information on the samples analysed are provided below. A general overview of the petrology, mineralogy, and stratigraphic position of samples discussed here is given in Chapter 3 and Appendix 1.

## 4.4 Method

### 4.4.1 Sampling

Mafic samples containing zircons were collected from the most fractionated outcrops of both the Dead Horse Metabasalt and Cobbold Metadolerite. These outcrops are commonly found in contact with surrounding metasedimentary units. Metasedimentary samples containing detrital zircons were collected from fine-grained, locally massive sandstone and psammitic layers of the Daniel Creek Formation. Where possible, samples of metasedimentary rock were collected from outcrops near fractionated mafic samples. Samples used for monazite analysis were collected from metasedimentary rocks of the lower Etheridge Group at Gum Flats and Robinhood (Fig. 4.1).

### 4.4.2 Laser ablation ICPMS analysis of zircon

The use of Laser Ablation Inductively-Coupled Plasma Mass-Spectrometry (LA-ICPMS) for the U-Pb dating of zircon has become increasingly popular in recent years due to its availability, low cost, and fast through-put of samples relative to other dating techniques. As such, this technique has been increasingly applied in numerous geochronological studies worldwide (eg. Hirata & Nesbitt, 1995; Horn *et al*., 2000; Berry *et al*., 2001; Li *et al*., 2001; Tiepolo, 2003; Jackson *et al*., 2004).

The LA-ICPMS technique is best suited to projects requiring a large number of analyses or the analysis of large zircons, due to the relatively large beam diameter (30-50 μm) of the laser ablation microprobe. As such, the technique is unsuitable for high-resolution analysis of grains, or the analysis of grains containing complex zoning. Difficulties cited in using the laser ablation technique include the induced fractionation of Pb relative to U during the ablation, transport, and ionisation processes, as well as the difficulty in correcting for common-Pb based on $^{204}$Pb due to isobaric interference from $^{204}$Hg (Jackson *et al*., 2004). Various methods have been

described in order to overcome these issues (eg. Hirata & Nesbitt, 1995; Horn *et al*., 2000; Li *et al*., 2001). However, collecting laser ablation data in time-resolved mode does, at least in part, provide information to recognise these problems where they occur. By using time-resolved analysis of the grains, zones with differing U-Pb ratios can be identified and the data reduced accordingly.

#### 4.4.2.1 Sample preparation

The majority of analysed samples were crushed using a jaw crusher and chrome-steel ring-mill at the University of Tasmania School of Earth Sciences. Individual zircons were then hand picked from panned separates of the appropriate density and mounted in epoxy for analysis. The mounts were polished to expose the zircon grains. Three mafic samples were cut from thin section blocks and prepared as 1-inch round mounts. Limited cathodoluminescence (CL) imaging on several samples was performed on the Cameca SX-100 Electron Micro-Probe (EMP), and the FEI Quanta 600 Scanning Electron Microscope (SEM) at the University of Tasmania Central Science Laboratory. CL imaging was conducted to reveal the internal structures of the zircons for the purpose of interpreting zircon growth and metamorphic histories, as well as choosing appropriate sites for LA-ICPMS analysis on some grains. Back-scattered electron (BSE) imaging was also carried out on the University of Tasmania SEM. This was designed to reveal any structures not apparent in the CL images, as well as to identify included phases and surface features for the purpose of choosing appropriate sites for analysis. Internal structures of zircons revealed using CL imaging were also apparent, though generally less distinct. The Mineral Liberation Analyser (MLA) attached to the SEM at the University of Tasmania was used for rapid, accurate location of zircons in mounts cut from sample blocks. Metamorphic and/or igneous rims identified from the imaging techniques on some individual igneous zircons were too thin for analysis by LA-ICPMS.

#### 4.4.2.2 Laser ablation ICPMS operating parameters

Samples were analysed using the HP 4500Plus ICPMS coupled with a Merchantek 266 nm frequency-quadrupled Nd:YAG Laser Ablation system (LA-ICPMS) at the University of Tasmania School of Earth Sciences. A combination of Ar and He gas

was used to transport the ablated material to the ICPMS for isotopic quantification. Isotopic masses collected using the LA-ICPMS system were $^{96}Zr$, $^{146}Nd$, $^{178}Hf$, $^{202}Hg$, $^{204}Pb$, $^{206}Pb$, $^{207}Pb$, $^{208}Pb$, $^{232}Th$, and $^{238}U$. Zircons were analysed with a 30 µm diameter beam, a laser repetition rate of 5 Hz, and a power setting of 0.2 mJ. The ICPMS was operated in a time-resolved mode, collecting one point per mass per sweep of the mass range with a dwell time of 10 msec/mass. Immediately prior to analysis grains were ablated at 1 Hz for 3-4 sec in order to remove any surface Pb contamination. Each analysis then consisted of a measurement of average background intensities (counts per second) on each mass for 30 sec prior to ablation, followed by 30 sec of ablation (Fig. 4.2). This was followed by an approximate two minute wash-out period during which the signal intensity returned to background level before the next zircon grain was analysed. Sample runs consisted of 12 unknowns bracketed by 6 standard analyses. Zircons from the international standards Temora and 91500 were analysed as unknowns to monitor drift and data quality during the period of the analyses (Black *et al*., 2003; Wiedenbeck *et al*., 2004).

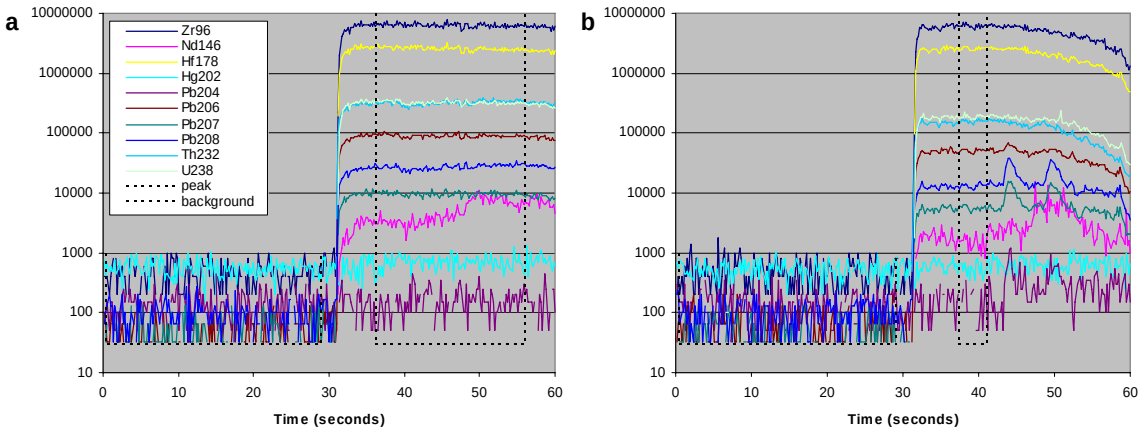


**Figure 4.2: Examples of count rates for element isotopes of single zircon grains analysed by LA-ICP-MS; (a) grain 1, and (b) grain 5, both from Sample 6.**

### 4.4.2.3 Data reduction and presentation

Raw data produced by the ICPMS was collected and reduced using the LAMTRACE program (van Achterbach *et al*., 2001) with the assistance of Dr. Sebastien Meffre. Time-resolved spectra from each analysis were then examined for changes in the ratio of $^{207}Pb/^{206}Pb$, which may indicate zones of Pb-loss or common-Pb. Net count rates for each mass were obtained by subtracting average background count rates from

average signal intensities taken ~30 sec after beginning ablation once the signal had stabilised (Fig. 4.2). Homogeneous standard grains with low common-Pb produced near-steady signals with no resolvable change in the signal intensities of measured isotopic masses (e.g. Fig. 4.2a).

Analysed isotopic masses were used to obtain the isotopic ratios $^{207}Pb/^{206}Pb$, $^{206}Pb/^{238}U$, $^{207}Pb/^{235}U$, and $^{208}Pb/^{232}Th$. The $^{207}Pb/^{206}Pb$ ratio was used for the majority of age estimates, with the remaining three isotopic ratios used to estimate discordance and identify grains containing high common-Pb. Subsequently, individual grains containing zones with widely differing U-Pb isotopic ratios illustrated in their time-resolved spectra were discarded before calculating sample weighted mean ages. This was done to limit the presence of common-Pb affected grains in weighted mean age calculations, as the presence of common-Pb can significantly raise the $^{207}Pb/^{206}Pb$ and $^{208}Pb/^{232}Th$ ages of a sample, in addition to greatly increasing a sample's $^{208}Pb/^{232}Th$ age relative to its $^{206}Pb/^{238}U$ age (Griffin *et al*., 2006). The $^{207}Pb/^{206}Pb$ ratio is used to represent the age of individual grains, as it is the least susceptible to common-Pb contamination and laser induced fractionation of the U-Pb isotopic system, and has been successfully used to represent U-Pb zircon ages in numerous other studies of eastern Australian Proterozoic terranes (e.g. Page & Sun, 1998; Page *et al*., 2005a; Griffin *et al*., 2006).

Sample ages were calculated from populations of $^{204}Pb$-corrected analyses. In many samples the MSWD (Mean Square of Weighted Deviates) was sufficiently high, and the probability of equivalence was sufficiently low that simple weighted mean ages were unrepresentative of the crystallisation age. High MSWD and low probabilities of equivalence may suggest the data represent the amalgamation of zircons from more than one age population. Therefore, to calculate a more realistic weighted mean age, analyses with high common-Pb, and analyses with $^{207}Pb/^{206}Pb$ ages significantly different from the sample mean were excluded until the remaining data were within analytical uncertainty of one another.

In addition to common-Pb, zircons in a number of igneous samples experienced appreciable Pb-loss, recognisable by the skewing of analyses towards younger ages in the U-Pb concordia diagrams (Ireland *et al*., 1998). Consequently, analysis of zircons that have been affected by Pb-loss will return values that represent the minimum age of their growth. As zircon is an effectively closed system below 900 °C, Pb-loss will

generally only occur as a result of radiation damage, intense metamorphism, alteration, or hydrothermal fluid activity (Mezger & Krogstad, 1997). Although no distinct measurable overgrowths were observed in this study, cumulative probability diagrams in some samples show small groupings of grains with ages below ca. 1600 Ma, possibly relating to periods of regional metamorphism and/or late stage alteration.

Ablation- and transport-related elemental fractionation of U relative to Pb was encountered during the analysis of individual grains. Therefore corrections were made by matching peak and background signal intensities between sample and standard analyses with identical time intervals. A calibration standard (NIST-612) was also used to correct for elemental fractionation, as well as the mass bias between the U-Pb and U-Th isotopic systems.

In addition to the calculated weighted mean age method outlined above, age populations and provenance were also determined using cumulative probability diagrams, as they illustrate a spectrum of zircon-forming events which have affected a sample population. The diagrams used in this study were constructed with *Isoplot* version 3.0 (Ludwig, 2003). For this study, the cumulative probability diagrams were primarily used to ascertain provenance ages from detrital zircons in metasedimentary samples. Probability diagrams are also presented for samples of igneous rocks, in order to show that the data are either normally distributed, or that in some cases the samples contain inherited zircons from earlier events. For populations of detrital zircons, peaks on the probability diagrams approximate the time of zircon-forming events. Therefore, approximate ages were taken from discrete peaks, rounded to the nearest 10 Ma, and quoted as ca. ages. As probability diagrams do not allow an exact age determination or the estimation of error, ages within 2σ (up to 30 Ma) of the ca. age were considered to belong to the zircon-forming event. In addition to these limitations, Raetz *et al*. (2002) also cautioned against interpretation of subtle 'shoulders' occurring on peaks in probability diagrams. These 'shoulders' are associated with either the overlapping of normally distributed populations producing artificial distributions, or may represent younger Pb-loss.

The $^{207}Pb/^{206}Pb$ and $^{238}U/^{206}Pb$ ratios for individual analyses are listed in Tables 4.1, 4.2, and 4.4. The remaining isotopic ratios are listed in Appendix 2. Individual zircon analyses for each sample are illustrated in inverse-concordia (Tera & Wasserburg, 1972) diagrams constructed using *Isoplot* version 3.0 (Ludwig, 2003).

| Label | U (ppm) | Th/U | $^{238}U/^{206}Pb$ | ± 1 σ | $^{207}Pb/^{206}Pb$ | ± 1 σ | $^{207}Pb/^{206}Pb$ Age (Ma) | ± 1 σ | Label | U (ppm) | Th/U | $^{238}U/^{206}Pb$ | ± 1 σ | $^{207}Pb/^{206}Pb$ | ± 1 σ | $^{207}Pb/^{206}Pb$ Age (Ma) | ± 1 σ |
|---|---|---|---|---|---|---|---|---|---|---|---|---|---|---|---|---|---|
| Sample: 6 (North Ortona) | | | | | | | | | Sample: 161 (South Ortona) | | | | | | | | |
| 1 | 1380 | 0.55 | 3.43854 | 0.02169 | 0.10082 | 0.00139 | 1639 | 26 | 1 | 928 | 1.31 | 3.31022 | 0.02297 | 0.10428 | 0.00243 | 1702 | 43 |
| 2 | 786 | 0.45 | 3.32941 | 0.02348 | 0.10133 | 0.00171 | 1649 | 31 | 2 | 975 | 1.21 | 3.39684 | 0.01872 | 0.10514 | 0.00260 | 1717 | 45 |
| 3 | 592 | 0.45 | 3.51061 | 0.02082 | 0.10091 | 0.00149 | 1641 | 27 | 3 | 1178 | 1.39 | 3.27110 | 0.02101 | 0.10473 | 0.00251 | 1710 | 44 |
| 5 | 763 | 0.50 | 3.43964 | 0.04360 | 0.10501 | 0.00363 | 1714 | 64 | 4 | 721 | 0.81 | 3.15846 | 0.02300 | 0.11359 | 0.00309 | 1858 | 49 |
| 6 | 1160 | 0.51 | 3.49649 | 0.02286 | 0.09939 | 0.00145 | 1613 | 27 | 5 | 728 | 0.85 | 3.38442 | 0.06632 | 0.10659 | 0.00614 | 1742 | 106 |
| 9 | 393 | 0.39 | 3.52829 | 0.03040 | 0.10455 | 0.00235 | 1706 | 41 | 6 | 867 | 1.11 | 3.36499 | 0.04053 | 0.11082 | 0.00545 | 1813 | 89 |
| 11 | 1242 | 0.52 | 3.38635 | 0.02229 | 0.10061 | 0.00154 | 1635 | 28 | 7 | 691 | 0.99 | 3.37809 | 0.02424 | 0.10608 | 0.00293 | 1733 | 51 |
| 12 | 1440 | 0.59 | 3.47525 | 0.05986 | 0.10227 | 0.00243 | 1666 | 44 | 8 | 934 | 1.10 | 3.38314 | 0.02499 | 0.10231 | 0.00298 | 1666 | 54 |
| | | | | | | | | | 10 | 832 | 0.96 | 3.37840 | 0.02458 | 0.10147 | 0.00259 | 1651 | 47 |
| Sample: 8 (North Ortona) | | | | | | | | | 11 | 594 | 0.99 | 3.19677 | 0.03367 | 0.10409 | 0.00311 | 1698 | 55 |
| 1 | 907 | 0.52 | 3.50303 | 0.06825 | 0.09979 | 0.00316 | 1620 | 59 | 12 | 688 | 0.85 | 3.21242 | 0.07736 | 0.12024 | 0.00655 | 1960 | 97 |
| 2 | 1216 | 0.46 | 3.47197 | 0.05489 | 0.10138 | 0.00334 | 1650 | 61 | 13 | 1071 | 1.09 | 3.30011 | 0.04005 | 0.10629 | 0.00244 | 1729 | 86 |
| 3 | 1615 | 0.52 | 3.47089 | 0.02976 | 0.10143 | 0.00139 | 1650 | 25 | 14 | 532 | 0.82 | 3.35719 | 0.05300 | 0.10990 | 0.00325 | 1620 | 157 |
| 4 | 1485 | 0.64 | 3.52365 | 0.03277 | 0.10060 | 0.00142 | 1635 | 26 | 18 | 944 | 0.98 | 3.30281 | 0.06093 | 0.10638 | 0.00330 | 1788 | 102 |
| 5 | 321 | 0.28 | 3.46139 | 0.04239 | 0.09860 | 0.00228 | 1598 | 43 | 19 | 516 | 0.98 | 3.21390 | 0.06801 | 0.12985 | 0.00484 | 1923 | 189 |
| 9 | 1308 | 0.52 | 3.47374 | 0.03050 | 0.09993 | 0.00136 | 1623 | 25 | 21 | 1396 | 1.27 | 3.38298 | 0.02559 | 0.10300 | 0.00167 | 1691 | 73 |
| 10 | 1233 | 0.51 | 3.51337 | 0.03502 | 0.10076 | 0.00150 | 1638 | 28 | 23 | 1120 | 1.08 | 3.32767 | 0.02990 | 0.10825 | 0.00252 | 1640 | 83 |
| 12 | 1312 | 0.50 | 3.43505 | 0.03080 | 0.10163 | 0.00147 | 1654 | 27 | 24 | 1509 | 1.19 | 3.32550 | 0.04315 | 0.12232 | 0.00383 | 1726 | 86 |
| | | | | | | | | | 25 | 798 | 1.18 | 3.28632 | 0.02875 | 0.13978 | 0.00292 | 1622 | 136 |
| Sample: 159 (South Ortona) | | | | | | | | | 26 | 1164 | 1.03 | 3.42314 | 0.03399 | 0.11085 | 0.00280 | 1723 | 84 |
| 2 | 763 | 1.09 | 3.21678 | 0.08550 | 0.10239 | 0.00335 | 1668 | 60 | 27 | 823 | 1.34 | 3.22662 | 0.06095 | 0.11783 | 0.00401 | 1740 | 185 |
| 3 | 1353 | 1.40 | 3.47188 | 0.06250 | 0.10668 | 0.00304 | 1743 | 52 | 28 | 1003 | 1.10 | 3.37757 | 0.03255 | 0.10356 | 0.00250 | 1534 | 101 |
| 4 | 956 | 1.05 | 3.14738 | 0.11802 | 0.10480 | 0.00490 | 1711 | 86 | 29 | 931 | 1.02 | 3.33597 | 0.02634 | 0.10990 | 0.00225 | 1685 | 91 |
| 6 | 1102 | 0.74 | 3.30541 | 0.09539 | 0.10426 | 0.00338 | 1701 | 60 | 30 | 972 | 1.08 | 3.29344 | 0.04555 | 0.10810 | 0.00290 | 1707 | 91 |
| 9 | 791 | 0.99 | 3.29305 | 0.07296 | 0.10374 | 0.00313 | 1692 | 56 | | | | | | | | | |
| 10 | 852 | 0.85 | 3.39516 | 0.06513 | 0.10679 | 0.00307 | 1745 | 53 | Sample: 172 (South Ortona)† | | | | | | | | |
| 11 | 624 | 0.85 | 3.35760 | 0.06367 | 0.10596 | 0.00328 | 1731 | 57 | 1 | 885 | 1.00 | 3.45526 | 0.02272 | 0.10360 | 0.00270 | 1633 | 12 |
| 14 | 907 | 1.04 | 3.08833 | 0.02553 | 0.10709 | 0.00178 | 1675 | 63 | 3 | 729 | 0.75 | 3.58031 | 0.02525 | 0.10338 | 0.00271 | 1578 | 12 |
| 15 | 1168 | 0.92 | 3.50227 | 0.03919 | 0.10591 | 0.00194 | 1716 | 90 | 4 | 1035 | 1.17 | 3.67439 | 0.03857 | 0.10435 | 0.00365 | 1537 | 17 |
| 16 | 1017 | 1.04 | 3.29107 | 0.02902 | 0.10149 | 0.00166 | 1695 | 65 | 5 | 610 | 0.77 | 3.34659 | 0.03465 | 0.12465 | 0.00344 | 1643 | 18 |
| 18 | 433 | 0.74 | 3.14006 | 0.02897 | 0.10658 | 0.00228 | 1673 | 134 | 6 | 326 | 0.82 | 3.45754 | 0.04375 | 0.11125 | 0.00578 | 1617 | 23 |
| 19 | 1290 | 0.78 | 3.39091 | 0.02620 | 0.10706 | 0.00188 | 1766 | 52 | 7 | 341 | 0.95 | 3.43572 | 0.04298 | 0.11080 | 0.00457 | 1628 | 22 |
| 20 | 1125 | 0.67 | 3.54371 | 0.04584 | 0.10108 | 0.00223 | 1683 | 88 | 8 | 369 | 0.99 | 3.41198 | 0.03521 | 0.11793 | 0.00370 | 1625 | 18 |
| 22 | 1933 | 1.61 | 3.40948 | 0.02426 | 0.10291 | 0.00144 | 1705 | 42 | 9 | 869 | 1.15 | 3.60062 | 0.03756 | 0.11336 | 0.00447 | 1551 | 18 |

† $^{207}Pb$ corrected $^{206}Pb/^{238}U$ age used

**Table 4.1: $^{204}$Pb-corrected U-Pb isotope data for zircons from mafic samples analysed by LA-ICP-MS.**

| Label | U (ppm) | Th/U | $^{238}U/^{206}Pb$ | ± 1 σ | $^{207}Pb/^{206}Pb$ | ± 1 σ | $^{207}Pb/^{206}Pb$ Age (Ma) | ± 1 σ |
|---|---|---|---|---|---|---|---|---|
| Sample 172 cont. | | | | | | | | |
| 10 | 871 | 1.17 | 3.38377 | 0.08569 | 0.14061 | 0.00782 | 1594 | 42 |
| 12 | 789 | 0.94 | 3.44792 | 0.02810 | 0.11088 | 0.00323 | 1623 | 14 |
| Sample: 264 (Robinhood) | | | | | | | | |
| 1 | 543 | 0.69 | 3.49765 | 0.02636 | 0.11173 | 0.00221 | 1828 | 36 |
| 2 | 689 | 0.81 | 3.59838 | 0.03115 | 0.11066 | 0.00291 | 1810 | 48 |
| 3 | 1001 | 1.06 | 3.72763 | 0.03729 | 0.10240 | 0.00267 | 1668 | 48 |
| 4 | 942 | 0.68 | 3.82156 | 0.04405 | 0.09782 | 0.00251 | 1583 | 48 |
| 5 | 576 | 1.06 | 3.66790 | 0.04348 | 0.10765 | 0.00330 | 1760 | 56 |
| 6 | 1076 | 0.88 | 3.49178 | 0.03690 | 0.10345 | 0.00206 | 1687 | 37 |
| 7 | 1336 | 0.50 | 3.32458 | 0.03832 | 0.10005 | 0.00206 | 1625 | 38 |
| 8 | 309 | 0.57 | 3.23130 | 0.04903 | 0.10460 | 0.00333 | 1707 | 59 |
| 9 | 80 | 1.01 | 2.42525 | 0.03838 | 0.14085 | 0.00475 | 2238 | 58 |
| 12 | 281 | 0.52 | 2.17207 | 0.04862 | 0.16538 | 0.00460 | 2511 | 47 |
| 13† | 567 | 0.55 | 3.51020 | 0.07069 | 0.10114 | 0.00405 | 1645 | 74 |
| 14† | 425 | 0.39 | 3.55985 | 0.05578 | 0.10350 | 0.00403 | 1688 | 72 |
| 15† | 1033 | 0.61 | 3.46529 | 0.07569 | 0.10424 | 0.00395 | 1701 | 70 |
| 16† | 310 | 1.03 | 3.61637 | 0.05296 | 0.09761 | 0.00319 | 1579 | 61 |
| 17† | 471 | 0.46 | 3.34630 | 0.03188 | 0.11583 | 0.00262 | 1662 | 16 |
| 18† | 525 | 0.27 | 2.16517 | 0.02274 | 0.18229 | 0.00319 | 2373 | 29 |
| 19† | 183 | 0.48 | 2.00459 | 0.02064 | 0.18315 | 0.00351 | 2580 | 33 |
| 20† | 622 | 0.73 | 3.41448 | 0.05158 | 0.11755 | 0.00321 | 1627 | 25 |
| 21† | 522 | 0.55 | 3.29980 | 0.05100 | 0.11479 | 0.00426 | 1687 | 27 |
| 22† | 545 | 0.85 | 3.51859 | 0.03058 | 0.11706 | 0.00260 | 1581 | 14 |
| 23† | 887 | 0.83 | 3.46150 | 0.07221 | 0.11078 | 0.00421 | 1618 | 34 |
| 24† | 270 | 1.70 | 2.86727 | 0.02780 | 0.12284 | 0.00262 | 1918 | 19 |
| 25† | 577 | 0.52 | 3.34983 | 0.06589 | 0.11108 | 0.00427 | 1669 | 33 |
| 27† | 827 | 0.39 | 3.41125 | 0.04256 | 0.10635 | 0.00296 | 1649 | 21 |
| 28† | 1067 | 0.90 | 3.44777 | 0.04220 | 0.11547 | 0.00306 | 1615 | 20 |
| 29† | 603 | 0.82 | 3.29492 | 0.03473 | 0.11183 | 0.00249 | 1695 | 18 |
| 30† | 759 | 0.42 | 3.47160 | 0.04808 | 0.10679 | 0.00332 | 1620 | 23 |
| 31† | 280 | 0.43 | 2.08527 | 0.02060 | 0.17394 | 0.00312 | 2500 | 29 |
| 32† | 743 | 0.78 | 3.46577 | 0.03628 | 0.10436 | 0.00202 | 1627 | 17 |
| 33† | 943 | 0.94 | 3.46982 | 0.04491 | 0.10855 | 0.00203 | 1618 | 21 |
| Sample 264 cont. | | | | | | | | |
| 34† | 1011 | 0.33 | 3.34757 | 0.03030 | 0.10607 | 0.00207 | 1680 | 15 |
| 35† | 231 | 1.66 | 2.91730 | 0.03002 | 0.12089 | 0.00277 | 1890 | 20 |
| Sample: 299 (Gum Flats)† | | | | | | | | |
| 1 | 243 | 0.51 | 3.17749 | 0.12306 | 0.10572 | 0.01235 | 1768 | 71 |
| 2 | 281 | 0.52 | 3.15655 | 0.18044 | 0.10157 | 0.01655 | 1787 | 105 |
| 3 | 326 | 0.69 | 3.15224 | 0.12472 | 0.10861 | 0.01093 | 1776 | 72 |
| 4 | 305 | 0.56 | 3.41636 | 0.15077 | 0.10489 | 0.01159 | 1649 | 73 |
| 5 | 258 | 0.72 | 3.39601 | 0.08148 | 0.10222 | 0.00685 | 1664 | 41 |
| 6 | 368 | 0.65 | 3.38777 | 0.09773 | 0.10950 | 0.00895 | 1655 | 49 |
| 9 | 180 | 0.31 | 3.47504 | 0.14300 | 0.11721 | 0.01339 | 1601 | 68 |
| 10 | 132 | 0.50 | 3.16112 | 0.13732 | 0.09654 | 0.01296 | 1795 | 80 |
| 12 | 656 | 0.94 | 3.37208 | 0.08156 | 0.10219 | 0.00659 | 1675 | 41 |
| Sample: 300 (Gum Flats)† | | | | | | | | |
| 1 | 189 | 0.51 | 3.38082 | 0.10398 | 0.10027 | 0.00895 | 1675 | 53 |
| 2 | 340 | 0.48 | 3.32990 | 0.08824 | 0.10536 | 0.00789 | 1690 | 46 |
| 3 | 439 | 0.81 | 3.53499 | 0.08974 | 0.10434 | 0.00755 | 1596 | 41 |
| 6 | 233 | 0.58 | 3.43074 | 0.09496 | 0.10457 | 0.00892 | 1643 | 47 |
| 7 | 164 | 0.51 | 3.49340 | 0.12892 | 0.10862 | 0.01188 | 1607 | 61 |
| 8 | 262 | 0.47 | 3.27915 | 0.09905 | 0.09746 | 0.00780 | 1731 | 53 |
| 9 | 488 | 0.72 | 3.36752 | 0.08096 | 0.10868 | 0.00732 | 1665 | 41 |
| 10 | 484 | 0.66 | 3.31547 | 0.08072 | 0.09845 | 0.00694 | 1710 | 43 |
| 11 | 759 | 0.88 | 3.55586 | 0.25926 | 0.11906 | 0.02137 | 1561 | 116 |
| Sample: 318 (Gum Flats)† | | | | | | | | |
| 2 | 984 | 0.52 | 3.15251 | 0.10253 | 0.09801 | 0.00738 | 1797 | 59 |
| 3 | 782 | 0.14 | 3.32110 | 0.17171 | 0.09596 | 0.01434 | 1712 | 90 |
| 5 | 1103 | 0.06 | 3.52616 | 0.14308 | 0.10262 | 0.01090 | 1604 | 66 |
| 6 | 995 | 0.03 | 3.47630 | 0.12181 | 0.09701 | 0.00865 | 1636 | 57 |
| 9 | 1453 | 0.00 | 3.60127 | 0.15747 | 0.09618 | 0.01198 | 1582 | 70 |
| 11 | 1296 | 0.00 | 3.47211 | 0.09984 | 0.09771 | 0.00894 | 1636 | 48 |
| 12 | 770 | 0.86 | 3.43003 | 0.18420 | 0.10515 | 0.01576 | 1643 | 90 |

† $^{207}Pb$ corrected $^{206}Pb/^{238}U$ age used

**Table 4.1 cont.**

| Label | U (ppm) | Th/U | $^{238}U/^{206}Pb$ | ± 1 σ | $^{207}Pb/^{206}Pb$ | ± 1 σ | $^{207}Pb/^{206}Pb$ Age (Ma) | ± 1 σ |
|---|---|---|---|---|---|---|---|---|
| Sample: 135 (Mount Hogan Granite) | | | | | | | | |
| 1 | 121 | 0.60 | 3.24252 | 0.07732 | 0.10131 | 0.00390 | 1648 | 71 |
| 3 | 594 | 0.92 | 3.92466 | 0.10001 | 0.10208 | 0.00372 | 1662 | 67 |
| 6 | 451 | 0.51 | 3.84811 | 0.15532 | 0.09760 | 0.00490 | 1579 | 94 |
| 7 | 584 | 0.68 | 3.61199 | 0.06022 | 0.09428 | 0.00233 | 1514 | 47 |
| 8 | 849 | 1.29 | 3.95138 | 0.23402 | 0.10420 | 0.00608 | 1700 | 107 |
| 9 | 1575 | 0.04 | 3.53854 | 0.06760 | 0.09531 | 0.00244 | 1534 | 48 |
| 11 | 429 | 1.40 | 3.85101 | 0.04808 | 0.09650 | 0.00252 | 1557 | 49 |
| Sample: 208 (Ropewalk Granite) | | | | | | | | |
| 1 | 513 | 0.35 | 3.52801 | 0.02143 | 0.09619 | 0.00188 | 1552 | 37 |
| 3 | 331 | 0.36 | 3.58848 | 0.02533 | 0.09729 | 0.00186 | 1573 | 36 |
| 5 | 550 | 0.45 | 3.57387 | 0.02195 | 0.09829 | 0.00202 | 1592 | 38 |
| 7 | 693 | 0.40 | 3.73633 | 0.04530 | 0.09579 | 0.00405 | 1544 | 80 |
| 11 | 469 | 0.46 | 3.57227 | 0.02370 | 0.09503 | 0.00206 | 1529 | 41 |
| 12 | 218 | 0.74 | 3.59033 | 0.03718 | 0.09498 | 0.00267 | 1528 | 53 |
| Sample: 209 (Ropewalk Granite) | | | | | | | | |
| 2 | 796 | 0.90 | 3.72600 | 0.02379 | 0.09557 | 0.00179 | 1539 | 35 |
| 3 | 431 | 1.12 | 3.59818 | 0.02415 | 0.09401 | 0.00189 | 1508 | 38 |
| 4 | 717 | 1.22 | 3.79178 | 0.02233 | 0.09362 | 0.00179 | 1501 | 36 |
| 5 | 721 | 1.17 | 3.70523 | 0.02290 | 0.09475 | 0.00171 | 1523 | 34 |
| 6 | 1509 | 1.70 | 3.74483 | 0.02015 | 0.09446 | 0.00147 | 1517 | 29 |
| 8 | 265 | 0.89 | 3.72748 | 0.03162 | 0.09407 | 0.00235 | 1510 | 47 |
| 10 | 1063 | 1.51 | 3.65562 | 0.03688 | 0.09632 | 0.00291 | 1554 | 57 |
| 11 | 351 | 1.53 | 3.80165 | 0.05440 | 0.09717 | 0.00454 | 1571 | 88 |
| 12 | 399 | 1.02 | 3.73943 | 0.06756 | 0.09945 | 0.00436 | 1614 | 82 |
| Sample: 210 (Ropewalk Granite) | | | | | | | | |
| 1 | 644 | 0.97 | 3.57072 | 0.03651 | 0.09872 | 0.00263 | 1600 | 50 |
| 2 | 260 | 0.70 | 3.63488 | 0.03318 | 0.09372 | 0.00234 | 1502 | 47 |
| 3 | 275 | 1.15 | 3.49572 | 0.02400 | 0.10100 | 0.00229 | 1643 | 42 |
| 4 | 390 | 0.67 | 3.60791 | 0.03002 | 0.09325 | 0.00204 | 1493 | 41 |
| 5 | 285 | 2.12 | 3.72676 | 0.03045 | 0.09421 | 0.00241 | 1512 | 48 |
| 6 | 309 | 0.46 | 3.54898 | 0.02856 | 0.09396 | 0.00232 | 1507 | 47 |
| 7 | 489 | 0.20 | 3.77140 | 0.02887 | 0.09337 | 0.00212 | 1495 | 43 |
| 8 | 531 | 0.79 | 3.74129 | 0.04016 | 0.09911 | 0.00228 | 1607 | 43 |
| 9 | 530 | 0.80 | 3.61350 | 0.02486 | 0.09631 | 0.00209 | 1554 | 41 |
| 10 | 314 | 2.14 | 3.68651 | 0.03227 | 0.09689 | 0.00257 | 1565 | 50 |
| 11 | 531 | 0.76 | 3.72087 | 0.03112 | 0.09479 | 0.00215 | 1524 | 43 |
| 12 | 195 | 1.04 | 3.68916 | 0.03940 | 0.09383 | 0.00271 | 1505 | 55 |

**Table 4.2: $^{204}$Pb-corrected U-Pb isotope data for zircons from granitic samples analysed by LA-ICPMS.**

### 4.4.2.4 Source of Pb-loss and common-Pb in igneous zircons

The presence of significant radiogenic Pb-loss coupled with possible low-T Pb-loss due to alteration or chemical weathering, have contributed to the partial resetting of isotopic compositions in some analyses. This has resulted in the scattering of individual isotopic ages within most igneous samples, and large errors for some individual analyses (Table 4.1). Radiogenic Pb-loss was most likely caused by a combination of radiation damage to the crystal lattice, and to a lesser extent partial

recrystallisation due to metamorphism. Pb-loss due to radiation damage of the zircon crystal lattice (metamictization) is caused by the α-decay of $^{238}U$ and fission products (Woodhead *et al*., 1991; Mezger & Krogstad, 1997). Significantly, the likelihood of radiation damage to the crystal lattice will increase with age, U-concentration, and the length of time below the zircons annealing temperature of about 600-650 °C (Mezger & Krogstad, 1997). Recrystallisation associated with post-depositional orogenesis may have also affected the crystal structure of the igneous zircons (Hoskin & Black, 2000). However, due to the low grade of metamorphism in the study area, metamorphic recrystallisation was unlikely to have been the factor controlling radiogenic Pb-loss in these samples. Regardless of the cause, zircons containing appreciable Pb-loss appear discordant on inverse-concordia diagrams, and will provide an erroneously young age. Consequently, individual isotopic analyses that showed >10% discordance were omitted from the calculated ages, and are not shown here. A full list of analyses, including those analyses considered too discordant for use, is given in Appendix 2.

Common-Pb appears to be a significant problem affecting the igneous zircons collected for this study, and it is unclear whether the problem is caused totally by inheritance and inclusions in individual zircon grains, or by an analytical issue related to Pb being retained in the analytical system between analyses. In the former case, inclusions within small zircon grains similar to those analysed in this study are difficult to avoid using the laser ablation method, as the laser ablates though a significant part of the zircon. However, areas containing inclusions of common-Pb can be avoided during data reduction, as areas free of contamination can be preferentially selected using time-resolved spectra.

The problem of common-Pb is harder to deal with when the contamination comes from within the analytical system itself. This problem was encountered during the second analytical run and required correction that impacted on the accuracy of the calculated ages, resulting in the use of $^{206}Pb/^{238}U$ ages instead of preferred $^{207}Pb/^{206}Pb$ ages (S. Meffre, pers. comm., 2005). As a result, samples analysed over the course of two sessions incorporated these errors into the weighted mean age calculations, resulting in the overcompensation of analytical errors for some crystallisation ages (indicated by MSWD values much less than unity). As I was unable to further correct for this problem, the errors are incorporated into the calculated ages of this study.

However, meaningful results, albeit with slightly greater error bars, were still obtained via careful attention to each spectra for analysed zircon.

### 4.4.3 EMPA analysis of monazite

As monazite occurs as an accessory phase in many igneous and metamorphic rocks, and contains high amounts of Th and U coupled with low common-Pb, it has become a useful mineral for U-Th-Pb geochronology. Numerous studies over the past decade have used electron microprobe U-Th-Pb dating of monazite as a substitute for techniques such as LA-ICPMS and SHRIMP, as it does not involve the separation of grains from their host rock, and thus can provide ages with some textural context (e.g. Montel *et al*., 1996, 2000; Cocherie *et al*., 1998; Williams *et al*., 1999; Shaw *et al*., 2001; Williams & Jercinovic, 2002; Kelsey *et al*., 2003; Dahl *et al*., 2005; Berry *et al*., 2005).

One of the key benefits of the EMPA technique for dating monazites is that the relatively small beam size used (commonly 1-3 μm) allows numerous spot analyses to be done on individual monazite grains of less than 10-20 μm in size, a population not typically sampled by other techniques. This technique also allows for the analysis of thin sections containing relatively few monazite grains (generally four or greater). By combining EMPA monazite-dated grains with back-scattered electron (BSE) images of the surrounding metamorphic fabric, ages can then be tied to specific structural events and/or mineral assemblages, making this an important tool for deciphering the metamorphic and structural history of igneous and metamorphic terranes.

#### 4.4.3.1 Sample preparation

Spot analyses were obtained from monazite grains in thin section, from metasedimentary schists of the lower Etheridge Group that were collected from areas that had experienced amphibolite facies metamorphism (Fig. 4.1). Samples were prepared as polished thin sections before being coated with graphite. Individual monazite grains were identified and their positions recorded for automated runs by BSE imaging using the FEI Quanta 600 SEM housed at the University of Tasmania Central Science Laboratory. BSE images of the areas immediately surrounding

monazite grains were collected for three samples, in order to relate individual monazites ages to particular structural fabrics in each of the samples.

#### 4.4.3.2 Electron microprobe operating parameters

Samples were analysed using the Cameca SX-100 EMP at the University of Tasmania Central Science Laboratory under the supervision of Mr. David Steele and Dr. Karsten Gömann. Five wavelength dispersive spectrometers were used for each analysis, with a configuration involving one PET, one Large-LIF, one TAP, and two Large-PET crystals. Values for Si, Al, K, Fe, Ca, Y, Th, U, Pb, P and 11 rare earth elements (REEs) were measured on each spot to help facilitate matrix corrections using the PAP method (Pouchou & Pichoir, 1984). Standard operating procedure for the analysis of monazite grains involved an accelerating voltage of 20 kV, 2-3 μm beam diameter, and a 100 nA beam current. Total counting times of 180 s (Pb), 40 s (Th) and 150 s (U) were used. X-ray lines on the EMP were calibrated using standard synthetic oxides, glasses and minerals. In particular, Huttonite (71.59 % Th), $UO_2$ (88.15 % U), and K227 Pb-glass (73.99 % Pb) were used for Th, U and Pb respectively. The EMP calibration was regularly checked using the monazite standard RGL04B (1563 ± 3 Ma; Rubatto *et al*., 2001). Analyses were obtained over the course of two sessions in automated runs. Automation and data collection was performed using software supplied by Cameca.

#### 4.4.3.3 Data reduction and presentation

Age calculations based on measured U, Th and Pb concentrations (ppm) are used to iteratively solve the age equation of Suzuki *et al*. (1991), assuming that there is no uncertainty on the decay constants:

$$0 = \left[a\,Th\left(e^{\lambda\,232Th\,t}-1\right)+b\,U\left(e^{\lambda\,238U\,t}-1\right)+c\,U\left(e^{\lambda\,235U\,t}-1\right)-Pb\right]^2 \qquad (4.1)$$

where the values a, b, and c are 'molecular constants' with $a$ = 208/232, $b$ = (0.9928 x 206)/238.04, and $c$ = (0.0072 x 207)/238.04, $\lambda^x$ are decay constants of $^{232}$Th, $^{238}$U and $^{235}$U, $t$ = the age of the sample in Ma, and Th, U, Pb are the measured concentrations in ppm. By applying equation 4.1 to each analysis, an age can be obtained for each

spot analysed. Minimum age uncertainties were calculated for each analysed spot, derived by the propagation of X-ray counting errors through the age equation, with analytical uncertainties (1σ) being taken as equal to the square root of the peak plus background counts. Individual analyses showing signs of chemical contamination (e.g. K > 0.02 wt%, P > 13.0 wt%, total wt% < 97.0) were omitted from age calculations. Individual spot analyses are listed in Table 4.5, with errors quoted at the 1σ level. Errors in sample weighted mean age calculations are quoted as 95% confidence limits (Table 4.6). Weighted mean ages and cumulative probability diagrams were calculated using *Isoplot* version 3.0 (Ludwig, 2003). Discrete age populations within samples were identified using a similar method to that used for detrital zircon populations (Section 4.4.2.3). Monazite analyses with similar calculated ages were first identified using the cumulative probability diagrams in Figure 4.15. Approximate ages were taken from discrete peaks, and analyses lying within the range of each peak were then selected for weighted mean age calculations. In determining the weighted mean age, the youngest and/or oldest analysis in each group was omitted until the calculated age was statistically acceptable. As a result, more than one acceptable weighted mean age was calculated for some samples, which may reflect the presence of a number of discrete thermal events within the Etheridge Group.

## 4.5 LA-ICPMS U-Pb zircon dating results

Complete individual isotopic analyses for zircons from each sample are listed in Appendix 2, and are summarised in Tables 4.1, 4.2, and 4.4. A summary of the weighted mean ages calculated from each mafic and felsic sample are listed in Table 4.3. An initial 'test run' analysis on CMD samples 6 and 8 appears to indicate a relatively simple age population for the mafic rocks. However, the combined affects of common-Pb and Pb-loss appeared to have had a variable response on the zircons and their calculated ages. Subsequent analyses were then used to confirm initial ages and determine whether a more complex age distribution exists, as well as to determine the pattern of detrital zircon ages in the surrounding metasedimentary package, and to test the accuracy of the LA-ICPMS method on samples of various Palaeoproterozoic granitoids in the Etheridge Group against established ages.

U-Pb isotopic analyses were conducted on zircons from a total of 9 mafic, 4 granitic, and 2 metasedimentary samples, from numerous locations within the lower-grade area of the Etheridge Group (Fig. 4.1). Weighted mean ages and associated errors for individual samples of the mafic rocks are relatively large compared to other established dating methods due to the small number of zircons obtained from each mafic sample, coupled with the significant open-system processes that affected the chemical composition of many grains. Errors in weighted mean age calculations are quoted as 95 % confidence limits, although analytical errors for individual analyses in data tables and in the Tera-Wasserburg concordia diagrams (Tera & Wasserburg, 1972) are at the 1σ level.

### 4.5.1 Mafic rocks

#### 4.5.1.1 Sample 6 (CMD – North Ortona)

Zircons from this sample were collected from a late-stage felsic differentiate of a metadolerite sill near Ortona station, and are all of igneous origin. The zircons are moderately uniform in size and elongation, averaging ~130 x 60 μm. Most grains are euhedral, and generally characterised by first-order prismatic faces. Terminations are either sharp on grain edges and broken surfaces, or are only very slightly rounded. Individual grains are morphologically simple, consisting of only a primary igneous growth phase, and are either poorly or strongly luminescent in CL images. The relatively low metamorphic grade (greenschist facies) has precluded the growth of metamorphic rims.

Only 12 zircon grains were recovered from this sample. Of these, eight were essentially free of common-Pb and Pb-loss. These grains have a $^{204}$Pb-corrected $^{207}$Pb/$^{206}$Pb weighted mean age of 1645 ± 22 Ma, free of significant scatter (MSWD = 0.75, probability of equivalence = 0.63; Fig. 4.3). This age is most likely associated with crystallisation of the late-stage felsic differentiate, and represents the emplacement age for the metadolerite sill.

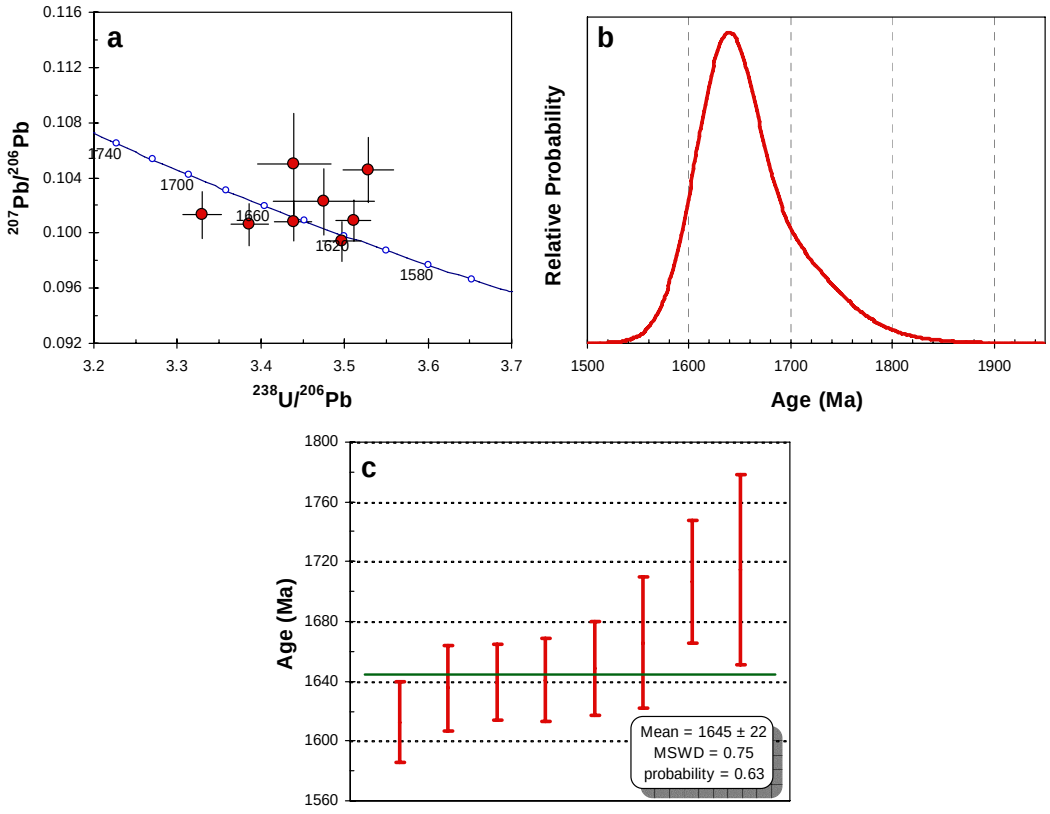


**Figure 4.3: (a) Tera-Wasserburg U-Pb concordia plot, (b) cumulative probability plot, and (c) weighted average plot for zircon analyses from sample 6. Data points in (a) represent analyses used in the determination of weighted mean ages. All error bars are 1σ.**

### 4.5.1.2 Sample 8 (CMD – North Ortona)

Zircons from sample 8 are morphologically similar to those in sample 6, and were also collected from a late-stage felsic differentiate within a metadolerite sill near Ortona station. Individual grains have weak cathodoluminescence, and contain no major rims or inclusions. Grains are relatively uniform in size and shape, but are generally smaller than those of sample 6 (averaging ~100 x 50 µm) and possess either prismatic or pyramidal faces.

The zircons of sample 8 define a single age distribution (Fig. 4.4b). The 8 coherent zircon analyses from this sample define a $^{204}Pb$-corrected $^{207}Pb/^{206}Pb$ weighted mean age of 1637 ± 21 Ma (MSWD = 0.28, probability of equivalence = 0.96; Fig. 4.4c). As with sample 6, the weighted mean age for sample 8 is interpreted as the crystallisation age of the felsic differentiate within the metadolerite sill, and also represents the emplacement age of the metadolerite.

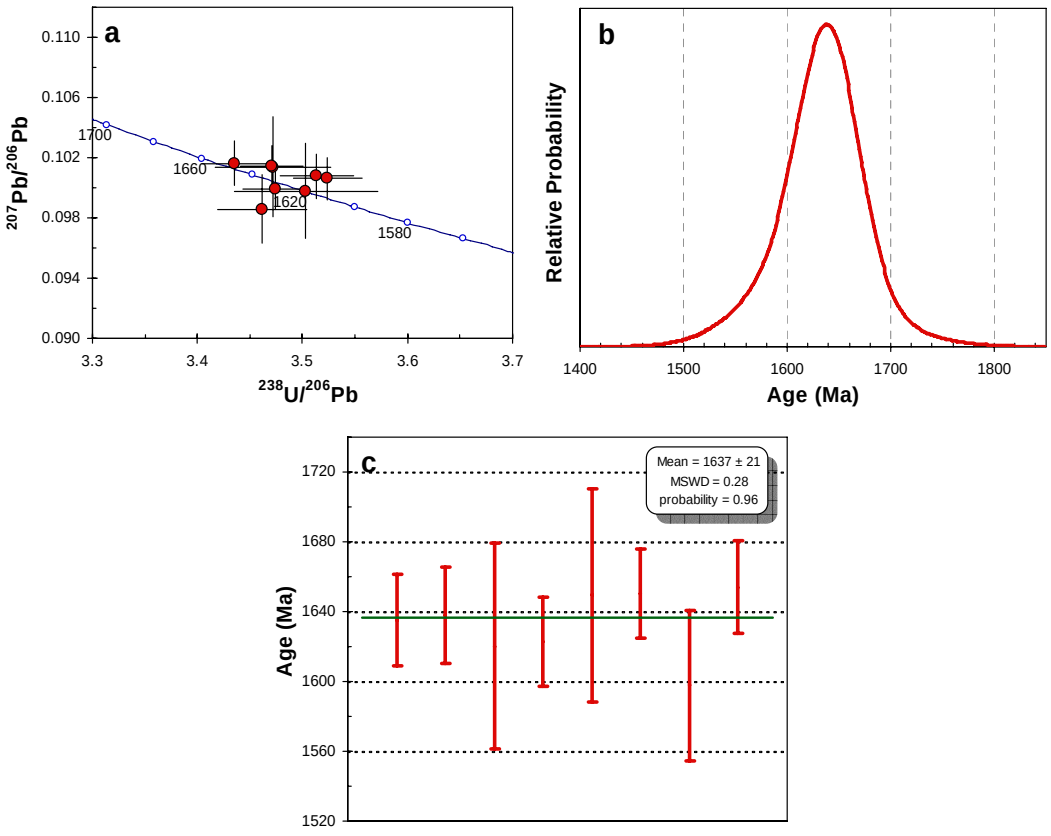


**Figure 4.4: (a) Tera-Wasserburg U-Pb concordia plot, (b) cumulative probability plot, and (c) weighted average plot for zircon analyses from sample 8. All error bars are 1σ.**

### 4.5.1.3 Sample 159 (CMD – South Ortona)

Zircons from sample 159 were collected from a felsic differentiate within a metadolerite sill south of Ortona station (Fig. 4.1). All separated zircons have igneous morphologies and are generally short with pyramidal to prismatic and lesser rounded edges (averaging ~100 x 60 µm). As with samples 6 and 8, metamorphic or recrystallization rims were not detected on the igneous zircons.

Some 24 zircons from sample 159 were analysed in two separate sessions. Although the isotopic data appear to form a single peak in the cumulative probability diagram (Fig. 4.5b), the isotopic ages for all analyses are significantly scattered and several have been affected by a combination of Pb-loss and common-Pb. By omitting two analyses with individual isotopic ages below 1500 Ma, one anomalous analysis at 1703 Ma with an extremely high associated error, one analysis with an isotopic age of 3376 ± 201 Ma, and several discordant analyses, the remaining 14 analyses yield an age of 1713 ± 32 Ma (MSWD = 0.25, probability of equivalence = 0.997).

The calculated age for this sample is significantly older than the previously suggested upper age limit for the onset of sedimentation in the eastern Etheridge Group (ca. 1700 Ma; Black *et al*., 2005). However, it is within error of the age of another sample from the same sill (see 161 below) and is regarded here as the crystallisation age.

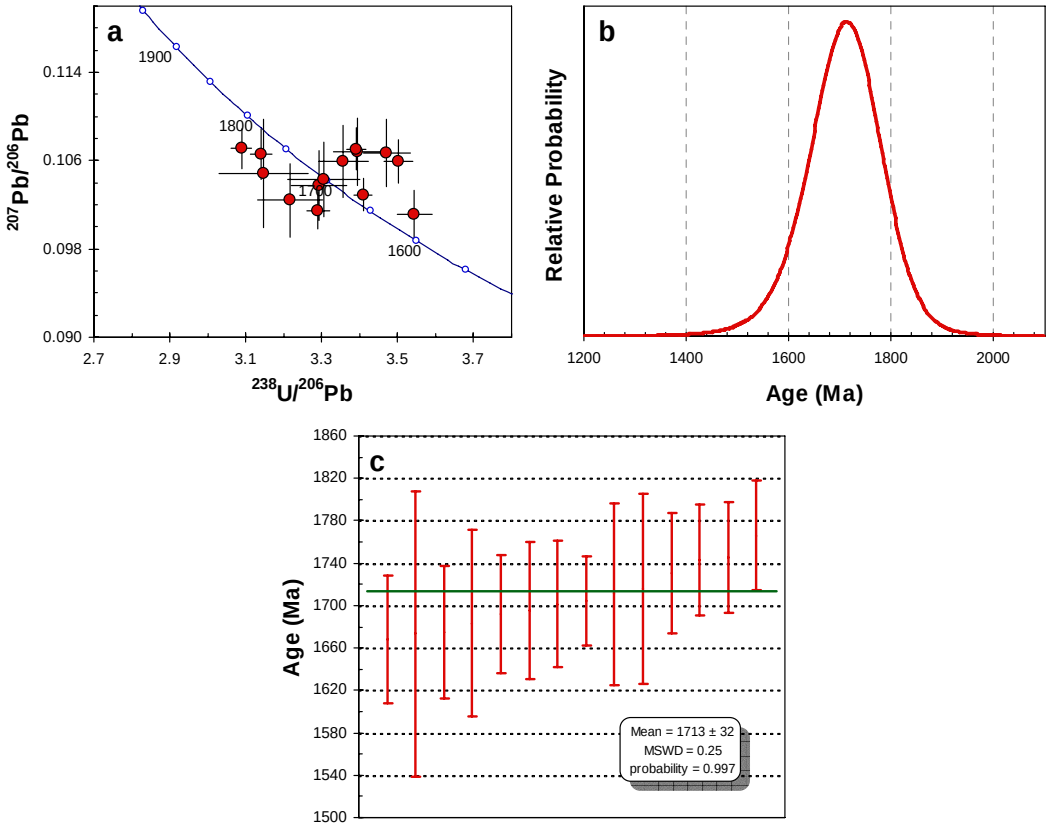


**Figure 4.5: (a) Tera-Wasserburg U-Pb concordia plot, (b) cumulative probability plot, and (c) weighted average plot for zircon analyses from sample 159. All error bars are 1σ.**

### 4.5.1.4 Sample 161 (CMD – South Ortona)

Sample 161 was collected 10 m east of sample 159 within the same metadolerite sill and, as such, contains zircons that are morphologically indistinguishable from sample 159. The majority of separated zircons are elongate with prismatic and lesser rounded edges (averaging up to ~120 x 80 µm). Metamorphic zircons occurring either as discrete grains or rims were not detected.

Some 30 zircons were analysed in two separate sessions for sample 161. After omitting analyses containing significant Pb-loss, the remaining 24 analyses form a broad single peak in the cumulative probability diagram (Fig. 4.6b). As with sample 159, the isotopic ages for all analyses are significantly scattered and several have been

affected by either minor Pb-loss or common-Pb. The 24 acceptable analyses combine to give a weighted mean age of 1719 ± 27 Ma (MSWD = 1.12, probability of equivalence = 0.31; Fig. 4.6c).

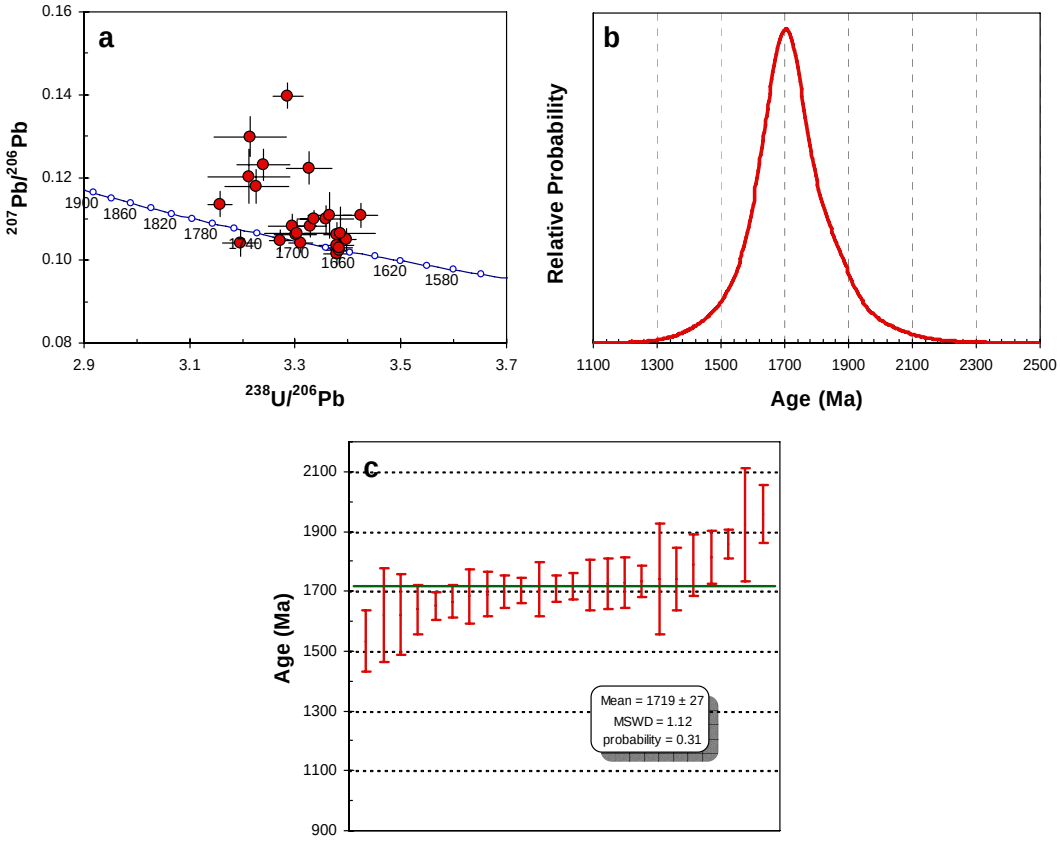


**Figure 4.6: (a) Tera-Wasserburg U-Pb concordia plot, (b) cumulative probability plot, and (c) weighted average plot for zircon analyses from sample 161. All error bars are 1σ.**

The correlation in calculated ages for samples 159 and 161 indicate that they represent a real crystallisation event, despite the presence of significant common-Pb and Pb-loss in some analyses affecting the calculated ages. The 1719 ± 27 Ma age is within error of the oldest magmatic zircon ages obtained for the Etheridge Group (Black *et al.*, 2005). Consequently, these zircons may be xenocrystal and derived from the same leucogneiss source as the ca. 1710-1700 Ma zircons analysed by Black *et al.* (2005), or they may represent an earlier phase of emplacement and crystallisation of mafic rocks. If the former is the case, then leucogneiss similar to that found in the Einasleigh Metamorphics must underlie the Etheridge Group metasediments in this area, and mafic material forming the CMD sills would have passed through the leucogneiss prior to emplacement. However, given that the analyses of the euhedral (igneous)

zircon grains from both samples 159 and 161 form relatively tight isotopic populations, it is highly unlikely that they were inherited.

#### 4.5.1.5 Sample 172 (CMD – South Ortona)

Zircons from sample 172 were collected from a late-stage felsic differentiate within a metadolerite sill separate but adjacent to the sill containing samples 159 and 161 (Fig. 4.1). Individual grains possess igneous morphologies and are short, with pyramidal to rounded edges (averaging ~100 x 50 μm). Metamorphic or recrystallised rims were not detected on the zircons in this sample.

The diagram of isotopic age distribution for the zircons of sample 172 defines a single peak with a broad younger shoulder (Fig. 4.7b). Some 12 grains were analysed for this sample, however the oldest and youngest values were omitted from subsequent age calculations due to significant common-Pb contamination. Due to the presence of minor common-Pb contamination coupled with some Pb-loss in the remaining analyses, the use of $^{204}$Pb-corrected $^{207}$Pb/$^{206}$Pb ages was not possible, so $^{207}$Pb-corrected $^{206}$Pb/$^{238}$U ages were used instead. The seven analyses defining the dominant peak in Figure 4.7b have a $^{207}$Pb-corrected $^{206}$Pb/$^{238}$U weighted mean age of 1628 ± 13 Ma (MSWD = 0.32, probability of equivalence = 0.930). Although the MSWD is significantly below unity, this value cannot be improved further by the omission or retention of more analyses. This age is younger than any previously dated sample for the Cobbold Metadolerite; however the use of the $^{207}$Pb-corrected $^{206}$Pb/$^{238}$U weighted mean age in addition to the presence of minor Pb-loss in some analyses could indicate that this value is a minimum crystallisation age for the dolerite.

Three zircons analysed from this sample returned ages younger than 1600 Ma, and although two grains suffered minor Pb-loss their resultant analyses are acceptable. The three grains combine to give a weighted mean age of 1561 ± 54 Ma; however they are significantly scattered (MSWD = 2.2). Although the ages of the younger grains are consistent with the established age for metamorphism in the Etheridge Group at ca. 1550 Ma, their clear igneous morphologies suggest they are unlikely to be metamorphic in origin. It is possible that these grains experienced complete resetting of their isotopic ages due to metamorphism, as similar ages have been

obtained from recrystallised igneous zircons in a meta-granitoid from the eastern Etheridge Group (Hoskin & Black, 2000). However, the low-grade of metamorphism experienced by sample 172 makes this unlikely.

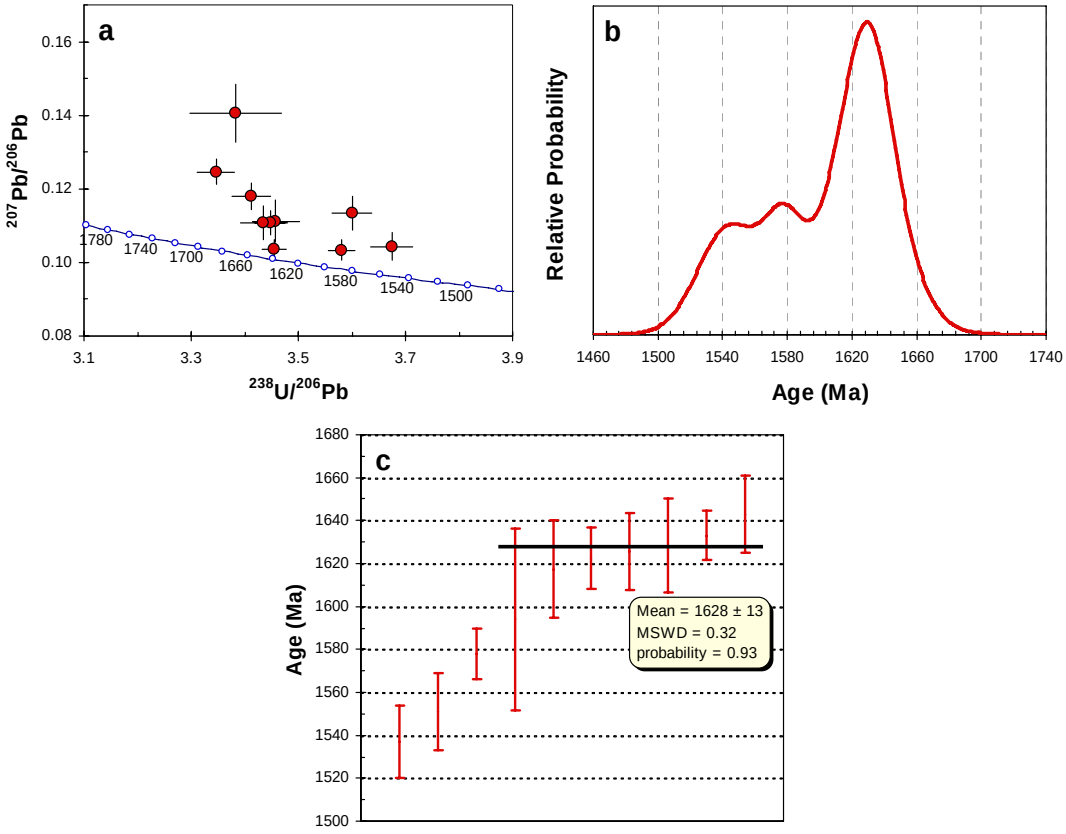


**Figure 4.7: (a) Tera-Wasserburg U-Pb concordia plot, (b) cumulative probability plot, and (c) weighted average plot for zircon analyses from sample 172. All error bars are 1σ.**

### 4.5.1.6 Sample 264 (DHM – Robinhood)

Sample 264 was collected from an amphibolite-facies outcrop of a Dead Horse Metabasalt flow SW of Robinhood station (Fig. 4.1). The sample contained a number of coarse-grained felsic segregations that appear consistent with the fractionation of a felsic component prior to pervasive metamorphism and re-crystallisation. Zircons collected were all of igneous origin. Small unbroken grains are moderately uniform in size and elongation, averaging ~100 x 50 µm. A number of larger, broken grains were also found, and vary in dimension up to ~110 x 80 µm. All grains are euhedral and generally characterised by first-order pyramidal, or lesser prismatic faces. Terminations are either sharp on grain edges and broken surfaces, or are only very slightly rounded (smaller grains) or rounded (larger grains). Individual grains are

morphologically simple, consisting of only a primary igneous growth phase; however larger grains contain some form of compositional zoning. Although the metamorphic grade experienced by sample 264 is significantly higher compared to other mafic samples in this study, no significant metamorphic rims or zoning were detected on the analysed zircons.

Some 35 analyses were conducted on the separated zircons from sample 264 over two separate sessions. Three analyses were omitted due to a combination of significant Pb-loss and common-Pb. As with sample 172, the presence of significant common-Pb contamination coupled with minor Pb-loss in several grains prevented the use of $^{204}$Pb corrected $^{207}$Pb/$^{206}$Pb ages, so $^{207}$Pb-corrected $^{206}$Pb/$^{238}$U ages were instead used for selected analyses (Table 4.1). Sample 264 is unique among the amphibolite samples analysed in this study, as it appears to contain a spectrum of isotopic ages that suggest a significant inherited component in the sample. There is a large spread in the isotopic age distribution (Fig. 4.8b), with the majority of analyses scattered between 1600 and 2600 Ma. Based on individual isotopic ages, the analyses falling between 1580 and 1710 Ma can be separated into a number of relatively distinct groups. However, only the most statistically acceptable groupings were used in order to determine weighted mean ages.

The youngest group (Group 1) contains 7 analyses that yield a weighted mean age of 1602 ± 17 Ma (MSWD = 0.74, probability of equivalence = 0.62). This age is within error of the crystallisation age determined for the younger phase of mafic intrusions represented by sample 172. However, the large isotopic errors for some Group 1 analyses and similarities in Th/U values to the Group 2 analyses may indicate that these zircons were partially reset by later metamorphism (Hoskin & Black, 2000). The next oldest group (Group 2) contains 15 analyses that yield a weighted mean age of 1663 ± 13 Ma (MSWD = 1.05, probability of equivalence = 0.40). As this group contains the majority of concordant analyses, the 1663 ± 13 Ma age represents the best estimate for the crystallisation age of this rock. Combining the Group 1 and 2 analyses did not return a statistically acceptable grouping.

The remaining analyses are separated into three groups based on isotopic ages. The two younger groups (Groups 3 and 4) contain 3 and 2 analyses respectively, with weighted mean ages of 1809 ± 50 Ma (MSWD = 0.52, probability of equivalence = 0.60) for Group 3, and 1905 ± 27 Ma (MSWD = 1.02, probability of equivalence =

0.31) for Group 4. The two groups most likely represent inherited sources, and may reflect the peperitic incorporation of Barramundi-aged material from adjacent metasediments into the magma. The oldest group (Group 5) contains 3 analyses that combine for a weighted mean age of 2531 ± 110 Ma (MSWD = 1.7, probability of equivalence = 0.18). This age may represent zircons inherited from a much older (pre-Barramundi?) source that were subsequently incorporated into the ca. 1660 Ma phase of magmatism. The significance of this age is discussed in more detail below. A further three analyses returned ages between 2200 and 2700 Ma, but do not form a statistically acceptable grouping.

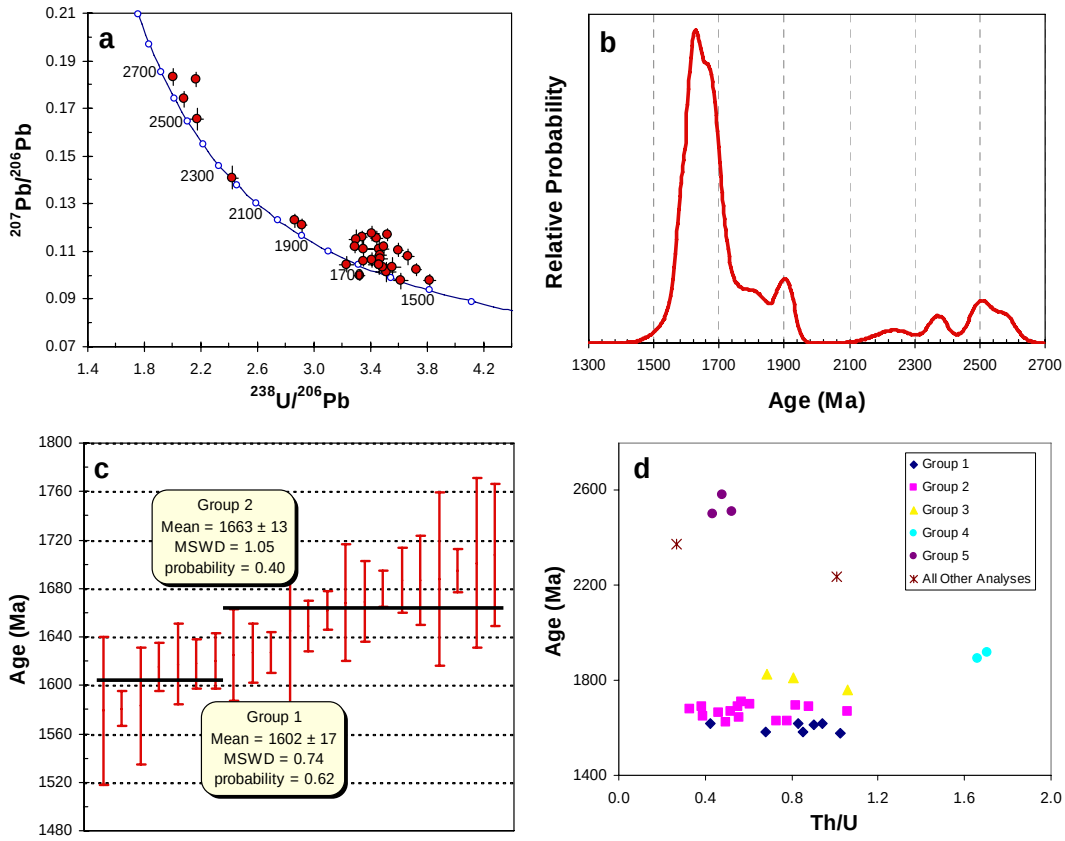


**Figure 4.8: (a) Tera-Wasserburg U-Pb concordia plot, (b) cumulative probability plot, (c) weighted average plot for Group 1 and 2 analyses (see text for explanation), and (d) Th/U versus age diagram for analyses from sample 264. All error bars are 1σ.**

The age groups outlined above are also distinguished by their Th/U characteristics (Fig. 4.8d). The younger groups (Groups 1, 2, and 3) have fairly distributed Th/U values (0.33-1.06, average = 0.71), whereas Group 4 analyses have Th/U values of 1.66 and 1.70 (average = 1.68). Th/U values for Group 5 also form a distinct group, ranging from 0.43 to 0.52 (average = 0.48). The difference in Th/U values, as well as the range in values for the younger groups, is partially a consequence of the younger

zircons possessing higher U and Th relative to Group 4 and 5 (averaging 770 ppm U and 541 ppm Th for Groups 1 and 2, compared to averages of 248 ppm U and 119 ppm Th for Group 5). Zircon morphology may also be linked to the distribution in isotopic ages in this sample, as analyses conducted on larger grains returned ages above ca. 1700 Ma.

It is possible that the spectrum of isotopic ages obtained for sample 264 may indicate that eruption of the metabasalt occurred sometime around the crystallisation of the Group 1 zircons (ca. 1600 Ma). However, the weighted mean age obtained for the Group 1 zircons is questionable, as in addition to the possibility of some isotopic re-setting occurring within the grains, the majority of analyses contained some common-Pb. Due to these effects, the use of $^{207}Pb$-corrected $^{206}Pb/^{238}U$ ages rather than the preferred $^{207}Pb/^{206}Pb$ ages was required. Consequently, I conclude that the Group 2 age of 1663 ± 13 Ma is the best estimate of the crystallisation age of this rock.

#### 4.5.1.7 Sample 299 (CMD – Gum Flats)

Sample 299 was collected from an outcrop of the Cobbold Metadolerite south of Gum Flats station (Fig. 4.1). Initial attempts to separate zircons from the sample using the milling method described above did not return an adequate number of grains. Therefore the sample was prepared for analysis as a 1 inch polished round mount, with all zircons analysed *in situ*. Individual zircon morphologies were difficult to distinguish due to the impingement of other minerals; however where visible, morphologies were typical of igneous rocks.

Eleven zircons were analysed for sample 299, with one discordant analysis omitted due to Pb-loss. $^{207}Pb$-corrected $^{206}Pb/^{238}U$ isotopic ages were again used in preference to $^{207}Pb/^{206}Pb$ ages due to common-Pb contamination (Table 4.1). The isotopic data form a broad single peak in the cumulative probability diagram (Fig. 4.9b), reflecting the higher analytical error associated with in situ analysis (Table 4.1). However, despite this variation the data combine to form a statistically acceptable weighted mean age from 9 grains of 1687 ± 38 Ma (MSWD = 1.04, probability of equivalence = 0.40; Fig. 4.9c). This age is similar to the crystallisation of the Dead Horse Metabasalt unit and associated metadolerite sills and supports correlation of the Cobbold Metadolerite with this unit.

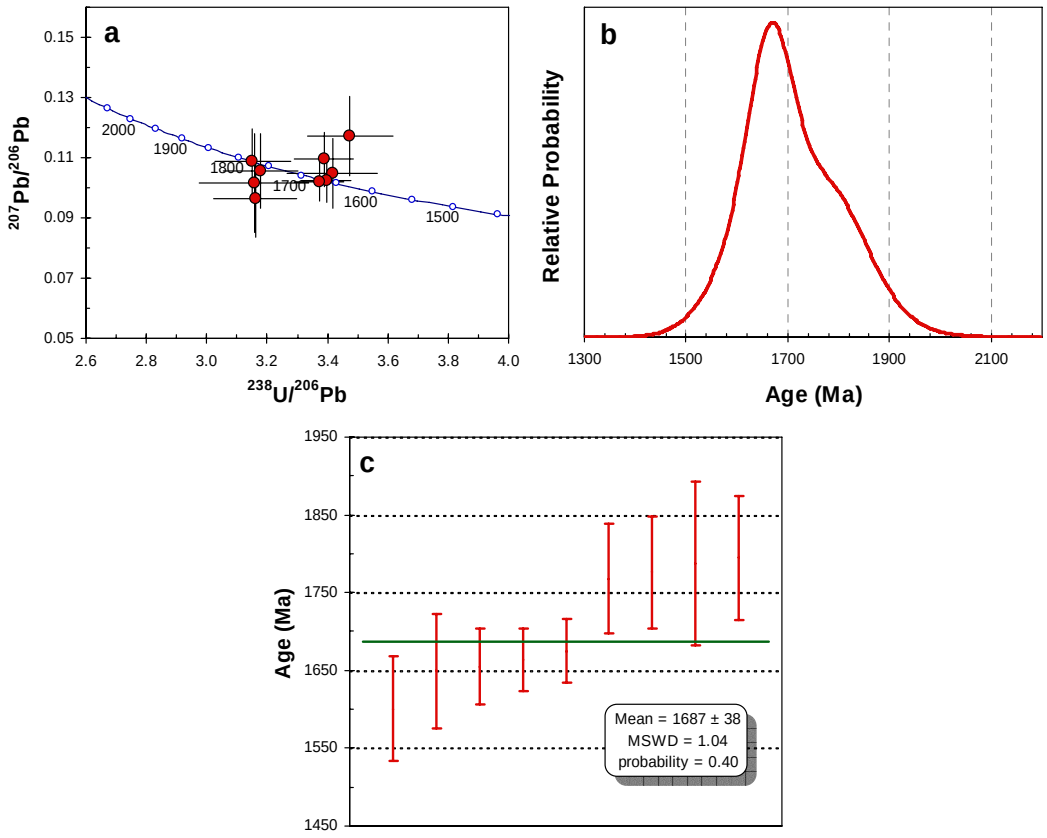


**Figure 4.9: (a) Tera-Wasserburg U-Pb concordia plot, (b) cumulative probability plot, and (c) weighted average plot for zircon analyses from sample 299. All error bars are 1σ.**

### 4.5.1.8 Sample 300 (CMD – Gum Flats)

Sample 300 was collected from an outcrop of the Cobbold Metadolerite close to sample 299 (Fig. 4.1). As with sample 299, this sample was prepared for analysis as a 1 inch round mount, and all zircons were analysed *in situ*. Problems encountered in sample 299 in distinguishing individual zircon morphologies were also encountered in this sample, but where visible, morphologies suggested an igneous origin.

12 zircons were analysed for sample 300; however three discordant analyses were omitted (Fig. 4.10). $^{206}Pb/^{238}U$ ages were used in preference to $^{207}Pb/^{206}Pb$ ages due to minor common-Pb contamination in some analyses. The analyses from 9 grains combine to form a statistically acceptable weighted mean age of 1662 ± 32 Ma (MSWD = 0.95, probability of equivalence = 0.48). This age corresponds well with the crystallisation ages sample 299 and Dead Horse Metabasalt listed above.

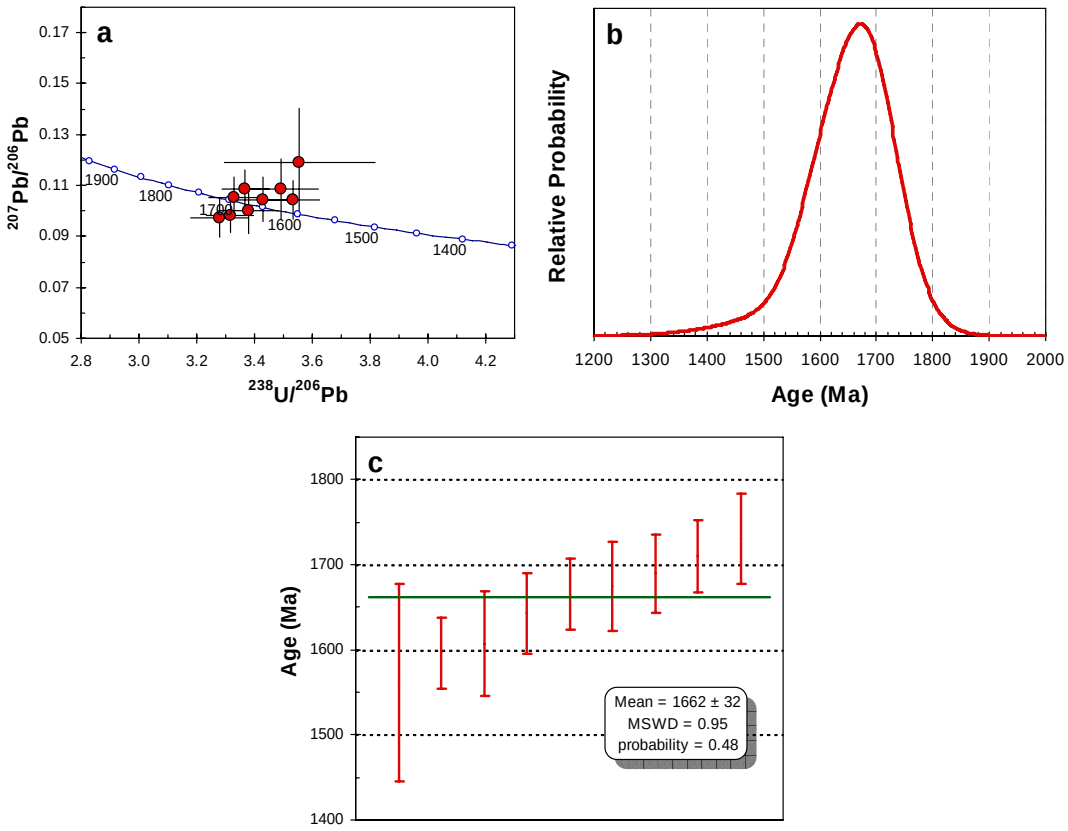


**Figure 4.10: (a) Tera-Wasserburg U-Pb concordia plot, (b) cumulative probability plot, and (c) weighted average plot for zircon analyses from sample 300. All error bars are 1σ.**

### 4.5.1.9 Sample 318 (Einasleigh Metamorphics – Gum Flats)

Sample 318 was collected from an amphibolite outcrop in the Einasleigh Metamorphics, east of Percyvale station (Fig. 4.1). As with samples 299 and 300, this sample was prepared for analysis as a 1 inch round mount, and all zircons were analysed *in situ*.

12 zircons were analysed for sample 318; however five analyses were omitted due to significant Pb-loss (Fig. 4.11). Due to the presence of common-Pb throughout the analysed zircons, $^{207}Pb$-corrected $^{206}Pb/^{238}U$ ages were again used in preference to $^{207}Pb/^{206}Pb$ ages. The 7 acceptable analyses form a statistically acceptable weighted mean age of 1658 ± 69 Ma (MSWD = 1.4, probability of equivalence = 0.23), which correlates with the inferred crystallisation age for the Dead Horse Metabasalt and Cobbold Metadolerite samples listed above.

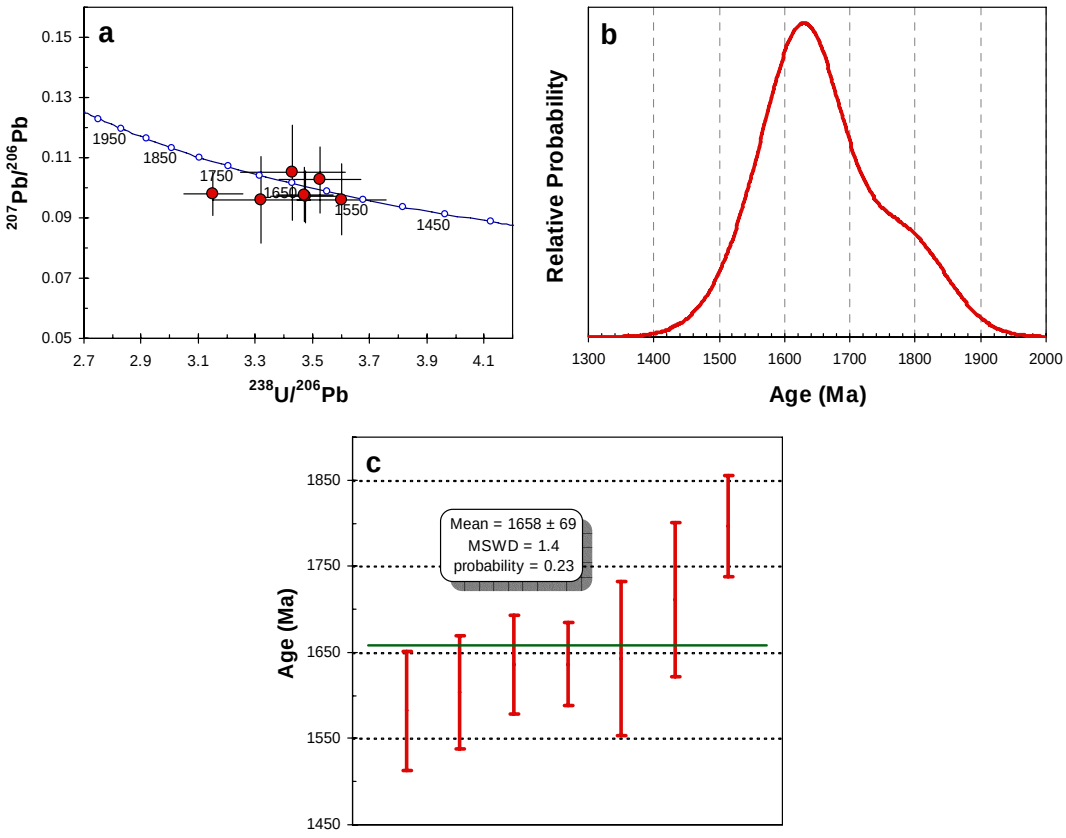


**Figure 4.11: (a) Tera-Wasserburg U-Pb concordia plot, (b) cumulative probability plot, and (c) weighted average plot for zircon analyses from sample 318. All error bars are 1σ.**

### 4.5.2 Summary of LA-ICPMS zircon ages from mafic samples

The igneous zircons from mafic rocks of the lower Etheridge Group define a number of key crystallisation ages (Table 4.3). The most significant of these relates to the eruption of the Dead Horse Metabasalt unit and associated feeder dykes and sills of the Cobbold Metadolerite. Four samples (samples 264, 299, 300 and 318), including a sample of Dead Horse Metabasalt amphibolite, returned magmatic ages of 1687 ± 38, 1663 ± 13, 1662 ± 32 and 1658 ± 69 Ma (Table 4.3). These ages combine to produce an approximate crystallisation age for the Dead Horse Metabasalt and associated metadolerite of ca. 1665 Ma. Two samples collected from Cobbold Metadolerite sills near 'Ortona' station returned crystallisation ages of 1645 ± 22 and 1637 ± 21 Ma (Table 4.3). These ages do not appear to be associated with the age of eruption of the Dead Horse Metabasalt, and may instead suggest an extended period of magmatism in the Etheridge Group. However the errors associated with the calculated ages do not

provide sufficient resolution to determine if these ages definitively date a second discrete pulse of mafic activity.

| Stratigraphic unit | Sample | Age (Ma) ± 95%[1] | No. of analyses[2] | MSWD | Prob. of Equivalence | Comment |
|---|---|---|---|---|---|---|
| Mafic samples | | | | | | |
| Cobbold Metadolerite | 6 | 1645 ± 22 | 8 | 0.75 | 0.63 | Magmatic age |
| Cobbold Metadolerite | 8 | 1637 ± 21 | 8 | 0.28 | 0.96 | Magmatic age |
| Cobbold Metadolerite | 159 | 1713 ± 32 | 14 | 0.25 | 0.997 | Magmatic age? |
| Cobbold Metadolerite | 161 | 1719 ± 27 | 24 | 1.12 | 0.31 | Magmatic age? |
| Cobbold Metadolerite | 172 | 1628 ± 13 | 7 | 0.32 | 0.93 | Magmatic age |
| | | 1561 ± 54 | 3 | 2.2 | 0.11 | Metamorphic age? |
| Dead Horse Metabasalt | 264 | 1663 ± 13 | 15 | 1.05 | 0.4 | Magmatic age |
| | | 1602 ± 17 | 7 | 0.74 | 0.62 | Partially re-set or metamorphic age |
| | | 1809 ± 50 | 3 | 0.52 | 0.6 | Inherited age |
| | | 1905 ± 27 | 2 | 1.02 | 0.31 | Inherited age |
| | | 2524 ± 64 | 3 | 1.7 | 0.18 | Inherited age |
| Cobbold Metadolerite | 299 | 1687 ± 38 | 9 | 1.04 | 0.4 | Magmatic age |
| Cobbold Metadolerite | 300 | 1662 ± 32 | 9 | 0.95 | 0.48 | Magmatic age |
| Einasleigh Metamorphics | 318 | 1658 ± 69 | 7 | 1.4 | 0.23 | Magmatic age |
| Granitic samples | | | | | | |
| Mt Hogan Granite | 135 | 1565 ± 46 | 6 | 1.02 | 0.4 | *1549 ± 25 Ma (Black & Withnall, 1993)* |
| Ropewalk Granite | 208 | 1558 ± 34 | 6 | 0.37 | 0.87 | Magmatic age |
| | 209 | 1524 ± 27 | 9 | 0.34 | 0.95 | Magmatic age |
| | 210 | 1544 ± 33 | 12 | 1.30 | 0.21 | Magmatic age |
| | | *1539 ± 16* | *27* | *0.83* | *0.71* | *Combined 208, 209, & 210 age 1550 +7/-5 Ma (Black & McCulloch, 1990)* |

[1] Pooled age from *n* analyses calculated using *Isoplot* version 3.0 (Ludwig, 2003)
[2] Number of analyses in pooled age

**Table 4.3: Summary of weighted mean ages calculated from individual LA-ICPMS igneous zircon analyses in Tables 4.1 and 4.2.**

Two Cobbold Metadolerite samples from the same sill (samples 159 and 161) returned older crystallisation ages of 1713 ± 32 and 1719 ± 27 Ma (Table 4.3). These ages are problematic, as they are older than the inferred maximum depositional age of the Etheridge Group (ca. 1700 Ma; Black *et al*., 2005). However, they are within error of the calculated age for the volcanic source of the Einasleigh Metamorphics leucogneiss (1706 ± 6 Ma; Black *et al*., 2005). Consequently, it is possible that the age of the leucogneiss represents a volcanic age that is not at the base of the sequence and that some parts of the lower Etheridge Group formed at or before ca. 1715 Ma.

Sample 172 returned a crystallisation age of 1628 ± 13 Ma (Table 4.3). It probably represents the last component of igneous activity within the basin before the onset of metamorphism. However, as noted above this age may be erroneously young, and since it is within error of the ca. 1640 Ma samples may relate to this pulse of magmatic activity within the Etheridge Group.

In addition to their magmatic ages, sample 264 contains zircons with isotopic ages that suggest inheritance from the host lower Etheridge Group metasediments. In addition, samples 172 and 264 contained zircon populations that have been reset to ages of 1561 ± 54 and 1602 ± 17 Ma respectively (Table 4.3), possibly due to post-depositional tectonothermal events. The significance of these ages, and the inherited ages in sample 264, are discussed in more detail below.

### 4.5.3 Granitoids

#### 4.5.3.1 Sample 135 (Mt Hogan Granite – Gum Flats)

Sample 135 was collected from an outcrop of the Mt Hogan Granite located approximately 10 km southwest of Gum Flats (Fig. 4.1). Relatively few zircons were recovered from this sample, and they are moderately uniform in size and elongation, averaging ~150 x 70 μm. The majority of grains have prismatic or pyramidal terminations that are typical of igneous growth. Euhedral zoning is also evident in some larger grains.

The majority of zircons analysed had very discordant isotopic compositions (Fig. 4.12a) due to low-temperature exchange of Pb. All analyses affected in this way returned ages in excess of 1700 Ma, and were omitted before calculating the crystallisation age of the rock. In order to calculate a preferred age for the crystallisation of the granite, the concordant individual ages were combined and their mean age determined. The analyses containing the six youngest isotopic ages yield the most statistically acceptable weighted mean age of 1565 ± 46 Ma (MSWD = 1.02, probability of equivalence = 0.40). This age is within error of the previously published age for the crystallisation of the Mt Hogan Granite (1549 ± 25 Ma; Black & Withnall, 1993).

#### 4.5.3.2 Samples 208, 209 and 210 (Ropewalk Granite - Robinhood)

Three samples were collected from outcrops of the Ropewalk Granite, south of Forsayth (Fig. 4.1). Zircons collected from these samples are mineralogically indistinguishable, and are of predominantly igneous origin. A range of zircon shapes is present across all three samples, from elongated grains (typically ~170 x 50 μm) of igneous origin, to equant grains (~120 μm) of possible metamorphic origin. The

majority of igneous grains have unmodified crystal faces, and very few possess rounded edges. Equant grains are generally well-rounded, and are less luminescent. As analysis was primarily focussed on determining the age of igneous crystallisation, grains of probable igneous origin were preferentially selected for analysis.

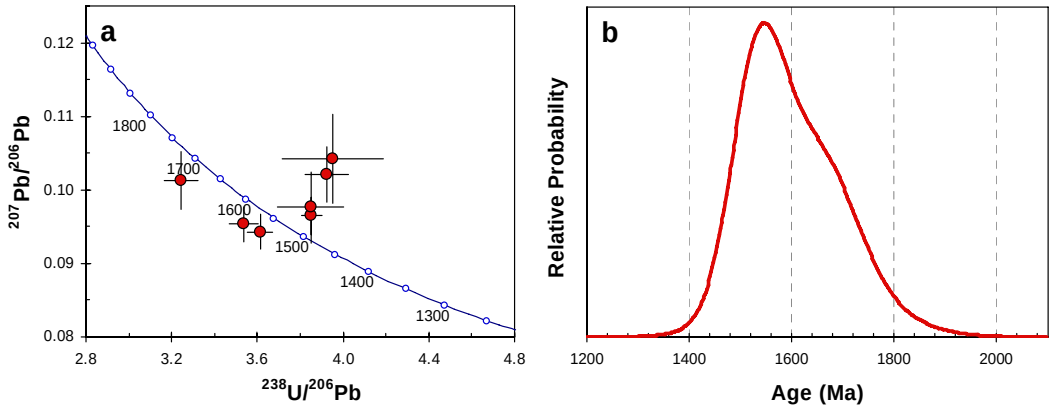


**Figure 4.12: (a) Tera-Wasserburg U-Pb concordia plot, and (b) cumulative probability plot for zircon analyses from sample 135. All error bars are 1σ.**

In sample 208, six grains were significantly discordant, and were subsequently omitted from the weighted mean age calculation. The remaining 6 analyses returned a $^{207}Pb/^{206}Pb$ weighted mean age of 1558 ± 34 Ma (MSWD = 0.37, probability of equivalence = 0.87). Three discordant analyses were also omitted from sample 209. The 9 acceptable analyses returned a $^{207}Pb/^{206}Pb$ weighted mean age of 1524 ± 27 Ma (MSWD = 0.34, probability of equivalence = 0.95). Although this age is younger than that calculated for other granitic bodies crystallising at around this time, it remains within error of the inferred ca. 1550 Ma age for Palaeoproterozoic felsic magmatism in the Etheridge Group (Black & McCulloch, 1990). In sample 210, all 12 analysed grains were free of significant Pb-loss and common-Pb (Fig. 4.13c), and returned a $^{207}Pb/^{206}Pb$ weighted mean age of 1544 ± 33 Ma (MSWD = 1.30, probability of equivalence = 0.21).

As the three samples are all assigned to the same granitic unit, I have combined the individual isotopic data in order to produce a more accurate age estimate for the Ropewalk Granite (Fig. 4.13d). Combining the three samples yields a weighted mean age from 27 analyses of 1539 ± 16 Ma (MSWD = 0.83, probability of equivalence = 0.71). As with the Mt Hogan Granite, this age is within error of the ca. 1550 Ma age for felsic magmatism in the Etheridge Group, and the 1550 +7/-5 Ma SHRIMP age calculated for the nearby Forsayth Granite (Black & McCulloch, 1990). Therefore, I

suggest that the ca. 1539 Ma calculated age represents the crystallisation age of the granite and provides some evidence that the Ropewalk Granite is the youngest Mesoproterozoic granitoid in the area.

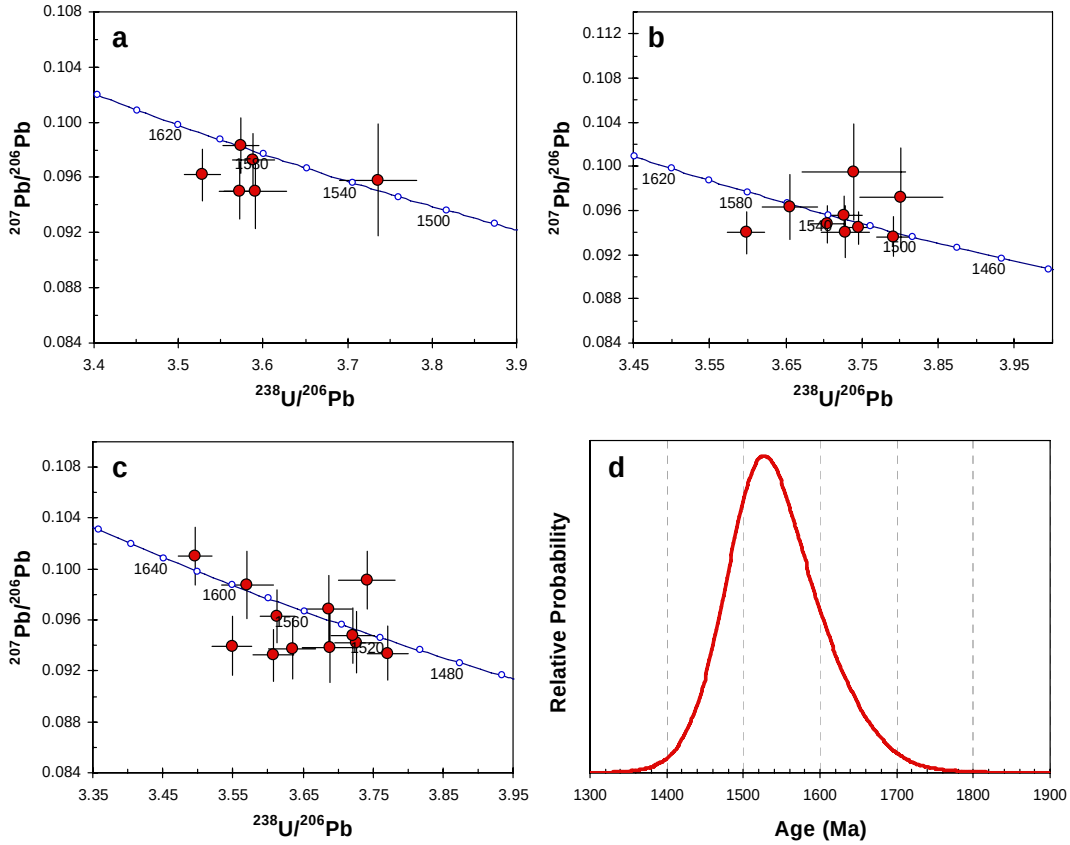


**Figure 4.13: Tera-Wasserburg U-Pb concordia diagrams for samples (a) 208, (b) 209, and (c) 210. (d) Cumulative probability plot for analyses from all three samples. All error bars are 1σ.**

### 4.5.4 Metasedimentary rocks

Prior to this study, little attention had been given to the provenance of zircons from metasedimentary rocks in the Etheridge Group. The work of Black *et al.* (2005) focussed on the U-Pb SHRIMP dating of zircons collected from high-grade leucogneiss of the Einasleigh Metamorphics in the area near Percyvale (Fig. 4.1). They found detrital zircon populations in a number of samples; however they could define no significant age groupings, and concluded the detrital grains were most likely derived from various sedimentary protoliths.

This study, involving two metasedimentary samples from lower-grade areas of the Daniel Creek Formation, represents the first attempt to directly determine the detrital zircon ages for the metasedimentary unit that directly underlies the Dead Horse

Metabasalt member. The resultant pattern of detrital ages is then compared to detrital populations found in sedimentary units surrounding the key mafic igneous units of the Eastern Mt Isa Succession and Broken Hill Block, in order to determine if any similarities in the detrital zircon patterns exist between the terranes.

| Label | $^{238}U/^{206}Pb$ | ± 1 σ | $^{207}Pb/^{206}Pb$ | ± 1 σ | $^{207}Pb/^{206}Pb$ Age (Ma) | ± 1 σ | Label | $^{238}U/^{206}Pb$ | ± 1 σ | $^{207}Pb/^{206}Pb$ | ± 1 σ | $^{207}Pb/^{206}Pb$ Age (Ma) | ± 1 σ |
|---|---|---|---|---|---|---|---|---|---|---|---|---|---|
| Sample: 184 (North Ortona) | | | | | | | Sample: 255 (South Head) | | | | | | |
| 7 | 3.01503 | 0.05063 | 0.11254 | 0.00977 | 1841 | 157 | 1 | 1.86501 | 0.01597 | 0.19819 | 0.00276 | 2811 | 23 |
| 10 | 1.99686 | 0.08782 | 0.19902 | 0.01637 | 2818 | 134 | 2 | 2.78281 | 0.02425 | 0.12481 | 0.00228 | 2026 | 32 |
| 11 | 1.90243 | 0.04112 | 0.18647 | 0.01093 | 2711 | 97 | 5 | 1.96781 | 0.02195 | 0.18821 | 0.00361 | 2727 | 32 |
| 15 | 1.92486 | 0.02078 | 0.18643 | 0.00374 | 2711 | 33 | 6 | 1.82846 | 0.02320 | 0.19362 | 0.00411 | 2773 | 35 |
| 18 | 2.24737 | 0.03448 | 0.17267 | 0.00486 | 2395 | 165 | 7 | 2.12700 | 0.02364 | 0.17301 | 0.00389 | 2587 | 38 |
| 19 | 2.13325 | 0.02709 | 0.17506 | 0.00456 | 2607 | 43 | 8 | 1.64084 | 0.01768 | 0.23173 | 0.00483 | 3064 | 33 |
| 20 | 1.93982 | 0.04455 | 0.19781 | 0.00726 | 2506 | 175 | 12 | 1.77776 | 0.01735 | 0.20882 | 0.00366 | 2896 | 28 |
| 23 | 2.23554 | 0.02951 | 0.18004 | 0.00535 | 2468 | 93 | 13 | 2.04021 | 0.01734 | 0.17528 | 0.00250 | 2609 | 24 |
| 24 | 2.08654 | 0.02246 | 0.17005 | 0.00403 | 2558 | 40 | 14 | 3.20727 | 0.05233 | 0.11541 | 0.00403 | 1886 | 63 |
| 26 | 2.05373 | 0.02016 | 0.17351 | 0.00356 | 2592 | 34 | 15 | 1.92504 | 0.02027 | 0.20840 | 0.00394 | 2782 | 70 |
| 29 | 1.94793 | 0.01875 | 0.18163 | 0.00362 | 2668 | 33 | 16 | 2.46464 | 0.02025 | 0.14288 | 0.00241 | 2262 | 29 |
| 32 | 2.85767 | 0.07009 | 0.12380 | 0.00503 | 2012 | 72 | 17 | 2.32150 | 0.02695 | 0.15702 | 0.00422 | 2424 | 46 |
| 33 | 2.25277 | 0.05961 | 0.17951 | 0.00840 | 2593 | 170 | 20 | 2.75826 | 0.03080 | 0.11691 | 0.00323 | 1910 | 50 |
| 36 | 2.10689 | 0.01761 | 0.16244 | 0.00279 | 2481 | 29 | 21 | 2.86951 | 0.02854 | 0.11891 | 0.00252 | 1940 | 38 |
| 37 | 2.10470 | 0.02184 | 0.16092 | 0.00357 | 2465 | 38 | 22 | 1.90356 | 0.01692 | 0.19138 | 0.00313 | 2754 | 27 |
| 41 | 2.01535 | 0.03934 | 0.16679 | 0.00389 | 2526 | 39 | 23 | 2.91840 | 0.02588 | 0.12296 | 0.00217 | 2000 | 31 |
| 42 | 2.16961 | 0.02316 | 0.15304 | 0.00210 | 2380 | 23 | 24 | 2.85486 | 0.02718 | 0.11717 | 0.00239 | 1913 | 37 |
| 43 | 1.92539 | 0.02335 | 0.19354 | 0.00293 | 2772 | 25 | 26 | 2.89766 | 0.02796 | 0.12388 | 0.00231 | 2013 | 33 |
| 44 | 2.89384 | 0.04585 | 0.11535 | 0.00215 | 1885 | 34 | 27 | 1.98405 | 0.01704 | 0.17999 | 0.00266 | 2653 | 25 |
| 45 | 3.00580 | 0.10859 | 0.11247 | 0.00447 | 1840 | 72 | 29 | 1.69155 | 0.06546 | 0.21064 | 0.00606 | 2910 | 47 |
| 46 | 2.01589 | 0.04169 | 0.17337 | 0.00302 | 2590 | 29 | 30 | 2.12648 | 0.04905 | 0.16699 | 0.00256 | 2528 | 26 |
| 47 | 2.26635 | 0.04325 | 0.16993 | 0.00260 | 2557 | 26 | 31 | 2.05717 | 0.03346 | 0.16358 | 0.00267 | 2493 | 27 |
| 48 | 2.18789 | 0.06672 | 0.18146 | 0.00479 | 2666 | 44 | 32 | 2.95561 | 0.03785 | 0.11502 | 0.00232 | 1880 | 36 |
| 49 | 2.77960 | 0.03437 | 0.11753 | 0.00188 | 1919 | 29 | 33 | 2.15862 | 0.02496 | 0.16080 | 0.00179 | 2464 | 19 |
| 50 | 2.00042 | 0.02360 | 0.17323 | 0.00225 | 2589 | 22 | 35 | 2.04325 | 0.02359 | 0.17701 | 0.00203 | 2625 | 19 |
| 52 | 2.99473 | 0.07834 | 0.11889 | 0.00245 | 1940 | 37 | 36 | 2.05450 | 0.03322 | 0.17034 | 0.00233 | 2561 | 23 |
| 54 | 2.22529 | 0.04850 | 0.17946 | 0.00299 | 2648 | 28 | 37 | 2.62953 | 0.04868 | 0.12827 | 0.00266 | 2074 | 37 |
| 55 | 2.58325 | 0.04207 | 0.13124 | 0.00211 | 2115 | 28 | 38 | 2.86244 | 0.04625 | 0.12155 | 0.00225 | 1979 | 33 |
| 61 | 2.07194 | 0.01833 | 0.16292 | 0.00201 | 2486 | 21 | 39 | 2.97520 | 0.03232 | 0.11423 | 0.00142 | 1868 | 22 |
| 63 | 2.17455 | 0.04451 | 0.17896 | 0.00341 | 2643 | 32 | 40 | 2.79044 | 0.02884 | 0.11713 | 0.00164 | 1913 | 25 |
| 64 | 1.90561 | 0.06983 | 0.17117 | 0.00497 | 2569 | 49 | 41 | 2.72581 | 0.02724 | 0.11974 | 0.00164 | 1952 | 25 |
| 66 | 2.18630 | 0.06753 | 0.16246 | 0.00353 | 2481 | 37 | 43 | 2.87008 | 0.02873 | 0.12122 | 0.00151 | 1974 | 22 |
| 67 | 1.89469 | 0.06671 | 0.18644 | 0.00517 | 2711 | 46 | 44 | 2.57433 | 0.02958 | 0.13246 | 0.00181 | 2131 | 24 |
| 68 | 2.10895 | 0.05405 | 0.16389 | 0.00332 | 2496 | 34 | 45 | 1.84628 | 0.02486 | 0.19790 | 0.00247 | 2809 | 20 |
| 69 | 1.96970 | 0.09003 | 0.17287 | 0.00593 | 2586 | 57 | 46 | 2.01090 | 0.02182 | 0.17923 | 0.00217 | 2646 | 20 |
| 70 | 2.76208 | 0.08952 | 0.12781 | 0.00332 | 2068 | 46 | 48 | 1.82326 | 0.02828 | 0.20844 | 0.00363 | 2893 | 28 |
| 71 | 2.65503 | 0.07883 | 0.12456 | 0.00504 | 2023 | 72 | 49 | 3.03088 | 0.03731 | 0.11434 | 0.00152 | 1870 | 24 |
| 72 | 2.23728 | 0.07181 | 0.15502 | 0.00353 | 2402 | 39 | 50 | 2.11984 | 0.03586 | 0.16441 | 0.00283 | 2502 | 29 |
| 73 | 2.08899 | 0.09390 | 0.16490 | 0.00531 | 2507 | 54 | 51 | 1.93153 | 0.02150 | 0.19347 | 0.00209 | 2772 | 18 |
| | | | | | | | 52 | 2.52505 | 0.03398 | 0.13393 | 0.00202 | 2150 | 26 |
| | | | | | | | 54 | 1.88531 | 0.03612 | 0.18554 | 0.00312 | 2703 | 28 |
| | | | | | | | 55 | 2.09824 | 0.03403 | 0.17692 | 0.00257 | 2624 | 24 |
| | | | | | | | 56 | 1.89127 | 0.02336 | 0.18672 | 0.00240 | 2713 | 21 |
| | | | | | | | 57 | 2.04890 | 0.02926 | 0.16912 | 0.00268 | 2549 | 27 |
| | | | | | | | 58 | 2.12961 | 0.02396 | 0.16742 | 0.00203 | 2532 | 20 |
| | | | | | | | 61 | 2.10855 | 0.02799 | 0.16239 | 0.00201 | 2481 | 21 |
| | | | | | | | 62 | 1.96878 | 0.03215 | 0.17437 | 0.00279 | 2600 | 27 |
| | | | | | | | 63 | 2.87696 | 0.05598 | 0.11963 | 0.00192 | 1951 | 29 |

**Table 4.4: $^{204}$Pb-corrected U-Pb isotope data for detrital zircons from metasedimentary samples analysed by LA-ICP-MS.**

#### 4.5.4.1 Sample 184 (Daniel Creek Formation – North Ortona)

Zircons collected from sample 184 are generally poorly- to well rounded with many containing pitted exteriors indicating a detrital origin involving varying degrees of abrasion and transportation prior to deposition. Poorly rounded grains are generally elongate, appearing to preserve almost unmodified crystal faces, and may have originally been derived from an igneous source. Overall, the grains are approximately uniform in size, averaging ~100 x 60 μm.

75 zircons from sample 184 were analysed over three sessions. However, 36 analyses showed significant discordance in their isotopic values due to common-Pb and/or Pb-loss, and were omitted from subsequent analysis. The discarded analyses included one grain which returned a $^{207}Pb/^{206}Pb$ age of 1602 ± 32 Ma that may be metamorphic in origin (Appendix 2). A summary of the isotopic values for the concordant analyses is presented in Table 4.4. Inverse U-Pb concordia and relative probability diagrams for sample 184 are illustrated in Fig. 4.14. In the relative probability diagram (Fig. 4.14c) there exists a large spread in individual zircon ages between ca. 1800 and 2800 Ma, with a significant peak between ca. 2400 and 2700 Ma. A minor peak formed by several analyses also occurs at ca. 2400 Ma. This result suggests a largely Archaean source for the Daniel Creek Formation.

#### 4.5.4.2 Sample 255 (Daniel Creek Formation – South Head)

Sample 255 was collected from an outcrop of the Daniel Creek Formation at South Head, approximately 60 km north-west of sample 184 (Fig. 4.1). As with sample 184, zircons collected from sample 255 are generally poorly to well-rounded, with the majority containing pitted exteriors indicating a detrital origin involving varying degrees of abrasion and transportation. Moderately to well-rounded zircons dominate this sample, with the remainder of a similar nature to the poorly-rounded, elongated grains of sample 184. Overall the grains show a slight bimodality in size and shape, ranging from somewhat equant, rounded grains (averaging ~110 x 100 μm) to poorly-rounded, elongated grains (averaging ~170 x 60 μm). Numerous zircons of both varieties contain small (<10 μm) inclusions, the majority of which contain Pb.

63 zircons from sample 255 were analysed, however 15 analyses were discarded due to significant discordance. Isotopic values for the concordant analyses are summarised

in Table 4.4. Inverse U-Pb concordia and relative probability diagrams for sample 255 are illustrated in Fig. 4.14. Significant groupings in the relative probability diagram (Fig. 4.14d) occur at ca. 1900 to 2000, and 2500 to 2800 Ma. Four other analyses, including two at ca. 2270 Ma, one at ca. 2420, and one at ca. 3060 Ma were also recorded but do not form statistically significant groups. The significance of these inheritance ages is discussed in more detail below.

The majority of isotopic values for analyses from sample 255 are much more concordant than for sample 184, with only 15 discordant analyses recorded. However, the removal of these analyses from the relative probability diagram has little effect on the inheritance pattern of this sample.

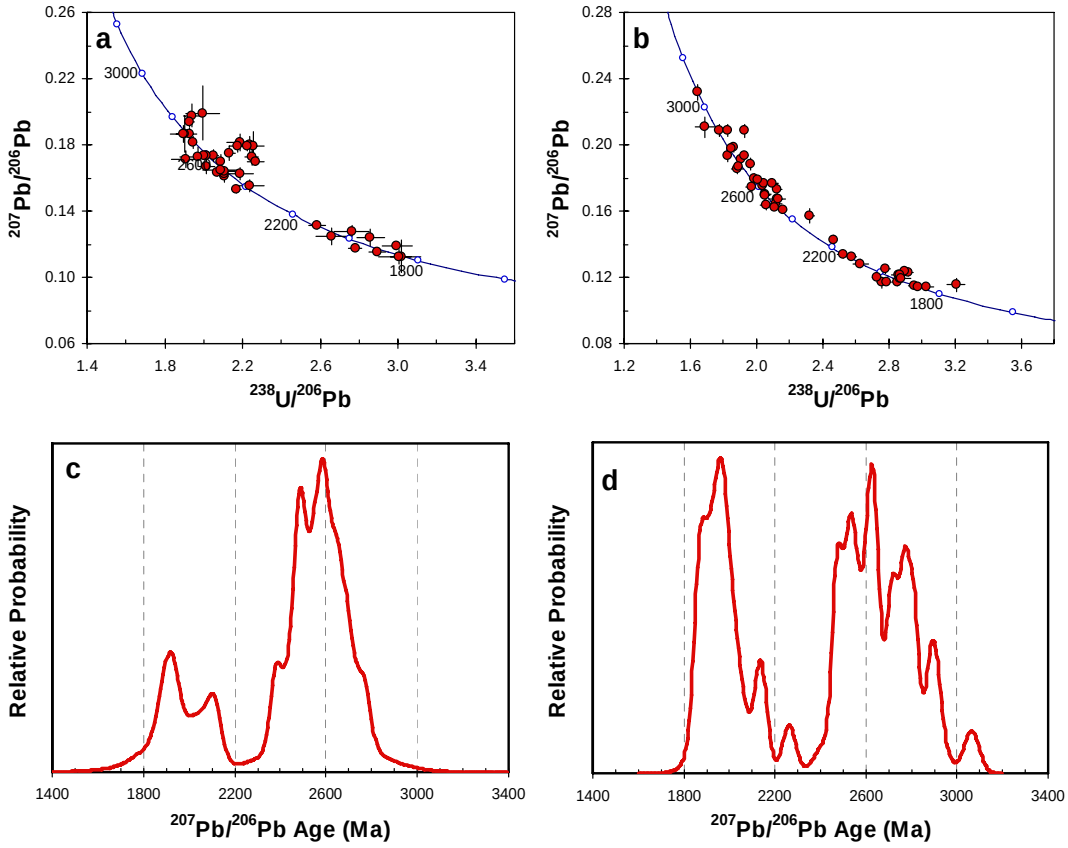


**Figure 4.14: Tera-Wasserburg U-Pb concordia diagrams for analyses from (a) sample 184, and (b) sample 255. Cumulative probability distribution diagrams for (c) sample 184, and (d) sample 255.**

## 4.6 EMPA monazite dating results

Metapelite samples from areas that experienced amphibolite facies metamorphism or higher were preferentially selected for in situ monazite analysis. Initial analysis of

monazite grains was conducted on three samples (samples 283, 288, and 308) in order to test the validity of the in situ method for the Etheridge Group metapelites, as well as give an initial estimation as to the metamorphic ages they record. Subsequent analyses were then conducted to expand on the age data collected from the initial analysis. Two samples (304 and 306) from the Robinhood area were also included to compare the EMPA monazite ages of this study to EMPA monazite ages reported by Cihan *et al*. (2006). A small percentage of analyses were discarded from subsequent age calculations based primarily on weight percent oxide totals, and low Pb abundances. Remaining analyses were then used to calculate weighted mean ages for each sample, and where appropriate for distinct age groups within each sample. Complete individual monazite analyses are listed in Appendix 2, and are summarised in Table 4.5. Weighted mean age calculations for each sample are summarised in Table 4.6.

### 4.6.1 Sample 283 (Einasleigh Metamorphics – Gum Flats)

Sample 283 is a strongly foliated mica schist from the Einasleigh Metamorphics south of Gum Flats (Fig. 4.1). It contains small 10-20 μm monazite grains that are in textural equilibrium with the surrounding $S_1$ metamorphic assemblage. 30 analyses were conducted on 14 grains, with the results forming a single distinct group in the corresponding cumulative probability diagram (Fig. 4.15a). Of the 30 analyses, 6 were discarded before final weighted mean age calculations due to low weight percent oxide totals (Appendix 2).

A single analysis returned a calculated age of 1626 ± 14 Ma (Table 4.5). This analysis is not associated with the dominant metamorphic events in the Etheridge Group which are believed to have occurred between ca. 1590 and 1550 Ma, and may instead reflect partial resetting of a detrital monazite. Omitting this analysis, and four younger analyses which do not form part of the prominent peak in the cumulative probability diagram (Fig. 4.15a), the remaining 20 analyses combine to give a weighted mean age of 1537 ± 18 Ma. The MSWD for this age is relatively high (5.1), suggesting that this group may incorporate more than one discrete age population. This age is within error of the crystallisation ages determined for granitoids of the Forsayth Batholith (ca. 1550 Ma), and may relate to this period of elevated heat-flow and associated metamorphism in the Etheridge Group.

| Grain | Spot | Pb (ppm) | Th (ppm) | U (ppm) | Age (Ma) | ± 1 σ |
|---|---|---|---|---|---|---|
| **Sample: 283 (Einasleigh Metamorphics - Gum Flats)** | | | | | | |
| 1 | 1 | 5089 | 52457 | 5260 | 1548 | 20 |
| 2 | 1 | 5408 | 49031 | 10206 | 1385 | 16 |
| | 2 | 6164 | 55394 | 8622 | 1549 | 17 |
| | 3 | 5875 | 53319 | 8356 | 1532 | 17 |
| 3 | 1 | 6696 | 52446 | 11549 | 1548 | 16 |
| | 2 | 4133 | 58526 | 2143 | 1363 | 21 |
| 4 | 1 | 4953 | 62293 | 2099 | 1539 | 21 |
| | 2 | 5309 | 55221 | 6287 | 1486 | 18 |
| | 3 | 5360 | 54667 | 6345 | 1505 | 19 |
| | 4 | 7895 | 75448 | 10935 | 1498 | 13 |
| 5 | 1 | 8175 | 67754 | 11373 | 1626 | 14 |
| 6 | 1 | 6602 | 80115 | 7828 | 1338 | 14 |
| 7 | 1 | 6855 | 55023 | 10766 | 1584 | 16 |
| 8 | 1 | 5508 | 49196 | 8128 | 1527 | 18 |
| 9 | 1 | 2632 | 27154 | 2613 | 1562 | 36 |
| 10 | 1 | 6552 | 67910 | 5932 | 1590 | 17 |
| 11 | 1 | 5525 | 64064 | 4109 | 1523 | 18 |
| | 2 | 5280 | 55377 | 5968 | 1496 | 18 |
| 12 | 1 | 5188 | 55882 | 5119 | 1518 | 19 |
| 13 | 1 | 5514 | 55818 | 6323 | 1526 | 18 |
| | 2 | 5732 | 56016 | 6533 | 1564 | 18 |
| 14 | 1 | 5075 | 65591 | 7819 | 1198 | 15 |
| | 2 | 9261 | 94275 | 10150 | 1538 | 12 |
| | 3 | 6858 | 59669 | 11177 | 1496 | 15 |
| **Sample: 288 (Daniel Creek Formation - Gum Flats)** | | | | | | |
| 1 | 1 | 8140 | 105243 | 1916 | 1573 | 14 |
| 2 | 1 | 2709 | 26435 | 2849 | 1599 | 36 |
| | 2 | 1714 | 16390 | 2316 | 1509 | 50 |
| 3 | 1 | 1550 | 15452 | 2901 | 1320 | 46 |
| | 2 | 6140 | 27852 | 18216 | 1444 | 15 |
| | 3 | 6860 | 29335 | 20195 | 1473 | 14 |
| Sample 288 cont. | | | | | | |
| 5 | 1 | 6803 | 94588 | 1630 | 1473 | 15 |
| 6 | 1 | 3429 | 38713 | 1871 | 1632 | 28 |
| | 2 | 5788 | 72701 | 1602 | 1598 | 18 |
| 7 | 1 | 2492 | 28301 | 2623 | 1441 | 32 |
| 8 | 1 | 5505 | 27473 | 16011 | 1423 | 15 |
| 9 | 1 | 1364 | 9089 | 2672 | 1581 | 59 |
| 10 | 1 | 3709 | 49496 | 2213 | 1409 | 22 |
| 11 | 1 | 4254 | 51922 | 2008 | 1560 | 22 |
| 12 | 1 | 6365 | 82547 | 2152 | 1530 | 16 |
| 13 | 1 | 8088 | 110927 | 1523 | 1509 | 13 |
| 14 | 1 | 522 | 15872 | 4164 | 397 | 28 |
| **Sample: 304 (Lane Creek Formation - Robinhood)** | | | | | | |
| 1 | 1 | 3971 | 31220 | 6550 | 1572 | 23 |
| | 2 | 4057 | 32294 | 7338 | 1506 | 22 |
| 2 | 1 | 4102 | 29297 | 7688 | 1563 | 23 |
| 3 | 1 | 4972 | 37710 | 8649 | 1567 | 19 |
| 4 | 1 | 4926 | 39491 | 8749 | 1512 | 19 |
| 5 | 1 | 4117 | 34547 | 7079 | 1495 | 21 |
| 6 | 1 | 1943 | 18665 | 3100 | 1426 | 39 |
| 7 | 1 | 5351 | 45922 | 7879 | 1563 | 18 |
| 8 | 1 | 2914 | 27393 | 4652 | 1444 | 28 |
| 9 | 1 | 4692 | 37574 | 8353 | 1511 | 19 |
| 10 | 1 | 4489 | 33782 | 8064 | 1553 | 21 |
| 11 | 1 | 4608 | 36840 | 8003 | 1527 | 20 |
| 12 | 1 | 3163 | 27057 | 4958 | 1532 | 28 |
| | 2 | 3158 | 25831 | 5121 | 1550 | 28 |
| 13 | 1 | 2183 | 20364 | 3857 | 1399 | 34 |
| 14 | 1 | 3563 | 36056 | 4546 | 1482 | 24 |
| 15 | 1 | 3840 | 37206 | 5295 | 1488 | 23 |
| 16 | 1 | 3738 | 38212 | 4426 | 1503 | 24 |
| 17 | 1 | 4187 | 33965 | 7453 | 1502 | 21 |

**Table 4.5: U-Th-Pb data and calculated ages for monazite analyses from metasedimentary samples analysed by EMP.**

| Grain | Spot | Pb (ppm) | Th (ppm) | U (ppm) | Age (Ma) | ± 1 σ |
|---|---|---|---|---|---|---|
| **Sample: 306 (Corbett Formation - Robinhood)** | | | | | | |
| 1 | 1 | 1637 | 30505 | 2088 | 958 | 28 |
| | 2 | 2475 | 25587 | 2619 | 1536 | 34 |
| 2 | 1 | 1725 | 12906 | 3266 | 1523 | 46 |
| | 2 | 1704 | 13030 | 3337 | 1486 | 45 |
| 3 | 1 | 2655 | 26010 | 3343 | 1518 | 32 |
| 4 | 1 | 2990 | 30989 | 4152 | 1424 | 27 |
| | 2 | 1821 | 15729 | 3111 | 1476 | 43 |
| | 3 | 2195 | 19423 | 3432 | 1505 | 37 |
| 5 | 1 | 3109 | 27168 | 4879 | 1513 | 28 |
| 6 | 1 | 3113 | 33429 | 3255 | 1501 | 28 |
| | 2 | 3095 | 33881 | 2950 | 1513 | 28 |
| **Sample: 308 (Daniel Creek Formation - Gum Flats)** | | | | | | |
| 1 | 1 | 5714 | 50089 | 9780 | 1464 | 17 |
| 2 | 1 | 14739 | 178379 | 8278 | 1537 | 9 |
| | 2 | 5695 | 44867 | 10331 | 1512 | 17 |
| 3 | 1 | 7716 | 66909 | 13572 | 1457 | 13 |
| 4 | 1 | 10056 | 69389 | 19957 | 1548 | 11 |
| | 2 | 7937 | 65681 | 13458 | 1515 | 13 |
| 5 | 1 | 2415 | 29820 | 1500 | 1492 | 36 |
| | 2 | 5587 | 80015 | 1686 | 1414 | 17 |
| 6 | 1 | 2545 | 36769 | 1182 | 1355 | 31 |
| 7 | 1 | 8575 | 69362 | 14992 | 1514 | 13 |
| **Sample: 324 (Einasleigh Metamorphics - Gum Flats)** | | | | | | |
| 1 | 1 | 5025 | 48698 | 6013 | 1551 | 19 |
| | 2 | 5062 | 46273 | 6874 | 1548 | 19 |
| 2 | 1 | 4099 | 40866 | 4302 | 1577 | 23 |
| | 2 | 3561 | 40152 | 3141 | 1505 | 25 |
| 3 | 1 | 5085 | 45301 | 7266 | 1546 | 19 |
| | 2 | 5130 | 43998 | 7470 | 1570 | 19 |
| | 3 | 5098 | 44104 | 7609 | 1549 | 19 |
| 4 | 1 | 4011 | 46564 | 2727 | 1544 | 23 |
| | 2 | 4966 | 44831 | 6923 | 1547 | 19 |
| | 3 | 3321 | 38455 | 2491 | 1522 | 27 |
| | 4 | 4759 | 43830 | 6451 | 1542 | 20 |
| 5 | 1 | 4174 | 46660 | 3369 | 1542 | 24 |
| | 2 | 3844 | 42677 | 3290 | 1532 | 25 |
| | 3 | 5092 | 48922 | 6402 | 1537 | 20 |
| | 4 | 5990 | 53494 | 7730 | 1595 | 18 |
| 6 | 1 | 4165 | 45763 | 3617 | 1539 | 24 |
| | 2 | 5355 | 46923 | 8558 | 1501 | 18 |
| 7 | 1 | 4035 | 36852 | 6064 | 1499 | 23 |
| | 2 | 3847 | 34123 | 5643 | 1536 | 25 |
| 8 | 1 | 4075 | 34996 | 6488 | 1520 | 23 |
| | 2 | 4262 | 37577 | 5864 | 1575 | 23 |
| | 3 | 4240 | 44369 | 4502 | 1522 | 23 |
| 9 | 1 | 4827 | 37444 | 7787 | 1597 | 21 |
| 10 | 1 | 4303 | 37460 | 6143 | 1567 | 23 |

**Table 4.5 cont.**

| Sample | Grains/Analyses | Age (Ma) | Error (95% C.I.) | MSWD | Prob. of Equivalence | Comment |
|---|---|---|---|---|---|---|
| 283 | 13/20 | 1537 | ± 18 | 5.1 | - | Metamorphic age ($M_2$) |
| 288 | 5/6 | 1585 | ± 18 | 1.06 | 0.38 | Metamorphic age ($M_1$) |
| 304 | 12/16 | 1527 | ± 16 | 2.0 | 0.012 | Metamorphic age ($M_2$?) |
| 306 | 6/10 | 1497 | ± 20 | 1.17 | 0.31 | Metamorphic age? |
| 308 | 4/6 | 1529 | ± 17 | 1.6 | 0.15 | Metamorphic age ($M_2$?) |
| 324 | 10/24 | 1546 | ± 11 | 1.6 | 0.038 | Metamorphic age ($M_2$) |

**Table 4.6: Summary of weighted mean ages calculated from EMPA monazite analyses in Table 4.5. All weighted mean ages calculated using *Isoplot* version 3.0 (Ludwig, 2003).**

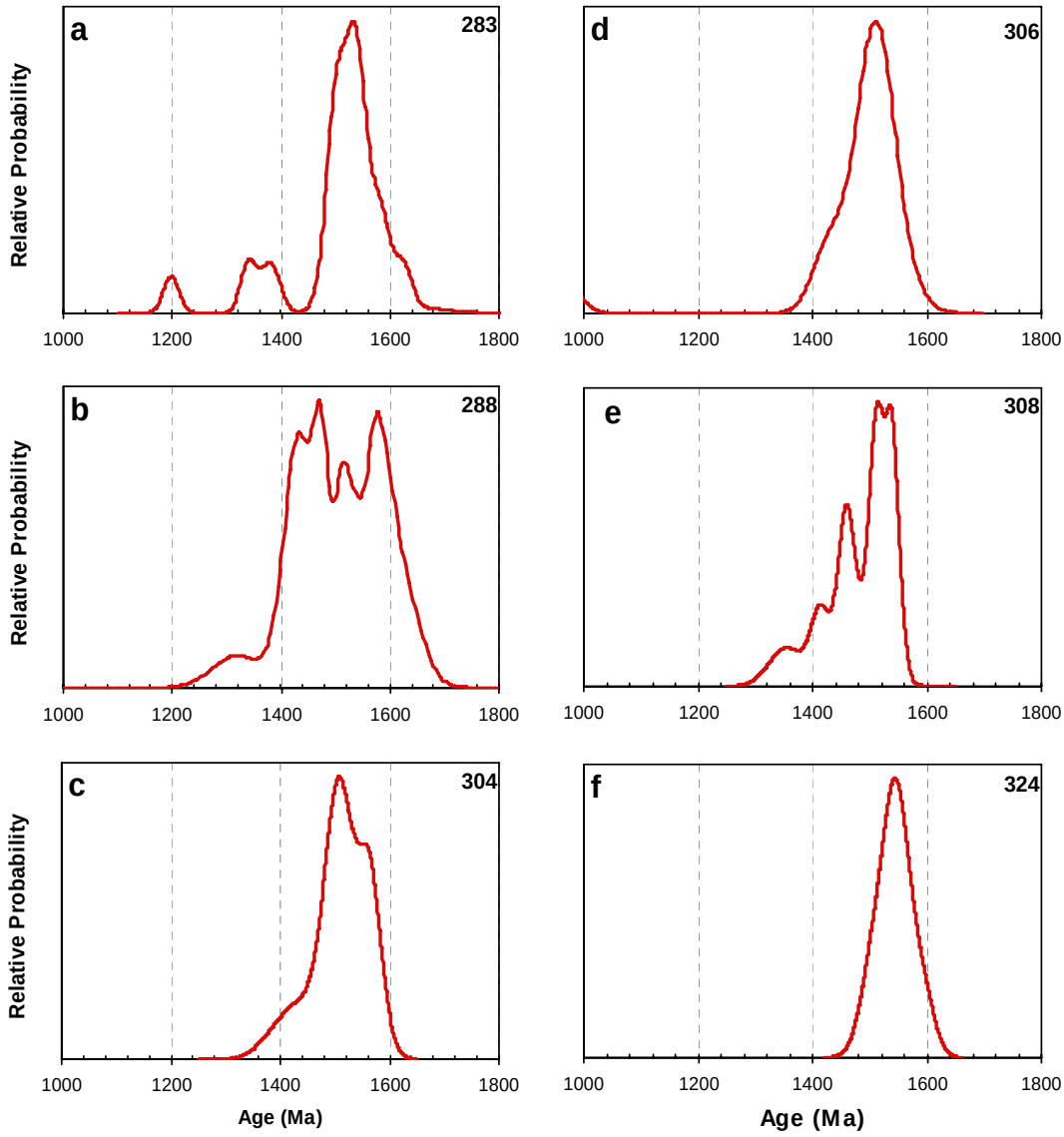


**Figure 4.15: Cumulative probability diagrams for U-Th-Pb monazite ages from (a) sample 283, (b) sample 288, (c) sample 304, (d) sample 306, (e) sample 308, and (f) sample 324.**

### 4.6.2 Sample 288 (Daniel Creek Formation – Gum Flats)

Sample 288, a muscovite-biotite mica schist from the Daniel Creek Formation near Gum Flats (Fig. 4.1), contains small irregularly shaped monazites that vary from 5 to 30 μm in size. All identifiable monazite grains in this sample lie parallel to the dominant $S_1$ fabric. A total of 31 analyses were conducted on 22 grains in this sample, with the analyses forming a broad double-peaked distribution on the cumulative probability diagram (Fig. 4.15b). Of the 31 analyses, 14 were discarded before final weighted mean age calculations due to low Th and total weight percent oxide values (Appendix 2).

When combined, the 17 remaining analyses do not form a statistically acceptable weighted mean age, suggesting that combined the analyses represent a spectrum of mixed ages. Therefore, to determine the pooled age of this sample, analyses were excluded until a statistically acceptable age was obtained. Using this method, the analyses that returned the six oldest ages (on five grains) combined to give a statistically valid weighted mean age of 1585 ± 18 Ma (MSWD = 1.06). This group includes one analysis of 1632 ± 28 Ma which may relate to an earlier stage of monazite growth, but importantly places an upper limit on the onset of metamorphism in this sample. The remaining analyses combine for a weighted mean age of 1472 ± 31 Ma. However, the MSWD for this pooled age is relatively high (5.7). This suggests that either more than one discrete age population is included in this sample, or that at least some monazites were affected by some Pb-loss at a later date.

The ca. 1585 Ma age is of regional significance, as it not only correlates with recent estimates for the age of medium-pressure/temperature metamorphism ($M_1$) and orogenesis in the Etheridge Group (Black *et al*., 2005; Cihan *et al*., 2006), but is also coeval with the age of regional-scale orogenesis and peak metamorphism in the Mt Isa Eastern Succession (Page & Sun, 1998). However, the ca. 1585 Ma age presented here must be treated with some caution, as it is based on a limited dataset. Consequently, it is considered to represent a maximum estimate for $M_1$.

### 4.6.3 Sample 304 (Lane Creek Formation – Robinhood)

Sample 304 is a muscovite-biotite mica schist from the Lane Creek Formation near Robinhood (Fig. 4.1). BSE images reveal that the sample contains small irregularly

shaped monazites which vary from 5 to 30 μm in size (Fig. 4.16a). In total, 27 analyses were conducted on 23 grains, with the analyses forming one large double-peaked population with a broad younger shoulder on the cumulative probability diagram (Fig. 4.15c). Eight of the 27 analyses were discarded before final weighted mean age calculations due to low weight percent oxide totals and low Th (Appendix 2).

The 16 oldest analyses form the dominant age population in Figure 4.15c. They combine to give a weighted mean age of 1527 ± 16 Ma (MSWD = 2.0), which is within error of the metamorphic age calculated for sample 283 (Table 4.6). However, the relatively high MSWD suggests that this age may contain a mix of ca. 1550 Ma and ca. 1500 Ma monazites. This hypothesis is further demonstrated by discarding the oldest six analyses from this group, which improves the calculated weighted mean age to 1500 ± 13 Ma (MSWD = 1.16). Regardless, the 1527 ± 16 Ma metamorphic age is preferred as it includes all analyses that lie within the dominant peak of the probability diagram for this sample.

### 4.6.4 Sample 306 (Corbett Formation – Robinhood)

Sample 306 is a muscovite-biotite-garnet-staurolite schist belonging to the Corbett Formation in the Robinhood area (Fig. 4.1). Monazites in this sample are irregularly shaped but are generally elongated, varying from 10 to 30 μm in width, and up to 150 μm in length (Fig. 4.16b). Elongated monazite grains are aligned in the dominant $S_3$ fabric. In total, 13 analyses were conducted on 8 grains; however 2 analyses were discarded before final weighted mean age calculations due to low weight percent oxide totals and high K values that suggest chemical alteration has occurred (Appendix 2). The remaining 11 analyses form a single peak with a minor young shoulder on the cumulative probability diagram (Fig. 4.15d).

Of the remaining 11 analyses, 10 combine to give a weighted mean age of 1497 ± 20 Ma (MSWD = 1.17, probability of equivalence = 0.31), which is the most statistically acceptable estimate that can be produced from the available data. This age is too young to be linked to the period of granitoid emplacement and associated metamorphism that occurred around ca. 1550 Ma in the lower Etheridge Group. However, monazite analyses returning similar ages were identified in two

metasedimentary samples collected approximately 10 km north of sample 306 by Cihan *et al*. (2006), which they attributed to a thermal pulse or hydrothermal activity occurring after or during the late stages of the ca. 1550 Ma event. It is possible then that the weighted mean age is representative of this event; however the dominant foliation (N-S trend) is consistent with a later stage of folding in the area ($F_3$ of Cihan *et al*., 2006).

A single analysis returned a calculated age of 958 ± 28 Ma (Table 4.5). This age is anomalous, as the analysis of another part of the same grain returned an age of 1536 ± 34 Ma (Table 4.5). It is possible that this grain experienced some Pb-loss, as reflected by the younger calculated age for part of the grain.

### 4.6.5 Sample 308 (Daniel Creek Formation – Gum Flats)

Sample 308 is a strongly foliated, fine-grained mica schist from the Daniel Creek Formation at Gum Flats (Fig. 4.1). As with the other monazite-dating samples described above it contains small, irregularly shaped grains of monazite that are generally less than 15 μm wide. In this sample, 10 analyses on 7 grains were attempted (Table 4.5). Unfortunately, the majority of analyses from this sample show some signs of alteration, with all but three analyses containing a combination of K > 0.02 wt%, P > 13.00 wt%, and weight percent oxide totals of less than 97 (Appendix 2). In addition broad younger shoulders on the cumulative probability diagram suggest Pb-loss may have affected a number of analyses (Fig. 4.15e).

Despite these limitations, the calculated ages are consistent with ages obtained from other samples, and are therefore retained for the weighted mean age calculations. Of the 10 analyses attempted, the four youngest ages were omitted until a statistically acceptable group of six analyses was formed. The six analyses are spread over four grains, and combine to give a weighted mean age of 1529 ± 17 (MSWD = 1.6). This age is within error of ages obtained from samples 304 and 283, and may therefore relate to the late stages of the high-temperature $M_2$ event at ca. 1550 Ma. The remaining four analyses are distributed over a large range from ca. 1500 Ma to ca. 1300 Ma corresponding to the broad younger shoulder of the cumulative probability diagram (Fig. 4.15e), and do not form a statistically acceptable group.

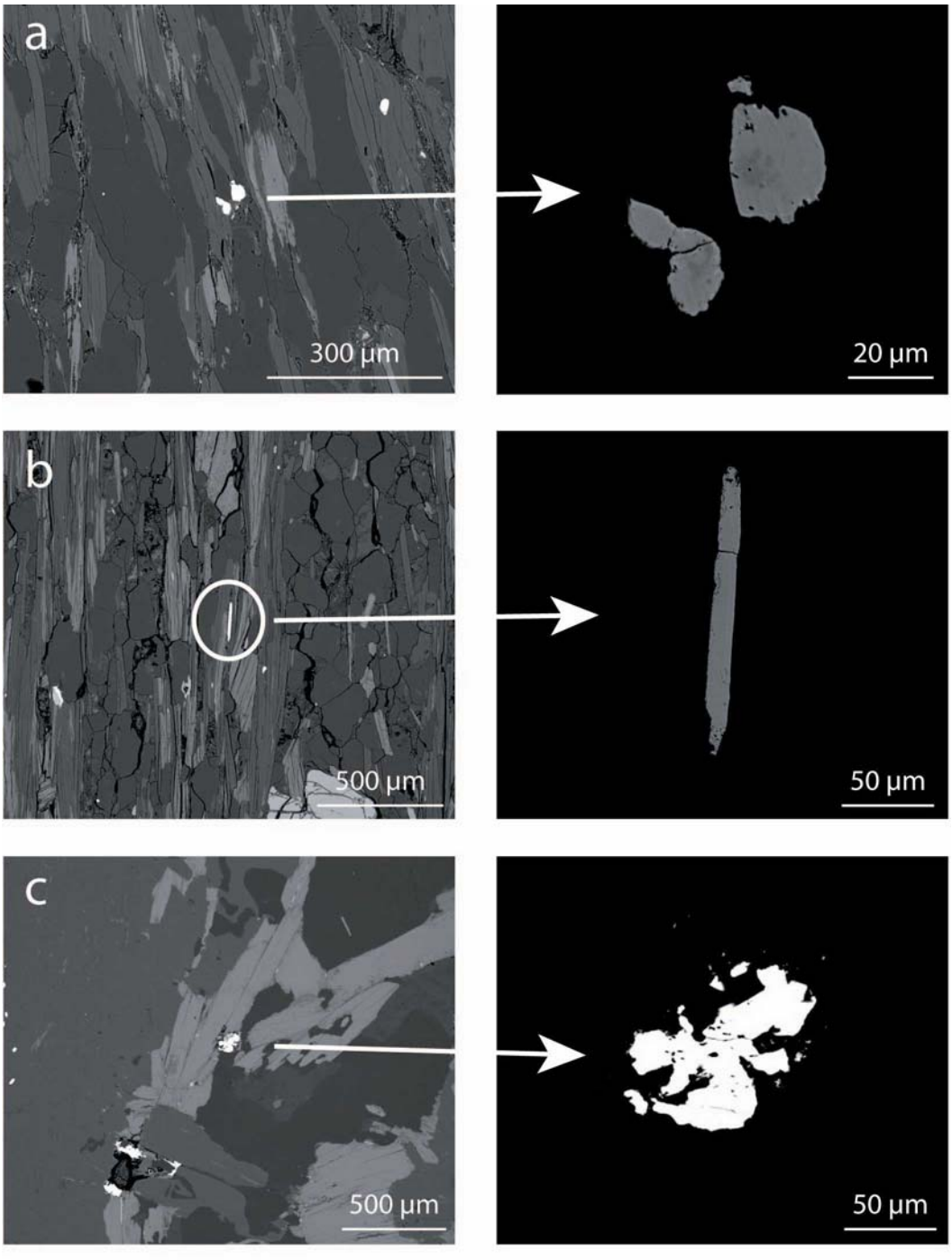


**Figure 4.16: Backscattered electron (BSE) images of monazite grains and their textural settings for (a) sample 304, (b) sample 306, and (c) sample 324.**

### 4.6.6 Sample 324 (Einasleigh Metamorphics – Gum Flats)

Sample 324, a coarse-grained muscovite-biotite mica schist from the Einasleigh Metamorphics north of Gum Flats (Fig. 4.1), contains moderately sized irregularly shaped monazites varying from 20 to 50 µm in width. All analysed monazite grains in

this sample show corroded margins (Fig.4.16c); however, for the most part their chemistry remains largely unaffected. Some 27 analyses were conducted on 11 grains, with the analyses combining to form a single, symmetric peak on the cumulative probability diagram (Fig. 4.15f). Of the 27 analyses, 3 were discarded before final weighted mean age calculations, due to low weight percent oxide totals, and high K values (Appendix 2).

The 24 acceptable analyses combine to give a weighted mean age of 1546 ± 11 Ma (MSWD = 1.6). This value is consistent with the established age for the high-temperature metamorphic event at ca. 1550 Ma ($M_2$) that is also associated with significant felsic magmatism in the lower Etheridge Group (Black & McCulloch, 1990; Black & Withnall, 1993).

## 4.7 Discussion

### 4.7.1 Significance of a younger (ca. 1500 Ma) age population recorded in the metamorphic monazites of the lower Etheridge Group

The occurrence of a distinct monazite age population at ca. 1500 Ma in sample 306, coupled with mixed age populations occurring in other samples, may suggest that a relatively weak metamorphic or hydrothermal event occurred at this time. Little geochronological evidence concerning the presence of a metamorphic event around ca. 1500 Ma has been uncovered in previous studies of the Etheridge Group. Black *et al*. (1979) presented Rb-Sr total rock isochron data that dated $M_2$ in the Etheridge Group to 1469 ± 20 Ma. However, subsequent U-Pb zircon dating (e.g. Black & Withnall, 1993) suggested that this age is probably related to cooling and may not have geological significance. Black *et al*. (2005) presented U-Pb zircon data from leucogneiss of the Einasleigh Metamorphics that gave metamorphic zircon ages ranging from 1560-1550 Ma to as low as 1500 Ma. The cause of these relatively young zircon ages in their study was not considered to be diagnostic of a younger (ca. 1500 Ma) event, but rather was attributed to the incomplete isotopic resetting of the zircons by partial recrystallization (Hoskin & Black, 2000).

The ca. 1500 Ma monazite age recorded in mica schist from the Corbett Formation (sample 306), and in mixed age populations containing ca. 1500 Ma analyses (samples 283 and 288; Table 4.5) has also been identified previously through

individual monazite ages in metasediments from the Robertson River Subgroup near Robinhood (Cihan *et al*., 2006). The possible regional extent of this age suggests that a thermal pulse or foliation forming event may have affected the lower Etheridge Group at this time. However, this event has a limited spatial distribution and is not chronologically related to any dated intrusive body. Consequently, the existence and significance of this event await clarification by future work.

Significantly, similar activity is recorded in other Proterozoic basins in northern Australia, including the Mt Isa Eastern Succession. In this region, younger plutons of the Williams and Naraku Batholiths are associated with major regional metasomatism and record U-Pb zircon ages ranging from ca. 1510 to 1490 Ma (Page & Sun, 1998; Wyborn, 1998). The prevalence of the ca. 1510-1490 Ma igneous and/or metamorphic ages in the Mt Isa Inlier and its existence in the Georgetown Inlier, suggests that a thermal event of regional significance occurred at this time, producing I-type granitoids in the Mt Isa Eastern Succession, but only crystallising or recrystallising monazites and developing a localised N-S trending structural fabric in the metasediments of the lower Etheridge Group in the Georgetown Inlier.

In summary, the majority of metamorphic monazites analysed in this study lie within the dominant $S_1$ foliation, which is observable throughout the lower Etheridge Group in the central region of the Georgetown Inlier. The monazites record a single ca. 1540 Ma event that would appear to be related to $S_1$ in some samples (e.g. samples 283 and 288 were sampled far from granitoids), or is perhaps younger than $S_1$ as indicated by the lack of aligned monazite grains in other samples (e.g. samples 304, 308, and 324: all sampled near granitoids suggesting late heating). Based on this evidence, I prefer the interpretation that the monazites recrystallised as a result of later heating associated with $M_2$ and the emplacement of the Forsayth Batholith at ca. 1550 Ma, as they do not appear to be associated with a distinct post-$S_1$ foliation. A localised foliation-forming event ($D_3$) is also proposed for the ca. 1500 Ma monazites. The implications of these results are discussed further in Chapter 5.

### 4.7.2 Significance of detrital zircon populations in metasedimentary samples, and comparison to other Proterozoic terranes of northeastern Australia

The age distributions of detrital zircon populations in metasediments of the Etheridge Group have previously been reported by Black & McCulloch (1990), Black & Withnall (1993), and Black *et al*. (2005). The inheritance patterns in samples 184, 255, and 264 presented here provide a useful comparison to these published detrital zircon populations, as well as to the inheritance patterns observed in the metasediments of other Palaeoproterozoic basins in eastern Australia. These broad similarities are discussed in more detail below.

Leucogneiss from the Einasleigh Metamorphics north of Gum Flats analysed by Black *et al*. (2005) contained inherited zircons that these authors suggested were most likely derived from a number of sedimentary protoliths. They defined a maximum age limit of ca. 1700 Ma for the leucogneiss and its equivalents, based on the presence of substantial detrital populations at ca. 1700 Ma in some samples of leucogneiss. Four samples from their study contained inherited zircon populations that have some similarities to the inheritance patterns of the Daniel Creek Formation samples (Fig 4.17). Three leucogneiss samples contained no ages younger than 1700 Ma, and their detrital patterns were thought to reflect the contribution of many different source terranes. The remaining sample contained a significant concentration of younger ages which they related to at least three episodes of crystallisation and recrystallization between 1570 and 1500 Ma. The most obvious similarities between the two lithologies are the presence of a major ca. 2600 Ma component and ca. 1800-2000 Ma component, coupled with the relative lack of ages between 2000 and 2400 Ma in three samples (Fig 4.17). The similarity in the inheritance patterns between the Daniel Creek Formation samples of this study and the Einasleigh Metamorphics leucogneiss of Black *et al*. (2005) indicates that both lithologies have shared a similar provenance.

Inherited zircons were also reported in samples of Proterozoic granite from the Georgetown Inlier by Black & McCulloch (1990) and Black & Withnall (1993). As with the metasedimentary samples, the inherited zircons present a similar age distribution. Demonstrating this relationship is a sample of the Lighthouse Granite analysed by Black & Withnall (1993), which contains a number of inherited grains forming a similar inheritance pattern to that of sample 264, a sample of Dead Horse Metabasalt amphibolite (Fig. 4.18). The authors suggested that their inheritance

patterns reflected the input of material from numerous sources into the source magma of the Lighthouse Granite. This hypothesis may also account for the pattern observed in sample 264, indicating the passage of mafic magmas though similar sedimentary rocks.

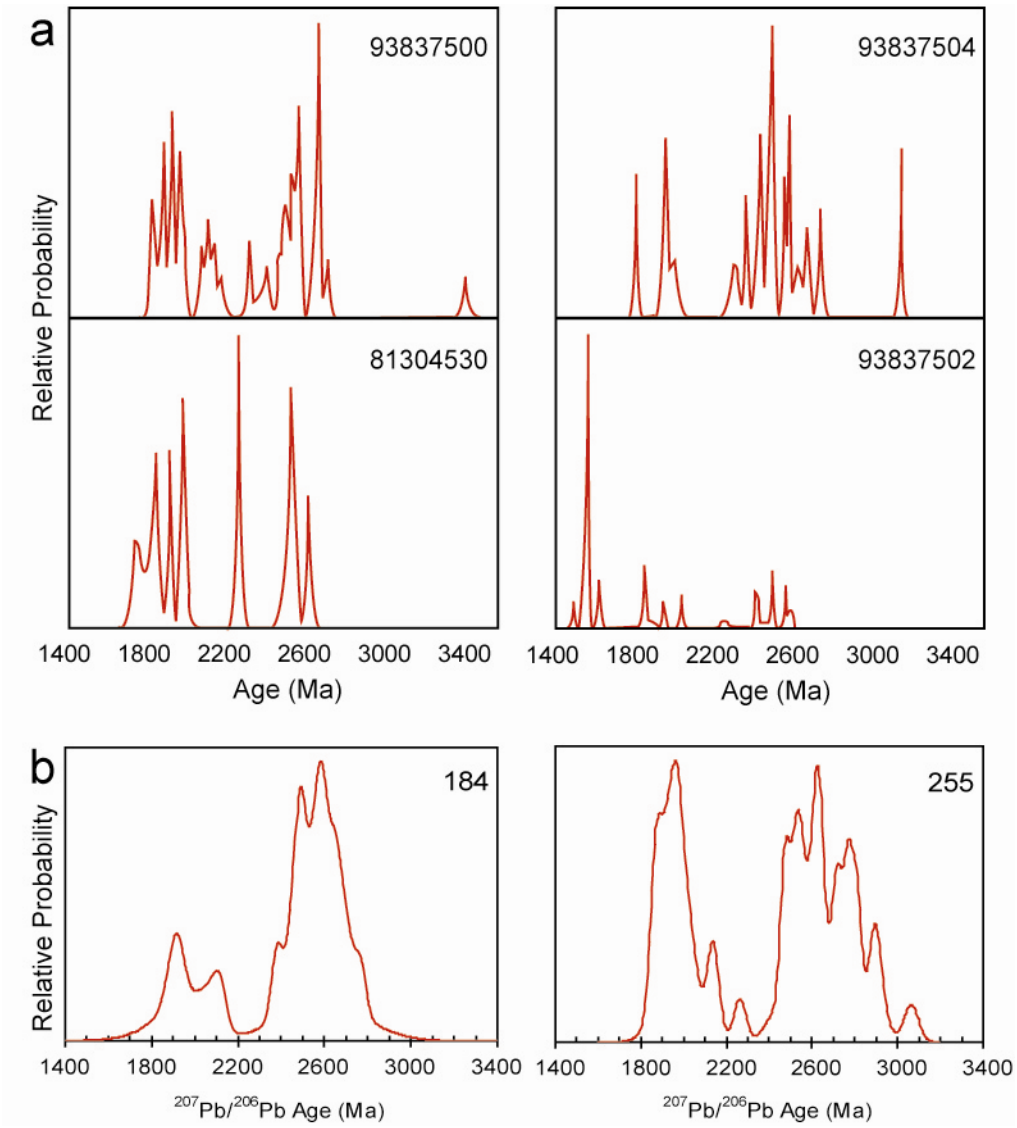


**Figure 4.17: (a) Cumulative probability diagrams for four leucogneiss samples from the Einasleigh Metamorphics (after Black *et al.*, 2005). Also shown for comparison in (b) are detrital zircon age data for Daniel Creek Formation samples 184 and 255 (this study).**

An alternative hypothesis that may account for the detrital populations between 2500 and 2000 Ma is that the inherited grains were sourced from now unexposed late-Archaean/early-Proterozoic basement rocks underlying the Etheridge Group, similar to that proposed for inherited populations in the Mt Isa Eastern Succession (Giles & Nutman, 2003). This would account for the regional extent of the ca. 2500-2000 Ma ages that have been obtained from the U-Pb zircon studies of numerous lithologies

across the region (e.g. Black & McCulloch, 1990; Black & Withnall, 1993; Black *et al*., 2005; and this study).

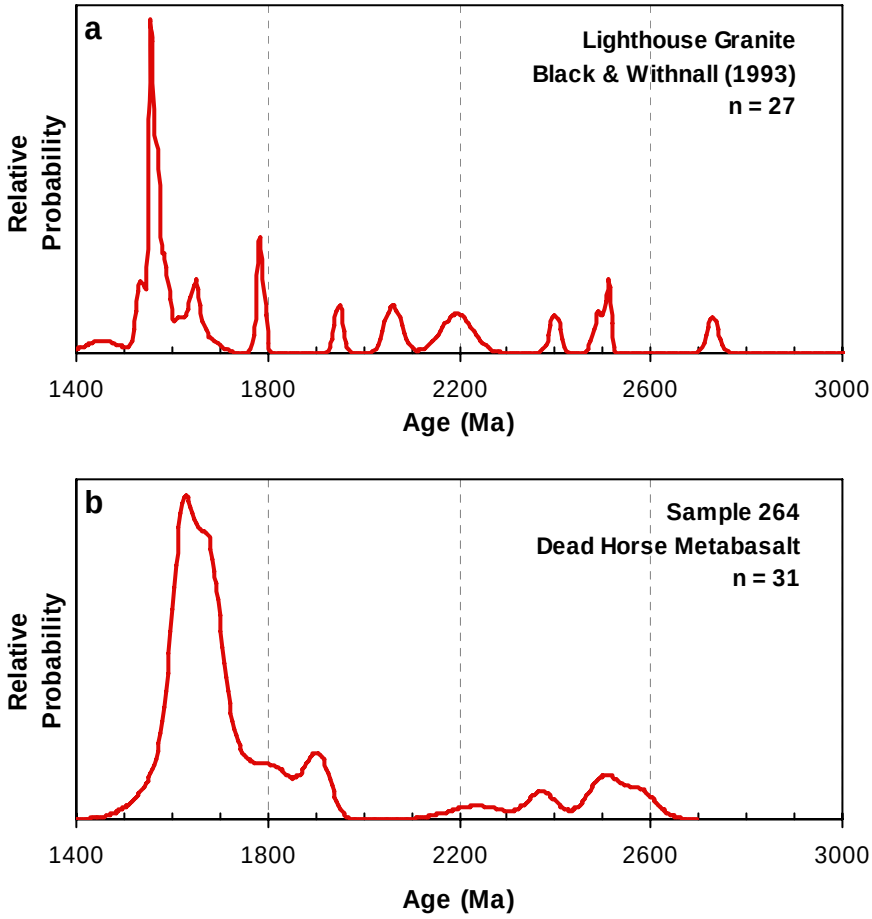


**Figure 4.18: Comparison of cumulative probability diagrams for (a) a sample of the Lighthouse Granite (Black & Withnall, 1993) and (b) sample 264 from the Dead Horse Metabasalt (this study).**

The inheritance patterns of the Etheridge Group metasediments share a number of traits common to rocks of both the Broken Hill Group and Mt Isa Eastern Succession, including: (i) a significant late-Archaean to earliest Palaeoproterozoic component (ca. 3100-2500 Ma); (ii) an absent or relatively insignificant early Palaeoproterozoic component (ca. 2400-2100 Ma); and (iii) a significant mid-Palaeoproterozoic component (ca. 2100-1800 Ma). In the Broken Hill Group of the Willyama Inlier (Willis *et al*., 1983) the spectrum of inheritance patterns listed above has been recognised in numerous samples of metasedimentary and gneissic rocks, including lithologies associated with and hosting the Pb-Zn-Ag orebody at Broken Hill (Fig. 4.19; Page & Laing, 1992; Raetz *et al*., 2002; Page *et al*., 2005a). However, the absence in the Daniel Creek Formation of the ca. 1800-1700 Ma detrital population

present in both the Broken Hill Group and Mt Isa Eastern Succession (Fig. 4.19 and 4.20 respectively), may also have important implications for the prospectivity of the Etheridge Group. In particular, that the Dead Horse Metabasalt-Daniel Creek Formation horizon within the Etheridge Group did not share the same provenance as the otherwise lithologically similar terranes further west.

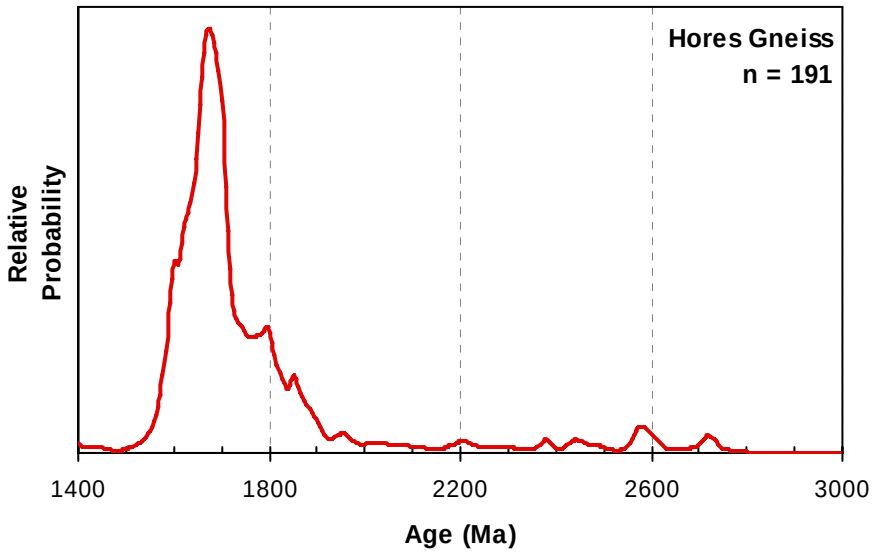


**Figure 4.19: Compilation of U-Pb SHRIMP detrital zircon analyses for four samples of the Hores Gneiss in the Broken Hill Group (Page & Laing, 1992). The dominant peak at ca. 1680 Ma represents the inferred crystallisation age of the host rock.**

The metasediments of the Broken Hill Group were also found to contain a large abundance of detrital zircons aged between ca. 1870 and 1780 Ma (Page *et al*., 2005a). These zircons were thought to have been sourced from terranes adjacent to the Willyama Inlier that contained rocks formed during the Barramundi Orogeny (ca. 1870-1850 Ma; Scott *et al*., 2000; Page *et al*., 2005a), and between ca. 1820 and 1780 Ma (Page *et al*., 2005a). As with the metasediments of the Etheridge Group, the late-Archaean component present in the metasediments of the Broken Hill Group has been attributed to incorporation of detrital zircons from unexposed basement material into the metasediments (Page *et al*., 2005b).

The analysis of metasedimentary and meta-igneous rocks from the Mt Isa Eastern Succession by Page & Sun (1998) and Giles & Nutman (2003) revealed detrital zircon age populations consistent with the inheritance patterns described above (Fig 4.20). In both cases their analyses showed broad similarities across the length of the terrane, as well as correlations with the detrital populations in metasediments from the rest of the

Mt Isa Inlier (Scott *et al*., 2000). In particular, Giles & Nutman (2003) described two significant detrital populations occurring at ca. 2600-2300 Ma and ca. 1750-1720 Ma (Fig. 4.20). The older population of detrital ages overlaps with and may relate to the population thought to represent late-Archaean basement inheritance in both the Etheridge Group and Broken Hill Group. The younger detrital population is believed to have originated locally, as metasedimentary and magmatic rocks of ca. 1780-1720 Ma age are widely exposed in the Kalkadoon-Leichhardt Belt further west (Giles & Nutman, 2003). The absence of a detrital population at ca. 2000 Ma is significant, as this peak is present in the metasediments of the Etheridge Group. However, its absence could be accounted for if the source for this population was localised to the Etheridge Group, in a similar way to the localised sourcing of Barramundi-age material into the Willyama Inlier and Mt Isa Eastern Succession.

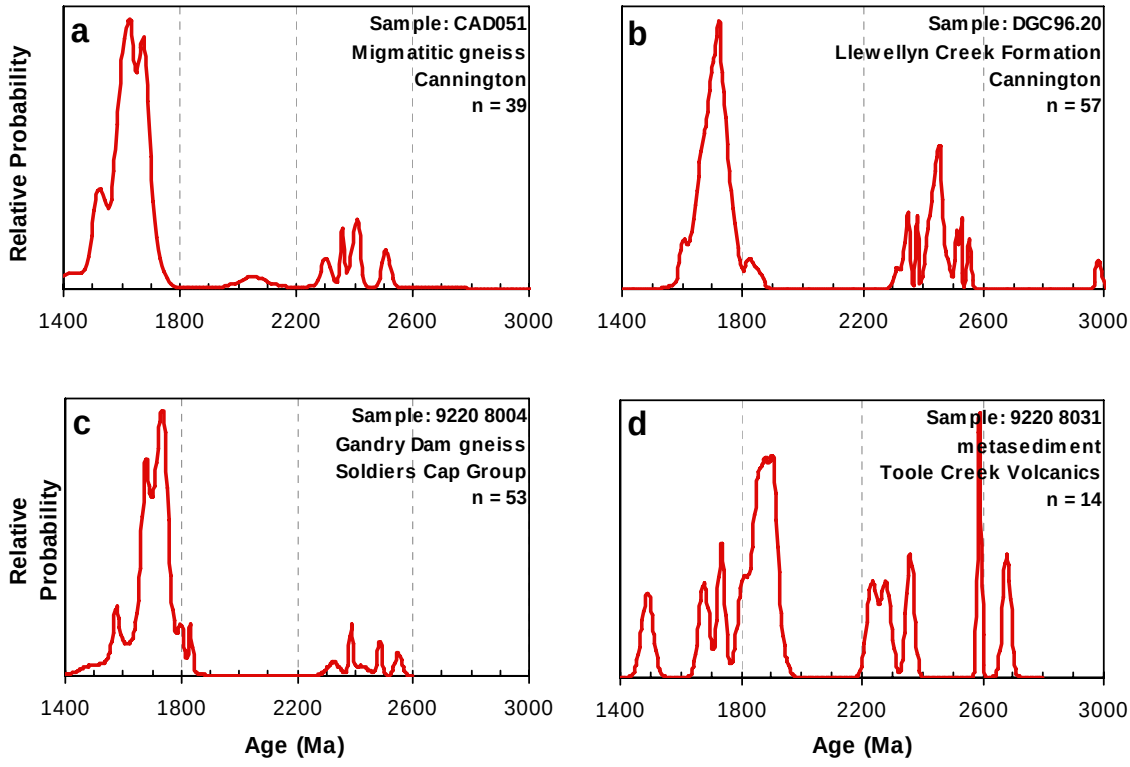


**Figure 4.20: Cumulative probability diagrams for selected metasedimentary samples from the Mt Isa Eastern Succession. Data sources: (a) and (b) Giles & Nutman (2003), (c) and (d) Page & Sun (1998).**

From the overview of inheritance patterns in the Palaeoproterozoic terranes of northeastern Australia outlined above, it is clear that a small but significant component that occurs throughout is the detrital population of late-Archaean age (between 3000 and 2500 Ma). This component has been inferred to represent the

addition of material from unexposed or eroded Archaean rocks that were basement to the Palaeoproterozoic terranes. A similar inheritance pattern was identified in the Belt Supergroup of western USA and southern Canada by Blewett *et al*. (1998), and may have important implications for reconstructions of the Rodinia supercontinent involving north Queensland (e.g. Ross *et al*., 1992; Brookfield, 1993). The presence of this Archaean component throughout the Proterozoic basins of northeastern Australia, including the Georgetown Inlier, indicates that these terranes may have shared a common Archaean basement, and would therefore all lie within the Proterozoic framework of the North Australian Craton.

## 4.8 Conclusions

### 4.8.1 Magmatic history of the lower Etheridge Group

New igneous zircon ages obtained from mafic rocks of the lower Etheridge Group, combined with previously reported data, provide important geochronological constraints on the early depositional and magmatic history of the Georgetown Inlier. The mafic rocks were emplaced in at least two discrete pulses, with the most significant period of emplacement related to the eruption of the Dead Horse Metabasalt member and associated doleritic sills at ca. 1670 Ma.

The ca. 1670 Ma crystallisation and emplacement age of the Dead Horse Metabasalt and related Cobbold Metadolerite intrusions is based on the combination of pooled zircon ages in four samples (Samples 264, 299, 300, and 318). This age is of regional significance, as it closely resembles established ages for similar Fe-rich tholeiitic intrusive units in the Mt Isa Eastern Succession (Toole Creek Volcanics, 1658 ± 8 Ma; Page & Sun, 1998) and felsic volcanics spatially and temporally associated with Fe-rich tholeiitic rocks in the Broken Hill Group (Hores Gneiss, 1685 ± 3 Ma; Page *et al*., 2005a). The significance of the association between these mafic units is discussed in more detail in subsequent chapters. Mafic magmatism in the Etheridge Group may have continued until ca. 1620 Ma, although evidence for this younger age is less robust than for the main ca. 1670 Ma event. Subsequent magmatic activity in the Palaeoproterozoic was limited to the intrusion of felsic granitoids associated with the Forsayth Batholith at ca. 1550 Ma.

The oldest mafic rocks found in the basin crystallised at about 1715 Ma (1713 ± 32 Ma and 1719 ± 27 Ma). They were closely followed by volcanism recorded in zircons of a leucogneiss from the Einasleigh Metamorphics at 1705 Ma (Black *et al*., 2005). Alternatively, these zircons may have been derived from the same juvenile volcanic source that provided zircons to the sedimentary precursor of the leucogneiss dated by Black *et al*. (2005). However, the tight grouping of isotopic ages for these clearly igneous zircons suggests they are unlikely to be inherited.

Late-stage felsic differentiates in two Cobbold Metadolerite sills yielded ages of ca. 1640 Ma. A late-stage felsic differentiate in a dolerite sill also crystallised at 1630 Ma and may form the last stage of this cycle of magmatism. The range of ages suggests a period of mafic magmatism spanning roughly 80 million years. It is not clear if this was a continuous event or was made up of a number of magmatic pulses of activity, however based on the distribution of pooled ages and the stratigraphic distribution of the mafic rocks the latter is most likely. The reported ages strongly support the inclusion of the lower Etheridge Group with the Calvert Superbasin (ca. 1730-1670 Ma) (Betts & Giles 2006). The ca. 1670 Ma Dead Horse Metabasalt may reflect the rejuvenation of the basin at the start of the Isa Superbasin cycle.

Isotopic zircon ages calculated for samples of the Mt Hogan and Digger Creek Granites yielded ages of 1565 ± 46 Ma and 1539 ± 16 Ma respectively. These ages are consistent with the established ages for both granites (Black & McCulloch, 1990; Black & Withnall, 1993), and place them within the timeframe of the emplacement of the regionally extensive Forsayth Batholith, and the associated low-pressure thermal event ($M_2$).

Inherited zircons were found in one mafic sample, revealing the presence of two significant age populations which may have been derived from adjacent metasedimentary rocks. The inherited sources include Barramundi-aged material (ca. 1800-1900 Ma) and a late Archaean-earliest Proterozoic component (ca. 2600 Ma). These provenance ages are of regional significance, as they are also found in metasediments from both the Etheridge Group and other Proterozoic basins of eastern Australia. No zircons were found that were coeval with deposition implying a very low component of volcanic activity during deposition of the Daniels Creek Formation.

### 4.8.2 Metamorphic history of the lower Etheridge Group

In the metapelites of the lower Etheridge Group, metamorphic monazite grew in response to a number of relatively distinct metamorphic and/or thermal events. A possible later stage of monazite growth was minor in comparison, and does not appear to be associated with a metamorphic fabric. There is little evidence for crystallisation of metamorphic monazite at ca. 1585 Ma, the previously proposed age for $D_1$ in these rocks. Only one sample analysed had a significant monazite population at this age and that sample also contained a much larger population of a younger age. The ca. 1585 Ma age is of regional importance, as it approximates the age of similar medium pressure-temperature metamorphism in the Mt Isa Eastern Succession and Broken Hill Block that occurred between ca. 1600 and 1580 Ma (Page & Sun, 1998; Page *et al*., 2005a; Cihan *et al*., 2006; Sayab, 2006). However, more work is required to constrain the age of this event in the lower Etheridge Group.

The majority of samples analysed in this study contain monazite formed at ca. 1530 Ma (1546 ± 11 Ma, 1537 ± 18 Ma, 1529 ± 17 Ma, and 1527 ± 16 Ma). These ages lie within error of the published ca. 1550 Ma age of high-temperature, low-pressure metamorphism ($M_2$) which is associated with the intrusion of voluminous granitoids throughout the lower Etheridge Group. Consequently they may represent crystallisation ages associated with this event. In some samples this age is related to monazite that is younger than $S_1$ but in at least two samples the monazites are aligned in the local $S_1$ and appear to be related to the earliest foliation in the area.

The results of this study, and to a lesser extent in Cihan *et al*. (2006), suggest a discrete younger event ($D_3$) dated by monazite at ca. 1500 Ma based on observed structural relationships in a small area west of Robinhood Station. The occurrence of this age may relate to the intrusion of a granitic body younger than the ca. 1550 Ma Forsayth Batholith, but this hypothesis remains to be tested. The ca. 1500 Ma age is coeval with granitoid magmatism in the Mt Isa Eastern Succession at ca. 1510-1500 Ma (Page & Sun, 1998), and may suggest a further link in the post-depositional histories of the two terranes.

### 4.8.3 The timing of deposition, and provenance ages in the lower Etheridge Group: implications for the regional tectonic history of the Georgetown Inlier

Based on the combination of new igneous and detrital zircon ages, and metamorphic monazite ages from a number of sources, the timing and duration of sediment deposition, and major periods of magmatism and metamorphism in the Etheridge Group can be identified. Deposition of the earliest sedimentary units had commenced by ca. 1715 Ma. At ca. 1670 Ma, significant volumes of tholeiitic mafic magmas were intruded into, and erupted onto the existing sedimentary package in response to continued or reinvigorated rifting. The tholeiitic magmatism continued as a probable series of discrete pulses until ca. 1630 Ma. The ca. 1670 Ma age of peak tholeiitic magmatism in the lower Etheridge Group is also broadly temporally equivalent to similar episodes of tholeiitic magmatism in the Mt Isa Eastern Succession and Broken Hill Group, which may suggest a regional correlation between the terranes at this time.

Regional-scale orogenesis involving the lower Etheridge Group is generally regarded to have reached its peak ($M_1$) at ca. 1580 Ma, coeval with medium pressure/temperature metamorphism in the Mt Isa Eastern Succession. However this was not the most common metamorphic age detected in this study. In response to the orogenesis and associated crustal thickening, voluminous S-type granitoids were emplaced at ca. 1550 Ma, forming a part of the regionally extensive Forsayth Batholith. The majority of crystallisation ages from monazites found in this study were between ca. 1550 and ca. 1525 Ma, and correlate with the period of high-temperature thermal metamorphism ($M_2$) reported previously. Later periods of elevated heat flow led to the development of monazites at ca. 1500 Ma, and appear restricted to west of Robinhood Station.

Detrital zircon populations in metasedimentary and mafic rocks of the lower Etheridge Group define a number of provenance ages, including two significant groups at ca. 2700-2500 Ma and ca. 2000-1800 Ma. Detrital patterns similar to those observed in the Etheridge Group metasediments are also found in metasedimentary rocks from the Mt Isa Eastern Succession and Broken Hill Group, and suggest that these sedimentary units had a similar provenance. The similarity in these provenance ages, coupled with the similar age for major periods of tholeiitic magmatism and

metamorphism across the Georgetown Inlier, Mt Isa Eastern Succession, and Broken Hill Group suggest that all three terranes were proximal to one another, and most likely shared a similar tectonic history from ca. 1700 to 1500 Ma. This implies that the Georgetown Inlier was a part of the North Australian Craton during the Palaeoproterozoic.

# Chapter 5.

# Thermobarometric conditions of early- to mid-Proterozoic metamorphic events in the lower Etheridge Group

## 5.1 Introduction

Proterozoic rocks of the Georgetown Inlier display a range of metamorphic assemblages indicating significant variation in metamorphism across the inlier. In the central Georgetown Inlier, there is a general eastward increase in metamorphic grade, from lower greenschist facies through to upper amphibolite and locally granulite facies (Withnall, 1996). In areas of higher metamorphic grade, such as those of the amphibolite and granulite facies, the mineral assemblages are particularly suited to the application of geothermometry and geobarometry techniques.

In this chapter, quantitative determinations of the pressure and temperature conditions at the time of formation are presented for the major Mesoproterozoic metamorphic events that affected the lower Etheridge Group. In previous studies (e.g. Boger & Hansen, 2004; Cihan *et al*., 2006) it has been suggested that the lower Etheridge Group experienced a period of high-temperature, medium-pressure, mid- to upper-amphibolite facies metamorphism ($M_1$), followed by a period of retrogression, and then a low-pressure thermal event ($M_2$). The results of this study, coupled with EMPA metamorphic monazite dating (Chapter 4) will be used to test this hypothesis.

Later metamorphic events affecting the Georgetown Inlier have less well constrained ages, but were also less intense and generally formed only local crenulations in the dominant metamorphic fabric (Withnall, 1996). Metamorphic assemblages for these later events were not observed, and their thermobarometric characteristics are not presented here.

## 5.2 Previous work

Previous studies describe at least six phases of deformation that have affected the Etheridge Group. Of these, only the first two were considered to have occurred in conjunction with the major mid-Proterozoic prograde metamorphic events (Davis, 1995; Withnall, 1996; Boger & Hansen, 2004). The first event ($M_1$) has previously

been considered to involve medium-pressure, high-temperature conditions, ranging from lower greenschist facies in the west to upper amphibolite facies and locally granulite facies in the east of the terrane (Bell & Rubenach, 1983; Withnall, 1996). This event was followed by a low-pressure thermal event ($M_2$) that was associated with the emplacement of Mesoproterozoic granites, and also locally graded into upper amphibolite facies (Withnall, 1996). However, recent metamorphic and geochronological studies have subsequently questioned the separation of these two events (Boger & Hansen, 2004; Black *et al*. 2005).

The pressure conditions during mid-Proterozoic metamorphism in the Etheridge Group were considered to be intermediate between those of the classic low-pressure (Buchan) and medium-pressure (Barrovian) facies series (Withnall, 1996). Withnall (1996; and references therein) observed numerous features in the lower Etheridge Group that are characteristic of a medium-pressure terrane. These included the existence of a distinct biotite isograd in the metapelites, the co-existence of albite and hornblende in mafic rocks, and co-existing quartz and clinozoisite in amphibolite facies calc-silicate rocks.

A first attempt at determining the *P-T* conditions for $M_{1\text{-}2}$ in the Etheridge Group was made by Withnall (1996) using a petrogenetic grid constructed from the plotting of experimental equilibrium curves and stability fields of minerals in pelitic rocks. Using this method, amphibolite facies *P-T* estimates for the Etheridge Group were estimated to range from lower amphibolite facies conditions of 3.5 kbar and 530 °C, to upper amphibolite-granulite facies conditions as high as 5.0 kbar and 820 °C (McNaughton & Wilson, 1983; Withnall, 1996).

More recent work has attempted to constrain the *P-T* conditions during the peak of metamorphism for both $M_1$ and $M_2$. Boger & Hansen (2004), using mineral textures coupled with thermodynamic modelling, indicated that the $M_1$ and $M_2$ events were separate and unrelated. They determined peak *P-T* conditions for $M_1$ of 8.0-9.0 kbar and 750-800 °C from metapelites at Einasleigh. However, they noted that rocks of the Robertson River area only reached 7.0-8.0 kbar and 600-650 °C during $M_1$. They also regard $M_2$ as a low-pressure thermal event, caused by the emplacement of the Forsayth Batholith and associated granitoids. *P-T* conditions at the time of $M_2$ in rocks of the Robertson River area were determined to be 3.0-4.0 kbar and 600-650 °C.

Further constraints on the *P-T* conditions for $M_1$ and $M_2$ were presented by Cihan *et al*. (2006) from four samples of amphibolite grade Robertson River Metamorphics metapelites near Robinhood. They analysed FIA (Foliation Intersection Axis) trends in garnet and staurolite porphyroblasts, as well as average *P-T* conditions and monazite ages from the metapelites. Their results produced *P-T* estimates for $M_1$ that correlate with those of Boger & Hansen (2004); however in addition to the two established prograde metamorphic events, they described a period of retrogressive metamorphism immediately following $M_1$. Based on monazite ages, they determined that this metamorphic 'event' occurred over an approximate 45 Ma period, over which time the thickened orogenic pile was exhumed and weakened, forming crustal rocks amenable to granite intrusion at ca. 1550 Ma.

## 5.3 Objectives of the thermobarometric study

Although previous studies over the past two decades have touched on the Proterozoic metamorphic history of the Georgetown Inlier, few authors have directly studied the pressure and temperature conditions at the time of formation for mineral assemblages in metapelites of the lower Etheridge Group. Therefore, it is the objective of this chapter to:

- Determine the pressure and temperature conditions of metamorphism for a number of amphibolite facies-grade samples from the central Georgetown Inlier.
- Where possible, correlate these conditions with ages determined from U-Th-Pb metamorphic monazite dating in Chapter 4.
- Synthesize the early- to mid-Proterozoic thermobarometric history of the lower Etheridge Group.

Details of the sampling and analytical techniques used and additional petrographic and mineralogical information on samples analysed is provided below. A detailed overview of the petrology, mineralogy, stratigraphic, and textural relationship of the metasedimentary units referred to in this chapter is given in Chapter 3.

## 5.4 Method

Electron Microprobe (EMP) analysis of metamorphic mineral assemblages combined with a number of directly calibrated geothermometers and geobarometers are used to determine the pressure-temperature conditions of the earliest two metamorphic events to have affected rocks from higher grade areas of the lower Etheridge Group. EMP analysis has proved successful in determining the metamorphic conditions of a number of terranes that have reached varying levels of metamorphic grade, though it is generally best suited to terranes that have experienced metamorphic conditions of at least amphibolite facies, and where clear equilibrium assemblages can be obtained (e.g. Clarke *et al*., 2000; Boger & Hansen, 2004; Fitzherbert *et al*., 2004).

### 5.4.1 Sample selection

Metasedimentary samples from the lower Etheridge Group were selected on the basis that they contained mineral assemblages that appeared representative of metamorphic events. First preference was given to samples that also contained dated metamorphic monazite grains. Also analysed were metasedimentary samples of similar grade from the same localities that also possess mineral assemblages in apparent textural equilibrium. The locations of all samples analysed are presented in Figures 5.1 and 5.2.

### 5.4.2 Analytical technique

In situ microprobe analyses of individual minerals were obtained using the Cameca SX-100 EMP housed at the University of Tasmania. Data was acquired using five wavelength dispersive spectrometers (one TAP, one PET, two LPET, and one LLIF) at operating conditions of 15 kV accelerating voltage, 20 nA electron beam and a beam diameter of 5 µm. PAP data reduction was performed using software supplied by Cameca. Analyses with total weight-percent oxide in the range 98-101 % were accepted as representing the true chemical composition of anhydrous minerals. Minerals with high $Fe^{3+}$ content (e.g. epidote) and minerals with high contents of hydroxide, water, or volatile elements (e.g. biotite, hornblende, epidote, phengitic white mica, and chlorite) were tested against appropriate compositional ranges.

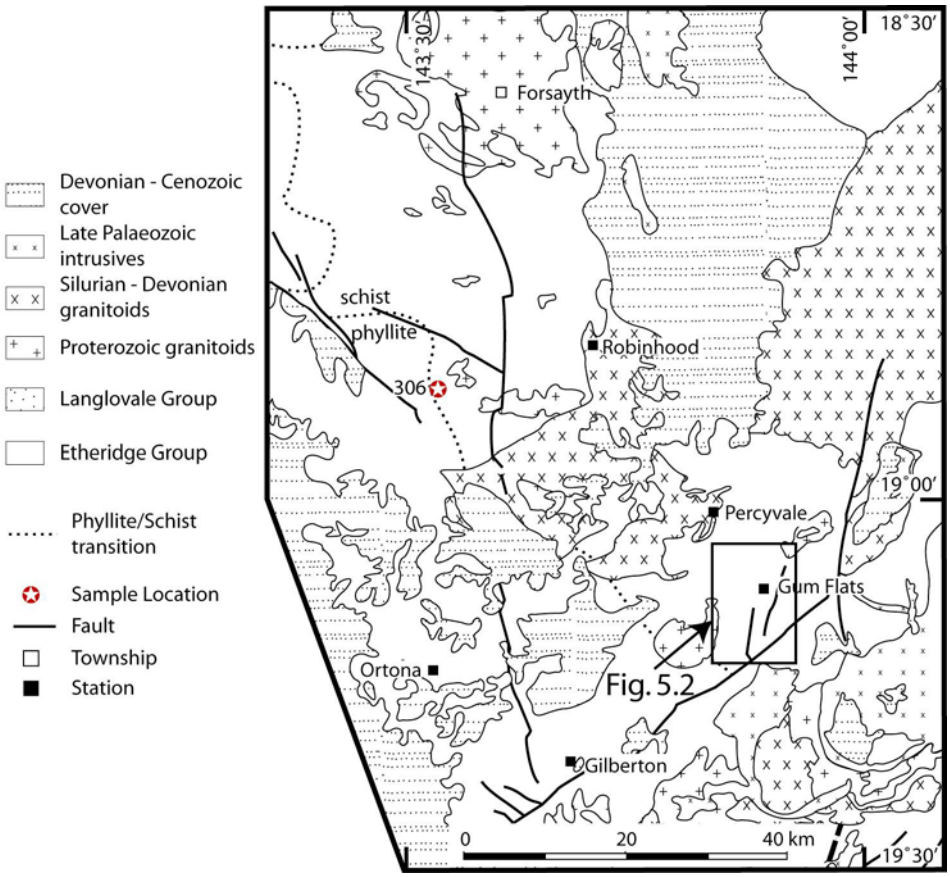


**Figure 5.1: Simplified geological map of the central Georgetown Inlier. Phyllite/schist transition boundary in Etheridge Group metasediments is after Withnall (1996).**

### 5.4.3 Data reduction and presentation

Cations per formula unit for each mineral analysed were calculated from weight-percent oxide totals obtained from the microprobe (Table 5.1). A number of directly calibrated geothermometers and geobarometers were then used in the quantitative determination of *P-T* conditions for each mineral assemblage. The methods involve cationic exchange and net transfer equilibria, as well as the average *P-T* method of THERMOCALC (Powell & Holland, 1988). The average *P-T* method involves the determination of all end-member reactions that can be calculated for a mineral assemblage, based on the internally consistent thermodynamic dataset of Holland & Powell (1998), and the calculation of the most favourable conditions of formation within a specified temperature or pressure window. An advantage of using THERMOCALC is that error propagation is applied to all calculations, thereby providing the user with uncertainties on all *P-T* estimations. THERMOCALC also incorporates the largest possible number of phases, which becomes useful when

temperature estimates vary significantly within an individual sample. All errors quoted for THERMOCALC outputs are at 95% confidence. Representative THERMOCALC outputs and results are listed in Appendix 3.

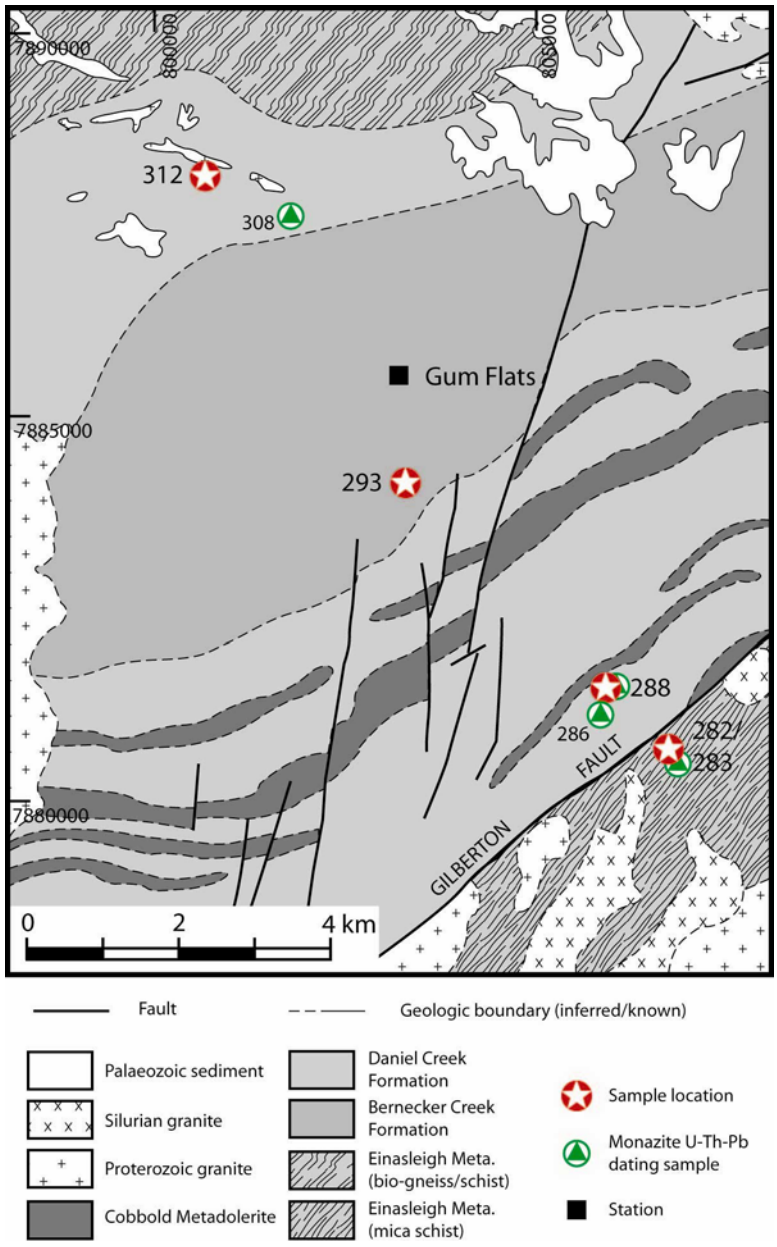


**Figure 5.2: Detailed geological map of the area surrounding Gum Flats station (modified after Withnall *et al.*, 2003a).**

The computer program AX (Holland & Powell, 2000) was used to estimate ferric iron content for each of the microprobe analyses used in thermobarometric calculations. This involved the recalculation of $Fe^{2+}$ as determined by microprobe analysis to achieve perfect stoichiometry. Mineral end-member activities required for average *P-T* calculations using THERMOCALC were also determined by AX. The chemistry of individual minerals is detailed below, and the analyses of all minerals used in

geothermometry and geobarometry calculations in this chapter are listed in Table 5.1. Mineral abbreviations are after Kretz (1983), and Holland & Powell (1998).

| Sample | 282 | | | | | | | 283 | | | | | | 288 | | | | | | Garnet traverse | | | | | | | | | |
|---|---|---|---|---|---|---|---|---|---|---|---|---|---|---|---|---|---|---|---|---|---|---|---|---|---|---|---|---|---|
| Mineral | gt | gt | gt[c] | gt[r] | bi | bi | mu | pl | pl | gt | gt[c] | gt[r] | bi | bi | mu | mu | gt | gt[r] | gt | gt[c] | gt[c] | gt | gt | gt[r] | bi | bi | mu | mu | ilm | ilm | chl |
| $SiO_2$ | 35.75 | 36.00 | 36.04 | 35.95 | 33.21 | 33.70 | 43.99 | 61.15 | 61.76 | 36.02 | 36.11 | 36.19 | 29.45 | 30.46 | 44.80 | 45.30 | 36.22 | 35.61 | 35.51 | 36.17 | 35.71 | 35.76 | 36.03 | 35.98 | 35.86 | 32.45 | 30.08 | 46.98 | 45.58 | 0.61 | 3.23 | 24.87 |
| $TiO_2$ | 0.00 | 0.00 | 0.01 | 0.00 | 1.94 | 1.75 | 0.63 | 0.00 | 0.00 | 0.00 | 0.00 | 0.01 | 1.85 | 1.81 | 0.44 | 0.22 | 0.04 | 0.04 | 0.01 | 0.04 | 0.01 | 0.07 | 0.06 | 0.07 | 0.05 | 0.10 | 0.19 | 0.30 | 0.31 | 51.91 | 48.96 | 0.05 |
| $Al_2O_3$ | 20.62 | 20.67 | 20.76 | 20.96 | 18.61 | 19.34 | 33.11 | 21.98 | 22.55 | 20.99 | 20.73 | 21.04 | 17.84 | 15.32 | 33.88 | 32.74 | 20.93 | 20.85 | 20.90 | 20.80 | 20.97 | 21.02 | 21.17 | 21.01 | 21.06 | 19.28 | 20.43 | 33.94 | 34.89 | 0.49 | 2.82 | 22.26 |
| $Cr_2O_3$ | 0.00 | 0.00 | 0.01 | 0.05 | 0.00 | 0.02 | 0.02 | 0.00 | 0.00 | 0.00 | 0.00 | 0.01 | 0.01 | 0.01 | 0.02 | 0.01 | 0.00 | 0.01 | 0.03 | 0.01 | 0.03 | 0.02 | 0.02 | 0.02 | 0.02 | 0.01 | 0.03 | 0.01 | 0.02 | 0.00 | 0.00 | 0.05 |
| $FeO^{total}$ | 32.27 | 32.21 | 33.11 | 32.43 | 21.21 | 19.06 | 2.17 | 0.21 | 0.08 | 32.86 | 32.95 | 33.09 | 25.51 | 18.90 | 2.16 | 2.08 | 32.26 | 34.01 | 33.56 | 33.51 | 33.33 | 32.90 | 32.92 | 33.06 | 33.06 | 25.72 | 24.20 | 2.07 | 1.44 | 43.64 | 42.58 | 27.14 |
| MnO | 6.71 | 6.60 | 5.79 | 6.36 | 0.25 | 0.24 | 0.03 | 0.02 | 0.00 | 5.80 | 5.91 | 5.65 | 0.28 | 0.16 | 0.09 | 0.14 | 8.06 | 6.75 | 7.20 | 6.95 | 7.19 | 7.86 | 8.10 | 7.81 | 7.66 | 1.91 | 0.26 | 0.00 | 0.02 | 3.34 | 1.45 | 0.34 |
| MgO | 2.17 | 2.12 | 2.40 | 2.35 | 7.58 | 8.12 | 0.78 | 0.02 | 0.00 | 2.31 | 2.25 | 2.17 | 7.77 | 7.99 | 0.85 | 1.02 | 1.71 | 1.64 | 1.48 | 1.57 | 1.65 | 1.73 | 1.66 | 1.54 | 1.48 | 7.90 | 10.11 | 0.76 | 0.70 | 0.01 | 0.41 | 11.02 |
| CaO | 0.96 | 1.04 | 0.97 | 0.99 | 0.32 | 0.24 | 0.00 | 3.61 | 4.01 | 0.95 | 1.01 | 1.08 | 0.19 | 0.40 | 0.00 | 0.03 | 1.31 | 1.39 | 1.33 | 1.24 | 1.26 | 1.24 | 1.20 | 1.30 | 1.32 | 0.45 | 0.08 | 0.03 | 0.00 | 0.00 | 0.01 | 0.03 |
| NaO | 0.03 | 0.00 | 0.03 | 0.01 | 0.23 | 0.20 | 0.28 | 8.85 | 9.05 | 0.01 | 0.00 | 0.00 | 0.23 | 0.46 | 0.50 | 0.43 | 0.04 | 0.00 | 0.05 | 0.02 | 0.03 | 0.03 | 0.04 | 0.02 | 0.06 | 0.02 | 0.03 | 0.88 | 0.92 | 0.01 | 0.06 | 0.02 |
| $K_2O$ | 0.00 | 0.01 | 0.01 | 0.00 | 5.89 | 7.53 | 10.55 | 0.12 | 0.15 | 0.03 | 0.00 | 0.02 | 2.63 | 3.52 | 10.70 | 10.30 | 0.01 | 0.01 | 0.03 | 0.03 | 0.01 | 0.00 | 0.00 | 0.00 | 0.02 | 2.27 | 3.39 | 9.39 | 9.78 | 0.10 | 0.76 | 0.51 |
| Total | 98.51 | 98.65 | 99.12 | 99.10 | 89.23 | 90.19 | 91.56 | 95.96 | 97.61 | 98.95 | 98.66 | 99.37 | 85.75 | 79.03 | 93.44 | 92.27 | 100.6 | 100.3 | 100.1 | 100.3 | 100.2 | 100.6 | 101.2 | 100.8 | 100.6 | 90.11 | 88.80 | 94.36 | 93.66 | 100.1 | 100.3 | 86.3 |
| number ox. | 12 | 12 | 12 | 12 | 22 | 22 | 22 | 8 | 8 | 12 | 12 | 12 | 22 | 22 | 22 | 22 | 12 | 12 | 12 | 12 | 12 | 12 | 12 | 12 | 12 | 22 | 22 | 22 | 22 | 6 | 6 | 28 |
| Si | 2.96 | 2.97 | 2.96 | 2.95 | 5.38 | 5.38 | 6.14 | 2.81 | 2.80 | 2.96 | 2.95 | 2.96 | 5.04 | 5.51 | 6.13 | 6.26 | 2.95 | 2.92 | 2.92 | 2.96 | 2.93 | 2.92 | 2.93 | 2.93 | 2.93 | 5.25 | 4.92 | 6.30 | 6.16 | 0.03 | 0.16 | 5.40 |
| Ti | 0.00 | 0.00 | 0.00 | 0.00 | 0.24 | 0.21 | 0.07 | 0.00 | 0.00 | 0.00 | 0.00 | 0.00 | 0.24 | 0.25 | 0.05 | 0.02 | 0.00 | 0.00 | 0.00 | 0.00 | 0.00 | 0.00 | 0.00 | 0.00 | 0.00 | 0.01 | 0.02 | 0.03 | 0.03 | 1.96 | 1.80 | 0.01 |
| Al | 2.01 | 2.01 | 2.01 | 2.03 | 3.56 | 3.64 | 5.45 | 1.19 | 1.20 | 2.03 | 2.02 | 2.03 | 3.60 | 3.26 | 5.47 | 5.33 | 2.01 | 2.02 | 2.03 | 2.00 | 2.03 | 2.02 | 2.03 | 2.02 | 2.03 | 3.68 | 3.94 | 5.36 | 5.56 | 0.03 | 0.16 | 5.69 |
| Cr | 0.00 | 0.00 | 0.00 | 0.00 | 0.00 | 0.00 | 0.00 | 0.00 | 0.00 | 0.00 | 0.00 | 0.00 | 0.00 | 0.00 | 0.00 | 0.00 | 0.00 | 0.00 | 0.00 | 0.00 | 0.00 | 0.00 | 0.00 | 0.00 | 0.00 | 0.00 | 0.00 | 0.00 | 0.00 | 0.00 | 0.00 | 0.01 |
| Fe | 2.23 | 2.22 | 2.27 | 2.23 | 2.87 | 2.55 | 0.25 | 0.01 | 0.00 | 2.26 | 2.28 | 2.27 | 3.65 | 2.86 | 0.25 | 0.24 | 2.20 | 2.33 | 2.31 | 2.29 | 2.29 | 2.25 | 2.24 | 2.25 | 2.26 | 3.48 | 3.31 | 0.23 | 0.16 | 1.83 | 1.74 | 4.93 |
| Mn | 0.47 | 0.46 | 0.40 | 0.44 | 0.03 | 0.03 | 0.00 | 0.00 | 0.00 | 0.40 | 0.41 | 0.39 | 0.04 | 0.03 | 0.01 | 0.02 | 0.56 | 0.47 | 0.50 | 0.48 | 0.50 | 0.54 | 0.56 | 0.54 | 0.53 | 0.26 | 0.04 | 0.00 | 0.00 | 0.14 | 0.06 | 0.06 |
| Mg | 0.27 | 0.26 | 0.29 | 0.29 | 1.83 | 1.93 | 0.16 | 0.00 | 0.00 | 0.28 | 0.28 | 0.26 | 1.98 | 2.15 | 0.17 | 0.21 | 0.21 | 0.20 | 0.18 | 0.19 | 0.20 | 0.21 | 0.20 | 0.19 | 0.18 | 1.91 | 2.47 | 0.15 | 0.14 | 0.00 | 0.03 | 3.57 |
| Ca | 0.09 | 0.09 | 0.08 | 0.09 | 0.05 | 0.04 | 0.00 | 0.18 | 0.19 | 0.08 | 0.09 | 0.10 | 0.03 | 0.08 | 0.00 | 0.01 | 0.11 | 0.12 | 0.12 | 0.11 | 0.11 | 0.11 | 0.10 | 0.11 | 0.12 | 0.08 | 0.01 | 0.00 | 0.00 | 0.00 | 0.00 | 0.01 |
| Na | 0.00 | 0.00 | 0.00 | 0.00 | 0.07 | 0.06 | 0.07 | 0.79 | 0.80 | 0.00 | 0.00 | 0.00 | 0.08 | 0.16 | 0.13 | 0.12 | 0.01 | 0.00 | 0.01 | 0.01 | 0.01 | 0.00 | 0.01 | 0.00 | 0.01 | 0.01 | 0.01 | 0.23 | 0.24 | 0.00 | 0.01 | 0.01 |
| K | 0.00 | 0.00 | 0.00 | 0.00 | 1.22 | 1.53 | 1.88 | 0.01 | 0.01 | 0.00 | 0.00 | 0.00 | 0.58 | 0.81 | 1.87 | 1.82 | 0.00 | 0.00 | 0.00 | 0.00 | 0.00 | 0.00 | 0.00 | 0.00 | 0.00 | 0.47 | 0.71 | 1.61 | 1.69 | 0.01 | 0.05 | 0.14 |
| Total | 8.04 | 8.02 | 8.04 | 8.03 | 15.25 | 15.38 | 14.04 | 4.99 | 5.00 | 8.03 | 8.03 | 8.02 | 15.24 | 15.10 | 14.09 | 14.02 | 8.05 | 8.07 | 8.07 | 8.04 | 8.06 | 8.07 | 8.06 | 8.05 | 8.06 | 15.14 | 15.44 | 13.91 | 13.99 | 4.00 | 3.99 | 19.82 |

[c], core analysis; [r], rim analysis

**Table 5.1: Representative electron microprobe analyses.**

| Sample | 293 | | | | | | | | | 306 | | | Garnet traverse | | | | | | | 312 | | | | Garnet traverse | | | | | |
|---|---|---|---|---|---|---|---|---|---|---|---|---|---|---|---|---|---|---|---|---|---|---|---|---|---|---|---|---|---|
| Mineral | gt | gt | gt[c] | gt[r] | bi | bi | mu | ep | pl | pl | st | st | gt[r] | gt | gt[c] | gt | gt[r] | bi | mu | rt | rt | chl | hbl | hbl | gt[r] | gt | gt[c] | gt | gt[r] | pl | pl | ttn |
| $SiO_2$ | 35.29 | 35.53 | 35.53 | 35.24 | 34.16 | 34.24 | 44.15 | 36.35 | 46.53 | 44.99 | 27.52 | 27.74 | 36.09 | 36.50 | 36.43 | 36.76 | 36.32 | 34.33 | 33.54 | 44.96 | 0.80 | 0.30 | 24.03 | 50.46 | 44.10 | 37.28 | 36.96 | 37.21 | 37.05 | 47.69 | 48.04 | 30.15 |
| $TiO_2$ | 0.16 | 0.07 | 0.17 | 0.01 | 2.42 | 2.74 | 0.80 | 0.06 | 0.00 | 0.00 | 0.56 | 0.56 | 0.02 | 0.24 | 0.05 | 0.07 | 0.04 | 1.51 | 1.38 | 0.46 | 92.70 | 93.43 | 0.12 | 0.14 | 0.30 | 0.05 | 0.07 | 0.21 | 0.23 | 0.03 | 0.02 | 34.89 |
| $Al_2O_3$ | 20.21 | 20.50 | 20.35 | 20.47 | 15.91 | 16.34 | 28.35 | 23.46 | 24.56 | 26.22 | 54.23 | 54.03 | 20.78 | 20.88 | 21.08 | 20.87 | 21.19 | 19.08 | 18.53 | 36.19 | 0.78 | 2.37 | 22.81 | 4.94 | 11.07 | 21.47 | 21.10 | 21.16 | 20.90 | 26.53 | 26.09 | 3.86 |
| $Cr_2O_3$ | 0.02 | 0.00 | 0.00 | 0.00 | 0.00 | 0.06 | 0.05 | 0.00 | 0.02 | 0.01 | 0.02 | 0.01 | 0.04 | 0.02 | 0.03 | 0.02 | 0.03 | 0.02 | 0.00 | 0.00 | 0.01 | 0.00 | 0.00 | 0.01 | 0.02 | 0.02 | 0.01 | 0.01 | 0.06 | 0.00 | 0.00 | 0.09 |
| $FeO^{total}$ | 17.51 | 19.69 | 17.62 | 19.65 | 21.21 | 19.48 | 4.61 | 11.23† | 0.14 | 0.23 | 13.40 | 13.57 | 33.67 | 33.31 | 32.50 | 33.02 | 34.11 | 17.51 | 17.73 | 0.89 | 3.41 | 0.43 | 25.32 | 14.67 | 18.03 | 13.82 | 20.62 | 19.59 | 19.67 | 0.03 | 0.02 | 0.74 |
| MnO | 16.43 | 14.18 | 16.84 | 14.36 | 0.71 | 0.47 | 0.17 | 0.41 | 0.05 | 0.03 | 0.23 | 0.22 | 4.46 | 4.53 | 5.35 | 4.88 | 4.58 | 0.09 | 0.08 | 0.01 | 0.09 | 0.02 | 0.15 | 0.65 | 0.62 | 10.57 | 7.09 | 7.06 | 7.17 | 0.01 | 0.01 | 0.17 |
| MgO | 0.78 | 0.86 | 0.82 | 0.89 | 8.94 | 9.19 | 1.99 | 0.01 | 0.00 | 0.00 | 1.45 | 1.37 | 1.65 | 1.88 | 2.16 | 2.18 | 1.87 | 10.48 | 10.89 | 0.56 | 0.09 | 0.06 | 14.05 | 13.29 | 9.27 | 0.56 | 0.49 | 0.50 | 0.49 | 0.01 | 0.00 | 0.00 |
| CaO | 8.47 | 7.99 | 7.82 | 7.60 | 0.06 | 0.16 | 0.15 | 22.66 | 14.32 | 16.77 | 0.00 | 0.00 | 2.47 | 2.67 | 2.58 | 2.78 | 2.58 | 0.65 | 0.58 | 0.00 | 0.12 | 0.20 | 0.01 | 12.25 | 11.21 | 16.78 | 16.81 | 13.72 | 14.52 | 14.57 | 14.57 | 27.93 |
| NaO | 0.00 | 0.02 | 0.01 | 0.00 | 0.11 | 0.13 | 0.18 | 0.01 | 4.91 | 3.68 | 0.01 | 0.02 | 0.01 | 0.02 | 0.03 | 0.01 | 0.00 | 0.20 | 0.21 | 1.11 | 0.03 | 0.06 | 0.00 | 0.42 | 0.74 | 0.00 | 0.01 | 0.04 | 0.02 | 4.39 | 4.77 | 0.02 |
| $K_2O$ | 0.00 | 0.01 | 0.00 | 0.02 | 9.48 | 9.85 | 10.98 | 0.01 | 0.29 | 0.29 | 0.00 | 0.00 | 0.00 | 0.01 | 0.00 | 0.00 | 0.03 | 5.13 | 5.30 | 9.68 | 0.04 | 0.13 | 0.05 | 0.35 | 0.98 | 0.02 | 0.01 | 0.00 | 0.02 | 0.38 | 0.31 | 0.00 |
| Total | 98.88 | 98.85 | 99.16 | 98.25 | 93.02 | 92.67 | 91.43 | 94.20 | 90.80 | 92.22 | 97.43 | 97.52 | 99.20 | 100.1 | 100.2 | 100.6 | 100.8 | 89.00 | 88.25 | 93.86 | 98.07 | 97.01 | 86.54 | 97.18 | 96.35 | 100.7 | 100.2 | 100.3 | 100.1 | 99.97 | 93.65 | 94.34 | 97.84 |
| number ox. | 12 | 12 | 12 | 12 | 22 | 22 | 22 | 13 | 8 | 8 | 48 | 48 | 12 | 12 | 12 | 12 | 12 | 22 | 22 | 22 | 2 | 2 | 28 | 23 | 23 | 12 | 12 | 12 | 12 | 8 | 8 | 20 |
| Si | 2.91 | 2.93 | 2.92 | 2.92 | 5.45 | 5.44 | 6.31 | 3.19 | 2.37 | 2.27 | 7.99 | 8.05 | 2.96 | 2.97 | 2.95 | 2.97 | 2.94 | 5.43 | 5.38 | 6.05 | 0.01 | 0.00 | 5.14 | 7.43 | 6.72 | 2.95 | 2.96 | 2.97 | 2.96 | 2.35 | 2.35 | 4.01 |
| Ti | 0.01 | 0.00 | 0.01 | 0.00 | 0.29 | 0.33 | 0.09 | 0.00 | 0.00 | 0.00 | 0.12 | 0.12 | 0.00 | 0.01 | 0.00 | 0.00 | 0.00 | 0.18 | 0.17 | 0.05 | 0.96 | 0.96 | 0.02 | 0.02 | 0.03 | 0.00 | 0.00 | 0.01 | 0.01 | 0.00 | 0.00 | 3.49 |
| Al | 1.97 | 1.99 | 1.97 | 2.00 | 2.99 | 3.06 | 4.77 | 2.42 | 1.48 | 1.56 | 18.56 | 18.48 | 2.01 | 2.00 | 2.02 | 1.99 | 2.02 | 3.56 | 3.50 | 5.74 | 0.01 | 0.04 | 5.75 | 0.86 | 1.99 | 2.00 | 1.97 | 1.99 | 1.95 | 1.54 | 1.51 | 0.61 |
| Cr | 0.00 | 0.00 | 0.00 | 0.00 | 0.00 | 0.01 | 0.01 | 0.00 | 0.00 | 0.00 | 0.01 | 0.00 | 0.00 | 0.00 | 0.00 | 0.00 | 0.00 | 0.00 | 0.00 | 0.00 | 0.00 | 0.00 | 0.00 | 0.00 | 0.00 | 0.00 | 0.00 | 0.00 | 0.00 | 0.00 | 0.00 | 0.01 |
| Fe | 1.21 | 1.36 | 1.21 | 1.36 | 2.83 | 2.59 | 0.55 | 0.82 | 0.01 | 0.01 | 3.25 | 3.29 | 2.31 | 2.26 | 2.20 | 2.23 | 2.31 | 2.31 | 2.38 | 0.10 | 0.04 | 0.00 | 4.53 | 1.81 | 2.30 | 0.91 | 1.11 | 1.38 | 1.32 | 0.00 | 0.00 | 0.08 |
| Mn | 1.15 | 0.99 | 1.17 | 1.01 | 0.10 | 0.06 | 0.02 | 0.03 | 0.00 | 0.00 | 0.06 | 0.05 | 0.31 | 0.31 | 0.37 | 0.33 | 0.31 | 0.01 | 0.01 | 0.00 | 0.00 | 0.00 | 0.03 | 0.08 | 0.08 | 0.71 | 0.51 | 0.48 | 0.48 | 0.49 | 0.00 | 0.02 |
| Mg | 0.10 | 0.11 | 0.10 | 0.11 | 2.12 | 2.17 | 0.42 | 0.00 | 0.00 | 0.00 | 0.63 | 0.59 | 0.20 | 0.23 | 0.26 | 0.26 | 0.23 | 2.47 | 2.60 | 0.11 | 0.00 | 0.00 | 4.48 | 2.92 | 2.10 | 0.07 | 0.06 | 0.08 | 0.06 | 0.00 | 0.00 | 0.00 |
| Ca | 0.75 | 0.71 | 0.69 | 0.67 | 0.01 | 0.03 | 0.02 | 2.13 | 0.78 | 0.91 | 0.00 | 0.00 | 0.22 | 0.23 | 0.22 | 0.24 | 0.22 | 0.11 | 0.10 | 0.00 | 0.00 | 0.00 | 0.00 | 1.93 | 1.83 | 1.42 | 1.43 | 1.17 | 1.24 | 1.25 | 0.77 | 0.79 | 3.98 |
| Na | 0.00 | 0.00 | 0.00 | 0.00 | 0.03 | 0.04 | 0.05 | 0.00 | 0.49 | 0.36 | 0.01 | 0.01 | 0.00 | 0.00 | 0.00 | 0.00 | 0.00 | 0.06 | 0.07 | 0.29 | 0.00 | 0.00 | 0.00 | 0.12 | 0.22 | 0.00 | 0.00 | 0.00 | 0.01 | 0.00 | 0.42 | 0.45 | 0.00 |
| K | 0.00 | 0.00 | 0.00 | 0.00 | 1.93 | 2.00 | 2.00 | 0.00 | 0.02 | 0.02 | 0.00 | 0.00 | 0.00 | 0.00 | 0.00 | 0.00 | 0.00 | 1.03 | 1.08 | 1.66 | 0.00 | 0.00 | 0.01 | 0.07 | 0.19 | 0.00 | 0.00 | 0.00 | 0.00 | 0.02 | 0.02 | 0.00 |
| Total | 8.09 | 8.08 | 8.08 | 8.08 | 15.75 | 15.72 | 14.24 | 8.60 | 5.14 | 5.13 | 30.61 | 30.60 | 8.03 | 8.02 | 8.04 | 8.03 | 8.05 | 15.16 | 15.28 | 14.01 | 1.03 | 1.02 | 19.97 | 15.22 | 15.46 | 8.05 | 8.05 | 8.05 | 8.04 | 8.05 | 5.10 | 5.13 | 12.20 |

[c], core analysis; [r], rim analysis

† total Fe in epidote reported as $Fe^{3+}$

**Table 5.1 cont.**

## 5.5 Metamorphic Petrology

Etheridge Group sedimentary rocks that have been metamorphosed to amphibolite facies conditions are located in the areas surrounding Gum Flats and Robinhood stations, and include the Einasleigh Metamorphics, Bernecker Creek Formation, Daniel Creek Formation, and Corbett Formation members (Fig. 5.1 and 5.2). These rocks contain variable amounts of quartz, biotite, muscovite, garnet, and more locally plagioclase feldspar, epidote, staurolite, and calcite. Aluminosilicate minerals were not observed, most likely due to the period of retrogression following peak metamorphism rather than unfavourable bulk rock compositions. Chlorite was observed in numerous samples as a retrograde mineral pseudomorphing large porphyroblasts, possibly of either an aluminosilicate mineral or staurolite.

Timing relationships between minerals are implied from the presence of inclusions, the growth of one mineral on or around another, or via the formation of overgrowths/coronas of finer-grained minerals along the margins of coarser-grained ones. Minerals found as inclusions, or minerals partially or wholly enveloped by other minerals, are implied to precede those that enclose them. The notation of metamorphic events and their associated structural fabrics (i.e. $M_1$, $S_1$, etc.) follows the notation used by Withnall (1996) and Withnall *et al*. (1997), except where indicating the retrograde event that followed $M_1$, which is denoted $M_{1R}$.

Sample 306, a muscovite-biotite-garnet-staurolite schist belonging to the Corbett Formation was collected from the Robinhood area (Fig. 5.1). The sample contains small aligned plates of biotite and muscovite which together with elongate quartz grains define a dominant schistosity that trends NW-SE and corresponds to the $D_3$ event of Cihan *et al*. (2006). Porphyroblasts of garnet and staurolite are enclosed by the foliation, forming large strain shadows containing biotite, muscovite and granoblastic quartz (Fig. 5.3a). Porphyroblasts of both garnet and staurolite are inclusion-rich and of variable size, however staurolite porphyroblasts are generally larger and occasionally enclose or partly enclose small garnet porphyroblasts (Fig. 5.3b). Garnet porphyroblasts are anhedral to subhedral in shape and have diameters ranging up to 1 mm. Within garnet, small elongate quartz inclusions define an earlier ($S_1$) foliation that is commonly orthogonal to the external schistosity (Fig. 5.3c). Examples where the internal foliation of the quartz inclusions is in whole or part continuous with the external schistosity are rare. This inclusion trail morphology is

more difficult to recognise in staurolite due to the larger size of the quartz inclusions (Fig. 5.3b), however $S_1$ is still partially visible within some larger grains. The staurolite porphyroblasts are generally subhedral to euhedral, and are between 2 and 5 mm in diameter. Monazite grains lying within $S_3$ assemblage minerals record a metamorphic age of 1497 ± 20 Ma, which I infer to date this event (see Chapter 4).

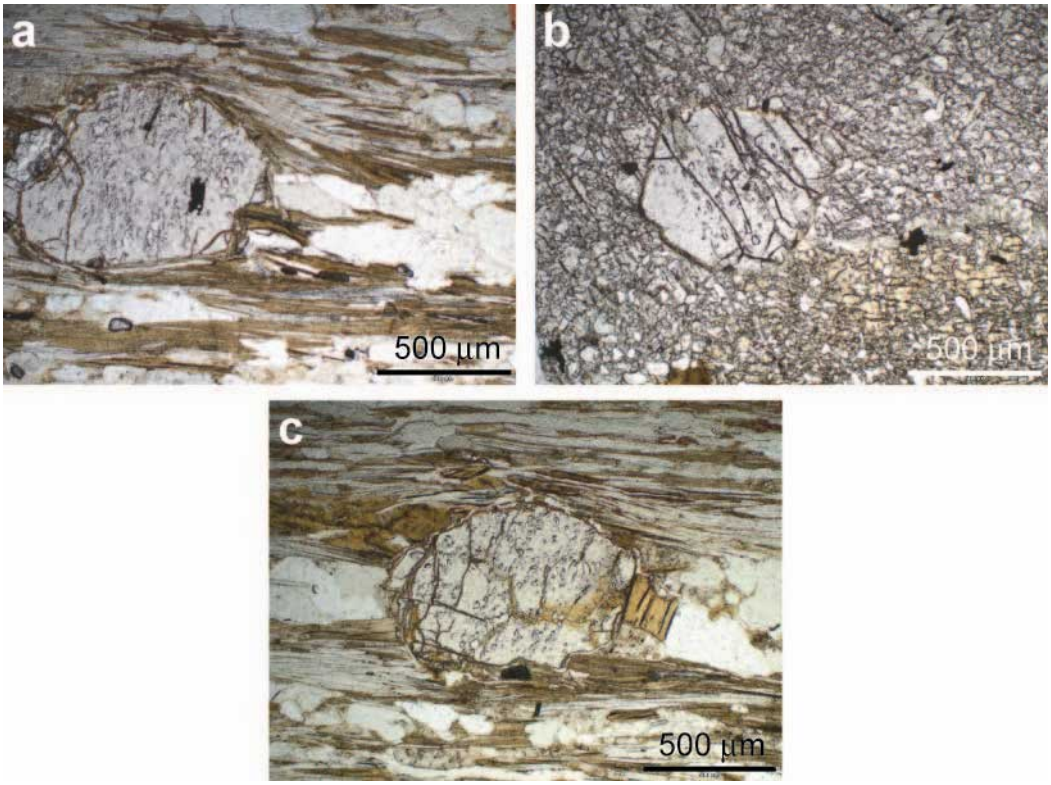


**Figure 5.3: Textural relationships preserved in sample 306 of the Corbett Formation from the Robinhood station area. (a) Photomicrograph of biotite-muscovite-quartz strain shadows on garnet and truncation by external foliation. (b) Photomicrograph of staurolite porphyroblast containing small garnet inclusion. (c) Photomicrograph of garnet porphyroblast containing inclusion trails of quartz. Note the high angle of the inclusion trails to the external schistosity.**

All remaining samples were collected from the Gum Flats area (Fig. 5.2). They are compositionally similar, with relative variations in the abundance of the main rock-forming minerals, and the level of metamorphism attained being their key differences. Samples 282 and 283 are biotite-muscovite-garnet-bearing schists from the Einasleigh Metamorphics. The rocks contain small aligned plates of biotite and muscovite which define the main layer-parallel schistosity ($S_1$). In both samples, quartz, along with minor amounts of variably sericitised plagioclase constitute the remainder of the matrix. Garnet porphyroblasts are more common in sample 282, whereas muscovite is more common and garnet less common in sample 283. Garnet is the only

porphyroblast-forming mineral in both samples, and is commonly anhedral to subhedral with diameters ranging up to 1 mm. Small, randomly aligned laths of biotite, blocky plagioclase, and quartz commonly surround garnet (Fig. 5.4a). No strain shadows surrounding garnet porphyroblasts, or inclusion trails within porphyroblasts, are recognised in either sample. Monazite grains lying between and within $S_{1\text{-}2}$ assemblage minerals in sample 283 record a metamorphic age as reported in Chapter 4. The primary metamorphic age was determined from 13 grains as being 1537 ± 18 Ma, which lies at the younger end of the inferred age spectrum for deformation and associated peak metamorphism in the Etheridge Group (c. 1580-1550 Ma; Withnall, 1996; Black *et al*., 2005).

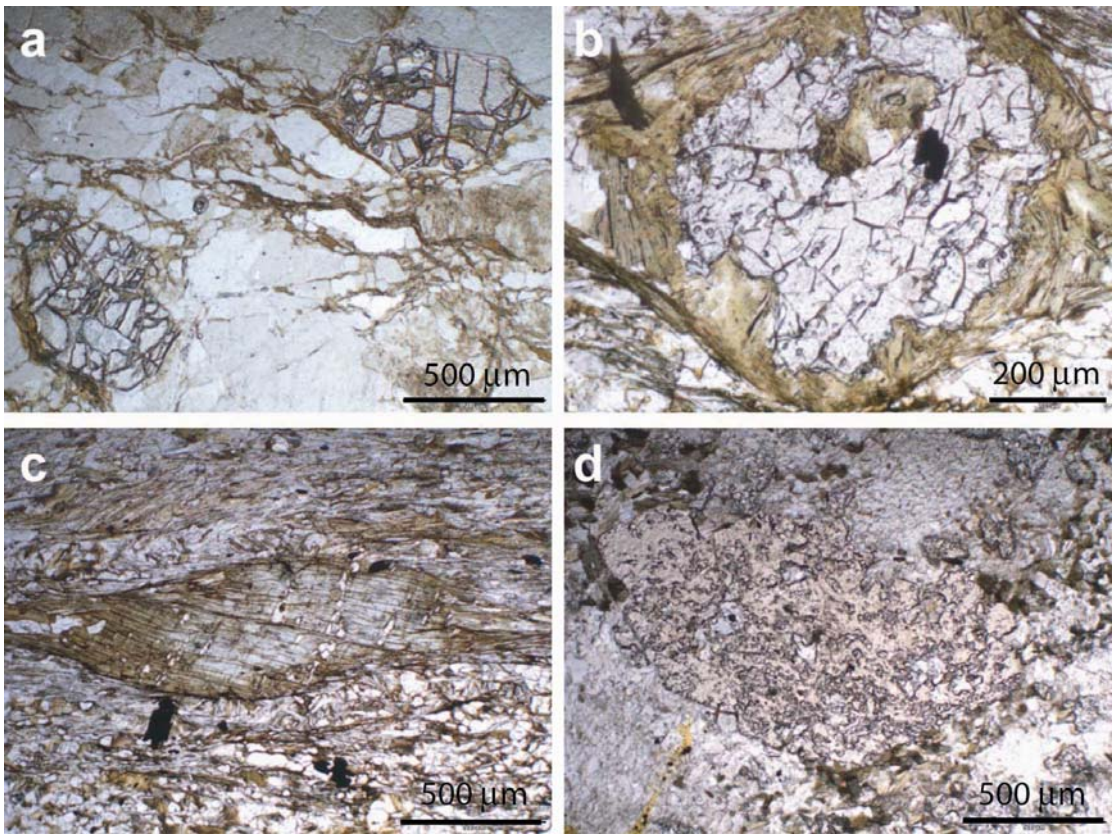


**Figure 5.4: Textural relationships preserved in metapelite samples from the Gum Flats area. (a) Photomicrograph of matrix biotite, muscovite, and quartz surrounding garnet porphyroblast (sample 282). (b) Photomicrograph of inclusion trail in garnet porphyroblast, orthogonal to the external schistosity; surrounding and replacing garnet are low-strain biotite plates (sample 288). (c) Photomicrograph of chlorite porphyroblast surrounded by biotite rims and containing inclusion trails of quartz. Note the high angle of the inclusion trails to the external schistosity (sample 288). (d) Photomicrograph of garnet porphyroblast with poikiloblastic texture in Bernecker Creek Formation calc-silicate (sample 293).**

Sample 288 is a biotite-muscovite-garnet-bearing schist from the Daniel Creek Formation. It contains small aligned laths of biotite and muscovite which again define the dominant layer-parallel schistosity ($S_1$). Small flattened grains of quartz constitute the remainder of the matrix. Porphyroblasts of garnet and chlorite are enclosed by this foliation, and form large symmetrical strain shadows containing biotite and blocky quartz (Fig. 5.4b and 5.4c). The garnet porphyroblasts are anhedral to subhedral, and are less than 1 mm in diameter. They are also commonly enclosed by thin coronas of biotite. Inclusion trails of quartz are found within most garnet porphyroblasts. Their orientation varies from sub-parallel, to more commonly orthogonal to the external schistosity. Other large porphyroblasts occurring throughout the sample were of a prograde metamorphic mineral, possibly staurolite, which has subsequently been pseudomorphed by retrograde chlorite. The porphyroblasts are commonly tabular, anhedral, and range up to 3 mm in diameter. They contain inclusion trails of quartz which commonly define a foliation orthogonal to the matrix foliation (Fig. 5.4c). Six analyses on five monazite grains lying within the dominant $S_1$ schistosity record a metamorphic age of 1585 ± 18 Ma (Chapter 4), which I associate with the pervasive $M_1$ event.

Sample 293 is a biotite-muscovite-garnet-bearing schist from the Bernecker Creek Formation. In this rock, biotite again defines the dominant foliation ($S_1$); however the foliation is weaker relative to previous samples. Small, blocky to elongated grains of plagioclase, and lesser quartz and calcite define the remainder of the matrix, suggesting the sedimentary precursor of this rock may have been calc-silicate in composition. Fine-grained epidote is accessory. Coarse-grained garnet forms inclusion-rich porphyroblasts of variable size surrounded by fine-grained biotite and blocky quartz grains. The garnet porphyroblasts are anhedral to subhedral and have diameters ranging between 1 and 3 mm. Within garnet, numerous small elongate quartz inclusions define a foliation that is generally consistent with the matrix foliation, giving the garnet a poikiloblastic texture (Fig. 5.4d).

Sample 312 is a garnet-hornblende-bearing calc-silicate gneiss from the Daniel Creek Formation. The sample contains garnet-hornblende-quartz-plagioclase as the peak metamorphic assemblage along with calcite, with secondary actinolite and accessory clinozoisite. Small, elongated grains of hornblende define a weak layer-parallel foliation, and are the most common form of hornblende in this sample. Fine-grained

blocky quartz and plagioclase up to 1 mm in length constitute the remainder of the matrix. Both garnet and hornblende form porphyroblasts in this sample, with garnet more numerous. Garnet porphyroblasts have diameters up to 4 mm, are anhedral to subhedral, and contain large inclusions of quartz. Hornblende porphyroblasts have diameters up to 2 mm, are commonly anhedral, and also contain numerous large quartz inclusions similar to garnet.

## 5.6 Mineral Chemistry

This section describes the mineral chemistry for each sample analysed. Iron values for all analyses were obtained as $Fe^{2+}$, except for epidote group minerals in which all iron was assumed to be $Fe^{3+}$. Chemical compositions of minerals analysed by electron microprobe and selected for thermobarometric analysis are shown in Table 5.1 and are summarized in Table 5.2.

| | 282 | 283 | 288 | 293 | 306 | 312 |
|---|---|---|---|---|---|---|
| Garnet | | | | | | |
| $X_{alm}$ | 0.75-0.72 | 0.76-0.74 | 0.77-0.71 | 0.43-0.38 | 0.78-0.71 | 0.44-0.29 |
| $X_{spss}$ | 0.17-0.13 | 0.15-0.13 | 0.19-0.12 | 0.37-0.29 | 0.13-0.06 | 0.23-0.15 |
| $X_{gr}$ | 0.04-0.03 | 0.03 | 0.04-0.03 | 0.25-0.20 | 0.08-0.06 | 0.49-0.37 |
| $X_{py}$ | 0.10-0.07 | 0.10-0.08 | 0.09-0.05 | 0.03 | 0.10-0.06 | 0.03-0.02 |
| $X_{Fe}$ | 0.92-0.87 | 0.90-0.89 | 0.93-0.89 | 0.93-0.92 | 0.92-0.88 | 0.96-0.93 |
| Staurolite | | | | | | |
| $X_{Fe}$ | | | | | 0.88-0.84 | |
| Hornblende | | | | | | |
| $X_{Ca}$ | | | | | | 1.00-0.86 |
| $X_{Al}$ | | | | | | 0.88-0.09 |
| Biotite | | | | | | |
| $X_{Fe}$ | 0.64-0.54 | 0.65-0.55 | 0.64-0.55 | 0.57-0.54 | 0.64-0.46 | |
| Muscovite | | | | | | |
| $X_{Fe}$ | 0.61 | 0.59-0.52 | 0.87-0.54 | 0.68-0.57 | 0.63-0.47 | |
| $X_{K}$ | 0.96 | 0.95-0.93 | 0.88-0.85 | 0.98-0.97 | 0.85-0.84 | |
| Plagioclase | | | | | | |
| $X_{alb}$ | 0.83-0.80 | | 0.92 | | | |
| $X_{an}$ | | | | 0.72-0.62 | 0.67 | 0.70-0.42 |

**Table 5.2: Summary of electron microprobe data listed in Table 5.1.**

### 5.6.1 Silicates

#### 5.6.1.1 Garnet

A single generation of garnet porphyroblast growth is recognised in sample 306 from the Robinhood area. Porphyroblasts from this sample form an almandine-rich solid solution. Individual porphyroblasts are weakly zoned (Fig. 5.5a), with average values

of $Alm_{71}Spss_{13}Py_8Gr_8$ for cores, and $Alm_{76}Spss_{10}Py_7Gr_7$ for rims (Alm = almandine, Spss = Spessartine, Py = Pyrope, Gr = Grossular). End-member components between individual porphyroblasts show small but significant variation, with $X_{alm}$ [Fe/(Fe + Mg + Mn + Ca)] varying from 0.71 to 0.78, $X_{spss}$ varying from 0.06 to 0.13, and $X_{py}$ varying from 0.06 to 0.10. The ratio of Fe:Mg [$X_{Fe}$ = Fe/(Fe + Mg)] remains almost constant ($X_{Fe}$ *c*. 0.89-0.91) across all analysed garnet grains implying that the grains grew over a relatively small temperature range, with rim temperatures ($X_{Fe}$ = 0.89) generally cooler than core temperatures ($X_{Fe}$ = 0.91; Fig. 5.5a). Relatively rapid decrease in $X_{py}$ and associated increase in $X_{alm}$ along some garnet rims (Fig. 5.5a), suggests diffusion zoning occurred, possibly involving adjacent biotite.

Garnet porphyroblasts from mica schists of the Einasleigh Metamorphics and Daniel Creek Formation in the south of the Gum Flats area (samples 282, 283, and 288) also possess similar almandine-rich compositions to those of the Robinhood area. In samples 282 and 283, a single generation of porphyroblast growth was recognised, with end-member compositions remaining relatively consistent between grains ($X_{alm}$ = 0.73-0.76, $X_{spss}$ = 0.13-0.17, $X_{py}$ = 0.07-0.10, $X_{gr}$ = 0.03-0.04). Minor zoning was observed across individual garnet porphyroblasts, with end-member component values of $Alm_{74}Spss_{13}Py_{10}Gr_3$ for cores and $Alm_{73}Spss_{15}Py_9Gr_3$ for rims. Garnet porphyroblasts in sample 288 are relatively more Mn-rich ($X_{spss}$ = 0.12-0.19) than those of the Einasleigh Metamorphics samples, but otherwise show limited variation between grains in two end-member components ($X_{alm}$ = 0.71-0.76, $X_{gr}$ = 0.03-0.04), and greater variation in Mg ($X_{py}$ = 0.05-0.09), suggesting growth occurred over a limited temperature range at near constant pressure. Individual porphyroblasts are weakly zoned with high $X_{spss}$ cores (Fig. 5.5b), and high $X_{alm}$ rims. $X_{Fe}$ is also relatively constant ($X_{Fe}$ *c*. 0.91-0.92) across all analysed grains.

Garnet compositions in the two remaining samples (samples 293 and 312) differ significantly from those described above. In both cases, the garnet porphyroblasts are significantly enriched in both Mn and Ca relative to Fe, suggesting that both samples were possibly derived from calcareous sediments, or that some amount of calcareous material was present in the sedimentary precursors of the rocks. The composition of garnet porphyroblasts in sample 293 varies from $X_{alm}$ = 0.38 to 0.43, with variation mostly observed within individual grains, rather than between grains. Within-grain variation is observed between other end-members, particularly spessartine ($X_{spss}$ =

0.29-0.37), and grossular ($X_{gr}$ = 0.22-0.25). Significant enrichment in the grossular component in sample 293 ($X_{gr}$ = 0.22-0.25) relative to other metapelite samples detailed above ($X_{gr}$ = 0.03-0.04) also suggests a calc-silicate origin for the rock. Similar compositional variation is observed in sample 312, with $X_{alm}$ varying from 0.29 to 0.44. The dominant compositional variation in this sample is again in the form of core to rim zoning (Fig. 5.5c), with representative end-member compositions of $Alm_{44}Spss_{15}Py_3Gr_{38}$ from a core analysis and $Alm_{29}Spss_{23}Py_2Gr_{46}$ from a rim analysis. $X_{Fe}$ is also consistent across all analyses ($X_{Fe}$ *c*. 0.93-0.95).

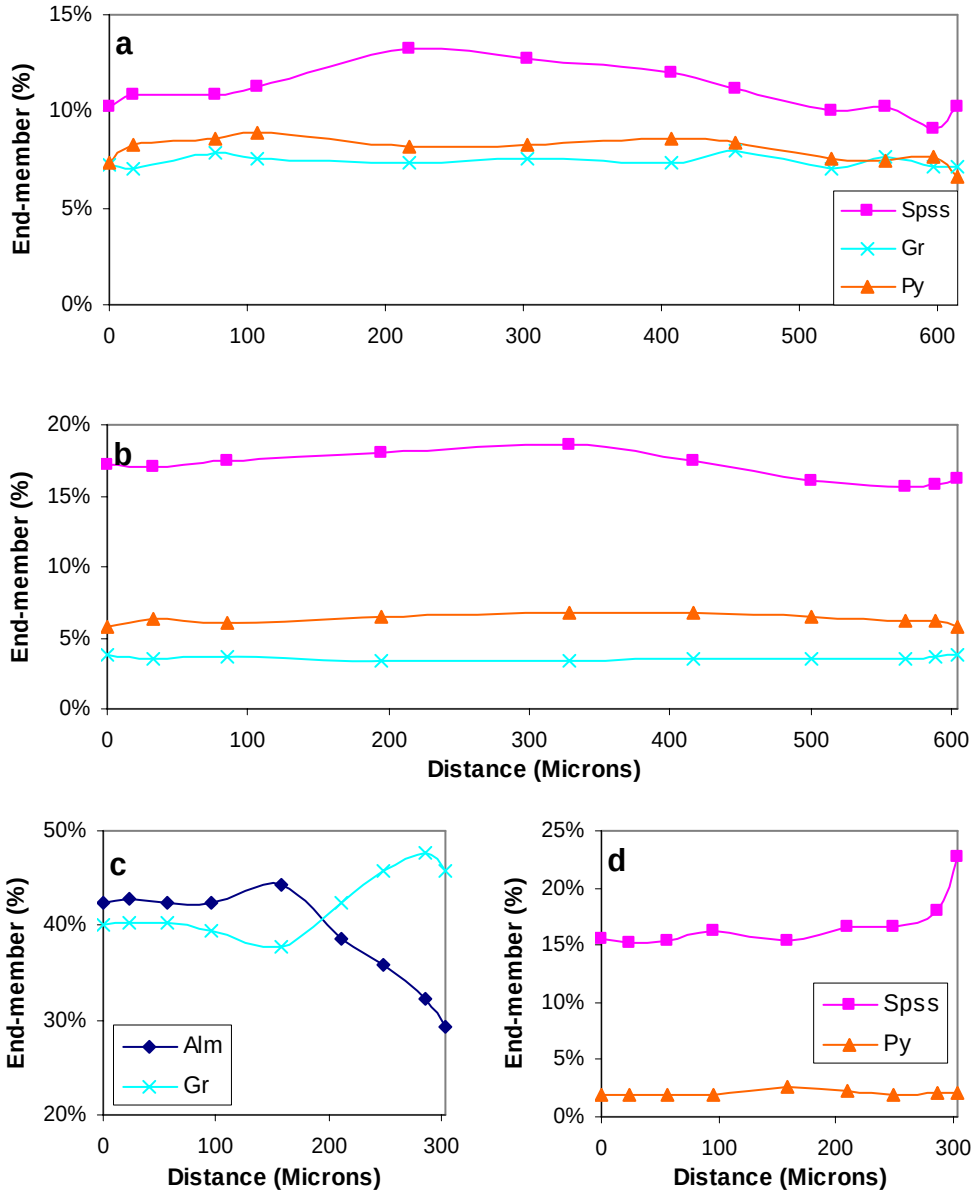


**Figure 5.5: Compositional zoning across garnet porphyroblasts. (a) Plot of values for traverse of garnet porphyroblast from sample 306. (b) Plot of values for traverse of garnet porphyroblast**

**from sample 288. (c) Plot of values for almandine and grossular components in traverse of garnet porphyroblast from sample 312. (d) Plot of values for spessartine and pyrope components in traverse of garnet porphyroblast from sample 312. In all plots: Alm = Almandine, Spss = Spessartine, Py = Pyrope, and Gr = Grossular.**

### 5.6.1.2 Feldspar

Plagioclase is found in samples 282, 288, 293, and 312. In samples 282 and 288 plagioclase is an albite-rich solid solution with $X_{alb}$ = 0.81-0.83 [$X_{alb}$ = Na/(Na + Ca)] in sample 282, and $X_{alb}$ = 0.92 in sample 288. Plagioclase in samples 293 and 312 consists of an anorthite-rich solid solution, which again suggests a calc-silicate origin for the rocks. Plagioclase compositions vary between $X_{an}$ = 0.62 to 0.72 [$X_{an}$ = Ca/(Na + Ca)] in sample 293, and $X_{an}$ = 0.42 to 0.70 in sample 312.

### 5.6.1.3 Epidote group minerals

Epidote group minerals only occur in samples 293 and 312. Epidote in sample 293 is relatively Fe-rich, with $X_{Fe}^{3+}$ = 0.25 [$X_{Fe}^{3+}$ = $Fe^{3+}/(Fe^{3+}+Al)$]. In sample 312, greater variation in $Fe^{3+}$ and Al is observed, with $X_{Fe}^{3+}$ ranging from 0.15 to 0.23.

### 5.6.1.4 Staurolite

Staurolite is only identified in sample 306. Compositional variation is limited within staurolite, with $X_{Mg}$ [$X_{Mg}$ = Mg/(Mg + Fe)] for all analyses falling within the range of 0.84 to 0.88. Mg also shows some minor variation between core ($X_{Mg}$ = 0.16) and rim analyses ($X_{Mg}$ = 0.14), and may reflect some compositional heterogeneity or zoning. Zn values were not measured in this study, but are likely to be low given very low Na values. Chlorite porphyroblasts in sample 288 may have originally been staurolite, but were completely pseudomorphed by subsequent retrogression.

### 5.6.1.5 Amphibole

Sample 312 is the only analysed sample containing amphibole. Two compositionally distinct Ca-rich amphiboles are identified in this sample. ‘Common’ hornblende is found as large phenocrysts throughout, often associated with garnet with which it defines the prograde metamorphic mineral assemblage. In this sample, hornblende

shows some compositional variation between individual grains, with compositions ranging between magnesio-hornblende ($X_{Ca}$ = 0.97-0.88 [$X_{Ca}$ = Ca/(Ca + Na)]; $X_{Al}$ = 0.17-0.50 [$X_{Al}$ = Al/(Al + Mg)]), ferro-hornblende ($X_{Ca}$ = 0.89; $X_{Al}$ = 0.49), pargasite ($X_{Ca}$ = 1.00; $X_{Al}$ = 0.88) and ferro-pargasite ($X_{Ca}$ = 0.86; $X_{Al}$ = 0.54). Secondary amphibole in the form of actinolite was also identified, and has a narrow compositional range ($X_{Ca}$ = 0.98-0.97; $X_{Al}$ = 0.15-0.09). In addition to the hornblende porphyroblasts, both hornblende and actinolite occur as small, elongate grains within the matrix of the sample.

#### 5.6.1.6 Biotite

Biotite occurs in all samples with the exception of sample 312. Despite its occurrence in all mica schist samples, it has a moderate compositional range. In the Gum Flats area, $X_{Fe}$ values for biotite lie within the range of 0.54 to 0.65 for all samples, and it is possible that more than one stage of biotite growth in present. In sample 306 from the Robinhood area, biotite shows a large compositional range, with $X_{Fe}$ falling between 0.46 and 0.64. As with the samples from Gum Flats, it is possible that more than one stage of biotite growth is present in this sample. However, Fe-Mg exchange between biotite and adjacent garnet ($X_{Fe}$ = 0.92-0.88) may in part account for the compositional variation. $TiO_2$ values for biotite across all samples vary significantly, ranging from less than 1 wt% in sample 288 through to up to 3 wt% in samples 283 and 293.

#### 5.6.1.7 White Mica

White mica in all samples is muscovite, with Fe and Mg constituting up to 0.4 cations per formula unit based on 22 oxygens. Si mostly constitutes 6.0-6.3 cations per formula unit (22 oxygens); however phengitic compositions are not observed, as the ratio of Si to Al is typically close to 6:5. Fe in most samples is in excess of Mg with measured $X_{Fe}$ values typically between 0.5 and 0.7. The exception is two analyses in sample 306 which have $X_{Fe}$ values of 0.47. Substitution of Na for K is low in most samples with $X_K$ [$X_K$ = K/(K + Na)] typically between 0.93 and 0.98. Muscovite in samples 288 and 306 both contain lower K:Na, with $X_K$ varying between 0.85 and 0.88 in sample 288, and between 0.84 and 0.85 in sample 306. Na typically constitutes

less than 0.15 cations per formula unit (22 oxygens) in samples with high K:Na ratios (greater than 0.90), but varies between 0.2 and 0.3 cations per formula unit in samples 288 and 306.

#### 5.6.1.8 Titanite (Sphene)

Sphene is only found in sample 312. All analyses contain between 3.49 and 3.69 Ti, 3.95 and 3.99 Ca, and between 0.35 and 0.61 Al cations per formula unit (20 oxygens).

#### 5.6.1.9 Chlorite

Chlorite was identified and analysed in samples 288 and 306. The composition of chlorite in both samples lies within the range of ripidolite (after Deer *et al*., 1992), with $X_{Fe}$ values of 0.50 and 0.58, and 5.14 to 5.40 Si cations per formula unit (28 oxygens).

### 5.6.2 Non-silicates

#### 5.6.2.1 Ilmenite

Ilmenite is only found in sample 288. Individual analyses are compositionally indistinguishable within the sample, containing on average 2 cations per formula unit (4 oxygens) of both Ti and Fe.

#### 5.6.2.2 Rutile

Rutile is only found in sample 306. Although essentially consisting of $TiO_2$, analysed rutile contains minor amounts of both Al (up to 2 wt%) and Fe (up to 3 wt%).

## 5.7 Thermobarometry results

Temperature estimates were made using five geothermometer calibrations. These included the average *P-T* (pressure-temperature) method of THERMOCALC (Powell & Holland, 1988), the garnet-biotite exchange thermometers of Ferry & Spear (1978), Perchuck & Lavrent´eva (1983), and Bhattacharya *et al*. (1992), and the garnet-hornblende exchange thermometer of Graham & Powell (1984). Across all analysed

samples containing biotite, reasonable correlation between garnet-biotite thermometer methods was observed. However, temperature and to a lesser extent pressure estimates obtained using the average *P-T* method of THERMOCALC returned significant differences. THERMOCALC temperature estimates were in the order of 50-100 °C higher than those obtained using other methods (Table 5.3). However, as all THERMOCALC temperature estimates were obtained from independent sets of reactions and contain low associated errors, the estimates obtained are considered reliable, and may therefore reflect maximum recorded temperature conditions. Of the three remaining garnet-biotite thermometers, the temperature estimates obtained using the method of Perchuck & Lavrent´eva (1983) are preferred, based on a recent assessment of the reliability of numerous garnet-biotite thermometer calibrations (Wu & Cheng, 2006). Subsequently, only temperature estimates produced using this method are discussed below and presented in Table 5.3, along with estimates obtained from THERMOCALC average *P-T* calculations.

Pressure estimates using net-exchange barometers were limited due to unfavourable mineral assemblages in biotite-grade samples. Subsequently only two geobarometers were used. These were the average *P-T* method of THERMOCALC, and for sample 312 the net-transfer barometer of Kohn & Spear (1990). Pressure estimates using THERMOCALC were obtained, with varying degrees of success, from all samples except sample 283. Pressure estimates obtained using THERMOCALC for samples containing biotite (all samples except 283 and 312) have relatively high errors (Table 5.3). For sample 312, where more than one method for estimating pressure was used, the THERMOCALC estimates also had relatively high calculated errors. However, in this sample the net-transfer barometer estimates lie within error, or correlate with THERMOCALC estimates (Table 5.3), and are therefore considered reliable.

*P-T* estimates in metapelites of lower- to mid-amphibolite grade from both the Gum Flats area (samples 282, 283, 288, and 293) and the Robinhood area (sample 306) are limited by the dominant mineral assemblage garnet-biotite-muscovite-quartz. Application of four calibrations of the garnet-biotite thermometer (Perchuk & Lavrent`eva, 1983; Ferry & Spear, 1978; Bhattacharya *et al.*, 1992) to these samples was reasonably successful, as estimates for $M_1$ were made by pairing almandine-rich garnet porphyroblast cores with adjacent $S_1$ biotite grains (e.g. Fig. 5.3a). In samples 282 and 283, temperature estimates for $M_1$ conditions calculated using the method of

Perchuk & Lavrent`eva (1983) vary between 522 and 558 °C, with assumed pressures between 4 and 6 kbar (Table 5.3). Slightly higher temperature estimates were obtained for $S_1$ assemblages in sample 288, at an assumed pressure of 5.5 kbar (566 to 568 °C). Temperature estimates for mineral assemblages in sample 288 that returned average *P-T* conditions analogous to $M_2$ were obtained using the garnet-biotite thermometer of Perchuk & Lavrent`eva (1983), and returned estimates of 483 and 484 °C at an assumed pressure of 3 kbar (Table 5.3).

| Sample | Lithology (GDA94 grid co-ordinates) | Mineral Assemblage | Assumed *P* (kbar) | Assumed *T* (°C) | Calculated Result *T* (°C) | Calculated Result *P* (kbar) | Method |
|---|---|---|---|---|---|---|---|
| 282 | Einasleigh Metamorphics | gt-bi-mu-pl-qz | - | - | 726 ± 45, 768 ± 75 | 6.9 ± 1.5, 7.3 ± 2.3 | 1 |
| | 0806720 7880664 | *(M1 assemblage)* | 4 | - | 551, 558 | | 2a, 2b |
| | (Easting Northing) | | 6 | - | 522, 522 | | 2a, 2b |
| 283 | Einasleigh Metamorphics | gt-bi-mu-pl-qz | 4.5 | - | 557, 552 | | 2a, 2b |
| | 0806700 7880664 | *(M1 assemblage)* | | | | | |
| 288 | Daniel Creek Formation | gt-bi-mu-pl-qz | - | - | 642 ± 31 | 7.6 ± 1.3 | 1 |
| | 0805845 7881526 | *(M1 assemblage)* | 5.5 | - | 568, 566 | | 2a, 2b |
| | | gt-bi-mu-chl-qz | - | - | 557 ± 117 | 3.1 ± 1.7 | 1 |
| | | *(M2 assemblage)* | 3 | | 484, 483 | | 2a, 2b |
| 293 | Bernecker Creek Formation | gt-bi-ep-pl-mu-qz | - | - | 624 ± 69 | 6.3 ± 1.8 | 1 |
| | 0803330 7884267 | *(M1 assemblage)* | | | | | |
| | | gt-bi-ep-pl-mu-qz | - | - | 559 ± 35 | 5.1 ± 1.0 | 1 |
| | | *(M1R assemblage)* | 5.5 | - | 426, 424 | | 2a, 2b |
| | | | 6.5 | - | 418, 419 | | 2a, 2b |
| 306 | Corbett Formation | gt-bi-mu-st-pl-qz | - | - | 574 ± 18 | 6.3 ± 2.5 | 1 |
| | 0766403 7908517 | *(M1 assemblage)* | 6.5 | | 523, 526 | | 2a, 2b |
| 312 | Daniel Creek Formation | gt-hbl-pl-qz | - | - | 649 ± 69, 631 ± 69 | 7.1 ± 1.8, 6.4 ± 1.7 | 1 |
| | 0800551 7888325 | *(M1 assemblage)* | - | 650 | | 6.5 | 4 |
| | | | 6 | - | 659 | | 3 |
| | | gt-act-pl-cz-qz | - | - | 562 ± 51, 564 ± 60 | 5.3 ± 1.4, 5.5 ± 1.6 | 1 |
| | | *(M1R assemblage)* | - | 550 | | 5.2 | 4 |
| | | | 5.5 | - | 512 | | 3 |

**Table 5.3: Pressure and temperature estimates calculated from a variety of thermobarometric techniques to the mineral assemblages of selected samples from the lower Etheridge Group metasediments. Methods: 1- THERMOCALC average *P-T* method (Powell & Holland, 1988); 2a- Perchuk & Lavrent`eva (1983) (Perchuk *et al.*, 1981); 2b- Perchuk & Lavrent`eva (1983) (Hewitt & Wones, 1975); 3- Graham & Powell (1984); 4- Kohn & Spear (1990). Mineral abbreviations after Kretz (1983). THERMOCALC output files are listed in Appendix 3.**

The application of the THERMOCALC average *P-T* method to $S_1$ and retrograde mineral assemblages in sample 282 and 288 was successful, and is illustrated best by the clear separation of *P-T* estimates for both $M_1$ and $M_2$ in sample 288 (Table 5.3). Subsequently, estimates made using THERMOCALC for these samples are considered to best represent the maximum *P-T* conditions reached during each event. For sample 282, THERMOCALC returns average *P-T* conditions of 6.9 ± 1.5 kbar

and 726 ± 45 °C, and 7.3 ± 2.3 kbar and 768 ± 75 °C (Table 5.3). These values are significantly higher than those of the garnet-biotite thermometers, and therefore represent maximum estimates for $M_1$ *P-T* conditions in this sample.

In sample 288, THERMOCALC returned conditions of 7.6 ± 1.3 kbar and 642 ± 31 °C from an independent set of five reactions for an $M_1$ assemblage (Table 5.3; Appendix 3). This temperature estimate is noticeably higher than the calculated garnet-biotite exchange thermometer estimates, and represents a maximum estimate for the temperature conditions during $M_1$. A THERMOCALC average *P-T* estimate was also obtained from a later assemblage containing chlorite, and returned conditions of 3.1 ± 1.7 kbar and 557 ± 117 °C from an incomplete independent set of three reactions (Table 5.3; Appendix 3). These conditions are low enough that they are analogous to calculated *P-T* conditions for $M_2$ in the Robertson River Subgroup near Robinhood (Cihan *et al.*, 2006); therefore I suggest that this estimate is more likely to represent early $M_2$ rather than retrograde $M_1$ conditions. Temperature estimates for $M_2$ using garnet-biotite exchange thermometers returned values lower than the THERMOCALC temperature estimate; however they remain within error of this value (Table 5.3).

Temperature conditions estimated for sample 293 using garnet-biotite exchange thermometers returned average temperatures approximately 100 °C below that of samples 282/283 and 288 (Table 5.3). They vary between 418 and 426 °C for assumed pressures of 5.5-6.5 kbar, and may represent $M_{1R}$ temperatures. Two estimates of average *P-T* conditions were calculated from equilibrium assemblages using THERMOCALC. In both cases estimates produced an independent set of reactions (Appendix 3). Maximum $M_1$ conditions experienced by this rock are best represented by the average *P-T* estimates of 6.3 ± 1.8 kbar and 624 ± 69 °C (Table 5.3). Although of lower pressure, this estimate corresponds to the average *P-T* conditions estimated for sample 288. The second equilibrium assemblage produced a *P-T* estimate of 5.1 ± 1.0 kbar and 559 ± 35 °C (Table 5.3), which is significantly lower than the inferred maximum $M_1$ conditions. This assemblage may have been influenced by later retrogression related to $M_{1R}$, as the calculated *P-T* estimates correlate with estimates obtained from $M_{1R}$ assemblages in sample 312.

Estimated *P-T* conditions for an $M_1$ mineral assemblage containing garnet and staurolite in sample 306 are close to those previously inferred to represent the peak

$M_1$ conditions in the area (Boger & Hansen, 2004; Cihan *et al*., 2006). The average *P-T* method of THERMOCALC gives conditions of 6.3 ± 2.5 kbar and 574 ± 18 °C from an independent set of five reactions (Table 5.3; Appendix 3). As with previous samples, temperature estimates using the garnet-biotite thermometers of Perchuk & Lavrent`eva (1983) returned estimates lower than the average *P-T* method. Estimates for paired garnet and $M_1$ biotite are 523 and 526 °C for an assumed pressure of 6.5 kbar (Table 5.3).

For sample 312, the methods of Kohn & Spear (1990) and Graham & Powell (1984) were used in addition to the average *P-T* method of THERMOCALC for *P-T* estimates, due to the absence of biotite and muscovite and the presence of hornblende. Close correlation is observed between the THERMOCALC estimates and the exchange method estimates (Table 5.3). Due to the presence of both $M_1$ hornblende and retrograde $M_{1R}$ actinolite, *P-T* estimates for both $M_1$ and $M_{1R}$ were calculated. For $M_1$, THERMOCALC returned average *P-T* conditions of 7.1 ± 1.8 kbar and 649 ± 69 °C, and 6.4 ± 1.7 kbar and 631 ± 69 °C. The garnet-hornblende exchange thermometer of Graham & Powell (1984) gave slightly lower temperature estimates for $M_1$ ranging up to 659 °C at an assumed pressure of 6 kbar from several garnet-hornblende pairs. Pressure conditions calculated by the garnet-hornblende-plagioclase-quartz Fe and Mg exchange barometers of Kohn & Spear (1990) gave estimates of up to 6.5 kbar for an assumed temperature of 650 °C (Table 5.3).

Average *P-T* conditions calculated by THERMOCALC from minerals considered representative of $M_{1R}$ in sample 312, including $S_2$ actinolite, returned estimates below that calculated for $M_1$. Using the average *P-T* method, two independent sets of reactions were produced giving conditions of 5.3 ± 1.4 kbar and 562 ± 51 °C, and 5.5 ± 1.6 kbar and 564 ± 60 °C (Table 5.3). As with the estimates produced for $M_1$, the garnet-hornblende exchange thermometer of Graham & Powell (1984) gave a slightly lower temperature estimate for $M_{1R}$ of 512 °C at an assumed pressure of 5.5 kbar. Pressure conditions calculated using the garnet-hornblende-plagioclase-quartz Fe and Mg exchange barometer of Kohn & Spear (1990) correlate well with the average *P* estimate, returning a calculated pressure of 5.2 kbar at an assumed temperature of 550 °C (Table 5.3).

## 5.8 Discussion

### 5.8.1 Limitations on the interpretation of *P-T* estimates using the exchange and net transfer methods.

The use of exchange and net transfer calculations in thermobarometric analysis require that the compositions analysed are in equilibrium at some point in their evolution. Typically, compositions in equilibrium are assumed, often conveniently, to represent peak metamorphic assemblages. However, in terranes that have experienced multiple recrystallising events, or relatively long cooling histories, equilibrium assemblages are often difficult to identify due to compositional heterogeneities in the phases of interest. The compositional heterogeneity within crystals is caused by a combination of exchange and net transfer reactions (hence their use in thermobarometric studies), and is often represented by chemical zoning in minerals (Spear, 1993). Zoning can occur during the prograde history of a mineral ('growth zoning'), and during its cooling history ('diffusion zoning').

The compositional zoning within crystals can have significant effects on *P-T* estimates, especially if the correct mineral compositions are not selected for particular stages of mineral growth (Spear, 1993). Garnet porphyroblasts from samples analysed in this study demonstrate the effects of diffusion and possibly also growth zoning (Fig. 5.5). The limited effects of diffusion on the garnet porphyroblasts analysed are visible on garnet rims in Figure 5.5. The diffusive zoning is a consequence of the Fe-Mg equilibrium exchange between garnet and adjacent biotite. However, net transfer reactions involving the consumption/production of metastable phases such as garnet and biotite, have also played an important role. This is demonstrated by the observed range in biotite compositions (e.g. Sample 306), and the compositional variation across the garnet porphyroblast in Sample 306 (Fig. 5.5a).

Consequently, there is significant risk in the compositions selected for analysis not being in equilibrium. Therefore, it is reasonable to suggest that *P-T* estimates obtained from reactions which involve garnet and other potentially zoned minerals, such as the garnet-biotite exchange thermometer used in this study, be treated with some caution.

### 5.8.2 Widespread retrograde assemblages in Etheridge Group metasediments from Gum Flats: evidence of an extended period of retrogression following peak metamorphism?

Widespread retrogression of prograde ($M_1$) metamorphic minerals, most notably staurolite to chlorite, and associations of other low-grade metamorphic minerals co-existing with higher-grade minerals, notably actinolite and hornblende, suggests a period of retrograde metamorphism immediately followed $M_1$ in the Etheridge Group metasediments near Gum Flats. These relationships are also supported by average *P-T* calculations from two samples (samples 293 and 312; Table 5.3), involving inferred retrograde assemblages that produced estimates consistent with a decrease in both pressure and temperature from $M_1$.

Numerous outcrops of Daniel Creek Formation metasediments from both the Gum Flats and Ortona areas contain chlorite porphyroblasts that I interpret to have formed via complete replacement of $M_1$ staurolite. In sample 288, the pairing of chlorite to an adjacent garnet rim, muscovite, biotite and quartz located in the strain shadow of the porphyroblast (Fig. 5.4c), allowed for the calculation of average *P-T* conditions of 3.1 ± 1.7 kbar and 557 ± 117 °C. I infer that these conditions mark the start of $M_2$ metamorphism, as well as the end of the decreasing *P-T* path representing $M_{1R}$. However, it is also possible that these conditions were reached later, between ca. 1550-1500 Ma. An $M_1$ assemblage from the same sample involving a garnet core, adjacent $S_1$ biotite, muscovite and plagioclase returned a maximum average *P-T* estimate for $M_1$ of 7.6 ± 1.3 kbar and 642 ± 31 °C, which also provides a tying point between maximum $M_1$ *P-T* conditions and initial *P-T* conditions for $M_2$ (Fig. 5.6).

In sample 312 coexisting $M_1$ hornblende and actinolite may suggest progressive metamorphism, with hornblende forming at higher grades. However, using the same method as for sample 288, actinolite when paired with an adjacent garnet rim, plagioclase and epidote returned average *P-T* conditions consistent with the retrograde $M_{1R}$ event (5.5 ± 1.6 kbar, 564 ± 60 °C). given that these conditions are significantly different from assumed $M_1$ estimates made by pairing hornblende with garnet cores (7.1 ± 1.8 kbar, 649 ± 69 °C), it is reasonable to assume that the co-existence of hornblende and actinolite may not indicate immiscibility but rather a later stage of retrogressive metamorphism, with $M_1$ hornblende replaced by actinolite and possibly clinozoisite.

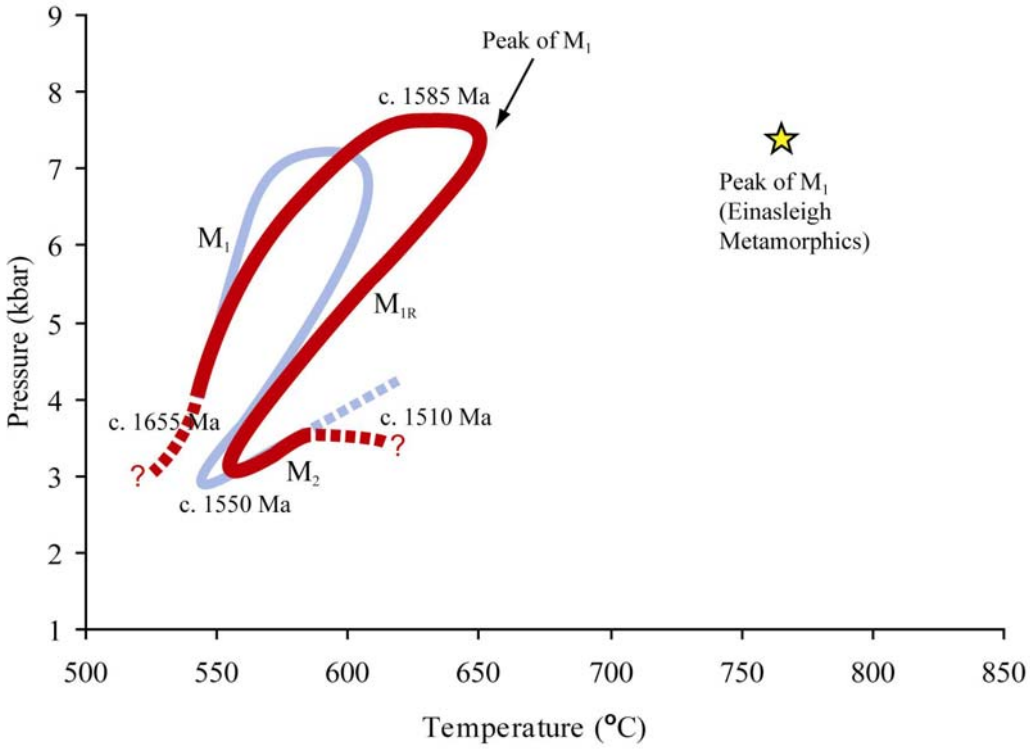


**Figure 5.6: *P-T-t* diagram for the lower Etheridge Group metasediments of the Gum Flats area (in red). *P-T-t* path in blue represents metamorphic history for Robertson River Subgroup metasediments near Robinhood (after Cihan *et al.*, 2006). Yellow star indicates maximum average *P-T* estimate obtained for $M_1$ from mica schist of the Einasleigh Metamorphics at Gum Flats (Sample 282; Table 5.3).**

As the number of samples successfully analysed in this study was relatively small, and their mineral assemblages relatively limited, only a small number of geothermometer and geobarometers calibrations were successfully applied. Despite these limitations, the average *P-T* conditions calculated for representative mineral assemblages, and to a lesser extent the garnet-biotite and garnet-hornblende exchange thermometers used, provide an indication of the differing metamorphic conditions that were experienced during both the $M_1$ and $M_{1R}$ events. From the results obtained, it appears that retrogression following $M_1$ in the Gum Flats area involved an approximate decrease in pressure and temperature of up to 4 kbar and 200 °C, possibly associated with uplift and extrusion immediately following $M_1$.

Indirect evidence for the presence of a retrograde $M_{1R}$ event in the metasediments of the Etheridge Group was also recently reported by Cihan *et al*. (2006) using EMPA ages obtained from $M_1$ (1586 ± 6 Ma) and inferred $M_2$ (1542 ± 8 Ma) monazites and

associated average *P-T* estimates. Based on these weighted-average monazite ages, in addition to microstructural data including the retrogression of $M_1$ staurolite to andalusite, they inferred that an extended period of retrogression may have lasted for as long as ~45 Ma. Although *P-T* estimates from their study were produced from analysis of metasediments of the Robertson River Subgroup at Robinhood, their *P-T-t* path is broadly analogous to the path *P-T-t* path for Gum Flats (Fig. 5.6). The correlation of *P-T* estimates was also confirmed by the analysis of $M_1$ minerals in sample 306, collected from the same locality, which returned average *P-T* estimates that lay upon the prograde path of $M_1$ from their study (Fig. 5.6).

### 5.8.3 Summary and timing of *P-T* conditions during mid-Proterozoic prograde and retrograde metamorphism in the lower Etheridge Group metasediments, and regional implications

Quantitative estimates obtained through the use of several directly calibrated barometers and thermometers and the average *P-T* method of THERMOCALC support the premise that the mid-Proterozoic (ca. 1600-1550 Ma) metamorphic evolution of the metapelites from the southern extensions of the lower Etheridge Group began with burial and metamorphism to mid-crustal pressures and temperatures ($M_1$). This was followed by a period of retrogression ($M_{1R}$), then a low-pressure, high-temperature thermal overprint ($M_2$). Although sample 306 was overprinted by a later metamorphic fabric ($S_3$), I was unable to obtain a reliable *P-T* estimate for this event. In the Gum Flats area, $M_1$ in Bernecker Creek Formation and Daniel Creek Formation metasediments resulted in *P-T* conditions of up to 7.6 kbar and 650 °C, and facilitated the development of a weak to strong layer-parallel schistosity ($S_1$). The garnet-hornblende gneiss (sample 312) reached similar peak metamorphic conditions for $M_1$, recording conditions of up to 7.1 ± 1.8 kbar and 649 ± 69 °C.

Estimates obtained for $M_1$ in samples of the Einasleigh Metamorphics (samples 282 and 283) are consistent with this unit experiencing on average higher metamorphic conditions than those experienced in the Bernecker Creek Formation and Daniel Creek Formation. For sample 282, $M_1$ average *P-T* estimates of up to 7.3 ± 2.3 kbar and 768 ± 78 °C were calculated (Table 5.3). A gradual decrease from the peak metamorphic conditions of $M_1$ is indicated in a number of samples by the replacement

of prograde metamorphic minerals. Examples of this include garnet by biotite and staurolite porphyroblasts pseudomorphed by chlorite. Initial *P-T* conditions at the onset of $M_2$ in the metasediments at Gum Flats are best represented by the average *P-T* estimate of 3.1 ± 1.7 kbar and 557 ± 117 °C obtained from sample 288 (Table 5.3).

The average *P-T* estimate for $M_1$ from sample 288 appears anomalously high when compared to the average *P-T* estimate for sample 293, given their relative stratigraphic positions (Fig. 5.2; Table 5.3). However, it is possible that prior to displacement along the Gilberton Fault during the Late Ordovician or Early Silurian (Withnall, 1989), the rocks surrounding sample 288 were in proximity to biotite-gneiss of the (higher-grade) Einasleigh Metamorphics, at a similar stratigraphic position to that now observed for sample 312. Removing the suggested ~50 km of dextral displacement along the Gilberton Fault (Withnall *et al*., 1980) would place the Daniel Creek Formation rocks surrounding sample 288 in proximity to Einasleigh Metamorphics biotite-gneiss and layered migmatites that now lie ~20 km southwest of Gilberton (Withnall *et al*., 2003a). Consequently, this suggests that outcrops of the Bernecker Creek Formation surrounding Gum Flats Station are of a relatively lower metamorphic grade than those of the Daniel Creek Formation schists proximal to schist/gneiss of the Einasleigh Metamorphics further north (Fig. 5.2), and that this difference may be related to the orogenic event that promoted $M_1$.

The major metamorphic events of the lower Etheridge Group ($M_1$ and $M_2$) have previously been estimated to have occurred within a ~30 million year period between 1580 and 1550 Ma (Withnall *et al*., 1997; Black *et al*., 2005). However, metamorphic monazite dating from Cihan *et al*. (2006) and this study infer that $M_1$ may have occurred slightly earlier (ca. 1590-1580 Ma). In sample 288, monazite that had grown within an $M_1$ assemblage returned a weighted mean age of 1585 ± 18 Ma, and correlates well with the estimated age of 1586 ± 6 Ma for $M_1$ from Cihan *et al*. (2006). This age is also coeval with the onset of major orogenesis in the Mt Isa Eastern Succession (Page & Sun, 1998; Sayab, 2006), as well as $D_1$ in the Yambo and Coen Inliers (Blewett & Black, 1998; Blewett *et al*., 1998; Fig. 1.1). As discussed in Chapter 4, monazites recording $M_2$ conditions yielded ages between ca. 1550 Ma and 1525 Ma, suggesting that the grains may have been affected by partial resetting during a later event. For example, sample 283 recorded a weighted mean age within a mixed $M_{1\text{-}2}$ assemblage of 1537 ± 18 Ma. This age is within error of the proposed age for $M_2$

from Cihan *et al*. (2006) of 1542 ± 8 Ma. However, due to the younger weighted mean age and spread of individual U-Th-Pb ages from individual grains, I suggest that the 1537 ± 18 Ma age may represent a partially reset $M_2$ age, possibly influenced by a later (ca. 1500 Ma) event.

The metamorphic history for the lower Etheridge Group metasediments at Gum Flats is illustrated in the *P-T-t* diagram shown in Fig. 5.6. Also shown is the *P-T-t* path for metasediments of the Robertson River Subgroup at Robinhood as proposed by Cihan *et al*. (2006). From the diagram, it is apparent that all rocks of the lower Etheridge Group experienced a similar 'clockwise' metamorphic history, beginning with a prograde metamorphic path leading to medium *P-T* metamorphism ($M_1$), followed by an extended period of retrograde metamorphism ($M_{1R}$), and then low-*P*, high-*T* metamorphism ($M_2$). The key difference between the two areas relates to level of metamorphism attained, with the metasediments at Gum Flats generally reaching higher temperatures for a given pressure during $M_1$ (Fig. 5.6). The highest $M_1$ conditions are recorded by the metasediments of the Einasleigh Metamorphics (Samples 282 and 283), reflecting their evolution at different crustal conditions before faulting along the Gilberton Fault led to their juxtaposition alongside the Daniel Creek Formation in the Palaeozoic.

The clockwise *P-T-t* path suggested here is not unique to the lower Etheridge Group. A similar metamorphic history has been proposed for the rocks of the Mt Isa Eastern Succession based on FIA trends and thermobarometric estimates (Sayab, 2006). The metamorphic history of this area involved similar mid-Proterozoic medium pressure-temperature conditions for $M_1$ that were followed by decompression, retrogression, and a later thermal overprint. In the case of Mt Isa this thermal overprint was associated with the emplacement of the Williams and Naraku Batholiths between ca. 1550-1500 Ma (Page & Sun, 1998). The emplacement of these batholiths may correlate with a late-stage 'thermal pulse' which was suggested by Cihan *et al*. (2006), and may have also led to the development of new metamorphic monazite and the partial resetting of $M_2$ monazite ages in this study. If this is the case, the evidence presented here, along with the growing collection of geochronological data indicating a coeval $M_1$ event across terranes (e.g. Blewett & Black, 1998; Blewett *et al*., 1998; Page & Sun, 1998; Cihan *et al*., 2006), would suggest that the Proterozoic cratons of

Northeastern Australia may have shared a similar metamorphic history spanning the period between ca. 1600 and ca. 1500 Ma.

# Chapter 6.

# Geochemical, Sm-Nd isotopic characteristics and petrogenesis of Palaeoproterozoic mafic rocks from the lower Etheridge Group, Georgetown Inlier, north Queensland

## 6.1 Introduction

Crustal blocks of Palaeoproterozoic – Mesoproterozoic age in eastern and northern Australia include the Curnamona Province in western New South Wales, the Mt Isa Inlier in western Queensland, and the Georgetown Inlier in north Queensland. Rock sequences in these inliers, including products of prominent and widespread mafic magmatism, are generally considered to have formed in major intra-cratonic basins developed in rift settings (e.g., Scott *et al*. 2000). These inliers, and several others further west in Northern Territory and central Australia, have been considered once to have formed a contiguous crustal block known as the North Australian Craton (Myers *et al*., 1996; Tyler *et al*., 1998; Scott *et al*., 2000; Betts & Giles 2006).

Whether the assembly and subsequent dispersion of these Palaeoproterozoic – Mesoproterozoic crustal blocks involved dominantly intraplate processes with limited or no lateral accretion (e.g., Etheridge *et al*. 1987), or processes analogous to those occurring via plate tectonics on the modern Earth (e.g. Myers *et al*. 1996; McDonald *et al*. 1997; Scott *et al*. 2000; Dawson *et al*. 2002; Betts *et al*. 2002; Giles *et al*. 2002, 2004; Betts & Giles 2006) is still debated. Giles, Betts and co-workers proposed that plate margin processes may affect basin evolution within continental blocks, and as summarised in Betts & Giles (2006), these authors have argued that the North Australian Craton was bordered on its southern margin by a S-dipping subduction zone from 1800-1600 Ma, and on its eastern margin by W-dipping subduction zone from 1600-1500 Ma.

Knowledge of the timing and composition of mafic magmatism in each of the inliers that are considered to have comprised the North Australian Craton is vital to developing a clearer understanding of the possible temporal and spatial links between these inliers, and their tectonic setting at the time of the mafic magmatism. To that end, I report here a detailed geochemical study of the widespread mafic rocks of late Palaeoproterozoic age in the Georgetown Inlier of north Queensland.

## 6.2 Previous Work

Previous geochemical studies of mafic rocks within the lower Etheridge Group include the work of McNaughton & Wilson (1983), Black & McCulloch (1984), Withnall (1985) and Knutson & Stephenson (1989). McNaughton & Wilson (1983) analysed 13 mafic granulites from the Einasleigh Metamorphics near Einasleigh, and concluded that the immobile element concentrations of the rocks were virtually indistinguishable from those of modern MORB, and that the igneous precursors of the mafic rocks were probably derived from a mantle source similar to that which underlies modern mid-ocean ridges.

As part of a broader study of the Nd isotopic compositions of Palaeoproterozoic mafic rocks in central and northern Australia, Black & McCulloch (1984) made a reconnaissance study of the Sm-Nd isotope characteristics of mafic rocks from the Georgetown Inlier. Based on the analysis of $T_{DM}$ ages from several Cobbold Metadolerites, they concluded that the mafic igneous rocks of the lower Etheridge Group were emplaced at 2490 ± 70 Ma, and were derived from partial melting of a depleted upper mantle source ($\varepsilon_{Nd} = +4.0 \pm 0.5$).

The studies of both Withnall (1985) and Knutson & Stephenson (1989) incorporated major and some trace element analyses of the mafic rocks. Withnall (1985) presented analyses of 52 mafic samples collected from the lower Etheridge Group. Knutson & Stephenson (1989) reported compositions for 11 mafic samples collected from the lower Etheridge Group. Lithologies analysed in both studies included greenschist and amphibolite facies metabasalt and metadolerite, amphibolite and 'mafic granulite'. Withnall (1985) concluded that the mafic rocks within the lower Etheridge Group are basaltic, and compare closely with K-poor Tertiary continental tholeiites of Greenland and Baffin Island, and relatively incompatible-element depleted Karoo mafic rocks of southern Africa, both suites being generated during extension of continental crust.

## 6.3 Objectives of the geochemical study

As there has been no comprehensive geochemical study of the mafic rocks of the lower Etheridge Group to date, and conflicting interpretations (MORB-like vs. continental tholeiites) exist for the geochemical character or likely tectonic setting of eruption of these igneous rocks, the key objectives of this geochemical study are:

- To investigate the geochemical character of the mafic rocks of the lower Etheridge Group, and if possible, to infer the likely tectonic setting of their formation.
- To assess whether any significant differences exist between the various mafic rocks of the lower Etheridge Group.
- To investigate the petrogenesis and chemical characteristics of the parental magmas to the mafic rocks in order to make a comparative study with similarly aged mafic rocks from the Mt. Isa and Broken Hill Inliers (Chapter 7).

Details of the sampling and analytical techniques used and additional petrographic information on samples analysed are provided below. A detailed overview of the petrology, mineralogy, stratigraphic, and textural relationships between the DHM and CMD is given in Chapter 3.

## 6.4 Methods

### 6.4.1 Sampling

In areas of semi-continuous outcrop, mafic rocks were collected along traverses with an approximate sample spacing of 100 m, except where detailed sampling to monitor geochemical variations across several thick sills used a much closer (20 m) sample spacing. Thin sections were prepared for all samples, and least altered samples were chosen for whole rock analysis on the basis of geographic spread. Samples showing a foliation, oxidation, veining, or more than 1-2 modal% carbonate or sulphides were excluded from analysis.

For ease of reference, mafic rocks from the lower Etheridge Group are separated into five domains based on their location (Fig. 6.1), and to a lesser extent their grade of metamorphism. The ‘Ortona’, ‘South Head’ and ‘Stockyard’ domains contain samples of greenschist facies DHM and CMD, whereas the ‘Robinhood’ and ‘Gum Flats’ domains contain samples of amphibolite facies CMD. Some 88 samples were analysed by XRF, 25 by ICPMS, and 10 for Nd-isotopes by MC-ICPMS using the methods described below. A full list of analyses and sample locations is given in Tables 6.1 and 6.3 along with average compositions for each domain (Table 6.2).

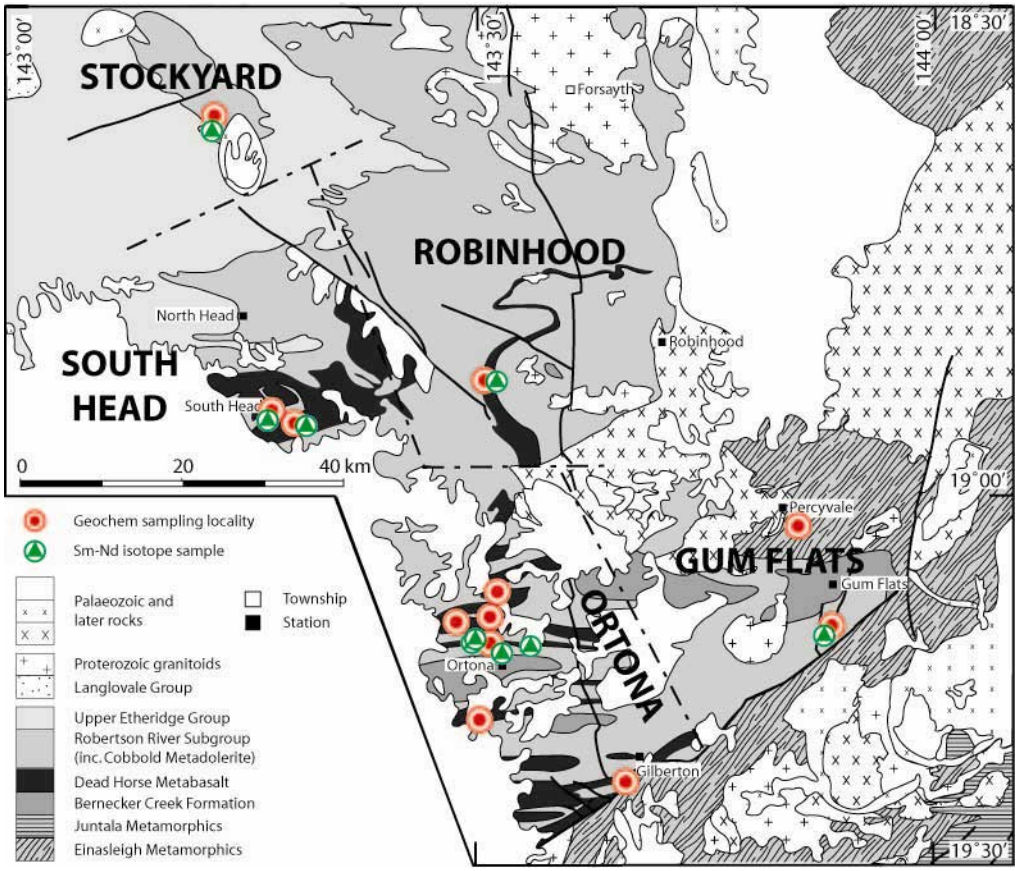


**Figure 6.1: Simplified geological map of the central Georgetown Inlier showing key sampling locations, and the location of sample domains.**

### 6.4.2 Major, trace, and rare earth element analytical techniques

Samples were prepared for analysis using a jaw crusher and tungsten-carbide ring-mill. For XRF analysis, samples were prepared as glass discs for major element-, and pressed powder discs for some trace element analysis. All samples were analysed using a Phillips PW1480 XRF system at the University of Tasmania School of Earth Sciences. Sample preparation, instrument operating conditions, and calibration procedures of the analyses follow the method of Norrish & Hutton (1969).

A representative collection of samples was also analysed for low-level trace elements and rare earth elements (REE) using the HP 4500Plus Inductively Coupled Plasma Mass Spectrometer (ICPMS) at the School of Earth Sciences, University of Tasmania. Samples for ICPMS analysis were digested using a low-pressure $HF/HNO_3$ Savillex digestion. For both XRF and ICPMS analysis, in-house standards TASBAS, BHVO-1, Tafahi and BIR-1 were analysed as unknowns in order to monitor instrumental drift and data quality during the analytical period. Precision for both methods (determined by repeated analysis of the standards and presented as relative standard deviation [%

RSD] for the period of analysis) is better than 5% except for Li, Sc, V, and Zn (5-14%). Analytical accuracy (presented as expected value/average measured value) is better than 5%. Conservative estimation of the detection limits is less than 50 ppb for all elements analysed by ICPMS. Total analytical blank is less than 10 ppb for most elements except for Li, Sc, V, Zn, Mo, and Pb (21-215 ppb), making blank corrections mostly less than 0.1% for mafic samples. Both XRF and ICPMS methods were used for 14 trace elements (Sc, V, Cr, Mn, Ni, Cu, Zn, Sr, Y, Zr, Nb, Ba, Ce, and Nd) on 25 samples. The difference between the two methods is generally less than 10% for all elements, except for Zr and Cr in some samples (up to 30% lower for ICPMS) due to incomplete digestion of chromite and zircon. Samples which returned ICPMS Zr values that varied by more than 15% from their XRF values were re-analysed using a high-pressure $HF/H_2SO_4$ PicoTrace digestion, in order to ensure complete digestion of zircon.

### 6.4.3 Sm-Nd isotope analytical technique

All Sm-Nd analyses were carried out on the NU Instruments MC-ICPMS in the School of Earth Sciences at the University of Melbourne by Dr. Roland Maas. Sample preparation followed Maas *et al*. (2005), and involved the dissolution of whole rock sample powders in Krogh-type high-pressure bombs. Initial digestions with $HF\text{-}HNO_3$ (48 hrs) were followed by digestion with 6M HCl (12 hrs). A mixed tracer solution spike of $^{149}Sm$-$^{150}Nd$ was added to each sample, and samples were prepared for mass spectrometry using a combination of cation exchange and resin methods (Pin *et al*., 1994; Maas *et al*., 2005).

Sm and Nd concentrations in spike and unknown samples were adjusted to yield a mean of 6.59 and 28.8 ppm respectively, based on 3 analyses of international standard BCR-1 run in the same batch. Total laboratory blanks of Sm and Nd for dissolutions were lower than 50 pg. Uncertainties in $^{147}Sm/^{144}Nd$ and $^{143}Nd/^{144}Nd$ are considered to be better than ± 0.2% (2σ) and ± 0.004% (2σ) respectively (R. Maas, pers. comm., 2006). $^{143}Nd/^{144}Nd$ ratios were normalised to 0.7219 for $^{146}Nd/^{144}Nd$, and are reported relative to La Jolla Nd = 0.511860.

| Sample: | 6 | 8 | 22 | 23 | 60 | 72 | 74 | 80 | 82 | 83 | 85 | 86 |
|---|---|---|---|---|---|---|---|---|---|---|---|---|
| Unit: | CMD | CMD | CMD | CMD | CMD | DHM | DHM | DHM | DHM | DHM | CMD | CMD |
| Rock type: | Dolerite | Dolerite | Dolerite | Dolerite | Dolerite | Basalt | Basalt | Basalt | Basalt | Basalt | Dolerite | Dolerite |
| Domain: | Ortona | Ortona | Ortona | Ortona | Ortona | Ortona | Ortona | Ortona | Ortona | Ortona | Ortona | Ortona |
| Method^: | ICPMS | XRF | ICPMS | XRF | XRF | XRF | ICPMS | XRF | XRF | XRF | XRF | XRF |
| $SiO_2$ | 53.64 | 40.18 | 47.14 | 46.73 | 48.50 | 48.21 | 48.73 | 45.31 | 46.27 | 47.66 | 49.15 | 47.62 |
| $TiO_2$ | 1.20 | 1.70 | 1.65 | 1.92 | 1.13 | 1.47 | 1.47 | 1.64 | 1.44 | 1.52 | 1.71 | 2.05 |
| $Al_2O_3$ | 12.95 | 13.58 | 13.15 | 13.41 | 15.35 | 13.75 | 14.25 | 15.46 | 14.05 | 14.90 | 12.67 | 12.48 |
| $Fe_2O_3$* | 13.13 | 6.81 | 15.82 | 18.31 | 13.32 | 15.79 | 15.27 | 17.52 | 15.49 | 16.08 | 17.40 | 17.75 |
| MnO | 0.21 | 0.33 | 0.23 | 0.25 | 0.19 | 0.23 | 0.30 | 0.31 | 0.22 | 0.25 | 0.25 | 0.24 |
| MgO | 5.18 | 4.43 | 7.99 | 5.90 | 6.93 | 6.53 | 7.74 | 7.49 | 6.87 | 6.09 | 5.12 | 5.51 |
| CaO | 7.69 | 11.17 | 9.09 | 8.57 | 9.59 | 9.36 | 5.01 | 4.60 | 11.18 | 5.29 | 8.32 | 9.48 |
| $Na_2O$ | 3.53 | 5.65 | 1.86 | 2.14 | 2.73 | 2.14 | 3.64 | 3.84 | 1.54 | 4.21 | 2.74 | 2.99 |
| $K_2O$ | 0.46 | 0.82 | 0.15 | 0.13 | 0.11 | 0.36 | 0.05 | 0.05 | 0.03 | 0.03 | 0.10 | 0.06 |
| $P_2O_5$ | 0.11 | 0.14 | 0.15 | 0.18 | 0.10 | 0.15 | 0.12 | 0.14 | 0.13 | 0.14 | 0.14 | 0.15 |
| LOI | 1.66 | 15.02 | 2.69 | 2.54 | 2.37 | 2.09 | 3.40 | 3.57 | 2.94 | 4.03 | 2.47 | 1.67 |
| Total | 99.76 | 99.82 | 99.91 | 100.07 | 100.33 | 100.07 | 99.97 | 99.94 | 100.15 | 100.20 | 100.07 | 100.00 |
| Cs | 0.36 | | 0.38 | | | | 0.08 | | | | | |
| Rb | 19.85 | 21.8 | 6.50 | 4.2 | 3.4 | 16.5 | 0.61 | 1.1 | | | 1.5 | |
| Ba | 75 | 166 | 39 | 69 | 147 | 91 | 40 | 20 | 55 | 22 | 85 | 85 |
| Th | 1.82 | | 1.30 | 2 | | | 0.59 | | | | | |
| U | 0.61 | | 0.36 | | | | 0.20 | | | | | |
| Nb | 5.7 | 7 | 7.1 | 7 | 4 | 6 | 6.2 | 5 | 5 | 7 | 5 | 6 |
| Ta | 0.58 | | 0.57 | | | | 0.40 | | | | | |
| La | 10.09 | 8 | 8.58 | 7 | 4 | 5 | 5.21 | 10 | 2 | 2 | 4 | 5 |
| Ce | 23.26 | 18 | 20.38 | 16 | 10 | 14 | 13.63 | 18 | 13 | 7 | 13 | 16 |
| Pb | 8.95 | 4 | 9.24 | 12 | 1 | 8 | 1.74 | 2 | | 3 | 6 | 2 |
| Pr | 3.17 | | 2.92 | | | | 2.16 | | | | | |
| Sr | 131.78 | 95 | 172.14 | 148 | 453 | 151 | 33.75 | 76 | 86 | 39 | 208 | 192 |
| Nd | 13.91 | 9.0 | 13.53 | 13.8 | 7.8 | 11.5 | 10.88 | 12.2 | 10.4 | 7.3 | 9.7 | 10.0 |
| Sm | 3.79 | | 3.68 | | | | 3.41 | | | | | |
| Zr | 136 | 78 | 94 | 100 | 56 | 93 | 96 | 92 | 86 | 99 | 87 | 94 |
| Hf | 2.69 | | 2.10 | | | | 1.52 | | | | | |
| Eu | 1.17 | | 1.03 | | | | 0.69 | | | | | |
| Gd | 4.50 | | 4.02 | | | | 4.31 | | | | | |
| Tb | 0.83 | | 0.68 | | | | 0.77 | | | | | |
| Dy | 5.27 | | 4.04 | | | | 4.84 | | | | | |
| Y | 30.89 | 9.9 | 20.74 | 29.2 | 19.7 | 28.2 | 25.35 | 30.2 | 25.8 | 22.0 | 28.2 | 29.7 |
| Ho | 1.16 | | 0.84 | | | | 1.01 | | | | | |
| Er | 3.38 | | 2.28 | | | | 2.84 | | | | | |
| Tm | 0.51 | | 0.31 | | | | 0.41 | | | | | |
| Yb | 3.28 | | 1.98 | | | | 2.42 | | | | | |
| Lu | 0.48 | | 0.28 | | | | 0.34 | | | | | |
| V | 403.80 | 412 | 462.71 | 486 | 303 | 405 | 351.66 | 524 | 418 | 363 | 553 | 624 |
| Cr | 72 | 121 | 84 | 59 | 189 | 137 | 125 | 184 | 135 | 145 | 35 | 3 |
| Ni | 60 | 39.9 | 74 | 94.2 | 103.2 | 71.8 | 82 | 90.3 | 86.6 | 84.7 | 51.5 | 56.4 |
| Cu | 270 | 70 | 194 | 109 | 152 | 149 | 192 | 199 | 196 | 80 | 230 | 219 |
| Zn | 106.75 | 17 | 135.81 | 155 | 100 | 168 | 111.35 | 138 | 126 | 111 | 130 | 132 |
| Ga | 18.04 | | 21.26 | | | | 20.30 | | | | | |
| Zr/Nb | 23.91 | 11.00 | 13.18 | 14.13 | 15.44 | 16.02 | 15.53 | 19.25 | 17.45 | 13.93 | 17.38 | 15.23 |
| Y/Nb | 5.35 | 1.39 | 2.83 | 4.11 | 5.47 | 4.86 | 4.03 | 6.29 | 5.27 | 3.10 | 5.64 | 4.79 |
| Ti/V | 20.87 | 24.71 | 27.27 | 23.65 | 22.43 | 21.68 | 19.51 | 18.76 | 20.61 | 25.08 | 18.57 | 19.67 |
| Zr/Y | 4.47 | 7.89 | 4.66 | 3.43 | 2.82 | 3.29 | 3.85 | 3.06 | 3.31 | 4.50 | 3.08 | 3.18 |
| Ti/Zr | 52.59 | 130.46 | 105.72 | 114.70 | 122.34 | 94.60 | 91.33 | 106.48 | 100.80 | 92.11 | 118.08 | 129.96 |
| Ti/Y | 235.02 | 1029.17 | 492.30 | 394.00 | 345.28 | 311.66 | 351.78 | 325.77 | 334.05 | 414.09 | 363.86 | 413.08 |
| Th/Nb | 0.32 | | 0.18 | 0.23 | | | 0.10 | | | | | |
| Nb/La | 0.57 | 0.93 | 0.83 | 1.03 | 0.88 | 1.29 | 1.19 | 0.48 | 2.13 | 3.55 | 1.25 | 1.32 |
| Ta/Yb | 0.18 | | 0.29 | | | | 0.17 | | | | | |
| $(La/Sm)n^{\dagger}$ | 1.67 | | 1.47 | | | | 0.96 | | | | | |
| $(Gd/Yb)n^{\dagger}$ | 1.11 | | 1.64 | | | | 1.44 | | | | | |
| $(Eu/Eu^*)n^{\dagger}$ | 0.86 | | 0.82 | | | | 0.55 | | | | | |

^ Method used to obtain trace and rare earth element compositions, all major element data obtained by XRF

† Normalising values after Boynton (1984)

**Table 6.1: Major (wt%), trace (ppm) and rare earth element (ppm) compositions for mafic rocks of the lower Etheridge Group.**

| Sample: | 87 | 88 | 89 | 90 | 100 | 101 | 102 | 103 | 104 | 106 | 107 | 108 |
|---|---|---|---|---|---|---|---|---|---|---|---|---|
| Unit: | DHM | CMD | DHM | DHM | DHM | CMD | DHM | DHM | DHM | CMD | DHM | CMD |
| Rock type: | Basalt | Dolerite | Basalt | Basalt | Basalt | Dolerite | Basalt | Basalt | Basalt | Dolerite | Basalt | Dolerite |
| Domain: | Ortona | Ortona | Ortona | Ortona | Ortona | Ortona | Ortona | Ortona | Ortona | Ortona | Ortona | Ortona |
| Method^: | XRF | XRF | ICPMS | XRF | ICPMS | ICPMS | XRF | ICPMS | XRF | ICPMS | XRF | ICPMS |
| $SiO_2$ | 50.63 | 50.70 | 50.54 | 48.57 | 49.40 | 48.85 | 46.40 | 49.27 | 47.01 | 46.11 | 42.02 | 48.49 |
| $TiO_2$ | 1.41 | 1.42 | 1.43 | 1.67 | 1.54 | 2.07 | 1.70 | 1.42 | 1.42 | 2.31 | 2.23 | 1.41 |
| $Al_2O_3$ | 12.97 | 13.71 | 13.08 | 12.97 | 14.89 | 13.01 | 14.57 | 14.04 | 14.11 | 11.78 | 11.64 | 13.98 |
| $Fe_2O_3$* | 15.08 | 14.40 | 14.97 | 17.34 | 14.90 | 16.90 | 16.72 | 15.60 | 15.67 | 18.37 | 17.22 | 15.43 |
| MnO | 0.23 | 0.22 | 0.22 | 0.25 | 0.22 | 0.23 | 0.25 | 0.24 | 0.24 | 0.23 | 0.41 | 0.22 |
| MgO | 6.81 | 6.25 | 5.43 | 6.22 | 5.80 | 5.35 | 6.31 | 6.87 | 6.44 | 4.92 | 2.83 | 6.00 |
| CaO | 7.67 | 7.42 | 8.65 | 8.51 | 6.59 | 8.47 | 6.01 | 6.36 | 9.09 | 8.83 | 11.47 | 9.62 |
| $Na_2O$ | 2.76 | 3.91 | 2.74 | 1.85 | 4.35 | 3.25 | 3.91 | 4.01 | 2.98 | 2.38 | 1.75 | 2.38 |
| $K_2O$ | 0.05 | 0.06 | 0.07 | 0.10 | 0.09 | 0.09 | 0.04 | 0.06 | 0.05 | 0.20 | 0.01 | 0.17 |
| $P_2O_5$ | 0.13 | 0.12 | 0.14 | 0.16 | 0.15 | 0.22 | 0.19 | 0.15 | 0.16 | 0.18 | 0.22 | 0.13 |
| LOI | 2.27 | 1.84 | 2.52 | 2.44 | 2.08 | 1.94 | 3.41 | 2.11 | 2.71 | 4.29 | 9.99 | 2.06 |
| Total | 100.00 | 100.05 | 99.79 | 100.08 | 100.00 | 100.38 | 99.51 | 100.13 | 99.88 | 99.61 | 99.80 | 99.88 |
| Cs | | | 0.16 | | 0.31 | 1.45 | | 0.07 | | 1.11 | | 0.31 |
| Rb | | | 1.60 | 2.3 | 0.91 | 1.68 | | 0.45 | | 9.64 | | 5.92 |
| Ba | 27 | 30 | 39 | 36 | 40 | 128 | 14 | 26 | 23 | 468 | 5 | 141 |
| Th | 2 | | 0.94 | | 0.72 | 1.09 | | 0.63 | | 1.06 | | 0.59 |
| U | | | 0.31 | | 0.29 | 0.38 | | 0.21 | | 0.32 | | 0.20 |
| Nb | 6 | 5 | 5.9 | 7 | 7.5 | 9 | 8 | 5.6 | 6 | 6.7 | 8 | 4.8 |
| Ta | | | 0.39 | | 0.48 | 0.61 | | 0.41 | | 0.53 | | 0.44 |
| La | | | 6.12 | 4 | 4.67 | 9.37 | 3 | 4.54 | 4 | 8.39 | 9 | 5.54 |
| Ce | 8 | 8 | 15.28 | 13 | 12.84 | 24.24 | 5 | 11.20 | 16 | 20.50 | 25 | 13.98 |
| Pb | 3 | | 2.64 | 4 | 1.89 | 2.34 | 4 | 0.33 | | 2.72 | 4 | 1.19 |
| Pr | | | 2.29 | | 2.07 | 3.76 | | 1.68 | | 3.15 | | 2.20 |
| Sr | 37 | 38 | 88.52 | 121 | 97.64 | 99.00 | 39 | 29.95 | 126 | 338.48 | 85 | 173.38 |
| Nd | 6.0 | 7.9 | 11.22 | 12.4 | 10.59 | 17.74 | 5.8 | 7.89 | 10.2 | 14.96 | 18.0 | 10.59 |
| Sm | | | 3.45 | | 3.62 | 5.46 | | 2.50 | | 4.55 | | 3.29 |
| Zr | 90 | 82 | 87 | 110 | 115 | 152 | 111 | 91 | 91 | 113 | 152 | 84 |
| Hf | | | 2.05 | | 1.72 | 3.32 | | 1.83 | | 2.84 | | 1.87 |
| Eu | | | 1.09 | | 1.16 | 1.68 | | 0.57 | | 1.48 | | 1.21 |
| Gd | | | 4.27 | | 4.71 | 6.80 | | 3.14 | | 5.59 | | 4.32 |
| Tb | | | 0.75 | | 0.86 | 1.21 | | 0.60 | | 0.99 | | 0.76 |
| Dy | | | 4.73 | | 5.38 | 7.82 | | 3.83 | | 6.16 | | 4.89 |
| Y | 23.0 | 23.4 | 25.83 | 33.4 | 29.53 | 42.27 | 22.9 | 18.90 | 27.1 | 33.77 | 42.1 | 27.42 |
| Ho | | | 1.01 | | 1.16 | 1.64 | | 0.80 | | 1.30 | | 1.06 |
| Er | | | 2.82 | | 3.27 | 4.69 | | 2.25 | | 3.69 | | 3.06 |
| Tm | | | 0.40 | | 0.47 | 0.69 | | 0.34 | | 0.53 | | 0.47 |
| Yb | | | 2.56 | | 2.95 | 4.35 | | 2.26 | | 3.39 | | 2.90 |
| Lu | | | 0.36 | | 0.41 | 0.62 | | 0.34 | | 0.50 | | 0.42 |
| V | 358 | 379 | 373.04 | 448 | 398.26 | 365.45 | 410 | 417.17 | 379 | 686.83 | 476 | 400.41 |
| Cr | 138 | 127 | 82 | 70 | 146 | 98 | 64 | 135 | 132 | 1 | 3 | 82 |
| Ni | 73.7 | 71 | 61 | 49.2 | 73 | 55 | 66.2 | 79 | 79.7 | 50 | 24 | 69 |
| Cu | 123 | 139 | 181 | 182 | 114 | 156 | 230 | 25 | 95 | 241 | 95 | 206 |
| Zn | 125 | 107 | 166.26 | 137 | 155.92 | 111.91 | 134 | 119.50 | 123 | 146.20 | 185 | 111.65 |
| Ga | | | 17.57 | | 15.50 | 12.31 | | 19.55 | | 21.84 | | 19.39 |
| Zr/Nb | 15.72 | 15.67 | 14.76 | 15.97 | 15.27 | 16.86 | 14.05 | 16.30 | 16.45 | 16.79 | 19.77 | 17.52 |
| Y/Nb | 4.04 | 4.50 | 4.41 | 4.84 | 3.92 | 4.83 | 2.90 | 3.39 | 4.93 | 5.01 | 5.47 | 5.83 |
| Ti/V | 23.57 | 22.37 | 21.60 | 22.37 | 21.73 | 26.21 | 24.85 | 22.06 | 22.53 | 23.86 | 28.06 | 21.03 |
| Zr/Y | 3.90 | 3.48 | 3.35 | 3.30 | 3.89 | 3.49 | 4.85 | 4.81 | 3.34 | 3.35 | 3.62 | 3.00 |
| Ti/Zr | 94.18 | 104.13 | 98.40 | 90.93 | 80.75 | 81.90 | 91.74 | 93.28 | 94.31 | 123.12 | 87.81 | 100.20 |
| Ti/Y | 366.90 | 362.68 | 329.64 | 300.03 | 314.47 | 285.62 | 444.67 | 448.25 | 314.93 | 412.23 | 317.47 | 300.96 |
| Th/Nb | 0.33 | | 0.16 | | 0.10 | 0.12 | | 0.11 | | 0.16 | | 0.12 |
| Nb/La | | | 0.96 | 1.97 | 1.60 | 0.96 | 2.47 | 1.23 | 1.57 | 0.80 | 0.91 | 0.87 |
| Ta/Yb | | | 0.15 | | 0.16 | 0.14 | | 0.18 | | 0.16 | | 0.15 |
| $(La/Sm)n^{\dagger}$ | | | 1.12 | | 0.81 | 1.08 | | 1.14 | | 1.16 | | 1.06 |
| $(Gd/Yb)n^{\dagger}$ | | | 1.35 | | 1.29 | 1.26 | | 1.12 | | 1.33 | | 1.20 |
| $(Eu/Eu^*)n^{\dagger}$ | | | 0.87 | | 0.86 | 0.84 | | 0.62 | | 0.90 | | 0.98 |

**Table 6.1 cont.**

| Sample: | 109 | 110 | 112 | 113 | 114 | 115 | 120 | 121 | 128 | 129 | 130 | 148 |
|---|---|---|---|---|---|---|---|---|---|---|---|---|
| Unit: | CMD | CMD | CMD | CMD | CMD | CMD | CMD | CMD | CMD | CMD | CMD | DHM |
| Rock type: | Dolerite | Dolerite | Dolerite | Dolerite | Dolerite | Dolerite | Dolerite | Dolerite | Dolerite | Dolerite | Dolerite | Basalt |
| Domain: | Ortona | Ortona | Ortona | Ortona | Ortona | Ortona | Ortona | Ortona | Ortona | Ortona | Ortona | Ortona |
| Method^: | ICPMS | XRF | ICPMS | ICPMS | XRF | ICPMS | XRF | ICPMS | XRF | XRF | ICPMS | ICPMS |
| $SiO_2$ | 49.82 | 48.28 | 50.91 | 46.92 | 49.20 | 46.38 | 47.23 | 47.71 | 49.06 | 49.21 | 50.50 | 46.60 |
| $TiO_2$ | 1.70 | 1.54 | 1.20 | 0.93 | 1.49 | 0.90 | 1.08 | 1.08 | 1.13 | 1.24 | 1.78 | 2.41 |
| $Al_2O_3$ | 12.40 | 12.37 | 14.34 | 15.81 | 13.23 | 14.93 | 14.06 | 14.46 | 13.65 | 13.35 | 12.91 | 12.78 |
| $Fe_2O_3$* | 16.86 | 17.15 | 13.49 | 13.22 | 16.63 | 13.34 | 14.72 | 14.44 | 15.06 | 15.08 | 17.50 | 18.72 |
| MnO | 0.27 | 0.26 | 0.20 | 0.18 | 0.24 | 0.19 | 0.21 | 0.21 | 0.22 | 0.20 | 0.20 | 0.30 |
| MgO | 4.76 | 5.99 | 6.29 | 8.45 | 5.76 | 9.87 | 8.63 | 7.55 | 7.37 | 6.51 | 3.92 | 6.49 |
| CaO | 9.34 | 9.58 | 8.71 | 9.99 | 8.05 | 8.97 | 9.44 | 8.88 | 7.03 | 8.34 | 6.83 | 6.01 |
| $Na_2O$ | 2.49 | 2.38 | 2.23 | 1.85 | 2.85 | 1.80 | 1.64 | 2.70 | 2.64 | 2.40 | 2.84 | 1.81 |
| $K_2O$ | 0.14 | 0.05 | 0.43 | 0.20 | 0.05 | 0.30 | 0.17 | 0.10 | 1.19 | 1.77 | 1.37 | 0.06 |
| $P_2O_5$ | 0.16 | 0.14 | 0.12 | 0.09 | 0.14 | 0.09 | 0.09 | 0.11 | 0.10 | 0.10 | 0.21 | 0.26 |
| LOI | 2.55 | 2.11 | 2.40 | 2.78 | 2.30 | 3.12 | 2.78 | 2.79 | 2.24 | 1.58 | 2.38 | 4.10 |
| Total | 100.49 | 99.86 | 100.32 | 100.42 | 99.95 | 99.89 | 100.04 | 100.04 | 99.69 | 99.79 | 100.43 | 99.54 |
| Cs | 3.87 | | 1.13 | 0.75 | | 0.74 | | 0.26 | | | 0.36 | 0.18 |
| Rb | 2.34 | | 18.02 | 7.98 | | 12.93 | 8 | 3.43 | 42 | 59 | 44.02 | 1.07 |
| Ba | 110 | 83 | 217 | 116 | 34 | 216 | 87 | 47 | 118 | 73 | 58 | 17 |
| Th | 0.68 | 2 | 2.13 | 0.35 | | 0.36 | | 0.46 | | | 1.12 | 1.34 |
| U | 0.23 | | 0.61 | 0.13 | | 0.13 | | 0.16 | | | 0.36 | 0.47 |
| Nb | 6.2 | 5 | 5.7 | 3.5 | 5 | 3.8 | 4 | 4.3 | 5 | 4 | 6.5 | 10.3 |
| Ta | 0.46 | | 0.41 | 0.25 | | 0.24 | | 0.30 | | | 0.65 | 0.67 |
| La | 6.19 | 7 | 8.80 | 3.39 | 3 | 3.42 | | 4.13 | 3 | | 9.74 | 10.7 |
| Ce | 15.62 | 12 | 19.33 | 8.66 | 11 | 8.77 | 9 | 10.87 | 10 | 10 | 24.90 | 26.8 |
| Pb | 4.00 | 29 | 2.95 | 0.70 | 5 | 0.79 | | 0.82 | 2 | 4 | 3.36 | 3.56 |
| Pr | 2.44 | | 2.74 | 1.37 | | 1.40 | | 1.72 | | | 3.79 | 4.18 |
| Sr | 142.46 | 121 | 158.83 | 145.56 | 170 | 120.67 | 101 | 119.96 | 87 | 95 | 107.34 | 83 |
| Nd | 11.83 | 10.4 | 11.86 | 6.72 | 10.2 | 6.68 | 5.5 | 8.29 | 9.8 | 6.8 | 18.29 | 20.2 |
| Sm | 3.71 | | 3.29 | 2.14 | | 2.15 | | 2.64 | | | 5.48 | 6.15 |
| Zr | 91 | 84 | 88 | 54 | 86 | 54 | 53 | 69 | 58 | 66 | 106 | 165 |
| Hf | 2.33 | | 2.07 | 1.38 | | 1.38 | | 1.63 | | | 3.04 | 4.36 |
| Eu | 1.42 | | 1.05 | 0.80 | | 0.78 | | 0.93 | | | 1.78 | 2.10 |
| Gd | 4.71 | | 3.93 | 2.68 | | 2.70 | | 3.39 | | | 6.83 | 7.46 |
| Tb | 0.85 | | 0.67 | 0.49 | | 0.49 | | 0.61 | | | 1.23 | 1.38 |
| Dy | 5.53 | | 4.23 | 3.10 | | 3.05 | | 3.79 | | | 7.79 | 8.44 |
| Y | 30.35 | 29.2 | 23.59 | 16.99 | 27.2 | 16.74 | 17.5 | 20.75 | 20.1 | 22.7 | 41.76 | 48.0 |
| Ho | 1.19 | | 0.91 | 0.66 | | 0.65 | | 0.83 | | | 1.65 | 1.81 |
| Er | 3.46 | | 2.54 | 1.87 | | 1.86 | | 2.30 | | | 4.68 | 5.25 |
| Tm | 0.51 | | 0.38 | 0.28 | | 0.27 | | 0.34 | | | 0.68 | 0.79 |
| Yb | 3.25 | | 2.35 | 1.82 | | 1.73 | | 2.13 | | | 4.32 | 4.90 |
| Lu | 0.48 | | 0.34 | 0.26 | | 0.25 | | 0.31 | | | 0.63 | 0.74 |
| V | 469.85 | 418 | 319.42 | 264.66 | 463 | 248.05 | 307 | 307.95 | 346 | 348 | 518.94 | 521 |
| Cr | 21 | 53 | 166 | 92 | 55 | 95 | 127 | 92 | 103 | 58 | 5 | 112 |
| Ni | 41 | 92.2 | 86 | 193 | 63.8 | 242 | 191.1 | 150 | 87.8 | 74.3 | 44 | 59 |
| Cu | 242 | 171 | 157 | 120 | 225 | 106 | 137 | 137 | 280 | 263 | 256 | 122 |
| Zn | 134.52 | 207 | 106.28 | 83.79 | 135 | 84.29 | 112 | 95.42 | 82 | 68 | 95.40 | 183 |
| Ga | 20.28 | | 19.28 | 16.91 | | 16.40 | | 17.63 | | | 22.86 | 18.83 |
| Zr/Nb | 14.68 | 16.76 | 15.35 | 15.40 | 16.78 | 14.24 | 13.84 | 16.12 | 12.91 | 15.42 | 16.35 | 16.85 |
| Y/Nb | 4.79 | 5.84 | 4.35 | 5.00 | 5.33 | 4.32 | 4.61 | 4.84 | 4.47 | 5.28 | 6.12 | 4.83 |
| Ti/V | 22.39 | 22.04 | 21.93 | 20.97 | 19.33 | 21.93 | 21.08 | 21.41 | 19.55 | 21.40 | 23.08 | 27.70 |
| Zr/Y | 3.06 | 2.87 | 3.53 | 3.08 | 3.15 | 3.30 | 3.01 | 3.33 | 2.89 | 2.92 | 2.67 | 3.49 |
| Ti/Zr | 112.10 | 109.83 | 81.99 | 103.86 | 104.46 | 99.93 | 123.17 | 93.82 | 116.36 | 112.17 | 100.25 | 88.45 |
| Ti/Y | 343.46 | 315.20 | 289.28 | 319.88 | 328.76 | 329.64 | 370.22 | 312.59 | 336.35 | 327.60 | 267.76 | 308.64 |
| Th/Nb | 0.11 | 0.30 | 0.37 | 0.10 | | 0.09 | | 0.11 | | | 0.17 | 0.13 |
| Nb/La | 1.00 | 0.72 | 0.65 | 1.03 | 1.65 | 1.11 | | 1.04 | 1.41 | | 0.67 | 0.96 |
| Ta/Yb | 0.14 | | 0.17 | 0.14 | | 0.14 | | 0.14 | | | 0.15 | 0.14 |
| $(La/Sm)n^{\dagger}$ | 1.05 | | 1.68 | 0.99 | | 1.00 | | 0.99 | | | 1.12 | 1.09 |
| $(Gd/Yb)n^{\dagger}$ | 1.17 | | 1.35 | 1.19 | | 1.26 | | 1.29 | | | 1.28 | 1.23 |
| $(Eu/Eu^*)n^{\dagger}$ | 1.04 | | 0.89 | 1.03 | | 0.98 | | 0.96 | | | 0.89 | 0.95 |

**Table 6.1 cont.**

| Sample: | 151 | 152 | 153 | 154 | 172 | 174 | 175 | 179 | 181 | 188 | 192 | 194 |
|---|---|---|---|---|---|---|---|---|---|---|---|---|
| Unit: | DHM | CMD | DHM | DHM | CMD | CMD | CMD | CMD | CMD | CMD | CMD | CMD |
| Rock type: | Basalt | Dolerite | Basalt | Basalt | Dolerite | Granophyre | Dolerite | Dolerite | Dolerite | Dolerite | Dolerite | Dolerite |
| Domain: | Ortona | Ortona | Ortona | Ortona | Ortona | Ortona | Ortona | Ortona | Ortona | Ortona | Stockyard | Stockyard |
| Method^: | XRF | XRF | XRF | XRF | XRF | XRF | XRF | XRF | ICPMS | XRF | XRF | XRF |
| $SiO_2$ | 47.34 | 49.35 | 43.68 | 47.63 | 57.80 | 59.89 | 49.61 | 48.31 | 47.28 | 48.17 | 48.40 | 49.15 |
| $TiO_2$ | 1.38 | 1.40 | 2.15 | 1.38 | 0.87 | 1.06 | 1.63 | 1.01 | 0.84 | 1.55 | 1.57 | 1.40 |
| $Al_2O_3$ | 13.95 | 11.08 | 14.69 | 13.86 | 13.14 | 12.96 | 13.06 | 14.07 | 15.31 | 13.57 | 13.57 | 14.07 |
| $Fe_2O_3$* | 15.36 | 15.26 | 19.81 | 16.89 | 10.59 | 6.73 | 14.49 | 12.66 | 11.89 | 14.54 | 15.33 | 13.80 |
| MnO | 0.22 | 0.24 | 0.29 | 0.26 | 0.18 | 0.16 | 0.23 | 0.20 | 0.15 | 0.21 | 0.29 | 0.20 |
| MgO | 6.71 | 7.30 | 6.89 | 7.29 | 4.69 | 1.84 | 5.93 | 7.64 | 8.49 | 5.41 | 6.42 | 6.54 |
| CaO | 10.12 | 11.87 | 5.68 | 7.14 | 7.89 | 4.48 | 9.33 | 9.56 | 10.54 | 11.95 | 10.57 | 11.04 |
| $Na_2O$ | 2.41 | 1.14 | 3.06 | 2.72 | 2.71 | 6.06 | 1.59 | 2.41 | 1.81 | 1.01 | 2.35 | 2.28 |
| $K_2O$ | 0.08 | 0.09 | 0.06 | 0.05 | 0.23 | 0.36 | 0.46 | 0.62 | 0.59 | 0.02 | 0.29 | 0.20 |
| $P_2O_5$ | 0.13 | 0.11 | 0.21 | 0.11 | 0.11 | 0.20 | 0.15 | 0.09 | 0.08 | 0.15 | 0.15 | 0.15 |
| LOI | 2.22 | 2.04 | 3.43 | 2.70 | 1.73 | 6.12 | 3.21 | 2.88 | 3.01 | 3.74 | 0.80 | 0.82 |
| Total | 99.90 | 99.88 | 99.95 | 100.03 | 99.94 | 99.86 | 99.69 | 99.45 | 99.99 | 100.32 | 99.74 | 99.65 |
| Cs | | | | | | | | | 1.41 | | | |
| Rb | | 2 | 1 | | 10 | 18 | 27 | 27 | 30.3 | | 5 | 2 |
| Ba | 65 | 119 | 13 | 43 | 77 | 112 | 112 | 61 | 74 | 12 | 184 | 77 |
| Th | 2 | | | | | 14 | 2 | | 0.44 | | | |
| U | | | | | | | | | 0.13 | | | |
| Nb | 5 | 2 | 8 | 5 | 7 | 13 | 8 | 3 | 2.45 | 5 | 6 | 5 |
| Ta | | | | | | | | | 0.25 | | | |
| La | 4 | 4 | 7 | 5 | 9 | 34 | 10 | | 3.25 | 4 | 9 | 5 |
| Ce | 10 | 9 | 10 | 7 | 21 | 71 | 21 | 13 | 7.71 | 15 | 19 | 14 |
| Pb | 2 | 4 | 2 | 3 | 9 | 10 | 17 | 6 | 2.91 | 3 | 5 | 3 |
| Pr | | | | | | | | | 1.17 | | | |
| Sr | 65 | 359 | 24 | 51 | 131 | 126 | 295 | 184 | 118 | 66 | 190 | 176 |
| Nd | 7.5 | 8.7 | 11.6 | 7.3 | 14 | 32.9 | 14.4 | 6.6 | 5.63 | 9.7 | 11.7 | 11.2 |
| Sm | | | | | | | | | 1.81 | | | |
| Zr | 80 | 70 | 129 | 87 | 163 | 199 | 104 | 52 | 42 | 94 | 78 | 75 |
| Hf | | | | | | | | | 1.18 | | | |
| Eu | | | | | | | | | 0.79 | | | |
| Gd | | | | | | | | | 2.29 | | | |
| Tb | | | | | | | | | 0.41 | | | |
| Dy | | | | | | | | | 2.65 | | | |
| Y | 24.1 | 23.0 | 29.9 | 22.0 | 33.9 | 34.9 | 22.2 | 19.1 | 14.8 | 27.4 | 24.7 | 22.9 |
| Ho | | | | | | | | | 0.57 | | | |
| Er | | | | | | | | | 1.65 | | | |
| Tm | | | | | | | | | 0.24 | | | |
| Yb | | | | | | | | | 1.55 | | | |
| Lu | | | | | | | | | 0.23 | | | |
| V | 405 | 387 | 447 | 427 | 213 | 174 | 390 | 340 | 311 | 414 | 415 | 382 |
| Cr | 156 | 142 | 78 | 146 | 40 | 2 | 39 | 190 | 167 | 106 | 117 | 137 |
| Ni | 96.1 | 88.5 | 66.4 | 83.7 | 46.2 | 5.9 | 52 | 132.2 | 171 | 57.55 | 72.1 | 65.5 |
| Cu | 156 | 190 | 62 | 164 | 161 | 119 | 85 | 145 | 92 | 108 | 132 | 121 |
| Zn | 109 | 123 | 164 | 132 | 124 | 26 | 161 | 76 | 45 | 118 | 161 | 100 |
| Ga | | | | | | | | | 15.76 | | | |
| Zr/Nb | 16.10 | 30.55 | 16.28 | 17.49 | 22.59 | 15.14 | 12.80 | 15.14 | 13.28 | 18.62 | 14.05 | 14.54 |
| Y/Nb | 4.87 | 10.11 | 3.78 | 4.45 | 4.70 | 2.65 | 2.74 | 5.52 | 4.66 | 5.42 | 4.46 | 4.44 |
| Ti/V | 20.43 | 21.68 | 28.81 | 19.39 | 24.47 | 36.45 | 25.04 | 17.82 | 16.21 | 22.44 | 22.67 | 21.99 |
| Zr/Y | 3.30 | 3.02 | 4.31 | 3.93 | 4.81 | 5.70 | 4.68 | 2.74 | 2.85 | 3.43 | 3.15 | 3.27 |
| Ti/Zr | 103.91 | 120.73 | 100.05 | 95.62 | 31.97 | 31.91 | 94.12 | 115.52 | 123.70 | 98.93 | 120.95 | 112.18 |
| Ti/Y | 343.19 | 364.82 | 430.97 | 375.95 | 153.81 | 182.04 | 440.06 | 316.93 | 352.06 | 339.66 | 380.96 | 367.21 |
| Th/Nb | 0.34 | | | | | 1.03 | 0.22 | | 0.18 | | | |
| Nb/La | 1.37 | 0.53 | 1.18 | 1.08 | 0.82 | 0.38 | 0.84 | | 0.75 | 1.17 | 0.60 | 0.97 |
| Ta/Yb | | | | | | | | | 0.16 | | | |
| $(La/Sm)n^{\dagger}$ | | | | | | | | | 1.13 | | | |
| $(Gd/Yb)n^{\dagger}$ | | | | | | | | | 1.19 | | | |
| $(Eu/Eu^*)n^{\dagger}$ | | | | | | | | | 1.19 | | | |

**Table 6.1 cont.**

| Sample: | 195 | 196 | 197 | 199 | 200 | 201 | 202 | 221 | 222 | 224 | 226 | 227 |
|---|---|---|---|---|---|---|---|---|---|---|---|---|
| Unit: | CMD | CMD | CMD | CMD | CMD | CMD | CMD | CMD | CMD | CMD | CMD | CMD |
| Rock type: | Dolerite | Dolerite | Dolerite | Dolerite | Dolerite | Dolerite | Dolerite | Dolerite | Dolerite | Dolerite | Dolerite | Dolerite |
| Domain: | Stockyard | Stockyard | Stockyard | Stockyard | Stockyard | Stockyard | Stockyard | South Head | South Head | South Head | South Head | South Head |
| Method^: | XRF | ICPMS | XRF | XRF | XRF | XRF | XRF | XRF | XRF | XRF | XRF | XRF |
| $SiO_2$ | 49.28 | 49.31 | 48.63 | 48.51 | 49.13 | 49.14 | 49.20 | 45.39 | 49.12 | 47.16 | 48.85 | 45.41 |
| $TiO_2$ | 1.51 | 1.44 | 1.20 | 1.56 | 1.17 | 1.30 | 1.06 | 1.29 | 1.51 | 1.85 | 1.55 | 1.29 |
| $Al_2O_3$ | 13.25 | 14.01 | 14.23 | 13.86 | 13.83 | 14.02 | 13.58 | 13.82 | 13.24 | 14.16 | 13.54 | 14.43 |
| $Fe_2O_3$* | 14.31 | 14.07 | 12.79 | 14.77 | 13.25 | 13.69 | 13.75 | 15.37 | 16.32 | 18.58 | 15.72 | 15.78 |
| MnO | 0.21 | 0.22 | 0.20 | 0.22 | 0.27 | 0.21 | 0.21 | 0.25 | 0.24 | 0.42 | 0.24 | 0.34 |
| MgO | 6.37 | 6.56 | 7.47 | 6.28 | 7.86 | 7.02 | 7.38 | 6.03 | 5.97 | 6.41 | 6.24 | 7.64 |
| CaO | 11.12 | 11.36 | 11.00 | 10.79 | 9.57 | 10.32 | 10.44 | 9.68 | 8.58 | 5.79 | 10.11 | 8.88 |
| $Na_2O$ | 2.43 | 2.21 | 2.96 | 2.45 | 3.26 | 3.45 | 3.26 | 2.36 | 2.87 | 2.63 | 2.41 | 2.05 |
| $K_2O$ | 0.42 | 0.25 | 0.23 | 0.32 | 0.39 | 0.26 | 0.23 | 0.32 | 0.18 | 0.10 | 0.15 | 0.08 |
| $P_2O_5$ | 0.15 | 0.14 | 0.11 | 0.15 | 0.10 | 0.12 | 0.09 | 0.13 | 0.14 | 0.17 | 0.15 | 0.12 |
| LOI | 0.42 | 0.81 | 0.77 | 0.73 | 0.94 | 0.48 | 0.49 | 4.89 | 1.48 | 2.36 | 0.87 | 4.28 |
| Total | 99.47 | 100.38 | 99.59 | 99.64 | 99.77 | 100.01 | 99.69 | 99.53 | 99.65 | 99.63 | 99.83 | 100.30 |
| Cs | | 0.55 | | | | | | | | | | |
| Rb | 13 | 4.04 | 2 | 8 | 16 | 1 | 2 | 24 | 12 | 2 | 4 | 2 |
| Ba | 258 | 108 | 180 | 150 | 444 | 157 | 133 | 138 | 328 | 47 | 75 | 153 |
| Th | | 0.68 | 2 | | 2 | | | | | | | |
| U | | 0.21 | | | | | | | | | | |
| Nb | 5 | 5.43 | 4 | 5 | 4 | 4 | 4 | 6 | 4 | 7 | 4 | 3 |
| Ta | | 0.52 | | | | | | | | | | |
| La | 5 | 5.92 | 6 | 5 | 4 | 3 | 5 | 6 | 3 | 9 | 8 | 8 |
| Ce | 14 | 14.7 | 13 | 14 | 16 | 13 | 12 | 13 | 16 | 16 | 9 | 13 |
| Pb | 4 | 3.05 | 4 | 5 | 6 | 4 | 11 | 12 | 2 | 5 | 2 | 3 |
| Pr | | 2.25 | | | | | | | | | | |
| Sr | 189 | 178 | 235 | 180 | 223 | 149 | 150 | 256 | 395 | 39 | 111 | 160 |
| Nd | 11.1 | 10.9 | 6.6 | 11.4 | 10.8 | 9.2 | 7.3 | 10.1 | 10.9 | 13.5 | 10.6 | 9.5 |
| Sm | | 3.22 | | | | | | | | | | |
| Zr | 80 | 76 | 67 | 81 | 59 | 61 | 57 | 80 | 90 | 116 | 95 | 77 |
| Hf | | 2.06 | | | | | | | | | | |
| Eu | | 1.16 | | | | | | | | | | |
| Gd | | 3.89 | | | | | | | | | | |
| Tb | | 0.68 | | | | | | | | | | |
| Dy | | 4.25 | | | | | | | | | | |
| Y | 24.6 | 22.7 | 20.4 | 24.3 | 19.5 | 19.8 | 20.5 | 27.3 | 28.7 | 35.9 | 30.7 | 24.3 |
| Ho | | 0.90 | | | | | | | | | | |
| Er | | 2.58 | | | | | | | | | | |
| Tm | | 0.37 | | | | | | | | | | |
| Yb | | 2.28 | | | | | | | | | | |
| Lu | | 0.34 | | | | | | | | | | |
| V | 405 | 393 | 349 | 411 | 355 | 384 | 364 | 498 | 461 | 564 | 473 | 389 |
| Cr | 82 | 136 | 242 | 145 | 272 | 180 | 106 | 89 | 73 | 78 | 142 | 128 |
| Ni | 51.9 | 65 | 92.2 | 62.5 | 97 | 83.3 | 71.5 | 52.3 | 63.2 | 55.4 | 62.7 | 138.5 |
| Cu | 105 | 112 | 107 | 145 | 91 | 59 | 74 | 234 | 215 | 159 | 169 | 65 |
| Zn | 120 | 106 | 101 | 127 | 108 | 103 | 139 | 160 | 136 | 155 | 130 | 128 |
| Ga | | 18.67 | | | | | | | | | | |
| Zr/Nb | 16.53 | 15.84 | 17.91 | 15.79 | 16.10 | 15.29 | 14.46 | 14.37 | 20.77 | 16.95 | 21.81 | 24.42 |
| Y/Nb | 5.08 | 4.87 | 5.43 | 4.73 | 5.33 | 5.01 | 5.18 | 4.93 | 6.60 | 5.26 | 7.05 | 7.68 |
| Ti/V | 22.37 | 21.94 | 20.62 | 22.74 | 19.75 | 20.30 | 17.47 | 15.52 | 19.61 | 19.67 | 19.65 | 19.87 |
| Zr/Y | 3.26 | 3.26 | 3.30 | 3.34 | 3.02 | 3.06 | 2.79 | 2.92 | 3.15 | 3.22 | 3.09 | 3.18 |
| Ti/Zr | 112.98 | 114.77 | 106.87 | 115.14 | 119.05 | 128.78 | 111.07 | 97.13 | 100.11 | 95.83 | 97.89 | 100.02 |
| Ti/Y | 367.89 | 373.62 | 352.55 | 384.76 | 359.61 | 393.51 | 309.90 | 283.21 | 315.33 | 308.85 | 302.60 | 318.17 |
| Th/Nb | | 0.12 | 0.51 | | 0.49 | | | | | | | |
| Nb/La | 0.90 | 0.92 | 0.68 | 1.05 | 1.02 | 1.24 | 0.86 | 0.88 | 1.67 | 0.78 | 0.54 | 0.42 |
| Ta/Yb | | 0.23 | | | | | | | | | | |
| $(La/Sm)n^{\dagger}$ | | 1.16 | | | | | | | | | | |
| $(Gd/Yb)n^{\dagger}$ | | 1.38 | | | | | | | | | | |
| $(Eu/Eu^*)n^{\dagger}$ | | 1.00 | | | | | | | | | | |

**Table 6.1 cont.**

| Sample: | 228 | 229 | 230 | 231 | 232 | 233 | 234 | 236 | 237 | 240 | 241 | 242 |
|---|---|---|---|---|---|---|---|---|---|---|---|---|
| Unit: | DHM | DHM | DHM | DHM | DHM | DHM | DHM | DHM | CMD | DHM | CMD | CMD |
| Rock type: | Basalt | Basalt | Basalt | Basalt | Basalt | Basalt | Basalt | Basalt | Dolerite | Basalt | Dolerite | Dolerite |
| Domain: | South Head | South Head | South Head | South Head | South Head | South Head | South Head | South Head | South Head | South Head | South Head | South Head |
| Method^: | XRF | XRF | XRF | XRF | XRF | XRF | ICPMS | XRF | XRF | XRF | ICPMS | XRF |
| $SiO_2$ | 47.58 | 48.83 | 49.03 | 46.10 | 47.69 | 47.19 | 51.53 | 48.48 | 48.60 | 49.16 | 48.66 | 49.91 |
| $TiO_2$ | 2.18 | 2.45 | 1.19 | 1.29 | 1.13 | 1.15 | 1.18 | 1.13 | 1.15 | 1.20 | 1.46 | 1.46 |
| $Al_2O_3$ | 13.42 | 12.58 | 13.70 | 14.83 | 13.84 | 14.08 | 12.97 | 13.95 | 14.06 | 14.22 | 13.49 | 13.07 |
| $Fe_2O_3$* | 18.43 | 19.50 | 14.18 | 15.14 | 14.21 | 14.79 | 14.56 | 14.17 | 14.37 | 13.57 | 15.61 | 14.54 |
| MnO | 0.27 | 0.27 | 0.20 | 0.22 | 0.21 | 0.23 | 0.24 | 0.22 | 0.22 | 0.21 | 0.22 | 0.19 |
| MgO | 5.83 | 6.34 | 6.51 | 6.64 | 7.40 | 8.02 | 7.76 | 7.32 | 7.51 | 7.06 | 7.46 | 7.12 |
| CaO | 6.86 | 6.59 | 12.57 | 11.99 | 12.40 | 10.04 | 6.49 | 10.29 | 9.26 | 10.49 | 7.41 | 8.22 |
| $Na_2O$ | 2.76 | 1.00 | 0.96 | 1.75 | 0.48 | 2.32 | 2.57 | 2.33 | 2.35 | 1.98 | 3.00 | 2.54 |
| $K_2O$ | 0.42 | 0.10 | 0.03 | 0.03 | 0.04 | 0.08 | 0.09 | 0.10 | 0.10 | 0.14 | 0.08 | 0.05 |
| $P_2O_5$ | 0.24 | 0.25 | 0.12 | 0.12 | 0.11 | 0.10 | 0.10 | 0.10 | 0.10 | 0.11 | 0.14 | 0.13 |
| LOI | 1.60 | 2.36 | 1.73 | 1.85 | 2.57 | 1.80 | 2.74 | 2.10 | 2.27 | 2.20 | 2.70 | 2.21 |
| Total | 99.59 | 100.27 | 100.22 | 99.96 | 100.08 | 99.80 | 100.23 | 100.19 | 99.99 | 100.34 | 100.23 | 99.44 |
| Cs | | | | | | | 0.22 | | | | 0.24 | |
| Rb | 30 | 3 | | | 1 | | 1.16 | 2 | 2 | 4 | 1.83 | |
| Ba | 326 | 55 | 19 | 25 | 17 | 91 | 36 | 147 | 56 | 168 | 70 | 21 |
| Th | | | | | | | 0.37 | | | | 0.70 | 2 |
| U | | | | | | | 0.13 | | | | 0.27 | |
| Nb | 8 | 9 | 3 | 4 | 3 | 3 | 3.53 | 3 | 3 | 4 | 6.00 | 5 |
| Ta | | | | | | | 0.37 | | | | 0.48 | |
| La | 14 | 10 | 6 | 2 | 5 | 4 | 3.44 | 7 | 5 | 6 | 6.07 | 6 |
| Ce | 25 | 18 | 10 | 10 | 9 | 5 | 9.08 | 8 | 8 | 9 | 15.4 | 13 |
| Pb | 4 | 3 | 2 | | | | 0.45 | | | | 1.21 | |
| Pr | | | | | | | 1.46 | | | | 2.41 | |
| Sr | 54 | 137 | 313 | 163 | 270 | 110 | 103 | 134 | 105 | 179 | 57 | 63 |
| Nd | 17.5 | 14.2 | 6.6 | 7.6 | 7.3 | 6.7 | 7.31 | 6.7 | 6.6 | 7.7 | 11.8 | 10.6 |
| Sm | | | | | | | 2.44 | | | | 3.66 | |
| Zr | 166 | 151 | 64 | 68 | 57 | 64 | 60 | 56 | 60 | 69 | 98 | 91 |
| Hf | | | | | | | 1.69 | | | | 2.74 | |
| Eu | | | | | | | 0.58 | | | | 1.15 | |
| Gd | | | | | | | 3.12 | | | | 4.52 | |
| Tb | | | | | | | 0.57 | | | | 0.80 | |
| Dy | | | | | | | 3.63 | | | | 4.97 | |
| Y | 46.3 | 41.3 | 20.9 | 23.3 | 20.3 | 20.3 | 20.0 | 19.8 | 20.9 | 22.1 | 27.3 | 24.6 |
| Ho | | | | | | | 0.78 | | | | 1.06 | |
| Er | | | | | | | 2.24 | | | | 3.05 | |
| Tm | | | | | | | 0.35 | | | | 0.47 | |
| Yb | | | | | | | 2.12 | | | | 2.88 | |
| Lu | | | | | | | 0.32 | | | | 0.44 | |
| V | 445 | 494 | 410 | 437 | 381 | 414 | 360 | 374 | 374 | 366 | 411 | 418 |
| Cr | 86 | 75 | 160 | 172 | 190 | 207 | 193 | 205 | 216 | 168 | 117 | 102 |
| Ni | 70.5 | 57.8 | 104.3 | 108.4 | 125.4 | 115.9 | 104 | 104.2 | 104.2 | 91.8 | 79 | 70.6 |
| Cu | 198 | 179 | 173 | 190 | 158 | 154 | 132 | 151 | 168 | 146 | 150 | 182 |
| Zn | 192 | 224 | 105 | 124 | 109 | 117 | 126 | 108 | 113 | 101 | 123 | 116 |
| Ga | | | | | | | 11.24 | | | | 18.32 | |
| Zr/Nb | 20.92 | 15.90 | 24.77 | 16.79 | 17.34 | 23.78 | 19.64 | 20.90 | 23.33 | 17.86 | 19.39 | 18.00 |
| Y/Nb | 5.85 | 4.35 | 8.13 | 5.75 | 6.22 | 7.60 | 7.11 | 7.41 | 8.13 | 5.73 | 5.39 | 4.88 |
| Ti/V | 29.36 | 29.70 | 17.38 | 17.68 | 17.79 | 16.64 | 19.63 | 18.09 | 18.42 | 19.65 | 21.31 | 20.95 |
| Zr/Y | 3.57 | 3.66 | 3.05 | 2.92 | 2.79 | 3.13 | 2.76 | 2.82 | 2.87 | 3.12 | 3.60 | 3.69 |
| Ti/Zr | 78.95 | 97.24 | 111.97 | 113.53 | 119.66 | 108.54 | 130.00 | 121.37 | 114.87 | 104.38 | 89.47 | 96.37 |
| Ti/Y | 282.20 | 355.54 | 341.25 | 331.83 | 333.62 | 339.53 | 359.00 | 342.05 | 329.78 | 325.44 | 321.71 | 355.71 |
| Th/Nb | | | | | | | 0.11 | | | | 0.12 | 0.32 |
| Nb/La | 0.58 | 1.00 | 0.45 | 1.93 | 0.73 | 0.65 | 1.03 | 0.40 | 0.56 | 0.62 | 0.99 | 0.83 |
| Ta/Yb | | | | | | | 0.17 | | | | 0.17 | |
| $(La/Sm)n^{\dagger}$ | | | | | | | 0.89 | | | | 1.04 | |
| $(Gd/Yb)n^{\dagger}$ | | | | | | | 1.19 | | | | 1.27 | |
| $(Eu/Eu^*)n^{\dagger}$ | | | | | | | 0.64 | | | | 0.86 | |

**Table 6.1 cont.**

| Sample: | 243 | 249 | 250 | 251 | 253 | 256 | 260 | 261 | 262 | 268 | 269 | 270 |
|---|---|---|---|---|---|---|---|---|---|---|---|---|
| Unit: | DHM | CMD | DHM | DHM | DHM | DHM | DHM | DHM | DHM | DHM | DHM | DHM |
| Rock type: | Basalt | Dolerite | Basalt | Basalt | Basalt | Basalt | Amphibolite | Amphibolite | Amphibolite | Amphibolite | Amphibolite | Amphibolite |
| Domain: | South Head | South Head | South Head | South Head | South Head | South Head | Robinhood | Robinhood | Robinhood | Robinhood | Robinhood | Robinhood |
| Method^: | XRF | ICPMS | ICPMS | XRF | XRF | XRF | XRF | XRF | XRF | XRF | ICPMS | XRF |
| $SiO_2$ | 50.37 | 49.30 | 47.65 | 49.23 | 49.42 | 49.32 | 47.72 | 50.28 | 47.91 | 46.33 | 50.04 | 49.64 |
| $TiO_2$ | 1.44 | 1.89 | 1.62 | 1.51 | 1.52 | 1.92 | 1.33 | 1.40 | 1.80 | 2.28 | 1.43 | 2.03 |
| $Al_2O_3$ | 13.18 | 12.61 | 12.36 | 13.10 | 13.48 | 11.61 | 14.91 | 14.03 | 13.06 | 12.02 | 13.14 | 12.87 |
| $Fe_2O_3$* | 14.44 | 16.23 | 16.71 | 15.71 | 15.58 | 16.03 | 14.67 | 14.95 | 17.16 | 19.84 | 15.45 | 17.81 |
| MnO | 0.20 | 0.28 | 0.29 | 0.24 | 0.22 | 0.21 | 0.23 | 0.21 | 0.24 | 0.26 | 0.25 | 0.25 |
| MgO | 6.69 | 5.61 | 5.08 | 6.66 | 5.74 | 4.49 | 7.04 | 6.17 | 6.73 | 6.05 | 6.59 | 5.53 |
| CaO | 9.36 | 8.76 | 11.42 | 8.58 | 9.35 | 6.30 | 9.80 | 8.31 | 9.86 | 10.13 | 9.65 | 9.66 |
| $Na_2O$ | 2.24 | 2.87 | 1.71 | 2.66 | 1.54 | 0.67 | 2.77 | 3.93 | 1.85 | 1.95 | 2.54 | 0.86 |
| $K_2O$ | 0.04 | 0.34 | 0.13 | 0.05 | 0.05 | 0.05 | 0.15 | 0.11 | 0.28 | 0.17 | 0.23 | 0.46 |
| $P_2O_5$ | 0.14 | 0.18 | 0.17 | 0.13 | 0.14 | 0.19 | 0.11 | 0.13 | 0.19 | 0.14 | 0.12 | 0.21 |
| LOI | 2.10 | 2.06 | 2.71 | 2.56 | 3.19 | 8.85 | 1.09 | 0.29 | 0.51 | 0.52 | 0.64 | 0.41 |
| Total | 100.20 | 100.13 | 99.85 | 100.43 | 100.23 | 99.64 | 99.82 | 99.81 | 99.59 | 99.69 | 100.08 | 99.73 |
| Cs | | 0.77 | 0.19 | | | | | | | | 2.29 | |
| Rb | | 13.2 | 2.99 | | | 2 | 7 | 1 | 9 | 9 | 10.8 | 12 |
| Ba | 13 | 146 | 87 | 30 | 43 | 55 | 118 | 109 | 146 | 160 | 124 | 198 |
| Th | | 0.72 | 0.73 | | | | | | 2 | 2 | 0.40 | |
| U | | 0.27 | 0.25 | | | | | | | | 0.17 | |
| Nb | 5 | 7.79 | 6.42 | 5 | 5 | 8 | 4 | 5 | 6 | 4 | 4.70 | 7 |
| Ta | | 0.63 | 0.53 | | | | | | | | 0.39 | |
| La | 7 | 7.65 | 6.41 | 7 | 10 | 9 | 4 | 7 | 8 | 6 | 4.32 | 11 |
| Ce | 13 | 19.4 | 16.7 | 15 | 19 | 19 | 13 | 19 | 17 | 14 | 11.3 | 24 |
| Pb | | 2.53 | 1.99 | | 3 | 4 | 9 | 3 | 7 | 6 | 1.14 | 28 |
| Pr | | 3.07 | 2.63 | | | | | | | | 1.79 | |
| Sr | 48 | 139 | 43 | 168 | 290 | 85 | 245 | 310 | 153 | 343 | 185 | 310 |
| Nd | 9.2 | 15.2 | 13.1 | 9.3 | 13.3 | 12.5 | 9.8 | 11.9 | 16.2 | 8.7 | 9.10 | 17 |
| Sm | | 4.60 | 4.12 | | | | | | | | 3.04 | |
| Zr | 93 | 124 | 110 | 82 | 98 | 130 | 79 | 91 | 98 | 82 | 73 | 129 |
| Hf | | 3.36 | 3.00 | | | | | | | | 2.03 | |
| Eu | | 1.61 | 1.43 | | | | | | | | 1.10 | |
| Gd | | 5.86 | 5.20 | | | | | | | | 3.92 | |
| Tb | | 1.05 | 0.93 | | | | | | | | 0.73 | |
| Dy | | 6.41 | 5.81 | | | | | | | | 4.53 | |
| Y | 25.2 | 35.6 | 32.9 | 27.3 | 28.6 | 35.4 | 25.7 | 27.3 | 32.6 | 27.5 | 25.6 | 39.1 |
| Ho | | 1.36 | 1.27 | | | | | | | | 1.01 | |
| Er | | 3.84 | 3.66 | | | | | | | | 2.91 | |
| Tm | | 0.58 | 0.55 | | | | | | | | 0.44 | |
| Yb | | 3.55 | 3.52 | | | | | | | | 2.71 | |
| Lu | | 0.53 | 0.51 | | | | | | | | 0.42 | |
| V | 432 | 495 | 503 | 481 | 412 | 546 | 422 | 413 | 475 | 999 | 456 | 538 |
| Cr | 98 | 71 | 34 | 79 | 67 | 36 | 273 | 104 | 107 | 7 | 104 | 97 |
| Ni | 65.5 | 67 | 46 | 66 | 67.2 | 40.3 | 84.4 | 63.9 | 109.1 | 94.7 | 73 | 52.9 |
| Cu | 187 | 178 | 242 | 188 | 123 | 170 | 222 | 162 | 183 | 486 | 203 | 152 |
| Zn | 120 | 142 | 129 | 124 | 127 | 134 | 144 | 119 | 156 | 167 | 114 | 152 |
| Ga | | 20.47 | 20.73 | | | | | | | | 18.21 | |
| Zr/Nb | 18.16 | 19.43 | 16.65 | 16.96 | 18.28 | 17.35 | 21.10 | 19.49 | 15.20 | 19.35 | 16.79 | 18.16 |
| Y/Nb | 4.90 | 5.43 | 4.92 | 5.63 | 5.36 | 4.71 | 6.84 | 5.87 | 5.07 | 6.47 | 6.21 | 5.49 |
| Ti/V | 19.99 | 22.88 | 19.32 | 18.83 | 22.10 | 21.06 | 18.89 | 20.33 | 22.74 | 13.68 | 18.79 | 22.60 |
| Zr/Y | 3.71 | 3.58 | 3.38 | 3.01 | 3.41 | 3.68 | 3.09 | 3.32 | 3.00 | 2.99 | 2.70 | 3.31 |
| Ti/Zr | 92.40 | 92.09 | 88.03 | 110.10 | 93.34 | 88.25 | 100.52 | 92.61 | 110.42 | 166.04 | 120.04 | 94.10 |
| Ti/Y | 342.48 | 329.29 | 297.83 | 331.50 | 318.53 | 325.07 | 310.17 | 307.36 | 330.93 | 496.91 | 324.64 | 311.17 |
| Th/Nb | | 0.09 | 0.11 | | | | | | 0.26 | 0.47 | 0.08 | |
| Nb/La | 0.73 | 1.02 | 1.00 | 0.75 | 0.56 | 0.88 | 0.87 | 0.70 | 0.82 | 0.77 | 1.09 | 0.63 |
| Ta/Yb | | 0.18 | 0.15 | | | | | | | | 0.14 | |
| $(La/Sm)n^{\dagger}$ | | 1.05 | 0.98 | | | | | | | | 0.89 | |
| $(Gd/Yb)n^{\dagger}$ | | 1.33 | 1.19 | | | | | | | | 1.17 | |
| $(Eu/Eu^*)n^{\dagger}$ | | 0.95 | 0.95 | | | | | | | | 0.97 | |

**Table 6.1 cont.**

| Sample: | 296 | 299 | 300 | 301 |
|---|---|---|---|---|
| Unit: | CMD | CMD | CMD | CMD |
| Rock type: | Amphibolite | Amphibolite | Amphibolite | Amphibolite |
| Domain: | Gum Flats | Gum Flats | Gum Flats | Gum Flats |
| Method^: | XRF | ICPMS | XRF | ICPMS |
| | | | | |
| $SiO_2$ | 48.99 | 47.96 | 48.50 | 50.27 |
| $TiO_2$ | 0.84 | 2.85 | 2.66 | 1.56 |
| $Al_2O_3$ | 14.50 | 12.37 | 13.03 | 13.64 |
| $Fe_2O_3$* | 11.59 | 21.11 | 20.20 | 13.43 |
| MnO | 0.22 | 0.35 | 0.33 | 0.20 |
| MgO | 8.04 | 3.28 | 3.18 | 6.95 |
| CaO | 12.26 | 7.60 | 7.76 | 10.53 |
| $Na_2O$ | 1.62 | 2.76 | 2.78 | 1.98 |
| $K_2O$ | 0.64 | 0.58 | 0.57 | 0.39 |
| $P_2O_5$ | 0.09 | 0.28 | 0.33 | 0.16 |
| LOI | 1.59 | 0.54 | 0.42 | 0.83 |
| Total | 100.38 | 99.68 | 99.76 | 99.94 |
| | | | | |
| Cs | | 1.54 | | 2.60 |
| Rb | 42 | 15.2 | 23 | 20.2 |
| Ba | 76 | 81 | 122 | 119 |
| Th | | 1.39 | 3 | 1.08 |
| U | | 0.29 | | 0.22 |
| Nb | 4 | 11.6 | 8 | 5.82 |
| Ta | | 0.67 | | 0.54 |
| La | 4 | 7.75 | 8 | 7.69 |
| Ce | 10 | 20.3 | 26 | 17.4 |
| Pb | 21 | 7.75 | 10 | 14.2 |
| Pr | | 3.18 | | 2.79 |
| Sr | 150 | 192 | 172 | 160 |
| Nd | 5.8 | 16.0 | 16.3 | 13.2 |
| Sm | | 5.28 | | 3.86 |
| Zr | 41 | 124 | 118 | 91 |
| Hf | | 3.45 | | 2.53 |
| Eu | | 2.17 | | 1.35 |
| Gd | | 6.54 | | 4.39 |
| Tb | | 1.19 | | 0.78 |
| Dy | | 7.24 | | 4.64 |
| Y | 19.5 | 39.4 | 38.8 | 24.0 |
| Ho | | 1.57 | | 0.96 |
| Er | | 4.52 | | 2.68 |
| Tm | | 0.65 | | 0.40 |
| Yb | | 4.18 | | 2.34 |
| Lu | | 0.61 | | 0.35 |
| V | 327 | 84 | 55 | 382 |
| Cr | 164 | 8 | 8 | 127 |
| Ni | 104.9 | 5 | 4.7 | 97 |
| Cu | 123 | 78 | 24 | 190 |
| Zn | 178 | 260 | 204 | 110 |
| Ga | | 22.75 | | 18.49 |
| | | | | |
| Zr/Nb | 10.47 | 11.37 | 15.28 | 17.46 |
| Y/Nb | 4.93 | 3.89 | 5.03 | 4.58 |
| Ti/V | 15.38 | 203.59 | 288.81 | 24.48 |
| Zr/Y | 2.12 | 2.92 | 3.04 | 3.81 |
| Ti/Zr | 121.61 | 146.12 | 135.22 | 102.18 |
| Ti/Y | 258.18 | 427.03 | 410.89 | 389.57 |
| Th/Nb | | 0.12 | 0.43 | 0.18 |
| Nb/La | 1.13 | 1.50 | 0.93 | 0.76 |
| Ta/Yb | | 0.16 | | 0.23 |
| $(La/Sm)n^{\dagger}$ | | 0.92 | | 1.25 |
| $(Gd/Yb)n^{\dagger}$ | | 1.26 | | 1.51 |
| $(Eu/Eu*)n^{\dagger}$ | | 1.13 | | 1.00 |

**Table 6.1 cont.**

| | Ortona | | | South Head | | Stockyard | Robinhood | Gum Flats |
|---|---|---|---|---|---|---|---|---|
| | metabasalt | metadolerite | granophyre | metabasalt | metadolerite | metadolerite | DHM amphibolite | CMD amphibolite |
| No. of analyses | 17 | 28 | 1 | 14 | 9 | 9 | 6 | 4 |
| $SiO_2$ | 47.37 | 48.67 | 59.89 | 48.68 | 48.04 | 48.97 | 48.65 | 48.93 |
| $TiO_2$ | 1.63 | 1.43 | 1.06 | 1.49 | 1.49 | 1.36 | 1.71 | 1.98 |
| $Al_2O_3$ | 13.88 | 13.49 | 12.96 | 13.38 | 13.60 | 13.82 | 13.34 | 13.39 |
| $Fe_2O_3$* | 16.38 | 14.81 | 6.73 | 15.50 | 15.84 | 13.97 | 16.65 | 16.58 |
| MnO | 0.26 | 0.22 | 0.16 | 0.23 | 0.27 | 0.23 | 0.24 | 0.28 |
| MgO | 6.40 | 6.36 | 1.84 | 6.54 | 6.67 | 6.88 | 6.35 | 5.36 |
| CaO | 7.57 | 9.09 | 4.48 | 9.48 | 8.52 | 10.69 | 9.57 | 9.54 |
| $Na_2O$ | 2.92 | 2.50 | 6.06 | 1.78 | 2.56 | 2.74 | 2.32 | 2.29 |
| $K_2O$ | 0.07 | 0.36 | 0.36 | 0.10 | 0.16 | 0.29 | 0.23 | 0.55 |
| $P_2O_5$ | 0.16 | 0.13 | 0.20 | 0.14 | 0.14 | 0.13 | 0.15 | 0.22 |
| LOI | 3.29 | 2.94 | 6.12 | 2.74 | 2.57 | 0.70 | 0.58 | 0.85 |
| Total | 99.94 | 100.00 | 99.86 | 100.07 | 99.86 | 99.77 | 99.79 | 99.94 |
| Cs | 0.16 | 1.01 | | 0.21 | 0.51 | 0.55 | 2.29 | 2.07 |
| Rb | 3 | 16 | 18 | 6 | 8 | 6 | 8 | 25 |
| Ba^ | 34 | 109 | 112 | 79 | 115 | 188 | 142 | 100 |
| Th | 1 | 1 | 14 | 1 | 1 | 1 | 1 | 2 |
| U | 0.30 | 0.30 | | 0.19 | 0.27 | 0.21 | 0.17 | 0.25 |
| Nb^ | 6 | 5 | 13 | 5 | 5 | 5 | 5 | 7 |
| Ta | 0.47 | 0.44 | | 0.45 | 0.56 | 0.52 | 0.39 | 0.60 |
| La | 5 | 6 | 34 | 7 | 6 | 5 | 7 | 7 |
| Ce | 13 | 15 | 71 | 13 | 14 | 14 | 16 | 19 |
| Pb | 3 | 6 | 10 | 3 | 4 | 5 | 9 | 13 |
| Pr | 2.48 | 2.49 | | 2.05 | 2.74 | 2.25 | 1.79 | 2.98 |
| Sr | 72 | 163 | 126 | 150 | 147 | 185 | 258 | 169 |
| Nd | 11 | 11 | 33 | 10 | 11 | 10 | 12 | 13 |
| Sm | 3.83 | 3.50 | | 3.28 | 4.13 | 3.22 | 3.04 | 4.57 |
| Zr^ | 104 | 86 | 199 | 90 | 92 | 70 | 92 | 94 |
| Hf | 2.30 | 2.15 | | 2.34 | 3.05 | 2.06 | 2.03 | 2.99 |
| Eu | 1.12 | 1.18 | | 1.01 | 1.38 | 1.16 | 1.10 | 1.76 |
| Gd | 4.78 | 4.31 | | 4.16 | 5.19 | 3.89 | 3.92 | 5.47 |
| Tb | 0.87 | 0.77 | | 0.75 | 0.92 | 0.68 | 0.73 | 0.98 |
| Dy | 5.44 | 4.86 | | 4.72 | 5.69 | 4.25 | 4.53 | 5.94 |
| Y | 28 | 25 | 35 | 27 | 28 | 22 | 30 | 30 |
| Ho | 1.16 | 1.04 | | 1.02 | 1.21 | 0.90 | 1.01 | 1.26 |
| Er | 3.29 | 2.96 | | 2.95 | 3.45 | 2.58 | 2.91 | 3.60 |
| Tm | 0.48 | 0.43 | | 0.45 | 0.52 | 0.37 | 0.44 | 0.53 |
| Yb | 3.02 | 2.76 | | 2.82 | 3.21 | 2.28 | 2.71 | 3.26 |
| Lu | 0.44 | 0.40 | | 0.42 | 0.48 | 0.34 | 0.42 | 0.48 |
| V | 419 | 398 | 174 | 433 | 454 | 384 | 550 | 212 |
| Cr^ | 117 | 87 | 2 | 126 | 113 | 157 | 115 | 77 |
| Ni^ | 72 | 91 | 6 | 83 | 77 | 73 | 80 | 53 |
| Cu^ | 139 | 174 | 119 | 171 | 169 | 105 | 235 | 104 |
| Zn | 140 | 111 | 26 | 131 | 134 | 118 | 142 | 188 |
| Ga | 18.35 | 18.50 | | 15.98 | 19.39 | 18.67 | 18.21 | 20.62 |
| Zr/Nb | 16.31 | 16.35 | 15.14 | 18.95 | 19.83 | 15.61 | 18.35 | 13.64 |
| Y/Nb | 4.43 | 4.92 | 2.65 | 5.98 | 6.15 | 4.95 | 5.99 | 4.61 |
| Ti/V | 22.87 | 21.91 | 36.45 | 20.52 | 19.76 | 21.09 | 19.50 | 133.07 |
| Zr/Y | 3.77 | 3.51 | 5.70 | 3.22 | 3.25 | 3.16 | 3.07 | 2.97 |
| Ti/Zr | 94.40 | 104.50 | 31.91 | 104.13 | 98.20 | 115.75 | 113.95 | 126.28 |
| Ti/Y | 354.85 | 362.22 | 182.04 | 330.42 | 318.29 | 365.56 | 346.86 | 371.42 |
| Th/Nb | 0.18 | 0.19 | 1.03 | 0.11 | 0.18 | 0.37 | 0.27 | 0.24 |
| Nb/La | 1.50 | 0.95 | 0.38 | 0.81 | 0.85 | 0.91 | 0.82 | 1.08 |
| Ta/Yb | 0.16 | 0.16 | | 0.16 | 0.17 | 0.23 | 0.14 | 0.19 |
| $(La/Sm)n^{\dagger}$ | 1.02 | 1.20 | | 0.93 | 1.05 | 1.16 | 0.89 | 1.09 |
| $(Gd/Yb)n^{\dagger}$ | 1.28 | 1.27 | | 1.19 | 1.30 | 1.38 | 1.17 | 1.39 |
| $(Eu/Eu^*)n^{\dagger}$ | 0.77 | 0.95 | | 0.80 | 0.91 | 1.00 | 0.97 | 1.06 |

^ XRF values preferred

† Normalising values after Boynton (1984)

**Table 6.2: Average geochemical compositions for mafic rocks by domain within the central Georgetown Inlier. Domains are illustrated in Fig. 6.1.**

## 6.5 Results

### 6.5.1 Affinities and classification of the Etheridge Group mafic rocks

This study shows that Etheridge Group mafic rocks are a sequence of comagmatic metabasalts and metadolerites that resemble modern, relatively evolved, low-K tholeiites matching those generated during the early stage of continental rifting.

Mobility of the alkali elements during metamorphism compromises classification using the total alkalis – $SiO_2$ diagram, yet the Etheridge Group mafic rocks (excluding several granophyres) cluster in the subalkaline basalt field (Fig. 6.2a). On the $Zr/TiO_2$ versus Nb/Y diagram of Winchester & Floyd (1977) (Fig. 6.2b), in which $Zr/TiO_2$ effectively proxies for variations in $SiO_2$, and Nb/Y reflects alkalinity, both the DHM and CMD show a tight and overlapping distribution, and they are confidently assigned as subalkaline mafic suites. Further, the pronounced clustering of the DHM and CMD samples, despite the observed variation in crystallisation ages (Chapter 4) and spatial distribution, suggests that these units may be comagmatic. Most DHM and CMD have 5-8% MgO and are thus relatively evolved, in keeping with the apparent absence of olivine phenocrysts in samples from either group.

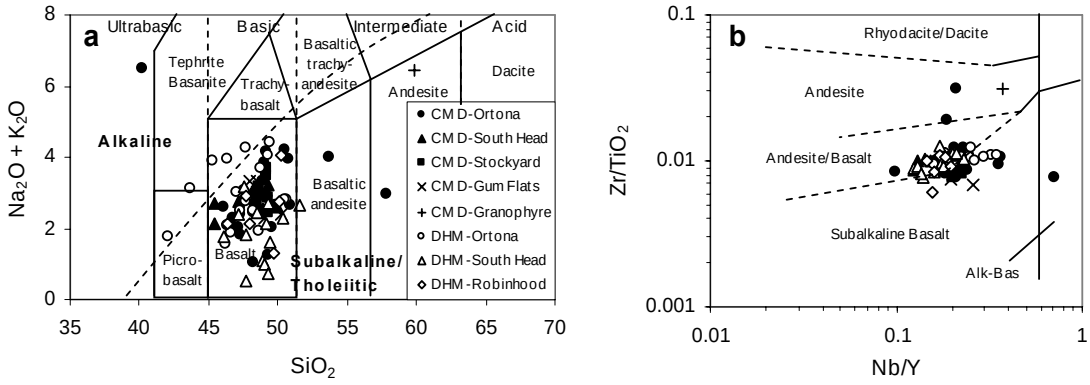


**Figure 6.2: (a) Total Alkalis-Silica (TAS) volcanic rock classification diagram (Le Bas *et al.*, 1986). (b) $Zr/TiO_2$ versus Nb/Y volcanic rock classification diagram (Winchester and Floyd, 1977).**

Strong Fe-, Ti- and V-enrichment with advancing fractionation (Figs. 6.3 and 6.4) shows clearly that both the DHM and CMD suites have tholeiitic affinities. Consistently low $K_2O$ contents in both CMD and DHM (average values for $K_2O$ in both the DHM and CMD 0.08 and 0.31 wt% respectively for greenschist facies samples; Table 2) suggest probable low-K tholeiite affinities. This is strongly supported by the Ti/Zr values that cluster between 80 and 120 for the majority of samples (Fig. 6.5a), a range typical of low-K tholeiites (Pearce, 1983).

Total iron (as $Fe_2O_3$) contents for both the DHM and CMD vary significantly, but predominantly lie within the range of 13 to 18 wt% (Table 6.1), defining a strong Fe-enrichment trend between 4 and 9 wt% MgO (Fig. 6.3). Four samples of the CMD do not follow this trend, and include three felsic differentiates and one granophyre sample, all from Ortona. However, one of the felsic differentiates has an LOI value

>15 wt%, and was probably subject to greater than average element mobility (Sample 8; Table 6.1).

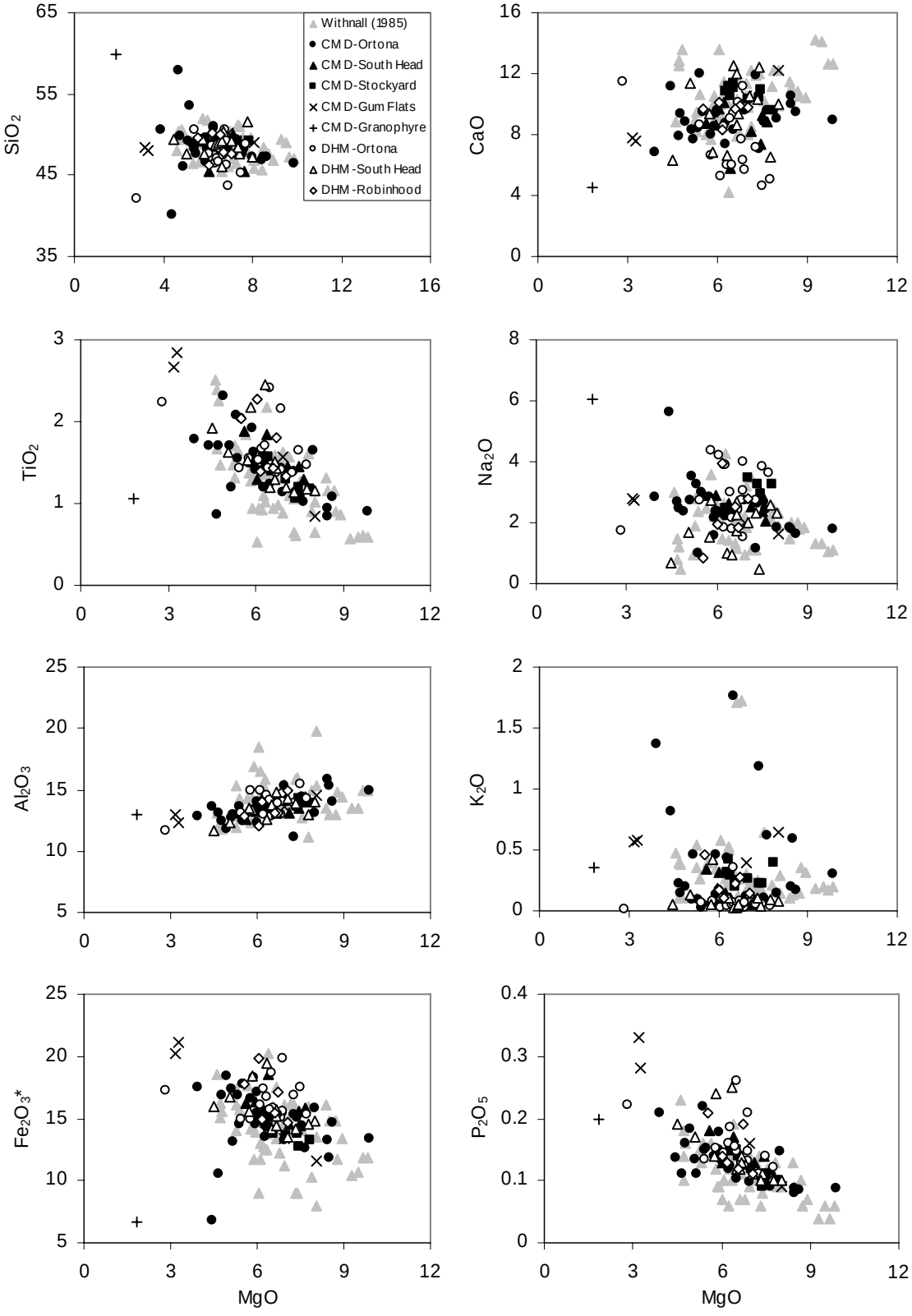


**Figure 6.3: Major element compositions of the lower Etheridge Group mafic rocks plotted against MgO. Additional Etheridge Group mafic rock data from Withnall (1985).**

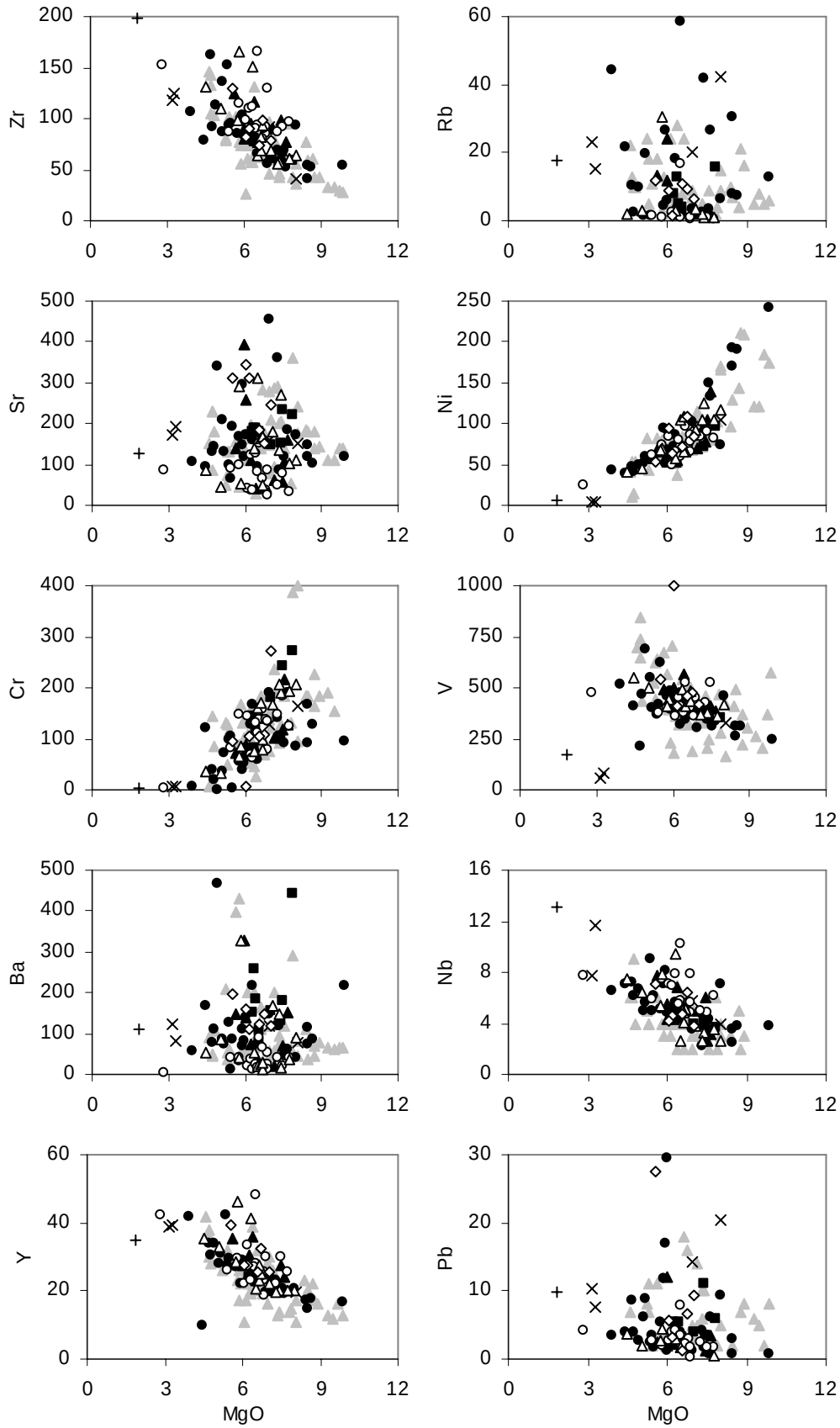


**Figure 6.4: Selected trace element compositions (in ppm) of the lower Etheridge Group mafic rocks plotted against MgO. Symbols as for Figure 6.3.**

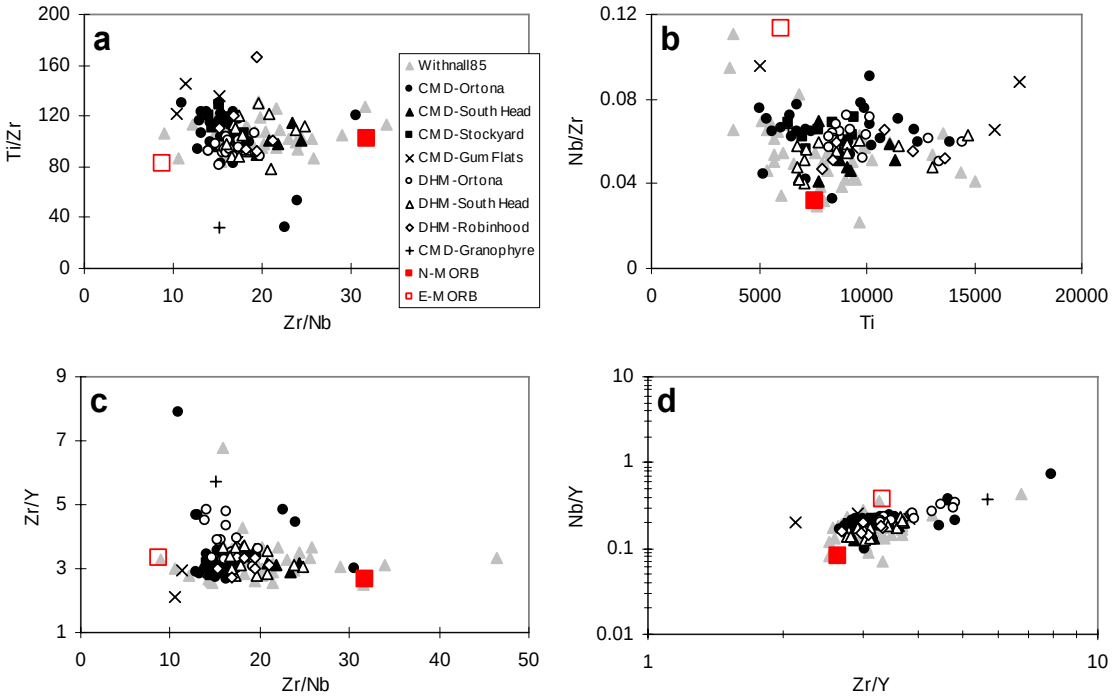


**Figure 6.5: Selected immobile trace element diagrams for mafic rocks of the lower Etheridge Group. Additional Etheridge Group mafic rock data from Withnall (1985). Average N-MORB and E-MORB values after Sun and McDonough (1989).**

Despite the regionally extensive spread of samples collected for this study, variation diagrams for major and trace elements within the DHM and CMD show significant overlap between the DHM and CMD (Figs. 6.3 and 6.4). The majority of samples have basaltic $SiO_2$ contents (45-53 wt%), with granophyres from CMD sills having higher $SiO_2$ contents (to 60 wt%). MgO ranges from 10 – 2 wt%, and most elements/oxides regarded as immobile during alteration show good correlations against MgO (e.g. $TiO_2$, $Al_2O_3$, $Fe_2O_3$, $P_2O_5$, Cr, Ni, V, Zr, Y, Nb; Figs. 6.3 and 6.4). The pronounced overlap on all immobile element – MgO diagrams (Fig. 6.4) is also consistent with the DHM and CMD having being derived from chemically similar parent magmas.

### 6.5.2 Trace- and rare earth element characteristics of the Etheridge Group mafic rocks

MORB-normalised trace-element diagrams and chondrite-normalised REE diagrams are presented in Figures 6.6 and 6.7 respectively for 25 representative samples of the DHM and CMD (Table 6.1). Although Rb, Ba, Pb, K and Sr were all likely to have been mobile to variable extents during post-magmatic alteration (as shown by the

scatter of points on element-MgO diagrams), K, Pb and Sr are included on the N-MORB-normalised plots to emphasise a number of points regarding element budgets during low-grade metamorphism.

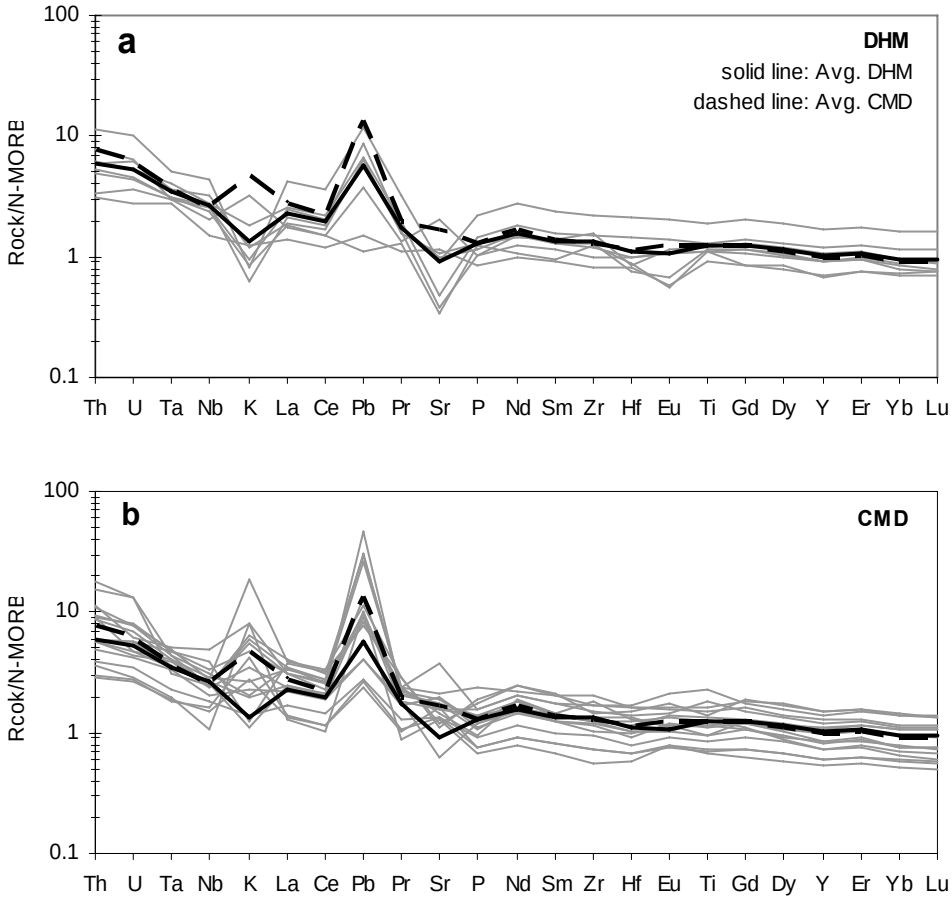


**Figure 6.6: MORB-normalised trace element diagrams for representative samples of the DHM and CMD. Normalising values after Sun and McDonough (1989).**

N-MORB-normalised multi-element patterns for eight well preserved DHM (Fig. 6.6a) show similar shapes, with the most notable differences being for the mobile elements Sr and Eu, both reflecting albitisation of plagioclase (see below). A striking feature of all patterns is the significant negative K anomalies. I believe these reflect chlorite-albite-silica alteration of glass and glassy mesostasis in the basalts, a feature not seen in the dolerites, which consequently show generally higher $K_2O$ contents (Fig. 6.6b), probably close to their primary values. Six of the eight basalts show strong positive Pb anomalies, a feature also characteristic of the majority of CMD patterns (Fig. 6.6b), and these are considered to be primary. These patterns show slight enrichment in LILE (Th, U, and La) relative to the similarly incompatible high field strength elements Ta and Nb.

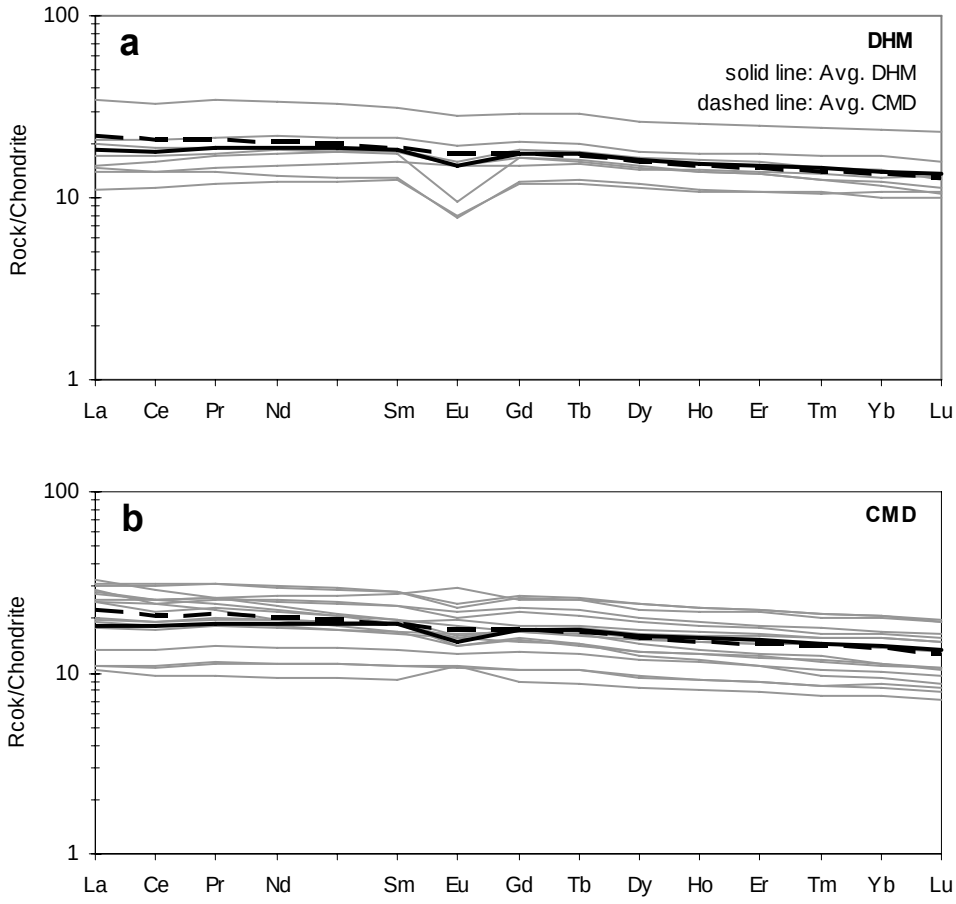


**Figure 6.7: Chondrite-normalised REE diagrams for representative samples of the DHM and CMD. Normalising values after Boynton (1984).**

Chondrite-normalised REE patterns for the DHM and CMD (Fig. 6.7) range from weakly LREE-enriched to moderately LREE-depleted (avg. $(La/Sm)_n$ = 1.11; range 0.81-1.68), with flat to weakly HREE-enriched HREE patterns (avg. $(Gd/Yb)_n$ = 1.28; range 1.11-1.64). Chondrite-normalised REE diagrams display the expected upward shift to higher total REE values with increased fractionation, as shown in Figure 6.8, in which all 25 representative samples are grouped in order of their MgO contents. DHM and CMD samples from both the South Head and Ortona areas (Fig. 6.8) have similar REE patterns; however, the metabasalts show more pronounced negative Eu-anomalies (avg. $(Eu/Eu^*)_n$ = 0.80 for DHM and 0.96 for CMD samples; Fig. 6.7a; Table 6.1). There is no significant difference in extent of fractionation between the Ortona DHM and CMD for which REE were analysed. Thus the significant negative Eu anomalies in the metabasalts relative to compositionally similar (in terms of major elements and other REE apart from Eu) metadolerites presumably reflects increased leaching of plagioclase-hosted and thus relatively mobile Eu (compared to the

immobile +3 valence state adjacent REE) during albitisation. Plagioclase is always albitised in the basalts, whereas calcic plagioclase is often preserved in the dolerites.

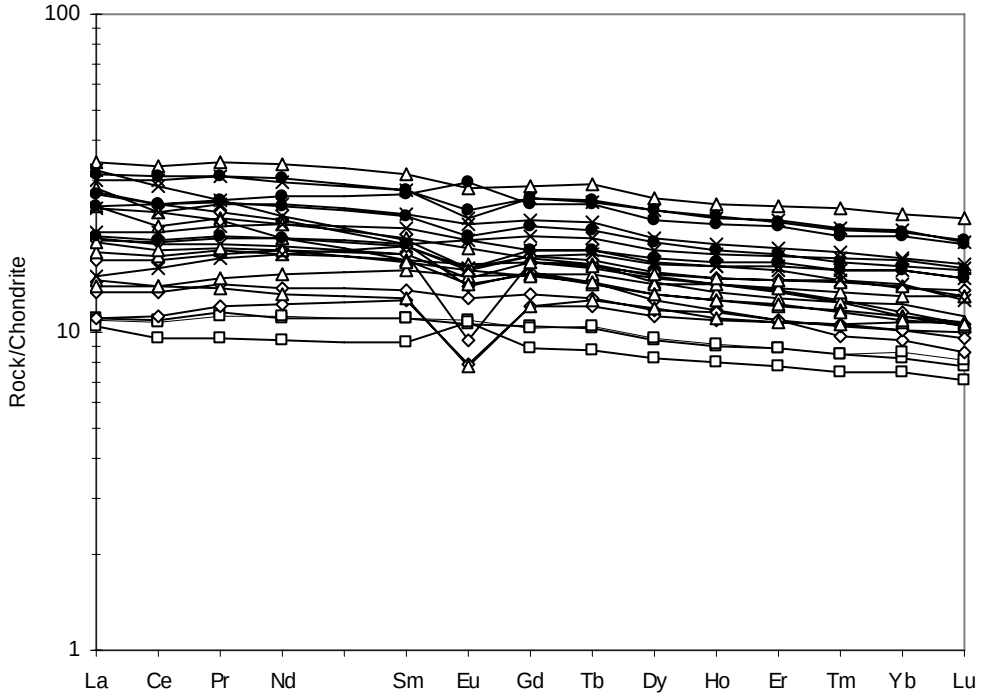


**Figure 6.8: Chondrite-normalised REE diagram for representative samples of the Etheridge Group mafic rocks grouped according to MgO wt% values. Symbols: squares = >8 wt% MgO; diamonds = 8-7 wt% MgO; triangles = 7-6 wt% MgO; crosses = 6-5 wt% MgO; filled circles = <5 wt% MgO. Normalising values after Boynton (1984).**

Three CMD samples from Ortona (Samples 6, 22, and 112) and one CMD amphibolite from Gum Flats (Sample 301) show distinct LREE-enriched, slightly HREE-depleted patterns ($(La/Sm)_n$ = 1.67, 1.47, 1.68, and 1.25 respectively). These samples have among the highest La/Nb and Th/Nb values for Etheridge Group mafic rocks, which may suggest (Pearce, 1983; James *et al*., 1987) that the LREE-enrichment reflects some crustal contamination.

A simple mixing relationship between the Etheridge Group mafic rocks and the host metasediments of the lower Etheridge Group could account for this variation. In Figure 6.9, a clear trend towards increasing degrees of contamination by the host metasediments is apparent, with the most contaminated dolerite sill-margin samples showing up to 20% assimilation of sedimentary material. However, the majority of samples contain less than 10% sedimentary material. A granophyric sample from the margin of a CMD sill (sample 174) shows approximately 40% assimilation of sedimentary material, and also lies within the field of the lower Etheridge Group

metasediments (Fig. 6.9). This relationship suggests that the lower Etheridge Group metasediments may have been the only contaminant of the mafic rocks.

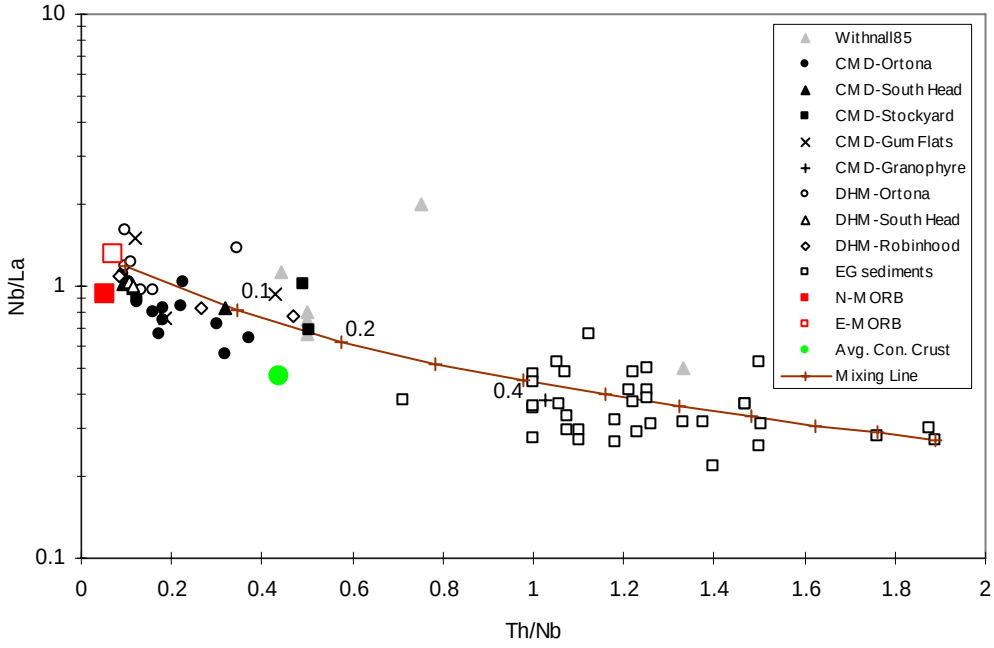


**Figure 6.9: Th/Nb versus Nb/La diagram for mafic and metasedimentary rocks of the lower Etheridge Group showing possible mixing curve between the lithologies. The mixing curve was calculated using the following parameters for the uncontaminated Etheridge Group mafic rocks (Th/Nb = 0.096, Nb/La = 1.189, Th = 1 ppm, Nb = 6 ppm, and La = 5 ppm), and for the Etheridge Group metasediments (Th/Nb = 1.889, Nb/La = 0.273, Th = 17 ppm, Nb = 9 ppm, and La = 33 ppm). Additional Etheridge Group mafic data after Withnall (1985). Lower Etheridge Group metasedimentary data available from the Geoscience Australia OZCHEM Database. Average N-MORB and E-MORB values after Sun and McDonough (1989). Average continental crust value after Weaver and Tarney (1984).**

Fractionation-independent Zr/Nb values mainly range from 12-20 and show no significant regional or stratigraphic variation, with CMD overlapping the compositional field of the DHM. The same applies to a variety of immobile element ratios shown in Figure 6.5, strongly supporting the suggestion from major and trace element data and REE patterns that the DHM are comagmatic with the CMD, and that the latter were likely feeders to the basalts. Dolerite sills emplaced after eruption of the DHM into the overlying Lane Creek Formation are compositionally identical to those emplaced during the main magmatic episode.

### 6.5.3 Compositional variations across-sill for CMD, and across stratigraphic for DHM

Wholerock geochemical data were measured for a series of samples taken systematically across the outcropping width of a DHM flow near 'Ortona' (650 m thick), and a thick CMD sill at Stockyard Creek (395 m thick). Detailed sampling was also carried out across the full width of the best exposed basalt-dolerite pile outcrops along the Gilbert River at South Head (~ 3000 m true thickness).

Figure 6.10 illustrates the chemical variations across the sills. Marginal samples have MgO contents < 7%, in keeping with the generally evolved nature of the magmas that formed the CMD and DHM. There appears to have been no significant accumulation of olivine in the lower sections of any sill sampled, in accordance with the absence of olivine in the relatively evolved marginal variants of each sill, although each sill shows generally higher MgO contents in its lower third to lower half. $TiO_2$ and $Fe_2O_3$ are generally higher in the upper half of both sills. The antithetic relationship between the more compatible (e.g. Ni) and more incompatible (e.g. Zr) elements is as expected from limited in-situ fractionation of a single magma batch.

Relative to many mafic sills 500-1000 m thick that have crystallised essentially in-situ, the sampled sills in the Lower Etheridge Group show surprisingly limited internal fractionation, with only relatively rare and small volumes of more felsic granophyres with ~60 wt% $SiO_2$. This may indicate that the sills were essentially open system conduits in which continuous provision of magma essentially added to and thickened the sills, rather than having been static, closed system bodies.

The thick (>3000 m) interlayered basalt-dolerite sequence at South Head (Fig. 6.10a and d) shows a slight decrease in MgO from the base to the top of the sequence, and sharp increase in $Fe_2O_3$ and $TiO_2$ in basalts from near the top of the pile, the latter probably reflecting expulsion of relatively late stage fractionation products from a deeper stagnating magma chamber.

The compositional variation between CMD sills emplaced stratigraphically below, within, and above the DHM is insignificant (Table 6.2; Figure 6.11). The CMD sill emplaced within the Lane Creek Formation at Stockyard Creek, above the level of the DHM, is compositionally similar (including REE) to CMD sills within and beneath the DHM, suggesting no significant change in the source mantle or partial melting/fractionation processes over the time interval represented by the stratigraphic

section from the DHM to the Lane Creek Formation (keeping in mind that many sills in the Bernecker Creek Formation and Daniel Creek Formation *below* the DHM may have been emplaced pre-, syn- or post-DHM).

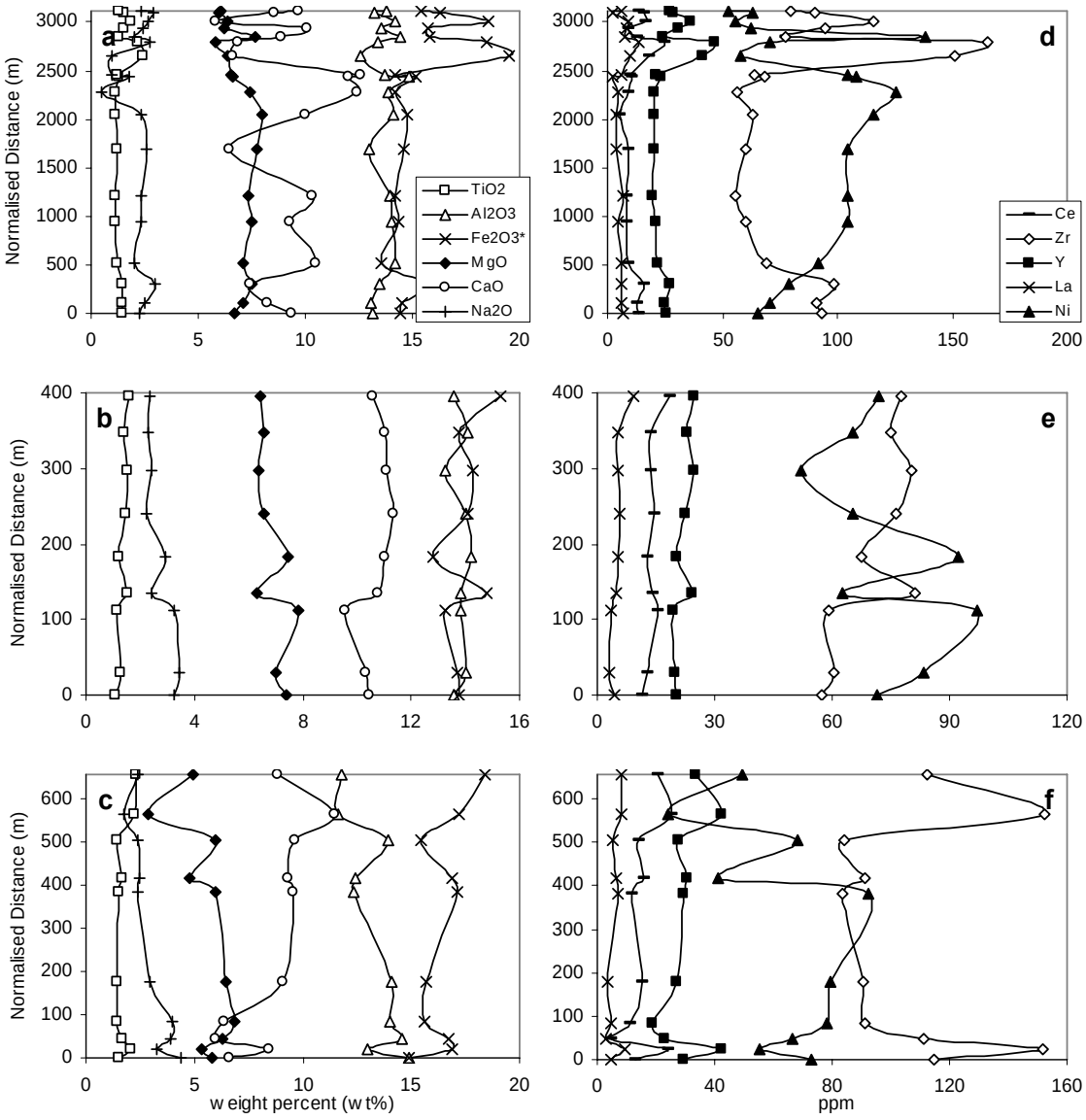


**Figure 6.10: Major oxide (wt %) and trace element (ppm) variation with stratigraphic height for selected CMD sills and DHM layers. (a) and (d): interlayered CMD and DHM sequence along Gilbert River at South Head; (b) and (e): CMD sill at Stockyard Creek; (c) and (f): CMD sill at Ortona.**

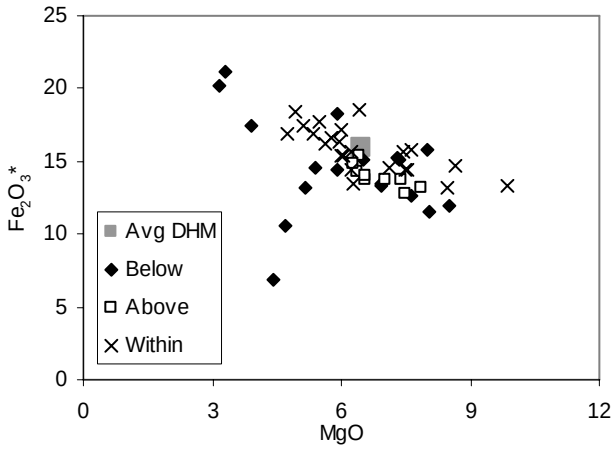


**Figure 6.11: MgO versus $Fe_2O_3$* showing geochemical variation in CMD sills emplaced stratigraphically below, within and above the level of the DHM.**

### 6.5.4 Sm-Nd radiogenic isotope geochemistry of representative Etheridge Group mafic rocks

The relative immobility of both Sm and Nd compared to Rb, Sr, U and Pb makes the Sm-Nd isotopic system particularly useful for determining both the petrogenetic characteristics and age of older (Proterozoic to Achaean) terranes that may have been affected by multiple stages of deformation (e.g. Black & McCulloch, 1984; Zhao & McCulloch, 1995; Blewett *et al*., 1998). In general, concentrations of both Sm and Nd in igneous rocks increase with increasing degrees of differentiation; however the Sm/Nd ratio decreases with fractionation, since Nd is more incompatible than Sm. Similarly, tholeiitic basalts that have assimilated crustal material (which is always LREE-enriched) will have lower Sm/Nd than unmodified magmas from the same source. Thus Sm-Nd isotopic systematics are useful for evaluating crustal interaction in mafic magmas.

For this study, three samples of DHM and seven samples of CMD were analysed for their Sm and Nd isotopic compositions (Table 6.3). Initial isotopic compositions for the individual samples are listed in the form of $\varepsilon_{Nd}(T)$ values, which were calculated for each sample assuming a magmatic age of 1.67 Ga, and the chondritic uniform reservoir (CHUR) to have a present-day $^{147}Sm/^{144}Nd$ value of 0.1967 and a $^{143}Nd/^{144}Nd$ value of 0.512638 (Wasserburg *et al*., 1981).

| Sample No. | | Sm (ppm) | Nd (ppm) | $^{147}Sm/^{144}Nd$ | $^{143}Nd/^{144}Nd$ | εNd(t) | $f_{Sm/Nd}$ | $T_{DM}$ (Ga) | La/Sm |
|---|---|---|---|---|---|---|---|---|---|
| **MAFIC** | | | | | | | | | |
| Dead Horse Metabasalt (DHM) | | | | | | εNd(1.67 Ga) | | | |
| 100 | | 3.52 | 10.43 | 0.2042 | 0.512937 | 4.2 | 0.04 | 3.39 | 1.33 |
| 234 | | 2.39 | 7.49 | 0.1926 | 0.512798 | 4.0 | -0.02 | 2.53 | 1.44 |
| 269 | | 2.94 | 9.15 | 0.1941 | 0.512824 | 4.2 | -0.01 | 2.52 | 1.47 |
| Cobbold Metadolerite (CMD) | | | | | | | | | |
| 6 | | 3.87 | 14.58 | 0.1605 | 0.512388 | 2.9 | -0.18 | 2.17 | 2.60 |
| 113 | | 2.10 | 6.70 | 0.1895 | 0.512781 | 4.3 | -0.04 | 2.31 | 1.61 |
| 181 | | 1.76 | 5.67 | 0.1879 | 0.512717 | 3.4 | -0.04 | 2.55 | 1.84 |
| 196 | | 3.19 | 11.03 | 0.1749 | 0.512590 | 3.8 | -0.11 | 2.19 | 1.86 |
| 249 | | 4.68 | 15.46 | 0.1828 | 0.512692 | 4.0 | -0.07 | 2.25 | 1.64 |
| 299 | | 5.19 | 16.20 | 0.1936 | 0.512737 | 2.6 | -0.02 | 3.11 | 1.49 |
| 301 | | 3.73 | 13.25 | 0.1701 | 0.512618 | 5.3 | -0.14 | 1.85 | 2.06 |
| *Black and McCulloch (1984)* | | | | | | | | | |
| 73303006 | CMD | 2.48 | 8.52 | 0.1757 | 0.512492 | 1.7 | | 2.63 | |
| 79300232 | CMD | 1.76 | 5.59 | 0.1905 | 0.512807 | 4.6 | | 2.24 | |
| 82303067 | Qtz diorite | 45.75 | 247.70 | 0.1116 | 0.5116 | -2.0 | | 2.30 | |
| 82303068 | Granophyre | 4.74 | 27.43 | 0.1045 | 0.511358 | -5.2 | | 2.49 | |
| 80303065 | Mafic granulite | 2.48 | 7.62 | 0.1971 | 0.51287 | 4.5 | | 2.56 | |
| 80303066 | Mafic granulite | 2.11 | 6.52 | 0.1958 | 0.512815 | 3.7 | | 2.84 | |
| *Knutson and Sun (1997)* | | | | | | | | | |
| 92836540 | Amphibolite | 3.67 | 11.96 | 0.1857 | 0.512718 | 4.0 | | 2.34 | |
| 92836504B | CMD | 5.93 | 29.04 | 0.1235 | 0.511674 | -3.0 | | 2.48 | |
| **FELSIC** | | | | | | | | | |
| *Black and McCulloch (1984)* | | | | | | εNd(1.685 Ga) | | | |
| 73303024 | Einasleigh Metamorphics | 7.52 | 42.77 | 0.1063 | 0.511376 | -5.1 | | 2.51 | |
| 73303001 | Einasleigh Metamorphics | 7.56 | 43.02 | 0.1064 | 0.511364 | -5.4 | | 2.52 | |
| 79300058 | Candlow Formation | 1.19 | 5.76 | 0.1251 | 0.511916 | 1.4 | | 2.11 | |
| 79300059 | Candlow Formation | 1.14 | 5.33 | 0.1291 | 0.511965 | 1.5 | | 2.13 | |
| 79300060 | Candlow Formation | 1.62 | 6.84 | 0.1434 | 0.511885 | -3.2 | | 2.73 | |
| 79300060 | Candlow Formation | 1.66 | 7.06 | 0.1420 | 0.511897 | -2.6 | | 2.65 | |
| 79300062 | Candlow Formation | 1.33 | 6.85 | 0.1171 | 0.51175 | -0.1 | | 2.20 | |
| 79300062 | Candlow Formation | 1.28 | 6.67 | 0.1162 | 0.511721 | -0.5 | | 2.22 | |
| *Knutson and Sun (1997)* | | | | | | | | | |
| 92836520 | Corbett Formation schist | 9.29 | 54.22 | 0.1036 | 0.511363 | -4.8 | | 2.46 | 7.23 |
| 92836536 | Townley Formation schist | 8.83 | 48.30 | 0.1105 | 0.511719 | 0.7 | | 2.11 | 8.61 |

*$f_{Sm/Nd} = [(^{147}Sm/^{144}Nd)_{sample}/(^{147}Sm/^{144}Nd)_{CHUR}]-1$*
*CHUR (chondrite uniform reservoir): $^{147}Sm/^{144}Nd = 0.1967$, $^{143}Nd/^{144}Nd = 0.512638$*
*DM (depleted mantle): $^{147}Sm/^{144}Nd = 0.2137$, $^{143}Nd/^{144}Nd = 0.51315$*
*$\lambda$ = decay constant of $^{147}Sm = 6.54 \times 10^{-12}$*

**Table 6.3: Sm-Nd isotopic data and depleted mantle model ages for rocks of the lower Etheridge Group. Sm and Nd ppm values for mafic rocks of this study taken from MC-ICPMS analyses.**

The analysed Etheridge Group mafic rocks show only a limited range in initial Nd isotopic compositions, with 7 analyses having $\varepsilon_{Nd}(T)$ values between +3.4 and +4.3. Samples 6 and 299 have isotopic compositions of +2.9 and +2.6 respectively, whereas sample 301 had the highest $\varepsilon_{Nd}(T)$ value of +5.3 (Table 3). The $\varepsilon_{Nd}(T)$ values for these samples are identical to those for samples of the CMD and related rocks reported by Black & McCulloch (1984), and clearly indicate that the majority of these Georgetown Inlier mafic rocks are broadly co-magmatic and were derived from partial melting of a depleted upper mantle source.

### 6.5.5 Sm-Nd isochron age for mafic igneous rocks of the lower Etheridge Group

The $^{147}Sm/^{144}Nd$ and $^{143}Nd/^{144}Nd$ values for the Etheridge Group igneous rocks show a relatively good linear correlation on the Sm-Nd isochron diagram (Fig. 6.12).

However, contamination by crustal material in a number of samples (see below), as well as the relatively short isochron, have affected the determination of a reliable Sm-Nd isochron age. For this reason (i.e. crustal contamination in mafic samples), mafic samples from the Etheridge Group analysed by Black & MuCulloch (1984) were not used in constructing the isochron in Figure 6.12. The isochron produced by the ten Etheridge Group samples corresponds to a poorly constrained age of 1691 ± 370 Ma (MSWD = 16 based on the Model 3 solution of *Isoplot* (Ludwig, 2003) and an initial $^{143}Nd/^{144}Nd$ of 0.51065 ± 0.00046 ($\varepsilon_{Nd}(T)$ = +4.0).

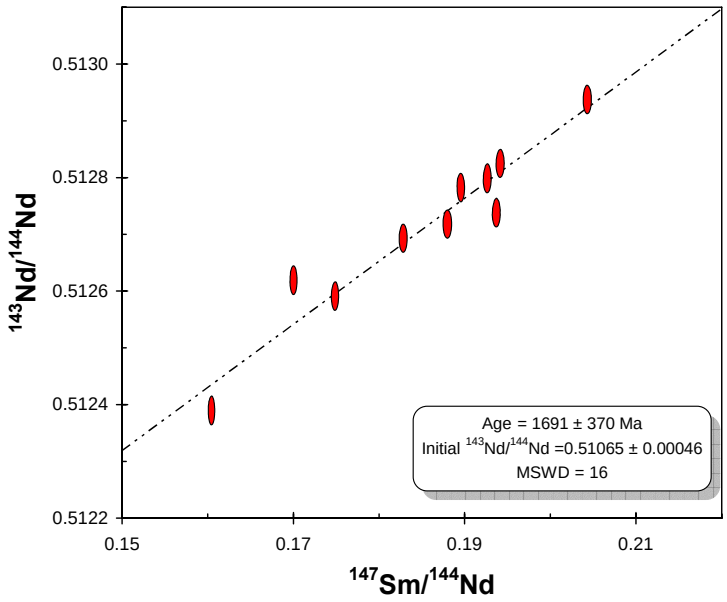


**Figure 6.12: $^{147}Sm/^{144}Nd$-$^{143}Nd/^{144}Nd$ whole rock isochron of the Etheridge Group mafic rocks. Model 3 solution isochron age and initial $^{143}Nd/^{144}Nd$ ratio calculated using *Isoplot* version 3.0 (Ludwig, 2003). Data point error ellipses are 2σ.**

A number of factors have contributed to the large error in the age calculation; the first and possibly most significant being the relatively limited spread in Sm/Nd across the sample range. Second, data points in Figure 6.12 that lie furthest from the Sm-Nd isochron correspond to those samples considered to have been significantly modified by crustal contamination prior to crystallisation. Unless all analysed samples contain crustal contaminants from a similar source, it would be expected that the Sm/Nd values for those contaminated samples would shift from the Sm-Nd isochron, compared to samples that were produced by simple fractionation from the depleted mantle-derived, unmodified parental magma. Nevertheless, despite the large error associated with the Sm-Nd isochron, the calculated age approximates the inferred crystallisation age of the DHM.

Nd depleted mantle model ages ($T_{DM}$) were calculated for the Etheridge Group mafic rocks using the equation of Faure (1986), a depleted mantle reservoir with a present-day $^{147}Sm/^{144}Nd = 0.2137$, and $^{143}Nd/^{144}Nd = 0.51315$ (Goldstein *et al*., 1984). The Nd model ages give an estimate of the average crustal residence time of the source material of a particular sample, and hence the time at which the sample is believed to have separated from its mantle source (either depleted mantle or CHUR). Knowledge of this reference reservoir is essential in order to calculate the correct model age, as is the assumption that Sm/Nd has not been modified following extraction from the source. Subsequently, the Nd model age can also give an indication as to the probable time of crust formation. As the Etheridge Group mafic samples all have $\varepsilon_{Nd}(T) > 0$, a depleted mantle source for the mafic rocks is inferred, and as such all model ages were calculated in reference to the depleted mantle.

The $T_{DM}$ ages for each sample are listed in Table 3. $T_{DM}$ ages range from 3.39 to 1.85 Ga for all samples, however the majority of ages lie between 2.17 and 2.55 Ga (average = 2.36 Ga). The majority of $T_{DM}$ ages from this study cover a similar range to those calculated from CMD and other Etheridge Group rocks by Black & McCulloch (1984) and Knutson & Sun (1997) (Fig. 6.13; Table 6.3), and mostly likely represent the time at which the mantle source last underwent melt extraction that imposed its depleted characteristics.

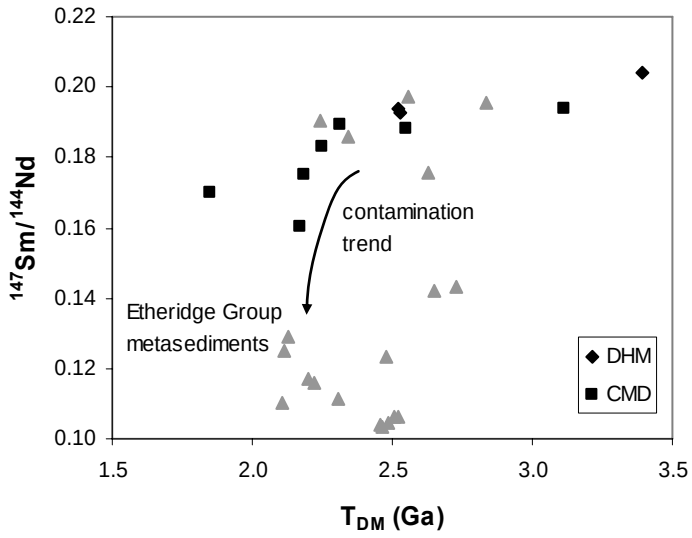


**Figure 6.13: $T_{DM}$ model ages versus $^{147}Sm/^{144}Nd$ for Etheridge Group mafic rocks. Additional samples (grey triangles) from Black and McCulloch (1984) and Knutson and Sun (1997). $T_{DM}$ ages and $^{147}Sm/^{144}Nd$ values listed in Table 6.3.**

In the $T_{DM}$ versus $^{147}Sm/^{144}Nd$ diagram (Fig. 6.13), younger $T_{DM}$ ages correspond to a general decrease in $^{147}Sm/^{144}Nd$, possibly relating to the contamination of the Sm-Nd system by small amounts of crustal material. Those samples that may have involved some contamination by crustal material also deviate slightly from the evolution curve. The evolution of the Nd isotopic composition in the mafic samples is illustrated in Figure 6.14. The evolution lines for the majority of samples cross near $\varepsilon_{Nd}(T) = +4$ and ~1.7 Ga, again indicating that the samples are geochemically related and share a near isochronous relationship. Samples that have been contaminated by crustal material would show a decrease in their $\varepsilon_{Nd}$ values over time, relative to the uncontaminated mafic rocks that were simply derived from a depleted mantle source. Sample 299 is an example of this, as it contains U-Pb dated zircons that have returned a weighted mean age of 1687 ± 38 Ma. However, the $\varepsilon_{Nd}(T)$ value and $T_{DM}$ age for this sample produce a Nd evolution line that lies below the cross-over point for the Etheridge Group mafic rocks at ca. 1.7 Ga (Fig. 6.14). Contamination by material with a lower $^{147}Sm/^{144}Nd$ and hence a lower $\varepsilon_{Nd}$ than uncontaminated Etheridge Group mafic rocks, such as Archaean crustal rocks or the metasedimentary rocks of the lower Etheridge Group, could account for this difference.

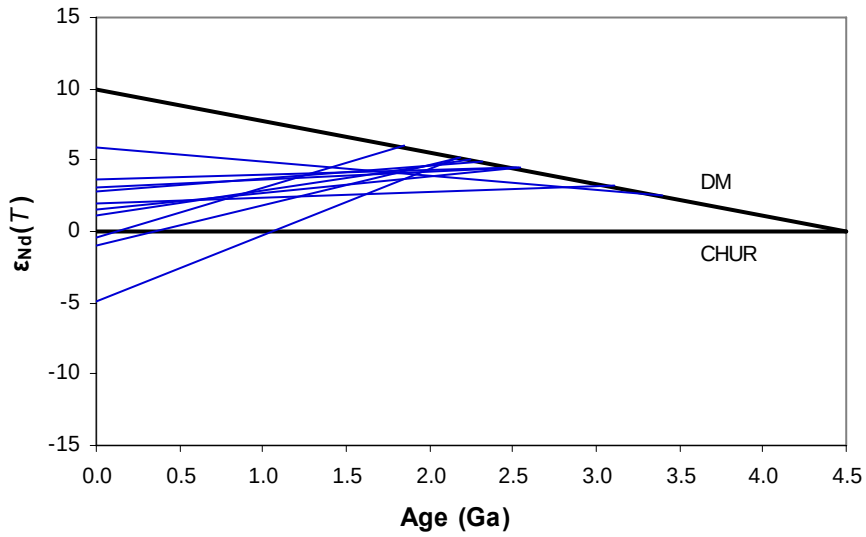


**Figure 6.14: Nd isotope evolution diagram for Etheridge Group mafic rocks. Model ages indicate the source was early Palaeoproterozoic. Evolution lines for uncontaminated samples cross at ~1.7 Ga, indicating an isochronous relationship. Depleted mantle curve (DM) assumes a linear evolution of the depleted mantle from CHUR ($\varepsilon_{Nd} = 0$) at 4.56 Ga to a present-day value of +10 (Goldstein *et al.*, 1984; Jahn & Condie, 1995; Blewett *et al.*, 1998). $T_{DM}$ ages and $\varepsilon_{Nd}(T)$ values listed in Table 6.3.**

The distribution of $\varepsilon_{Nd}(T)$ values is partially reflected in the $^{147}Sm/^{144}Nd$ values for each sample, with a relative decrease in $^{147}Sm/^{144}Nd$ corresponding to a decrease in $\varepsilon_{Nd}(T)$ (Fig. 6.15). This relationship is consistent with limited crustal contamination by a typical upper crustal component with $^{147}Sm/^{144}Nd$ <~1.50, and a $\varepsilon_{Nd}(T)$ value below +2.5 (Fig. 6.16). Importantly, Sample 6, which has the lowest $\varepsilon_{Nd}(T)$ and $^{147}Sm/^{144}Nd$ values, is a felsic differentiate from a CMD sill at Ortona. Sample 6 has the highest La/Sm of analysed CMD (2.60; Table 6.3), indicating that crustal contamination was a possible cause of the relatively lower $^{147}Sm/^{144}Nd$, as addition of crustal material to the host magma generally leads to higher La/Sm values (Marsh, 2004; Lightfoot & Keays, 2005). The effect of this contamination is illustrated in Figure 6.16, where the representative Etheridge Group mafic rocks follow a simple mixing trend towards increasing degrees of contamination by the host metasediments of the lower Etheridge Group.

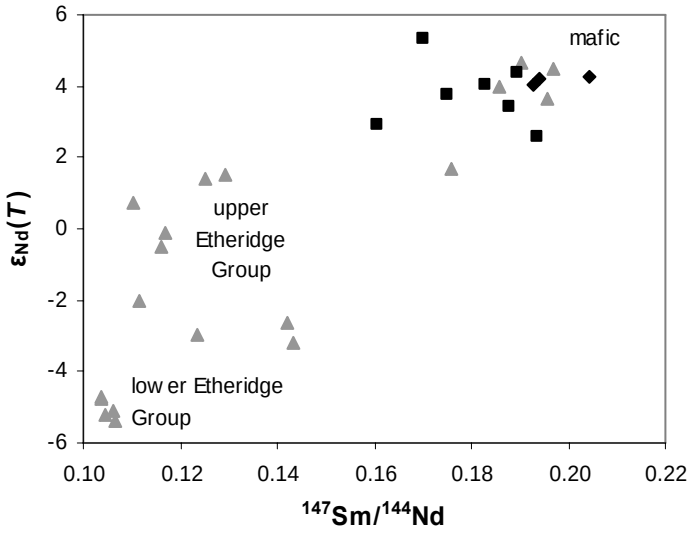


**Figure 6.15: $^{147}Sm/^{144}Nd$ versus $\varepsilon_{Nd}(T)$ for mafic rocks of the lower Etheridge Group. Symbols as in Figure 6.13.**

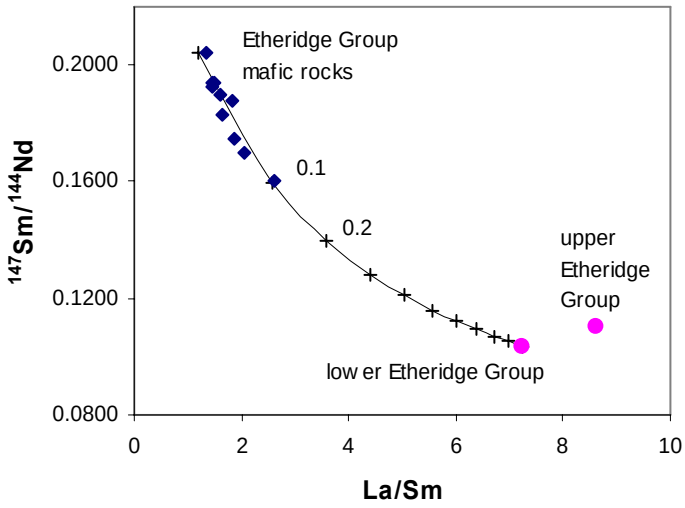


**Figure 6.16: La/Sm versus $^{147}Sm/^{144}Nd$ diagram showing simple mixing curve for the Etheridge Group mafic rocks. The mixing curve was calculated using the following parameters for the uncontaminated Etheridge Group mafic rocks (La/Sm = 1.33, $^{147}Sm/^{144}Nd$ = 0.2042, La = 4.67 ppm, Sm = 3.52 ppm, and Nd = 10.43 ppm), and for the lower Etheridge Group metasediments (La/Sm = 7.23, $^{147}Sm/^{144}Nd$ = 0.1036, La = 67.95 ppm, Sm = 9.29 ppm, and Nd = 54.22 ppm). Etheridge Group metasedimentary data from Knutson and Sun (1997). La/Sm and $^{147}Sm/^{144}Nd$ data from Table 6.3.**

### 6.5.6 Fractionation of the depleted mantle source of the Etheridge Group mafic rocks modelled using $\varepsilon_{Nd}(T)$ values

The fractionation factor $f^{Sm/Nd}$ is a measure of the $^{147}Sm/^{144}Nd$ ratio of a given reservoir relative to CHUR, and is therefore the $^{147}Sm/^{144}Nd$ equivalent to the $\varepsilon_{Nd}$ parameter (Rollinson, 1993). Consequently, $f^{Sm/Nd}$ can be used to estimate the level of enrichment or depletion of a given sample relative to CHUR, as well as estimate the fractionation history of the source. The $f^{Sm/Nd}$ value of an individual sample is calculated by the equation of DePaolo (1988):

$$f^{Sm/Nd} = \frac{\left(^{147}Sm/^{144}Nd\right)_{sample}}{\left(^{147}Sm/^{144}Nd\right)^{0}_{CHUR}} - 1 \qquad (6.1)$$

The $f^{Sm/Nd}$ values for individual Etheridge Group mafic samples are listed in Table 6.3. The calculated $\varepsilon_{Nd}(T)$ and $f^{Sm/Nd}$ values for the Etheridge Group mafic rocks can be used to estimate the $^{147}Sm/^{144}Nd$ value of the depleted mantle source, and hence the

amount of depletion of the source relative to CHUR at the time of crystallisation. Using the average value for $\varepsilon_{Nd}(T)$ of +4.0, derived from the Sm-Nd isochron of Figure 6.12, the $f^{Sm/Nd}$ value of the source can be estimated using the equation of DePaolo (1988):

$$f_{Sm/Nd}^{source} = \frac{\varepsilon_{Nd}(T_X)}{Q(T_S - T_X)} \qquad (6.2)$$

where $Q$ = 25.09 $Ga^{-1}$ (Rollinson, 1993), $T_S$ = model age of the magma source = 4.5 Ga (Goldstein *et al*., 1984), and $T_X$ = crystallisation age of the Etheridge Group mafic rocks = 1.67 Ga. Based on these values, the $f^{Sm/Nd}$ value of the source was calculated to be +0.06, which equates to an initial $^{147}Sm/^{144}Nd$ for the source of 0.2085, calculated using the following equation (DePaolo, 1988):

$$f_{source}^{Sm/Nd} = \frac{\left(^{147}Sm/^{144}Nd\right)_{source} - \left(^{147}Sm/^{144}Nd\right)_{CHUR}}{\left(^{147}Sm/^{144}Nd\right)_{CHUR}} \qquad (6.3)$$

rearranged to solve for $^{147}Sm/^{144}Nd$:

$$\left(\frac{^{147}Sm}{^{144}Nd}\right)_{source} = \left[f_{source}^{Sm/Nd} \times \left(\frac{^{147}Sm}{^{144}Nd}\right)_{CHUR}\right] + \left(\frac{^{147}Sm}{^{144}Nd}\right)_{CHUR} \qquad (6.4)$$

The calculated $f^{Sm/Nd}$ value indicates that the depleted mantle source of the Etheridge Group mafic rocks had a Sm/Nd ratio that was ~6 % higher than CHUR at the time of crystallisation of the mafic rocks.

The $f^{Sm/Nd}$ values obtained for both the source and sampled rocks can then be used to estimate the amount of depletion in the Sm/Nd value from the crystallised rocks relative to their depleted mantle source. The depletion factor ($\alpha_{Sm/Nd}$) is calculated from the following equation (DePaolo, 1988):

$$\alpha_{Sm/Nd} = \frac{1 + f^{Sm/Nd}_{sample}}{1 + f^{Sm/Nd}_{source}} \qquad (6.5)$$

Using the values of $f^{Sm/Nd}$ = +0.06 for the depleted mantle source, and $f^{Sm/Nd}$ = -0.06 for the Etheridge Group mafic samples (average of the 10 samples, Table 3), a value of 0.890 was calculated for $\alpha_{Sm/Nd}$. This indicates that the Sm/Nd value of the mafic rocks decreased by ~11 % from that of the depleted mantle source, which was originally depleted in Sm/Nd by ~6 % relative to CHUR (Fig. 6.17). A relatively low degree of partial melting coupled with significant fractional crystallisation of a tholeiitic parental magma could account for the observed depletion (DePaolo, 1988). This evidence, in addition to the calculated $T_{DM}$ and crystallisation ages, indicates that the Etheridge Group mafic rocks had a relatively short residence time in the upper crust during the Palaeoproterozoic, but did assimilate some crustal material from host metasediments during emplacement.

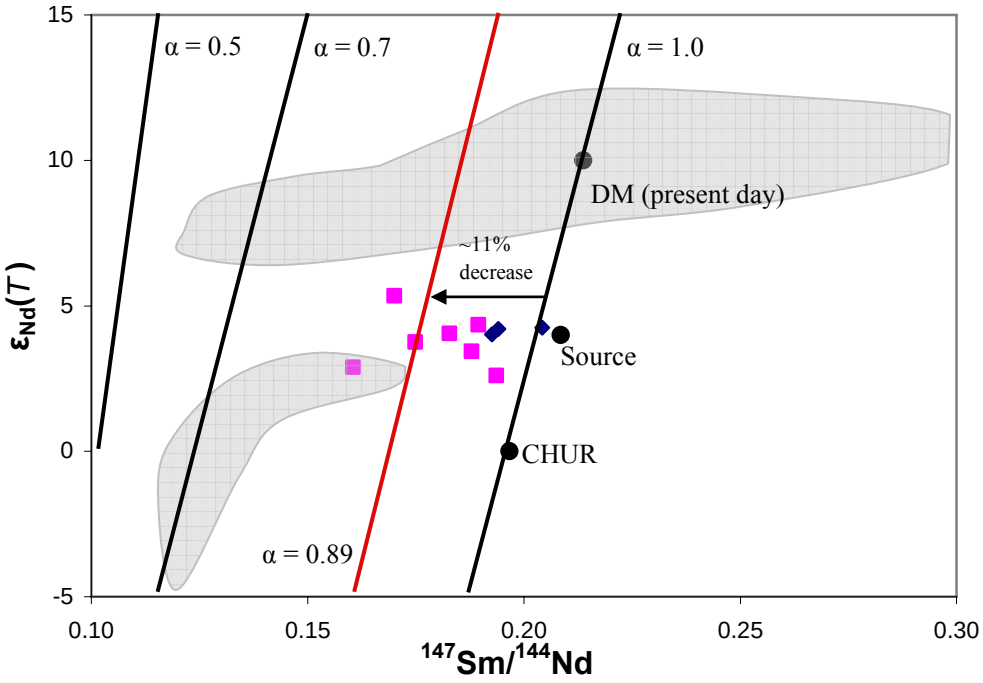


**Figure 6.17: $^{147}Sm/^{144}Nd$ versus $\varepsilon_{Nd}(T)$ diagram showing the effects of Sm/Nd fractionation (α) associated with partial melting for the Etheridge Group mafic rocks (after DePaolo, 1988). For explanation of $\alpha_{Sm/Nd}$, $\varepsilon_{Nd}(T)$, and $^{147}Sm/^{144}Nd$ values of source see text and Figure 6.12. $\alpha_{Sm/Nd}$ values calculated for a present day depleted mantle $^{147}Sm/^{144}Nd$ ratio of 0.2317 (DePaolo, 1988). Shaded areas represent tholeiitic MORB and tholeiitic basalt fields of DePaolo (1988).**

## 6.6 Similarities to modern continental and oceanic tholeiitic flood basalt provinces: implications for the tectonic setting of the Etheridge Group mafic rocks

The tectonic setting for the eruption and emplacement of the Etheridge Group mafic rocks is reasonably well constrained to a continental-rift setting leading to break-up. This is based partially on regional geological and lithological evidence, and also on the geochemical evidence presented above and by previous authors (e.g. Withnall, 1985). Despite this well constrained setting, at present little work has been done in order to determine the processes that affected the evolution of the magma. To address this issue, in this section the mafic rocks of the Etheridge Group are compared to a number of major Phanerozoic tholeiitic flood basalt provinces (Table 6.4). A number of these provinces (e.g. Karoo, East Greenland) have been associated with Phanerozoic continental rifting, and as such, may provide a close modern analogue to the processes that affected the genesis of the Etheridge Group mafic rocks.

The relatively primitive, Fe-enriched nature of the Etheridge Group tholeiites, coupled with the apparent lack of contamination by subduction-related material, precludes the possibility that the tholeiites formed in a back-arc basin setting proximal to a volcanic arc. For example, contemporaneous Mg-rich and Fe-rich metatholeiites found in the Olary Domain, western Curnamona Province display geochemical characteristics typical of back-arc basin basalts. These include relatively elevated LREE/HREE, Nb/Y, Zr/Y, and more evolved Nd-isotope values ($\varepsilon_{Nd} < +2$) compared to more primitive tholeiites (Rutherford *et al*., 2006; Chapter 7). It has been proposed that the geochemically distinct character of the Olary Domain metatholeiites is a consequence of refertilisation of the lithospheric mantle by a subduction-related component (Rutherford *et al*., 2006); a feature common to tholeiites formed in back-arc basins (Ishizuka *et al*., 2006; Haraguchi & Ishii, 2007).

In contrast, otherwise geochemically-related Fe-rich tholeiites of the Broken Hill Domain (Rutherford *et al*., 2006), and contemporaneous Etheridge Group tholeiites are relatively primitive, and do not show the same level of LREE or isotopic enrichment. The geochemical characteristics and relationship between the mafic suites is expanded upon in Chapter 7. Although the geochemical characteristics of the Etheridge Group tholeiites precludes formation in a back-arc basin setting, a tectonic model involving a more distal back-arc setting (Giles *et al*., 2002), and thus not

involving fluids from a subducting slab effecting the geochemistry of the mafic rocks, may form a realistic interpretation for the development of the mafic rocks. This model is discussed in more detail in Chapter 8.

In general, the mafic rocks of the Etheridge Group appear relatively Fe-rich when compared to modern examples of rift-related tholeiites (Table 6.4). Although possessing lower Nb/Zr values than N-MORB (Galapagos suite in Fig. 6.18), the range of Nb/Zr values for the Etheridge Group rocks and their trend of increasing Ti values with advancing fractionation are typical of basalts from volcanic rifted passive margins (e.g. E Greenland) and of tholeiitic basalts erupted during plume-head related Large Igneous Province eruptions such as those basalts forming the Siberian Traps and Ontong Java Plateau (Fig. 6.18). Significantly, the basalts of all of these three terranes were formed by processes that involved the presence of a mantle plume source (Neal *et al*., 1997; Saunders *et al*., 1997; Sharma, 1997).

In the Zr/Nb versus Zr/Y diagram (Fig. 6.19) the Etheridge Group mafic rocks plot predominately within the field of continental within-plate basalts erupted in Large Igneous Provinces, for example, central Karoo (Marsh *et al*., 1997) and the Ontong Java Plateau. In this diagram, values for continental within-plate basalts erupted in rift settings, such as for the central Karoo basalts, plot between the values for average N- and E-MORB, and above average Primitive Mantle.

An intra-cratonic LIP or volcanic passive margin setting for the emplacement of the Etheridge Group tholeiites is further supported by the close correlation in their incompatible element ratios to tholeiitic rocks emplaced both onshore and offshore during plume-triggered rifting of East Greenland-Faeroe Islands margin in the North Atlantic Igneous Province (Fig. 6.20; Saunders *et al*., 1997). The onshore and offshore lavas of East Greenland show a clear transition from continental lithosphere-influenced to MORB-type oceanic magmatism, illustrated by changes in the incompatible element compositions across the region (Fig. 6.21; Fitton *et al*., 1995, 2000). Older pre- to syn-rift lavas are represented by onshore lava suites from both East Greenland and the Faeroe Islands (Fig. 6.20a), and additionally by ODP drillsites which preferentially sampled lower series lavas from the seaward-dipping reflector sequences (SDRS) along the East Greenland continental margin (Sites 989 and lower portion of 917; Fig. 6.20c). The rift-margin lavas show enriched compositions (Zr/Nb < 20), consistent with evolution involving fractional crystallisation and assimilation of

crustal material in deep crustal magma reservoirs beneath the continental lithosphere (Fitton *et al*., 2000). Younger lavas of the middle and upper SDRS (Sites 990 and upper portion of 917) represent later stages of rifting leading to continental break-up and eruption of oceanic crust, and preferentially have compositions more consistent with N-type MORB (Zr/Nb > 20; Fig. 6.21a).

| | Karoo tholeiite | East Greenland tholeiite | Galapagos tholeiitic MORB | Oceanic tholeiite | Continental tholeiite |
|---|---|---|---|---|---|
| No. of analyses | 24 | 22 | 75 | 74 | 44 |
| $SiO_2$ | 50.50 | 48.20 | 49.69 | 49.26 | 50.18 |
| $TiO_2$ | 1.07 | 2.84 | 2.34 | 1.34 | 1.35 |
| $Al_2O_3$ | 14.05 | 13.21 | 14.87 | 14.53 | 16.06 |
| $Fe_2O_3$* | 11.89 | 13.88 | 13.57 | 12.54 | 12.08 |
| MnO | 0.17 | 0.19 | 0.16 | 0.20 | 0.18 |
| MgO | 7.46 | 8.00 | 6.82 | 6.95 | 6.83 |
| CaO | 10.07 | 10.55 | 8.34 | 12.08 | 9.96 |
| $Na_2O$ | 2.30 | 2.36 | 2.45 | 2.28 | 2.29 |
| $K_2O$ | 0.67 | 1.72 | 0.20 | 0.33 | 0.76 |
| $P_2O_5$ | 0.12 | 0.28 | 0.37 | 0.25 | 0.20 |
| LOI | - | 1.50 | - | 0.38 | 2.33 |
| Nb | 14 | 17 | 13 | 5 | 11 |
| Zr | 109 | 210 | 305 | 79 | 134 |
| Sr | 205 | 292 | 62 | 148 | 266 |
| Cr | 349 | 318 | 102 | 178 | 192 |
| Ba | 235 | 88 | 73 | 18 | - |
| Sc | 35 | 30 | 44 | 49 | 32 |
| V | 295 | 373 | 358 | 332 | 228 |
| La | - | 15 | 11 | 5 | 15 |
| Ce | - | 36 | 24 | 12 | 35 |
| Nd | - | 23 | 23 | 9 | 19 |
| Y | 21 | 30 | 96 | 27 | 25 |
| Rb | 30 | 5 | 2 | 10 | 15 |
| Pb | - | 2 | 14 | - | - |
| Zn | - | 110 | 229 | - | 106 |
| Cu | - | 198 | 1592 | - | 89 |
| Ni | 95 | 194 | 43 | 98 | 106 |
| K (ppm) | 5527 | 14309 | 1675 | 2706 | 6268 |
| Ti (ppm) | 6435 | 17040 | 14040 | 8028 | 8114 |
| P (ppm) | 538 | 1234 | 1625 | 1085 | 861 |

**Table 6.4: Average geochemical compositions for various unaltered tholeiitic suites. Karoo analyses from Marsh *et al.* (1997); East Greenland analyses from Peate *et al*. (2003); Galapagos MORB analyses from Schilling *et al*. (1976), Fisk *et al*. (1982), Embley *et al*. (1988), Ridley *et al*. (1994), and Perfit *et al*. (1999); oceanic tholeiite (Ontong Java Plateau) analyses from Mahoney *et al*. (1993); continental tholeiite (Siberian Traps) analyses from Lightfoot *et al*. (1990).**

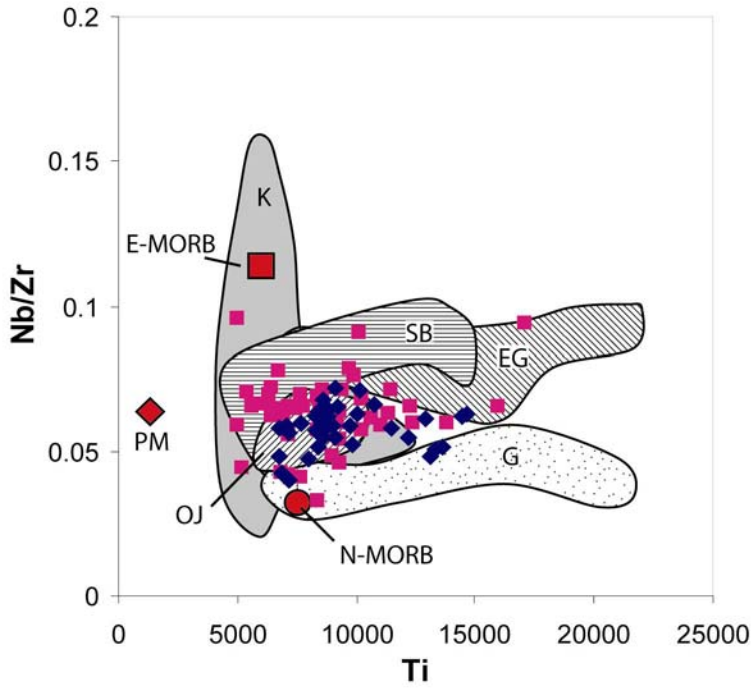


**Figure 6.18: Ti (ppm) versus Nb/Zr for Etheridge Group mafic rocks and selected Phanerozoic flood basalt provinces (data sources as for Table 6.4). CMD = pink squares; DHM = blue diamonds. PM = Primitive Mantle; K = Karoo Igneous Province; SB = Siberian Traps; EG = East Greenland; G = Galapagos spreading centre; OJ = Ontong Java plateau. Average N-MORB, E-MORB, and Primitive Mantle values after Sun and McDonough (1989). Fractional crystallisation on this diagram will produce horizontal vectors.**

In Figure 6.21, incompatible trace element ratios from the suite of Etheridge Group tholeiites show a clear association with the older, onshore and lower series lavas from the East Greenland margin and Faeroe Islands (Zr/Nb = 10-30). This suggests that the differentiation processes which influenced the evolution of the Etheridge Group tholeiites were similar to those of East Greenland, and that emplacement/eruption of the mafic rocks occurred in a similar tectonic setting, in a developing rift in attenuating continental crust along a volcanic passive margin.

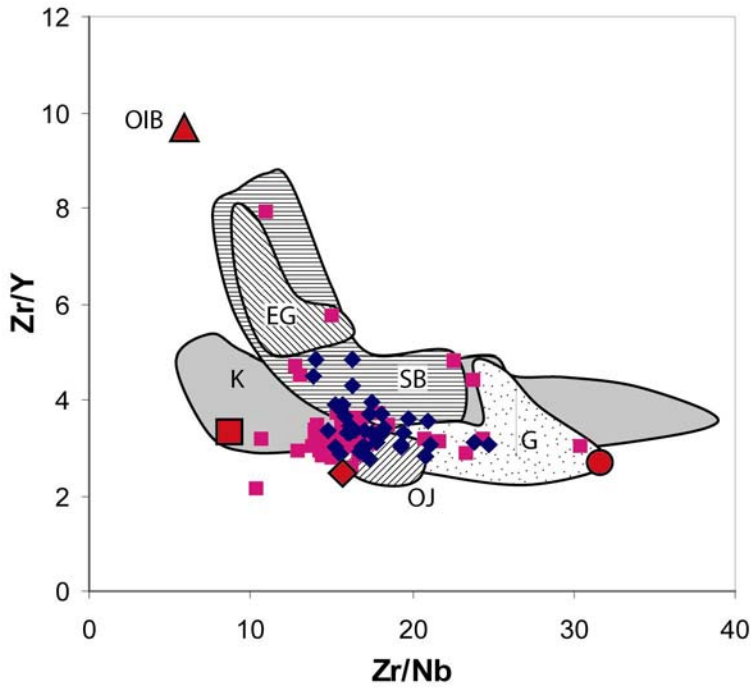


**Figure 6.19: Zr/Nb versus Zr/Y for Etheridge Group mafic rocks and selected Phanerozoic flood basalt provinces (data sources as for Table 6.4). OIB = Oceanic Island Basalt. Average OIB value after Sun and McDonough (1989). All other symbols and fields as in Figure 6.18.**

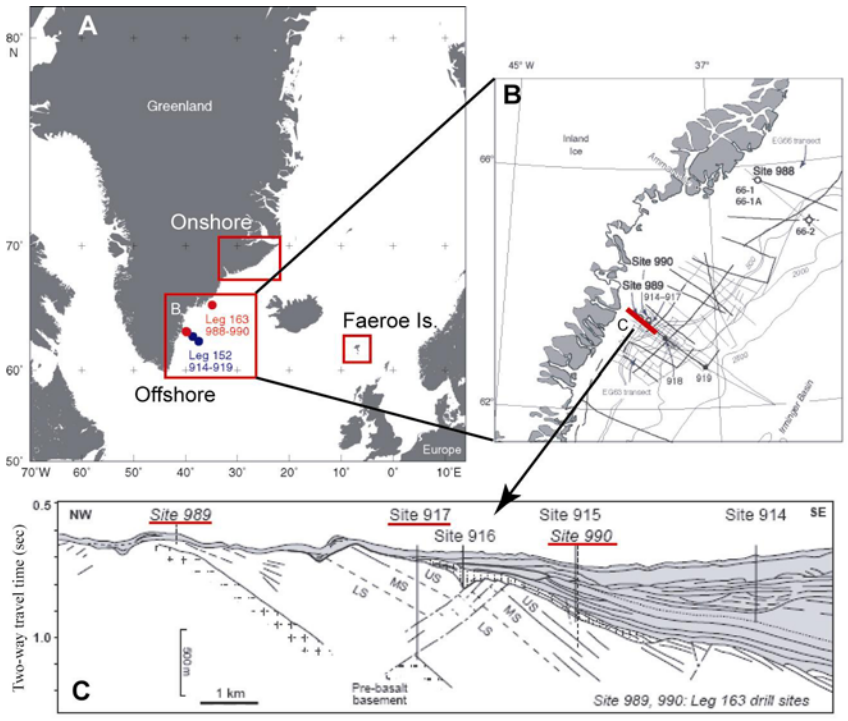


**Figure 6.20: (A) Location of East Greenland and Faeroe Islands lavas erupted during Palaeogene plume-triggered rifting in the North Atlantic. (B) Location of ODP drillsites along Southeast Greenland margin (after Larsen *et al.*, 1999). (C) Section across the Southeast Greenland margin**

**at 63°N showing location of ODP drillsites (after Larsen *et al.*, 1999). Analyses from underlined sites in (C) represent East Greenland offshore lavas.**

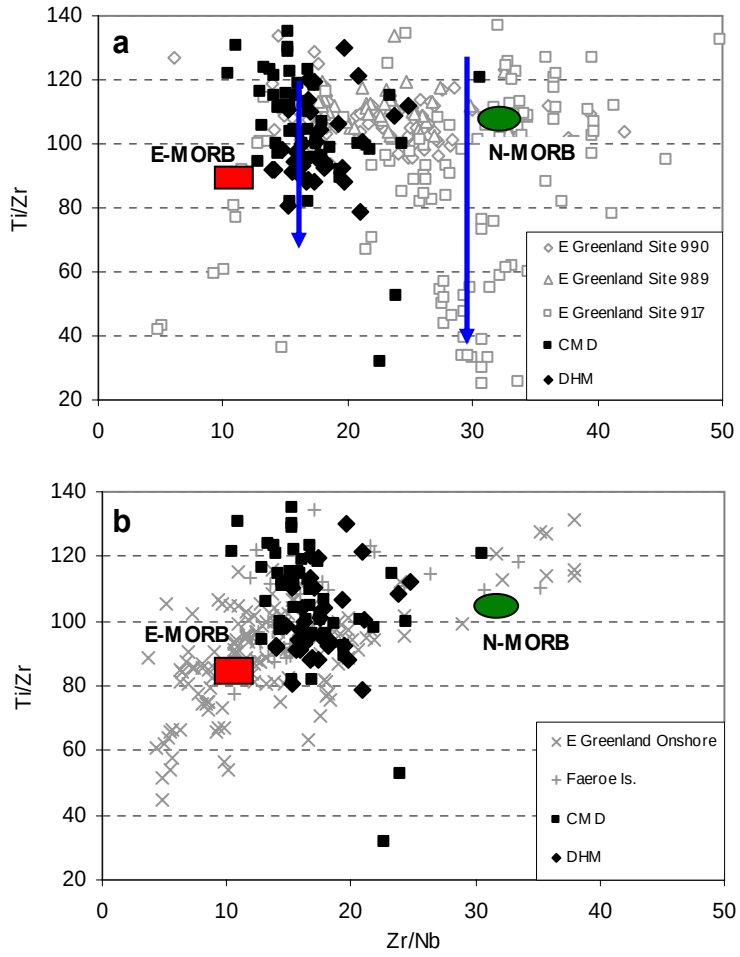


**Figure 6.21: Zr/Nb versus Ti/Zr for mafic rocks of the Etheridge Group, and comparison to (a) East Greenland offshore lavas, and (b) East Greenland and Faeroe Island onshore lavas. Blue arrows in (a) denote progressive fractionation from more primitive to more evolved compositions. Data for East Greenland offshore lavas from Larsen *et al.* (1998), Larsen *et al.* (1999), Fitton *et al.* (2000), and Philipp *et al.* (2001). Data for East Greenland onshore lavas from Noe-Nygaard and Pedersen (1974), Brooks *et al.* (1976), Thirlwall *et al.* (1994), Hansen and Nielsen (1999), and Momme *et al.* (2002). Data for Faeroe Islands lavas from Waagstein *et al.* (1984), and Hald and Waagstein (1991).**

## 6.7 Conclusions

The extrusive (DHM) and intrusive (CMD) mafic igneous rocks of the lower Etheridge Group share a common geochemical history, were likely derived from the same parental magmas, and possess geochemical characteristics typical of relatively evolved, low-K, Fe-rich continental tholeiites and tholeiites during strong extension of continental crust leading to continental break-up. The mafic rocks were most likely

emplaced over a relatively short timeframe, from melts derived directly from a depleted convecting asthenospheric mantle source, and limited assimilation of upper crustal material from the host lower Etheridge Group metasediments. Trace and REE data indicate that the rocks were generated by partial melting of a mantle source similar to that which provides modern MORB, and evolved along a tholeiitic trend of Fe-enrichment that produced rare evolved samples with >20 wt% $Fe_2O_3^{total}$. A poorly constrained Sm-Nd isochron age, coupled with $\varepsilon_{Nd}(T)$ and $T_{DM}$ values indicate that the mafic rocks crystallised at ~1.7 Ga, which correlates with crystallisation ages determined from U-Pb igneous zircons analysed by LA-ICPMS. $T_{DM}$ model ages also indicate that the source of the mafic rocks may have formed during the early Palaeoproterozoic (ca. 2.36 Ga).

Despite their relatively widespread spatial distribution, the Etheridge Group mafic rocks show only limited geochemical variation. Little, if any, geochemical variation is observed between CMD sills emplaced below, within, or above the level of the DHM. Individual sills of the CMD (<1000 m thick) show little variation in MgO, indicating that individual sills were emplaced relatively rapidly.

In several samples of the mafic rocks, REE values show distinct LREE-enriched HREE-depleted chondrite-normalised patterns and LILE enrichment relatively to similarly incompatible Nb, consistent with small degrees of contamination by the host metasediments (Fig. 6.7; Fig. 6.9). The presence of this contamination is also illustrated by $^{147}Sm/^{144}Nd$ isotopic values which show a trend towards increasing degrees of contamination by an upper crustal component (Fig. 6.16).

A continental rifting environment at a volcanic passive margin provides the appropriate conditions for the emplacement of the Etheridge Group mafic rocks. During opening of the rift system that contained the lower Etheridge Group metasediments, the underlying depleted mantle melted due to decompression and tholeiitic magma was introduced into the upper crust as sills and lava-sill packages.

Similar relatively Fe-rich tholeiitic basalts of similar age to the lower Etheridge Group mafic rocks are recorded from the Eastern Succession of the Mt Isa Inlier, and the from the Broken Hill Inlier. The following chapter investigates further these correlations and their implications for the geological evolution of eastern Australia in the Palaeoproterozoic.

# Chapter 7.

# Geochemical comparison of Fe-rich tholeiites from the lower Etheridge Group, Broken Hill Group and Mt Isa Eastern Succession: their genesis and implications for the eastern margin of Palaeoproterozoic Australia

## 7.1 Introduction

The Palaeoproterozoic basins of northeastern and eastern Australia host large amounts of variably deformed and metamorphosed Fe-rich tholeiitic rocks. Their origin has been the focus of considerable debate in recent years (e.g. Phillips *et al*., 1985; Withnall, 1985; Etheridge *et al*., 1987; Williams, 1998b; Rutherford *et al*., 2006); however at present the most accepted hypothesis is that the rocks were derived from partial melts of widespread asthenospheric convection accreting material to the base of Archaean and earliest Palaeoproterozoic lithosphere (Scott *et al*., 2000; Giles *et al*., 2002). Emplacement and/or extrusion of the mafic rocks occurred during one or more episodes of crustal thinning associated with the second cycle of Palaeoproterozoic regional extension and sedimentation across northeastern Australia (ca. 1730-1650 Ma; Etheridge *et al*., 1987; Betts *et al*., 2002; Giles *et al*., 2002). The widespread occurrence of the high-Fe tholeiites, coupled with complementary geochronological, sedimentary, and geophysical evidence, has led several authors to imply a shared evolution for the terranes of Palaeoproterozoic northeastern Australia (e.g. Black *et al*., 1998; Williams, 1998b; Giles *et al*., 2002; Betts & Giles, 2006; MacCready *et al*., 2006). However to date, none of these studies have provided a comparative geochemical study of the Fe-rich tholeiitic rocks found in each terrane.

Both the Broken Hill Block and Mt Isa Eastern Succession host world-class base-metal ore deposits. Therefore, the geochemical comparison of Fe-rich tholeiites from northeastern Australia is not only of regional significance, but may also be of significant economic importance for the Georgetown Inlier, as mineralisation is often spatially associated with areas containing significant tholeiitic magmatism. Subsequently, by using the new geochemical data from the mafic rocks of the Georgetown Inlier presented in Chapter 6, along with previously published data from mafic rocks of the Mt Isa Eastern Succession and Broken Hill Block, I provide a detailed geochemical overview of the similarities and differences between the

Georgetown, Mt Isa, and Broken Hill Fe-rich tholeiites. The implications for base-metal mineralisation in the Georgetown Inlier will also be discussed.

The first section of this chapter reviews the Palaeoproterozoic Broken Hill and Mt Isa Eastern Succession volcano-sedimentary basins, providing detailed summaries of the Fe-rich tholeiitic rocks found in each terrane. This is followed by a geochemical comparison of the ca. 1690-1660 Ma Fe-rich tholeiites that occur in the Georgetown Inlier, Mt Isa Eastern Succession, and Curnamona Province. The results of this study are then combined with similar work that has focussed on comparing the geochronology and lithostratigraphy of the Proterozoic terranes, with the aim of proposing a regional tectonic model for the formation and evolution of the Proterozoic sedimentary basins of eastern Australia.

## 7.2 Objectives

The objectives of the comparative geochemical study of the Fe-rich tholeiitic rocks from the Georgetown Inlier, Mt Isa Eastern Succession, and Broken Hill Block are:

- To compare the geochemistry of the mafic igneous rocks; and evaluate possible implications for regional constructions of the Proterozoic margin of eastern Australia, as well as the Palaeoproterozoic position of the Georgetown Inlier.
- To further constrain the petrogenesis and tectonic setting of the Fe-rich tholeiites from the Georgetown Inlier, as described in Chapter 6.
- To determine whether the Proterozoic rocks of the Georgetown Inlier were also a suitable host for major base-metal mineralisation based on their relationships with the Mt Isa Eastern Succession and Broken Hill Block.

## 7.3 Regional Geology of the Broken Hill Block and Mt Isa Eastern Succession: a review

The Broken Hill Block of western New South Wales, and the Mt Isa Eastern Succession of western Queensland, form disjunct parts of regionally extensive Proterozoic volcano-sedimentary sequences in eastern Australia (Fig. 7.1). Both sequences share several key features, including the occurrence of ca. 1690-1660 Ma Fe-rich tholeiites (Phillips *et al*., 1985; James *et al*., 1987; Williams, 1998b), and the

presence of major 'Broken Hill-type' Pb-Zn-Ag deposits associated with zones of high metamorphic grade (Walters, 1998; Williams, 1998a). To aid the geochemical study, a review of the regional geology of the Broken Hill Block and Mt Isa Eastern Succession is presented below. This is followed by a detailed description of the location and petrology of significant Fe-rich mafic-igneous units from each terrane.

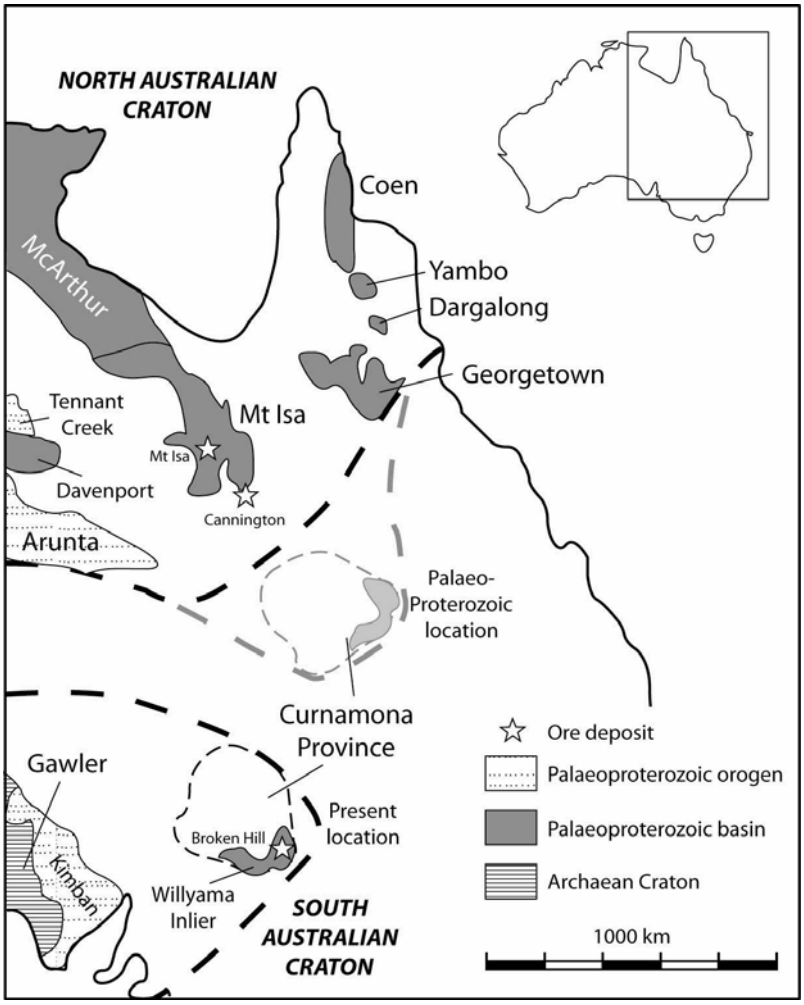


**Figure 7.1: Palaeoproterozoic terranes of eastern Australia. Palaeoproterozoic location of the Curnamona Province after Giles *et al.* (2004). Figure adapted after Myers *et al.* (1996) and Betts & Giles (2006).**

### 7.3.1 Broken Hill Block

The Broken Hill Block of the Willyama Inlier in western New South Wales represents the easternmost part of the regionally extensive Curnamona Province (Fig. 7.1; Willis *et al*., 1983), and has been the focus of considerable research for the past 100 years (e.g. Mawson, 1912; Vernon, 1969; Willis *et al*., 1983), due in large part to the world-class stratiform Pb-Zn-Ag orebodies at Broken Hill. The Broken Hill Block is

composed of metamorphosed and multiply-deformed volcano-sedimentary rocks intruded by bimodal igneous volcanics. This package is thought to be approximately 6-7 km in thickness (Fig. 7.2; Willis *et al*., 1983). The sequence is unconformably overlain by Neoproterozoic sediments of the Adelaide Fold Belt, and is thought to have been deposited onto Archaean continental crust (James *et al*., 1987).

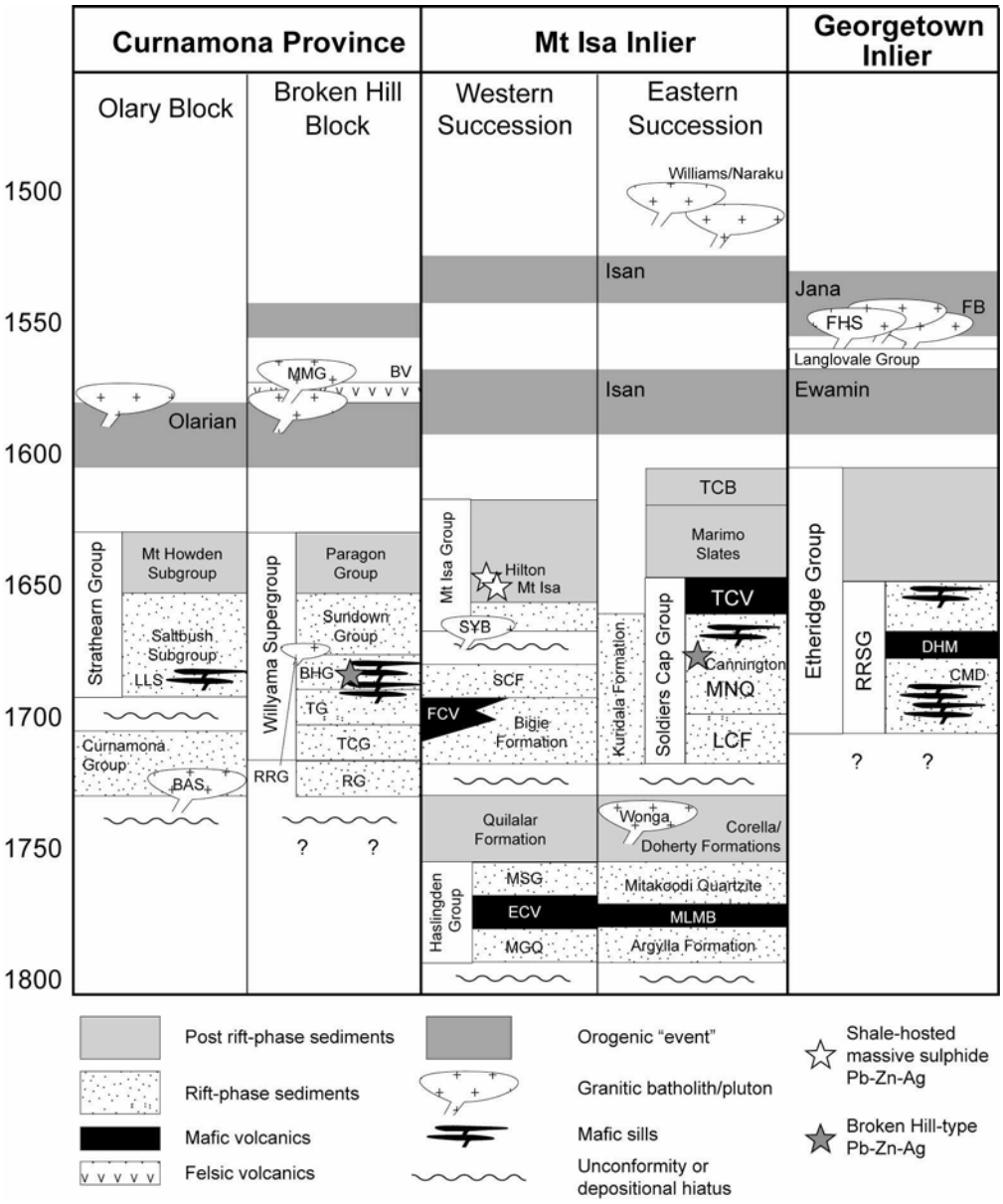


**Figure 7.2: Simplified time-space diagram showing tectonostratigraphic evolution of eastern Australian Proterozoic terranes between 1800 and 1600 Ma. BAS: Basso Suite; LLS: Lady Louise Suite; RG: Redan Gneiss; TCG: Thorndale Composite Gneiss; TG: Thackaringa Group; BHG: Broken Hill Group; RRG: Rasp Ridge Gneiss; BV: Benagerie Volcanics; MMG: Mundi Mundi Granite; MGQ: Mount Guide Quartzite; ECV: Eastern Creek Volcanics; MSG: Myally Subgroup; FCV: Fiery Creek Volcanics; SCF: Surprise Creek Formation; SYB: Sybella Granite; MLMB: Magna Lynn Metabasalt; LCF: Llewellyn Creek Formation; MNQ: Mount Norna Quartzite; TCV: Toole Creek Volcanics; TCB: Tommy Creek Beds; RRSG: Robertson River**

**Subgroup; CMD: Cobbold Metadolerite; DHM: Dead Horse Metabasalt; FB: Forsayth Batholith; FHS: Forest Home Suite. Data summarised from Withnall *et al.* (1988a), Page *et al.* (2005b), Betts *et al.* (2006), Betts & Giles (2006), and Rutherford *et al.* (2006).**

The lithostratigraphy of the Broken Hill Block has been defined by Willis *et al*. (1983), and revised by Raetz *et al*. (2002) (Fig. 7.2). The lowermost sequence comprises paragneiss (Redan and Farmcote Gneiss) belonging to the Redan Geophysical Zone (Raetz *et al*., 2002). The Redan Geophysical Zone is overlain by migmatites (Clevedale Migmatite) and feldspathic metasedimentary composite gneiss (Thorndale Composite Gneiss) that are thought to represent interlayered immature siliciclastic sediment and felsic volcanics deposited in a shallow shelf environment (Willis *et al*., 1983). The overlying Thackaringa Group is the main outcropping lithology in the Broken Hill region and is characterised by quartzo-feldspathic granite gneiss and albite-quartz rocks (Himalaya Formation), psammo-pelitic rocks (Cues Formation), and lesser amounts of amphibolites and basic gneiss (Willis *et al*., 1983; Raetz *et al*., 2002). The basal sequence of the overlying Broken Hill Group comprises turbiditic, thinly-bedded metasediments and mafic gneiss (Allendale Formation), overlain by mafic and felsic gneiss (Parnell Formation), pelitic metasediments (Freyers Metasediments), and mafic and felsic gneisses and pelitic metasediments (Silver King Formation) (Willis *et al*., 1983; Page & Laing, 1992). The uppermost member of the group is the Hores Gneiss, comprising felsic gneiss ('Potosi gneiss'; Page & Laing, 1992), mafic gneiss and rare pelite, which hosts to the major Pb-Zn-Ag orebody at Broken Hill (Willis *et al*., 1983). The Thackaringa and Broken Hill Groups are thought to represent a period of deepening shelf sedimentation proximal to a propagating continental-rift environment, during which there was widespread bimodal magmatism, with most of the mafic granulites being regarded as sills (Willis *et al*., 1983; James *et al*., 1987). No stratabound magmatic rocks of either mafic or felsic nature are identified above the level of the Broken Hill Group (Fig. 7.2; James *et al*., 1987). Pelitic and psammo-pelitic metasediments are the primary lithologies in the overlying Sundown and Paragon Groups, and were thought to have been deposited in a continental slope to deep water environment (Willis *et al*., 1983).

Numerous studies involving zircon U-Pb SHRIMP analyses have been published over the past two decades in order to constrain an approximate depositional age for the Broken Hill Group (e.g. Stevens, 1986; Page & Laing, 1992; Donaghy *et al*., 1998;

Nutman & Ehlers, 1998; Page *et al*., 2000; Raetz *et al*., 2002; Page *et al*., 2005a). At present, near-consensus exists that deposition had commenced by ca. 1690 Ma (e.g. Page & Laing, 1992; Raetz *et al*., 2002; Page *et al*., 2005a), although Nutman & Ehlers (1998) argued for deposition between ca. 1720-1690 Ma. Page & Laing (1992) analysed samples of the Hores Gneiss at a number of locations across the terrane, and were able to define a major zircon population at 1690 ± 5 Ma which they ascribed to deposition of the volcano-sedimentary precursor to the gneiss.

The rocks of the Broken Hill Group are believed to have undergone at least three periods of deformation and metamorphism in the early Proterozoic (James *et al*., 1987; Raetz *et al*., 2002; Gibson & Nutman, 2004). The first two deformation events involved extension and subsequent folding, with the latter coinciding with peak low-pressure and high-temperature metamorphic conditions in the upper amphibolite to granulite facies (James *et al*., 1987; Page & Laing, 1992; Gibson & Nutman, 2004). The third deformation event also produced folding, but resulted in the formation of retrograde assemblages where the intensity of this event was greatest (Gibson & Nutman, 2004). As with the depositional age of the Broken Hill Group, there is also debate as to the age (and relevance) of the tectono-metamorphic events that affected the terrane during the Proterozoic. Page & Laing (1992) obtained a metamorphic age of 1600 ± 8 Ma which they ascribed to $M_2$, determined from the analysis of metamorphic overgrowths surrounding the magmatic cores of zircons from the granulite facies rocks surrounding Broken Hill. They also inferred that $M_1$ preceded this event by a short time interval, and that both events were compressional. This age also corresponds to the early stages of the inter-cratonic Olarian Orogeny (Raetz *et al*., 2002). Based on the U-Pb zircon analysis of three amphibolites and one granulite from the Clevedale Migmatite and Thorndale Composite Gneiss, Gibson & Nutman (2004) suggested the first tectono-metamorphic event occurred between ca. 1690 Ma and 1670 Ma, some 70 million years earlier than the $M_1$ age suggested by Page & Laing (1992). However, it is possible that the zircons analysed by Gibson & Nutman (2004) were magmatic rather than metamorphic in origin, and consequently date the crystallisation age of the rocks. Evidence for the third deformation event is best preserved in retrograde amphibolite facies assemblages in areas of high $D_3$ strain (Gibson & Nutman, 2004). $^{40}Ar/^{39}Ar$ hornblende and Pb-Pb apatite ages indicate

metamorphism associated with this event occurred between 1590-1560 Ma (Harrison & McDougall, 1981; Gulson, 1984).

#### 7.3.1.1 Metamorphosed Fe-rich tholeiites of the Broken Hill Group

Mafic or 'basic' gneisses in the Broken Hill Block are confined to the lower half of the sequence, below the Sundown Group (Fig. 7.2; James *et al*., 1987; Raetz *et al*., 2002). They commonly occur as tabular or lenticular bodies 0.5-200 m in thickness and 1-2000 m in length, but are generally up to 1000 m long and up to 40 m wide within the Broken Hill Group (Phillips *et al*., 1985). They are mostly conformable to bedding, and are generally considered to be sills, although discordant examples also exist (James *et al*., 1987). High-Fe (>10 wt% $Fe_2O_3^{total}$) tholeiitic basic gneisses are common in the Broken Hill and Thackaringa Groups, with the most Fe-rich examples occurring proximal to areas of mineralisation (Phillips *et al*., 1985), including along the main Broken Hill line of lode. The exceptionally high-Fe contents from these areas (up to 25 wt% $Fe_2O_3^{total}$) were thought to be a product of hydrothermal alteration that occurred synchronous with mineralisation and prior to regional deformation in the Broken Hill Block (Phillips *et al*., 1985). However, a more detailed geochemical study by James *et al*. (1987) suggested that even the most extreme Fe-rich rocks may have evolved by a process of fractional crystallisation along a strong Fe-enrichment trend.

The basic gneisses, including the Fe-rich tholeiites, are commonly composed of plagioclase and hornblende with or without quartz, epidote, garnet, ilmenite and clinopyroxene, and orthopyroxene is a common phase in the granulites. In the Broken Hill area, their mineralogy is indicative of amphibolite to low-granulite facies metamorphism (James *et al*., 1987). Due to the high level of recrystallization, most primary igneous features have been generally obliterated; however, Stroud *et al*. (1983) and James *et al*. (1987) indicated that some igneous textures and contacts may have been preserved, particularly in the lower grade northwest part of the Broken Hill Block.

### 7.3.2 Mt Isa Eastern Succession

The Mt Isa Eastern Succession represents the easternmost part of the regionally extensive Mt Isa Inlier in western Queensland (Fig. 7.1). It is interpreted to have formed as a product of Palaeoproterozoic intracratonic rifting, in a similar tectonic environment to that proposed for the Broken Hill and Georgetown regions (O'Dea *et al*., 1997; Page & Sun, 1998; Williams, 1998b). The rocks of the Eastern Succession, in particular those belonging to the informally named Maronan Supergroup (Beardsmore *et al*., 1988), have come under increasing scrutiny over the past two decades, due to the discoveries of major base-metal deposits within the succession. These include the Broken Hill-type Pb-Zn-Ag orebody at Cannington, smaller Pb-Zn deposits at Pegmont and Fairmile, and major Cu-Au deposits such as Ernest Henry (Williams, 1998a). The succession is composed of a number of lithologically distinct units including metamorphosed siliciclastic volcano-sedimentary and mafic volcanic rocks of the Maronan Supergroup, metasedimentary and bimodal volcanic rocks of the Tommy Creek Beds, the Argylla, Corella and Doherty Formations (collectively termed the Mary Kathleen Group), and younger granitic rocks of the Williams and Naraku Batholiths (Fig. 7.2; Beardsmore *et al*., 1988; Page & Sun, 1998).

Using U-Pb SHRIMP zircon ages and crustal Sm-Nd isotope signatures calculated from a diverse range of lithologies, Page & Sun (1998) inferred that the Mt Isa Eastern Succession was most likely deposited as two tectonostratigraphic packages over a period of ~170 million years, between ca. 1770-1600 Ma. The older sequence, deposited between ca. 1770-1725 Ma, included sediments and bimodal volcanics belonging to the Mary Kathleen Group. The younger sequence included metasediments and bimodal volcanics of the Maronan Supergroup, and metasediments of the Tommy Creek Beds deposited between ca. 1720-1600 Ma (Page & Sun, 1998). Deposition of sediments and the emplacement of bimodal volcanics, including Fe-rich tholeiites belonging to the Soldiers Cap Group of the Maronan Supergroup, are thought to have commenced ca. 1670 Ma. This age approximates inferred or calculated ages for the deposition of other key volcano-sedimentary sequences containing base-metal mineralisation in northeastern Australia including the Broken Hill Group (ca. 1690 Ma; Page *et al*., 2005a), and the Mt Isa Group of the Mt Isa Western Succession (ca. 1655 Ma; Page & Sun, 1998), as well as metasedimentary rocks of the lower Etheridge Group (ca. 1700-1650 Ma) (Fig. 7.2).

At least three major episodes of deformation are thought to have affected the Mt Isa Eastern Succession (Laing, 1998). There is general consensus that the last two events were compressional, the latter corresponding to the later stages of the Isan Orogeny between ca. 1540 and 1500 Ma (Page & Sun, 1998; Betts *et al*., 2000; Betts & Giles, 2006). Peak metamorphic conditions within the Mt Isa Inlier are suggested to have occurred during the earlier stage of the Isan Orogeny between ca. 1600 and 1570 Ma, which led to metamorphism ranging from amphibolite to granulite facies in the Soldiers Cap Group (Page & Bell, 1986; Page & Sun, 1998). The estimated age of the first deformation event is controversial. Oliver *et al*. (1991) and Oliver (1995) proposed that the first event occurred between ca. 1750 and 1730 Ma and involved extension coupled with magmatic underplating, leading to the emplacement of the Eastern Creek Volcanics in the Mt Isa Western Succession. However, a metamorphic age of 1584 ± 17 Ma obtained from overgrowths on the rims of zircons sampled from felsic gneisses that formed by partial melting at the base of the Soldiers Cap Group led Page & Sun (1998) to suggest that this age may represent metamorphism associated with the first deformation event. This age is also broadly coincident with the ca. 1600 Ma timing of high-grade metamorphism at Broken Hill (Page & Laing, 1992).

#### 7.3.2.1 Metamorphosed mafic igneous rocks of the Mt Isa Eastern Succession

Bimodal volcanic rocks occur throughout the Mt Isa Eastern Succession, and locally dominate parts of the ca. 1670 Ma Soldiers Cap Group (Fig. 7.2; Beardsmore *et al*., 1988; Page & Sun, 1998; Hatton & Davidson, 2004). The lithostratigraphy of the Soldiers Cap Group was originally proposed by Derrick *et al*. (1976), and comprises a basal sequence of turbiditic pelite and lesser metadolerite (Llewellyn Creek Formation) conformably overlain by massively bedded quartzite, psammo-pelite, pelite and intercalated metadolerite, and lesser metabasalt (Mt Norna Quartzite). The Mt Norna Quartzite is conformably overlain by a 2800 m-thick sequence of metadolerite and metabasalt, and minor interbedded quartzite, pelite, and ironstone termed the Toole Creek Volcanics (Derrick *et al*., 1976; Hatton & Davidson, 2004).

Williams (1998b) defined amphibolites of the Soldiers Cap Group as high-Fe metatholeiites, as they commonly contain between 11 and 19 wt% $Fe_2O_3^{total}$. The Fe-enriched nature of these tholeiites has led a number of authors to suggest an intra-

cratonic rift setting for the rocks (Glikson & Derrick, 1978; Williams, 1998b). The amphibolites are commonly composed of hornblende and plagioclase with lesser biotite, locally developed garnet and quartz, and accessory titanite or ilmenite (Williams, 1998b). Despite the high levels of recrystallization experienced by the mafic rocks, igneous features indicative of a syn-sedimentary to diagenetic depositional origin are preserved, including basalt pillows and peperitic contacts (Hatton & Davidson, 2004).

#### 7.3.2.2 Other mafic igneous rocks of the Mt Isa Inlier

Mafic igneous rocks of comparable geochemistry to the Fe-rich tholeiites of the Toole Creek Volcanics occur within the Eastern Creek Volcanics and Fiery Creek Volcanics of the Mt Isa Western Succession, and the Marraba Volcanics and Magna Lyn Metabasalt of the lower Eastern Succession (Fig. 7.2; Page & Sun, 1998; Giles *et al*., 2002). Due to their age and stratigraphic location, the mafic rocks of the Eastern Creek Volcanics are unlikely to have been associated with the ca. 1670 Ma magmatism that generated the Fe-rich tholeiites of the Soldiers Cap Group, being some 100 million years older. However, their geochemistry and close spatial relationship to the large Cu and Pb-Zn-Ag orebody at Mt Isa are noteworthy, and as such, a representative suite of samples from this unit is included in the comparative geochemistry section.

The Eastern Creek Volcanics are a suite of meta-igneous, sedimentary, and volcaniclastic rocks deposited between ca. 1780 and 1750 Ma in an intra-continental rift setting (Gulson *et al*., 1983; Wyborn, 1987). Although their age suggests that they are unlikely to be related to post-1700 Ma tholeiitic suites from other terranes, the high-Fe Eastern Creek Volcanics are comparable in age to other volcano-sedimentary packages including the Nungbalgarri, Bartalumba and Seigal Volcanics of the Palaeoproterozoic McArthur Basin of northern Australia, and the Magna Lyn and Marraba Volcanics of eastern-central Mt Isa (Giles *et al*., 2002).

The Magna Lyn Metabasalt and Marraba Volcanics also contain Fe-rich metabasalt and amphibolite, which may be equivalent to the Fe-rich tholeiites of the Eastern Creek Volcanics (Giles *et al*., 2002). Both units contain basalt with >10 wt% $Fe_2O_3^{total}$ (Ozchem, 2000; Hatton, 2004). Metabasalts from the ca. 1710 Ma Fiery Creek

Volcanics (Page & Sun, 1998) also display the high-Fe values characteristic of Proterozoic tholeiitic volcanism, including some mafic rocks that are extremely Fe-rich (>15 wt% $Fe_2O_3^{total}$; Ozchem, 2000; Hatton, 2004). However, representative samples from this unit have <3 wt% MgO and were likely affected by some degree of crustal assimilation.

## 7.4 Geochemical comparison of Fe-rich tholeiites and basic gneisses from the Etheridge Group, Mt Isa Eastern Succession, and Broken Hill Group.

### 7.4.1 Data sources used for comparative geochemistry

Geochemical data from mafic rocks of the Soldiers Cap Group and other mafic units of the Mt Isa Inlier were obtained from Davidson (1994), Williams (1998b), Scott *et al*. (2000), Hatton (2004) and the Geoscience Australia Ozchem Database (Ozchem, 2000). Geochemical data for basic gneisses from the Broken Hill Group were obtained from the Geological Survey of New South Wales Broken Hill whole rock geochemical database (1998), and A.J. Crawford (unpublished data). Sample numbers where listed for samples from the Ozchem database are those provided by Ozchem. Analyses obtained from the Ozchem database are reproduced along with all other geochemical analyses for the Broken Hill and Mt Isa mafic rocks in Appendix 5.

### 7.4.2 Comparative major, trace, and rare earth element geochemistry

The Fe-rich tholeiites of the Etheridge Group possess whole-rock chemical compositions remarkably similar to contemporaneous Fe-rich mafic rocks from both the Broken Hill Group of the Willyama Inlier and Soldiers Cap Group of the Mt Isa Eastern Succession. A possible geochemical link between the mafic rocks of the Broken Hill and Soldiers Cap Groups has been postulated in some previous studies (e.g. Williams, 1998b; Scott *et al*., 2000; Giles *et al*., 2002). Subsequently, a significant geochemical correlation between the mafic rocks from these terranes has important implications for the location, timing of deposition, and regional tectonic setting of the Georgetown Inlier during the Palaeoproterozoic.

In order to accurately demonstrate the geochemical similarities that exist between the mafic rocks of the Broken Hill Group (BHG), Soldiers Cap Group (SCG; including the Toole Creek Volcanics), and Etheridge Group (EG), their key major and trace

element values are illustrated in Figures 7.3 and 7.4. Representative samples from the Eastern Creek Volcanics (ECV) are also provided for comparison (Fig. 7.5; Scott *et al*., 2000; Ozchem, 2000). In comparing magmas from these sequences, I have concentrated on rocks with >4 wt% MgO to avoid sample compositions compromised by strong assimilation and/or fractionation. Based on their sampling location, mafic gneiss and amphibolite from the BHG are separated into two distinct groups: BHG-L, for rocks sampled along the line of lode at Broken Hill; and BHG-R, for 'regional' BHG mafic rocks (i.e. samples collected away from areas of significant mineralisation; Crawford, A.J., pers. comm., 2006).

From the variation diagrams, it is apparent that the EG mafic rocks possess major and trace element compositions virtually indistinguishable from those of the BHG-R and SCG. These three suites are also relatively Fe-rich and Ti-poor when compared with a suite of modern MORB (Fig. 7.3b, 7.3c, 7.4b, and 7.4c), suggesting that the mantle source for the mafic suites may have been slightly more Fe-rich than the N-MORB source. Compositional variation between the suites, where visible, is limited to samples of BHG-L, which on average possess higher $Fe_2O_3^{total}$ and $TiO_2$, and generally have lower MgO values relative to the other suites (Fig. 7.3c). Samples of the SCG are also marginally depleted in $Fe_2O_3^{total}$ relative to the other suites (Fig. 7.4c), however this effect may be partially a consequence of the sampling criterion, as only 'regional' SCG samples were included (i.e. samples collected away from areas of mineralisation and extreme alteration). Samples from the ECV correlate reasonably well with the other tholeiitic suites in the majority of major element variation diagrams (Fig. 7.5a-d), as would be expected for tholeiitic mafic rocks. The ECV samples follow the same major geochemical trends as the other mafic suites, but generally show a greater variation in some major and trace element values as they move towards more evolved (lower MgO) compositions (Fig. 7.5).

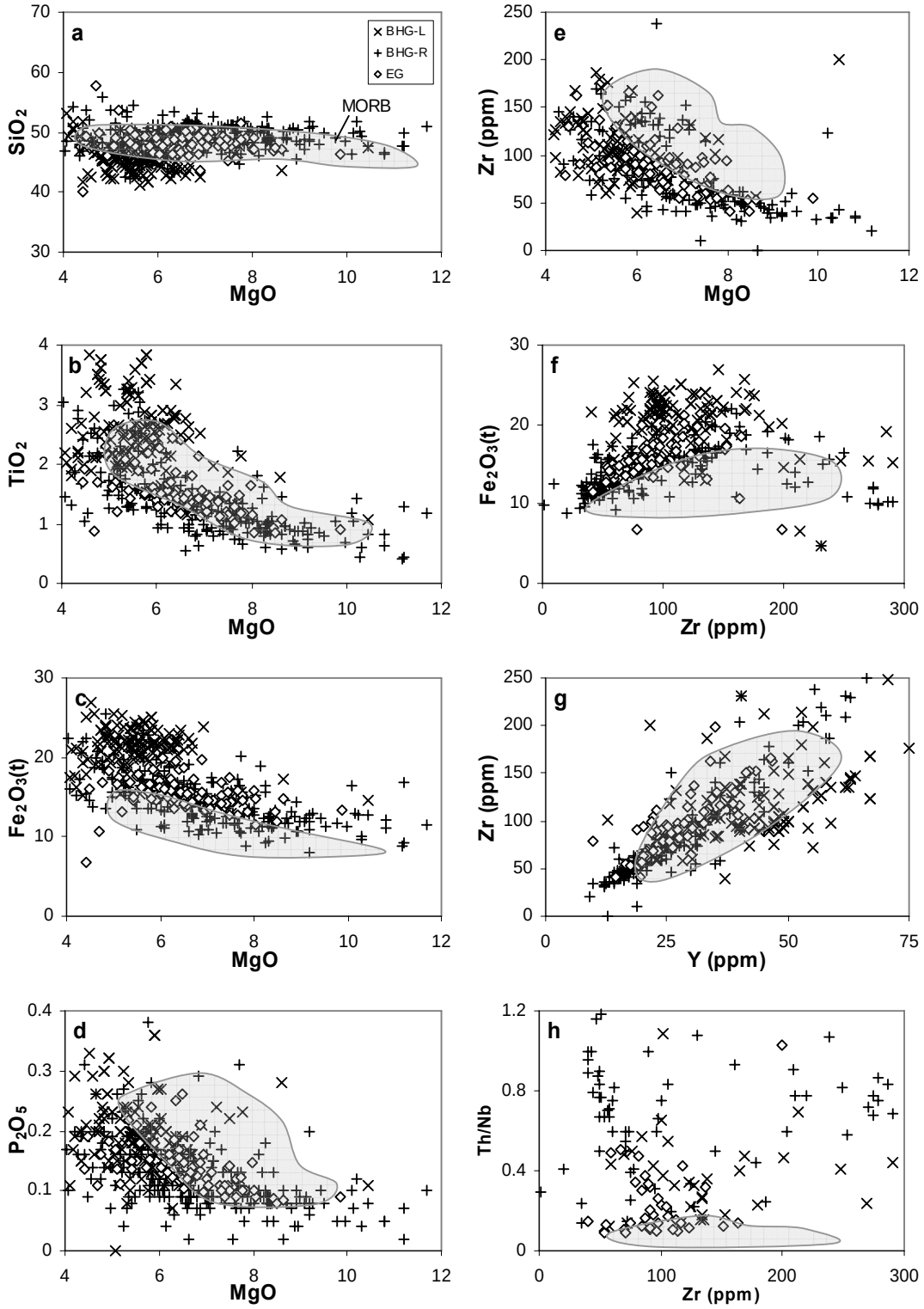


**Figure 7.3: Selected major element oxides (in weight per cent) versus MgO and selected trace element variation diagrams for mafic rocks of the Broken Hill Group (BHG-L and BHG-R) and Etheridge Group (EG). Etheridge Group mafic rocks defined by 88 samples of the Dead Horse Metabasalt and Cobbold Metadolerite (this study; Appendix 4). For Broken Hill data source see text; data listed in Appendix 5. MORB field defined by 200+ samples from the East Pacific Rise (23°N-23°S; numerous sources; Appendix 5).**

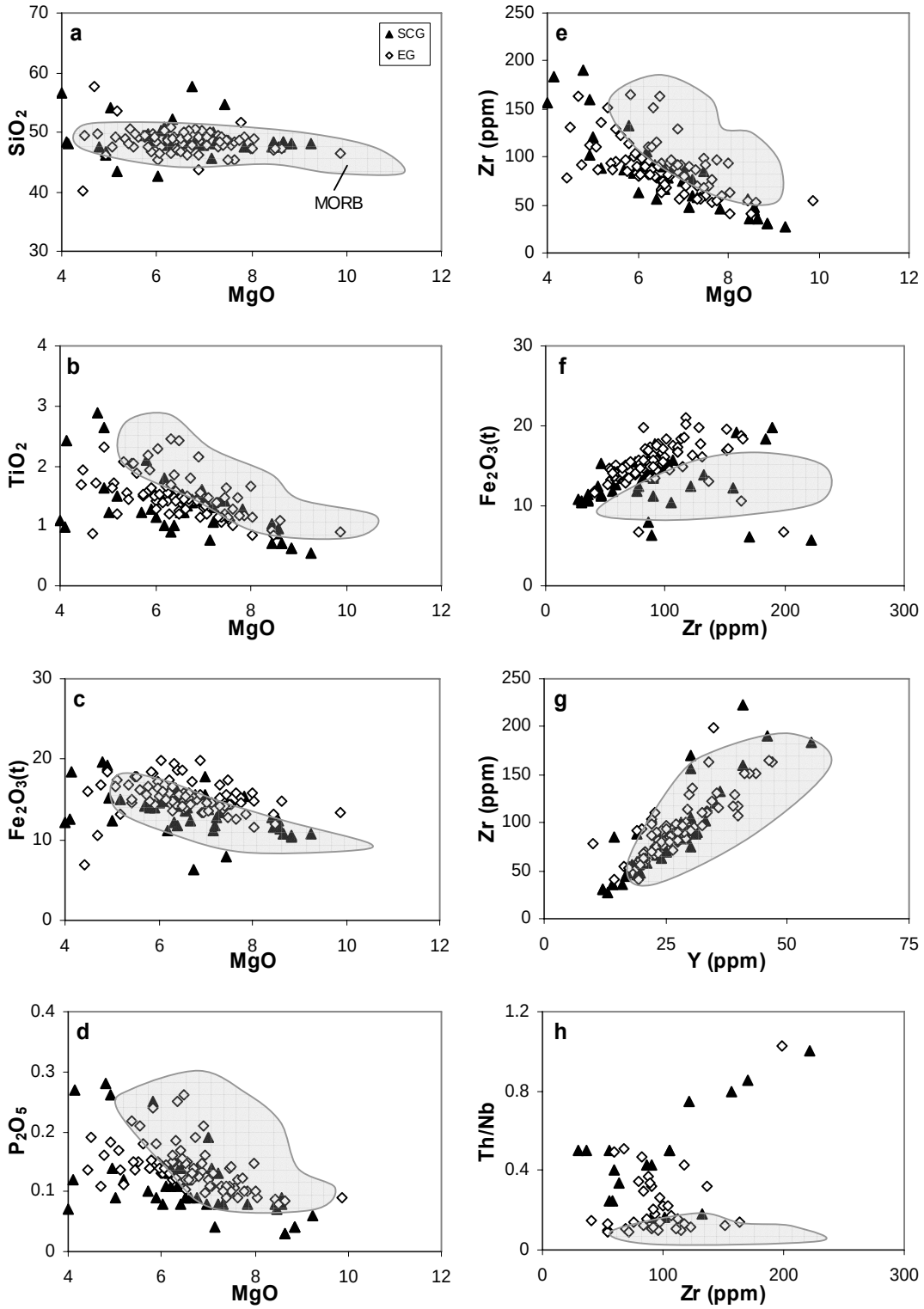


**Figure 7.4: Selected major element oxides (in weight per cent) versus MgO and selected trace element variation diagrams for mafic rocks of the Soldiers Cap Group (SCG) and Etheridge Group (EG). For SCG data source see text; data listed in Appendix 5. Etheridge Group and MORB data sources as in Fig. 7.3.**

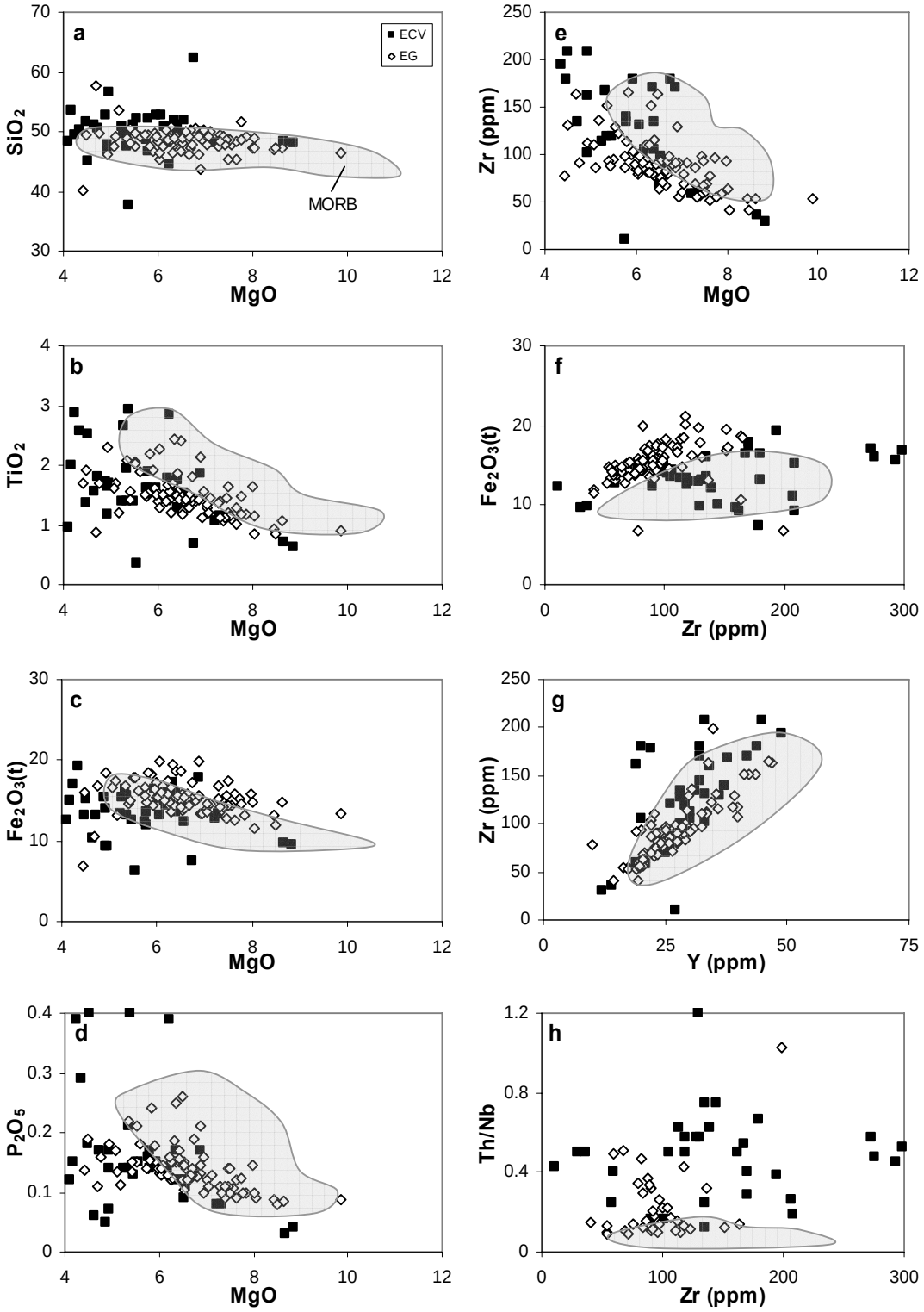


**Figure 7.5: Selected major element oxides (in weight per cent) versus MgO and selected trace element variation diagrams for mafic rocks of the Eastern Creek Volcanics (ECV) and Etheridge Group (EG). For ECV data source see text; data listed in Appendix 5. Etheridge Group and MORB data sources as in Fig. 7.3.**

Trace element variation diagrams also support a geochemical relationship between the EG, SCG and BHG mafic rocks (Fig. 7.3e-h, 7.4e-h). Significantly, the tight correlation in immobile incompatible element values across the compositional range (denoted by MgO values) is consistent with the mafic rocks experiencing very similar fractionation histories, and derivation from similar parental magmas and mantle sources. The immobile incompatible element values for the mafic suites (e.g. Fig. 7.3e and 7.4e) are also consistent with a less depleted mantle source than for typical N-MORB. Zr values for the ECV are relatively higher compared to the other suites at the same stage of their evolution (e.g. Fig. 7.5e-h), suggesting that the composition of the parental magma for this suite may have differed from those of the other suites, an assertion strongly supported by REE data (see later). Variable assimilation of crustal material is the most likely reason for variation in Th/Nb values for each mafic suite (Fig. 7.3h, 7.4h, and 7.5h). In Chapter 6 the observed trend in Th/Nb values for the EG tholeiites was consistent with a local, upper-crustal contaminant. However, the contaminants of the Broken Hill and Mt Isa mafic suites are more difficult to evaluate, although the observed trend for the SCG suggests this suite may have assimilated a similar late-stage upper-crustal contaminant to the EG tholeiites (Fig. 7.4h).

The strong similarities in the immobile incompatible trace elements from the mafic rocks of the EG, SCG (Toole Creek Volcanics), BHG-R, and BHG-L are also illustrated by the MORB-normalised multi-element diagram (Fig. 7.6). The MORB-normalised profiles are broadly similar, with the majority of the averaged patterns appearing near-identical across the EG, SCG, BHG-R and BHG-L. The majority of incompatible trace element values for both the ECV and FCV are elevated relative to the other suites, again suggesting a different source. The average values for mafic rocks from the BHG-R, BHG-L and SCG suites also lie with the observed compositional range of the EG tholeiites.

Similarities in both the geochemistry and fractionation history across the mafic suites are also reflected in their chondrite-normalised REE patterns (Fig. 7.7). Average REE values for the Dead Horse Metabasalt (DHM) and Cobbold Metadolerite (CMD) units lie between average values for the BHG and SCG tholeiites, and these values also lie within the range of all analysed EG tholeiites (indicated by the dashed line). Average REE values for both the ECV and FCV show significant enrichment in LREE relative to the other suites, suggesting more enriched parental magmas and a more enriched

source composition. Comparable fractionation histories and parent magmas for the EG, SCG, and BHG tholeiites are suggested by similar levels of LREE enrichment (avg. $(La/Sm)_n$ = 1.11, 1.15, and 1.06), and HREE depletion (avg. $(Gd/Yb)_n$ = 1.27, 1.32, and 1.16).

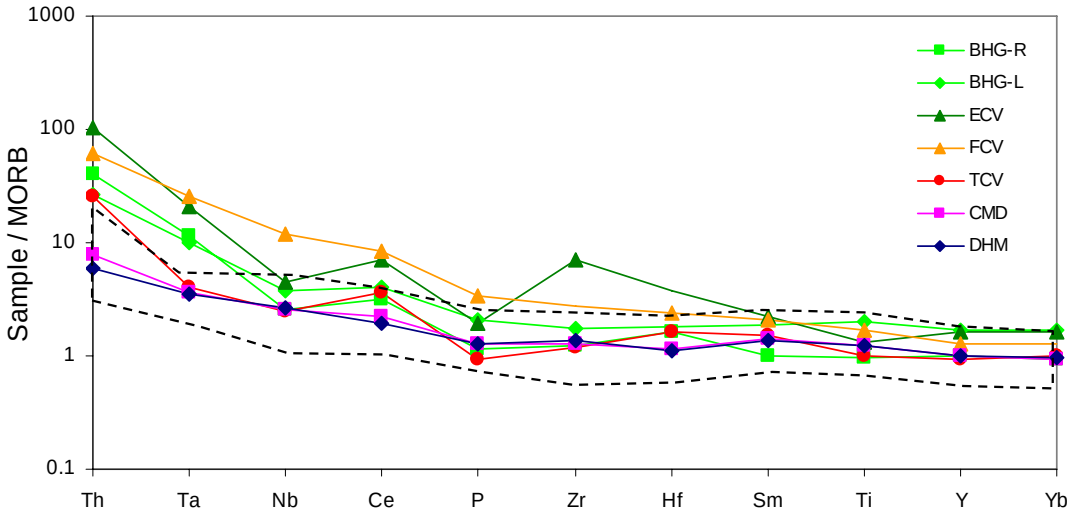


**Figure 7.6: MORB-normalised trace element diagram for average values of mafic rocks from the Broken Hill Group (BHG-R and BHG-L), Etheridge Group (CMD and DHM), and Toole Creek, Eastern Creek and Fiery Creek Volcanics (Mt Isa). Data from individual Etheridge Group samples from this study lie within the field denoted by the dashed line. Normalising values after Pearce (1983).**

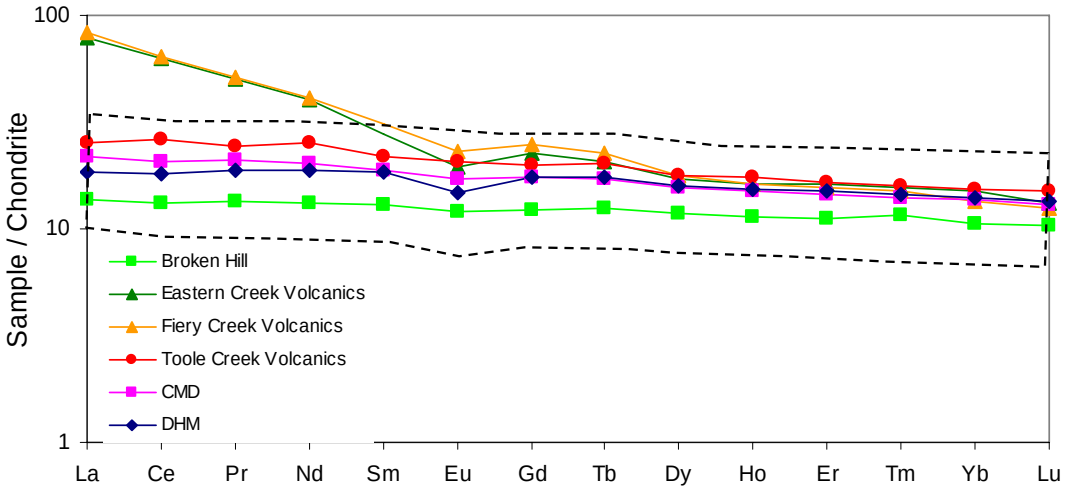


**Figure 7.7: Chondrite-normalised REE diagram for average values of mafic rocks from the Broken Hill Group, Etheridge Group, and Toole Creek, Eastern Creek and Fiery Creek Volcanics (Mt Isa). Symbols and fields as in Figure 7.6. Normalising values after Boynton (1984).**

Although the MORB-normalised trace element and chondrite-normalised REE patterns suggest near-geochemically identical tholeiitic parent magmas for the EG, SCG and BHG mafic suites, they cannot implicitly indicate that the rocks were derived from a common source. Therefore, a number of immobile trace element ratio diagrams are presented to better discriminate between the mafic suites (Fig. 7.8). The close association of the mafic suites in the Zr/Nb versus Ti/Zr and Zr/Nb versus Zr/Y variation diagrams (Fig. 7.8) again suggests that the mafic rocks may have been sourced from similar parental magmas, as Zr/Nb is a fractionation-insensitive ratio that is believed to reflect mantle source values (Pearce, 1983). The large variation in Ti/Zr values relative to Zr/Nb for the BHG tholeiites is probably fractionation-related due to removal of Fe-Ti oxides with advancing fractionation. In summary, the Palaeoproterozoic mafic suites show remarkable similarity in their key immobile incompatible trace element and REE contents. In the following section, the Sm-Nd isotope geochemistry of these suites is compared.

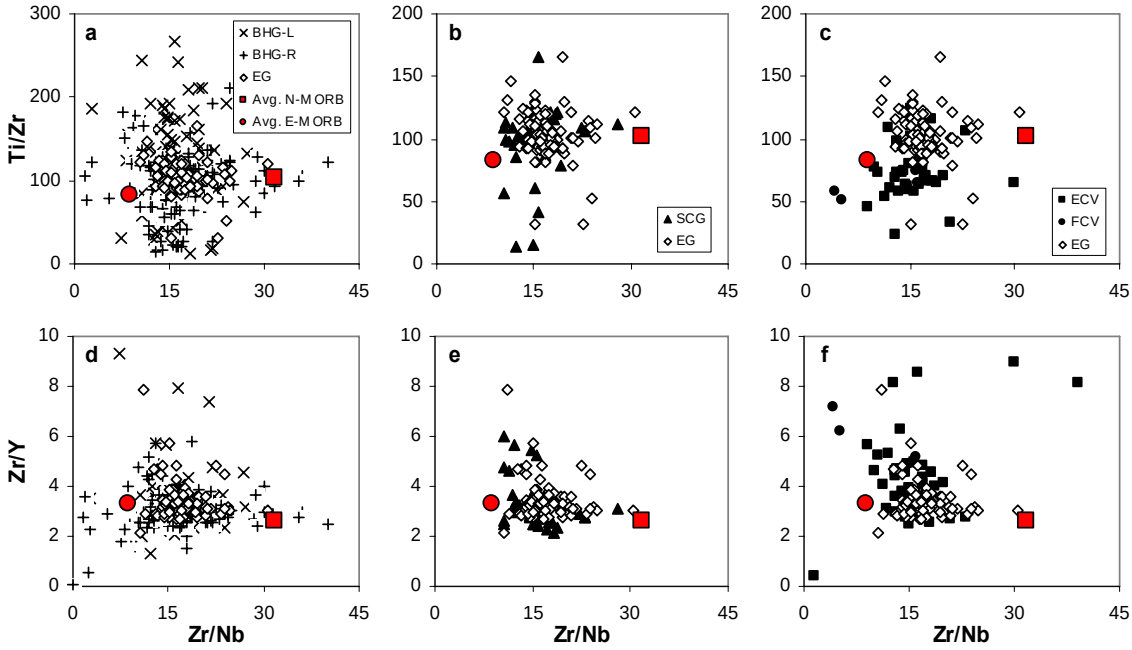


**Figure 7.8: (a) Zr/Nb versus Ti/Zr, and (b) Zr/Nb versus Zr/Y for mafic rocks of the Broken Hill Group, Etheridge Group, and Toole Creek, Eastern Creek and Fiery Creek Volcanics (Mt Isa). Data sources as in Figures 7.3, 7.4, and 7.5. Average N-MORB and E-MORB values after Sun & McDonough (1989). Average Continental Crust values after Weaver & Tarney (1984).**

### 7.4.3 Sm-Nd isotope geochemistry

Comparison of the Sm-Nd whole-rock isotope characteristics for tholeiitic rocks of the BHG, SCG, and EG is compromised to some extent by the paucity of available data. However, some conclusions can still be drawn from the available analyses. Only one Sm-Nd isotope analysis was available from the mafic rocks of the SCG, that being for a garnetiferous mafic rock in the Mt Norna Quartzite member (Page & Sun, 1988; Fig. 7.2). No Sm-Nd isotope analyses were available for mafic rocks of the BHG; however a recent study of tholeiitic metabasalts from the ca. 1685 Ma Lady Louise Suite (LLS) of the Curnamona Province (Conor & Fanning, 2001) by Rutherford *et al*. (2006) provided Sm-Nd analysis of 24 samples. Based on their age and geochemical characteristics, the metabasalts of the LLS have been correlated to those of the BHG (Page *et al*., 2005b; Rutherford *et al*., 2006), and are subsequently included here for comparison. The Sm-Nd data for both the SCG and LLS are summarised in Table 7.1, and individual analyses are listed in Appendix 5.

| Sample | No. of analyses | Sm (ppm) | Nd (ppm) | Age | $^{147}Sm/^{144}Nd$ | $^{143}Nd/^{144}Nd$ | $\varepsilon_{Nd}(T)$ | $T_{DM}$ (Ga) | Data Source |
|---|---|---|---|---|---|---|---|---|---|
| Etheridge Group | 10 | 3.3 | 11.0 | 1.67 | 0.1850 | 0.512708 | 3.9 | 2.49 | Table 6.3 |
| Soldiers Cap Group | | | | | | | | | |
| Mt Norna Quartzite | 1 | 6.9 | 26.1 | 1.67 | 0.1603 | 0.512265 | 0.5 | 2.51 | Page & Sun (1998) |
| Lady Louise Suite | | | | | | | | | |
| Plumbargo | 2 | 3.4 | 13.1 | 1.685 | 0.1687 | 0.512339 | 0.2 | 2.77 | Rutherford et al. (2006) |
| Outalpa | 9 | 3.4 | 12.4 | 1.685 | 0.1651 | 0.512327 | 0.8 | 2.63 | |
| Waukaloo | 2 | 2.9 | 9.9 | 1.685 | 0.1766 | 0.512509 | 1.8 | 2.62 | |
| Mingary | 9 | 2.1 | 6.7 | 1.685 | 0.1916 | 0.512663 | 1.6 | 2.98 | |
| Mundi | 2 | 4.8 | 14.5 | 1.685 | 0.2023 | 0.512747 | 0.9 | n/a | |

*CHUR (chondrite uniform reservoir): $^{147}Sm/^{144}Nd = 0.1967$, $^{143}Nd/^{144}Nd = 0.512638$*
*DM (depleted mantle): $^{147}Sm/^{144}Nd = 0.2137$, $^{143}Nd/^{144}Nd = 0.51315$*
*$\lambda$ = decay constant of $^{147}Sm = 6.54 \times 10^{-12}$*

**Table 7.1: Summary of Sm-Nd isotope data for mafic rocks of the Etheridge Group, Soldiers Cap Group, and Lady Louise Suite (Curnamona Province). Individual analyses listed in Table 6.3 (Etheridge Group); for all other analyses see Appendix 5.**

$^{147}Sm/^{144}Nd$ ratios are variable within each terrane but mostly lie between 0.16 and 0.22, consistent with their tholeiitic nature (Fig. 7.9a). Samples from the LLS with lower $^{147}Sm/^{144}Nd$ ratios may have been contaminated at some stage during their genesis or reflect source heterogeneity, as they plot along a trend towards decreasing (negative) $\varepsilon_{Nd}$ values (Fig. 7.9a; Rutherford *et al*., 2006). The correlation in the range of $^{147}Sm/^{144}Nd$ ratios between the EG and LLS samples is also reflected in their $T_{DM}$ ages (Fig. 7.9b).

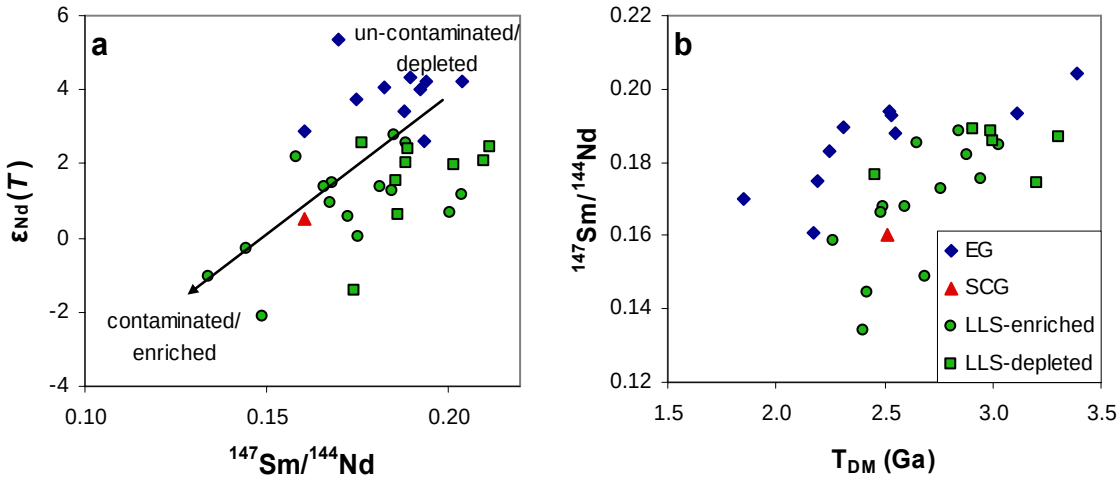


**Figure 7.9: (a) $^{147}Sm/^{144}Nd$ versus $\varepsilon_{Nd}(T)$, and (b) $T_{DM}$ model ages versus $^{147}Sm/^{144}Nd$ for samples from the Etheridge Group (EG), Soldiers Cap Group (SCG), and Lady Louise Suite (LLS). Data sources as for Table 7.1.**

Initial $\varepsilon_{Nd}$ values [$\varepsilon_{Nd}(T)$] for metabasalts from the LLS were calculated for an assumed crystallisation age of 1685 Ma (Rutherford *et al*., 2006), and the SCG sample for an assumed age of 1670 Ma (Page & Sun, 1998). $\varepsilon_{Nd}(T)$ values for the EG tholeiites (5.3-2.6; Table 6.3) are higher on average than those of both the LLS (1.8-0.2) and SCG (0.5) (Table 7.1), indicating that the EG tholeiites experienced little contamination by crustal material relative to the other suites (Chapter 6). Although some form of crustal contamination or late-stage assimilation of crustal material can account for the differing $\varepsilon_{Nd}(T)$ and $^{147}Sm/^{144}Nd$ values between the EG and LLS samples (Fig. 7.9), Rutherford *et al*. (2006) suggested that the observed variation in LLS geochemistry could not be adequately explained by crustal contamination, and was rather an effect of limited source heterogeneity. They demonstrated that some of the most isotopically primitive samples from the LLS (i.e. those samples with $\varepsilon_{Nd}(T)$ values > 0) were also displaced towards higher La/Sm values (Fig. 7.10).

Rutherford *et al*. (2006) proposed that tholeiites showing this relationship were most likely derived from a geochemically enriched, isotopically depleted lithospheric mantle source beneath the Olary Domain (western Curnamona Province) that had incorporated a subduction-related component. Their hypothesis is also supported by distinct, elevated REE profiles for the most enriched LLS samples (Fig. 7.11). They concluded that the enriched magma produced in the Olary Domain of the Curnamona Province during the ca. 1.7-1.67 Ga period of lithospheric thinning was absent, or at

least less obvious from the more depleted magmas emplaced within the Broken Hill Block to the east.

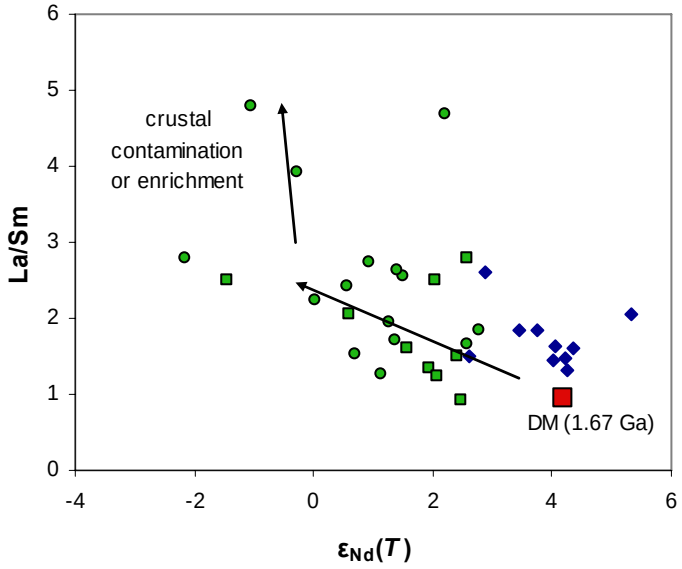


**Figure 7.10: $\varepsilon_{Nd}(T)$ versus La/Sm for mafic rocks of the Etheridge Group and Lady Louise Suite. DM = Depleted Mantle $\varepsilon_{Nd}$ value at 1.67 Ga, derived from DePaolo (1981). All other data sources and symbols as in Figure 7.9.**

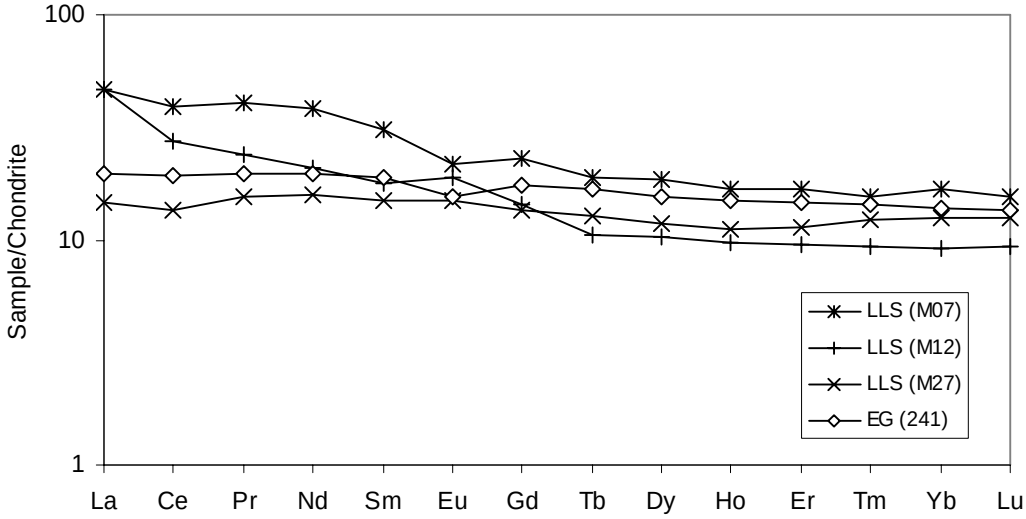


**Figure 7.11: Chondrite-normalised REE compositions for representative tholeiitic samples from the Etheridge Group (sample 241) and Lady Louise Suite (samples M07, M12 and M27; data from Rutherford *et al.*, 2006). Samples M07 and M12 are 'enriched' tholeiites from the Olary Domain, western Curnamona Province. Sample M27 is a 'depleted' tholeiite from the Broken Hill Domain, eastern Curnamona Province. Normalising values after Boynton (1984).**

Conversely, the EG tholeiites of this study possess relatively flat REE profiles similar to the BHG, as well as trace element and isotopic values consistent with the late-stage assimilation of relatively minor amounts of crustal material into a geochemically and isotopically depleted magma (Chapter 6). Compositional variation between the most geochemically primitive and evolved EG tholeiites was also shown to be the result of magmatic fractionation. There is no strong evidence for the existence of a relatively enriched mantle source.

Despite the limited Sm-Nd isotopic datasets for the mafic rocks of the Curnamona Province and SCG, it is still possible to draw a meaningful relationship from the available data. The Nd isotope evolution diagram (Fig. 7.12) shows that the tholeiitic magmas which produced the mafic rocks in each terrane were derived from a relatively depleted mantle source over a similar time interval, but each evolved to unique isotopic characteristics based on the extent of crustal contamination and/or prior enrichment of the depleted mantle source. Variably enriched to depleted tholeiitic magma which forms the LLS in the western Curnamona Province produced mafic rocks with $T_{DM}$ ages ranging from 3.31 to 2.26 Ga (Fig. 7.12; Rutherford *et al*., 2006). These model ages overlap with those of both the EG (3.39 to 1.85 Ga; Table 6.3), and the single analysed mafic igneous rock from the SCG (2.51 Ga; Page & Sun, 1998). The overlap in $T_{DM}$ ages for these terranes coupled with similar crystallisation ages of their mafic rocks is significant, as it suggests that the processes which led to the emplacement of tholeiitic magma in each terrane occurred over a similar timescale, producing geochemically similar intrusive and/or extrusive igneous rocks.

Although the dominant Nd isotope evolution trajectories for each mafic suite differ significantly (Fig. 7.12), there is some inter-regional correlation between individual analyses. A number of processes have been suggested which together may account for the observed variation. Page & Sun (1998) suggested that alteration may have affected the Sm-Nd systematics of some samples from the SCG, including the mafic sample from the Mt Norna Quartzite (Table 7.1). However, without access to additional Sm-Nd data from this area it is impossible to predict whether the Nd isotope evolution trajectory of this sample is representative of the SCG mafic rocks. Alternatively, for the LLS metabasalts an anomalous enriched component in the source is proposed, with little or no additional input from crustal material (Rutherford *et al*., 2006). Despite these differences, the majority of the available geochemical and isotopic

evidence suggests that tholeiitic mafic rocks emplaced ca. 1.69-1.67 Ga throughout the eastern Australian Proterozoic terranes are geochemically linked, and may have even been derived from a geochemically similar, relatively depleted upper-mantle source. The significance of this relationship, for both the Georgetown Inlier and the North Australian Craton, is discussed below.

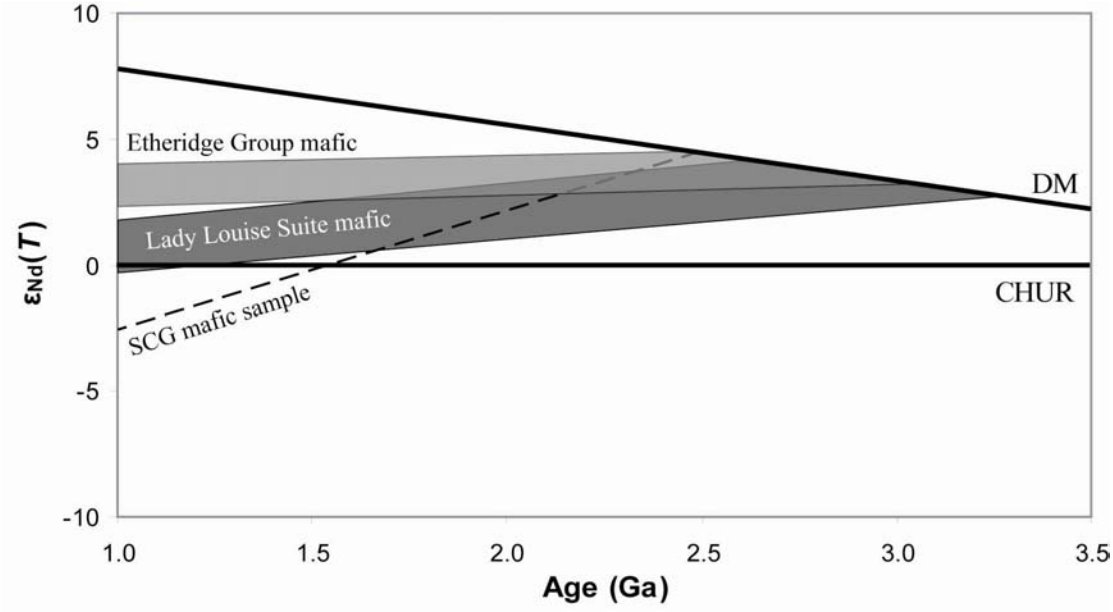


**Figure 7.12: Nd isotope evolution diagram for mafic rocks of the Etheridge Group, Soldiers Cap Group (SCG), and Lady Louise Suite (Curnamona Province; Fig. 7.1). Depleted mantle curve (DM) assumes a linear evolution of the depleted mantle from CHUR ($\varepsilon_{Nd} = 0$) at 4.56 Ga to a present-day value of +10 (Goldstein *et al*., 1984; Jahn & Condie, 1995; Blewett *et al*., 1998). Data sources as for Table 7.1.**

## 7.5 Discussion

### 7.5.1 Variation in the level of Fe-enrichment: the effect of source or setting?

The generation of ca. 1670 Ma Fe-rich tholeiitic melts with remarkably similar geochemistry within Broken Hill Block, Mt Isa Eastern Succession, and Georgetown Inlier has important implications for lithospheric evolution on the eastern margin of the North Australian Craton during the Palaeoproterozoic. However, before this issue can be addressed the origin and evolution of the individual tholeiitic melts must be considered.

Strongly Fe-rich tholeiitic basalts (>15 wt% $Fe_2O_3^{total}$), such as those found in the Proterozoic terranes of eastern Australia, are rare and generally restricted to extensional tectonic settings (Brooks *et al*., 1991). Numerous conditions have been

suggested to account for the development of Fe-enriched assemblages during the fractionation of tholeiitic melts, including the composition of the upper mantle source, low oxygen fugacity ($fO_2$) and closed system fractionation in the melt, and the relatively high density of Fe-rich liquids (Sinton *et al*., 1983; James *et al*., 1987; Brooks *et al*., 1991). Continental rift settings are highlighted as favourable environments, as they are thought to contain high-level magma chambers that are well removed from their mantle sources and thus are more likely to develop as relatively closed systems (Sinton *et al*., 1983; Brooks *et al*., 1991).

It is beyond the scope of this study to assess the viability of each of these conditions in influencing the general level of Fe-enrichment in tholeiitic melts. However, based on the combination of geochemistry and lithostratigraphic evidence, reasonable assumptions can be made regarding the possible contributions from each of these conditions to Fe-enrichment in the tholeiitic rocks of this study. Brooks *et al*. (1991) suggested that the trend towards strong Fe-enrichment of a tholeiitic liquid was a direct result of differentiation in a closed system at a relatively low $fO_2$ state. For this to occur, the low $fO_2$ state would need to have been inherited from the source or magma chamber. Additionally, the low oxidation state would be maintained so long as little to no replenishment of the magma took place, essentially implying fractionation as a closed system. If replenishment of the magma did take place, equally low $fO_2$ magma would be required to maintain the reduced state. If these conditions were imposed on the BHG, SCG, and EG suites, then based on the near-identical nature of the Fe-enrichment trends for each terrane (Fig. 7.3 and 7.4), similar low $fO_2$ conditions coupled with little to no replenishment of the source magmas would have been required to produce the trends observed.

Based on the conditions for Fe-enrichment discussed above, I prefer a scenario whereby the Fe-rich tholeiites of the BHG, SCG, and EG were derived from a geochemically similar upper-mantle source, and evolved along a unique tholeiitic fractionation trend towards strong Fe-enrichment (up to 20 wt% $Fe_2O_3^{total}$). The Fe-enrichment observed in each terrane was accommodated by fractionation within a closed system at a relatively low oxidation state, which suppressed magnetite crystallisation until relatively late in the fractionation sequence.

### 7.5.2 Base metal mineralisation in the lower Etheridge Group: is there a world-class Broken Hill-type deposit in the Georgetown Inlier?

The geochronological, geochemical, and lithostratigraphic similarities between the Etheridge Group, Mt Isa Eastern Succession, and Broken Hill Block suggest that the Proterozoic rocks of the Georgetown Inlier were also a suitable host for base-metal mineralisation. Numerous small stratabound and/or stratiform base metal deposits are found within the lower Etheridge Group, and are hosted by the Einasleigh Metamorphics (Bain *et al*., 1990). Further west in the Robertson River Subgroup, a zone of high Zn, Pb and Cu has been reported in the lowermost part of the Daniel Creek Formation, 8 km northwest of Gilberton (Onley, 1978). However, no other significant base metal deposits have been found in this part of the inlier (Withnall *et al*., 1997). Despite the presence of numerous small-scale deposits, world-class Broken Hill-type base metal deposits of a similar size to those found at Broken Hill and in the Mt Isa Eastern Succession (e.g. Cannington deposit) are not found in the Etheridge Group. The possible reasons for the absence of such a deposit in the Etheridge Group are discussed below.

Although debate concerning the exact lithological, geochemical, and regional relationships responsible for the development of Broken Hill-type deposits is ongoing, reasonable constraints can be placed on their genesis based on the relationships observed in existing deposits. Identification of these criteria is essential for determining the economic prospectivity of exploration sites, including the Georgetown Inlier. A comprehensive summary of the features associated with Broken Hill-type deposits was presented by Walters (1998); however, only the key geologic criteria are mentioned here.

Both the Broken Hill and Cannington deposits are hosted by quartzo-feldspathic sequences, with the host rock dominated by garnet quartzite that has been metamorphosed to upper amphibolite-granulite facies. The quartzite lies at the transition between a lower sequence consisting predominantly of quartzo-feldspathic units, and a dominantly psammopelitic to pelitic upper stratigraphy (Walters, 1998). Occurring proximal to the ore lodes at both Broken Hill and Cannington are concentrations of amphibolite and felsic igneous rocks (Fig. 7.13). At Broken Hill, the felsic igneous rocks are termed ‘Potosi’ gneiss (Stevens *et al*., 1988), whereas at Cannington the felsic igneous rocks are pegmatites (Williams & Smith, 2003). The

amphibolites are generally described as sills emplaced during the intrusion of tholeiitic magmas, introduced during rifting of the depositional basins. The magnetic response of the amphibolites has a variable association with mineralisation, as demonstrated by the poor magnetic response produced by magnetite in amphibolite in the Broken Hill main lode, whereas at Cannington magnetite has produced a direct magnetic target (Walters, 1998).

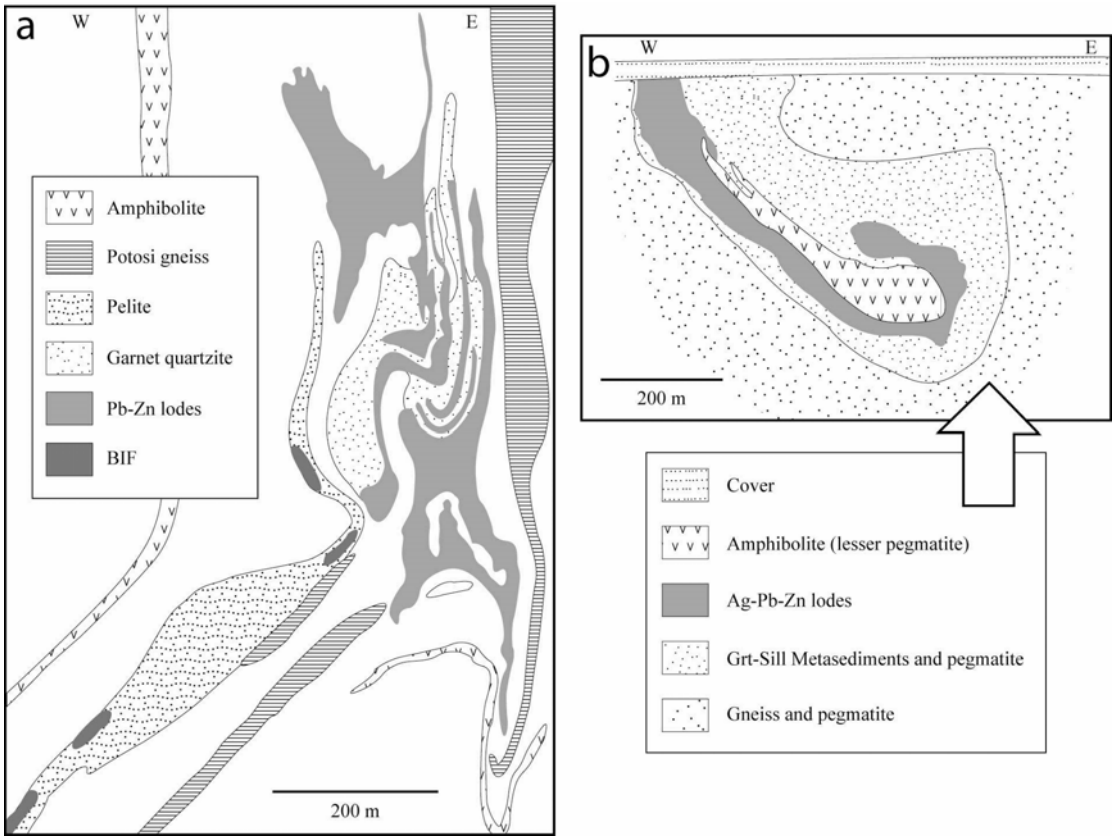


**Figure 7.13: Simplified cross-sections of (a) the Broken Hill Main Lode (in the region of the Zinc Corp main shaft; after Walters, 1998), and (b) Cannington deposit (southern zone, through 4800N; after Williams & Smith, 2003).**

In the Etheridge Group, base metal deposits hosted by the Einasleigh Metamorphics fall into four categories: stratabound Fe-Cu ± Ag sulphide deposits (e.g. Einasleigh), Fe-Zn sulphide deposits (e.g. Eveleigh), Fe-Pb-Zn-Cu ± Ag sulphide deposits (e.g. Mount Misery), and Cu/Fe/Si/Ba gossans in the Werrington area (Withnall *et al*., 1997). These deposits have features that suggest an affinity to Broken Hill-type mineralisation, as they are commonly associated with quartzite and quartzo-feldspathic units, and are concentrated at the transition between a lower calcareous quartzo-feldspathic sequence, and an upper psammopelitic sequence (Withnall *et al*., 1997). Concentrations of amphibolite (mafic gneiss) are also found in near-ore

sequences (Withnall *et al*., 1997), and quartzo-feldspathic gneiss associated with the deposits may also be of possible volcanic origin (Johnston, 1978; Oversby, 1981).

In the south-western extensions of the lower Etheridge Group (Fig. 2.6), the transition from lower quartzo-feldspathic sequences to upper psammopelitic to pelitic sequences are located at the contact between the Bernecker Creek and Daniel Creek Formations. Metadolerite sills belonging to the Cobbold Metadolerite member are locally intruded; however apart from sparse and volumetrically minor granophyric bodies representing late-stage felsic differentiates in the metadolerite, no other concentrations of contemporaneous felsic igneous or volcanic rocks are observed. Peak metamorphism in the area is also generally restricted to greenschist facies assemblages.

Taking these characteristics into consideration, lower Etheridge Group rocks in the south-western and western extensions of the Georgetown Inlier are an unlikely host for large Broken-Hill-type orebodies, as a number of key lithologic and metamorphic conditions have not been met. However, higher-grade equivalents represented by the Einasleigh Metamorphics further east appear conducive to mineralisation of this type, as exemplified by the numerous small base metal deposits already identified. It is therefore possible that the majority of mineralisation in the lower Etheridge Group was restricted to the eastern half of the succession, with the presence of possible volcaniclastic sequences (Black *et al*., 2005), and the influx of oxidised ore fluids restricted to this area alone. The prospectivity of the Einasleigh Metamorphics is further enhanced by the presence of elevated Na contents relative to other Etheridge Group rocks further west. This suggests a regional Na metasomatic event, perhaps associated with mineralisation, may have affected the Einasleigh Metamorphics during the Proterozoic (Black *et al*., 2005).

The absence of an exposed volcaniclastic sequence, coupled with low metamorphic grade in the central and western extensions of the lower Etheridge Group does not necessarily imply that mineralisation is absent from these areas. Leucogneiss in the Einasleigh Metamorphics dated by Black *et al*. (2005) contains zircons which they inferred were of possible volcaniclastic origin. If this volcaniclastic source is located within the Einasleigh Metamorphics, it is possible that this sequence may also occur within un-exposed equivalents of the Bernecker Creek and/or Daniel Creek Formations further west (Withnall *et al*., 1988a). Subsequently, if higher-grade equivalents of the Bernecker Creek and Daniel Creek Formations are located at depth

in the central and western parts of the inlier, they may provide a viable target for further exploration. High magnetic responses are also recorded in the central and south-western parts of the Etheridge Group, and are associated with exposed or partially exposed amphibolite (Withnall *et al*., 2003a), or amphibolite under cover (Withnall *et al*., 2003b). As these magnetic highs also occur proximal to exposed contacts between the Daniel Creek and Bernecker Creek Formations, they may also provide viable exploration targets.

## 7.6 Conclusions

The Fe-rich tholeiites of the lower Etheridge Group are hosted by late Palaeoproterozoic metasedimentary rocks, and show strong geochemical affinities with similarly aged mafic rocks from the Soldiers Cap Group and Broken Hill Group in the Mt Isa Eastern Succession and Broken Hill Block respectively. These affinities include the correlation of major and incompatible trace element values, and variation diagram trends that are virtually indistinguishable (e.g. Fig. 7.3 and 7.4). Compositional variation, where present, is limited to samples of Broken Hill Group mafic gneiss collected proximal to the main line-of-lode at Broken Hill. These rocks generally have higher $Fe_2O_3^{total}$ and $TiO_2$ compositions relative to other samples at a given stage of their evolution, and their unusual geochemistry may be related to processes responsible for the mineralisation (Phillips *et al*., 1985).

Similarities in the fractionation histories of the mafic suites are also supported by the near-identical trends in compatible and incompatible trace elements including Ni and Zr. In addition, similar REE and incompatible trace element patterns are also suggestive of similar fractionation histories for the mafic rocks (Fig. 7.6 and 7.7). They also imply the mafic rocks followed the same or very similar tholeiitic liquid lines of decent. By comparison, tholeiitic basalts from the Mt Isa Western Succession (represented by the Eastern Creek and Fiery Creek Volcanics) have higher incompatible trace element and LREE values, suggesting slightly more alkaline parent magmas than for the Broken Hill, Soldiers Cap, and Etheridge Group tholeiites. The correlation in immobile trace element ratios (e.g. Fig. 7.8) also suggests the Broken Hill, Soldiers Cap, and Etheridge Group tholeiites possessed similar initial geochemical compositions. This correlation, coupled with the observed similarities in

trace and rare earth element patterns, implies that the rocks were most likely derived from chemically similar parent magmas.

In addition to major, trace, and rare earth element geochemistry, the Etheridge Group tholeiites possess $^{147}Sm/^{144}Nd$ ratios and $T_{DM}$ model ages similar to the ca. 1685 Ma Lady Louise Suite, a suite of variable enriched tholeiitic basalts in the central-western Curnamona Province that have been correlated to the mafic rocks of the Broken Hill Group. In addition, a contemporaneous mafic igneous rock in the Soldiers Cap Group possesses a similar $T_{DM}$ age to those of the Etheridge Group tholeiites. The similarities in Sm-Nd systematics between the terranes suggest that separation of their parental magmas from a depleted mantle source occurred over a similar time-span, providing a further link for the correlation of the tholeiitic rocks from each terrane.

The geochemistry and geochemical similarities between similarly aged Fe-enriched tholeiites from the Broken Hill, Soldiers Cap and Etheridge Groups suggest they each formed from Fe-rich parental melts, with strong Fe-enrichment most likely occurring as a result of closed system fractionation under generally reduced conditions (low $fO_2$). Additional Fe-enrichment up to 25 wt% $Fe_2O_3^{total}$, observed in the tholeiites along the line-of-lode at Broken Hill, may be linked to mineralisation processes.

The geochemical similarities observed between the Fe-rich tholeiites of the Broken Hill, Soldiers Cap and Etheridge Groups are significant; and if Fe-rich tholeiites from both Mt Isa Eastern Succession and Broken Hill are associated with the development of significant mineralisation, may suggest that ore-forming processes also occurred within the lower Etheridge Group. The correlation of these Palaeoproterozoic mafic suites suggests that they were derived from similar depleted mantle sources. This relationship, coupled with other lithostratigraphic, geochronological, and structural evidence, suggests that the Etheridge Group was deposited in an extensional basin not far removed from the Mt Isa and Broken Hill terranes. This has important implications for the Palaeoproterozoic location of the Georgetown Inlier, as it implies that the terrane formed an integral part of the North Australian Craton during this time.

# Chapter 8.

# Summary and conclusions

## 8.1 Palaeoproterozoic evolution of the lower Etheridge Group

Sedimentary rocks of the lower Etheridge Group were deposited in a subsiding volcanic passive continental margin setting between ca. 1720 Ma and 1650 Ma. Deposition of the earliest sedimentary units had commenced by ca. 1715 Ma, determined from crystallisation ages for two samples of the Cobbold Metadolerite that were intruded into the lower Etheridge Group. This is the preferred maximum depositional age for the Etheridge Group, as it is within error of zircon SHRIMP ages obtained from samples of interbedded leucogneiss in the underlying Einasleigh Metamorphics, which have previously placed an upper limit on the depositional age of the Etheridge Group (Black *et al*., 2005).

Voluminous Fe-rich tholeiitic igneous rocks were emplaced into the lower Etheridge Group from around ca. 1670 Ma. The mafic rocks are assigned to two units: the extrusive Dead Horse Metabasalt (DHM), a 1000m-thick series of fine- to coarse-grained basalts and pillow lavas; and the intrusive Cobbold Metadolerite (CMD), a multitude of sills and lesser dykes. At least one later pulse of magmatic activity is observed where CMD sills are intruded into the Lane Creek Formation, the upper unit of the Robertson River Subgroup. These uppermost sills were not dated in this study due to an absence of granophyric differentiation; however CMD sills intruding the Bernecker Creek Formation, which is lower in the stratigraphic sequence, returned pooled ages of ca. 1645 Ma that may date the later generation of sills.

Following deposition, the lower Etheridge Group sedimentary rocks underwent an extended period of regional-scale orogenesis and metamorphism. At least two discrete tectonothermal events are recorded, with the intensity of each event generally increasing from west to east. EMPA dating of metamorphic monazite from this and a previous study (Cihan *et al*., 2006) suggests that the earliest orogenic event occurred at around ca. 1585 Ma. This event corresponds to the $D_1$ event of Withnall *et al*. (1988a), and was associated with regional-scale folding, and the development of a pervasive metamorphic fabric. In the area around ‘Gum Flats’, the metasediments of the Robertson River Subgroup record peak metamorphic conditions of up to 650 °C

and 7.5 kbar associated with this event. Samples of Einasleigh Metamorphics mica schist that are in fault-contact with Robertson River Subgroup metasediments in this area record *P-T* conditions of up to 750 °C and 7.5 kbar also associated with this event.

The second regionally significant tectonothermal event was associated with the emplacement of voluminous S-type granitoids, and corresponds to the $D_2$ event of Withnall *et al*. (1988a). LA-ICPMS analysis of igneous zircons collected from granitoid samples, coupled with EMPA monazite analysis of lower Etheridge Group metasediments indicate that this event occurred between ca. 1550 Ma and 1530 Ma. An estimate of the *P-T* conditions associated with this event was limited to a sample of mica schist from the Daniel Creek Formation that returned a retrograde $M_1$-early $M_2$ *P-T* estimate of 550 °C and 3 kbar. EMPA monazite analysis of a sample containing a later ($S_3$) foliation suggests a possible weak metamorphic event occurred at ca. 1500 Ma, and may date the previously unconstrained $D_3$ event of Withnall (1996).

## 8.2 Geochemical evolution of Fe-rich tholeiites within the lower Etheridge Group

The DHM and CMD are shown to be co-magmatic and share a common geochemical history. They possess geochemical characteristics typical of relatively evolved, low-K, Fe-rich continental tholeiites and basalts erupted in the early stages of development of volcanic passive margins, typified by the early Tertiary E Greenland margin. Trace element, REE and isotopic data indicate that the rocks were generated by partial melting of a depleted mantle source, and that the magmas continued to evolve along a trend of Fe-enrichment involving fractional crystallisation within a closed system. As a result, some samples show extreme Fe-rich compositions (>20 wt% $Fe_2O_3^{total}$). $\varepsilon_{Nd}(T)$ values average +4.0, suggesting the magma was originally derived from a depleted mantle source. A poorly constrained Sm-Nd isochron age, coupled with $\varepsilon_{Nd}(T)$ and $T_{DM}$ values, indicate that the mafic rocks crystallised at ~1.69 Ga. This correlates with U-Pb zircon crystallisation ages obtained from some of the mafic samples. $T_{DM}$ model ages also indicate that the mantle source of the mafic rocks formed during the early Palaeoproterozoic (ca. 2.36 Ga).

In several samples, REE values show distinct LREE-enriched patterns consistent with small degrees of crustal contamination. Trace element ratio diagrams (e.g. Fig. 6.14, 6.21) indicate that the crustal contaminant was derived from the host metasediments of the lower Etheridge Group, with the majority of samples showing less than 10% assimilation of sedimentary material.

Based on their geochemistry and geological setting (i.e. large volumes of sills), a continental rifting environment provides the appropriate conditions for the emplacement of the Etheridge Group mafic rocks. During opening of the rift-system and deposition of the lower Etheridge Group metasediments, tholeiitic magmas derived from convecting upper mantle melted due to decompression, and tholeiitic magma was introduced into the upper crust. Differentiation of the tholeiitic magma to the most Fe-rich (13-20 wt% $Fe_2O_3^{total}$) compositions occurred without the significant input of crustal material via processes associated with fractional crystallisation including partial melting, until emplacement within the overlying lower Etheridge Group sediments as the CMD member. During the initial period of sustained magmatism, batches of melt that reached the surface were erupted to form the DHM member.

## 8.3 Implications for the Palaeoproterozoic location of the Georgetown Inlier (ca. 1700-1500 Ma)

The lithological, geochemical, and geochronological similarities between the Georgetown Inlier, the Broken Hill Block, and the Mt Isa Eastern Succession have important implications for the Palaeoproterozoic position of the Georgetown Inlier. Such similarities, when found to occur over significant intervals of time, imply that the terranes must have been spatially associated. Both the Broken Hill Block and Mt Isa Eastern Succession have previously been included as integral parts within the North Australian Craton (NAC; Myers *et al*., 1996; Giles *et al*., 2002). Subsequently, the observed similarities suggest that the Georgetown Inlier also developed along the eastern-most section of the craton. Therefore, plate tectonic models for the evolution of the Australian Plate between ca. 1700 and 1500 Ma should incorporate the Georgetown Inlier in their construction.

The evolution of the eastern margin of the NAC between 1800 Ma and 1500 Ma was summarised by Betts & Giles (2006), following the studies of Wingate & Evans (2003) and Giles *et al*. (2004). Their model proposed that plate tectonic processes played an integral part in the development of the craton, and its constituent extensional basins. In particular, their model suggested that subduction processes along the southern margin of the NAC promoted the development of several extensional basins within the plate interior, corresponding to the sedimentary successions now located within the Broken Hill, Mt Isa, and Georgetown Inliers (Giles *et al*., 2002). Following deposition, the basins experienced similar, but not identical deformation histories corresponding to a number of regional- and local-scale orogenic events (Betts & Giles, 2006). A summary of this history for the eastern margin of the NAC is provided below; however particular attention is given to the location and tectonic processes responsible for the development of the Georgetown Inlier and its associated terranes.

### 8.3.1 Onset of deposition in the Georgetown Inlier, and renewed deposition in the Broken Hill Block and Mt Isa Eastern Succession (ca. 1740-1600 Ma)

By ca. 1740 Ma, a number of extensional basins had developed within the NAC in response to earlier periods of lithospheric extension (Betts & Giles, 2006). These basins included the McArthur basin, and both the Western and Eastern Successions of the Mt Isa Inlier (Fig. 8.1a). At ca. 1740 Ma, a depositional hiatus was recorded in these basins, and additionally in the Curnamona Province. This hiatus has been linked to the onset of collision between the Mawson continent (comprising the Gawler Craton and associated rocks in East Antarctica) and the NAC (Fig. 8.1a; Scott *et al*., 2000; Giles *et al*., 2002; Betts & Giles, 2006).

Sedimentation in the Mt Isa Eastern Succession and Curnamona Province had recommenced by ca. 1720 Ma (Page & Sun, 1998; Page *et al*., 2005a). By this time, deposition of the oldest exposed sedimentary units had also commenced within the Georgetown Inlier. This period of basin development and sedimentation was linked to the retreat (roll-back) of a north-dipping subduction zone along the southern margin of the NAC (Fig. 8.1a; Giles *et al*., 2002; Betts & Giles, 2006). The subsequent intrusion and eruption of geochemically related, Fe-rich tholeiitic rocks into the extensional basins between ca. 1680 Ma and 1660 Ma occurred as a result of

lithospheric thinning beneath the NAC. However, the amount of lithospheric thinning was not enough to induce the development of new oceanic crust.

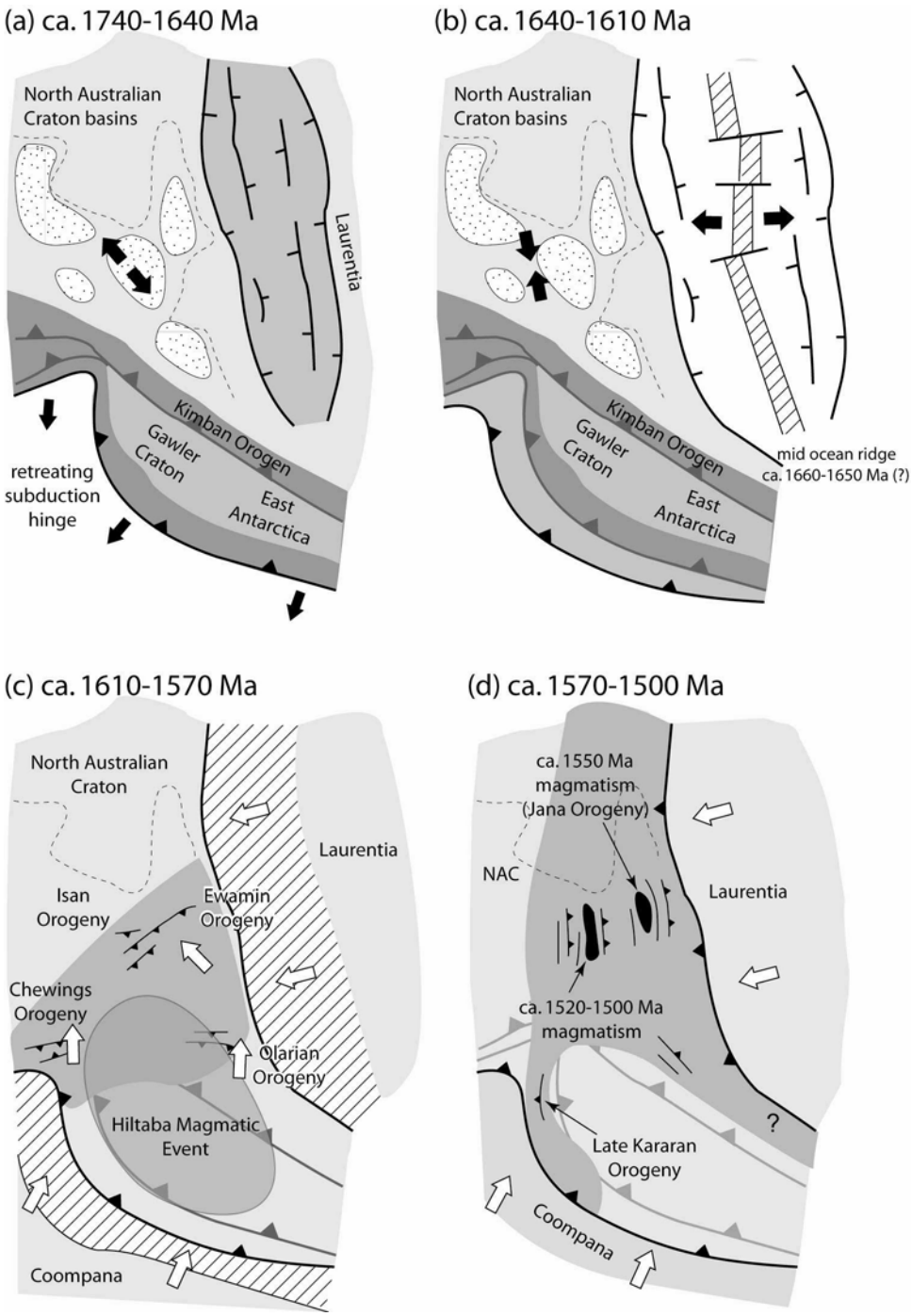


**Figure 8.1: Interpreted tectonic evolution of the eastern North Australian Craton between ca. 1740 and 1500 Ma. Regional scale tectonic processes, orogenic events, and their location follow the interpretation of Betts & Giles (2006), MacCready *et al.* (2006), and references therein. Figures modified after Betts & Giles (2006).**

A significant change in the style of sedimentation is recorded in the Mt Isa, Broken Hill and Georgetown extensional basins after ca. 1660 Ma, with sedimentary lithologies progressively changing from continental shelf-type sands and silts to deeper marine sediments including turbidites, muds and carbonaceous sediments (Willis *et al*., 1983; Withnall, 1996; Betts *et al*., 2006). This transition was co-incident with the start of the Isa Superbasin cycle, and was thought to coincide with the opening of an oceanic basin to the east of the Georgetown Inlier, with the locus of lithospheric extension shifting from beneath the NAC to the new spreading centre (Fig. 8.1b; Betts *et al*., 2003; Betts & Giles, 2006).

### 8.3.2 Orogenesis along the eastern margin of the North Australian Craton (ca. 1600-1500 Ma)

A series of regional-scale orogenic events are recorded within the extensional basins along the eastern margin of the NAC between ca. 1600-1500 Ma. The earliest regional-scale event occurred between ca. 1600-1580 Ma, and was associated with a period of contemporaneous north-south oriented thin-skinned deformation in the Broken Hill Block (Olarian Orogeny), Mt Isa Inlier (Isan Orogeny) and Georgetown Inlier (Page *et al*., 2005a; Betts & Giles, 2006; Giles *et al*., 2006). This event also produced peak metamorphic conditions in the Georgetown Inlier ($D_1$), and the development of upper amphibolite facies assemblages in the Mt Isa Eastern Succession ($D_2$; Giles *et al*., 2006; Sayab, 2006). Betts & Giles (2006) related this event to tectonic activity occurring along the southern margin of the NAC (Fig. 8.1c).

Subsequent orogenesis in the extensional basins of eastern Australia recorded a change from generally north-south oriented thin-skinned deformation to east-west oriented thick-skinned deformation, commencing at ca. 1565 Ma and continuing until ca. 1500 Ma (Betts & Giles, 2006; MacCready *et al*., 2006). In contrast to the ca. 1600-1580 Ma event, the timing of metamorphism and felsic magmatism associated with the later event differed between the terranes, suggesting that this event may have been partly diachronous across the craton. In the Georgetown Inlier, voluminous felsic magmatism dated to ca. 1550 Ma is associated with this event. In the Mt Isa Eastern Succession magmatism of this age is restricted to the Marramungee Granite (Page & Sun, 1998). This led MacCready *et al*. (2006) to suggest that thin-skinned deformation occurring in the Mt Isa Eastern Succession before ca. 1540 Ma may have been linked

to deep-crustal thickening and thick-skinned deformation beneath the Georgetown Inlier at ca. 1550 Ma.

Betts & Giles (2006) suggested that the onset of thick-skinned orogenesis and associated felsic magmatism in the Georgetown Inlier was related to westward subduction of oceanic crust along the eastern margin of the NAC, and the subsequent collision of the Laurentia continent with eastern Australia at ca. 1540 Ma (Fig. 8.1d). However, the absence of unambiguous arc-related rocks or igneous rocks with subduction signatures along the eastern margin of the NAC questions this interpretation. Regardless of the cause, the subsequent locus of crustal shortening shifted, and was accommodated by thick-skinned deformation in the Mt Isa Inlier (Betts *et al*., 2006; MacCready *et al*., 2006). This phase of deformation was later accompanied by the intrusion of ca. 1520-1500 Ma granitoids in the Mt Isa Eastern Succession (Williams and Naraku Granites; Page & Sun, 1998), and is also recorded by $S_3$ metamorphic monazite ages in the Georgetown Inlier (Cihan *et al*., 2006; and this study).

## 8.4 Conclusions

New geological data and interpretations presented in this thesis are combined with data from previous studies of the lower Etheridge Group to make the following important statements on the geologic characteristics and history of the Georgetown Inlier:

i) The mafic rocks hosted by metasediments of the lower Etheridge Group form two texturally distinct units: the extrusive Dead Horse Metabasalt, a 1000 m-thick series of fine- to coarse-grained basalts and pillow lavas; and the intrusive Cobbold Metadolerite, a multitude of sills and lesser dykes.

ii) The DHM and CMD are co-magmatic, and possess geochemical characteristics typical of relatively evolved, low-K, Fe-rich continental tholeiites and tholeiites erupted along volcanic passive margins such as the E Greenland margin during rifting and the early stages of ocean opening. The rocks evolved along a trend of strong Fe-enrichment, resulting in some samples containing in excess of 20 wt% $Fe_2O_3^{total}$.

iii) The mafic rocks possess Sm-Nd isotopic values consistent with derivation from a depleted mantle parent (initial $\varepsilon_{Nd}$ values between +2.6 and +5.3). $T_{DM}$ crustal residence ages range from 3.39 Ga to 1.85 Ga. Variation in the Sm/Nd isotopic ratio and observed trends in trace element values are consistent with a volumetrically minor amount of contamination by host metasediments of the lower Etheridge Group which occurred during the emplacement of the mafic rocks. As expected, those samples showing the strongest LREE-enrichment also show the lowest initial $\varepsilon_{Nd}$ values, recording this crustal contamination.

iv) The Etheridge Group mafic rocks show strong geochemical affinities to contemporaneous Fe-rich tholeiites from the Soldiers Cap Group and Broken Hill Group of the Mt Isa Eastern Succession and Broken Hill Block respectively. This implies that the mafic rocks of each terrane may have been derived from a similar depleted mantle source during breakup of continental crust along the eastern margin of the NAC.

v) The mafic rocks of the Etheridge Group crystallised between ca. 1715 Ma and ca. 1630 Ma in at least two distinct pulses. The most significant was related to the eruption of the DHM and associated CMD sills, occurring at ca. 1670 Ma. A later pulse was related to the intrusion of CMD sills into the upper Robertson River Subgroup, and occurred at ca. 1640 Ma. The crystallisation age of the DHM member is significant, as it approximates the inferred crystallisation ages of mafic rocks in both the Broken Hill Group (ca. 1685 Ma) and Soldiers Cap Group (ca. 1670-1650 Ma).

vi) The S-type Mt Hogan and Ropewalk Granites, part of the voluminous Forsayth Batholith, were intruded into the lower Etheridge Group at ca. 1550 Ma.

vii) Inheritance patterns produced from detrital zircon analyses of metasediments from the lower Etheridge Group, Broken Hill Group and Mt Isa Eastern Succession share some common components. These include a late-Archaean component (ca. 3100-2500 Ma), which may represent a common Archaean basement, and a significant mid-Palaeoproterozoic component (ca. 2100-1800 Ma). The similarities in inheritance patterns suggest a shared provenance for the sediments.

viii) Prograde metamorphism in the lower Etheridge Group had commenced by ca. 1600 Ma, and had reached peak medium *P-T* conditions at around ca. 1585 Ma. This age corresponds to inferred orogenic ages in both the Broken Hill Block and Mt Isa Eastern Succession. Following a period of retrogression, a second medium-*T*, low-*P* event occurred at ca. 1550-1530 Ma, associated with the intrusion of voluminous S-type felsic igneous rocks. A third, relatively weak metamorphic event is recorded at ca. 1500 Ma, and may relate to a similar period of thermal activity and granitoid emplacement in the Mt Isa Eastern Succession occurring between ca. 1520 and ca. 1500 Ma.

ix) Metasedimentary rocks of the Robertson River Subgroup near Gum Flats record peak metamorphic conditions of up to 650 °C and 7.5 kbar associated with $M_1$. Retrogressive metamorphism produced a clockwise *P-T* path for the metasediments, leading to initial *P-T* conditions for $M_2$ of 550 °C and 3 kbar.

x) The geochemical affinities of the Etheridge Group mafic rocks, coupled with geochronological and lithostratigraphic evidence, suggests that the Georgetown Inlier was proximal to the Mt Isa and Broken Hill Inliers during the Palaeoproterozoic. This further implies that the Georgetown Inlier formed the easternmost part of the NAC during the Proterozoic.

The combination of geochemical, geochronological, and tectonostratigraphic evidence presented in this thesis provides strong support to the hypothesis that the Georgetown Inlier was proximal to the sedimentary basins of northeastern Australia, in particular the Broken Hill Block and Mt Isa Eastern Succession, during the Palaeoproterozoic. Additionally, this relationship implies that the Georgetown Inlier formed the easternmost extension of the NAC during this time, and that the Georgetown Inlier is an integral component of the Proterozoic history of the Australian continent.

## 8.5 Suggestions for future work

Although compelling evidence is presented here and by other sources documenting the geochemical nature and affinities of the Etheridge Group Fe-rich tholeiites, additional work is required to resolve some remaining issues. In particular, a detailed isotopic analysis of the Fe-rich tholeiites from both the Mt Isa Eastern Succession and Broken Hill Block would categorically determine if these mafic rocks shared the same

depleted mantle source as the mafic rocks of the Etheridge Group, and would additionally determine if the rocks shared the same or similar crustal residence ages. Additional isotopic dating of the Fe-rich tholeiites from both the Soldiers Cap and Broken Hill Groups would provide an exact crystallisation age for the mafic rocks, and would also enable a more accurate comparison to the crystallisation age of the Etheridge Group mafic rocks.

Significant work is also required to resolve the tectonothermal history of the lower Etheridge Group, in particular the variation in thermobarometric conditions and its control on mineralogy across the group. Although evidence presented here and in previous studies indicates a clockwise *P-T-t* path for the Etheridge Group involving medium *P-T* metamorphic conditions, contemporaneous *P-T-t* paths proposed for the Mt Isa Inlier and Broken Hill Block involve anticlockwise *P-T-t* paths, with peak metamorphism reached during high-*T*, low-*P* conditions. Further detailed geochronological work is required to constrain the ages of the $M_1$ and $M_3$ events in the Etheridge Group, as only limited data for these two events was obtained over the course of this study. In particular, the ca. 1500 Ma monazite age has possible implications to a contemporaneous period of thermal activity in the Mt Isa Eastern Succession. Further investigation of these issues should determine if the orogenic history of the Georgetown Inlier approximated that of the Mt Isa Inlier and Broken Hill Block.

## Reference List

Bain, J.H.C., Withnall, I.W., Oversby, B.S. and Mackenzie, D.E. (1985). Geology of the Georgetown Region, Queensland. Australian Bureau of Mineral Resources 1:250 000 Scale map.

Bain, J.H.C., Withnall, I.W., Oversby, B.S. and Mackenzie, D.E. (1990). North Queensland Proterozoic inliers and Palaeozoic igneous provinces; regional geology and mineral deposits. Monograph Series – Australasian Institute of Mining and Metallurgy **14**: 963-978.

Beardsmore, T.J., Newbery, S.P. and Laing, W.P. (1988). The Maronan Supergroup: an inferred early volcano-sedimentary rift sequence in the Mount Isa Inlier, and its implications for ensialic rifting in the middle Proterozoic of northwest Queensland. Precambrian Research **40/41**: 487-507.

Bell, T.H. and Rubenach, M.J. (1983). Sequential porphyroblast growth and crenulation cleavage development during progressive deformation. Tectonophysics **92**: 171-194.

Berry, R.F., Jenner, G.A., Meffre, S. and Tubrett, M.N. (2001). A North American provenance for Neoproterozoic to Cambrian sandstones in Tasmania? Earth and Planetary Science Letters **192**: 207-222.

Berry, R.F., Holm, O.H. and Steele, D.A. (2005). Chemical U-Th-Pb monazite dating and the Proterozoic history of King Island, southeast Australia. Australian Journal of Earth Sciences **52**: 461-471.

Betts, P.G. and Giles, D. (2006). The 1800-1100 Ma tectonic evolution of Australia. Precambrian Research **144**: 92-125.

Betts, P.G. and Lister, G.S. (2001). Comparison of the 'strike-slip' versus the 'episodic rift-sag' models for the origin of the Isa Superbasin. Australian Journal of Earth Sciences **48**: 265-280.

Betts, P.G., Ailleres, L., Giles, D. and Hough, M. (2000). Deformation history of the Hampden Synform in the Eastern Fold Belt of the Mt Isa terrane. Australian Journal of Earth Sciences **47**: 1113-1125.

Betts, P.G., Giles, D., Lister, G.S. and Frick, L.R. (2002). Evolution of the Australian lithosphere. Australian Journal of Earth Sciences **49**: 661-695.

Betts, P.G., Giles, D. and Lister, G.S. (2003). Tectonic environment of shale-hosted massive sulphide Pb-Zn-Ag deposits of Proterozoic northeastern Australia. Economic Geology **98**: 557-576.

Betts, P.G., Giles, D., Mark, G., Lister, G.S., Goleby, B.R. and Aillères, L. (2006). Synthesis of the Proterozoic evolution of the Mt Isa Inlier. Australian Journal of Earth Sciences **53**: 187-211.

Bhattacharya, A., Mohanty, L., Maji, A., Sen, S.K. and Raith, M. (1992). Non-ideal mixing in the phlogopite-annite binary; constraints from experimental data on Mg-Fe partitioning and a reformulation of the biotite-garnet geothermometer. Contributions to Mineralogy and Petrology **111**: 87-93.

Black, L.P., Bell, T.H., Rubenach, M.J. and Withnall, I.W. (1979). Geochronology of discrete structural-metamorphic events in a multiply deformed Precambrian terrain. Tectonophysics **54**: 103-137.

Black, L.P. and McCulloch, M.T. (1984). Sm-Nd ages of the Arunta, Tennant Creek, and Georgetown Inliers of northern Australia. Australian Journal of Earth Sciences **31**: 49-60.

Black, L.P. and McCulloch, M.T. (1990). Recurrent felsic magmatism: an isotopic case history from the Georgetown Inlier, Queensland. Geochimica et Cosmochimica Acta **54**: 183-196.

Black, L.P. and Withnall, I.W. (1993). The ages of Proterozoic granites in the Georgetown Inlier of northeastern Australia, and their relevance to the dating of tectonothermal events. AGSO Journal of Australian Geology and Geophysics **14**: 331-341.

Black, L.P., Gregory, P., Withnall, I.W. and Bain, J.H.C. (1998). U-Pb zircon age for the Etheridge Group, Georgetown region, north Queensland: implications for relationship with the Broken Hill and Mt Isa sequences. Australian Journal of Earth Sciences **45**: 925-935.

Black, L.P., Kamo, S.L., Allen, C.M., Aleinikoff, J.N., Davis, D.W., Korsch, R.J. and Foudoulis, C. (2003). TEMORA 1: a new zircon standard for Phanerozoic U-Pb geochronology. Chemical Geology **200**: 155-170.

Black, L.P., Kamo, S.L., Allen, C.M., Davis, D.W., Aleinikoff, J.N., Valley, J.W., Mundil, R., Campbell, I.H., Korsch, R.J., Williams, I.S. and Foudoulis, C. (2004). Improved $^{206}Pb/^{238}U$ microprobe geochronology by the monitoring of a trace-element-related matrix effect; SHRIMP, ID-TIMS, ELA-ICP-MS and oxygen isotope documentation for a series of zircon standards. Chemical Geology **205**: 115-140.

Black, L.P., Withnall, I.W., Gregory, P., Oversby, B.S. and Bain, J.H.C. (2005). U-Pb ages from leucogneiss in the Etheridge Group and their significance for the early history of the Georgetown region, north Queensland. Australian Journal of Earth Sciences **52**: 385-401.

Blewett, R.S., Trail, D.S. and von Gnielinski, F.E. (1992). The stratigraphy of metamorphic rocks of the Ebagoola 1:250000 sheet area in Cape York Peninsula, North Queensland. Bureau of Mineral Resources, Australia, Record **1992/74**.

Blewett, R.S., Denaro, T.J., Knutson, J., Wellman, P., Mackenzie, D.E., Cruikshank, B.I., Wilford, J.R., von Gnielinski, F.E., Pain, C.F., Sun, S.-s. and Bultitude,

R.J. (1997). Coen Region. North Queensland Geology. Bain, J.H.C. and Draper, J.J. (eds.), Australian Geological Survey Organisation Bulletin, Canberra. **240:** 117-158.

Blewett, R.S. and Black, L.P. (1998). Structural and temporal framework of the Coen Region, north Queensland: implications for major tectonothermal events in east and north Australia. Australian Journal of Earth Sciences **45**: 597-609.

Blewett, R.S., Black, L.P., Sun, S.S., Knutson, J., Hutton, L.J. and Bain, J.H.C. (1998). U-Pb zircon and Sm-Nd geochronology of the Mesoproterozoic of North Queensland: implications for a Rodinian connection with the Belt supergroup of North America. Precambrian Research **89**: 101-127.

Boger, S.D. and Hansen, D. (2004). Metamorphic evolution of the Georgetown Inlier, northeast Queensland, Australia; evidence for an accreted Palaeoproterozoic terrane? Journal of Metamorphic Geology **22**: 511-527.

Boynton, W.V. (1984). Geochemistry of the rare earth elements: meteorite studies. Rare Earth Element Geochemistry. Henderson, P. (ed.), Elsevier, Amsterdam, 63-114.

Brookfield, M.E. (1993). Neoproterozoic Laurentia-Australia fit. Geology **21**: 683-686.

Brooks, C.K., Nielsen, T.F.D. and Petersen, T.S. (1976). The Blosserville Coast basalts of east Greenland: their occurrence, composition and temporal variations. Contributions to Mineralogy and Petrology **58**: 279-292.

Brooks, C.K., Larsen, L.M. and Nielsen, T.F.D. (1991). Importance of iron-rich tholeiitic magmas at divergent plate margins: A reappraisal. Geology **19**: 269-272.

Bultitude, R.J., Rees, I.D. and Garrad, P.D. (1995). Bellevue region, sheet 7764, part 7774, 1:100000 Map Commentary. Geological Survey of Queensland.

Burrett, C. and Berry, R.F. (2000). Proterozoic Australia-Western United States (AUSWUS) fit between Laurentia and Australia. Geology **28**: 103-106.

Cihan, M. and Parsons, A. (2005). The use of porphyroblasts to resolve the history of macro-scale structures: an example from the Robertson River Metamorphics, North-Eastern Australia. Journal of Structural Geology **27**: 1027-1045.

Cihan, M., Evins, P., Lisowiec, N. and Blake, K. (2006). Time constraints on deformation and metamorphism from EPMA dating of monazite in the Proterozoic Robertson River Metamorphics, NE Australia. Precambrian Research **145**: 1-23.

Clarke, D.B. (1970). Tertiary basalts of Baffin Bay: possible primary magma from the mantle. Contributions to Mineralogy and Petrology **25**: 203-224.

Clarke, G.L., Klepeis, K.A. and Daczko, N.R. (2000). Cretaceous high-*P* granulites at Milford Sound, New Zealand: metamorphic history and emplacement in a convergent margin setting. Journal of Metamorphic Geology **18**: 359-374.

Cocherie, A., Legendre, O., Peucat, J.J. and Kouamelan, A. (1998). Geochronology of polygenetic monazites constrained by in situ electron microprobe Th-U-Total Pb determination: implications for Pb behaviour in monazite. Geochimica et Cosmochimica Acta **62**: 2475-2497.

Coffin, M.F. and Eldholm, O. (1994). Large igneous provinces; crustal structure, dimensions, and external consequences. Reviews of Geophysics **32**: 1-36.

Compston, W. (1996). SHRIMP: Origins, impact and continuing evolution. Journal of the Royal Society of Western Australia **79**: 109-117.

Compston, W., Williams, I.S. Meyer, C.E., Boynton, W.V.E. and Schubert, G.E. (1984). U-Pb geochronology of zircons from lunar breccia 73217 using a sensitive high mass-resolution ion microprobe. Journal of Geophysical Research **89**: B525-534.

Connors, K.A. and Page, R.W. (1995). Relationships between magmatism, metamorphism and deformation in the western Mt Isa Inlier, Australia. Precambrian Research **71**: 131-153.

Conor, C.H.H. and Fanning, C.M. (2001). Geochronology of the Woman-in-White amphibolite, Olary Domain. MESA Journal of Primary Industries and Resources of South Australia **20**: 41-43.

Cox, K.G. and Hornung, G. (1967). The petrology of the Karoo basalts of Basutoland. American Mineralogist **51**: 1414-1432.

Crawford, A.J. and Stevens, B.P.J. (2006). A magmatic origin for the Broken Hill orebodies? Australian Earth Sciences Convention, Melbourne, Australia, Abstracts on CD-ROM.

Dahl, P.S., Hamilton, M.A., Jercinovic, M.J., Terry, M.P., Williams, M.L. and Frei, R. (2005). Comparative isotopic and chemical geochronometry of monazite, with implications for U-Th-Pb dating by electron microprobe: An example from metamorphic rocks of the eastern Wyoming Craton (U.S.A.). American Mineralogist **90**: 619-638.

Davidson, G.J. (1994). A geochemical and geological reconnaissance study of alteration, copper-gold ores, and iron-rich lithologies in the Cloncurry area, Mt Isa Inlier. Centre for Ore Deposit and Exploration Studies, University of Tasmania.

Davidson, G.J. (1998). Variation in copper-gold styles through time in the Proterozoic Cloncurry goldfield, Mt Isa Inlier: a reconnaissance view. Australian Journal of Earth Sciences **45**: 445-462.

Davis, B.K. (1995). Regional-scale foliation reactivation and reuse during formation of a macroscopic fold in the Robertson River Metamorphics, north Queensland, Australia. Tectonophysics **242**: 293-311.

Dawson, G.C., Bryan, K., Fletcher, I.R., McNaughton, N.J. and Rasmussen, B. (2002). Did late Palaeoproterozoic assembly of proto-Australia involve collision between the Pilbara, Yilgarn and Gawler cratons? Geochronological evidence from the Mount Barren Group in the Albany-Fraser Orogen of Western Australia. Precambrian Research **118**: 195-220.

Deer, W.A., Howie, R.A. and Zussman, J. (1992). An introduction to the rock-forming minerals, Longman Scientific & Technical, Essex, England.

DePaolo, D.J. (1981). Neodymium isotopes in the Colorado Front Range and crust-mantle evolution in the Proterozoic. Nature **291**: 193-196.

DePaolo, D.J. (1988). Neodymium isotope geochemistry: An introduction. Springer Verlag, New York.

Derrick, G.M., Wilson, I.H. and Hill, R.M. (1976). Revision of stratigraphic nomenclature in the Precambrian of northwest Queensland. V: Soldiers Cap Group. Queensland Government Mining Journal **77**: 601-604.

Donaghy, A.G., Hall, M., Gibson, G.M. and Nutman, A.P. (1998). The age of deposition and first deformation of the Palaeoproterozoic Willyama Supergroup, Broken Hill, Australia. Geological Society of Australia Abstracts **49**: 118.

Donchak, P.J.T. and Bultitude, R.J. (1998). Atherton, Queensland 1:250000 Geological Series (2nd edition). Geological Survey of Queensland, Explanatory Notes SE55-5.

Embley, R.W., Jonasson, I.R., Perfit, M.R., Franklin, J.M., Tivey, M.A., Malahoff, A., Smith, M.F. and Francis, T.J.G. (1988). Submersible investigation of an extinct hydrothermal system on the Galapagos Ridge: sulfide mound, stockwork zone, and differentiated lavas. Canadian Mineralogist **26**: 517-539.

Etheridge, M.A., Rutland, R.W.R. and Wyborn, L.A.I. (1987). Orogenesis and tectonic process in the Early to Middle Proterozoic of northern Australia. Proterozoic lithosphere evolution. Kroner, A. (ed.), American Geophysical Union Geodynamics Series **17:** 131-147.

Faure, G. (1986). Principles of isotope geology. John Wiley & Sons, New York.

Ferry, J.M. and Spear, F.S. (1978). Experimental calibration of the partitioning of Fe and Mg between biotite and garnet. Contributions to Mineralogy and Petrology **66**: 113-117.

Fisk, M.R., Bence, A.E. and Schilling, J.G. (1982). Major element chemistry of Galapagos Rift Zone magmas and their phenocrysts. Earth and Planetary

Science Letters **61**: 171-189.

Fitton, J.G., Saunders, A.D., Larsen, L.M., Fram, M.S., Demant, A., Sinton, C. and Leg 152 Shipboard Scientific Party (1995). Magma sources and plumbing systems during break-up of the SE Greenland margin: preliminary results from ODP Leg 152. Journal of the Geological Society **152**: 985-990.

Fitton, J.G., Larsen, L.M., Saunders, A.D., Hardarson, B.S. and Kempton, P.D. (2000). Paleogene continental to oceanic magmatism on the SE Greenland continental margin at 63°N: a review of the results of the Ocean Drilling Program Legs 152 and 163. Journal of Petrology **41**: 951-966.

Fitzherbert, J.A., Clarke, G.L., Marmo, B. and Powell, R. (2004). The origin and *P-T* evolution of peridotites and serpentinites of NE New Caledonia: prograde interaction between continental margin and the mantle wedge. Journal of Metamorphic Geology **22**: 327-344.

Gibson, G.M. and Nutman, A.P. (2004). Detachment faulting and bimodal magmatism in the Palaeoproterozoic Willyama Supergroup, south-central Australia: keys to recognition of a multiply deformed Precambrian metamorphic core complex. Journal of the Geological Society **161**: 55-66.

Giles, D., Betts, P.G. and Lister, G.S. (2002). Far-field continental backarc setting for the 1.80-1.67 Ga basins of northeastern Australia. Geology **30**: 823-826.

Giles, D. and Nutman, A.P. (2003). SHRIMP U-Pb zircon dating of the host rocks of the Cannington Ag-Pb-Zn deposit, southeastern Mt Isa Block, Australia. Australian Journal of Earth Sciences **50**: 295-309.

Giles, D., Betts, P.G. and Lister, G.S. (2004). 1.8-1.5 Ga links between the North and South Australian Cratons and the Palaeo- to Mesoproterozoic configuration of Australia. Tectonophysics **380**: 27-41.

Giles, D., Betts, P.G., Aillères, L., Hulscher, B., Hough, M. and Lister, G.S. (2006). Evolution of the Isan Orogeny at the southeastern margin of the Mt Isa Inlier. Australian Journal of Earth Sciences **53**: 91-108.

Glikson, A.Y. and Derrick, G.M. (1978). Geology and geochemistry of the Middle Proterozoic basic volcanic belts, Mt Isa/Cloncurry north-western Queensland. Bureau of Mineral Resources Record **1978/48**.

Goldstein, S.L., O'Nions, R.K. and Hamilton, P.J. (1984). A Sm-Nd isotopic study of atmospheric dust and particulates from major river systems. Earth and Planetary Science Letters **70**: 221-236.

Graham, C.M. and Powell, R. (1984). A garnet-hornblende geothermometer: calibration, testing, and application to the Pelona Schist, Southern California. Journal of Metamorphic Geology **2**: 13-31.

Griffin, W.L., Belousova, E.A., Walters, S.G. and O'Reilly, S.Y. (2006). Archaean and Proterozoic crustal evolution in the Eastern Succession of the Mt Isa district, Australia: U-Pb and Hf-isotope studies of detrital zircons. Australian Journal of Earth Sciences **53**: 125-149.

Griselin, M., Arndt, N.T. and Baragar, W.R.A. (1997). Plume-lithosphere interaction and crustal contamination during formation of Coppermine River basalts, Northwest Territories, Canada. Canadian Journal of Earth Sciences **34**: 958-975.

Gulson, B.L. (1984). Uranium-lead and lead-lead investigations of minerals from the Broken Hill lodes and mine sequence rocks. Economic Geology **79**: 476-490.

Gulson, B.L., Perkins, W.G. and Mizon, K.J. (1983). Lead isotope studies bearing on the genesis of copper ore bodies at Mount Isa, Queensland. Economic Geology **78**: 1466-1504.

Hald, N. and Waagstein, R. (1991). The dykes and sills of the Early Tertiary Faeroe Island Baalt Plateau. Transactions of the Royal Society of Edinburgh **82**: 373-388.

Hansen, H. and Nielsen, T. (1999). Crustal contamination in Paleogene East Greenland flood basalts: plumbing system evolution during continental rifting. Chemical Geology **157**: 89-118.

Haraguchi, S. and Ishii, T. (2007). Simultaneous boninitic and arc-tholeiitic volcanisms in the Izu forearc region during early arc volcanism, based on ODP Leg 125 Site 786. Contributions to Mineralogy and Petrology **153**: 509-531.

Harrison, T.M. and McDougall, I. (1981). Excess $^{40}Ar$ in metamorphic rocks from Broken Hill, New South Wales: Implications for $^{40}Ar/^{39}Ar$ age spectra and the thermal history of the region. Earth and Planetary Science Letters **55**: 123-149.

Hatton, O.J. (2004). Sedimentology, geochemistry, volcanology and basin evolution of the Soldiers Cap Group, Eastern Succession, Mt Isa Inlier, northwest Queensland, Australia. Ph.D. Thesis, University of Tasmania (unpublished).

Hatton, O.J. and Davidson, G.J. (2004). Soldiers Cap Group iron-formations, Mt Isa Inlier, Australia, as windows into the hydrothermal evolution of a base-metal-bearing Proterozoic rift basin. Australian Journal of Earth Sciences **51**: 85-106.

Hewitt, D.A. and Wones, D.R. (1975). Physical properties of some synthetic Fe-Mg-Al trioctahedral biotites. American Mineralogist **60**: 854-862.

Hirata, T. and Nesbitt, R.W. (1995). U-Pb isotope geochronology of zircon: evaluation of the laser probe-inductively coupled plasma-mass spectrometry technique. Geochimica et Cosmochimica Acta **59**: 2491-2500.

Holland, T.J.B. and Powell, R. (1995). Linearised calibrations of the Grt-Pl-$Al_2SiO_5$-

Qtz and Grt-Pl-Ms-Bt geobarometers for medium-grade metapelites (based on Holland & Powell (1995) data set) *Excel file*. http://www.earth.ox.ac.uk/~davewa/pt/th_tools.html

Holland, T.J.B. and Powell, R. (1998). An internally consistent thermodynamic data set for phases of petrological interest. Journal of Metamorphic Geology **16**: 309-343.

Holland, T.J.B. and Powell, R. (2000). Computer program *AX*. http://www.esc.cam.ac.uk/software.html

Horn, I., Rudnick, R.L. and McDonough, W.F. (2000). Precise elemental and isotope ratio determination by simultaneous solution nebulization and laser ablation-ICP-MS: application to U-Pb geochronology. Chemical Geology **164**: 281-301.

Hoskin, P.W.O. and Black, L.P. (2000). Metamorphic zircon formation by solid-state recrystallisation of protolith igneous zircon. Journal of Metamorphic Geology **18**: 423-439.

Ireland, T.R., Flōttmann, T., Fanning, C.M., Gibson, G.M. and Preiss, W.V. (1998). Development of the early Palaeozoic Pacific margin of Gondwana from detrital-zircon ages across the Delamerian Orogen. Geology **26**: 243-246.

Ishizuka, O., Kimura, J-.I., Li, Y.B., Stern, R.J., Reagan, M.K., Taylor, R.N., Ohara, Y., Bloomer, S.H., Ishii, T., Hargrove III, U.S. and Haraguchi, S. (2006). Early stages in the evolution of Izu-Bonin arc volcanism: New age, chemical, and isotope constraints. Earth and Planetary Science Letters **250**: 385-401.

Jackson, M.J., Scott, D.L. and Rawlings, D.J. (2000). Stratigraphic framework for the Leichhardt and Calvert Superbasins: review and correlations of the pre-1700 Ma successions between Mt Isa and McArthur River. Australian Journal of Earth Sciences **47**: 381-403.

Jackson, S.E., Pearson, N.J., Griffin, W.L. and Belousova, E.A. (2004). The application of laser ablation-inductively coupled plasma-mass spectrometry to in situ U-Pb zircon geochronology. Chemical Geology **211**: 47-69.

Jahn, B-.M. and Condie, K.C. (1995). Evolution of the Kaapvaal Craton as viewed from geochemical and Sm-Nd isotopic analyses of intracratonic pelites. Geochimica et Cosmochimica Acta **59**: 2239-2258.

Jakobsen, J.K., Veksler, I.V., Tegner, C. and Brooks, C.K. (2005). Immiscible iron- and silica-rich melts in basalt petrogenesis documented in the Skaergaard intrusion. Geology **33**: 885-888.

James, S.D., Pearce, J.A. and Oliver, R.A. (1987). The geochemistry of the Lower Proterozoic Willyama Complex volcanics, Broken Hill Block, New South Wales. Geochemistry and Mineralisation of Proterozoic Volcanic Suites. Pharaoh, T.C., Beckinsale, R.D. and Rickard, D. (eds.), Geological Society

Special Publication **33**: 395-408.

Johnson, W.H. (1978). Annual report for 1977 and final report for Authority to Prospect 1613M, Stockyard Creek, Queensland. CRA Exploration Pty Ltd. Unpublished report held by the Queensland Department of Mines and Energy as CR 6599.

Karlstrom, K.E., Ahall, K.-I., Harlan, S.S., Williams, M.L., McLelland, J. and Geissman, J.W. (2001). Long-lived (1.8-1.0 Ga) convergent orogen in the southern Laurentia, its extensions to Australia and Baltica, and implications for Rodinia. Precambrian Research **111**: 5-30.

Kelsey, D.E., Powell, R., Wilson, C.J.L. and Steele, D.A. (2003). (Th+U)-Pb monazite ages from Al-Mg-rich metapelites, Rauer Group, east Antarctica. Contributions to Mineralogy and Petrology **146**: 326-340.

Knutson, J. and Stephenson, P.J. (1989). East Australian volcanic geology; Northern Queensland. Intraplate volcanism in eastern Australia and New Zealand. Johnson, R.W., Knutson, J. and Taylor, S.R. (eds.), Cambridge University Press, Cambridge, UK: 89-97.

Knutson, J. and Sun, S.S. (1997). Sm-Nd isotope geochemistry. North Queensland Geology. Bain, J.H.C., Draper, J.J. (eds.), Australian Geological Survey Organisation Bulletin 240-Queensland Geology 9, 126.

Kohn, M.J. and Spear, F.S. (1989). Empirical calibration of geobarometers for the assemblage garnet + plagioclase + quartz. American Mineralogist **74**: 77-84.

Kohn, M.J. and Spear, F.S. (1990). Two new geobarometers for garnet amphibolites, with applications to southeastern Vermont. American Mineralogist **75**: 89-96.

Kretz, R. (1983). Symbols for rock-forming minerals. American Mineralogist **68**: 277-279.

Kroner, A. (1979). Precambrian crustal evolution in the light of plate tectonics and the undation theory. Geologie en Mijnbouw **58**: 231-240.

Kuno, H. (1969). Plateau basalts. The Earth's crust and upper mantle. Hart, P. (ed.), American Geophysical Union Geophysical Monograph **13**: 495-501.

Laing, W.P. (1998). Structural-metasomatic environment of the East Mt Isa Block base-metal-gold province. Australian Journal of Earth Sciences **45**: 413-428.

Larsen, H.C. and Jakobsdóttir, S. (1988). Distribution, crustal properties and significance of seawards-dipping sub-basement reflectors off E Greenland. Early Tertiary Volcanism and the Opening of the NE Atlantic. Morton, A.C. and Parson, L.M. (eds.), Geological Society Special Publication **39**: 95-114.

Larsen, L.M., Fitton, J.G. and Fram, M.S. (1998). Volcanic rocks of the Southeast Greenland margin in comparison with other parts of the North Atlantic

Tertiary Igneous Province. Proceedings ODP, Initial Reports, 152. Saunders, A.D., Larsen, H.C. and Wise, S.W., Jr. (eds.), College Station, Texas, 315-330.

Larsen, H.C., Duncan, R.A., Allan, J.F. and Brooks, K. (eds.) (1999a). Proceedings of the Ocean Drilling Program, Scientific Results, 163. College Station, Texas.

Larsen, L.M., Fitton, J.G. and Saunders, A.D. (1999b). Composition of volcanic rocks from the Southeast Greenland margin, Leg 163: major and trace element geochemistry. Proceedings ODP, Scientific Results, 163. Larsen, H.C., Duncan, R.A., Allan, J.F. and Brooks, K. (eds.), College Station, Texas, 63-75.

Le Bas, M.J., Le Maitre, R.W., Streckeisen, A. and Zanettin, B.A. (1986). Chemical classification of volcanic rocks based on the total alkali-silica diagram. Journal of Petrology **27**: 745-750.

Li, X.-H., Liang, X., Sun, M., Guan, H. and Malpas, J.G. (2001). Precise $^{206}Pb/^{238}U$ age determination on zircons by laser ablation microprobe-inductively coupled plasma-mass spectrometry using continuous laser ablation. Chemical Geology **175**: 209-219.

Lightfoot, P.C., Naldrett, A.J., Gorbachev, N.S., Doherty, W. and Fedorenko, V.A. (1990). Geochemistry of the Siberian Trap of the Noril'sk area, USSR, with implications for the relative contributions of crust and mantle to flood basalt magmatism. Contributions to Mineralogy and Petrology **104**: 631-644.

Lightfoot, P.C. and Keays, R.R. (2005). Siderophile and chalcophile metal variations in flood basalts from the Siberian Trap, Noril'sk region: implications for the origin of the Ni-Cu-PGE sulfide ores. Economic Geology **100**: 439-462.

Ludwig, K. (2003). *Isoplot* version 3.0 – a geochronological toolkit for Microsoft Excel. Berkeley Geochronology Centre, Special Publication No. 4, 71 pp. http://www.bgc.org/klprogrammenu.html

Maas, R., Kamenetsky, M.B., Sobolev, A.V., Kamenetsky, V.S. and Sobolev, N.V. (2005). Sr, Nd, and Pb isotope evidence for a mantle origin of alkali chlorides and carbonates in the Udachnaya kimberlite, Siberia. Geology **33**: 549-552.

MacCready, T. (2006). Structural evolution of the southern Mt Isa Valley. Australian Journal of Earth Sciences **53**: 27-40.

MacCready, T., Goleby, B.R., Goncharov, A., Drummond, B.J. and Lister, G.S. (2006). Shifts in the locus of crustal thickening during Mesoproterozoic orogenesis in the Mt Isa Terrane. Australian Journal of Earth Sciences **53**: 41-53.

Mackenzie, D.E., Henderson, G.A.M., Warnick, J.V. and Bain, J.H.C. (1985). Geology of the Croydon Region, Queensland, 1:250000 map, Bureau of Mineral Resources, Australia.

Mahoney, J. (1987). An isotopic survey of Pacific oceanic plateaus; implications for their nature and origin. Geophysical Monograph **43**: 207-220.

Mahoney, J., Storey, M., Duncan, R.A., Spencer, K.J. and Pringle, M.S. (1993). Geochemistry and geochronology of Leg 130 basement lavas: nature and origin of the Ontong Java Plateau. Proceedings of the Ocean Drilling Program, Scientific Results **130**: 3-22.

Mallikharjuna Rao, J., Poornachandra Rao, G.V.S., Widdowson, M. and Kelly, S.P. (2005). Evolution of Proterozoic mafic dyke swarms of the Bundelkhand Granite Massif, Central India. Current Science **88**: 502-506.

Manikyamba, C., Kerrich, R., Naqvi, S.M. and Ram Mohan, M. (2004). Geochemical systematics of tholeiitic basalts from the 2.7 Ga Ramagiri-Hungund composite greenstone belt, Dharwar craton. Precambrian Research **134**: 21-39.

Marsh, J.S. (2004). Rare earth element geochemistry of Insizwa Lobe of the Mount Ayliff Complex, Eastern Cape, South Africa. South African Journal of Science **100**: 556-560.

Marsh, J.S., Hooper, P.R., Rehacek, J., Duncan, R.A. and Duncan, A.R. (1997). Stratigraphy and age of Karoo basalts of Lesotho and implications for correlations within the Karoo Igneous Province. Large Igneous Provinces: Continental, Oceanic, and Planetary Flood Volcanism. Mahoney, J.J. and Coffin, M.F. (eds.), American Geophysical Union Monograph, Washington D.C. **100**: 247-272.

Mawson, D. (1912). Geological investigations in the Broken Hill area. Memoirs of the Royal Society of South Australia **11**: 211-319.

McDonald, G.D., Collerson, K.D. and Kinny, P.D. (1997). Late Archaean and early Proterozoic crustal evolution of the Mount Isa Block, Northwest Queensland, Australia. Geology **25**: 1095-1098.

McNaughton, N.J. (1980). An isotopic, geochemical and structural study of the Proterozoic Einasleigh Metamorphics, northern Queensland. Ph.D. thesis, University of Queensland (unpublished).

McNaughton, N.J. and Wilson, A.F. (1983). The geochemical and oxygen-isotope affinities of Proterozoic mafic granulites from the Einasleigh Metamorphics, northern Queensland. Precambrian Research **21**: 21-37.

Mezger, K. and Krogstad, E.J. (1997). Interpretation of discordant U-Pb zircon ages; an evaluation. Journal of Metamorphic Geology **15**: 127-140.

Momme, P., Tegner, C., Brooks, C.K. and Keays, R.R. (2002). The behaviour of Platinum-Group Elements in basalts from the East Greenland rifted margin. Contributions to Mineralogy and Petrology **143**: 133-153.

Montel, J., Foret, S., Veschambre, M., Nicollet, C. and Provost, A. (1996). Electron microprobe dating of monazite. Chemical Geology **131**: 37-53.

Montel, J.M., Kornprobst, J. and Vielzeuf, D. (2000). Preservation of old U-Th-Pb ages in shielded monazite: example from the Beni Bousera Hercynian kinzigites (Morocco). Journal of Metamorphic Geology **18**: 335-342.

Mutter, J.C. and Zehnder, C.M. (1988). Deep crustal structure and magnetic processes: the inception of seafloor spreading in the Norwegian-Greenland Sea. Early Tertiary Volcanism and the Opening of the NE Atlantic. Morton, A.C. and Parson, L.M. (eds.), Geological Society Special Publication **39**: 35-48.

Myers, J.S., Shaw, R.D. and Tyler, I.M. (1996). Tectonic evolution of Proterozoic Australia. Tectonics **15**: 1431-1446.

Neal, C.R., Mahoney, J., Kroenke, L.W., Duncan, R.A. and Petterson, M.G. (1997). The Ontong Java Plateau. Large Igneous Provinces: Continental, Oceanic, and Planetary Flood Volcanism. Mahoney, J.J. and Coffin, M.F. (eds.), American Geophysical Union Monograph, Washington D.C. **100**: 183-216.

Neudert, M.K. and Russell, R.E. (1981). Shallow water and hypersaline features from the Middle Proterozoic Mount Isa Sequence. Nature **293**: 284-286.

Noe-Nygaard, A. and Pedersen, A.K. (1974). Progressive chemical variation in a tholeiitic lava sequence at Kap Stosch, Northeastern Greenland. Bulletin of the Geological Society of Denmark **23**: 175-190.

Norrish, K. and Hutton, J.T. (1969). An accurate X-ray spectrographic method for the analysis of a wide range of geological samples. Geochimica et Cosmochimica Acta, **33**: 431-453.

Nutman, A.P. and Ehlers, K. (1998). Evidence for multiple Palaeoproterozoic thermal events and magmatism adjacent to the Broken Hill Pb-Zn-Ag orebody, Australia. Precambrian Research **90**: 203-238.

Nyblade, A.A. and Sleep, N.H. (2003). Long lasting epeirogenic uplift from mantle plumes and the origin of the Southern African Plateau. Geochemistry, Geophysics, Geosystems **4(12)**: 1105, doi:10.1029/2003GC000573.

O'Dea, M.G., Lister, G.S., MacCready, T., Betts, P.G., Oliver, K.S., Pound, K.S., Huang, W. and Valenta, R.K. (1997). Geodynamic evolution of the Proterozoic Mount Isa terrain. Orogeny Through Time. Burg, J.-P. and Ford, M. (eds.), Geological Society Special Publication **121**: 99-122.

Oliver, N.H.S. (1995). Hydrothermal history of the Mary Kathleen fold belt, Mt Isa Block, Queensland. Australian Journal of Earth Sciences **42**: 267-279.

Oliver, N.H.S., Holcombe, R.J., Hill, E.J. and Pearson, P.J. (1991). Tectono-metamorphic evolution of the Mary Kathleen fold belt, northwest Queensland:

a reflection of mantle plume processes? Australian Journal of Earth Sciences **38**: 425-456.

Onley, P.G. (1978). A-P 1497M, Einasleigh, Queensland. Annual report for 1977. Unpublished report held by the Queensland Department of Mines and Energy as CR 6724.

Oversby, B.S. (1981). Preliminary report on concordant barite and base-metal sulphide deposits in Proterozoic Einasleigh Metamorphics of the Werrington area, Georgetown Inlier, northeastern Australia. Geological Society of Australia, Abstracts **3**: 13.

OZCHEM 2000. Ozchem National Whole Rock Geochemistry GIS Database. Geoscience Australia, Canberra. http://www.ga.gov.au/oracle/#geochem

Page, R.W. (1988). Geochronology of Early to Middle Proterozoic Foldbelts in northern Australia: a review. Precambrian Research **40/41**: 1-19.

Page, R.W. and Bell, T.H. (1986). Isotopic and structural response of granite to successive deformation and metamorphism. Journal of Geology **94**: 365-379.

Page, R.W. and Laing, W.P. (1992). Felsic metavolcanic rocks related to the Broken Hill Pb-Zn-Ag orebody, Australia: Geology, depositional age, and timing of high-grade metamorphism. Economic Geology **87**: 2138-2168.

Page, R.W. and Sun, S.-s. (1998). Aspects of geochronology and crustal evolution in the Eastern fold belt, Mt Isa inlier. Australian Journal of Earth Sciences **45**: 343-362.

Page, R.W., Jackson, M.J. and Krassay, A.A. (2000). Constraining sequence stratigraphy in North Australian basins: SHRIMP U-Pb zircon geochronology between Mt. Isa and McArthur River. Australian Journal of Earth Sciences **47**: 431-459.

Page, R.W., Stevens, B.P.J., Gibson, G.M. and Conor, C.H.H. (2000). Geochronology of the Willyama Supergroup between Olary and Broken Hill, and comparison with northern Australia. Australian Geological Survey Organisation Record **2000/10**: 72-75.

Page, R.W., Griffin, T.J., Tyler, I.M. and Sheppard, S. (2001). Geochronological constraints on tectonic models for Australian Palaeoproterozoic high-K granites. Journal of the Geological Society **158**: 535-545.

Page, R.W., Stevens, B.P.J. and Gibson, G.M. (2005a). Geochronology of the sequence hosting the Broken Hill Pb-Zn-Ag orebody, Australia. Economic Geology **100**: 633-661.

Page, R.W., Conor, C.H.H., Stevens, B.P.J., Gibson, G.M., Preiss, W.V. and Southgate, P.N. (2005b). Correlation of Olary and Broken Hill Domains, Curnamona Province: possible relationship to Mount Isa and other North

Australian Pb-Zn-Ag-bearing successions. Economic Geology **100**: 663-676.

Pearce, J.A. (1983). The role of sub-continental lithosphere in magma genesis at destructive plate margins. Continental basalts and mantle xenoliths. Hawkesworth, C.J. and Norry, M.J. (eds.), Shiva, Nantwich, 230-249.

Peate, D.W., Baker, J.A., Blichert-Toft, J., Hilton, D.R., Storey, M., Kent, A.J.R., Brooks, C.K., Hansen, H., Pedersen, A.K. and Duncan, R.A. (2003). The Prinsen of Wales Bjerge Formation lavas, East Greenland: the transition from tholeiitic to alkalic magmatism during Palaeogene continental breakup. Journal of Petrology **44**: 279-304.

Peccerillo R. and Taylor, S.R. (1976). Geochemistry of Eocene calc-alkaline volcanic rocks from the Kastamonu area, Northern Turkey. Contributions to Mineralogy and Petrology **58**: 63-81.

Perchuk, L.L., Podlesskii, K.K. and Aranovich, L.Y. (1981). Calculation of thermodynamic properties of end-member minerals from natural parageneses. Themodynamics of minerals and melts. Saxena, S.K. (ed.). Springer-Verlag, New York, 111-129.

Perchuk, L.L. and Lavrent´eva I.V. (1983). Experimental investigation of exchange equilibria in the system cordierite-garnet-biotite. Kinetics and equilibrium in mineral reactions, advances in physical geochemistry. Saxena, S.K. (ed.). Springer-Verlag, New York, 199-239.

Perfit, M.R., Ridley, W.I. and Jonasson, I.R. (1999). Geologic, petrologic and geochemical relationships between magmatism and massive sulfide mineralization along the eastern Galapagos spreading center. Volcanic-associated massive sulfide deposits. Barry, T. and Hannington, M. (eds.), Reviews in Economic Geology, **8**: 75-100.

Philipp, H., Eckhardt, J.-D. and Puchelt, H. (2001). Platinum-Group Elements (PGE) in basalts of the seaward-dipping reflector sequence, SE Greenland coast. Journal of Petrology **42**: 407-432.

Phillips, G.N., Archibald, N.J. and Wall, V.J. (1985). Metamorphosed high-Fe tholeiites: their alteration and relationship to sulphide mineralization, Broken Hill, Australia. Transactions of the Geological Society of South Africa **88**: 49-59.

Pin, C., Briot, D., Bassin, C. and Poitrasson, F. (1994). Concomitant separation of strontium and samarium-neodymium for isotopic analysis in silicate samples, based on specific extraction chromatography. Analytica Chimica Acta **298**: 209-217.

Pouchou, L. and Pichoir, F. (1984). A new model for quantitative X-ray microanalysis. La Recherche Aerospatiale **3**: 167-192.

Powell, R. and Holland, T.J.B. (1988). An internally consistent dataset with uncertainties and correlations: 3. Applications to geobarometry, worked examples and a computer program. Journal of Metamorphic Geology **6**: 173-204.

Raetz, M., Krabbendam, M. and Donaghy, A.G. (2002). Compilation of U-Pb zircon data from the Willyama Supergroup, Broken Hill region, Australia: evidence for three tectonostratigraphic successions and four magmatic events? Australian Journal of Earth Sciences **49**: 965-983.

Raveggi, M., Giles, D., Foden, J. and Raetz, M. (2006). High Fe-Ti mafic magmatism and tectonic setting of the Broken Hill Inlier, NSW, Australia. Australian Earth Sciences Convention, Melbourne, Australia, Abstracts on CD-ROM.

Ridley, W.I., Perfit, M.R., Jonasson, I.R. and Smith, M. (1994). Hydrothermal alteration in oceanic ridge volcanics: a detailed study at the Galapagos fossil hydrothermal field. Geochimica et Cosmochimica Acta **58**: 2477-2494.

Rollinson, H. (1993). Using geochemical data: evaluation, presentation, and interpretation, Longman Scientific & Technical, Essex, England.

Ross, G.M., Parrish, R.R. and Winston, D. (1992). Provenance and U-Pb geochronology of the Mesoproterozoic Belt Supergroup (Northwestern United States): implication for age of deposition and pre-Panthalassa plate reconstructions. Earth and Planetary Science Letters **113**: 57-76.

Rubatto, D., Williams, I.S. and Buick, I.S. (2001). Zircon and monazite response to prograde metamorphism in the Reynolds Range, central Australia. Contributions to Mineralogy and Petrology **140**: 458-468.

Rudnick, R.L. (1992). Restites, Eu anomalies, and the lower continental crust. Geochimica et Cosmochimica Acta **56**: 963-970.

Rutherford, L., Barovich, K., Hand, M. and Foden, J. (2006). Continental *ca* 1.7-1.69 Ga Fe-rich metatholeiites in the Curnamona Province, Australia: a record of melting of a heterogeneous, subduction-modified lithosphere. Australian Journal of Earth Sciences **53**: 501-519.

Saunders, A.D., Fitton, J.G., Kerr, A.C., Norry, M.J. and Kent, R.W. (1997). The North Atlantic Igneous Province. Large Igneous Provinces: Continental, Oceanic, and Planetary Flood Volcanism. Mahoney, J.J. and Coffin, M.F. (eds.), American Geophysical Union Monograph, Washington D.C. **100**: 45-93.

Sayab, M. (2006). Decompression through clockwise *P-T* path: implications for early N-S shortening orogenesis in the Mesoproterozoic Mt Isa Inlier (NE Australia). Journal of Metamorphic Geology **24**: 89-105.

Schilling, J.G., Anderson, R.N. and Vogt, P.R. (1976). Rare earth, Fe and Ti variations along the Galapagos spreading center and their relationship to the

Galapagos mantle plume. Nature **261**: 108-113.

Scott, D.L., Rawlings, D.J., Page, R.W., Tarlowski, C.Z., Idnurm, M., Jackson, M.J. and Southgate, P.N. (2000). Basement framework and geodynamic evolution of the Palaeoproterozoic superbasins of north-central Australia: an integrated review of geochemical, geochronological and geophysical data. Australian Journal of Earth Sciences **47**: 341-380.

Self, S., Thordarson, T. and Keszthelyi, L. (1997). Emplacement of Continental Flood Basalt Lava Flows. Large Igneous Provinces: Continental, Oceanic, and Planetary Flood Volcanism. Mahoney, J. and Coffin, M.F. (eds.), American Geophysical Union Monograph, Washington D.C. **100**: 381-410.

Shaw, C.A., Karlstrom, K.E., Williams, M.L., Jercinovic, M.J. and McCoy, A.M. (2001). Electron microprobe monazite dating of ca. 1.7-1.63 and ca. 1.45-1.38 Ga deformation in the Homestake Shear Zone, Colorado: origin and evolution of a persistent intracontinental tectonic zone. Geology **29**: 739-742.

Sharma, M. (1997). Siberian Traps. Large Igneous Provinces: Continental, Oceanic, and Planetary Flood Volcanism. Mahoney, J. and Coffin, M.F. (eds.), American Geophysical Union Monograph, Washington D.C. **100**: 273-295.

Sinton, J.M., Wilson, D.S., Christie, D.M., Hey, R.N. and Delaney, J.R. (1983). Petrologic consequences of rift propagation on oceanic spreading ridges. Earth and Planetary Science Letters **62**: 193-207.

Spear, F.S. (1993). Metamorphic Phase Equilibria and Pressure-Temperature-Time Paths, Mineralogical Society of America Monograph, Washington D.C., U.S.A.

Stevens, B.P.J. (1986). Post-depositional history of the Willyama Supergroup in the Broken Hill block, NSW. Australian Journal of Earth Sciences **33**: 73-98.

Stevens, B.P.J., Barnes, R.G., Brown, R.E., Stroud, W.J. and Willis, I.L. (1988). The Willyama Supergroup in the Broken Hill and Eurowie Blocks, New South Wales. Precambrian Research **40-41**: 297-327.

Stroud, W.J., Willis, I.L., Bradley, G.M., Brown, R.E., Stevens, B.P.J. and Barnes, R.G. (1983). Amphibole and/or pyroxene-bearing rocks. Rocks of the Broken Hill Block: their Classification, Nature, Stratigraphic Distribution and Origin. Stevens, B.P.J. and Stroud, W.J. (eds.), Records of the NSW Geological Survey, **20**: 227-288.

Sun, S.S. and McDonough, W.F. (1989). Chemical and isotopic systematics of oceanic basalts: implications for mantle composition and processes. Magmatism in ocean basins. Saunders, A.D. and Norry, M.J. (eds.), Geological Society of London Special Publication, **42**: 313-345.

Suzuki, K., Adachi, M. and Tanaka, T. (1991). Middle Precambrian provenance of Jurassic sandstone in the Mino Terrane, central Japan: Th-U-total Pb evidence

from an electron microprobe monazite study. Sedimentary Geology **75**: 141-147.

Tera, F. and Wasserburg, G.J. (1972). U-Th-Pb systematics in three Apollo 14 basalts and the problem of initial Pb in lunar rocks. Earth and Planetary Science Letters **14**: 281-304.

Thirlwall, M.F., Upton, B.G.J. and Jenkins, C. (1994). Interaction between continental lithosphere and the Iceland Plume – Sr-Nd-Pb isotope geochemistry of Tertiary basalts, NE Greenland. Journal of Petrology **35**: 839-879.

Tiepolo, M. (2003). In situ Pb geochronology of zircon with laser ablation-inductively coupled plasma-sector field mass spectrometry. Chemical Geology **199**: 159-177.

Toplis, M.J. and Carroll, M.R. (1995). An experimental study of the influence of oxygen fugacity on Fe-Ti oxide stability, phase relations, and mineral-melt equilibria in ferro-basaltic systems. Journal of Petrology **36**: 1137-1170.

Tyler, I.M., Pirajno, F., Bagas, L., Myers, J.S. and Preston, W.A. (1998). The geology and mineral deposits of the Proterozoic in Western Australia. AGSO Journal of Australian Geology and Geophysics **17**: 223-244.

Tyler, I.M., Page, R.W. and Griffin, T.J. (1999). Depositional age and provenance of the Marboo Formation from SHRIMP U-Pb zircon geochronology; implications for the early Palaeoproterozoic tectonic evolution of the Kimberley region, Western Australia. Precambrian Research **95**: 225-243.

van Achterbergh, E., Ryan, C.G., Jackson, S.E. and Griffin, W.L. (2001). Data reduction software for LA-ICP-MS: appendix. Laser Ablation-ICP-Mass Spectrometry in the Earth Sciences: Principles and Applications. Sylvester, P.J. (ed.), Mineralogical Association of Canada (MAC) Short Course Series, Ottawa, Ontario, Canada, **29**: 239-243.

Vernon, R.H. (1969). The Willyama Complex, Broken Hill area. Journal of the Geological Society of Australia **16**: 20-65.

Waagstein, R., Hald, N., Jorgensen, O., Nielsen, P.H., Noe-Nygaard, A., Rasmussen, J. and Schönharting, G. (1984). Deep drilling on the Faeroe Islands. Bulletin of the Geological Society of Denmark **32**: 133-138.

Walters, S.G. (1998). Broken Hill-type deposits. AGSO Journal of Australian Geology & Geophysics **17**: 229-237.

Wasserburg, G.J., Jacobson, S.B., DePaolo, D.J., McCulloch, M.T. and Wen, J. (1981). Precise determinations of Sm/Nd ratios, Sm and Nd isotopic abundances in standard solutions. Geochimica et Cosmochimica Acta **45**: 2311-2323.

Weaver, B.L. and Tarney, J. (1984). Major and trace element composition of the

continental lithosphere. Physics and Chemistry of the Earth **15**: 39-68.

White, D.A. (1965). The geology of the Georgetown/Clarke River area, Queensland. Bureau of Mineral Resources, Australia Bulletin **71**.

White, R.S. and McKenzie, D. (1995). Mantle plumes and flood basalts. Journal of Geophysical Research **100**: 17543-17585.

Wiedenbeck, M., Hanchar, J.M., Peck, W.H., Sylvester, P., Valley, J., Whitehouse, M., Kronz, A., Morishita, Y., Nasdala, L., Fiebig, J., Franchi, I., Girard, J.P., Greenwood, R.C., Hinton, R., Kita, N., Mason, P.R.D., Norman, M., Ogasawara, M., Piccoli, P.M., Rhede, D., Satoh, H., Schulz-Dobrick, B., Skar, O., Spicuzza, M.J., Terada, K., Tindle, A., Togashi, S., Vennemann, T., Xie, Q. and Zheng, Y.F. (2004). Further characterisation of the 91500 zircon crystal. Geostandards and Geoanalytical Research **28**: 9-39.

Williams, M.L., Jercinovic, M.J. and Terry, M. (1999). High resolution "age" mapping, chemical analysis, and chemical dating of monazite using the electron microprobe: a new tool for tectonic analysis. Geology **27**: 1023-1026.

Williams, M.L. and Jercinovic, M.J. (2002). Microprobe monazite geochronology: putting absolute time into microstructural analysis. Journal of Structural Geology **24**: 1013-1028.

Williams, P.J. (1998a). Metalliferous economic geology of the Mt Isa Eastern Succession, Queensland. Australian Journal of Earth Sciences **45**: 329-341.

Williams, P.J. (1998b). Magmatic iron enrichment in high-iron metatholeiites associated with 'Broken Hill-type' Pb-Zn-Ag deposits, Mt Isa Eastern Succession. Australian Journal of Earth Sciences **45**: 389-396.

Williams, P.J. and Smith, M.J. (2003). Pb-Zn-(As) enrichments in amphibolites from the Broken Hill-type ore systems, NW Queensland: Products of retrograde hydrothermal dispersion. Geochemistry: Exploration, Environment, Analysis **3**: 245-261.

Willis, I.L., Brown, R.E., Stroud, W.J. and Stevens, B.P.J. (1983). The early Proterozoic Willyama Supergroup: stratigraphic subdivision and interpretation of high- to low-grade metamorphic rocks in the Broken Hill Block, New South Wales. Journal of the Geological Society of Australia **30**: 195-224.

Wilson, M. (1989). Igneous Petrogenesis. Kluwer Academic Publishers, The Netherlands.

Winchester, J.A. and Floyd, P.A. (1977). Geochemical discrimination of different magma series and their differentiation products using immobile elements. Chemical Geology **20**: 325-343.

Wingate, M.T.D. and Evans, D.A.D. (2003). Palaeomagnetic constraints of the Proterozoic tectonic evolution of Australia. Proterozoic of East Gondwana:

Supercontinent assembly and breakup. Yoshida, M., Windley, B. and Dasgupta, S. (eds.), Geological Society of London Special Publication, **206**: 77-91.

Withnall, I.W. (1983). The Robertson River Subgroup and Cobbold Metadolerite - revised Proterozoic units in the Georgetown Inlier, north Queensland. Queensland Government Mining Journal **84**: 182-190.

Withnall, I.W. (1984). Stratigraphy, structure and metamorphism of the Proterozoic Etheridge and Langlovale Groups, central Georgetown Inlier, north Queensland. Geological Survey of Queensland, Record **1984/59** (unpublished).

Withnall, I.W. (1985). Geochemistry and tectonic significance of Proterozoic mafic rocks from the Georgetown Inlier, north Queensland. BMR Journal of Australian Geology & Geophysics **9**: 339-351.

Withnall, I.W. (1989). Precambrian and Palaeozoic geology of the southeastern Georgetown Inlier, north Queensland, Queensland Department of Mines, Report **2**: 1-102.

Withnall, I.W. (1996). Stratigraphy, structure and metamorphism of the Proterozoic Etheridge and Langlovale Groups, Georgetown region, north Queensland. Australian Geological Survey Organisation Record **1996/15**.

Withnall, I.W. and Mackenzie, D.E. (1980). New and revised stratigraphic units in the Proterozoic Georgetown Inlier, north Queensland. Queensland Government Mining Journal **81**: 28-43.

Withnall, I.W., Bain, J.H.C. and Rubenach, M.J. (1980). The Precambrian geology of northeast Queensland. The Geology and Geophysics of Northeastern Australia. Henderson, R.A. and Stephenson, P.J. (eds.), Geological Society of Australia, Queensland Division, Brisbane, 109-127.

Withnall, I.W., Bain, J.H.C., Draper, J.J., Mackenzie, D.E. and Oversby, B.S. (1988a). Proterozoic stratigraphy and tectonic history of the Georgetown Inlier, northeastern Queensland. Precambrian Research **40/41**: 429-446.

Withnall, I.W., Lang, S.C., Jell, J.S., McLennan, T.P.T., Talent, J.A., Mawson, R., Fleming, P.J.G., Law, S.R., Macansh, J.D., Savory, P., Kay, J.R. and Draper, J.J. (1988b). Stratigraphy, sedimentology, biostratigraphy, and tectonics of the Ordovician to Carboniferous Broken River Province, north Queensland. Australian Sedimentologists Group Field Guide Series No. 5. Geological Society of Australia Inc.

Withnall, I.W., Black, L.P. and Harvey, K.J. (1991). Geology and geochronology of the Balcooma area – part of an early Palaeozoic magmatic belt in north Queensland. Australian Journal of Earth Sciences, **38**: 15-29.

Withnall, I.W., MacKenzie, D.E., Denaro, T.J., Bain, J.H.C., Oversby, B.S., Knutson,

J., Donchak, P.J.T., Champion, D.C., Wellman, P., Cruikshank, B.I., Sun, S.-s. and Pain, C.F. (1997). Chapter 3. Georgetown Region. North Queensland Geology. Bain, J.H.C. and Draper, J.J. (eds.), Australian Geological Survey Organisation Bulletin **240:** 19-116.

Withnall, I.W. and Blight, R.K.J. (2003). Geology of the Forsayth region, Queensland, 1:100000 map, Department of Natural Resources and Mines, Queensland.

Withnall, I.W., Blight, R.K.J. and Pascoe, G.S. (2003a). Geology of the Gilberton region, Queensland, 1:100000 map, Department of Natural Resources and Mines, Queensland.

Withnall, I.W., Blight, R.K.J. and Gatehouse, N.C. (2003b). Geology of the North Head region, Queensland, 1:100000 map, Department of Natural Resources and Mines, Queensland.

Woodhead, J.A., Rossman, G.R. and Silver, L.T. (1991). The metamictization of zircon: radiation dose dependent structural characteristics. American Mineralogist **76**: 74-82.

Wu, C-.M. and Cheng, B-.H. (2006). Valid garnet-biotite (GB) geothermometry and garnet-aluminium silicate-plagioclase-quartz (GASP) geobarometry in metapelitic rocks. Lithos **89**: 1-23.

Wyborn, L.A.I. (1987). The petrology and geochemistry of alteration assemblages in the Eastern Creek Volcanics, as a guide to copper and uranium mobility associated with regional metamorphism and deformation, Mount Isa, Queensland. Geochemistry and Mineralization of Proterozoic Volcanic Suites. Pharaoh, T.C., Beckinsale, R.D. and Rickard, D. (eds.), Geological Society Special Publication **33**: 425-434.

Wyborn, L.A.I. (1998). Younger *ca* 1500 Ma granites of the Williams and Naraku Batholiths, Cloncurry district, eastern Mt Isa Inlier: geochemistry, origin, metallogenic significance and exploration indicators. Australian Journal of Earth Sciences **45**: 397-411.

Wyborn, L.A.I. (2001). Broken Hill Block Synthesis. The Metallogenic Potential of Australian Proterozoic Granites. Budd, A.R., Wyborn, L.A.I. and Bastrakova, I.V. (eds.), Australian Geological Survey Organisation Record **2001/12**.

Wynne-Edwards, H.R. (1972). Proterozoic ensialic orogenesis; the millipede model of ductile plate tectonics. American Journal of Science **276**: 927-953.

Zhao, J. (1994). Geochemical and Sm-Nd isotopic study of amphibolites in the southern Arunta inlier, central Australia: Evidence for subduction at a Proterozoic continental margin. Precambrian Research **65**: 71-94.

Zhao, J.X. and McCulloch, M.T. (1995). Geochemical and Nd isotopic systematics of granites from the Arunta Inlier, central Australia: implications for Proterozoic

crustal evolution. Precambrian Research **71**: 265-299.

# APPENDIX

**Contents:**

# Appendix 1: Representative Thin Section Descriptions

The thin sections described below are representative of the lithologies discussed in Chapters 2 and 3. Where heterogeneities in the lithologies were observed more than one sample description is provided. Thin sections of samples used in geochemical, geochronological, and thermobarometric analysis are also described here. Sample locations including grid references are presented in Appendix 6.

**Einasleigh Metamorphics**

**282:** Einasleigh Metamorphics mica schist collected from outcrop south of Gilberton Fault near Gum Flats. Sample contains small abundant laths of quartz, fine-grained muscovite and biotite surrounding garnet porphyroblasts. Garnet porphyroblasts are generally small (up to 1 mm diameter), and subhedral to anhedral.

**283:** Very strongly foliated muscovite schist from same outcrop as sample 282. Sample contains quartz, abundant muscovite, anhedral biotite. Garnet porphyroblasts (up to 1 mm diameter) also occur, but are less common in this sample.

**317:** Biotite gneiss from outcrop near Percyvale. Contains coarse-grained subhedral biotite laths, quartz, andesine to albite, calcite, small garnet porphyroblasts, and accessory sphene and Fe-Ti oxide (possibly haematite). Thin discontinuous layers of retrogressive sericite have also replaced a prograde phase, possibly sillimanite.

**318:** Einasleigh Metamorphics amphibolite containing foliated euhedral but rounded olive hornblende, albite, and lesser quartz, clinopyroxene and Fe-Ti oxide. Sample is near granulite facies or high-grade amphibolite facies, but is probably equivalent to amphibolites from lower grade areas.

**324:** Coarse-grained muscovite-biotite-quartz mica-schist. Sample contains large clots of muscovite and biotite, in addition to quartz and lesser albite. Metamorphic monazite is accessory.

**Bernecker Creek Formation**

**7:** Psammitic rock with 60-70% fine-grained quartz. Abrupt change to pelitic texture containing micro-granular quartz. Small percentage of calcite and Fe-Ti oxide also present in psammitic section.

**10:** Fine-grained psammitic rock containing muscovite and quartz as the dominant matrix phases, along with accessory fine-grained albite, epidote and biotite.

**13:** Pelite containing fine-grained epidote occurring as bands of aligned prismatic grains. Some chlorite and lesser Fe-Ti oxide also associated with the epidote bands. Surrounding matrix comprises fine-grained quartz.

**124:** Psammo-pelitic rock containing up to 50% fine-grained quartz, and lesser fine-grained calcite, muscovite, and accessory Fe-Ti oxide.

**292:** Fine-grained mica schist containing layer-parallel foliation. Dominant phase is calcite, with lesser fine-grained biotite, muscovite, quartz, and feldspar also present.

**293:** Moderately to strongly foliated biotite-muscovite-garnet-bearing schist. Small elongated grains of plagioclase, quartz, and lesser calcite comprise the remainder of the matrix. Inclusion-rich garnet porphyroblasts are anhedral to subhedral and vary from 1 to 3 mm in diameter. The inclusions are

mainly quartz, and define a foliation that is generally consistent with the matrix foliation. The garnet porphyroblasts are surrounded by strain-shadows comprising quartz and fine-grained biotite.

**307:** Fine-grained biotite schist containing equigranular anhedral biotite, quartz, and lesser muscovite, feldspar, and accessory Fe-Ti oxide.

**Daniel Creek Formation**

**97:** Strongly foliated, very fine-grained muscovite schist, also containing quartz, biotite, and lesser calcite and albite. Small porphyroblasts of a prograde metamorphic mineral (possibly staurolite) have been pseudomorphed by chlorite. Muscovite-rich/quartz-poor and muscovite-poor/quartz-rich layering is visible consistent with small-scale changes to the clastic composition of the sedimentary precursor.

**184:** Low-grade, very fine-grained quartz-muscovite sandstone. Quartz dominates (~80 %) and is surrounded by sericitic muscovite, and accessory zircon. Patches of an opaque mineral (possibly haematite) are scattered throughout, comprising ~5 % of the sample.

**255:** Fine-grained sandstone containing ~80 % quartz surrounded by sericitic muscovite, and accessory zircon.

**288:** Moderately- to strongly-foliated biotite-muscovite-garnet-bearing schist. Small aligned laths of biotite and muscovite define the dominant layer-parallel schistosity ($S_1$). Small elongate quartz constitutes the remainder of the matrix. Garnet porphyroblasts are anhedral to subhedral, and are generally less than 1 mm in diameter. The other porphyroblast-forming phase has been completely pseudomorphed by retrograde chlorite. These porphyroblasts are commonly tabular, anhedral, and range up to 3 mm in diameter. Inclusion trails of quartz in these porphyroblasts commonly define a foliation orthogonal to the matrix foliation.

**308:** Strongly foliated, fine-grained biotite-muscovite-quartz mica schist. Biotite and muscovite define the layer-parallel schistosity, while quartz and lesser plagioclase comprise the remainder of the matrix. Metamorphic monazite is accessory.

**311:** Mica-schist containing fine- to coarse-grained biotite, muscovite, fine-grained quartz, small (up to 1 mm diameter) garnet porphyroblasts, and lesser feldspar and chlorite. A second small porphyroblast-forming phase (possibly of an aluminosilicate) has been sericitised.

**312:** Weakly foliated, garnet-hornblende-bearing calc-silicate gneiss. Peak metamorphic assemblage consists of garnet, hornblende, and fine-grained quartz and plagioclase. Lesser calcite, actinolite, and zoisite also occur. Small elongate hornblende defines a weak layer-parallel foliation, and is the most common form of hornblende in this sample. Garnet porphyroblasts have diameters up to 4 mm, are anhedral to subhedral, and contain large inclusions of quartz. Hornblende porphyroblasts have diameters up to 2 mm, are commonly anhedral, and also contain numerous large quartz inclusions.

**Dead Horse Metabasalt**

**72:** Foliated, low-greenschist facies metabasalt containing fine-grained actinolite, albite, chlorite, epidote, and accessory Fe-Ti oxide. A thin (less than 1 mm wide) quartz-calcite vein cuts the foliation. Igneous texture and some relic igneous clinopyroxene are locally preserved.

**74:** Relatively undeformed greenschist facies metabasalt containing sparse, fine-grained actinolite, albite, chlorite, relic igneous clinopyroxene and lesser plagioclase, and calcite. Accessory Fe-Ti oxide also common.

**80:** Greenschist facies metabasalt containing weak foliation denoted by alignment of elongate, fine-grained feldspar laths. Dominant minerals include chlorite, actinolite, albite, some relic igneous clinopyroxene, and accessory Fe-Ti oxide. Thin section contains one large relic clinopyroxene grain containing alteration rim of chlorite and Fe-Ti oxide.

**82:** Aphyric, greenschist facies metabasalt containing actinolite, albite, chlorite, epidote, accessory Fe-Ti oxide, and minor relic igneous clinopyroxene. Relic igneous texture is relatively well preserved.

**83:** Weakly foliated, aphyric, greenschist facies rock containing albite, actinolite, chlorite, epidote, and sparse very fine-grained Fe-Ti oxide. One, possibly two relic clinopyroxene grains are preserved, and outlines of larger replaced clinopyroxene grains are visible.

**87:** Weakly-foliated greenschist facies metabasalt. Aphyric, but well preserved sample containing chlorite, albite, fibrous actinolite, epidote/zoisite, and accessory Fe-Ti oxide.

**89:** Weakly foliated, low-greenschist facies metabasalt containing fine-grained albite, actinolite, chlorite, epidote, and accessory Fe-Ti oxide. Epidote has grown proximal to larger actinolite grains.

**90:** Upper-greenschist facies aphyric metabasalt containing pale-green actinolite, albite, clinozoisite, sphene, and accessory chlorite and Fe-Ti oxide.

**100:** Weakly-foliated greenschist facies metabasalt containing well preserved igneous texture. Contains actinolite, albite, chlorite, epidote, minor relic clinopyroxene, and accessory Fe-Ti oxide. Rare assemblage of igneous plagioclase and an altered olivine phenocryst is also observed.

**102, 103:** Fine-grained, weakly-foliated, greenschist facies metabasalts containing well preserved igneous texture. Rare olivine and clinopyroxene phenocrysts are replaced by epidote and chlorite respectively. Dominant phases are chlorite, albite, and actinolite, with lesser relic igneous minerals, epidote, and Fe-Ti oxide.

**104:** Greenschist facies metabasalt with well preserved igneous texture, including rare, largely replaced relic olivine and clinopyroxene phenocrysts. Mineral assemblage is albite, actinolite, clinopyroxene, olivine, chlorite, epidote, calcite, and lesser Fe-Ti oxide. Medium-grained calcite and chlorite vein cuts sample normal to section orientation.

**107:** Weakly foliated, fine-grained, lower-greenschist facies metabasalt containing medium-grained quartz, actinolite, chlorite, albite, calcite, and lesser relic clinopyroxene, and Fe-Ti oxide.

**111:** Low- to mid-greenschist facies metabasalt containing fine-grained actinolite, albite, quartz, chlorite, and minor epidote and Fe-Ti oxide. Relic igneous clinopyroxene and plagioclase form sub-ophitic texture.

**148:** Fine-grained greenschist facies metabasalt with near-aphyric texture containing fibrous actinolite and albite, and very fine-grained chlorite, quartz, and minor Fe-Ti oxide.

**151, 153, 154:** Aphyric greenschist facies metabasalts containing fine-grained actinolite, albite, chlorite, and relic clinopyroxene.

**228:** Aphyric greenschist facies metabasalt containing fine-grained actinolite and albite. Accessory minerals are biotite, quartz, and minor Fe-Ti oxide.

**229, 230, 236, 240:** Aphyric greenschist facies metabasalts containing fine-grained actinolite and albite. Accessory phases include quartz and minor chalcopyrite. Hematite and ilmenite (with possible limonite) form concentric growth bands around chalcopyrite grains.

**232, 243:** Coarser-grained aphyric metabasalts containing actinolite, albite, relic igneous clinopyroxene, and accessory chalcopyrite.

**233:** Well preserved, quenched pillow basalt metamorphosed to greenschist facies containing fine-grained actinolite, chlorite, and albite.

**234:** Fine-grained greenschist facies metabasalt, originally forming basalt pillow rim. Relic igneous plagioclase and olivine phenocrysts are almost completely replaced by quartz, calcite, and chlorite. Groundmass altered to anhedral chlorite and very fine-grained actinolite.

**250, 251:** Fine-grained, greenschist facies sub-ophitic metabasalts containing actinolite, albite, quartz, minor calcite and Fe-Ti oxide, and relic clinopyroxene and plagioclase altered to chlorite and epidote.

**253:** Aphyric greenschist facies metabasalt containing fine-grained actinolite, albite, chlorite, calcite, quartz, and accessory Fe-Ti oxide.

**256:** Aphyric lower-greenschist facies metabasalt containing fine-grained calcite, chlorite, albite, and accessory Fe-Ti oxide.

**260, 269:** Thoroughly recrystallised medium-grained, foliated amphibolite containing elongate hornblende in an albite-quartz groundmass.

**261:** Weakly foliated, fine-grained amphibolite containing hornblende, quartz, albite, and minor Fe-Ti oxide. Accessory chalcopyrite without Fe-oxide alteration rim also identified.

**262:** Medium- to coarse-grained amphibolite containing hornblende, albite, quartz, and Fe-Ti oxide.

**264:** Foliated, medium-grained amphibolite containing hornblende, albite, quartz, and accessory Fe-Ti oxide. Sample is cut by thin (10 mm thick) felsic vein of the same mineralogy as the host rock, however coarser-grained albite and quartz dominate.

**268:** Fine-grained, weakly-foliated amphibolite. Hornblende is the dominant phase, with minor phases including quartz, Fe-Ti oxide, and albite.

**270:** Strongly foliated amphibolite containing fine-grained hornblende, quartz, albite, and minor Fe-Ti oxide.

**Corbett Formation**

**278B:** Weakly foliated phyllite containing very fine-grained quartz, muscovite, lesser biotite, and accessory Fe-Ti oxide. Alternating muscovite-rich/quartz-poor and muscovite-poor/quartz-rich layers are common.

**306:** Foliated muscovite-biotite-schist collected near Robinhood, containing phenocrysts of staurolite after garnet. Small aligned laths of biotite and muscovite define the dominant $S_3$ foliation. Both garnet and staurolite porphyroblasts are inclusion-rich and variable in size; however staurolite is generally larger (2 to 5 mm in diameter), and partially encloses some garnet grains. Garnet porphyroblasts are small (up to 1 mm in diameter), anhedral to subhedral, and contain small inclusion trails of quartz that with staurolite define an earlier ($S_1$) foliation that is generally orthogonal to the external schistosity.

**Lane Creek Formation**

**245:** Chloritoid-bearing meta-siltstone containing very fine-grained quartz and fibrous muscovite. Lesser biotite and accessory Fe-Ti oxide are also present within the matrix.

**304:** Fine- to medium-grained mica-schist containing foliated, elongate muscovite, fine-grained blocky quartz, and lesser biotite. Large porphyroblasts of a prograde metamorphic mineral have been pseudomorphed by blocky quartz, muscovite and chlorite.

**Cobbold Metadolerite**

**6:** Mid-greenschist facies metadolerite containing actinolite, interstitial quartz, albite, epidote, sericitic muscovite, and accessory zircon. Sample is cut by late-stage tonalitic vein (10-20 mm wide) containing anhedral quartz, albite, and lesser actinolite and epidote.

**8:** Unusual syenite/quartz-free diorite containing plagioclase, K-feldspar, calcite, interstitial chlorite-actinolite, sphene, Fe-Ti oxide, and accessory zircon.

**22:** Low-greenschist facies metadolerite containing medium- to fine-grained actinolite, epidote, interstitial quartz, and lesser albite, and sericite.

**23:** Low- to mid-greenschist facies metadolerite containing abundant blue-green hornblende in addition to albite, epidote, interstitial quartz, and lesser sericitic muscovite.

**60:** Mid-greenschist facies metadolerite containing large (cm-size) actinolite, albite, and fine-grained epidote, chlorite, and Fe-Ti oxide.

**85, 86:** High-greenschist facies metadolerites containing medium- to coarse-grained hornblende, plagioclase-albite, and fine-grained epidote, quartz, and altered Fe-Ti oxide.

**88:** Fine-grained, weakly foliated metadolerite containing actinolite, albite, Fe-Ti oxide, and lesser epidote and chlorite.

**101:** Coarse-grained, well-preserved greenschist facies metadolerite containing blue-green actinolite, albite, and lesser epidote, chlorite, and Fe-Ti oxide. Several small grains of igneous clinopyroxene are also visible.

**106:** Low- to mid-greenschist facies metadolerite containing medium-grained brown hornblende rimmed by fibrous green actinolite, albite, quartz and apatite needles, and accessory Fe-Ti oxide.

**108, 109, 110, 112:** Coarse-grained greenschist facies metadolerites containing blue-green actinolite, albite, interstitial quartz, epidote, chlorite, and large altered Fe-Ti oxide.

**113, 114, 115:** Largely ophitic, coarse-grained low-greenschist facies metadolerites containing rare altered olivine, actinolite, albite, chlorite, epidote, interstitial quartz, and accessory Fe-Ti oxide.

**120, 121:** Low-greenschist facies metadolerites with coarse-grained actinolite overprinting clinopyroxene, albite, epidote, chlorite, and accessory Fe-Ti oxide. Preserved igneous texture is near-ophitic in places.

**128, 129:** Greenschist facies, well-preserved metadolerites containing actinolite after clinopyroxene, albite, interstitial quartz, and lesser epidote.

**130:** Greenschist facies metadolerite with pegmatoidal segregation showing myrmekitic texture. Sample contains fine- to medium-grained actinolite, albite, and lesser quartz, epidote, and Fe-Ti oxide.

**152:** Medium- to fine-grained greenschist facies metadolerite containing actinolite after clinopyroxene, albite, chlorite, interstitial quartz, and minor Fe-Ti oxide.

**159, 161:** Fine- to medium-grained greenschist facies metadolerites containing minor felsic segregations showing myrmekitic texture. Samples contain actinolite, albite, quartz, chlorite, lesser Fe-Ti oxide and igneous clinopyroxene.

**172:** Fine- to medium-grained greenschist facies metadolerite containing late-stage felsic differentiate with quartz, albite, chlorite, epidote, and accessory zircon. Mafic section contains medium-grained actinolite, chlorite, albite, and quartz.

**174:** Fine- to medium-grained granophyric sample showing myrmekitic texture. Sample contains albite, quartz, calcite, chlorite, and lesser biotite.

**175:** Fine- to medium-grained greenschist facies metadolerite containing actinolite, albite, quartz, and lesser chlorite and sericite.

**178:** Fine- to medium-grained greenschist facies metadolerite from CMD outcrop containing spheroidal clinozoisite-epidote xenoliths. Doleritic section contains actinolite, albite, and lesser igneous clinopyroxene.

**179:** Greenschist facies metadolerite containing actinolite after clinopyroxene, albite with sericitic alteration, chlorite, quartz, and lesser Fe-Ti oxide.

**181, 188:** Coarse-grained greenschist facies metadolerites containing actinolite after clinopyroxene, Fe-Ti oxide, and finer-grained albite, quartz and chlorite.

**192, 194, 195, 196, 197, 199, 200:** Mid- to high-greenschist facies metadolerites containing medium-grained actinolite, albite, quartz, and lesser calcite and Fe-Ti oxide. Fe-Ti oxide in sample 195 is mostly altered to sphene.

**201:** High-greenschist facies metadolerite, transitional to amphibolite. Sample contains fine-grained actinolite, albite, quartz, and lesser Fe-Ti oxide.

**202:** Very fine-grained feldspar-poor greenschist facies metadolerite from sill margin. Sample contains actinolite, albite, quartz, and accessory Fe-Ti oxide.

**215:** Amphibolite facies metadolerite containing clear, euhedral, medium-grained hornblende, albite with sericitic alteration, quartz, and accessory Fe-Ti oxide.

**221, 222:** Greenschist facies metadolerites containing coarse-grained actinolite, albite, chlorite, quartz, and accessory Fe-Ti oxide altered to sphene.

**224, 226:** Fine-grained greenschist facies metadolerites containing actinolite, albite, chlorite, quartz, and minor Fe-Ti oxide.

**227:** Fine-grained greenschist facies metadolerite or coarse metabasalt containing actinolite, albite, chlorite, and accessory Fe-Ti oxide.

**237:** Blocky holocrystalline greenschist facies metabasalt or fine-grained metadolerite containing actinolite, albite, sericite, and accessory Fe-Ti oxide.

**241:** Fine-grained greenschist facies metadolerite containing actinolite after clinopyroxene, albite, chlorite, calcite, minor igneous plagioclase, and accessory haematite surrounding chalcopyrite.

**242, 249:** Fine-grained greenschist facies metadolerites containing actinolite after clinopyroxene, albite, chlorite, calcite, and accessory Fe-Ti oxide and chalcopyrite.

**291:** Texturally well-preserved greenschist facies metadolerite containing fine-grained actinolite after clinopyroxene, albite, some igneous plagioclase, sericite, and accessory Fe-Ti oxide.

**296:** Greenschist facies metadolerite containing abundant, subhedral to anhedral actinolite after clinopyroxene, albite, and accessory Fe-Ti oxide.

**299, 300:** Strongly recrystallised amphibolite facies metadolerites containing blue-green hornblende, albite, quartz, lesser sericite, and small clusters of Fe-Ti oxide.

**301:** Fine-grained sub-ophitic strongly recrystallised amphibolite facies metadolerite containing hornblende after clinopyroxene, albite, quartz, lesser sericite, and accessory Fe-Ti oxide.

**Ropewalk Granite**

**208, 209, 210:** Medium- to coarse-grained biotite-muscovite granites. Biotite is the dominant mica, and accessory phases include quartz, sphene (absent in sample 208), alkali feldspar (accessory in sample 208), lesser plagioclase, and accessory zircon. All samples are weakly foliated; however the foliation is most intense in sample 210.

**Mount Hogan Granite**

**135:** Unfoliated medium- to coarse-grained granite containing quartz, microcline, fine-grained muscovite, and accessory zircon.

# APPENDIX 2:

# Zircon LA-ICPMS and EMPA Monazite data

**Table 1.** Zircon U-Pb LA-ICPMS data for mafic samples from the lower Etheridge Group.

| Sample/analysis | | U ppm | Th/U | 206Pb/238U | ± | 207Pb/235U | ± | 207Pb/206Pb | ± | 207Pb/206Pb age (Ma) | ± |
|---|---|---|---|---|---|---|---|---|---|---|---|
| 6 | 1 | 1380 | 0.55 | 0.2908 | 0.0018 | 4.027 | 0.056 | 0.1008 | 0.0014 | 1639 | 26 |
| | 2 | 786 | 0.45 | 0.3004 | 0.0021 | 4.158 | 0.067 | 0.1013 | 0.0017 | 1649 | 31 |
| | 3 | 592 | 0.45 | 0.2849 | 0.0017 | 3.956 | 0.061 | 0.1009 | 0.0015 | 1641 | 27 |
| | 4 | 397 | 0.39 | 0.2968 | 0.0025 | 4.563 | 0.091 | 0.1124 | 0.0022 | 1838 | 35 |
| | 5 | 763 | 0.50 | 0.2907 | 0.0037 | 4.067 | 0.145 | 0.1050 | 0.0036 | 1714 | 64 |
| | 6 | 1160 | 0.51 | 0.2860 | 0.0019 | 3.901 | 0.059 | 0.0994 | 0.0015 | 1613 | 27 |
| | 7 | 481 | 0.44 | 0.2849 | 0.0043 | 4.130 | 0.164 | 0.1105 | 0.0043 | 1807 | 72 |
| | 8 | 749 | 0.46 | 0.2848 | 0.0020 | 4.184 | 0.079 | 0.1068 | 0.0019 | 1745 | 32 |
| | 9 | 393 | 0.39 | 0.2834 | 0.0024 | 4.045 | 0.087 | 0.1046 | 0.0023 | 1706 | 41 |
| | 10 | 511 | 0.30 | 0.2638 | 0.0019 | 4.086 | 0.078 | 0.1131 | 0.0021 | 1850 | 33 |
| | 11 | 1242 | 0.52 | 0.2953 | 0.0019 | 4.074 | 0.058 | 0.1006 | 0.0015 | 1635 | 28 |
| | 12 | 1440 | 0.59 | 0.2877 | 0.0050 | 3.892 | 0.108 | 0.1023 | 0.0024 | 1666 | 44 |
| 8 | 1 | 907 | 0.52 | 0.2855 | 0.0056 | 3.831 | 0.140 | 0.0998 | 0.0032 | 1620 | 59 |
| | 2 | 1216 | 0.46 | 0.2880 | 0.0046 | 4.136 | 0.149 | 0.1014 | 0.0033 | 1650 | 61 |
| | 3 | 1615 | 0.52 | 0.2881 | 0.0025 | 3.991 | 0.059 | 0.1014 | 0.0014 | 1650 | 25 |
| | 4 | 1485 | 0.64 | 0.2838 | 0.0026 | 3.917 | 0.061 | 0.1006 | 0.0014 | 1635 | 26 |
| | 5 | 321 | 0.28 | 0.2889 | 0.0035 | 3.859 | 0.090 | 0.0986 | 0.0023 | 1598 | 43 |
| | 6 | 983 | 0.46 | 0.2702 | 0.0036 | 3.806 | 0.070 | 0.1025 | 0.0017 | 1670 | 31 |
| | 7 | 393 | 0.15 | 0.3542 | 0.0046 | 12.094 | 0.394 | 0.2467 | 0.0068 | 3164 | 44 |
| | 8 | 1146 | 0.57 | 0.2602 | 0.0091 | 3.583 | 0.173 | 0.1034 | 0.0046 | 1686 | 82 |
| | 9 | 1308 | 0.52 | 0.2879 | 0.0025 | 3.941 | 0.057 | 0.0999 | 0.0014 | 1623 | 25 |
| | 10 | 1233 | 0.51 | 0.2846 | 0.0028 | 3.901 | 0.059 | 0.1008 | 0.0015 | 1638 | 28 |
| | 11 | 831 | 0.43 | 0.2528 | 0.0026 | 3.505 | 0.057 | 0.1015 | 0.0015 | 1651 | 28 |
| | 12 | 1312 | 0.50 | 0.2911 | 0.0026 | 4.071 | 0.061 | 0.1016 | 0.0015 | 1654 | 27 |
| 159 | 1 | 1919 | 0.96 | 0.3436 | 0.0271 | 13.946 | 2.554 | 0.2823 | 0.0363 | 3376 | 201 |
| | 2 | 763 | 1.09 | 0.3109 | 0.0083 | 4.488 | 0.179 | 0.1024 | 0.0033 | 1668 | 60 |
| | 3 | 1353 | 1.40 | 0.2880 | 0.0052 | 4.391 | 0.136 | 0.1067 | 0.0030 | 1743 | 52 |
| | 4 | 956 | 1.05 | 0.3177 | 0.0119 | 4.816 | 0.267 | 0.1048 | 0.0049 | 1711 | 86 |
| | 5 | 1187 | 0.74 | 0.2624 | 0.0060 | 4.321 | 0.189 | 0.1171 | 0.0047 | 1913 | 72 |
| | 6 | 1102 | 0.74 | 0.3025 | 0.0087 | 4.506 | 0.192 | 0.1043 | 0.0034 | 1701 | 60 |
| | 7 | 1512 | 1.19 | 0.2798 | 0.0074 | 4.349 | 0.266 | 0.1104 | 0.0056 | 1806 | 92 |
| | 8 | 1257 | 0.99 | 0.2669 | 0.0054 | 4.289 | 0.160 | 0.1127 | 0.0039 | 1844 | 63 |
| | 9 | 791 | 0.99 | 0.3037 | 0.0067 | 4.456 | 0.161 | 0.1037 | 0.0031 | 1692 | 56 |
| | 10 | 852 | 0.85 | 0.2945 | 0.0057 | 4.524 | 0.151 | 0.1068 | 0.0031 | 1745 | 53 |
| | 11 | 624 | 0.85 | 0.2978 | 0.0056 | 4.492 | 0.152 | 0.1060 | 0.0033 | 1731 | 57 |
| | 12 | 741 | 0.98 | 0.2816 | 0.0067 | 4.511 | 0.174 | 0.1129 | 0.0037 | 1847 | 59 |
| | 13 | 2025 | 1.33 | 0.2669 | 0.0046 | 3.834 | 0.111 | 0.1082 | 0.0025 | 1720 | 62 |
| | 14 | 907 | 1.04 | 0.3238 | 0.0027 | 4.477 | 0.077 | 0.1071 | 0.0018 | 1675 | 63 |
| | 15 | 1168 | 0.92 | 0.2855 | 0.0032 | 3.908 | 0.085 | 0.1059 | 0.0019 | 1716 | 90 |
| | 16 | 1017 | 1.04 | 0.3039 | 0.0027 | 3.975 | 0.067 | 0.1015 | 0.0017 | 1695 | 65 |
| | 17 | 1468 | 0.94 | 0.2743 | 0.0049 | 3.821 | 0.118 | 0.1097 | 0.0036 | 1393 | 148 |
| | 18 | 433 | 0.74 | 0.3185 | 0.0029 | 4.351 | 0.096 | 0.1066 | 0.0023 | 1673 | 134 |
| | 19 | 1290 | 0.78 | 0.2949 | 0.0023 | 4.071 | 0.074 | 0.1071 | 0.0019 | 1766 | 52 |
| | 20 | 1125 | 0.67 | 0.2822 | 0.0036 | 3.620 | 0.083 | 0.1011 | 0.0022 | 1683 | 88 |
| | 21 | 722 | 0.88 | 0.2946 | 0.0036 | 3.961 | 0.104 | 0.1022 | 0.0027 | 1561 | 121 |
| | 22 | 1933 | 1.61 | 0.2933 | 0.0021 | 3.893 | 0.059 | 0.1029 | 0.0014 | 1705 | 42 |
| | 23 | 2115 | 0.89 | 0.2270 | 0.0063 | 3.219 | 0.163 | 0.1120 | 0.0058 | 1457 | 177 |
| | 24 | 1965 | 0.77 | 0.2817 | 0.0071 | 4.170 | 0.257 | 0.1198 | 0.0066 | 1703 | 329 |

| Sample/analysis | | U ppm | Th/U | 206Pb/238U | ± | 207Pb/235U | ± | 207Pb/206Pb | ± | 207Pb/206Pb age (Ma) | ± |
|---|---|---|---|---|---|---|---|---|---|---|---|
| 161 | 1 | 928 | 1.31 | 0.3021 | 0.0021 | 4.532 | 0.115 | 0.1043 | 0.0024 | 1702 | 43 |
| | 2 | 975 | 1.21 | 0.2944 | 0.0016 | 4.455 | 0.117 | 0.1051 | 0.0026 | 1717 | 45 |
| | 3 | 1178 | 1.39 | 0.3057 | 0.0020 | 4.602 | 0.116 | 0.1047 | 0.0025 | 1710 | 44 |
| | 4 | 721 | 0.81 | 0.3166 | 0.0023 | 5.170 | 0.150 | 0.1136 | 0.0031 | 1858 | 49 |
| | 5 | 728 | 0.85 | 0.2955 | 0.0058 | 4.821 | 0.304 | 0.1066 | 0.0061 | 1742 | 106 |
| | 6 | 867 | 1.11 | 0.2972 | 0.0036 | 4.477 | 0.221 | 0.1108 | 0.0054 | 1813 | 89 |
| | 7 | 691 | 0.99 | 0.2960 | 0.0021 | 4.490 | 0.118 | 0.1061 | 0.0029 | 1733 | 51 |
| | 8 | 934 | 1.10 | 0.2956 | 0.0022 | 4.259 | 0.122 | 0.1023 | 0.0030 | 1666 | 54 |
| | 9 | 1537 | 0.62 | 0.2720 | 0.0040 | 4.266 | 0.204 | 0.1014 | 0.0050 | 1650 | 91 |
| | 10 | 832 | 0.96 | 0.2960 | 0.0022 | 4.320 | 0.112 | 0.1015 | 0.0026 | 1651 | 47 |
| | 11 | 594 | 0.99 | 0.3128 | 0.0033 | 4.688 | 0.136 | 0.1041 | 0.0031 | 1698 | 55 |
| | 12 | 688 | 0.85 | 0.3113 | 0.0075 | 5.742 | 0.342 | 0.1202 | 0.0065 | 1960 | 97 |
| | 13 | 1071 | 1.09 | 0.3030 | 0.0037 | 4.048 | 0.088 | 0.1063 | 0.0024 | 1729 | 86 |
| | 14 | 532 | 0.82 | 0.2979 | 0.0047 | 4.070 | 0.109 | 0.1099 | 0.0032 | 1620 | 157 |
| | 15 | 1070 | 0.67 | 0.2864 | 0.0038 | 4.097 | 0.109 | 0.1104 | 0.0029 | 1805 | 85 |
| | 16 | 1346 | 1.10 | 0.2845 | 0.0025 | 3.748 | 0.073 | 0.1042 | 0.0019 | 1741 | 68 |
| | 17 | 779 | 1.05 | 0.3087 | 0.0048 | 5.066 | 0.185 | 0.1231 | 0.0039 | 1722 | 150 |
| | 18 | 944 | 0.98 | 0.3028 | 0.0056 | 4.223 | 0.122 | 0.1064 | 0.0033 | 1788 | 102 |
| | 19 | 516 | 0.98 | 0.3111 | 0.0066 | 5.033 | 0.230 | 0.1298 | 0.0048 | 1923 | 189 |
| | 20 | 846 | 1.04 | 0.2839 | 0.0038 | 4.071 | 0.143 | 0.1091 | 0.0034 | 1620 | 137 |
| | 21 | 1396 | 1.27 | 0.2956 | 0.0022 | 3.933 | 0.064 | 0.1030 | 0.0017 | 1691 | 73 |
| | 22 | 1899 | 1.04 | 0.2766 | 0.0032 | 3.696 | 0.094 | 0.1067 | 0.0027 | 1680 | 64 |
| | 23 | 1120 | 1.08 | 0.3005 | 0.0027 | 4.148 | 0.093 | 0.1082 | 0.0025 | 1640 | 83 |
| | 24 | 1509 | 1.19 | 0.3007 | 0.0039 | 4.704 | 0.144 | 0.1223 | 0.0038 | 1726 | 86 |
| | 25 | 798 | 1.18 | 0.3043 | 0.0027 | 5.761 | 0.124 | 0.1398 | 0.0029 | 1622 | 136 |
| | 26 | 1164 | 1.03 | 0.2921 | 0.0029 | 4.258 | 0.108 | 0.1108 | 0.0028 | 1723 | 84 |
| | 27 | 823 | 1.34 | 0.3099 | 0.0059 | 4.710 | 0.178 | 0.1178 | 0.0040 | 1740 | 185 |
| | 28 | 1003 | 1.10 | 0.2961 | 0.0029 | 3.977 | 0.101 | 0.1036 | 0.0025 | 1534 | 101 |
| | 29 | 931 | 1.02 | 0.2998 | 0.0024 | 4.368 | 0.090 | 0.1099 | 0.0022 | 1685 | 91 |
| | 30 | 972 | 1.08 | 0.3036 | 0.0042 | 4.257 | 0.123 | 0.1081 | 0.0029 | 1707 | 91 |
| 172* | 1 | 885 | 1.00 | 0.2894 | 0.0019 | 4.320 | 0.110 | 0.1036 | 0.0027 | 1633 | 12 |
| | 2 | 556 | 0.85 | 0.4308 | 0.0064 | 21.936 | 1.196 | 0.3683 | 0.0193 | 1652 | 76 |
| | 3 | 729 | 0.75 | 0.2793 | 0.0020 | 4.182 | 0.108 | 0.1034 | 0.0027 | 1578 | 12 |
| | 4 | 1035 | 1.17 | 0.2722 | 0.0029 | 4.227 | 0.154 | 0.1043 | 0.0036 | 1537 | 17 |
| | 5 | 610 | 0.77 | 0.2988 | 0.0031 | 5.378 | 0.147 | 0.1246 | 0.0034 | 1643 | 18 |
| | 6 | 326 | 0.82 | 0.2892 | 0.0037 | 4.839 | 0.252 | 0.1113 | 0.0058 | 1617 | 23 |
| | 7 | 341 | 0.95 | 0.2911 | 0.0036 | 4.791 | 0.201 | 0.1108 | 0.0046 | 1628 | 22 |
| | 8 | 369 | 0.99 | 0.2931 | 0.0030 | 4.991 | 0.161 | 0.1179 | 0.0037 | 1625 | 18 |
| | 9 | 869 | 1.15 | 0.2777 | 0.0029 | 4.721 | 0.178 | 0.1134 | 0.0045 | 1551 | 18 |
| | 10 | 871 | 1.17 | 0.2955 | 0.0075 | 6.474 | 0.419 | 0.1406 | 0.0078 | 1594 | 42 |
| | 11 | 1073 | 0.82 | 0.2400 | 0.0046 | 5.342 | 0.326 | 0.1449 | 0.0081 | 1296 | 28 |
| | 12 | 789 | 0.94 | 0.2900 | 0.0024 | 4.616 | 0.135 | 0.1109 | 0.0032 | 1623 | 14 |
| 264 | 1 | 567 | 0.55 | 0.2849 | 0.0057 | 4.081 | 0.173 | 0.1011 | 0.0041 | 1645 | 74 |
| | 2 | 425 | 0.39 | 0.2809 | 0.0044 | 4.031 | 0.186 | 0.1035 | 0.0040 | 1688 | 72 |
| | 3 | 1033 | 0.61 | 0.2886 | 0.0063 | 4.380 | 0.171 | 0.1042 | 0.0040 | 1701 | 70 |
| | 4 | 310 | 1.03 | 0.2765 | 0.0040 | 3.900 | 0.141 | 0.0976 | 0.0032 | 1579 | 61 |
| | 5 | 543 | 0.69 | 0.2859 | 0.0022 | 4.545 | 0.101 | 0.1117 | 0.0022 | 1828 | 36 |
| | 6 | 689 | 0.81 | 0.2779 | 0.0024 | 4.315 | 0.121 | 0.1107 | 0.0029 | 1810 | 48 |
| | 7 | 1001 | 1.06 | 0.2683 | 0.0027 | 3.956 | 0.126 | 0.1024 | 0.0027 | 1668 | 48 |

* $^{207}Pb$ corrected $^{206}Pb/^{238}U$ used

| Sample/analysis | | U ppm | Th/U | 206Pb/238U | ± | 207Pb/235U | ± | 207Pb/206Pb | ± | 207Pb/206Pb age (Ma) | ± |
|---|---|---|---|---|---|---|---|---|---|---|---|
| 264 | 8 | 942 | 0.68 | 0.2617 | 0.0030 | 3.670 | 0.101 | 0.0978 | 0.0025 | 1583 | 48 |
| | 9 | 576 | 1.06 | 0.2726 | 0.0032 | 4.217 | 0.128 | 0.1077 | 0.0033 | 1760 | 56 |
| | 10 | 1076 | 0.88 | 0.2864 | 0.0030 | 4.232 | 0.094 | 0.1035 | 0.0021 | 1687 | 37 |
| | 11 | 1336 | 0.50 | 0.3008 | 0.0035 | 4.345 | 0.104 | 0.1001 | 0.0021 | 1625 | 38 |
| | 12 | 309 | 0.57 | 0.3095 | 0.0047 | 4.663 | 0.179 | 0.1046 | 0.0033 | 1707 | 59 |
| | 13* | 80 | 1.01 | 0.4123 | 0.0065 | 8.212 | 0.286 | 0.1409 | 0.0048 | 2238 | 58 |
| | 14* | 392 | 0.63 | 0.3797 | 0.0053 | 8.886 | 0.204 | 0.1643 | 0.0034 | 2500 | 35 |
| | 15* | 404 | 0.98 | 0.4170 | 0.0137 | 10.525 | 0.422 | 0.1781 | 0.0045 | 2636 | 42 |
| | 16* | 281 | 0.52 | 0.4604 | 0.0103 | 10.919 | 0.372 | 0.1654 | 0.0046 | 2511 | 47 |
| | 17* | 471 | 0.46 | 0.2988 | 0.0028 | 4.596 | 0.104 | 0.1158 | 0.0026 | 1662 | 16 |
| | 18* | 525 | 0.27 | 0.4619 | 0.0049 | 11.162 | 0.214 | 0.1823 | 0.0032 | 2373 | 29 |
| | 19* | 183 | 0.48 | 0.4989 | 0.0051 | 12.168 | 0.236 | 0.1832 | 0.0035 | 2580 | 33 |
| | 20* | 622 | 0.73 | 0.2929 | 0.0044 | 4.566 | 0.129 | 0.1176 | 0.0032 | 1627 | 25 |
| | 21* | 522 | 0.55 | 0.3030 | 0.0047 | 4.551 | 0.175 | 0.1148 | 0.0043 | 1687 | 27 |
| | 22* | 545 | 0.85 | 0.2842 | 0.0025 | 4.381 | 0.090 | 0.1171 | 0.0026 | 1581 | 14 |
| | 23* | 887 | 0.83 | 0.2889 | 0.0060 | 4.160 | 0.158 | 0.1108 | 0.0042 | 1618 | 34 |
| | 24* | 270 | 1.70 | 0.3488 | 0.0034 | 5.657 | 0.119 | 0.1228 | 0.0026 | 1918 | 19 |
| | 25* | 577 | 0.52 | 0.2985 | 0.0059 | 4.486 | 0.178 | 0.1111 | 0.0043 | 1669 | 33 |
| | 26* | 1138 | 1.04 | 0.3032 | 0.0040 | 6.112 | 0.179 | 0.1497 | 0.0035 | 1621 | 22 |
| | 27* | 827 | 0.39 | 0.2931 | 0.0037 | 4.106 | 0.113 | 0.1064 | 0.0030 | 1649 | 21 |
| | 28* | 1067 | 0.90 | 0.2900 | 0.0035 | 4.418 | 0.121 | 0.1155 | 0.0031 | 1615 | 20 |
| | 29* | 603 | 0.82 | 0.3035 | 0.0032 | 4.540 | 0.094 | 0.1118 | 0.0025 | 1695 | 18 |
| | 30* | 759 | 0.42 | 0.2881 | 0.0040 | 4.163 | 0.130 | 0.1068 | 0.0033 | 1620 | 23 |
| | 31* | 280 | 0.43 | 0.4796 | 0.0047 | 11.153 | 0.201 | 0.1739 | 0.0031 | 2500 | 29 |
| | 32* | 743 | 0.78 | 0.2885 | 0.0030 | 4.019 | 0.085 | 0.1044 | 0.0020 | 1627 | 17 |
| | 33* | 943 | 0.94 | 0.2882 | 0.0037 | 4.177 | 0.079 | 0.1085 | 0.0020 | 1618 | 21 |
| | 34* | 1011 | 0.33 | 0.2987 | 0.0027 | 4.199 | 0.081 | 0.1061 | 0.0021 | 1680 | 15 |
| | 35* | 231 | 1.66 | 0.3428 | 0.0035 | 5.583 | 0.115 | 0.1209 | 0.0028 | 1890 | 20 |
| 299* | 1 | 243 | 0.51 | 0.3147 | 0.0122 | 4.782 | 0.523 | 0.1057 | 0.0123 | 1768 | 71 |
| | 2 | 281 | 0.52 | 0.3168 | 0.0181 | 4.747 | 0.753 | 0.1016 | 0.0165 | 1787 | 105 |
| | 3 | 326 | 0.69 | 0.3172 | 0.0126 | 4.729 | 0.485 | 0.1086 | 0.0109 | 1776 | 72 |
| | 4 | 305 | 0.56 | 0.2927 | 0.0129 | 4.175 | 0.469 | 0.1049 | 0.0116 | 1649 | 73 |
| | 5 | 258 | 0.72 | 0.2945 | 0.0071 | 4.329 | 0.279 | 0.1022 | 0.0069 | 1664 | 41 |
| | 6 | 368 | 0.65 | 0.2952 | 0.0085 | 4.416 | 0.361 | 0.1095 | 0.0090 | 1655 | 49 |
| | 7 | 285 | 0.67 | 0.2604 | 0.0138 | 3.699 | 0.467 | 0.1018 | 0.0125 | 1478 | 78 |
| | 8 | 180 | 0.31 | 0.2878 | 0.0118 | 4.526 | 0.534 | 0.1172 | 0.0134 | 1601 | 68 |
| | 9 | 132 | 0.50 | 0.3163 | 0.0137 | 4.302 | 0.556 | 0.0965 | 0.0130 | 1795 | 80 |
| | 10 | 340 | 0.73 | 0.2804 | 0.0099 | 3.898 | 0.397 | 0.1040 | 0.0108 | 1584 | 57 |
| | 11 | 656 | 0.94 | 0.2966 | 0.0072 | 4.285 | 0.290 | 0.1022 | 0.0066 | 1675 | 41 |
| 300* | 1 | 189 | 0.51 | 0.2958 | 0.0091 | 3.991 | 0.355 | 0.1003 | 0.0090 | 1675 | 53 |
| | 2 | 340 | 0.48 | 0.3003 | 0.0080 | 4.348 | 0.330 | 0.1054 | 0.0079 | 1690 | 46 |
| | 3 | 439 | 0.81 | 0.2829 | 0.0072 | 4.095 | 0.297 | 0.1043 | 0.0075 | 1596 | 41 |
| | 4 | 481 | 0.59 | 0.2476 | 0.0081 | 3.377 | 0.271 | 0.0989 | 0.0075 | 1412 | 46 |
| | 5 | 369 | 0.54 | 0.2454 | 0.0106 | 3.191 | 0.304 | 0.1016 | 0.0092 | 1396 | 60 |
| | 6 | 233 | 0.58 | 0.2915 | 0.0081 | 4.388 | 0.395 | 0.1046 | 0.0089 | 1643 | 47 |
| | 7 | 164 | 0.51 | 0.2863 | 0.0106 | 3.986 | 0.438 | 0.1086 | 0.0119 | 1607 | 61 |
| | 8 | 262 | 0.47 | 0.3050 | 0.0092 | 3.901 | 0.315 | 0.0975 | 0.0078 | 1731 | 53 |
| | 9 | 488 | 0.72 | 0.2970 | 0.0071 | 4.488 | 0.300 | 0.1087 | 0.0073 | 1665 | 41 |

* $^{207}$Pb corrected $^{206}$Pb/$^{238}$U used

| Sample/analysis | | U ppm | Th/U | 206Pb/238U | ± | 207Pb/235U | ± | 207Pb/206Pb | ± | 207Pb/206Pb age (Ma) | ± |
|---|---|---|---|---|---|---|---|---|---|---|---|
| 300* | 10 | 484 | 0.66 | 0.3016 | 0.0073 | 4.104 | 0.297 | 0.0984 | 0.0069 | 1710 | 43 |
| | 11 | 759 | 0.88 | 0.2812 | 0.0205 | 4.010 | 0.722 | 0.1191 | 0.0214 | 1561 | 116 |
| | 12 | 300 | 0.53 | 0.2429 | 0.0073 | 3.243 | 0.276 | 0.0974 | 0.0079 | 1389 | 42 |
| 318* | 1 | 1335 | 0.06 | 0.2622 | 0.0160 | 3.523 | 0.601 | 0.1037 | 0.0160 | 1485 | 91 |
| | 2 | 984 | 0.52 | 0.3172 | 0.0103 | 4.211 | 0.317 | 0.0980 | 0.0074 | 1797 | 59 |
| | 3 | 782 | 0.14 | 0.3011 | 0.0156 | 3.723 | 0.552 | 0.0960 | 0.0143 | 1712 | 90 |
| | 4 | 504 | 0.01 | 0.2295 | 0.0085 | 3.068 | 0.281 | 0.0998 | 0.0098 | 1312 | 49 |
| | 5 | 1103 | 0.06 | 0.2836 | 0.0115 | 3.786 | 0.399 | 0.1026 | 0.0109 | 1604 | 66 |
| | 6 | 995 | 0.03 | 0.2877 | 0.0101 | 3.653 | 0.332 | 0.0970 | 0.0087 | 1636 | 57 |
| | 7 | 1673 | 0.01 | 0.2588 | 0.0140 | 3.508 | 0.355 | 0.1024 | 0.0105 | 1469 | 78 |
| | 8 | 1347 | 0.00 | 0.2294 | 0.0118 | 3.260 | 0.417 | 0.1055 | 0.0140 | 1304 | 67 |
| | 9 | 1453 | 0.00 | 0.2777 | 0.0121 | 3.424 | 0.414 | 0.0962 | 0.0120 | 1582 | 70 |
| | 10 | 1441 | 0.00 | 0.2455 | 0.0080 | 3.270 | 0.278 | 0.1016 | 0.0088 | 1397 | 46 |
| | 11 | 1296 | 0.00 | 0.2880 | 0.0083 | 3.727 | 0.332 | 0.0977 | 0.0089 | 1636 | 48 |
| | 12 | 770 | 0.86 | 0.2915 | 0.0157 | 3.875 | 0.559 | 0.1052 | 0.0158 | 1643 | 90 |

* $^{207}$Pb corrected $^{206}$Pb/$^{238}$U used

**Table 2.** Zircon U-Pb LA-ICPMS data for samples of the Mount Hogan Granite (135) and Ropewalk Granite (208, 209, 210).

| Sample/analysis | | U ppm | Th/U | 206Pb/238U | ± | 207Pb/235U | ± | 207Pb/206Pb | ± | 207Pb/206Pb age (Ma) | ± |
|---|---|---|---|---|---|---|---|---|---|---|---|
| 135 | 1 | 121 | 0.60 | 0.3084 | 0.0074 | 4.404 | 0.174 | 0.1013 | 0.0039 | 1648 | 71 |
| | 2 | 442 | 0.59 | 0.1432 | 0.0023 | 2.199 | 0.072 | 0.1099 | 0.0034 | 1799 | 56 |
| | 3 | 594 | 0.92 | 0.2548 | 0.0065 | 3.692 | 0.149 | 0.1021 | 0.0037 | 1662 | 67 |
| | 4 | 635 | 1.86 | 0.2345 | 0.0058 | 3.379 | 0.183 | 0.1002 | 0.0048 | 1627 | 89 |
| | 5 | 618 | 0.69 | 0.2420 | 0.0058 | 3.948 | 0.178 | 0.1128 | 0.0049 | 1844 | 79 |
| | 6 | 451 | 0.51 | 0.2599 | 0.0105 | 3.483 | 0.232 | 0.0976 | 0.0049 | 1579 | 94 |
| | 7 | 584 | 0.68 | 0.2769 | 0.0046 | 3.689 | 0.103 | 0.0943 | 0.0023 | 1514 | 47 |
| | 8 | 849 | 1.29 | 0.2531 | 0.0150 | 3.823 | 0.332 | 0.1042 | 0.0061 | 1700 | 107 |
| | 9 | 1575 | 0.04 | 0.2826 | 0.0054 | 3.797 | 0.103 | 0.0953 | 0.0024 | 1534 | 48 |
| | 10 | 698 | 0.38 | 0.2110 | 0.0030 | 3.411 | 0.095 | 0.1117 | 0.0028 | 1827 | 45 |
| | 11 | 429 | 1.40 | 0.2597 | 0.0032 | 3.557 | 0.094 | 0.0965 | 0.0025 | 1557 | 49 |
| | 12 | 1068 | 2.92 | 0.1487 | 0.0034 | 3.251 | 0.104 | 0.1560 | 0.0044 | 2413 | 48 |
| 208 | 1 | 513 | 0.35 | 0.2834 | 0.0017 | 3.879 | 0.078 | 0.0962 | 0.0019 | 1552 | 37 |
| | 2 | 696 | 0.56 | 0.2522 | 0.0016 | 3.481 | 0.078 | 0.0968 | 0.0022 | 1564 | 42 |
| | 3 | 331 | 0.36 | 0.2787 | 0.0020 | 3.911 | 0.087 | 0.0973 | 0.0019 | 1573 | 36 |
| | 4 | 734 | 0.56 | 0.2543 | 0.0028 | 3.665 | 0.109 | 0.0997 | 0.0028 | 1619 | 53 |
| | 5 | 550 | 0.45 | 0.2798 | 0.0017 | 3.895 | 0.082 | 0.0983 | 0.0020 | 1592 | 38 |
| | 6 | 298 | 0.51 | 0.2306 | 0.0029 | 3.359 | 0.142 | 0.1014 | 0.0038 | 1650 | 69 |
| | 7 | 693 | 0.40 | 0.2676 | 0.0032 | 3.730 | 0.160 | 0.0958 | 0.0041 | 1544 | 80 |
| | 8 | 995 | 0.96 | 0.2285 | 0.0051 | 3.358 | 0.211 | 0.1017 | 0.0048 | 1656 | 88 |
| | 9 | 876 | 0.41 | 0.2350 | 0.0020 | 3.346 | 0.066 | 0.1003 | 0.0018 | 1630 | 33 |
| | 10 | 711 | 0.40 | 0.2581 | 0.0046 | 3.678 | 0.141 | 0.0981 | 0.0037 | 1589 | 71 |
| | 11 | 469 | 0.46 | 0.2799 | 0.0019 | 3.785 | 0.088 | 0.0950 | 0.0021 | 1529 | 41 |
| | 12 | 218 | 0.74 | 0.2785 | 0.0029 | 3.732 | 0.099 | 0.0950 | 0.0027 | 1528 | 53 |
| 209 | 1 | 854 | 0.37 | 0.2567 | 0.0016 | 3.482 | 0.074 | 0.0952 | 0.0020 | 1532 | 39 |
| | 2 | 796 | 0.90 | 0.2684 | 0.0017 | 3.635 | 0.072 | 0.0956 | 0.0018 | 1539 | 35 |
| | 3 | 431 | 1.12 | 0.2779 | 0.0019 | 3.701 | 0.078 | 0.0940 | 0.0019 | 1508 | 38 |
| | 4 | 717 | 1.22 | 0.2637 | 0.0016 | 3.487 | 0.072 | 0.0936 | 0.0018 | 1501 | 36 |
| | 5 | 721 | 1.17 | 0.2699 | 0.0017 | 3.627 | 0.070 | 0.0948 | 0.0017 | 1523 | 34 |
| | 6 | 1509 | 1.70 | 0.2670 | 0.0014 | 3.582 | 0.059 | 0.0945 | 0.0015 | 1517 | 29 |
| | 7 | 530 | 1.05 | 0.2503 | 0.0019 | 3.390 | 0.090 | 0.0957 | 0.0025 | 1541 | 49 |
| | 8 | 265 | 0.89 | 0.2683 | 0.0023 | 3.573 | 0.092 | 0.0941 | 0.0024 | 1510 | 47 |
| | 9 | 506 | 0.37 | 0.3465 | 0.0023 | 5.146 | 0.108 | 0.1043 | 0.0020 | 1702 | 36 |
| | 10 | 1063 | 1.51 | 0.2736 | 0.0028 | 3.830 | 0.126 | 0.0963 | 0.0029 | 1554 | 57 |
| | 11 | 351 | 1.53 | 0.2630 | 0.0038 | 3.584 | 0.159 | 0.0972 | 0.0045 | 1571 | 88 |
| | 12 | 399 | 1.02 | 0.2674 | 0.0048 | 3.741 | 0.179 | 0.0995 | 0.0044 | 1614 | 82 |
| 210 | 1 | 644 | 0.97 | 0.2801 | 0.0029 | 3.941 | 0.108 | 0.0987 | 0.0026 | 1600 | 50 |
| | 2 | 260 | 0.70 | 0.2751 | 0.0025 | 3.663 | 0.094 | 0.0937 | 0.0023 | 1502 | 47 |
| | 3 | 275 | 1.15 | 0.2861 | 0.0020 | 4.106 | 0.097 | 0.1010 | 0.0023 | 1643 | 42 |
| | 4 | 390 | 0.67 | 0.2772 | 0.0023 | 3.687 | 0.084 | 0.0932 | 0.0020 | 1493 | 41 |
| | 5 | 285 | 2.12 | 0.2683 | 0.0022 | 3.628 | 0.099 | 0.0942 | 0.0024 | 1512 | 48 |
| | 6 | 309 | 0.46 | 0.2818 | 0.0023 | 3.729 | 0.092 | 0.0940 | 0.0023 | 1507 | 47 |
| | 7 | 489 | 0.20 | 0.2652 | 0.0020 | 3.531 | 0.087 | 0.0934 | 0.0021 | 1495 | 43 |
| | 8 | 531 | 0.79 | 0.2673 | 0.0029 | 3.780 | 0.099 | 0.0991 | 0.0023 | 1607 | 43 |
| | 9 | 530 | 0.80 | 0.2767 | 0.0019 | 3.814 | 0.086 | 0.0963 | 0.0021 | 1554 | 41 |
| | 10 | 314 | 2.14 | 0.2713 | 0.0024 | 3.760 | 0.105 | 0.0969 | 0.0026 | 1565 | 50 |
| | 11 | 531 | 0.76 | 0.2688 | 0.0022 | 3.645 | 0.092 | 0.0948 | 0.0022 | 1524 | 43 |
| | 12 | 195 | 1.04 | 0.2711 | 0.0029 | 3.638 | 0.107 | 0.0938 | 0.0027 | 1505 | 55 |

**Table 3.** Zircon U-Pb LA-ICPMS data for metasediments of the Daniel Creek Formation, lower Etheridge Group.

| Sample/analysis | | U ppm | Th/U | 206Pb/238U | ± | 207Pb/235U | ± | 207Pb/206Pb | ± | 207Pb/206Pb age (Ma) | ± |
|---|---|---|---|---|---|---|---|---|---|---|---|
| 184 | 1 | 1724 | 1.19 | 0.1820 | 0.0038 | 6.322 | 0.161 | 0.2613 | 0.0037 | 3085 | 38 |
| | 2 | 764 | 0.87 | 0.3882 | 0.0062 | 10.542 | 0.350 | 0.2097 | 0.0069 | 2730 | 89 |
| | 3 | 231 | 0.81 | 0.5195 | 0.0056 | 12.773 | 0.252 | 0.1864 | 0.0037 | 2711 | 33 |
| | 4 | 800 | 0.35 | 0.3608 | 0.0041 | 7.771 | 0.182 | 0.1643 | 0.0038 | 2438 | 72 |
| | 5 | 552 | 1.21 | 0.3283 | 0.0091 | 7.968 | 0.355 | 0.1887 | 0.0077 | 2308 | 229 |
| | 6 | 290 | 0.41 | 0.4450 | 0.0068 | 9.918 | 0.293 | 0.1727 | 0.0049 | 2395 | 165 |
| | 7 | 476 | 0.28 | 0.4688 | 0.0060 | 10.723 | 0.280 | 0.1751 | 0.0046 | 2607 | 43 |
| | 8 | 277 | 1.01 | 0.5155 | 0.0118 | 14.036 | 0.557 | 0.1978 | 0.0073 | 2506 | 175 |
| | 9 | 824 | 0.47 | 0.3726 | 0.0071 | 9.894 | 0.440 | 0.2012 | 0.0093 | 2743 | 95 |
| | 10 | 4015 | 0.30 | 0.0993 | 0.0035 | 3.229 | 0.173 | 0.2369 | 0.0100 | 2532 | 215 |
| | 11 | 716 | 0.75 | 0.4473 | 0.0059 | 10.503 | 0.329 | 0.1800 | 0.0054 | 2468 | 93 |
| | 12 | 186 | 0.69 | 0.4793 | 0.0052 | 10.735 | 0.258 | 0.1701 | 0.0040 | 2558 | 40 |
| | 13 | 1259 | 0.59 | 0.2485 | 0.0022 | 5.022 | 0.087 | 0.1508 | 0.0025 | 1987 | 69 |
| | 14 | 175 | 0.32 | 0.4869 | 0.0048 | 11.173 | 0.264 | 0.1735 | 0.0036 | 2592 | 34 |
| | 15 | 1502 | 1.13 | 0.2194 | 0.0038 | 6.103 | 0.152 | 0.2070 | 0.0031 | 2485 | 61 |
| | 16 | 1085 | 0.86 | 0.2724 | 0.0061 | 6.958 | 0.205 | 0.1913 | 0.0042 | 2589 | 95 |
| | 17 | 238 | 0.25 | 0.5134 | 0.0049 | 12.367 | 0.262 | 0.1816 | 0.0036 | 2668 | 33 |
| | 18 | 1279 | 1.31 | 0.2106 | 0.0044 | 5.972 | 0.152 | 0.2117 | 0.0039 | 2525 | 70 |
| | 19 | 828 | 1.13 | 0.3567 | 0.0067 | 9.616 | 0.296 | 0.2000 | 0.0065 | 2452 | 110 |
| | 20 | 263 | 1.32 | 0.3499 | 0.0086 | 5.611 | 0.253 | 0.1238 | 0.0050 | 2012 | 72 |
| | 21 | 385 | 0.72 | 0.4439 | 0.0117 | 10.327 | 0.423 | 0.1795 | 0.0084 | 2593 | 170 |
| | 22 | 1689 | 1.07 | 0.1917 | 0.0020 | 5.025 | 0.092 | 0.1959 | 0.0034 | 1985 | 92 |
| | 23 | 2233 | 0.78 | 0.1257 | 0.0040 | 3.141 | 0.104 | 0.1901 | 0.0046 | 1841 | 146 |
| | 24 | 440 | 0.16 | 0.4746 | 0.0040 | 10.267 | 0.175 | 0.1624 | 0.0028 | 2481 | 29 |
| | 25 | 125 | 0.38 | 0.4751 | 0.0049 | 10.322 | 0.225 | 0.1609 | 0.0036 | 2465 | 38 |
| | 26 | 512 | 0.48 | 0.3219 | 0.0089 | 7.817 | 0.241 | 0.1843 | 0.0035 | 2556 | 101 |
| | 27 | 934 | 1.24 | 0.2643 | 0.0040 | 7.592 | 0.163 | 0.2124 | 0.0031 | 2645 | 49 |
| | 28 | 874 | 0.84 | 0.2254 | 0.0103 | 5.089 | 0.297 | 0.1640 | 0.0080 | 2497 | 83 |
| | 29 | 3530 | 0.58 | 0.0756 | 0.0015 | 1.718 | 0.071 | 0.1649 | 0.0071 | 2507 | 72 |
| | 30 | 504 | 0.65 | 0.2640 | 0.0058 | 4.729 | 0.200 | 0.1301 | 0.0075 | 2100 | 101 |
| | 31 | 918 | 0.72 | 0.2011 | 0.0044 | 4.363 | 0.184 | 0.1576 | 0.0073 | 2430 | 79 |
| | 32 | 271 | 0.64 | 0.4641 | 0.0085 | 14.263 | 0.578 | 0.2232 | 0.0094 | 3004 | 68 |
| | 33 | 1215 | 1.69 | 0.1405 | 0.0043 | 3.175 | 0.151 | 0.1641 | 0.0087 | 2499 | 89 |
| | 34 | 199 | 0.39 | 0.3317 | 0.0056 | 5.139 | 0.205 | 0.1125 | 0.0098 | 1841 | 157 |
| | 35 | 612 | 0.56 | 0.3178 | 0.0052 | 7.289 | 0.289 | 0.1666 | 0.0069 | 2523 | 69 |
| | 36 | 856 | 1.25 | 0.2261 | 0.0081 | 4.851 | 0.247 | 0.1558 | 0.0104 | 2411 | 113 |
| | 37 | 80 | 0.47 | 0.5008 | 0.0220 | 13.723 | 0.781 | 0.1990 | 0.0164 | 2818 | 134 |
| | 38 | 149 | 1.45 | 0.5256 | 0.0114 | 13.496 | 0.568 | 0.1865 | 0.0109 | 2711 | 97 |
| | 39 | 1110 | 0.96 | 0.1919 | 0.0060 | 3.930 | 0.188 | 0.1487 | 0.0087 | 2331 | 100 |
| | 40 | 602 | 0.45 | 0.3138 | 0.0037 | 5.556 | 0.080 | 0.1303 | 0.0016 | 2101 | 22 |
| | 41 | 185 | 0.91 | 0.4962 | 0.0097 | 11.080 | 0.264 | 0.1668 | 0.0039 | 2526 | 39 |
| | 42 | 150 | 0.43 | 0.4609 | 0.0049 | 9.587 | 0.133 | 0.1530 | 0.0021 | 2380 | 23 |
| | 43 | 280 | 0.66 | 0.5194 | 0.0063 | 13.266 | 0.224 | 0.1935 | 0.0029 | 2772 | 25 |
| | 44 | 193 | 0.47 | 0.3456 | 0.0055 | 5.333 | 0.109 | 0.1153 | 0.0021 | 1885 | 34 |
| | 45 | 37 | 1.35 | 0.3327 | 0.0120 | 4.872 | 0.240 | 0.1125 | 0.0045 | 1840 | 72 |
| | 46 | 189 | 0.34 | 0.4961 | 0.0103 | 11.537 | 0.250 | 0.1734 | 0.0030 | 2590 | 29 |
| | 47 | 183 | 0.75 | 0.4412 | 0.0084 | 10.112 | 0.212 | 0.1699 | 0.0026 | 2557 | 26 |
| | 48 | 469 | 0.54 | 0.4571 | 0.0139 | 10.885 | 0.368 | 0.1815 | 0.0048 | 2666 | 44 |
| | 49 | 150 | 1.95 | 0.3598 | 0.0044 | 5.686 | 0.092 | 0.1175 | 0.0019 | 1919 | 29 |
| | 50 | 231 | 0.53 | 0.4999 | 0.0059 | 11.737 | 0.165 | 0.1732 | 0.0023 | 2589 | 22 |
| | 51 | 440 | 1.31 | 0.3182 | 0.0058 | 7.806 | 0.154 | 0.1808 | 0.0023 | 2660 | 21 |

| Sample/analysis | | U ppm | Th/U | 206Pb/238U | ± | 207Pb/235U | ± | 207Pb/206Pb | ± | 207Pb/206Pb age (Ma) | ± |
|---|---|---|---|---|---|---|---|---|---|---|---|
| 184 | 52 | 298 | 0.31 | 0.3339 | 0.0087 | 5.442 | 0.164 | 0.1189 | 0.0025 | 1940 | 37 |
| | 53 | 298 | 0.76 | 0.4087 | 0.0112 | 10.088 | 0.325 | 0.1798 | 0.0046 | 2651 | 42 |
| | 54 | 384 | 0.46 | 0.4494 | 0.0098 | 10.933 | 0.238 | 0.1795 | 0.0030 | 2648 | 28 |
| | 55 | 212 | 0.39 | 0.3871 | 0.0063 | 6.879 | 0.126 | 0.1312 | 0.0021 | 2115 | 28 |
| | 56 | 2521 | 0.40 | 0.1161 | 0.0027 | 2.856 | 0.065 | 0.1836 | 0.0028 | 2686 | 25 |
| | 57 | 1255 | 0.95 | 0.1624 | 0.0039 | 4.187 | 0.113 | 0.1883 | 0.0028 | 2727 | 24 |
| | 58 | 2290 | 0.71 | 0.1251 | 0.0031 | 3.233 | 0.079 | 0.1907 | 0.0021 | 2748 | 18 |
| | 59 | 773 | 0.80 | 0.2713 | 0.0046 | 6.890 | 0.129 | 0.1918 | 0.0030 | 2758 | 26 |
| | 60 | 209 | 1.35 | 0.2753 | 0.0044 | 3.702 | 0.069 | 0.0988 | 0.0017 | 1602 | 32 |
| | 61 | 185 | 0.51 | 0.4826 | 0.0043 | 10.678 | 0.135 | 0.1629 | 0.0020 | 2486 | 21 |
| | 62 | 148 | 0.88 | 0.2486 | 0.0084 | 4.048 | 0.147 | 0.1199 | 0.0039 | 1955 | 58 |
| | 63 | 514 | 0.46 | 0.4599 | 0.0094 | 11.149 | 0.251 | 0.1790 | 0.0034 | 2643 | 32 |
| | 64 | 237 | 0.72 | 0.5248 | 0.0192 | 12.089 | 0.404 | 0.1712 | 0.0050 | 2569 | 49 |
| | 65 | 237 | 0.74 | 0.3724 | 0.0205 | 10.286 | 0.512 | 0.2066 | 0.0069 | 2879 | 54 |
| | 66 | 406 | 0.38 | 0.4574 | 0.0141 | 9.967 | 0.316 | 0.1625 | 0.0035 | 2481 | 37 |
| | 67 | 293 | 0.34 | 0.5278 | 0.0186 | 13.219 | 0.478 | 0.1864 | 0.0052 | 2711 | 46 |
| | 68 | 259 | 0.44 | 0.4742 | 0.0122 | 10.593 | 0.278 | 0.1639 | 0.0033 | 2496 | 34 |
| | 69 | 228 | 0.76 | 0.5077 | 0.0232 | 11.856 | 0.524 | 0.1729 | 0.0059 | 2586 | 57 |
| | 70 | 360 | 0.08 | 0.3620 | 0.0117 | 6.297 | 0.215 | 0.1278 | 0.0033 | 2068 | 46 |
| | 71 | 195 | 0.26 | 0.3766 | 0.0112 | 6.212 | 0.205 | 0.1246 | 0.0050 | 2023 | 72 |
| | 72 | 68 | 1.43 | 0.4470 | 0.0143 | 9.243 | 0.271 | 0.1550 | 0.0035 | 2402 | 39 |
| | 73 | 473 | 0.41 | 0.4787 | 0.0215 | 10.379 | 0.379 | 0.1649 | 0.0053 | 2507 | 54 |
| | 74 | 180 | 0.87 | 0.4511 | 0.0148 | 11.029 | 0.394 | 0.1792 | 0.0046 | 2646 | 43 |
| | 75 | 677 | 0.69 | 0.3956 | 0.0166 | 9.987 | 0.386 | 0.1897 | 0.0053 | 2740 | 46 |
| 255 | 1 | 722 | 0.44 | 0.5362 | 0.0046 | 14.255 | 0.216 | 0.1982 | 0.0028 | 2811 | 23 |
| | 2 | 439 | 0.04 | 0.3593 | 0.0031 | 5.992 | 0.110 | 0.1248 | 0.0023 | 2026 | 32 |
| | 3 | 1910 | 0.26 | 0.2199 | 0.0027 | 11.043 | 0.190 | 0.3751 | 0.0051 | 2030 | 140 |
| | 4 | 1773 | 0.48 | 0.2085 | 0.0029 | 6.527 | 0.110 | 0.2355 | 0.0046 | 1932 | 101 |
| | 5 | 200 | 0.53 | 0.5082 | 0.0057 | 12.625 | 0.258 | 0.1882 | 0.0036 | 2727 | 32 |
| | 6 | 101 | 0.83 | 0.5469 | 0.0069 | 14.152 | 0.294 | 0.1936 | 0.0041 | 2773 | 35 |
| | 7 | 139 | 1.29 | 0.4701 | 0.0052 | 10.883 | 0.246 | 0.1730 | 0.0039 | 2587 | 38 |
| | 8 | 111 | 0.62 | 0.6094 | 0.0066 | 18.919 | 0.407 | 0.2317 | 0.0048 | 3064 | 33 |
| | 9 | 1140 | 0.15 | 0.2731 | 0.0027 | 5.493 | 0.090 | 0.1508 | 0.0022 | 1962 | 53 |
| | 10 | 773 | 0.27 | 0.3747 | 0.0033 | 9.672 | 0.151 | 0.1934 | 0.0030 | 2444 | 55 |
| | 11 | 2377 | 0.11 | 0.1440 | 0.0019 | 4.341 | 0.099 | 0.2244 | 0.0037 | 2188 | 78 |
| | 12 | 235 | 0.88 | 0.5625 | 0.0055 | 15.753 | 0.305 | 0.2088 | 0.0037 | 2896 | 28 |
| | 13 | 792 | 0.47 | 0.4901 | 0.0042 | 11.458 | 0.174 | 0.1753 | 0.0025 | 2609 | 24 |
| | 14 | 56 | 1.30 | 0.3118 | 0.0051 | 4.751 | 0.163 | 0.1154 | 0.0040 | 1886 | 63 |
| | 15 | 242 | 1.30 | 0.5195 | 0.0055 | 14.335 | 0.261 | 0.2084 | 0.0039 | 2782 | 70 |
| | 16 | 461 | 0.31 | 0.4057 | 0.0033 | 7.731 | 0.141 | 0.1429 | 0.0024 | 2262 | 29 |
| | 17 | 95 | 0.76 | 0.4308 | 0.0050 | 9.017 | 0.245 | 0.1570 | 0.0042 | 2424 | 46 |
| | 18 | 897 | 0.78 | 0.2494 | 0.0038 | 5.060 | 0.086 | 0.1536 | 0.0034 | 1920 | 108 |
| | 19 | 212 | 0.75 | 0.3789 | 0.0054 | 10.020 | 0.209 | 0.2010 | 0.0043 | 2684 | 109 |
| | 20 | 145 | 0.79 | 0.3625 | 0.0040 | 5.619 | 0.151 | 0.1169 | 0.0032 | 1910 | 50 |
| | 21 | 304 | 1.15 | 0.3485 | 0.0035 | 5.513 | 0.121 | 0.1189 | 0.0025 | 1940 | 38 |
| | 22 | 408 | 1.27 | 0.5253 | 0.0047 | 13.539 | 0.224 | 0.1914 | 0.0031 | 2754 | 27 |
| | 23 | 625 | 0.26 | 0.3427 | 0.0030 | 5.609 | 0.104 | 0.1230 | 0.0022 | 2000 | 31 |
| | 24 | 444 | 0.38 | 0.3503 | 0.0033 | 5.449 | 0.110 | 0.1172 | 0.0024 | 1913 | 37 |
| | 25 | 428 | 0.17 | 0.4863 | 0.0045 | 11.434 | 0.205 | 0.1749 | 0.0028 | 2605 | 27 |
| | 26 | 683 | 0.37 | 0.3451 | 0.0033 | 5.673 | 0.111 | 0.1239 | 0.0023 | 2013 | 33 |

| Sample/analysis | | U ppm | Th/U | 206Pb/238U | ± | 207Pb/235U | ± | 207Pb/206Pb | ± | 207Pb/206Pb age (Ma) | ± |
|---|---|---|---|---|---|---|---|---|---|---|---|
| 255 | 27 | 770 | 0.58 | 0.5040 | 0.0043 | 12.140 | 0.172 | 0.1800 | 0.0027 | 2653 | 25 |
| | 28 | 338 | 0.58 | 0.5635 | 0.0324 | 14.008 | 0.768 | 0.1823 | 0.0069 | 2910 | 47 |
| | 29 | 190 | 0.74 | 0.5912 | 0.0229 | 16.831 | 0.623 | 0.2106 | 0.0061 | 2910 | 47 |
| | 30 | 706 | 0.36 | 0.4703 | 0.0108 | 10.572 | 0.264 | 0.1670 | 0.0026 | 2528 | 26 |
| | 31 | 498 | 0.04 | 0.4861 | 0.0079 | 10.688 | 0.231 | 0.1636 | 0.0027 | 2493 | 27 |
| | 32 | 77 | 0.86 | 0.3383 | 0.0043 | 5.246 | 0.104 | 0.1150 | 0.0023 | 1880 | 36 |
| | 33 | 723 | 0.02 | 0.4633 | 0.0054 | 10.106 | 0.134 | 0.1608 | 0.0018 | 2464 | 19 |
| | 34 | 893 | 0.74 | 0.3780 | 0.0051 | 11.079 | 0.157 | 0.2155 | 0.0025 | 2948 | 19 |
| | 35 | 608 | 0.33 | 0.4894 | 0.0057 | 11.817 | 0.155 | 0.1770 | 0.0020 | 2625 | 19 |
| | 36 | 327 | 0.23 | 0.4867 | 0.0079 | 11.329 | 0.182 | 0.1703 | 0.0023 | 2561 | 23 |
| | 37 | 278 | 0.39 | 0.3803 | 0.0070 | 6.407 | 0.142 | 0.1283 | 0.0027 | 2074 | 37 |
| | 38 | 359 | 1.54 | 0.3494 | 0.0056 | 5.790 | 0.116 | 0.1216 | 0.0022 | 1979 | 33 |
| | 39 | 476 | 0.25 | 0.3361 | 0.0037 | 5.205 | 0.071 | 0.1142 | 0.0014 | 1868 | 22 |
| | 40 | 285 | 1.00 | 0.3584 | 0.0037 | 5.714 | 0.081 | 0.1171 | 0.0016 | 1913 | 25 |
| | 41 | 213 | 0.74 | 0.3669 | 0.0037 | 5.975 | 0.086 | 0.1197 | 0.0016 | 1952 | 25 |
| | 42 | 588 | 0.60 | 0.4793 | 0.0088 | 11.990 | 0.266 | 0.1830 | 0.0033 | 2681 | 30 |
| | 43 | 392 | 0.83 | 0.3484 | 0.0035 | 5.750 | 0.076 | 0.1212 | 0.0015 | 1974 | 22 |
| | 44 | 261 | 0.19 | 0.3884 | 0.0045 | 7.021 | 0.110 | 0.1325 | 0.0018 | 2131 | 24 |
| | 45 | 160 | 0.72 | 0.5416 | 0.0073 | 14.584 | 0.222 | 0.1979 | 0.0025 | 2809 | 20 |
| | 46 | 194 | 0.71 | 0.4973 | 0.0054 | 12.154 | 0.151 | 0.1792 | 0.0022 | 2646 | 20 |
| | 47 | 407 | 0.34 | 0.3468 | 0.0032 | 6.682 | 0.090 | 0.1416 | 0.0019 | 2247 | 23 |
| | 48 | 289 | 0.67 | 0.5485 | 0.0085 | 15.213 | 0.292 | 0.2084 | 0.0036 | 2893 | 28 |
| | 49 | 531 | 0.26 | 0.3299 | 0.0041 | 5.122 | 0.075 | 0.1143 | 0.0015 | 1870 | 24 |
| | 50 | 514 | 0.34 | 0.4717 | 0.0080 | 10.649 | 0.224 | 0.1644 | 0.0028 | 2502 | 29 |
| | 51 | 408 | 0.82 | 0.5177 | 0.0058 | 13.633 | 0.181 | 0.1935 | 0.0021 | 2772 | 18 |
| | 52 | 159 | 0.66 | 0.3960 | 0.0053 | 7.203 | 0.123 | 0.1339 | 0.0020 | 2150 | 26 |
| | 53 | 435 | 0.62 | 0.4571 | 0.0064 | 11.833 | 0.181 | 0.1887 | 0.0031 | 2731 | 27 |
| | 54 | 183 | 1.02 | 0.5304 | 0.0102 | 13.249 | 0.276 | 0.1855 | 0.0031 | 2703 | 28 |
| | 55 | 330 | 0.40 | 0.4766 | 0.0077 | 11.529 | 0.197 | 0.1769 | 0.0026 | 2624 | 24 |
| | 56 | 192 | 0.61 | 0.5287 | 0.0065 | 13.477 | 0.196 | 0.1867 | 0.0024 | 2713 | 21 |
| | 57 | 154 | 0.47 | 0.4881 | 0.0070 | 11.234 | 0.204 | 0.1691 | 0.0027 | 2549 | 27 |
| | 58 | 275 | 0.47 | 0.4696 | 0.0053 | 10.641 | 0.137 | 0.1674 | 0.0020 | 2532 | 20 |
| | 59 | 393 | 0.31 | 0.3963 | 0.0093 | 8.403 | 0.187 | 0.1597 | 0.0033 | 2452 | 35 |
| | 60 | 947 | 0.45 | 0.3576 | 0.0051 | 11.199 | 0.187 | 0.2299 | 0.0029 | 3051 | 21 |
| | 61 | 307 | 0.51 | 0.4743 | 0.0063 | 10.477 | 0.147 | 0.1624 | 0.0020 | 2481 | 21 |
| | 62 | 251 | 0.90 | 0.5079 | 0.0083 | 12.017 | 0.223 | 0.1744 | 0.0028 | 2600 | 27 |
| | 63 | 660 | 0.01 | 0.3476 | 0.0068 | 5.599 | 0.113 | 0.1196 | 0.0019 | 1951 | 29 |

**Table 4.** Monazite EMPA data for metasedimentary samples from the lower Etheridge Group.

| Grain/analysis | | Si | Al | K | Fe | Ca | Sr | Pb | Y | Th | U | La | Ce | Pr | Nd | Sm | Eu | Gd | Dy | Yb | Er | P |
|---|---|---|---|---|---|---|---|---|---|---|---|---|---|---|---|---|---|---|---|---|---|---|
| **Sample 283: Einasleigh Metamorphics (Gum Flats)** | | | | | | | | | | | | | | | | | | | | | | |
| 1 | 1 | 0.12 | 0.00 | 0.01 | 0.06 | 1.04 | -0.01 | 0.61 | 2.08 | 5.23 | 1.11 | 10.65 | 21.24 | 2.47 | 9.05 | 1.45 | 0.14 | 1.15 | 0.58 | 0.07 | 0.16 | 12.59 |
| | 2 | 0.13 | 0.00 | -0.01 | 0.06 | 0.96 | -0.01 | 0.56 | 2.48 | 5.31 | 0.76 | 10.43 | 21.08 | 2.48 | 9.06 | 1.45 | 0.07 | 1.31 | 0.67 | 0.01 | 0.14 | 12.45 |
| | 3 | 0.11 | 0.00 | 0.02 | 0.04 | 0.92 | -0.02 | 0.51 | 2.40 | 5.25 | 0.53 | 10.81 | 22.47 | 2.55 | 9.11 | 1.44 | -0.01 | 1.23 | 0.66 | 0.04 | 0.15 | 12.56 |
| 2 | 1 | 0.08 | 0.00 | -0.01 | 0.04 | 0.96 | -0.01 | 0.55 | 1.88 | 4.74 | 0.97 | 10.86 | 21.74 | 2.47 | 8.94 | 1.46 | 0.13 | 1.17 | 0.56 | 0.08 | 0.16 | 12.48 |
| | 2 | 0.09 | -0.01 | -0.01 | 0.07 | 1.01 | -0.01 | 0.54 | 1.97 | 4.90 | 1.02 | 11.43 | 23.14 | 2.50 | 9.03 | 1.42 | 0.15 | 1.14 | 0.58 | 0.09 | 0.18 | 12.60 |
| | 3 | 0.08 | 0.00 | 0.00 | 0.06 | 1.04 | -0.01 | 0.62 | 1.52 | 5.54 | 0.86 | 11.02 | 22.52 | 2.53 | 9.25 | 1.42 | 0.18 | 1.11 | 0.50 | 0.04 | 0.11 | 12.45 |
| | 4 | 0.08 | 0.00 | 0.01 | 0.06 | 1.00 | -0.01 | 0.59 | 1.43 | 5.33 | 0.84 | 11.43 | 22.91 | 2.44 | 9.16 | 1.39 | 0.14 | 1.12 | 0.49 | 0.07 | 0.12 | 12.51 |
| 3 | 1 | 0.22 | 0.00 | -0.01 | 0.04 | 1.09 | -0.01 | 0.61 | 1.44 | 7.25 | 0.38 | 10.46 | 21.46 | 2.42 | 8.95 | 1.40 | 0.15 | 1.00 | 0.45 | 0.04 | 0.15 | 12.16 |
| | 2 | 0.08 | 0.01 | -0.01 | 0.04 | 1.15 | 0.00 | 0.67 | 1.72 | 5.24 | 1.15 | 10.90 | 22.12 | 2.50 | 9.07 | 1.47 | 0.10 | 1.16 | 0.56 | 0.06 | 0.14 | 12.76 |
| | 3 | 0.24 | 0.01 | 0.00 | 0.07 | 0.72 | 0.01 | 0.42 | 1.17 | 5.85 | 0.21 | 11.90 | 24.09 | 2.55 | 9.25 | 1.47 | 0.15 | 1.00 | 0.49 | 0.05 | 0.07 | 12.39 |
| 4 | 1 | 0.10 | 0.00 | 0.01 | 0.06 | 0.97 | 0.00 | 0.57 | 2.26 | 5.38 | 0.79 | 10.76 | 22.20 | 2.36 | 8.91 | 1.47 | -0.01 | 1.24 | 0.65 | 0.06 | 0.16 | 12.61 |
| | 2 | 0.31 | 0.00 | -0.01 | 0.06 | 0.74 | 0.01 | 0.50 | 1.06 | 6.23 | 0.21 | 11.19 | 22.94 | 2.62 | 9.16 | 1.48 | 0.18 | 1.06 | 0.45 | 0.02 | 0.07 | 12.25 |
| | 3 | 0.14 | 0.01 | 0.00 | 0.16 | 0.98 | 0.00 | 0.53 | 2.57 | 5.52 | 0.63 | 10.83 | 22.63 | 2.52 | 9.16 | 1.51 | 0.01 | 1.34 | 0.72 | 0.08 | 0.16 | 12.77 |
| | 4 | 0.14 | 0.00 | -0.01 | 0.07 | 0.98 | -0.01 | 0.54 | 2.55 | 5.47 | 0.63 | 10.46 | 21.87 | 2.49 | 9.10 | 1.44 | 0.06 | 1.34 | 0.74 | 0.05 | 0.18 | 12.68 |
| | 5 | 0.09 | 0.00 | -0.03 | 0.06 | 1.42 | 0.00 | 0.79 | 1.72 | 7.54 | 1.09 | 10.85 | 22.14 | 2.37 | 8.55 | 1.38 | 0.17 | 1.07 | 0.54 | 0.04 | 0.12 | 12.82 |
| 5 | 1 | 0.11 | 0.02 | -0.01 | 0.12 | 1.59 | -0.01 | 0.82 | 2.13 | 6.78 | 1.14 | 10.27 | 21.58 | 2.38 | 8.93 | 1.51 | 0.16 | 1.24 | 0.65 | 0.09 | 0.16 | 13.08 |
| 6 | 1 | 0.21 | 0.00 | 0.01 | 0.14 | 1.45 | 0.11 | 0.66 | 1.54 | 8.01 | 0.78 | 10.35 | 21.88 | 2.31 | 8.72 | 1.44 | -0.01 | 1.12 | 0.56 | 0.03 | 0.11 | 12.72 |
| 7 | 1 | 0.14 | -0.01 | 0.01 | 0.04 | 1.18 | 0.01 | 0.68 | 1.66 | 5.50 | 1.08 | 10.84 | 22.95 | 2.46 | 8.96 | 1.48 | -0.05 | 1.15 | 0.60 | 0.06 | 0.11 | 12.84 |
| 8 | 1 | 0.03 | -0.01 | 0.00 | 0.02 | 0.36 | 0.02 | 0.12 | 2.34 | 0.94 | 0.22 | 11.36 | 25.50 | 2.91 | 10.38 | 1.75 | 0.02 | 1.56 | 0.72 | 0.04 | 0.17 | 12.70 |
| | 2 | 0.11 | 0.00 | 0.01 | 0.02 | 0.93 | 0.00 | 0.55 | 2.29 | 4.92 | 0.81 | 11.65 | 22.86 | 2.45 | 8.93 | 1.45 | -0.13 | 1.12 | 0.61 | 0.13 | 0.16 | 12.54 |
| 9 | 1 | 0.11 | 0.00 | 0.01 | 0.13 | 0.39 | 0.00 | 0.26 | 0.84 | 2.72 | 0.26 | 13.70 | 24.64 | 2.58 | 9.87 | 1.65 | 0.04 | 1.31 | 0.40 | 0.02 | 0.01 | 12.49 |
| 10 | 1 | 0.15 | 0.00 | 0.01 | 0.10 | 1.23 | 0.01 | 0.65 | 1.41 | 6.79 | 0.59 | 11.67 | 22.88 | 2.44 | 8.36 | 1.23 | -0.03 | 1.02 | 0.49 | 0.06 | 0.14 | 12.63 |
| 11 | 1 | 0.20 | 0.00 | 0.02 | 0.25 | 0.91 | 0.00 | 0.55 | 1.39 | 6.41 | 0.41 | 11.87 | 23.63 | 2.48 | 8.76 | 1.36 | -0.06 | 1.10 | 0.51 | 0.03 | 0.06 | 12.39 |
| | 2 | 0.08 | 0.00 | 0.02 | 0.22 | 1.05 | 0.00 | 0.52 | 1.92 | 5.54 | 0.60 | 11.21 | 22.88 | 2.51 | 9.07 | 1.39 | -0.09 | 1.25 | 0.69 | 0.08 | 0.15 | 12.60 |
| 12 | 1 | 0.12 | 0.00 | 0.01 | 0.08 | 0.99 | 0.01 | 0.51 | 2.00 | 5.59 | 0.51 | 10.79 | 22.53 | 2.47 | 9.19 | 1.49 | -0.09 | 1.22 | 0.60 | 0.09 | 0.13 | 12.54 |
| 13 | 1 | 0.18 | 0.00 | 0.01 | 0.04 | 1.00 | -0.01 | 0.55 | 2.24 | 5.58 | 0.63 | 10.78 | 22.33 | 2.46 | 9.09 | 1.49 | -0.15 | 1.36 | 0.67 | 0.07 | 0.11 | 12.52 |
| | 2 | 0.16 | 0.00 | 0.01 | 0.02 | 1.00 | -0.01 | 0.57 | 2.27 | 5.60 | 0.65 | 10.59 | 22.06 | 2.44 | 9.08 | 1.43 | -0.18 | 1.28 | 0.68 | 0.03 | 0.13 | 12.54 |
| 14 | 1 | 0.33 | 0.00 | 0.02 | 0.14 | 1.07 | 0.02 | 0.50 | 1.51 | 6.56 | 0.78 | 10.98 | 22.51 | 2.42 | 8.90 | 1.52 | -0.04 | 1.26 | 0.59 | 0.03 | 0.11 | 12.27 |
| | 2 | 0.11 | 0.00 | 0.01 | 0.02 | 1.77 | -0.01 | 0.92 | 1.87 | 9.43 | 1.02 | 9.21 | 19.86 | 2.19 | 8.24 | 1.47 | -0.06 | 1.30 | 0.63 | 0.09 | 0.15 | 12.58 |
| | 3 | 0.09 | 0.00 | 0.01 | 0.07 | 1.29 | 0.00 | 0.68 | 1.86 | 5.97 | 1.12 | 10.37 | 21.75 | 2.49 | 8.91 | 1.56 | -0.11 | 1.35 | 0.66 | 0.06 | 0.16 | 12.54 |
| **Sample 288: Daniel Creek Formation (Gum Flats)** | | | | | | | | | | | | | | | | | | | | | | |
| 1 | 1 | 0.48 | 0.03 | 0.01 | 0.23 | 1.35 | 0.01 | 0.82 | 1.05 | 10.52 | 0.19 | 9.19 | 19.37 | 2.35 | 9.00 | 1.70 | 0.33 | 1.42 | 0.40 | 0.02 | 0.06 | 11.96 |
| 2 | 1 | 0.09 | 0.01 | -0.01 | 0.29 | 0.33 | 0.01 | 0.27 | 1.10 | 2.64 | 0.28 | 13.42 | 25.45 | 2.75 | 9.76 | 1.53 | 0.28 | 1.00 | 0.39 | 0.03 | 0.06 | 12.65 |
| | 2 | 0.11 | 0.03 | 0.02 | 0.38 | 0.28 | 0.01 | 0.18 | 0.89 | 1.64 | 0.23 | 13.28 | 25.67 | 2.88 | 10.00 | 1.49 | 0.34 | 0.80 | 0.35 | 0.04 | 0.11 | 12.60 |
| 3 | 1 | 0.07 | 0.01 | 0.00 | 0.41 | 0.34 | 0.00 | 0.16 | 0.98 | 1.55 | 0.29 | 13.17 | 24.72 | 2.82 | 10.04 | 1.56 | 0.32 | 0.96 | 0.35 | 0.05 | 0.06 | 12.47 |
| | 2 | 0.06 | 0.01 | 0.01 | 0.47 | 0.84 | 0.02 | 0.62 | 0.95 | 2.79 | 1.82 | 11.89 | 23.23 | 2.69 | 9.52 | 1.59 | 0.44 | 1.21 | 0.38 | 0.05 | 0.05 | 12.82 |
| | 3 | 0.05 | 0.01 | 0.00 | 0.39 | 0.41 | 0.02 | 0.69 | 1.10 | 2.93 | 2.02 | 12.53 | 22.46 | 2.62 | 9.43 | 1.45 | 0.38 | 1.09 | 0.25 | 0.02 | 0.06 | 12.29 |
| 4 | 1 | 0.26 | 0.10 | 0.00 | 0.85 | 1.53 | 0.07 | 0.09 | 0.76 | 3.17 | 0.19 | 12.81 | 20.03 | 2.97 | 10.35 | 1.60 | 0.27 | 0.90 | 0.32 | 0.02 | 0.08 | 10.89 |
| | 2 | 0.13 | 0.05 | -0.02 | 0.68 | 0.64 | 0.12 | 0.13 | 0.98 | 1.50 | 0.21 | 14.26 | 24.59 | 3.38 | 12.22 | 1.94 | 0.39 | 1.07 | 0.32 | 0.01 | 0.08 | 12.62 |
| | 3 | 0.14 | 0.03 | -0.01 | 0.51 | 1.24 | 0.00 | 0.13 | 0.93 | 1.16 | 0.32 | 13.47 | 23.94 | 2.76 | 10.07 | 1.58 | 0.33 | 0.90 | 0.36 | 0.07 | 0.07 | 13.29 |
| | 4 | 0.23 | 0.05 | 0.05 | 0.48 | 0.64 | 0.05 | 0.10 | 0.82 | 0.93 | 0.21 | 13.81 | 24.76 | 2.91 | 10.15 | 1.52 | 0.30 | 0.85 | 0.34 | 0.03 | 0.03 | 12.51 |
| | 5 | 0.11 | 0.01 | -0.01 | 0.30 | 0.92 | 0.03 | 0.28 | 1.53 | 1.23 | 0.71 | 12.45 | 24.96 | 2.91 | 10.20 | 1.62 | 0.30 | 1.05 | 0.52 | 0.01 | 0.10 | 13.21 |
| 5 | 1 | 0.39 | 0.08 | 0.00 | 1.45 | 0.45 | 0.04 | 0.06 | 1.11 | 2.73 | 0.20 | 13.29 | 24.94 | 2.65 | 9.44 | 1.35 | 0.21 | 0.89 | 0.32 | 0.07 | 0.09 | 11.98 |
| 6 | 1 | 0.28 | 0.09 | 0.01 | 0.39 | 0.36 | 0.00 | 0.13 | 0.96 | 0.72 | 0.28 | 13.59 | 26.69 | 2.90 | 10.08 | 1.54 | 0.31 | 0.91 | 0.34 | 0.06 | 0.07 | 12.80 |
| 7 | 1 | 0.19 | 0.02 | 0.11 | 0.14 | 0.62 | 0.01 | 0.45 | 0.94 | 5.20 | 0.27 | 11.81 | 23.02 | 2.64 | 9.40 | 1.40 | 0.25 | 0.85 | 0.37 | 0.03 | 0.07 | 12.28 |
| | 2 | 0.30 | 0.03 | 0.09 | 0.12 | 0.95 | 0.01 | 0.50 | 1.03 | 7.05 | 0.22 | 11.23 | 21.76 | 2.41 | 8.98 | 1.43 | 0.30 | 0.81 | 0.43 | 0.01 | 0.07 | 12.25 |
| 8 | 1 | 0.36 | 0.01 | 0.02 | 0.11 | 1.17 | 0.03 | 0.68 | 1.02 | 9.46 | 0.16 | 10.12 | 20.65 | 2.31 | 8.97 | 1.70 | 0.34 | 1.58 | 0.48 | 0.02 | 0.08 | 11.97 |
| 9 | 1 | 0.22 | 0.02 | 0.01 | 1.32 | 0.69 | 0.01 | 0.34 | 0.95 | 3.87 | 0.19 | 12.49 | 23.94 | 2.59 | 9.30 | 1.54 | 0.13 | 1.30 | 0.47 | 0.02 | -0.01 | 12.17 |
| | 2 | 0.32 | 0.01 | 0.01 | 0.98 | 1.10 | 0.03 | 0.57 | 0.97 | 7.27 | 0.16 | 10.90 | 21.73 | 2.41 | 8.91 | 1.63 | 0.10 | 1.39 | 0.49 | 0.03 | 0.05 | 11.96 |

| Grain/analysis | | S | As | O | Total (wt%) | Pb (ppm) | Th (ppm) | U (ppm) | Age (Ma) | ± 1 σ |
|---|---|---|---|---|---|---|---|---|---|---|
| **Sample 283: Einasleigh Metamorphics (Gum Flats)** | | | | | | | | | | |
| 1 | 1 | 0.00 | 0.01 | 26.26 | 96.08 | 6087 | 52270 | 11105 | 1444 | 16 |
| | 2 | 0.00 | 0.03 | 26.08 | 95.52 | 5548 | 53099 | 7602 | 1502 | 18 |
| | 3 | 0.01 | 0.02 | 26.43 | 97.23 | 5089 | 52457 | 5260 | 1548 | 20 |
| 2 | 1 | 0.01 | 0.02 | 26.01 | 95.31 | 5510 | 47424 | 9659 | 1465 | 17 |
| | 2 | 0.00 | 0.02 | 26.59 | 98.48 | 5408 | 49031 | 10206 | 1385 | 16 |
| | 3 | 0.00 | 0.00 | 26.19 | 97.06 | 6164 | 55394 | 8622 | 1549 | 17 |
| | 4 | 0.00 | 0.01 | 26.30 | 97.42 | 5875 | 53319 | 8356 | 1532 | 17 |
| 3 | 1 | 0.00 | 0.01 | 25.76 | 95.44 | 6091 | 72468 | 3765 | 1537 | 17 |
| | 2 | 0.00 | 0.01 | 26.59 | 97.52 | 6696 | 52446 | 11549 | 1548 | 16 |
| | 3 | 0.00 | 0.01 | 26.44 | 98.57 | 4133 | 58526 | 2143 | 1363 | 21 |
| 4 | 1 | 0.00 | 0.01 | 26.40 | 96.97 | 5712 | 53753 | 7855 | 1515 | 18 |
| | 2 | 0.00 | 0.02 | 26.04 | 96.60 | 4953 | 62293 | 2099 | 1539 | 21 |
| | 3 | 0.00 | 0.02 | 26.98 | 99.29 | 5309 | 55221 | 6287 | 1486 | 18 |
| | 4 | 0.00 | 0.00 | 26.58 | 97.37 | 5360 | 54667 | 6345 | 1505 | 19 |
| | 5 | 0.00 | 0.01 | 26.95 | 99.74 | 7895 | 75448 | 10935 | 1498 | 13 |
| 5 | 1 | 0.00 | 0.00 | 27.35 | 100.08 | 8175 | 67754 | 11373 | 1626 | 14 |
| 6 | 1 | 0.01 | 0.01 | 26.89 | 99.05 | 6602 | 80115 | 7828 | 1338 | 14 |
| 7 | 1 | 0.01 | 0.00 | 26.87 | 98.62 | 6855 | 55023 | 10766 | 1584 | 16 |
| 8 | 1 | 0.00 | 0.02 | 26.62 | 97.82 | 1297 | 9359 | 2236 | 1612 | 69 |
| | 2 | 0.00 | 0.01 | 26.50 | 98.06 | 5508 | 49196 | 8128 | 1527 | 18 |
| 9 | 1 | 0.00 | 0.01 | 26.30 | 97.74 | 2632 | 27154 | 2613 | 1562 | 36 |
| 10 | 1 | 0.00 | 0.01 | 26.66 | 98.53 | 6552 | 67910 | 5932 | 1590 | 17 |
| 11 | 1 | 0.00 | 0.01 | 26.49 | 98.83 | 5525 | 64064 | 4109 | 1523 | 18 |
| | 2 | 0.00 | 0.00 | 26.58 | 98.37 | 5280 | 55377 | 5968 | 1496 | 18 |
| 12 | 1 | 0.00 | 0.02 | 26.40 | 97.30 | 5188 | 55882 | 5119 | 1518 | 19 |
| 13 | 1 | 0.00 | 0.00 | 26.46 | 97.57 | 5514 | 55818 | 6323 | 1526 | 18 |
| | 2 | 0.01 | 0.01 | 26.38 | 96.95 | 5732 | 56016 | 6533 | 1564 | 18 |
| 14 | 1 | 0.01 | 0.01 | 26.35 | 97.90 | 5075 | 65591 | 7819 | 1198 | 15 |
| | 2 | 0.00 | 0.00 | 26.38 | 97.21 | 9261 | 94275 | 10150 | 1538 | 12 |
| | 3 | 0.00 | 0.02 | 26.37 | 97.35 | 6858 | 59669 | 11177 | 1496 | 15 |
| **Sample 288: Daniel Creek Formation (Gum Flats)** | | | | | | | | | | |
| 1 | 1 | 0.00 | 0.02 | 25.87 | 96.35 | 8140 | 105243 | 1916 | 1573 | 14 |
| 2 | 1 | 0.00 | 0.02 | 26.65 | 99.01 | 2709 | 26435 | 2849 | 1599 | 36 |
| | 2 | 0.01 | 0.03 | 26.50 | 97.85 | 1714 | 16390 | 2316 | 1509 | 50 |
| 3 | 1 | 0.00 | 0.01 | 26.14 | 96.47 | 1550 | 15452 | 2901 | 1320 | 46 |
| | 2 | 0.00 | 0.01 | 26.67 | 98.14 | 6140 | 27852 | 18216 | 1444 | 15 |
| | 3 | 0.00 | 0.03 | 25.77 | 96.00 | 6860 | 29335 | 20195 | 1473 | 14 |
| 4 | 1 | 0.24 | 0.02 | 24.72 | 92.25 | 873 | 31669 | 1918 | 512 | 28 |
| | 2 | 0.07 | 0.03 | 27.45 | 102.89 | 1282 | 14976 | 2144 | 1249 | 52 |
| | 3 | 0.56 | 0.02 | 28.37 | 100.24 | 1225 | 11611 | 3162 | 1189 | 53 |
| | 4 | 0.09 | 0.02 | 26.68 | 97.53 | 921 | 9273 | 2102 | 1216 | 68 |
| | 5 | 0.04 | 0.02 | 27.58 | 100.08 | 2808 | 12328 | 7092 | 1604 | 33 |
| 5 | 1 | 0.03 | 0.03 | 26.37 | 98.16 | 568 | 27343 | 2015 | 374 | 31 |
| 6 | 1 | 0.00 | 0.01 | 27.16 | 99.67 | 1289 | 7159 | 2763 | 1627 | 70 |
| 7 | 1 | 0.00 | 0.02 | 25.92 | 96.01 | 4416 | 51969 | 2651 | 1558 | 23 |
| | 2 | 0.01 | 0.03 | 26.00 | 96.00 | 4931 | 70475 | 2185 | 1374 | 18 |
| 8 | 1 | 0.01 | 0.02 | 25.86 | 97.11 | 6803 | 94588 | 1630 | 1473 | 15 |
| 9 | 1 | 0.00 | 0.01 | 26.27 | 97.87 | 3429 | 38713 | 1871 | 1632 | 28 |
| | 2 | 0.00 | 0.01 | 25.95 | 96.99 | 5788 | 72701 | 1602 | 1598 | 18 |

| Grain/analysis | | Si | Al | K | Fe | Ca | Sr | Pb | Y | Th | U | La | Ce | Pr | Nd | Sm | Eu | Gd | Dy | Yb | Er | P |
|---|---|---|---|---|---|---|---|---|---|---|---|---|---|---|---|---|---|---|---|---|---|---|
| 10 | 1 | 0.09 | 0.00 | 0.01 | 0.28 | 0.41 | 0.01 | 0.24 | 0.91 | 2.83 | 0.26 | 12.88 | 25.17 | 2.71 | 9.59 | 1.50 | 0.13 | 1.04 | 0.41 | 0.04 | 0.04 | 12.48 |
| 11 | 1 | 0.06 | 0.01 | 0.01 | 0.45 | 0.85 | 0.03 | 0.55 | 0.88 | 2.75 | 1.60 | 12.20 | 23.92 | 2.71 | 9.52 | 1.54 | 0.17 | 1.33 | 0.43 | 0.03 | 0.06 | 12.60 |
| 12 | 1 | 0.06 | 0.01 | 0.02 | 0.24 | 0.23 | 0.01 | 0.13 | 0.97 | 0.91 | 0.27 | 13.64 | 26.75 | 2.87 | 9.98 | 1.51 | 0.12 | 0.92 | 0.44 | 0.05 | 0.10 | 12.58 |
| 13 | 1 | 0.03 | 0.00 | 0.01 | 0.20 | 0.36 | 0.00 | 0.27 | 1.39 | 0.69 | 0.92 | 13.40 | 26.15 | 2.77 | 9.51 | 1.41 | 0.13 | 0.89 | 0.45 | 0.03 | 0.09 | 12.50 |
| | 2 | 0.04 | 0.00 | 0.00 | 0.18 | 0.29 | 0.01 | 0.26 | 1.16 | 0.68 | 0.87 | 13.62 | 26.56 | 2.75 | 9.69 | 1.36 | 0.13 | 0.91 | 0.42 | 0.01 | 0.05 | 12.57 |
| | 3 | 0.02 | 0.00 | 0.01 | 0.20 | 0.23 | 0.00 | 0.16 | 1.02 | 0.66 | 0.48 | 14.05 | 26.94 | 2.84 | 9.70 | 1.35 | 0.12 | 0.79 | 0.35 | 0.06 | 0.03 | 12.63 |
| 14 | 1 | 0.19 | 0.05 | 0.04 | 1.01 | 0.83 | 0.04 | 0.37 | 0.99 | 4.95 | 0.22 | 11.90 | 23.65 | 2.60 | 9.66 | 1.56 | 0.20 | 1.16 | 0.42 | 0.04 | 0.03 | 12.23 |
| 15 | 1 | 0.19 | 0.01 | 0.03 | 0.87 | 0.79 | 0.03 | 0.42 | 1.02 | 5.19 | 0.20 | 12.09 | 23.07 | 2.47 | 9.22 | 1.60 | 0.12 | 1.32 | 0.46 | 0.01 | 0.04 | 12.31 |
| 16 | 1 | 0.30 | 0.00 | 0.02 | 0.62 | 1.09 | 0.02 | 0.63 | 1.10 | 8.25 | 0.22 | 10.34 | 20.86 | 2.38 | 9.00 | 1.68 | 0.16 | 1.43 | 0.45 | 0.06 | 0.07 | 11.93 |
| 17 | 1 | 0.57 | 0.00 | 0.01 | 0.92 | 1.28 | 0.04 | 0.80 | 0.91 | 11.09 | 0.15 | 9.62 | 20.09 | 2.29 | 9.09 | 1.72 | 0.11 | 1.47 | 0.46 | 0.03 | 0.06 | 11.69 |
| 18 | 1 | 0.14 | 0.02 | 0.01 | 0.80 | 0.60 | 0.02 | 0.30 | 0.91 | 3.40 | 0.22 | 11.67 | 22.53 | 2.37 | 8.68 | 1.36 | 0.14 | 1.02 | 0.36 | 0.04 | 0.05 | 11.60 |
| 19 | 1 | 0.15 | 0.00 | 0.00 | 0.20 | 0.13 | 0.01 | 0.02 | 0.82 | 0.80 | 0.16 | 14.05 | 26.80 | 2.85 | 9.90 | 1.31 | 0.12 | 0.93 | 0.32 | 0.06 | 0.03 | 12.40 |
| | 2 | 0.39 | 0.16 | 0.01 | 0.34 | 0.36 | 0.02 | 0.05 | 1.33 | 1.59 | 0.42 | 13.26 | 25.38 | 2.74 | 9.72 | 1.46 | 0.06 | 1.13 | 0.52 | 0.05 | 0.05 | 12.37 |
| **Sample 304: Lane Creek Formation (Robinhood)** | | | | | | | | | | | | | | | | | | | | | | |
| 1 | 1 | 0.03 | 0.00 | 0.01 | 0.10 | 0.75 | 0.00 | 0.39 | 1.54 | 3.12 | 0.66 | 11.91 | 24.33 | 2.64 | 9.67 | 1.42 | -0.08 | 1.20 | 0.54 | 0.08 | 0.10 | 12.74 |
| | 2 | 0.02 | 0.00 | 0.00 | 0.06 | 0.35 | 0.00 | 0.06 | 1.60 | 0.63 | 0.14 | 13.59 | 25.79 | 2.71 | 9.80 | 1.65 | 0.00 | 1.37 | 0.63 | 0.06 | 0.07 | 12.93 |
| | 3 | 0.03 | 0.01 | 0.01 | 0.05 | 0.74 | 0.00 | 0.40 | 1.56 | 3.23 | 0.73 | 12.15 | 24.57 | 2.63 | 9.51 | 1.51 | -0.07 | 1.18 | 0.57 | 0.05 | 0.13 | 12.77 |
| 2 | 1 | 0.02 | 0.00 | 0.01 | 0.07 | 0.32 | -0.01 | 0.13 | 1.51 | 0.81 | 0.29 | 13.30 | 25.52 | 2.75 | 9.96 | 1.67 | -0.05 | 1.46 | 0.64 | 0.06 | 0.03 | 12.80 |
| | 2 | 0.03 | 0.00 | 0.03 | 0.04 | 0.69 | -0.01 | 0.41 | 1.57 | 2.93 | 0.77 | 12.03 | 24.58 | 2.68 | 9.61 | 1.55 | -0.08 | 1.26 | 0.54 | 0.05 | 0.11 | 12.81 |
| 3 | 1 | 0.05 | 0.00 | 0.03 | 0.07 | 0.87 | -0.02 | 0.49 | 1.56 | 3.77 | 0.86 | 11.42 | 23.65 | 2.64 | 9.69 | 1.51 | -0.09 | 1.20 | 0.62 | 0.07 | 0.12 | 12.92 |
| 4 | 1 | 0.06 | 0.01 | 0.04 | 0.08 | 0.88 | 0.00 | 0.49 | 1.65 | 3.95 | 0.87 | 11.25 | 23.46 | 2.63 | 9.55 | 1.53 | -0.10 | 1.16 | 0.54 | 0.02 | 0.17 | 12.73 |
| 5 | 1 | 0.07 | 0.00 | 0.01 | 0.09 | 0.76 | -0.01 | 0.41 | 1.40 | 3.45 | 0.71 | 12.09 | 24.36 | 2.63 | 9.35 | 1.47 | -0.10 | 1.09 | 0.51 | 0.08 | 0.10 | 12.59 |
| 6 | 1 | 0.16 | 0.04 | 0.09 | 0.52 | 0.95 | 0.01 | 0.49 | 1.70 | 4.19 | 0.80 | 11.14 | 23.21 | 2.54 | 9.30 | 1.54 | -0.13 | 1.26 | 0.58 | 0.02 | 0.09 | 12.62 |
| 7 | 1 | 0.11 | 0.00 | 0.03 | 0.06 | 0.94 | 0.00 | 0.53 | 1.77 | 4.59 | 0.79 | 11.03 | 22.95 | 2.55 | 9.34 | 1.47 | -0.10 | 1.26 | 0.64 | 0.05 | 0.13 | 12.73 |
| 8 | 1 | 0.06 | 0.00 | 0.03 | 0.08 | 0.57 | 0.01 | 0.19 | 1.45 | 1.87 | 0.31 | 12.35 | 25.00 | 2.82 | 9.74 | 1.50 | -0.03 | 1.11 | 0.56 | 0.03 | 0.10 | 12.59 |
| 9 | 1 | 0.94 | 0.22 | 0.08 | 1.66 | 0.83 | 0.08 | 0.25 | 1.45 | 3.45 | 0.39 | 10.83 | 22.55 | 2.58 | 9.40 | 1.45 | -0.07 | 1.08 | 0.48 | 0.06 | 0.07 | 12.00 |
| 10 | 1 | 0.12 | 0.03 | 0.07 | 0.58 | 0.59 | 0.01 | 0.29 | 1.53 | 2.74 | 0.47 | 11.83 | 24.84 | 2.78 | 9.83 | 1.57 | -0.10 | 1.38 | 0.65 | 0.04 | 0.07 | 12.78 |
| 11 | 1 | 0.05 | 0.01 | 0.08 | 0.09 | 0.84 | 0.00 | 0.46 | 1.66 | 3.76 | 0.84 | 11.61 | 23.50 | 2.50 | 9.28 | 1.47 | -0.12 | 1.20 | 0.56 | 0.04 | 0.14 | 12.61 |
| 12 | 1 | 0.11 | 0.00 | 0.02 | 0.06 | 0.76 | 0.00 | 0.44 | 1.69 | 3.38 | 0.81 | 11.51 | 23.96 | 2.70 | 9.52 | 1.52 | -0.14 | 1.22 | 0.61 | 0.05 | 0.12 | 12.81 |
| 13 | 1 | 0.12 | 0.03 | 0.07 | 0.27 | 0.66 | 0.00 | 0.28 | 1.97 | 2.77 | 0.45 | 11.54 | 24.12 | 2.72 | 9.58 | 1.54 | -0.09 | 1.30 | 0.67 | 0.08 | 0.07 | 12.84 |
| 14 | 1 | 0.07 | 0.00 | 0.02 | 0.04 | 0.83 | -0.02 | 0.46 | 1.63 | 3.68 | 0.80 | 11.55 | 23.96 | 2.59 | 9.37 | 1.55 | -0.09 | 1.19 | 0.58 | 0.03 | 0.13 | 12.65 |
| 15 | 1 | 0.06 | 0.00 | 0.03 | 0.18 | 0.60 | 0.00 | 0.31 | 1.63 | 2.71 | 0.50 | 12.02 | 24.77 | 2.70 | 9.66 | 1.51 | -0.06 | 1.30 | 0.59 | 0.05 | 0.05 | 12.81 |
| | 2 | 0.06 | 0.01 | 0.03 | 0.55 | 0.60 | 0.00 | 0.31 | 1.50 | 2.58 | 0.51 | 12.34 | 24.80 | 2.65 | 9.57 | 1.49 | -0.04 | 1.15 | 0.51 | 0.06 | 0.06 | 12.76 |
| 16 | 1 | 0.04 | 0.01 | 0.08 | 0.13 | 0.65 | 0.00 | 0.29 | 1.54 | 2.38 | 0.56 | 11.82 | 23.97 | 2.73 | 9.64 | 1.52 | -0.08 | 1.23 | 0.58 | 0.04 | 0.07 | 12.53 |
| 17 | 1 | 0.04 | 0.00 | 0.03 | 0.12 | 0.53 | -0.01 | 0.21 | 1.73 | 2.04 | 0.39 | 11.39 | 24.56 | 2.88 | 9.95 | 1.70 | -0.04 | 1.28 | 0.65 | 0.06 | 0.14 | 12.80 |
| 18 | 1 | 0.06 | 0.00 | 0.05 | 0.26 | 0.70 | 0.00 | 0.35 | 1.60 | 3.61 | 0.45 | 11.60 | 23.99 | 2.78 | 9.71 | 1.51 | -0.11 | 1.25 | 0.51 | 0.06 | 0.13 | 12.53 |
| 19 | 1 | 0.06 | 0.04 | 0.02 | 0.20 | 0.19 | -0.01 | 0.04 | 1.37 | 0.54 | 0.09 | 12.99 | 27.00 | 2.91 | 10.27 | 1.51 | 0.00 | 1.11 | 0.55 | 0.04 | 0.08 | 12.65 |
| 20 | 1 | 0.38 | 0.00 | 0.01 | 0.12 | 0.75 | 0.00 | 0.38 | 1.55 | 3.72 | 0.53 | 11.71 | 23.92 | 2.73 | 9.62 | 1.54 | -0.15 | 1.20 | 0.60 | 0.07 | 0.09 | 12.46 |
| 21 | 1 | 0.06 | -0.01 | 0.03 | 0.07 | 0.74 | 0.00 | 0.37 | 1.65 | 3.82 | 0.44 | 11.53 | 23.81 | 2.79 | 9.64 | 1.57 | -0.12 | 1.27 | 0.57 | 0.05 | 0.11 | 12.60 |
| 22 | 1 | 0.02 | 0.00 | 0.01 | 0.11 | 0.77 | -0.01 | 0.41 | 1.45 | 3.40 | 0.75 | 11.92 | 23.61 | 2.62 | 9.24 | 1.41 | -0.05 | 1.10 | 0.51 | 0.04 | 0.08 | 12.57 |
| 23 | 1 | 0.03 | 0.00 | 0.03 | 0.14 | 0.89 | -0.01 | 0.50 | 1.55 | 4.19 | 0.80 | 11.07 | 22.77 | 2.61 | 9.34 | 1.49 | -0.09 | 1.18 | 0.56 | 0.03 | 0.09 | 12.55 |
| **Sample 306: Corbett Formation (Robinhood)** | | | | | | | | | | | | | | | | | | | | | | |
| 1 | 1 | 0.34 | 0.01 | 0.02 | 0.13 | 0.24 | -0.01 | 0.16 | 0.87 | 3.05 | 0.21 | 12.42 | 26.15 | 2.86 | 10.14 | 1.56 | -0.01 | 0.91 | 0.37 | 0.03 | 0.05 | 12.15 |
| | 2 | 0.07 | 0.00 | 0.03 | 0.09 | 0.45 | 0.01 | 0.24 | 1.18 | 2.56 | 0.26 | 12.38 | 25.85 | 2.79 | 9.80 | 1.56 | 0.02 | 1.04 | 0.46 | 0.06 | 0.09 | 12.55 |
| 2 | 1 | 0.04 | 0.01 | 0.05 | 0.04 | 0.26 | -0.01 | 0.17 | 1.20 | 1.29 | 0.33 | 13.06 | 26.37 | 2.87 | 9.88 | 1.49 | -0.02 | 1.06 | 0.43 | 0.02 | 0.08 | 12.57 |
| | 2 | 0.04 | 0.00 | 0.03 | 0.04 | 0.29 | -0.01 | 0.17 | 1.18 | 1.30 | 0.33 | 13.20 | 26.47 | 2.92 | 9.70 | 1.43 | -0.02 | 1.07 | 0.49 | 0.04 | 0.08 | 12.57 |
| 3 | 1 | 0.07 | 0.00 | 0.01 | 0.06 | 0.53 | -0.01 | 0.26 | 1.30 | 2.60 | 0.33 | 12.44 | 25.41 | 2.79 | 9.51 | 1.39 | -0.02 | 1.00 | 0.51 | 0.03 | 0.09 | 12.52 |
| 4 | 1 | 0.10 | 0.00 | 0.01 | 0.06 | 0.55 | 0.00 | 0.29 | 1.18 | 3.10 | 0.42 | 12.50 | 25.02 | 2.69 | 9.57 | 1.42 | 0.05 | 1.00 | 0.39 | 0.03 | 0.08 | 12.59 |
| | 2 | 0.04 | 0.00 | 0.02 | 0.09 | 0.33 | -0.02 | 0.18 | 1.10 | 1.57 | 0.31 | 12.96 | 26.27 | 2.84 | 9.60 | 1.42 | 0.00 | 1.06 | 0.44 | 0.04 | 0.06 | 12.64 |
| | 3 | 0.06 | 0.00 | 0.03 | 0.12 | 0.40 | 0.01 | 0.21 | 1.11 | 1.94 | 0.34 | 12.88 | 25.80 | 2.73 | 9.54 | 1.47 | -0.02 | 0.99 | 0.45 | 0.07 | 0.11 | 12.71 |

| Grain/analysis | | S | As | O | Total (wt%) | Pb (ppm) | Th (ppm) | U (ppm) | Age (Ma) | ± 1 σ |
|---|---|---|---|---|---|---|---|---|---|---|
| 10 | 1 | 0.00 | 0.01 | 26.25 | 97.32 | 2492 | 28301 | 2623 | 1441 | 32 |
| 11 | 1 | 0.00 | 0.01 | 26.51 | 98.21 | 5505 | 27473 | 16011 | 1423 | 15 |
| 12 | 1 | 0.01 | 0.02 | 26.50 | 98.31 | 1364 | 9089 | 2672 | 1581 | 59 |
| 13 | 1 | 0.00 | 0.02 | 26.32 | 97.54 | 2748 | 6874 | 9188 | 1504 | 28 |
| | 2 | 0.00 | 0.02 | 26.43 | 98.03 | 2679 | 6790 | 8717 | 1531 | 30 |
| | 3 | 0.00 | 0.01 | 26.49 | 98.13 | 1616 | 6580 | 4807 | 1482 | 45 |
| 14 | 1 | 0.02 | 0.02 | 26.43 | 98.61 | 3709 | 49496 | 2213 | 1409 | 22 |
| 15 | 1 | 0.01 | 0.01 | 26.30 | 97.77 | 4254 | 51922 | 2008 | 1560 | 22 |
| 16 | 1 | 0.01 | 0.02 | 25.75 | 96.39 | 6365 | 82547 | 2152 | 1530 | 16 |
| 17 | 1 | 0.01 | 0.03 | 26.03 | 98.49 | 8088 | 110927 | 1523 | 1509 | 13 |
| 18 | 1 | 0.00 | 0.02 | 24.58 | 90.83 | 3020 | 33958 | 2231 | 1560 | 29 |
| 19 | 1 | 0.00 | 0.01 | 26.22 | 97.28 | 217 | 7981 | 1566 | 372 | 43 |
| | 2 | 0.00 | 0.00 | 26.69 | 98.11 | 522 | 15872 | 4164 | 397 | 28 |
| **Sample 304: Lane Creek Formation (Robinhood)** | | | | | | | | | | |
| 1 | 1 | 0.01 | 0.02 | 26.60 | 97.86 | 3971 | 31220 | 6550 | 1572 | 23 |
| | 2 | 0.01 | 0.01 | 26.87 | 98.34 | 698 | 6259 | 1365 | 1374 | 91 |
| | 3 | 0.00 | 0.02 | 26.71 | 98.57 | 4057 | 32294 | 7338 | 1506 | 22 |
| 2 | 1 | 0.00 | 0.00 | 26.65 | 98.00 | 1322 | 8066 | 2888 | 1556 | 60 |
| | 2 | 0.01 | 0.01 | 26.73 | 98.44 | 4102 | 29297 | 7688 | 1563 | 23 |
| 3 | 1 | 0.00 | 0.02 | 26.83 | 98.39 | 4972 | 37710 | 8649 | 1567 | 19 |
| 4 | 1 | 0.00 | 0.02 | 26.57 | 97.68 | 4926 | 39491 | 8749 | 1512 | 19 |
| 5 | 1 | 0.00 | 0.02 | 26.41 | 97.60 | 4117 | 34547 | 7079 | 1495 | 21 |
| 6 | 1 | 0.02 | 0.00 | 26.69 | 97.96 | 4931 | 41945 | 7970 | 1519 | 19 |
| 7 | 1 | 0.00 | 0.01 | 26.58 | 97.56 | 5351 | 45922 | 7879 | 1563 | 18 |
| 8 | 1 | 0.02 | 0.02 | 26.35 | 96.73 | 1943 | 18665 | 3100 | 1426 | 39 |
| 9 | 1 | 0.08 | 0.00 | 26.88 | 96.81 | 2531 | 34515 | 3889 | 1157 | 24 |
| 10 | 1 | 0.01 | 0.01 | 26.96 | 99.19 | 2914 | 27393 | 4652 | 1444 | 28 |
| 11 | 1 | 0.00 | 0.00 | 26.36 | 97.05 | 4692 | 37574 | 8353 | 1511 | 19 |
| 12 | 1 | 0.00 | 0.01 | 26.73 | 98.05 | 4489 | 33782 | 8064 | 1553 | 21 |
| 13 | 1 | 0.01 | 0.02 | 26.85 | 97.95 | 2893 | 27728 | 4455 | 1445 | 28 |
| 14 | 1 | 0.00 | 0.02 | 26.51 | 97.68 | 4608 | 36840 | 8003 | 1527 | 20 |
| 15 | 1 | 0.00 | 0.01 | 26.74 | 98.24 | 3163 | 27057 | 4958 | 1532 | 28 |
| | 2 | 0.00 | 0.01 | 26.73 | 98.28 | 3158 | 25831 | 5121 | 1550 | 28 |
| 16 | 1 | 0.00 | 0.02 | 26.12 | 95.93 | 2957 | 23751 | 5621 | 1469 | 27 |
| 17 | 1 | 0.00 | 0.02 | 26.56 | 97.06 | 2183 | 20364 | 3857 | 1399 | 34 |
| 18 | 1 | 0.00 | 0.02 | 26.37 | 97.54 | 3563 | 36056 | 4546 | 1482 | 24 |
| 19 | 1 | 0.00 | 0.02 | 26.61 | 98.27 | 490 | 5369 | 938 | 1242 | 104 |
| 20 | 1 | 0.00 | 0.01 | 26.62 | 98.02 | 3840 | 37206 | 5295 | 1488 | 23 |
| 21 | 1 | 0.00 | 0.00 | 26.42 | 97.57 | 3738 | 38212 | 4426 | 1503 | 24 |
| 22 | 1 | 0.00 | 0.02 | 26.17 | 96.22 | 4187 | 33965 | 7453 | 1502 | 21 |
| 23 | 1 | 0.00 | 0.00 | 26.11 | 95.93 | 5028 | 41937 | 8032 | 1542 | 19 |
| **Sample 306: Corbett Formation (Robinhood)** | | | | | | | | | | |
| 1 | 1 | 0.00 | 0.02 | 26.19 | 97.87 | 1637 | 30505 | 2088 | 958 | 28 |
| | 2 | 0.00 | 0.01 | 26.40 | 97.90 | 2475 | 25587 | 2619 | 1536 | 34 |
| 2 | 1 | 0.00 | 0.01 | 26.35 | 97.56 | 1725 | 12906 | 3266 | 1523 | 46 |
| | 2 | 0.00 | 0.02 | 26.38 | 97.76 | 1704 | 13030 | 3337 | 1486 | 45 |
| 3 | 1 | 0.00 | 0.02 | 26.30 | 97.18 | 2655 | 26010 | 3343 | 1518 | 32 |
| 4 | 1 | 0.00 | 0.03 | 26.41 | 97.51 | 2990 | 30989 | 4152 | 1424 | 27 |
| | 2 | 0.00 | 0.01 | 26.40 | 97.39 | 1821 | 15729 | 3111 | 1476 | 43 |
| | 3 | 0.00 | 0.02 | 26.50 | 97.50 | 2195 | 19423 | 3432 | 1505 | 37 |

| Grain/analysis | | Si | Al | K | Fe | Ca | Sr | Pb | Y | Th | U | La | Ce | Pr | Nd | Sm | Eu | Gd | Dy | Yb | Er | P |
|---|---|---|---|---|---|---|---|---|---|---|---|---|---|---|---|---|---|---|---|---|---|---|
| 5 | 1 | 0.07 | 0.00 | 0.02 | 0.24 | 0.60 | 0.01 | 0.31 | 1.91 | 2.72 | 0.49 | 10.93 | 23.77 | 2.86 | 10.67 | 1.93 | -0.02 | 1.37 | 0.60 | 0.04 | 0.14 | 12.54 |
| 6 | 1 | 1.14 | 0.65 | 0.04 | 0.30 | 0.63 | 0.31 | 0.10 | 0.73 | 3.08 | 0.11 | 12.37 | 23.55 | 2.60 | 9.29 | 1.61 | 0.11 | 1.05 | 0.33 | 0.04 | 0.02 | 11.63 |
| 7 | 1 | 3.51 | 3.63 | 0.36 | 1.34 | 0.52 | 0.07 | 0.12 | 0.61 | 2.11 | 0.16 | 11.26 | 21.81 | 2.63 | 9.66 | 1.31 | 0.03 | 0.84 | 0.25 | 0.04 | 0.08 | 10.51 |
| 8 | 1 | 0.13 | 0.00 | 0.00 | 0.03 | 0.56 | -0.01 | 0.31 | 1.30 | 3.34 | 0.33 | 12.67 | 24.58 | 2.70 | 9.65 | 1.55 | 0.02 | 1.22 | 0.45 | 0.04 | 0.06 | 12.52 |
| | 2 | 0.15 | 0.00 | 0.01 | 0.04 | 0.55 | -0.01 | 0.30 | 1.24 | 3.39 | 0.30 | 12.55 | 24.35 | 2.65 | 9.78 | 1.62 | 0.00 | 1.17 | 0.45 | 0.03 | 0.05 | 12.49 |
| **Sample 308: Daniel Creek Formation (Gum Flats)** | | | | | | | | | | | | | | | | | | | | | | |
| 1 | 1 | 0.31 | 0.01 | 0.04 | 0.08 | 1.54 | -0.02 | 0.57 | 1.60 | 5.01 | 0.98 | 11.03 | 21.81 | 2.67 | 9.75 | 1.55 | 0.23 | 1.08 | 0.54 | 0.04 | 0.09 | 13.50 |
| 2 | 1 | 0.34 | 0.02 | 0.04 | 0.08 | 2.96 | -0.01 | 1.48 | 1.69 | 17.84 | 0.83 | 8.28 | 16.47 | 1.86 | 6.45 | 1.07 | 0.30 | 1.03 | 0.49 | 0.04 | 0.08 | 12.48 |
| | 2 | 0.12 | 0.10 | 0.05 | 0.09 | 1.05 | -0.01 | 0.57 | 1.69 | 4.49 | 1.03 | 11.72 | 23.50 | 2.58 | 9.39 | 1.52 | 0.10 | 1.18 | 0.57 | 0.06 | 0.09 | 13.02 |
| 3 | 1 | 0.30 | 0.04 | -0.01 | 0.17 | 1.44 | 0.00 | 0.77 | 1.61 | 6.69 | 1.36 | 10.36 | 20.24 | 2.41 | 8.49 | 1.28 | 0.18 | 1.05 | 0.49 | 0.03 | 0.10 | 12.21 |
| 4 | 1 | 0.04 | 0.00 | 0.03 | 0.03 | 1.59 | -0.01 | 1.01 | 1.80 | 6.94 | 2.00 | 10.07 | 19.84 | 2.33 | 8.39 | 1.25 | 0.18 | 1.02 | 0.50 | 0.06 | 0.14 | 12.49 |
| | 2 | 0.04 | 0.01 | 0.04 | 0.05 | 1.36 | 0.00 | 0.80 | 1.42 | 6.57 | 1.35 | 10.62 | 20.48 | 2.45 | 8.72 | 1.36 | 0.25 | 1.06 | 0.45 | 0.09 | 0.12 | 12.41 |
| 5 | 1 | 0.18 | 0.01 | 0.09 | 0.25 | 0.33 | 0.00 | 0.25 | 0.88 | 2.98 | 0.15 | 11.66 | 23.82 | 2.87 | 10.33 | 1.68 | 0.28 | 1.08 | 0.40 | 0.04 | 0.10 | 12.34 |
| | 2 | 0.54 | 0.02 | 0.13 | 0.22 | 0.38 | 0.01 | 0.56 | 0.85 | 8.00 | 0.17 | 10.64 | 21.03 | 2.60 | 9.81 | 1.51 | 0.21 | 0.94 | 0.38 | 0.03 | 0.03 | 11.29 |
| 6 | 1 | 0.44 | 0.01 | 0.02 | 0.22 | 0.41 | -0.01 | 0.26 | 0.99 | 3.68 | 0.12 | 12.26 | 24.60 | 2.73 | 9.88 | 1.56 | 0.21 | 1.06 | 0.42 | 0.03 | 0.00 | 12.16 |
| 7 | 1 | 0.09 | 0.03 | -0.02 | 0.18 | 1.49 | -0.02 | 0.86 | 1.79 | 6.94 | 1.50 | 10.43 | 20.91 | 2.34 | 8.67 | 1.33 | 0.21 | 1.10 | 0.53 | 0.04 | 0.16 | 12.98 |
| **Sample 324: Einasleigh Metamorphics (Gum Flats)** | | | | | | | | | | | | | | | | | | | | | | |
| 1 | 1 | 0.12 | 0.00 | 0.02 | 0.18 | 0.88 | 0.01 | 0.50 | 1.65 | 4.87 | 0.60 | 12.04 | 23.03 | 2.44 | 8.99 | 1.43 | -0.07 | 1.20 | 0.58 | 0.05 | 0.12 | 12.39 |
| | 2 | 0.07 | 0.01 | 0.02 | 0.14 | 0.94 | 0.01 | 0.50 | 1.82 | 4.63 | 0.69 | 11.97 | 22.93 | 2.50 | 9.10 | 1.40 | -0.10 | 1.23 | 0.59 | 0.09 | 0.18 | 12.60 |
| | 3 | 0.40 | 0.00 | 0.03 | 0.20 | 0.76 | 0.01 | 0.59 | 1.60 | 6.85 | 0.39 | 11.90 | 22.72 | 2.40 | 8.58 | 1.38 | -0.08 | 1.17 | 0.57 | 0.06 | 0.13 | 11.98 |
| 2 | 1 | 0.14 | 0.00 | 0.01 | 0.10 | 0.61 | 0.01 | 0.41 | 1.58 | 4.09 | 0.43 | 12.44 | 23.80 | 2.63 | 9.18 | 1.40 | -0.11 | 1.15 | 0.54 | 0.05 | 0.08 | 12.28 |
| | 2 | 0.18 | 0.21 | 0.01 | 0.16 | 0.57 | 0.01 | 0.35 | 1.48 | 4.02 | 0.31 | 12.46 | 24.05 | 2.60 | 9.22 | 1.45 | -0.04 | 1.07 | 0.47 | 0.02 | 0.11 | 12.18 |
| 3 | 1 | 0.07 | -0.01 | 0.01 | 0.14 | 0.90 | 0.00 | 0.50 | 1.83 | 4.53 | 0.73 | 11.82 | 22.77 | 2.58 | 9.03 | 1.39 | -0.11 | 1.16 | 0.58 | 0.10 | 0.12 | 12.43 |
| | 2 | 0.10 | 0.00 | 0.00 | 0.10 | 0.87 | 0.01 | 0.51 | 1.79 | 4.40 | 0.75 | 12.02 | 23.37 | 2.50 | 9.10 | 1.34 | -0.11 | 1.13 | 0.60 | 0.09 | 0.15 | 12.56 |
| | 3 | 0.08 | 0.00 | 0.01 | 0.09 | 0.89 | 0.00 | 0.51 | 1.86 | 4.41 | 0.76 | 11.96 | 23.10 | 2.50 | 9.16 | 1.41 | -0.08 | 1.22 | 0.58 | 0.08 | 0.14 | 12.44 |
| 4 | 1 | 0.20 | 0.00 | 0.03 | 0.06 | 0.67 | 0.01 | 0.37 | 1.53 | 4.07 | 0.32 | 12.34 | 23.97 | 2.59 | 9.25 | 1.44 | -0.05 | 1.13 | 0.50 | 0.06 | 0.09 | 12.25 |
| 5 | 1 | 0.25 | 0.00 | 0.01 | 0.04 | 0.57 | 0.01 | 0.40 | 1.51 | 4.66 | 0.27 | 12.50 | 23.56 | 2.55 | 9.25 | 1.47 | -0.07 | 1.18 | 0.53 | 0.03 | 0.10 | 12.21 |
| | 2 | 0.09 | 0.00 | 0.01 | 0.02 | 0.86 | 0.02 | 0.49 | 1.79 | 4.48 | 0.69 | 12.15 | 23.13 | 2.66 | 8.95 | 1.43 | -0.08 | 1.14 | 0.59 | 0.09 | 0.09 | 12.47 |
| | 3 | 0.19 | 0.01 | 0.01 | 0.05 | 0.52 | 0.02 | 0.33 | 1.43 | 3.85 | 0.25 | 13.21 | 24.52 | 2.59 | 9.24 | 1.39 | -0.08 | 1.02 | 0.46 | 0.05 | 0.13 | 12.17 |
| | 4 | 0.06 | 0.00 | 0.02 | 0.14 | 0.91 | 0.02 | 0.47 | 1.75 | 4.38 | 0.65 | 12.10 | 23.23 | 2.58 | 9.01 | 1.36 | -0.10 | 1.18 | 0.57 | 0.07 | 0.14 | 12.54 |
| 6 | 1 | 0.26 | 0.00 | 0.01 | 0.15 | 0.58 | 0.01 | 0.41 | 1.48 | 4.67 | 0.34 | 12.27 | 23.40 | 2.63 | 9.36 | 1.46 | -0.06 | 1.15 | 0.48 | 0.06 | 0.09 | 12.29 |
| | 2 | 0.24 | 0.00 | 0.01 | 0.09 | 0.52 | 0.00 | 0.38 | 1.45 | 4.27 | 0.33 | 12.34 | 23.93 | 2.65 | 9.53 | 1.48 | -0.07 | 1.14 | 0.55 | 0.05 | 0.12 | 12.26 |
| | 3 | 0.17 | 0.00 | 0.01 | 0.10 | 0.80 | 0.02 | 0.50 | 1.83 | 4.89 | 0.64 | 11.64 | 22.73 | 2.54 | 9.20 | 1.41 | -0.12 | 1.15 | 0.56 | 0.06 | 0.11 | 12.39 |
| | 4 | 0.18 | 0.00 | 0.01 | 0.17 | 0.93 | 0.01 | 0.59 | 1.91 | 5.35 | 0.77 | 11.47 | 22.28 | 2.49 | 8.98 | 1.35 | -0.05 | 1.18 | 0.55 | 0.10 | 0.13 | 12.55 |
| 7 | 1 | 0.24 | 0.01 | 0.02 | 0.03 | 0.71 | 0.01 | 0.41 | 1.54 | 4.58 | 0.36 | 12.41 | 23.84 | 2.64 | 9.32 | 1.51 | -0.08 | 1.13 | 0.49 | 0.04 | 0.19 | 12.31 |
| | 2 | 0.09 | 0.01 | 0.01 | 0.02 | 1.00 | 0.00 | 0.53 | 2.49 | 4.69 | 0.86 | 11.50 | 22.59 | 2.58 | 9.19 | 1.41 | -0.23 | 1.30 | 0.70 | 0.11 | 0.21 | 12.53 |
| 8 | 1 | 0.09 | 0.00 | 0.00 | 0.00 | 0.68 | 0.00 | 0.40 | 1.56 | 3.69 | 0.61 | 12.38 | 23.62 | 2.63 | 9.41 | 1.49 | -0.07 | 1.05 | 0.53 | 0.04 | 0.08 | 12.47 |
| | 2 | 0.07 | 0.01 | 0.01 | 0.01 | 0.65 | 0.01 | 0.38 | 1.45 | 3.41 | 0.56 | 12.58 | 24.03 | 2.68 | 9.35 | 1.47 | -0.06 | 1.08 | 0.52 | 0.07 | 0.11 | 12.47 |
| | 3 | 0.07 | 0.00 | 0.00 | 0.02 | 0.65 | 0.00 | 0.37 | 1.46 | 3.38 | 0.53 | 12.53 | 23.79 | 2.58 | 9.18 | 1.41 | -0.07 | 1.12 | 0.49 | 0.05 | 0.10 | 12.29 |
| 9 | 1 | 0.04 | 0.00 | 0.00 | 0.01 | 0.74 | 0.00 | 0.40 | 1.73 | 3.50 | 0.65 | 12.21 | 23.53 | 2.66 | 9.36 | 1.35 | -0.09 | 1.12 | 0.51 | 0.07 | 0.15 | 12.59 |
| | 2 | 0.08 | 0.00 | 0.01 | 0.01 | 0.74 | 0.01 | 0.42 | 1.65 | 3.76 | 0.59 | 12.81 | 24.14 | 2.57 | 9.31 | 1.41 | -0.07 | 1.16 | 0.52 | 0.07 | 0.11 | 12.59 |
| | 3 | 0.11 | 0.01 | 0.00 | 0.01 | 0.77 | 0.00 | 0.42 | 1.78 | 4.44 | 0.45 | 12.05 | 23.01 | 2.55 | 9.16 | 1.37 | -0.14 | 1.12 | 0.56 | 0.06 | 0.12 | 12.47 |
| 10 | 1 | 0.05 | 0.00 | 0.01 | 0.15 | 0.78 | 0.00 | 0.48 | 1.81 | 3.74 | 0.78 | 12.45 | 23.57 | 2.58 | 9.15 | 1.39 | -0.16 | 1.12 | 0.62 | 0.06 | 0.16 | 12.80 |
| 11 | 1 | 0.09 | 0.00 | 0.01 | 0.07 | 0.69 | 0.01 | 0.43 | 1.75 | 3.75 | 0.61 | 12.35 | 23.78 | 2.58 | 9.44 | 1.44 | -0.08 | 1.12 | 0.55 | 0.04 | 0.12 | 12.52 |

| Grain/analysis | | S | As | O | Total (wt%) | Pb (ppm) | Th (ppm) | U (ppm) | Age (Ma) | ± 1 σ |
|---|---|---|---|---|---|---|---|---|---|---|
| 5 | 1 | 0.00 | 0.03 | 26.43 | 97.67 | 3109 | 27168 | 4879 | 1513 | 28 |
| 6 | 1 | 0.01 | 0.00 | 26.60 | 96.29 | 1001 | 30813 | 1075 | 646 | 27 |
| 7 | 1 | 0.00 | -0.12 | 30.03 | 100.88 | 1237 | 21070 | 1574 | 1028 | 36 |
| 8 | 1 | 0.00 | 0.00 | 26.41 | 97.88 | 3113 | 33429 | 3255 | 1501 | 28 |
| | 2 | 0.00 | 0.03 | 26.33 | 97.48 | 3095 | 33881 | 2950 | 1513 | 28 |
| **Sample 308: Daniel Creek Formation (Gum Flats)** | | | | | | | | | | |
| 1 | 1 | 0.00 | 0.00 | 28.01 | 100.45 | 5714 | 50089 | 9780 | 1464 | 17 |
| 2 | 1 | 0.01 | 0.02 | 26.98 | 100.84 | 14739 | 178379 | 8278 | 1537 | 9 |
| | 2 | 0.00 | 0.01 | 27.35 | 100.28 | 5695 | 44867 | 10331 | 1512 | 17 |
| 3 | 1 | 0.00 | 0.03 | 25.93 | 95.19 | 7716 | 66909 | 13572 | 1457 | 13 |
| 4 | 1 | 0.00 | 0.02 | 26.04 | 95.79 | 10056 | 69389 | 19957 | 1548 | 11 |
| | 2 | 0.00 | 0.02 | 25.90 | 95.55 | 7937 | 65681 | 13458 | 1515 | 13 |
| 5 | 1 | 0.00 | 0.02 | 25.91 | 95.64 | 2415 | 29820 | 1500 | 1492 | 36 |
| | 2 | 0.00 | 0.01 | 24.85 | 94.20 | 5587 | 80015 | 1686 | 1414 | 17 |
| 6 | 1 | 0.00 | 0.02 | 26.20 | 97.27 | 2545 | 36769 | 1182 | 1355 | 31 |
| 7 | 1 | 0.00 | 0.01 | 26.98 | 98.57 | 8575 | 69362 | 14992 | 1514 | 13 |
| **Sample 324: Einasleigh Metamorphics (Gum Flats)** | | | | | | | | | | |
| 1 | 1 | 0.00 | 0.01 | 26.24 | 97.37 | 5025 | 48698 | 6013 | 1551 | 19 |
| | 2 | 0.00 | 0.01 | 26.50 | 97.92 | 5062 | 46273 | 6874 | 1548 | 19 |
| | 3 | 0.00 | 0.02 | 26.07 | 97.81 | 5911 | 68474 | 3939 | 1552 | 17 |
| 2 | 1 | 0.00 | 0.01 | 26.07 | 97.01 | 4099 | 40866 | 4302 | 1577 | 23 |
| | 2 | 0.00 | 0.03 | 26.17 | 97.13 | 3561 | 40152 | 3141 | 1505 | 25 |
| 3 | 1 | 0.00 | 0.01 | 26.18 | 96.91 | 5085 | 45301 | 7266 | 1546 | 19 |
| | 2 | 0.00 | 0.01 | 26.46 | 97.85 | 5130 | 43998 | 7470 | 1570 | 19 |
| | 3 | 0.00 | 0.01 | 26.29 | 97.51 | 5098 | 44104 | 7609 | 1549 | 19 |
| 4 | 1 | 0.00 | 0.02 | 26.11 | 97.02 | 3706 | 40721 | 3246 | 1536 | 25 |
| 5 | 1 | 0.00 | 0.01 | 26.10 | 97.22 | 4011 | 46564 | 2727 | 1544 | 23 |
| | 2 | 0.00 | 0.01 | 26.29 | 97.44 | 4966 | 44831 | 6923 | 1547 | 19 |
| | 3 | 0.00 | 0.01 | 26.06 | 97.50 | 3321 | 38455 | 2491 | 1522 | 27 |
| | 4 | 0.00 | 0.00 | 26.38 | 97.55 | 4759 | 43830 | 6451 | 1542 | 20 |
| 6 | 1 | 0.00 | 0.01 | 26.20 | 97.31 | 4174 | 46660 | 3369 | 1542 | 24 |
| | 2 | 0.00 | 0.02 | 26.18 | 97.54 | 3844 | 42677 | 3290 | 1532 | 25 |
| | 3 | 0.00 | 0.01 | 26.21 | 96.97 | 5092 | 48922 | 6402 | 1537 | 20 |
| | 4 | 0.00 | 0.02 | 26.46 | 97.48 | 5990 | 53494 | 7730 | 1595 | 18 |
| 7 | 1 | 0.00 | 0.01 | 26.36 | 98.18 | 4165 | 45763 | 3617 | 1539 | 24 |
| | 2 | 0.01 | 0.01 | 26.57 | 98.41 | 5355 | 46923 | 8558 | 1501 | 18 |
| 8 | 1 | 0.00 | 0.01 | 26.22 | 96.95 | 4035 | 36852 | 6064 | 1499 | 23 |
| | 2 | 0.00 | 0.02 | 26.22 | 97.15 | 3847 | 34123 | 5643 | 1536 | 25 |
| | 3 | 0.00 | 0.02 | 25.88 | 95.92 | 3759 | 33789 | 5286 | 1546 | 25 |
| 9 | 1 | 0.00 | 0.00 | 26.31 | 96.95 | 4075 | 34996 | 6488 | 1520 | 23 |
| | 2 | 0.00 | 0.03 | 26.58 | 98.56 | 4262 | 37577 | 5864 | 1575 | 23 |
| | 3 | 0.00 | 0.03 | 26.21 | 96.71 | 4240 | 44369 | 4502 | 1522 | 23 |
| 10 | 1 | 0.00 | 0.02 | 26.75 | 98.47 | 4827 | 37444 | 7787 | 1597 | 21 |
| 11 | 1 | 0.00 | 0.03 | 26.40 | 97.76 | 4303 | 37460 | 6143 | 1567 | 23 |

# APPENDIX 3:

# Representative THERMOCALC outputs

**Sample 282**

Average P-T

Activities and their uncertainties

| | py | gr | alm | phl | ann | east | mu |
|---|---|---|---|---|---|---|---|
| a | 0.00121 | 3.50e-5 | 0.340 | 0.0353 | 0.0530 | 0.0390 | 0.720 |
| sd(a)/a | 0.71841 | 0.91713 | 0.15000 | 0.40638 | 0.35554 | 0.39308 | 0.10000 |

| | pa | cel | an | ab | q | H2O |
|---|---|---|---|---|---|---|
| a | 0.296 | 0.0210 | 0.280 | 0.820 | 1.00 | 1.00 |
| sd(a)/a | 0.14868 | 0.47619 | 0.15552 | 0.05000 | 0 | |

Independent set of reactions
1) gr + 2pa + 3q = 3an + 2ab + 2H2O
2) 3east + 6q = py + phl + 2mu
3) phl + east + 6q = py + 2cel
4) ann + 3an = gr + alm + mu
5) phl + 3an = py + gr + mu

Calculations for the independent set of reactions
(for x(H2O) = 1.0)

| | P(T) | sd(P) | a | sd(a) | b | c | ln_K | sd(ln_K) |
|---|---|---|---|---|---|---|---|---|
| 1 | 4.6 | 0.97 | 142.97 | 0.70 | -0.26761 | 8.562 | 8.479 | 1.076 |
| 2 | 5.1 | 3.14 | 13.93 | 1.24 | 0.01303 | -3.575 | -0.985 | 1.453 |
| 3 | 7.9 | 2.43 | 59.19 | 1.09 | 0.03692 | -4.185 | -7.856 | 1.320 |
| 4 | 5.7 | 1.15 | -34.73 | 1.16 | 0.12438 | -7.402 | -4.911 | 1.104 |
| 5 | 4.8 | 1.43 | 9.80 | 0.71 | 0.11083 | -7.110 | -10.143 | 1.323 |

Average PT (for x(H2O) = 1.0)

| | avP | sd | avT | sd | cor | fit |
|---|---|---|---|---|---|---|
| lsq | 6.9 | 1.5 | 726 | 45 | 0.718 | 1.13 |

| | P | sd(P) | T | sd(T) | cor | fit | e* | hat |
|---|---|---|---|---|---|---|---|---|
| py | 7.46 | 1.39 | 748 | 43 | 0.753 | 0.90 | -1.13 | 0.20 |
| gr | 7.63 | 1.76 | 731 | 42 | 0.675 | 1.06 | -0.53 | 0.50 |
| alm | 6.75 | 1.49 | 719 | 46 | 0.739 | 1.10 | 0.30 | 0.05 |
| phl | 6.98 | 1.48 | 730 | 46 | 0.721 | 1.12 | 0.29 | 0.07 |
| ann | 6.32 | 1.46 | 701 | 47 | 0.781 | 1.00 | -0.71 | 0.26 |
| east | 6.92 | 1.54 | 726 | 45 | 0.711 | 1.13 | 0.01 | 0.09 |
| mu | 6.98 | 1.51 | 729 | 46 | 0.730 | 1.13 | -0.13 | 0.04 |
| pa | 6.90 | 1.51 | 723 | 59 | 0.659 | 1.13 | -0.05 | 0.39 |
| cel | 6.35 | 1.40 | 719 | 40 | 0.719 | 0.91 | 1.20 | 0.17 |
| an | 7.19 | 1.60 | 728 | 44 | 0.695 | 1.11 | 0.27 | 0.13 |
| ab | 6.92 | 1.49 | 726 | 46 | 0.705 | 1.13 | 0.02 | 0.04 |
| q | 6.92 | 1.48 | 726 | 45 | 0.718 | 1.13 | 0 | 0 |
| H2O | 6.92 | 1.48 | 726 | 45 | 0.718 | 1.13 | 0 | 0 |

T = 726°C, sd = 45,
P = 6.9 kbars, sd = 1.5, cor = 0.718, sigfit = 1.13

Average P-T

Activities and their uncertainties

| | py | gr | alm | phl | ann | east | mu |
|---|---|---|---|---|---|---|---|
| a | 0.00146 | 3.40e-5 | 0.370 | 0.0277 | 0.0220 | 0.0520 | 0.720 |
| sd(a)/a | 0.70738 | 0.92604 | 0.15000 | 0.43777 | 0.46630 | 0.35756 | 0.10000 |

| | pa | cel | an | ab | q | H2O |
|---|---|---|---|---|---|---|
| a | 0.296 | 0.0210 | 0.330 | 0.800 | 1.00 | 1.00 |
| sd(a)/a | 0.14868 | 0.47619 | 0.13467 | 0.05000 | 0 | |

Independent set of reactions
1) 3east + 6q = py + phl + 2mu
2) 2east + 6q = py + mu + cel
3) phl + 3an = py + gr + mu
4) ann + 3an = gr + alm + mu
5) py + 2pa + 3cel = 3east + 2ab + 9q + 2H2O

Calculations for the independent set of reactions
(for x(H2O) = 1.0)

| | P(T) | sd(P) | a | sd(a) | b | c | ln_K | sd(ln_K) |
|---|---|---|---|---|---|---|---|---|
| 1 | 3.2 | 2.83 | 13.91 | 1.24 | 0.01289 | -3.547 | -1.903 | 1.372 |
| 2 | 6.1 | 2.12 | 36.56 | 1.12 | 0.02484 | -3.856 | -4.808 | 1.117 |
| 3 | 4.5 | 1.34 | 9.11 | 0.71 | 0.11171 | -7.128 | -10.235 | 1.313 |
| 4 | 5.6 | 1.11 | -35.56 | 1.16 | 0.12540 | -7.418 | -4.469 | 1.127 |
| 5 | 5.5 | 1.51 | 57.33 | 2.02 | -0.21869 | 9.460 | 11.238 | 1.947 |

Average PT (for x(H2O) = 1.0)

| | avP | sd | avT | sd | cor | fit |
|---|---|---|---|---|---|---|
| lsq | 7.3 | 2.3 | 768 | 75 | 0.754 | 1.64 |

| | P | sd(P) | T | sd(T) | cor | fit | e* | hat |
|---|---|---|---|---|---|---|---|---|
| py | 8.56 | 1.89 | 817 | 64 | 0.801 | 1.22 | -1.71 | 0.26 |
| gr | 7.96 | 2.80 | 772 | 75 | 0.703 | 1.60 | -0.46 | 0.52 |
| alm | 7.13 | 2.29 | 759 | 76 | 0.767 | 1.59 | 0.43 | 0.03 |
| phl | 7.39 | 2.34 | 770 | 79 | 0.758 | 1.64 | 0.15 | 0.09 |
| ann | 6.23 | 2.14 | 721 | 74 | 0.808 | 1.36 | -1.33 | 0.28 |
| east | 7.56 | 2.36 | 770 | 74 | 0.748 | 1.61 | 0.53 | 0.10 |
| mu | 7.45 | 2.34 | 773 | 78 | 0.765 | 1.62 | -0.22 | 0.03 |
| pa | 7.30 | 2.35 | 762 | 95 | 0.695 | 1.64 | -0.10 | 0.34 |
| cel | 6.61 | 2.07 | 759 | 64 | 0.749 | 1.39 | 1.56 | 0.17 |
| an | 7.53 | 2.47 | 769 | 75 | 0.733 | 1.63 | 0.20 | 0.10 |
| ab | 7.34 | 2.32 | 767 | 78 | 0.743 | 1.64 | 0.03 | 0.04 |
| q | 7.34 | 2.31 | 768 | 75 | 0.754 | 1.64 | 0 | 0 |
| H2O | 7.34 | 2.31 | 768 | 75 | 0.754 | 1.64 | 0 | 0 |

T = 768°C, sd = 75,
P = 7.3 kbars, sd = 2.3, cor = 0.754, sigfit = 1.64

## Sample 288

Average P-T (M1)

Activities and their uncertainties

| | py | gr | alm | phl | ann | east | mu |
|---|---|---|---|---|---|---|---|
| a | 0.000680 | 6.60e-5 | 0.350 | 0.0188 | 0.0540 | 0.0370 | 0.650 |
| sd(a)/a | 0.74867 | 0.82873 | 0.15143 | 0.48501 | 0.35355 | 0.40013 | 0.10000 |

| | pa | cel | an | ab | q | H2O |
|---|---|---|---|---|---|---|
| a | 0.660 | 0.0150 | 0.145 | 0.910 | 1.00 | 1.00 |
| sd(a)/a | 0.10061 | 0.66667 | 0.21931 | 0.05011 | 0 | |

Independent set of reactions
1) phl + east + 6q = py + 2cel
2) 2east + 6q = py + mu + cel
3) phl + 3an = py + gr + mu
4) ann + 3an = gr + alm + mu
5) py + 2pa + 3cel = 3east + 2ab + 9q + 2H2O

Calculations for the independent set of reactions
(for x(H2O) = 1.0)

| | P(T) | sd(P) | a | sd(a) | b | c | ln_K | sd(ln_K) |
|---|---|---|---|---|---|---|---|---|
| 1 | 7.7 | 2.77 | 59.16 | 1.09 | 0.03650 | -4.108 | -8.422 | 1.653 |
| 2 | 5.3 | 2.33 | 36.53 | 1.12 | 0.02455 | -3.804 | -5.330 | 1.287 |
| 3 | 6.9 | 1.34 | 8.20 | 0.71 | 0.11276 | -7.126 | -7.583 | 1.388 |
| 4 | 6.9 | 1.05 | -36.59 | 1.16 | 0.12658 | -7.414 | -2.395 | 1.130 |
| 5 | 5.3 | 1.86 | 56.79 | 2.02 | -0.21602 | 9.130 | 10.644 | 2.460 |

Average PT (for x(H2O) = 1.0)

| | avP | sd | avT | sd | cor | fit |
|---|---|---|---|---|---|---|
| lsq | 7.6 | 1.3 | 642 | 31 | 0.716 | 1.02 |

| | P | sd(P) | T | sd(T) | cor | fit | e* | hat |
|---|---|---|---|---|---|---|---|---|
| py | 8.08 | 1.36 | 656 | 34 | 0.750 | 0.84 | -0.95 | 0.19 |
| gr | 7.20 | 1.65 | 640 | 31 | 0.669 | 0.99 | 0.29 | 0.45 |
| alm | 7.55 | 1.34 | 639 | 33 | 0.738 | 1.01 | 0.17 | 0.06 |
| phl | 7.59 | 1.29 | 638 | 32 | 0.711 | 0.98 | -0.46 | 0.07 |
| ann | 7.29 | 1.44 | 629 | 39 | 0.783 | 0.97 | -0.40 | 0.34 |
| east | 8.07 | 1.33 | 646 | 31 | 0.713 | 0.73 | 1.20 | 0.08 |
| mu | 7.73 | 1.34 | 645 | 33 | 0.734 | 1.01 | -0.16 | 0.05 |
| pa | 7.63 | 1.33 | 640 | 38 | 0.678 | 1.02 | -0.06 | 0.22 |
| cel | 7.51 | 1.33 | 641 | 31 | 0.712 | 0.99 | 0.44 | 0.11 |
| an | 7.33 | 1.56 | 640 | 31 | 0.677 | 1.00 | -0.23 | 0.28 |
| ab | 7.64 | 1.32 | 642 | 33 | 0.703 | 1.02 | 0.03 | 0.06 |
| q | 7.65 | 1.31 | 642 | 31 | 0.716 | 1.02 | 0 | 0 |
| H2O | 7.65 | 1.31 | 642 | 31 | 0.716 | 1.02 | 0 | 0 |

T = 642°C, sd = 31,
P = 7.6 kbars, sd = 1.3, cor = 0.716, sigfit = 1.02

Average P-T (M2)

Activities and their uncertainties

| | py | alm | phl | ann | east | clin | daph |
|---|---|---|---|---|---|---|---|
| a | 0.000410 | 0.340 | 0.0348 | 0.0530 | 0.0640 | 0.0105 | 0.0520 |
| sd(a)/a | 0.77125 | 0.15000 | 0.40826 | 0.35086 | 0.33482 | 0.54900 | 0.35756 |

| | ames | mu | cel | q | H2O |
|---|---|---|---|---|---|
| a | 0.0110 | 0.730 | 0.0180 | 1.00 | 1.00 |
| sd(a)/a | 0.48074 | 0.15000 | 0.55556 | 0 | |

··INCOMPLETE·· independent set of reactions
1) 2east + 6q = py + mu + cel
2) py + 2ann + 3ames + 6q = 2alm + 3clin + 2mu
3) 10east + 3daph + 30q = 5alm + 3clin + 5mu + 5cel

Calculations for the independent set of reactions
(for x(H2O) = 1.0)

| | P(T) | sd(P) | a | sd(a) | b | c | ln_K | sd(ln_K) |
|---|---|---|---|---|---|---|---|---|
| 1 | 3.4 | 1.97 | 35.53 | 1.12 | 0.02616 | -3.871 | -6.634 | 1.172 |
| 2 | 3.0 | 5.20 | -68.25 | 2.50 | 0.01091 | -3.082 | 10.748 | 2.462 |
| 3 | 2.6 | 1.69 | -41.96 | 7.87 | 0.15461 | -19.191 | -4.365 | 4.890 |

Average PT (for x(H2O) = 1.0)

| | avP | sd | avT | sd | cor | fit |
|---|---|---|---|---|---|---|
| lsq | 3.1 | 1.7 | 557 | 117 | 0.189 | 0.42 |

| | P | sd(P) | T | sd(T) | cor | fit | e* | hat |
|---|---|---|---|---|---|---|---|---|
| py | 2.97 | 2.07 | 539 | 204 | 0.541 | 0.40 | 0.06 | 0.79 |
| alm | 3.09 | 1.75 | 556 | 122 | 0.141 | 0.42 | -0.01 | 0.04 |
| ann | 3.05 | 1.74 | 557 | 117 | 0.185 | 0.36 | -0.14 | 0.01 |
| east | 3.39 | 2.45 | 557 | 117 | 0.142 | 0.38 | 0.11 | 0.42 |
| clin | 2.93 | 1.85 | 573 | 133 | -0.013 | 0.33 | 0.18 | 0.28 |
| daph | 3.12 | 1.74 | 550 | 125 | 0.135 | 0.39 | 0.09 | 0.07 |
| ames | 3.01 | 1.75 | 558 | 117 | 0.180 | 0.27 | -0.28 | 0.02 |
| mu | 3.06 | 1.80 | 557 | 117 | 0.178 | 0.41 | 0.03 | 0.03 |
| cel | 3.30 | 2.28 | 557 | 117 | 0.150 | 0.39 | -0.09 | 0.29 |
| q | 3.09 | 1.73 | 557 | 117 | 0.189 | 0.42 | 0 | 0 |

T = 557°C, sd = 117,
P = 3.1 kbars, sd = 1.7, cor = 0.189, sigfit = 0.42

## Sample 293

Average P-T (M1)

Activities and their uncertainties

| | py | gr | alm | mu | pa | cel | an |
|---|---|---|---|---|---|---|---|
| a | 0.000165 | 0.0170 | 0.0510 | 0.510 | 0.163 | 0.0590 | 0.800 |
| sd(a)/a | 0.80398 | 0.49667 | 0.35625 | 0.15000 | 0.21332 | 0.26564 | 0.05025 |

| | ab | phl | ann | east | cz | ep | fep |
|---|---|---|---|---|---|---|---|
| a | 0.460 | 0.0350 | 0.0770 | 0.0310 | 0.240 | 0.710 | 0.0560 |
| sd(a)/a | 0.08748 | 0.39650 | 0.31321 | 0.42337 | 0.17328 | 0.10000 | 0.34963 |

| | q | H2O |
|---|---|---|
| a | 1.00 | 1.00 |
| sd(a)/a | 0 | |

Independent set of reactions
1) 4gr + 5pa + 6q = 5ab + 6cz + 2H2O
2) 2east + 6q = py + mu + cel
3) 3an + phl = py + gr + mu
4) cel + 3an + east = py + gr + 2mu
5) 2py + 3mu + 24cz = 5gr + 33an + 3east + 12H2O
6) 3an + ann = gr + alm + mu
7) alm + mu + 8ep + q = 8an + ann + 4fep + 2H2O

Calculations for the independent set of reactions
(for x(H2O) = 1.0)

| | P(T) | sd(P) | a | sd(a) | b | c | ln_K | sd(ln_K) |
|---|---|---|---|---|---|---|---|---|
| 1 | 7.8 | 3.11 | 66.08 | 2.59 | -0.23594 | 5.952 | 12.923 | 2.521 |
| 2 | 5.2 | 2.30 | 36.78 | 1.12 | 0.02446 | -3.834 | -5.266 | 1.207 |
| 3 | 5.4 | 1.07 | 8.98 | 0.71 | 0.11179 | -7.118 | -9.436 | 1.047 |
| 4 | 3.2 | 1.20 | -13.64 | 0.76 | 0.09984 | -6.813 | -7.157 | 1.121 |
| 5 | 5.0 | 0.57 | 1148.36 | 7.62 | -1.85662 | 71.345 | 15.532 | 5.533 |
| 6 | 5.6 | 0.72 | -35.67 | 1.16 | 0.12546 | -7.408 | -4.490 | 0.719 |
| 7 | 5.7 | 0.77 | 331.35 | 4.67 | -0.41406 | 17.430 | -9.490 | 1.733 |

Average PT (for x(H2O) = 1.0)

| | avP | sd | avT | sd | cor | fit |
|---|---|---|---|---|---|---|
| lsq | 6.3 | 1.8 | 624 | 69 | 0.929 | 2.01 |

| | P | sd(P) | T | sd(T) | cor | fit | e* | hat |
|---|---|---|---|---|---|---|---|---|
| py | 6.71 | 1.93 | 641 | 73 | 0.941 | 1.95 | -1.06 | 0.19 |
| gr | 6.39 | 1.91 | 628 | 71 | 0.934 | 2.00 | -0.40 | 0.12 |
| alm | 6.17 | 2.08 | 621 | 77 | 0.943 | 2.01 | 0.14 | 0.18 |
| mu | 6.74 | 1.64 | 640 | 62 | 0.932 | 1.76 | -1.46 | 0.03 |
| pa | 6.66 | 1.76 | 651 | 72 | 0.921 | 1.88 | 1.27 | 0.29 |
| cel | 5.41 | 1.23 | 593 | 46 | 0.934 | 1.31 | 3.33 | 0.07 |
| an | 6.44 | 1.84 | 623 | 68 | 0.889 | 1.98 | 0.48 | 0.22 |
| ab | 6.37 | 1.80 | 631 | 70 | 0.926 | 1.97 | -0.52 | 0.05 |
| phl | 5.68 | 1.77 | 602 | 67 | 0.937 | 1.84 | -1.48 | 0.09 |
| ann | 6.18 | 2.05 | 621 | 76 | 0.942 | 2.01 | -0.12 | 0.14 |
| east | 6.30 | 1.81 | 625 | 69 | 0.929 | 1.99 | 0.56 | 0.01 |
| cz | 6.43 | 1.82 | 622 | 68 | 0.894 | 1.97 | -0.75 | 0.36 |
| ep | 6.29 | 1.83 | 626 | 71 | 0.929 | 2.01 | 0.16 | 0.04 |
| fep | 6.31 | 1.84 | 627 | 72 | 0.928 | 2.00 | -0.27 | 0.11 |
| q | 6.26 | 1.82 | 624 | 69 | 0.929 | 2.01 | 0 | 0 |
| H2O | 6.26 | 1.82 | 624 | 69 | 0.929 | 2.01 | 0 | 0 |

T = 624°C, sd = 69,
P = 6.3 kbars, sd = 1.8, cor = 0.929, sigfit = 2.01

Average P-T (M1R)

Activities and their uncertainties

| | py | gr | alm | phl | ann | east | cz |
|---|---|---|---|---|---|---|---|
| a | 0.000178 | 0.0120 | 0.0490 | 0.0320 | 0.0890 | 0.0270 | 0.280 |
| sd(a)/a | 0.80159 | 0.53508 | 0.36184 | 0.41925 | 0.29541 | 0.44100 | 0.15552 |

| | ep | fep | an | ab | mu | pa | cel |
|---|---|---|---|---|---|---|---|
| a | 0.680 | 0.0470 | 0.800 | 0.450 | 0.610 | 0.239 | 0.0310 |
| sd(a)/a | 0.10000 | 0.36805 | 0.10000 | 0.09075 | 0.10000 | 0.17374 | 0.32258 |

| | q | H2O |
|---|---|---|
| a | 1.00 | 1.00 |
| sd(a)/a | 0 | |

Independent set of reactions
1) 2east + 6q = py + mu + cel
2) py + gr + mu = phl + 3an
3) py + gr + east + cel = 2phl + 3an
4) 5py + 12cz + 15cel = 8gr + 15east + 57q + 6H2O
5) alm + 3east + 6q = 2py + ann + 2mu
6) py + 2pa + 3cel = 3east + 2ab + 9q + 2H2O
7) 2py + 12gr + 18fep + 19pa + 6cel = 6east + 36ep + 19ab + 10H2O

Calculations for the independent set of reactions
(for x(H2O) = 1.0)

| | P(T) | sd(P) | a | sd(a) | b | c | ln_K | sd(ln_K) |
|---|---|---|---|---|---|---|---|---|
| 1 | 5.8 | 2.00 | 35.45 | 1.12 | 0.02569 | -3.766 | -5.378 | 1.239 |
| 2 | 4.6 | 0.93 | -6.79 | 0.71 | -0.11470 | 7.142 | 9.439 | 1.098 |
| 3 | 6.1 | 1.15 | -29.42 | 0.80 | -0.12665 | 7.446 | 12.589 | 1.421 |
| 4 | 5.0 | 1.90 | 94.13 | 11.03 | -0.53000 | 32.877 | 20.989 | 10.249 |
| 5 | 5.2 | 4.08 | 57.91 | 1.55 | -0.00043 | -3.177 | -6.823 | 2.140 |
| 6 | 4.6 | 1.29 | 58.68 | 2.02 | -0.21643 | 8.841 | 9.485 | 1.866 |
| 7 | 6.0 | 2.02 | -40.61 | 21.58 | -1.25471 | 34.993 | 122.689 | 11.192 |

Average PT (for x(H2O) = 1.0)

| | avP | sd | avT | sd | cor | fit |
|---|---|---|---|---|---|---|
| lsq | 5.1 | 1.0 | 559 | 35 | 0.889 | 1.18 |

| | P | sd(P) | T | sd(T) | cor | fit | e* | hat |
|---|---|---|---|---|---|---|---|---|
| py | 5.17 | 1.07 | 562 | 38 | 0.908 | 1.17 | -0.21 | 0.20 |
| gr | 5.08 | 1.02 | 559 | 36 | 0.895 | 1.18 | 0.02 | 0.09 |
| alm | 5.25 | 1.12 | 564 | 39 | 0.916 | 1.17 | -0.26 | 0.18 |

| | | | | | | | | |
|---|---|---|---|---|---|---|---|---|
| phl | 4.77 | 0.91 | 547 | 32 | 0.900 | 1.04 | -1.04 | 0.08 |
| ann | 5.21 | 1.09 | 563 | 38 | 0.911 | 1.17 | 0.21 | 0.12 |
| east | 5.12 | 0.97 | 560 | 34 | 0.889 | 1.16 | 0.44 | 0.02 |
| cz | 5.17 | 1.00 | 559 | 34 | 0.861 | 1.16 | -0.31 | 0.19 |
| ep | 5.07 | 0.98 | 558 | 35 | 0.890 | 1.18 | -0.11 | 0.02 |
| fep | 5.06 | 0.99 | 557 | 36 | 0.891 | 1.17 | 0.20 | 0.07 |
| an | 5.42 | 1.05 | 559 | 33 | 0.788 | 1.13 | 0.50 | 0.52 |
| ab | 5.18 | 0.97 | 565 | 35 | 0.885 | 1.15 | -0.39 | 0.07 |
| mu | 5.24 | 0.94 | 565 | 33 | 0.894 | 1.11 | -0.55 | 0.02 |
| pa | 5.33 | 0.94 | 576 | 36 | 0.882 | 1.09 | 0.74 | 0.27 |
| cel | 4.70 | 0.85 | 548 | 30 | 0.893 | 0.79 | 2.01 | 0.06 |
| q | 5.09 | 0.98 | 559 | 35 | 0.889 | 1.18 | 0 | 0 |
| H2O | 5.09 | 0.98 | 559 | 35 | 0.889 | 1.18 | 0 | 0 |

T = 559°C, sd = 35,
P = 5.1 kbars, sd = 1.0, cor = 0.889, sigfit = 1.18

## Sample 306

Average P-T

Activities and their uncertainties

| | phl | ann | east | py | alm | clin | daph |
|---|---|---|---|---|---|---|---|
| a | 0.0427 | 0.0180 | 0.0680 | 0.000920 | 0.380 | 0.0240 | 0.0260 |
| sd(a)/a | 0.37765 | 0.49008 | 0.32788 | 0.73345 | 0.15000 | 0.45567 | 0.44574 |

| | ames | mu | cel | mst | fst | q | H2O |
|---|---|---|---|---|---|---|---|
| a | 0.0320 | 0.780 | 0.0130 | 0.000330 | 0.560 | 1.00 | 1.00 |
| sd(a)/a | 0.40454 | 0.15000 | 0.76923 | 1.10096 | 0.20000 | 0 | |

Independent set of reactions
1) 27phl + 4mst = 21east + 13py + 2clin + 6cel
2) phl + east + 6q = py + 2cel
3) 16east + ames + 39q = 6phl + 10cel + 2mst
4) 5phl + 13cel + 2mst = 18east + 46q + 4H2O
5) 2phl + mu + 6q = py + 3cel
6) 97phl + 12fst = 16ann + 63east + 39py + 6clin + 18cel
7) 53phl + 10ann + 12mst = 45east + 39py + 6daph + 18mu
8) ann + 3east + 6q = 2phl + alm + 2mu

Calculations for the independent set of reactions
(for x(H2O) = 1.0)

| | P(T) | sd(P) | a | sd(a) | b | c | ln_K | sd(ln_K) |
|---|---|---|---|---|---|---|---|---|
| 1 | 4.3 | 32.44 | 664.67 | 9.57 | -0.29716 | 3.566 | -63.643 | 16.847 |
| 2 | 5.3 | 2.97 | 59.16 | 1.09 | 0.03650 | -4.108 | -9.835 | 1.776 |
| 3 | 5.2 | 2.41 | 55.14 | 8.82 | 0.37536 | -28.142 | -31.928 | 9.841 |
| 4 | 5.3 | 2.40 | 109.29 | 10.40 | -0.68364 | 34.386 | 39.869 | 11.969 |
| 5 | 6.7 | 3.95 | 81.78 | 1.14 | 0.04845 | -4.413 | -13.464 | 2.541 |
| 6 | 3.8 | 33.96 | 2910.55 | 29.62 | -1.14294 | 10.798 | -293.988 | 53.416 |
| 7 | 4.2 | 21.53 | 1576.22 | 29.44 | -1.01367 | 12.981 | -116.486 | 40.615 |
| 8 | 5.4 | 2.52 | -30.89 | 1.55 | 0.02643 | -3.787 | 4.311 | 1.375 |

Average PT (for x(H2O) = 1.0)

| | avP | sd | avT | sd | cor | fit |
|---|---|---|---|---|---|---|
| lsq | 6.3 | 2.5 | 574 | 18 | 0.297 | 1.45 |

| | P | sd(P) | T | sd(T) | cor | fit | e* | hat |
|---|---|---|---|---|---|---|---|---|
| phl | 6.26 | 2.50 | 575 | 19 | 0.282 | 1.45 | -0.30 | 0.06 |
| ann | 4.97 | 2.10 | 571 | 15 | 0.318 | 1.15 | -2.19 | 0.12 |
| east | 8.26 | 2.76 | 572 | 16 | 0.177 | 1.30 | 1.33 | 0.43 |
| py | 6.66 | 2.46 | 579 | 19 | 0.344 | 1.39 | -1.10 | 0.16 |
| alm | 5.65 | 2.57 | 567 | 20 | 0.409 | 1.39 | 0.68 | 0.16 |
| clin | 6.75 | 2.38 | 571 | 17 | 0.243 | 1.35 | -1.21 | 0.10 |
| daph | 6.46 | 2.45 | 581 | 21 | 0.313 | 1.41 | 0.71 | 0.28 |
| ames | 6.33 | 2.43 | 578 | 19 | 0.294 | 1.40 | 0.86 | 0.09 |
| mu | 6.12 | 2.78 | 574 | 18 | 0.192 | 1.45 | 0.13 | 0.15 |
| cel | 6.11 | 2.68 | 574 | 18 | 0.318 | 1.45 | 0.28 | 0.17 |
| mst | 5.98 | 2.49 | 571 | 18 | 0.335 | 1.41 | 0.89 | 0.11 |
| fst | 6.11 | 2.49 | 573 | 18 | 0.304 | 1.43 | -0.41 | 0.01 |
| q | 6.28 | 2.51 | 574 | 18 | 0.297 | 1.45 | 0 | 0 |
| H2O | 6.28 | 2.51 | 574 | 18 | 0.297 | 1.45 | 0 | 0 |

T = 574°C, sd = 18,
P = 6.3 kbars, sd = 2.5, cor = 0.297, sigfit = 1.45

## Sample 312

Average P-T (M1)

Activities and their uncertainties

| | an | tr | fact | ts | cz | ep | fep |
|---|---|---|---|---|---|---|---|
| a | 0.650 | 0.122 | 0.00310 | 0.000100 | 0.300 | 0.430 | 0.0280 |
| sd(a)/a | 0.05000 | 0.25406 | 0.70389 | 2.00000 | 0.14700 | 0.10000 | 0.41600 |

| | py | gr | alm | q | H2O |
|---|---|---|---|---|---|
| a | 6.90e-5 | 0.0570 | 0.0580 | 1.00 | 1.00 |
| sd(a)/a | 2.40772 | 0.34057 | 0.33810 | 0 | |

Independent set of reactions
1) 2cz + py + q = 2an + ts
2) 5ts + 12cz + 14q = 28an + 3tr + 8H2O
3) 6cz + 5py + 4gr + 15q = 18an + 3tr
4) 6cz + 4gr + 5alm + 15q = 18an + 3fact
5) 12ep + 4gr + 5alm + 15q = 18an + 3fact + 6fep

Calculations for the independent set of reactions
(for x(H2O) = 1.0)

| | P(T) | sd(P) | a | sd(a) | b | c | ln_K | sd(ln_K) |
|---|---|---|---|---|---|---|---|---|
| 1 | 8.4 | 4.06 | 17.73 | 2.22 | -0.08961 | 5.969 | 1.917 | 3.145 |

| | | | | | | | | |
|---|---|---|---|---|---|---|---|---|
| 2 | 4.2 | 1.61 | 737.93 | 11.31 | -1.37312 | 49.440 | 42.126 | 10.279 |
| 3 | 4.3 | 2.39 | 21.84 | 2.99 | -0.64277 | 39.258 | 52.524 | 12.205 |
| 4 | 7.5 | 0.63 | 327.07 | 6.19 | -0.75590 | 41.415 | 7.836 | 3.280 |
| 5 | 7.3 | 0.81 | 477.43 | 9.00 | -0.75528 | 41.258 | -10.713 | 4.202 |

Average PT (for x(H2O) = 1.0)

| | avP | sd | avT | sd | cor | fit |
|---|---|---|---|---|---|---|
| lsq | 7.1 | 1.8 | 649 | 69 | 0.942 | 1.37 |

| | P | sd(P) | T | sd(T) | cor | fit | e* | hat |
|---|---|---|---|---|---|---|---|---|
| an | 7.17 | 1.81 | 648 | 69 | 0.913 | 1.37 | 0.05 | 0.18 |
| tr | 7.17 | 1.75 | 649 | 69 | 0.942 | 1.36 | 0.22 | 0.00 |
| fact | 6.44 | 2.15 | 627 | 78 | 0.955 | 1.31 | -0.46 | 0.31 |
| ts | 7.29 | 1.29 | 652 | 51 | 0.942 | 0.98 | -1.90 | 0.01 |
| cz | 7.14 | 1.77 | 651 | 72 | 0.889 | 1.37 | 0.12 | 0.51 |
| ep | 7.10 | 1.81 | 646 | 72 | 0.943 | 1.37 | -0.13 | 0.04 |
| fep | 7.03 | 1.85 | 643 | 74 | 0.946 | 1.36 | 0.27 | 0.17 |
| py | 7.54 | 1.63 | 663 | 64 | 0.946 | 1.22 | -1.21 | 0.09 |
| gr | 7.13 | 2.35 | 648 | 96 | 0.967 | 1.37 | 0.01 | 0.38 |
| alm | 6.66 | 2.05 | 633 | 76 | 0.952 | 1.33 | 0.37 | 0.20 |
| q | 7.15 | 1.77 | 649 | 69 | 0.942 | 1.37 | 0 | 0 |
| H2O | 7.15 | 1.77 | 649 | 69 | 0.942 | 1.37 | 0 | 0 |

T = 649°C, sd = 69,
P = 7.1 kbars, sd = 1.8, cor = 0.942, sigfit = 1.37

Average P-T (M1)

Activities and their uncertainties

| | an | tr | fact | ts | cz | ep | fep |
|---|---|---|---|---|---|---|---|
| a | 0.700 | 0.131 | 0.00340 | 0.000100 | 0.290 | 0.450 | 0.0209 |
| sd(a)/a | 0.05000 | 0.25038 | 0.69188 | 2.00000 | 0.15123 | 0.10000 | 0.43906 |

| | py | gr | alm | q | H2O |
|---|---|---|---|---|---|
| a | 8.70e-5 | 0.0570 | 0.0580 | 1.00 | 1.00 |
| sd(a)/a | 2.14423 | 0.34057 | 0.33810 | 0 | |

Independent set of reactions
1) 2cz + py + q = 2an + ts
2) 6cz + 5py + 4gr + 15q = 18an + 3tr
3) 22cz + 5py + 19q = 38an + 3tr + 8H2O
4) 6cz + 4gr + 5alm + 15q = 18an + 3fact
5) 12ep + 4gr + 5alm + 15q = 18an + 3fact + 6fep

Calculations for the independent set of reactions
(for x(H2O) = 1.0)

| | P(T) | sd(P) | a | sd(a) | b | c | ln_K | sd(ln_K) |
|---|---|---|---|---|---|---|---|---|
| 1 | 7.3 | 3.39 | 10.35 | 2.22 | -0.08135 | 5.998 | 1.902 | 2.949 |
| 2 | 3.7 | 1.89 | 4.04 | 2.99 | -0.62442 | 39.558 | 53.116 | 10.909 |
| 3 | 3.9 | 0.99 | 759.03 | 7.21 | -1.74575 | 79.578 | 54.330 | 11.410 |
| 4 | 5.6 | 0.56 | 310.32 | 6.19 | -0.73863 | 41.698 | 9.651 | 3.264 |
| 5 | 5.4 | 0.74 | 461.51 | 9.00 | -0.73916 | 41.570 | -11.403 | 4.267 |

Average PT (for x(H2O) = 1.0)

| | avP | sd | avT | sd | cor | fit |
|---|---|---|---|---|---|---|
| lsq | 6.4 | 1.7 | 631 | 69 | 0.936 | 1.41 |

| | P | sd(P) | T | sd(T) | cor | fit | e* | hat |
|---|---|---|---|---|---|---|---|---|
| an | 6.46 | 1.75 | 631 | 69 | 0.906 | 1.40 | 0.06 | 0.17 |
| tr | 6.46 | 1.70 | 632 | 68 | 0.936 | 1.39 | 0.22 | 0.00 |
| fact | 5.59 | 1.99 | 605 | 74 | 0.950 | 1.30 | -0.61 | 0.29 |
| ts | 6.57 | 1.24 | 634 | 50 | 0.936 | 1.01 | -1.92 | 0.01 |
| cz | 6.45 | 1.71 | 627 | 72 | 0.877 | 1.40 | -0.18 | 0.52 |
| ep | 6.48 | 1.74 | 634 | 71 | 0.938 | 1.40 | 0.12 | 0.04 |
| fep | 6.54 | 1.78 | 637 | 74 | 0.940 | 1.40 | -0.27 | 0.17 |
| py | 6.83 | 1.62 | 646 | 65 | 0.941 | 1.27 | -1.14 | 0.12 |
| gr | 6.10 | 2.25 | 616 | 95 | 0.964 | 1.39 | 0.20 | 0.38 |
| alm | 5.83 | 1.93 | 612 | 73 | 0.947 | 1.33 | 0.49 | 0.19 |
| q | 6.44 | 1.72 | 631 | 69 | 0.936 | 1.41 | 0 | 0 |
| H2O | 6.44 | 1.72 | 631 | 69 | 0.936 | 1.41 | 0 | 0 |

T = 631°C, sd = 69,
P = 6.4 kbars, sd = 1.7, cor = 0.936, sigfit = 1.41

Average P-T (M1R)

Activities and their uncertainties

| | py | gr | alm | an | cz | ep | fep |
|---|---|---|---|---|---|---|---|
| a | 0.000133 | 0.0580 | 0.0600 | 0.720 | 0.400 | 0.560 | 0.0244 |
| sd(a)/a | 0.81046 | 0.33810 | 0.33326 | 0.15000 | 0.10800 | 0.10000 | 0.42719 |

| | tr | fact | q | H2O |
|---|---|---|---|---|
| a | 0.145 | 0.00350 | 1.00 | 1.00 |
| sd(a)/a | 0.25034 | 0.68808 | 0 | |

Independent set of reactions
1) 5py + 4gr + 6cz + 15q = 18an + 3tr
2) 21an + 6tr = 10py + 11gr + 27q + 6H2O
3) 4gr + 5alm + 6cz + 15q = 18an + 3fact
4) 4gr + 5alm + 12ep + 15q = 18an + 6fep + 3fact

Calculations for the independent set of reactions
(for x(H2O) = 1.0)

| | P(T) | sd(P) | a | sd(a) | b | c | ln_K | sd(ln_K) |
|---|---|---|---|---|---|---|---|---|
| 1 | 4.3 | 0.89 | 4.04 | 2.99 | -0.62442 | 39.558 | 49.807 | 5.150 |
| 2 | 4.0 | 1.34 | 558.15 | 4.74 | 0.40786 | -49.102 | -102.087 | 9.576 |
| 3 | 5.8 | 0.68 | 310.32 | 6.19 | -0.73863 | 41.698 | 8.076 | 4.071 |
| 4 | 5.6 | 0.84 | 461.51 | 9.00 | -0.73916 | 41.570 | -12.743 | 4.916 |

Average PT (for x(H2O) = 1.0)

| | avP | sd | avT | sd | cor | fit |
|---|---|---|---|---|---|---|
| lsq | 5.3 | 1.4 | 562 | 51 | 0.795 | 1.47 |

| | P | sd(P) | T | sd(T) | cor | fit | e* | hat |
|---|---|---|---|---|---|---|---|---|
| py | 6.22 | 1.10 | 596 | 41 | 0.854 | 0.97 | -1.39 | 0.35 |
| gr | 4.81 | 1.62 | 538 | 66 | 0.876 | 1.38 | 0.47 | 0.41 |
| alm | 4.96 | 1.19 | 552 | 43 | 0.805 | 1.21 | 0.84 | 0.06 |
| an | 5.47 | 1.74 | 561 | 51 | 0.539 | 1.46 | 0.12 | 0.74 |
| cz | 5.34 | 1.37 | 559 | 52 | 0.735 | 1.46 | -0.15 | 0.15 |
| ep | 5.30 | 1.38 | 560 | 52 | 0.799 | 1.46 | -0.12 | 0.02 |
| fep | 5.27 | 1.39 | 559 | 53 | 0.803 | 1.45 | 0.26 | 0.09 |
| tr | 5.39 | 1.36 | 564 | 50 | 0.801 | 1.43 | 0.26 | 0.01 |
| fact | 4.85 | 1.12 | 550 | 40 | 0.808 | 1.12 | -1.04 | 0.09 |
| q | 5.32 | 1.37 | 562 | 51 | 0.795 | 1.47 | 0 | 0 |
| H2O | 5.32 | 1.37 | 562 | 51 | 0.795 | 1.47 | 0 | 0 |

T = 562°C, sd = 51,
P = 5.3 kbars, sd = 1.4, cor = 0.795, sigfit = 1.47

Average P-T (M1R)

Activities and their uncertainties

| | py | gr | alm | an | cz | ep | fep |
|---|---|---|---|---|---|---|---|
| a | 0.000107 | 0.0570 | 0.0600 | 0.700 | 0.410 | 0.550 | 0.0330 |
| sd(a)/a | 0.81657 | 0.34057 | 0.33326 | 0.15000 | 0.10443 | 0.10000 | 0.40181 |

| | tr | fact | q | H2O |
|---|---|---|---|---|
| a | 0.137 | 0.00320 | 1.00 | 1.00 |
| sd(a)/a | 0.25036 | 0.69978 | 0 | |

Independent set of reactions
1) 5py + 4gr + 6cz + 15q = 18an + 3tr
2) 5py + 22cz + 19q = 38an + 3tr + 8H2O
3) 4gr + 5alm + 6cz + 15q = 18an + 3fact
4) 4gr + 5alm + 12ep + 15q = 18an + 6fep + 3fact

Calculations for the independent set of reactions
(for x(H2O) = 1.0)

| | P(T) | sd(P) | a | sd(a) | b | c | ln_K | sd(ln_K) |
|---|---|---|---|---|---|---|---|---|
| 1 | 4.8 | 1.01 | 21.84 | 2.99 | -0.64277 | 39.258 | 50.138 | 5.174 |
| 2 | 6.3 | 0.72 | 826.57 | 7.21 | -1.82119 | 79.288 | 45.812 | 7.416 |
| 3 | 7.6 | 0.77 | 327.07 | 6.19 | -0.75590 | 41.415 | 7.221 | 4.089 |
| 4 | 7.5 | 0.93 | 477.43 | 9.00 | -0.75528 | 41.258 | -11.422 | 4.856 |

Average PT (for x(H2O) = 1.0)

| | avP | sd | avT | sd | cor | fit |
|---|---|---|---|---|---|---|
| lsq | 5.5 | 1.6 | 564 | 60 | 0.800 | 1.74 |

| | P | sd(P) | T | sd(T) | cor | fit | e* | hat |
|---|---|---|---|---|---|---|---|---|
| py | 6.56 | 1.28 | 605 | 47 | 0.857 | 1.15 | -1.64 | 0.35 |
| gr | 5.10 | 2.01 | 546 | 82 | 0.878 | 1.70 | 0.35 | 0.41 |
| alm | 5.10 | 1.50 | 555 | 54 | 0.810 | 1.51 | 0.86 | 0.06 |
| an | 5.62 | 2.08 | 563 | 61 | 0.545 | 1.73 | 0.11 | 0.75 |
| cz | 5.47 | 1.65 | 565 | 62 | 0.744 | 1.74 | 0.06 | 0.14 |
| ep | 5.39 | 1.61 | 559 | 60 | 0.804 | 1.68 | -0.43 | 0.02 |
| fep | 5.30 | 1.57 | 555 | 59 | 0.809 | 1.62 | 0.85 | 0.09 |
| tr | 5.56 | 1.63 | 567 | 60 | 0.806 | 1.70 | 0.30 | 0.01 |
| fact | 4.98 | 1.45 | 552 | 51 | 0.813 | 1.43 | -1.08 | 0.09 |
| q | 5.48 | 1.64 | 564 | 60 | 0.800 | 1.74 | 0 | 0 |
| H2O | 5.48 | 1.64 | 564 | 60 | 0.800 | 1.74 | 0 | 0 |

T = 564°C, sd = 60,
P = 5.5 kbars, sd = 1.6, cor = 0.800, sigfit = 1.74

# Appendix 6: Sample Locations

| Sample # | Domain | Unit | GDA 94 grid co-ordinate Easting | Northing | Sample # | Domain | Unit | GDA 94 grid co-ordinate Easting | Northing |
|---|---|---|---|---|---|---|---|---|---|
| 6 | Ortona | Cobbold Metadolerite | 0764910 | 7876412 | 197 | Stockyard | Cobbold Metadolerite | 0735282 | 7941168 |
| 7 | Ortona | Bernecker Creek Formation | 0764782 | 7876443 | 199 | Stockyard | Cobbold Metadolerite | 0735252 | 7941109 |
| 8 | Ortona | Cobbold Metadolerite | 0764822 | 7876539 | 200 | Stockyard | Cobbold Metadolerite | 0735260 | 7941052 |
| 10 | Ortona | Bernecker Creek Formation | 0764782 | 7876533 | 201 | Stockyard | Cobbold Metadolerite | 0735261 | 7941003 |
| 13 | Ortona | Bernecker Creek Formation | 0764531 | 7876765 | 202 | Stockyard | Cobbold Metadolerite | 0735229 | 7940955 |
| 22 | Ortona | Cobbold Metadolerite | 0764081 | 7877964 | 208 | Robinhood | Ropewalk Granite | 0766287 | 7952017 |
| 23 | Ortona | Cobbold Metadolerite | 0763573 | 7879147 | 209 | Robinhood | Ropewalk Granite | 0769766 | 7938112 |
| 60 | Ortona | Cobbold Metadolerite | 0766289 | 7893968 | 210 | Robinhood | Ropewalk Granite | 0769256 | 7936256 |
| 72 | Ortona | Dead Horse Metabasalt | 0780166 | 7866980 | 215 | Robinhood | Cobbold Metadolerite | 0766619 | 7936146 |
| 74 | Ortona | Dead Horse Metabasalt | 0780606 | 7866385 | 221 | South Head | Cobbold Metadolerite | 0745832 | 7904637 |
| 80 | Ortona | Dead Horse Metabasalt | 0758921 | 7883022 | 222 | South Head | Cobbold Metadolerite | 0745814 | 7904652 |
| 82 | Ortona | Dead Horse Metabasalt | 0758968 | 7882795 | 224 | South Head | Cobbold Metadolerite | 0745760 | 7904752 |
| 83 | Ortona | Dead Horse Metabasalt | 0758990 | 7882593 | 226 | South Head | Cobbold Metadolerite | 0745706 | 7904811 |
| 85 | Ortona | Cobbold Metadolerite | 0759485 | 7882209 | 227 | South Head | Cobbold Metadolerite | 0745698 | 7904896 |
| 86 | Ortona | Cobbold Metadolerite | 0759644 | 7882155 | 228 | South Head | Dead Horse Metabasalt | 0745690 | 7904962 |
| 87 | Ortona | Dead Horse Metabasalt | 0759676 | 7881475 | 229 | South Head | Dead Horse Metabasalt | 0745600 | 7905105 |
| 88 | Ortona | Cobbold Metadolerite | 0759735 | 7881315 | 230 | South Head | Dead Horse Metabasalt | 0745525 | 7905294 |
| 89 | Ortona | Dead Horse Metabasalt | 0759838 | 7881284 | 232 | South Head | Dead Horse Metabasalt | 0745399 | 7905478 |
| 90 | Ortona | Dead Horse Metabasalt | 0759889 | 7881014 | 233 | South Head | Dead Horse Metabasalt | 0745299 | 7905707 |
| 97 | Ortona | Daniel Creek Formation | 0760433 | 7879591 | 234 | South Head | Dead Horse Metabasalt | 0745128 | 7906067 |
| 100 | Ortona | Dead Horse Metabasalt | 0761691 | 7880234 | 236 | South Head | Dead Horse Metabasalt | 0744865 | 7906543 |
| 101 | Ortona | Cobbold Metadolerite | 0761714 | 7880144 | 237 | South Head | Cobbold Metadolerite | 0744716 | 7906815 |
| 102 | Ortona | Dead Horse Metabasalt | 0761755 | 7880084 | 240 | South Head | Dead Horse Metabasalt | 0744501 | 7907232 |
| 103 | Ortona | Dead Horse Metabasalt | 0761806 | 7879995 | 241 | South Head | Cobbold Metadolerite | 0744406 | 7907452 |
| 104 | Ortona | Dead Horse Metabasalt | 0761837 | 7879961 | 242 | South Head | Cobbold Metadolerite | 0744302 | 7907651 |
| 106 | Ortona | Cobbold Metadolerite | 0762360 | 7879578 | 243 | South Head | Dead Horse Metabasalt | 0744217 | 7907752 |
| 107 | Ortona | Dead Horse Metabasalt | 0762299 | 7879600 | 245 | South Head | Lane Creek Formation | 0737343 | 7911863 |
| 108 | Ortona | Cobbold Metadolerite | 0762237 | 7879624 | 249 | South Head | Cobbold Metadolerite | 0741348 | 7906695 |
| 109 | Ortona | Cobbold Metadolerite | 0762155 | 7879663 | 250 | South Head | Dead Horse Metabasalt | 0741270 | 7906783 |
| 110 | Ortona | Cobbold Metadolerite | 0762008 | 7879755 | 251 | South Head | Dead Horse Metabasalt | 0741221 | 7906880 |
| 111 | Ortona | Dead Horse Metabasalt | 0761929 | 7879749 | 253 | South Head | Dead Horse Metabasalt | 0741010 | 7907251 |
| 112 | Ortona | Cobbold Metadolerite | 0765456 | 7879961 | 255 | South Head | Daniel Creek Formation | 0740889 | 7907568 |
| 113 | Ortona | Cobbold Metadolerite | 0765188 | 7879846 | 256 | South Head | Dead Horse Metabasalt | 0740889 | 7907568 |
| 114 | Ortona | Cobbold Metadolerite | 0765157 | 7879755 | 260 | Robinhood | Dead Horse Metabasalt | 0765214 | 7911170 |
| 115 | Ortona | Cobbold Metadolerite | 0765216 | 7879873 | 261 | Robinhood | Dead Horse Metabasalt | 0765269 | 7911303 |
| 120 | Ortona | Cobbold Metadolerite | 0764776 | 7879884 | 262 | Robinhood | Dead Horse Metabasalt | 0765424 | 7911326 |
| 121 | Ortona | Cobbold Metadolerite | 0764439 | 7879949 | 264 | Robinhood | Dead Horse Metabasalt | 0765535 | 7911389 |
| 124 | Ortona | Bernecker Creek Formation | 0760673 | 7877719 | 268 | Robinhood | Dead Horse Metabasalt | 0765747 | 7911590 |
| 128 | Ortona | Cobbold Metadolerite | 0764030 | 7876727 | 269 | Robinhood | Dead Horse Metabasalt | 0765675 | 7911505 |
| 129 | Ortona | Cobbold Metadolerite | 0764012 | 7876729 | 270 | Robinhood | Dead Horse Metabasalt | 0765625 | 7911442 |
| 130 | Ortona | Cobbold Metadolerite | 0764012 | 7876729 | 278B | Ortona | Corbett Formation | 0763205 | 7881161 |
| 135 | Gum Flats | Mt Hogan Granite | 0798215 | 7881440 | 282 | Gum Flats | Einasleigh Metamorphics | 0806726 | 7880850 |
| 148 | Ortona | Dead Horse Metabasalt | 0764368 | 7871563 | 283 | Gum Flats | Einasleigh Metamorphics | 0806706 | 7880850 |
| 151 | Ortona | Dead Horse Metabasalt | 0764327 | 7871479 | 288 | Gum Flats | Daniel Creek Formation | 0805845 | 7881526 |
| 152 | Ortona | Cobbold Metadolerite | 0764260 | 7871458 | 291 | Gum Flats | Cobbold Metadolerite | 0803601 | 7885196 |
| 153 | Ortona | Dead Horse Metabasalt | 0764252 | 7871356 | 292 | Gum Flats | Bernecker Creek Formation | 0803612 | 7885159 |
| 154 | Ortona | Dead Horse Metabasalt | 0764248 | 7871333 | 293 | Gum Flats | Bernecker Creek Formation | 0803330 | 7884267 |
| 159 | Ortona | Cobbold Metadolerite | 0765618 | 7869966 | 296 | Gum Flats | Cobbold Metadolerite | 0803182 | 7882632 |
| 161 | Ortona | Cobbold Metadolerite | 0765618 | 7869966 | 299 | Gum Flats | Cobbold Metadolerite | 0803317 | 7881548 |
| 172 | Ortona | Cobbold Metadolerite | 0765141 | 7870249 | 300 | Gum Flats | Cobbold Metadolerite | 0803334 | 7881548 |
| 174 | Ortona | Cobbold Metadolerite | 0763625 | 7878064 | 301 | Gum Flats | Cobbold Metadolerite | 0803598 | 7881489 |
| 175 | Ortona | Cobbold Metadolerite | 0763688 | 7878004 | 304 | Robinhood | Lane Creek Formation | 0766619 | 7936146 |
| 178 | Ortona | Cobbold Metadolerite | 0763728 | 7878008 | 306 | Ortona | Corbett Formation | 0766403 | 7908517 |
| 179 | Ortona | Cobbold Metadolerite | 0763728 | 7878008 | 307 | Gum Flats | Bernecker Creek Formation | 0802540 | 7885152 |
| 181 | Ortona | Cobbold Metadolerite | 0763628 | 7878039 | 308 | Gum Flats | Daniel Creek Formation | 0801829 | 7887568 |
| 184 | Ortona | Daniel Creek Formation | 0763245 | 7882389 | 311 | Gum Flats | Daniel Creek Formation | 0800748 | 7888073 |
| 188 | Ortona | Cobbold Metadolerite | 0763367 | 7881600 | 312 | Gum Flats | Daniel Creek Formation | 0800551 | 7888325 |
| 192 | Stockyard | Cobbold Metadolerite | 0735451 | 7941350 | 317 | Gum Flats | Einasleigh Metamorphics | 0800000 | 7892233 |
| 194 | Stockyard | Cobbold Metadolerite | 0735421 | 7941321 | 318 | Gum Flats | Einasleigh Metamorphics | 0799901 | 7892058 |
| 195 | Stockyard | Cobbold Metadolerite | 0735378 | 7941237 | 324 | Gum Flats | Einasleigh Metamorphics | 0798867 | 7893315 |
| 196 | Stockyard | Cobbold Metadolerite | 0735320 | 7941215 | | | | | |

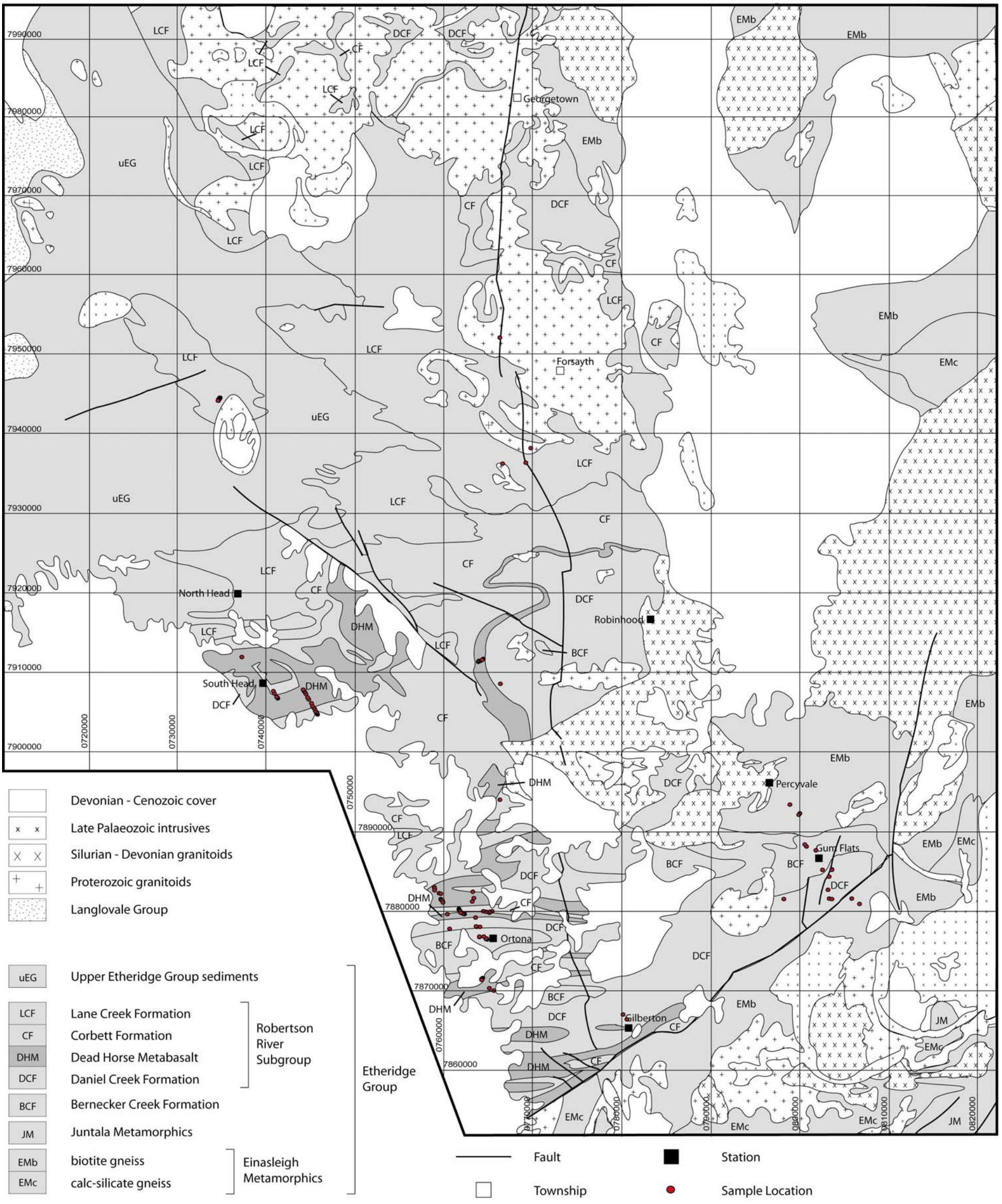
7990000
7980000
7970000
7960000
7950000
7940000
7930000
7920000
7910000
7900000
7890000
7880000
7870000
7860000
0720000
0730000
0740000
0750000
0760000
0770000
0780000
0790000
0800000
0810000
0820000
LCF
DCF
CF
DHM
BCF
uEG
EMb
EMc
JM
Georgetown
Forsayth
North Head
South Head
Robinhood
Percyvale
Gum Flats
Ortona
Gilberton
Devonian - Cenozoic cover
Late Palaeozoic intrusives
Silurian - Devonian granitoids
Proterozoic granitoids
Langlovale Group
uEG Upper Etheridge Group sediments
LCF Lane Creek Formation
CF Corbett Formation
DHM Dead Horse Metabasalt
DCF Daniel Creek Formation
Robertson River Subgroup
BCF Bernecker Creek Formation
JM Juntala Metamorphics
EMb biotite gneiss
EMc calc-silicate gneiss
Einasleigh Metamorphics
Etheridge Group
Fault
Station
Township
Sample Location